Impact on heat rate and subsequent emissions due to varying operation of coal fired power plants

Prepared by:

Patrick Udeme-Obong Akpan

AKPPAT001

Department of Mechanical Engineering

University of Cape Town

Supervisor:

A/Prof Wim Fuls

<June 2019>

Submitted to the Department of Mechanical Engineering at the University of Cape Town in fulfilment of the academic requirements for a **Doctor of Philosophy** degree in Mechanical Engineering

Key Words: Coal fired Power Plants, Heat rates, CO_2 emissions, Renewable Power Integration, Power Plant modelling and simulation, Energy Mix Modelling

Abstract

Energy mix modellers often use a constant emissions factor model, which more or less implies a constant heat rate, when trying to show the emissions reduction benefits of integrating renewable power generation system on the grid. This approach does not consider the fact that there is a deterioration in the heat rate with load for the Coal Fired Power Plants that need to accommodate the additional renewable supply. If varying heat rate were to be included in a study, it is often limited to plant specific cases. This PhD presents a novel Variable Turbine Cycle Heat Rate (V-TCHR) model for predicting the part load Turbine cycle heat rate (TCHR) response of various Coal Fired Power Plant (CFPP) architectures, without detail knowledge of the entire steam cycle parameters. A total of 192 process models of representative CFPP architectures were developed using a Virtual Plant software. The models had different combinations of the degree of reheat; the throttle temperature; throttle pressure; and condenser cooling technology. The part load response of all the models were simulated using the software. Results show that using a power law function in the form $TCHR = TCHR_{FL} \cdot X^{-\Re}$, with X being the low load fraction (0.4-1), best describes the response for all the architectures considered. The coefficient $TCHR_{FL}$ is simply the turbine cycle heat rate at full load, and the exponent $\Re$ can be determined from simple correlations which considers the degree of reheat, cooling technology, main/live steam enthalpy, and the boiler pressure mode of operation. Using this methodology, the TCHR at various part load can be adequately predicted within a 3% deviation. The novel V-TCHR model was implemented in an Energy mix modelling demonstration study to investigate the impact of including a varying emissions factor model on the daily fleet-wide CO_2 emissions of different power system networks, containing different levels of renewable power generation. The results show that a daily fleet-wide CO_2 emissions penalty of 2-9% is seen if a varying emissions factor model is not included in the Energy mix modelling. The CO_2 emissions penalty reported depends on: (a) the Renewable power penetration level in the power system network; (b) the varying load CO_2 emissions characteristics (and thus varying load heat rate) of the individual CFPPs on the network; and (c) How the Coal fired power plants are dispatched on the network. The knowledge presented in this PhD research provides an improved basis for: (a) Predicting the CO_2 emissions factor of various CFPPs configurations at varying loads; (b) Inclusion of a variable heat rate model for CFPPs in Energy mix modelling; (c) Determining the CO_2 emissions reduction impact/potentials of integrating Renewable power generation at various penetration levels; and (d) Calculating the fuel and CO_2 emissions penalty cost of CFPPs which is required for assessing the variable cost of integrating REPG systems.

Declaration

I, Patrick Udeme-obong Akpan, hereby declare the work contained in this dissertation to be my own. All information which has been gained from various journal articles, text books or other sources has been referenced accordingly. I have not allowed, and will not allow, anyone to copy my work with the intention of passing it off as their own work or part thereof.

.

Patrick Udeme-obong Akpan — 10th June, 2019.

Signed by candidate

Name **Date**

Declaration-Inclusion of Publications

I confirm that I have been granted permission by the University of Cape Town's Doctoral Degrees Board to include the following publications in my PhD thesis, and where co-authorships are involved, my co-authors have agreed that I may include the publications:

a) Akpan, P. U. and Fuls, W. F. "Application and limits of a constant effectiveness model for predicting the pressure of steam condensers at varying loads", Applied Thermal Engineering. 158 (2019) 113779.

b) Akpan, P. U. and Fuls, W. F. "Generic method for estimating final feed water temperature and extraction pressures in coal fired power plants", Applied Thermal Engineering (141), pp. 257-268.

Signed by candidate

10th June, 2019

Signature **Date**

Patrick Udeme-obong Akpan AKPPAT001

Student Name **Student Number**

Acknowledgements

I would love to acknowledge the following people for the support that was received during the PhD research:

- The almighty God for sustaining me and my family, and for bringing the right set of people that assisted me throughout the research.
- My darling and beautiful wife (Mrs. Bose Akpan), and my three lovely daughters (Inemesit, Uyaiabasi, Uduakabasi) for their patience, loving support throughout the program, and most especially for enduring my prolonged absence. Finally, we can smile and be together again.
- A/Prof Wim Fuls for guidance, mentorship, enhancement of my writing skills, and providing a strong research focus throughout the study. I do not regret working under your leadership. I am truly grateful I met your family.
- Eskom Power holdings for :
    - Providing the license for the Virtual Plant simulator used in the research, and
    - Hosting me during my field trips/ visits to 4 different power stations.
- The funding support obtained from:
    - NRF-TWAS Doctoral grant no SFH150903141411, and
    - PhD bursary from Eskom's Energy Efficiency Centre at University of Cape Town are highly appreciated.
- The University of Nigeria for granting me a study leave to pursue this PhD programme.
- The University of Cape Town for the Conference travel grant support received.
- Prof. Pieter Rousseau for opening the door to his network - this has provided me the opportunity to study at UCT. God bless you.
- Priyesh Gosai for assisting me with access to important data for validating my models.
- Shane Ferguson for assisting me with all the logistics and travel supports to attend workshops, conferences, and field trips.
- Rendani Khobo for assisting me with all the IT related problems, and for also helping me settle into student life at Cape Town.
- The assistance received from John Clark, Gary de Klerk, Christina Auret, Yusuf Khan, Pieter Rosslee, Gerto Prinsloo, and Excellent Gwebu are also highly appreciated.

- All my flat mates Tshenolo, Petrus, Mamagkooa, Mapaseka, and Louis for being such good neighbours.
- Obiora Anene for occasionally listening to my boring PhD story and for all the encouragements.
- My parents and in-laws for their prayers and well wishes.

Table of Contents

List of Figures

List of Tables

List of Nomenclature

General symbols

Symbol	Meaning	Units
A	Heat transfer area	$[m^2]$
$Approach$	Approach temperature	$[℃]$
A_{an}	Low pressure turbine exhaust annulus area	$[m^2]$
AR	Activity rate of the power plant	$[ton/yr]$
C_{adj}	Adjustment coefficient	$[℃]$
C_c,C_h	Heat capacity of cold and hot fluid respectively	$[W/K]$
C_{min}	Minimum heat capacity	$[W/K]$
$C_{\Re}$	Intercept of $\Re$ vs. h_{main} plot	$[-]$
$CO2_{penalty}$	CO_2 emissions penalty for a given CFPP	$[\%]$
$CO2_{fleet-penalty}$	Fleet-wide CO_2 emissions penalty	$[\%]$
$CO2_{tot-daily-fleet}$	Total daily fleet wide CO_2 emissions on the power system network	$[tons/day]$
$CO2_{tot,i}$	Hourly CO_2 emission rate from all the CFPPs dispatched at time t_i	$[tons/hr]$
$CO2_{unacct}$	Unaccounted daily fleet wide CO_2 emissions	$[tons/day]$
$CO2_{conv}$	Hourly CO_2 emissions from a CFPP based on the conventional/constant emissions factor model	$[tons/hr]$
$CO2_{V-TCHR}$	Hourly CO_2 emissions from a CFPP based on the V-TCHR based emissions factor model	$[tons/hr]$
$C_{reserve}$	Reserve generation capacity	$[\%]$
CE	Emissions device control efficiency	$[\%]$
DCA	Drain cooler approach	[℃]
DC	Drain cooling	[℃]
EF	Emissions factor	$[kg/kWh]$
E_{UC}	Unburnt carbon energy	$[MJ/kg]$
E_{system}	Total electricity demand from the power system network	$[MWh]$

Symbol	Meaning	Units
E_{REPG}	Total electricity generated by REPG systems	$[MWh]$
E_{CFPP}	Total electricity generated by CFPP systems	$[MWh]$
E_{solar}	Total electricity generated by solar power generators	$[MWh]$
E_{wind}	Total electricity generated by wind power generators	$[MWh]$
$Err_{T_{ci}}$	Correction function for the effect of varying load at various cooling fluid inlet temperatures.	$[-]$
Exh_{loss}	Exhaust losses	$[kg/kJ]$
f_{aux}	Ratio of auxiliary consumption to gross power generated	$[-]$
$f_{aux.FL}$	Ratio of auxiliary consumption to gross power generated at full load condition	$[-]$
f_{dea}^{as}	Steam flow mass fraction through the deaerator	$[-]$
f_{cond}^{as}	Steam flow mass fraction through the condenser	$[-]$
$FFWT$	Final feed water temperature	[°C]
$FFWP$	Final feed water pressure	$[MPa]$
f_{NOx}	The fraction of fuel NOx formed	$[\%]$
$f_{wind/REPG}$	Contribution of wind to total renewable power generation	$[\%]$
$f_{solar/REPG}$	Contribution of solar to total renewable power generation	$[\%]$
f_{REPG}	Renewable power penetration level on the grid	$[\%]$
$GUHR$	Gross unit heat rate	$[kJ/kWh]$
$Gen_{mech,losses}$	Generator mechanical losses	$[MW]$
$Gen_{elec,losses}$	Generator electrical losses	$[MW]$
h	Enthalpy	$[kJ/kg]$
h_{ELEP}	Low pressure turbine Expansion Line End Point enthalpy	$[kJ/kg]$
h_{main}	Live steam enthalpy	$[kJ/kg]$
I	Integral of the V-TCHR model with respect to X	$[kJ/kWh]$
n	Number of feed water heaters	$[-]$
$NUHR$	Net unit heat rate	$[kJ/kWh]$
LSB	Last stage bucket size of the low pressure turbine	$[m]$
$Loss_{boiler}$	Total boiler losses	$[\%]$

Symbol	Meaning	Units
$Loss_{uc}$	Unburnt carbon losses in the boiler	$[-]$
$L_{residual}$	The power system residual	$[MW]$
$L_{sys,max}$	Power system network maximum load demand	$[MW]$
L_{sys}	Power system load	$[MW]$
$\overline{L_{sys}}$	Normalized system load demand from a power system network	$[-]$
m	Steam mass flow rate	$[kg/s]$
$m_{off-design}$	Off design steam mass flow rate	$[kg/s]$
m_{thr}	Throttle (main) steam mass flow rate	$[kg/s]$
m_{coal}	Coal mass flow rate	$[kg/s]$
m_{CO_2}	Mass flow rate of CO_2	$[kg/s]$
m_{cond}	Condenser steam mass flow rate	$[kg/s]$
M_{air}	Molar mass of air	$[kg/kmol]$
M_C	Molar mass of carbon	$[kg/kmol]$
M_{CO_2}	Molar mass of CO_2	$[kg/kmol]$
NTU	Number of heat transfer units	$[-]$
n_C	Number of moles of Carbon in fuel	$[-]$
n_H	Number of moles of Hydrogen in fuel	$[-]$
n_O	Number of moles of Oxygen in fuel	$[-]$
n_N	Number of moles of Nitrogen in fuel	$[-]$
n_S	Number of moles of Sulphur in fuel	$[-]$
P	Pressure	$[MPa]$
P_{cond}	Condensing pressure	$[kPa]$
$P_{ext,i}$	Extraction pressure at the turbine flange for FWH number i	$[MPa]$
P_{ELEP}	LP turbine Expansion Line End Point pressure	$[kPa]$
P_{rat}	Reheat pressure ratio	$[-]$
P_{rat1}	1st reheat pressure ratio for double reheat CFPPs	$[-]$
P_{rat2}	2nd reheat pressure ratio for double reheat CFPPs	$[-]$
$P_{FWH,i}$	Extraction steam shell pressure for FWH number i	$[MPa]$

Symbol	Meaning	Units
P_{ref}	Reference condensing pressure for the V-TCHR model	$[kPa]$
P_{RH}	Reheater inlet pressure	$[MPa]$
P_{rh1}	Reheat pressure of reheater 1 for SRHs and DRHs	$[MPa]$
P_{rh2}	Reheat temperature of reheater 2 for DRHs only	$[MPa]$
P_{thr}	Throttle (live steam) pressure	$[MPa]$
ΔP	Pressure difference	$[MPa]$
ΔP_{boiler}	Steam pressure drop in the boiler	$[\%]$
$\Delta P_{ext,i}$	Extraction line pressure drop for FWH number i	$[\%]$
$\Delta P_{ext-pipe}$	Pressure drop along extraction pipe	$[\%]$
q_{actual}	Actual heat transfer	$[W]$
q_{max}	Theoretical maximum heat transfer rate	$[W]$
Q	Heat transfer rate	$[W]$
$Q_{in.cycle}$	Energy input per unit main steam flow into the steam cycle	$[kJ/kg]$
$Q_{out.cycle}$	Energy output per unit main steam flow from the steam cycle	$[kJ/kg]$
Q_{TCHI}	Heat input to the turbine steam cycle	$[MW]$
$Q_{TCHI,DRH}$	Turbine cycle Heat input for a double reheat CFPPs	$[MW]$
$Q_{TCHI,NRH}$	Turbine cycle Heat input for a non-reheat CFPPs	$[MW]$
$Q_{TCHI,SRH}$	Turbine cycle Heat input for the Single reheat CFPPs	$[MW]$
$\Re$	Exponential coefficient of the V-TCHR model	$[-]$
$\Re_{ref}$	Exponential coefficient of the V-TCHR model at the relevant reference condenser pressure	$[-]$
$S_{\Re}$	Slope of $\Re$ vs. h_{main} plot	$[kg/kJ]$
t	Time duration	$[h]$ or $[s]$
T	Temperature	$[℃]$
$T_{ci_{off-D}}$	Off design cooling fluid inlet temperature	$[℃]$
TAR	Theoretical air ratio	$[-]$
$T_{drybulb}$	Dry bulb temperature	$[℃]$
T_{ci} ,T_{co}	Inlet and outlet temperature of the cooling fluid	$[℃]$

Symbol	Meaning	Units
T_{hi}, T_{ho}	Inlet and outlet temperature of the condensing steam	$[℃]$
T_{hi}^{*}	Adjusted condensing steam temperature	$[℃]$
T^{*}	Average of dry bulb and wet bulb temperature	$[℃]$
T_{rh1}	Hot reheat temperature of reheater 1 for SRHs and DRHs	$[℃]$
T_{rh2}	Hot reheat temperature of reheater 2 for DRHs only	$[℃]$
T_{source}	Temperature of water from river/sea/ocean/pond	$[℃]$
$T_{sat,i}$	Extraction steam saturation temperature at FWH number i	$[℃]$
$T_{sat,FWH1}$	Saturation temperature at reheater inlet pressure	$[℃]$
T_{thr}	Throttle (live steam) temperature	$[℃]$
$\bar{T}_{N,i}$	Normalized feed water temperature rise factor across component, i	$[-]$
$TCHR$	Turbine cycle heat rate	$[kJ/kWh]$
$TCHR_{FL}$	Turbine cycle heat rate at full load i.e Turbine maximum continuous rating (TMCR)	$[kJ/kWh]$
TTD_{FWH1}	Terminal temperature difference for FWH on the HP turbine exhaust line.	$[℃]$
$T_{wetbulb}$	Wet bulb temperature	$[℃]$
ΔT	Temperature difference	$[K]$
$\Delta T_{FW,i}$	Feed water temperature rise across component i	$[℃]$
$\Delta T_{FWtotal}$	Total feed water temperature rise across all the components between the condenser exit and the economizer exit	$[℃]$
ΔT_{LM}	Log mean temperature difference	$[K]$
ΔT_{LM_D}	Log mean temperature difference at design/full load condition	$[K]$
ΔT_{rise}	Cooling fluid temperature rise	$[K]$
ΔT_{rise_D}	Cooling fluid temperature rise at design/full load condition	$[K]$
ΔT_{sat}^{p}	FWH extraction interval between successive extraction points using proposed method	$[℃]$

Symbol	Meaning	Units
ΔT_{sat}^{OCEM}	FWH extraction interval between successive extraction points using OCEM method	$[℃]$
ΔT_{TTD}	Terminal temperature difference	$[K]$
U	Overall heat transfer coefficient	$[W/m^2K]$
V_{an}	LP turbine exhaust Annulus velocity	$[m/s]$
v	Specific volume	$[m^3/kg]$
v_{ELEP}	Specific volume at expansion line end point	$[m^3/kg]$
W_{pumps}	Total pump work done	$[MW]$
W_{BFP}	Boiler feed pump work done	$[MW]$
W_{CEP}	Condensate extraction pump work done	$[MW]$
W_{CDP}	Condensate drain pump work done	$[MW]$
$W_{turbines}$	Total turbine work done	$[MW]$
W_{HP}	High pressure turbine work done	$[MW]$
W_{IP}	Intermediate pressure turbine work done	$[MW]$
W_{LP}	Low pressure turbine work done	$[MW]$
W_{aux}	Auxiliary power generation	$[MW]$
$W_{aux.FL}$	Auxiliary power generation at full load condition	$[MW]$
$W_{aux.fix.FL}$	Fixed component of auxillary power generation at full load condition	$[MW]$
$W_{aux.fix}$	Fixed component of auxillary power generation	$[MW]$
$W_{aux.var}$	Variable component of auxillary power generation	$[MW]$
$W_{aux.var.FL}$	Variable component of auxillary power generation at full load condition	$[MW]$
W_{gross}	Gross power generation	$[MW]$
$W_{gross.FL}$	Gross power generation at full load condition	$[MW]$
W_{net}	Net power generation	$[MW]$
$W_{net,FL}$	Net power generation at full load condition	$[MW]$
$W_{CFPP,avail}$	Net generation available capacity	$[MW]$

Symbol	Meaning	Units
$W_{CFPP,total}$	Total net generation for all CFPPs	$[MW]$
W_{solar}	Solar power generation on a power system network	$[MW]$
$\overline{W_{Solar}}$	Normalized solar power generation on a power system network	$[-]$
$W_{solar,max}$	Maximum solar power generated on a power system network	$[MW]$
W_{wind}	Wind power generation on a power system network	$[MW]$
$\overline{W_{wind}}$	Normalized wind power generation on a power system network	$[-]$
$W_{wind,max}$	Maximum wind power generated on a power system network	$[MW]$
W_{REPG}	Combined solar and wind power generation on a power system network	$[MW]$
W_{CFPP}	Power generated from CFPPs on a power system network	$[MW]$
$W_{T,NRH}$	Total work done in the non-reheat steam cycle	$[MW]$
$W_{T,SRH}$	Total work done in the single-reheat steam cycle	$[MW]$
X	Plant (low) load factor	$[-]$
x_C	Mass fraction of carbon in the fuel	$[-]$
x_{UC}	Mass fraction of unburnt carbon in the fuel	$[-]$
x_H	Mass fraction of Hydrogen in the fuel	$[-]$
x_O	Mass fraction of Oxygen in the fuel	$[-]$
x_N	Mass fraction of Nitrogen in the fuel	$[-]$
x_S	Mass fraction of Sulphur in the fuel	$[-]$
$x_{LP.exhaust}$	Steam quality at the exhaust of the LP turbine	$[-]$
$y_{O2/air}$	Mole fraction of oxygen in air	$[-]$

Greek symbols

β	Fraction of fixed component of auxillary power generation at full load condition	$[-]$
ε	Condenser effectiveness	$[-]$
η_{BFP}	Boiler feed pump isentropic efficiency	$[-]$
η_B	Boiler overall efficiency based on fuel HHV	$[-]$
$\eta_{B\cdot FL}$	Boiler efficiency at full load condition	$[-]$
η_{CEP}	Condensate extraction pump isentropic efficiency	$[-]$
η_{cycle}	Thermodynamic cycle efficiency	$[-]$
η_{IPT}	Intermediate pressure turbine isentropic efficiency	$[-]$
η_{HPT}	High pressure turbine isentropic efficiency	$[-]$
η_{LPT}	Low pressure turbine isentropic efficiency	$[-]$
η_G	Generator efficiency	$[-]$
$\eta_{plant_{FL}}$	Power plant efficiency at full load condition	$[-]$
$\theta_{\Re}$	condenser pressure based adjustment coefficient for VWO condenser pressure	

Acronyms and Abbreviations

Acronyms	**Meaning**
ACC	Air cooled condenser
APC	Auxillary power consumption
BFP	Boiler feed pump
CEP	Condensate extraction pump
CDP	Condensate drain pump
CFPPs	Coal fired power plants
DCA	Drains cooler approach
EM	Energy mix
FWHs	Feed water heaters

FFWT	Final feed water temperature
GSC	Gland steam condenser
HP	High pressure
HARP	Heater above reheat point
IDC	Indirect dry cooled
LMTD	Log mean temperature difference
LP	Low pressure
MCR	Maximum continuous rating
NTU	Number of transfer units
OCEM	Optimum cycle efficiency method
OEMs	Original equipment manufacturers
OTC	Once through condenser
SFC	Specific fuel consumption
SC	Sub-cooling
TCHBD	Turbine cycle heat balance diagram
TCHR	Turbine cycle heat rate
TMCR	Turbine maximum continuous rating
TTD	Terminal temperature difference
V-TCHR	Variable Turbine cycle heat rate
V-NUHR	Variable Net Unit heat rate
VWO	Valve wide open
WCC	Wet cooled condensers

1. Introduction

1.1 Research Background

Modern electrical power systems (see Figure 1.1) are typically made up of a complex network of generators (power plants), transmission and distribution systems, and demand/load centres (factories, residential and commercial users). The conventional generators typically include the hydro-electric power plants, Nuclear power plants, and thermal power plants fuelled by either coal, gas or low pour fuel oil (LPFO). Electricity is also generated from renewable sources such as solar, wind and tidal power plants.

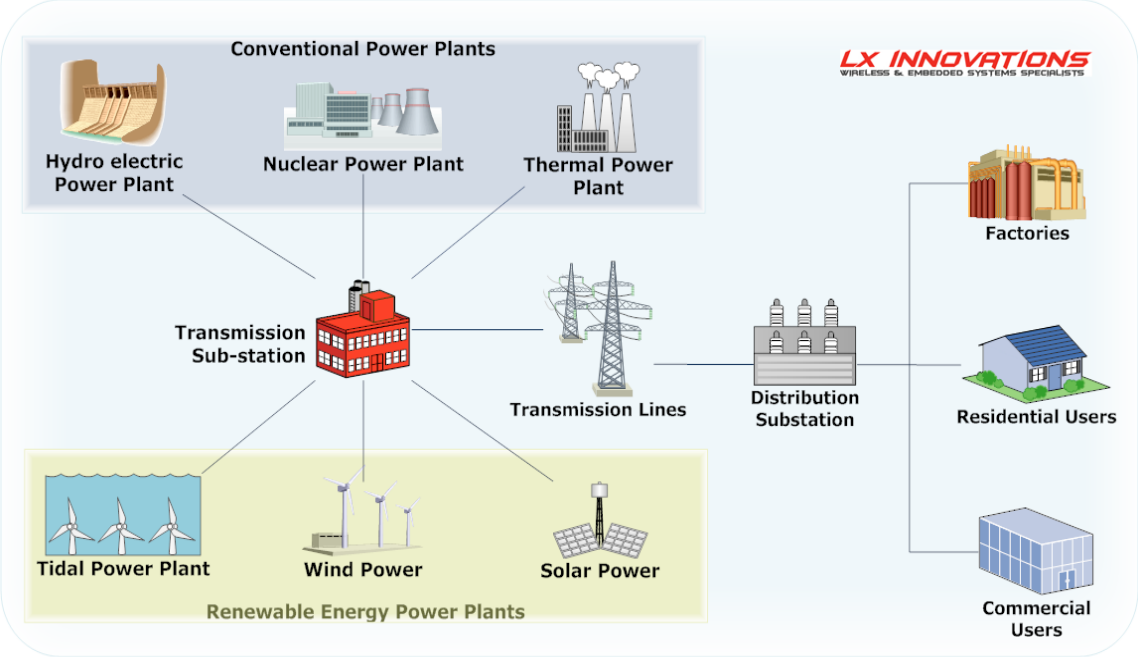

Figure 1.1 A typical electrical grid system set-up [1]

Electric Power generation in the world is largely produced from Coal fired Power Plants (CFPP) [2]. However, CFPPs are also known to be the largest stationary emitter of anthropocentric based emissions in the world [3][4][5] [6]. There have been a lot of concerns about the emissions that it produces and the effects those emissions have on the environment. The large scale deployment of Renewable Power generation systems (REPGs) has been proposed as a means to reduce the emissions from CFPPs [7].

There are two methods of combining REPG systems and CFPPs for electricity generation. The first method is known as Renewable Augmentation of Coal fired Power Plants. It is sometimes called Renewable aided power generation (RAPG) [8]. These are hybrid systems that have the REPG systems as an integral part of the coal power generation process. The most common type of RAPG system is the Solar Aided Power Generation (SAPG) system, in which there is a partial/total replacement of the extraction steam of the high/low pressure feed water heaters by the steam generated from a solar thermal field [8] - [9]. The second method is Coal fired Power Plants (CFPP) with Grid connected REPG systems [10] - [11]. In this approach, the REPG is not an integral part of the coal power generation process. The REPG generates its own power and then supplies a grid that already has CFPPs connected.

The latter of the two methods appear to be the most commonly used in electricity generation around the world. The increased use of grid connected REPG systems have caused more CFPPs to operate at increasingly low operating load and cycling modes, instead of operating as base load plants. These modes of operation adversely affects the life, availability, thermal performance (heat rate or efficiency) and emissions rate of the CFPPs [12][13]. These adverse effects on CFPPs have raised some concerns from CFPP operators, and amongst researchers as well.

Even though there are studies that have quantified and evaluated different aspects or issues pertaining the integration of variable REPG systems on the grid, there still remain some aspects of the impact of a large scale deployment of variable REPG systems on CFPPs that are yet to be fully understood. This study is concerned with how the REPG induced varying operation of CFPPs impacts the heat rate and subsequent emissions of CFPPs.

1.2 Problem Statement and Research Motivation

The study of the impact of large scale deployment of grid-connected REPG systems on the emissions of CFPPs is usually done by performing Energy mix modelling of the electric power system network. The generation levels for each CFPP in the network is first determined from the residual load. The residual load is determined by subtracting the total generation from the grid connected REPG systems from the total power system network load. Once this is done, then the fuel that is consumed or saved at that generation level is calculated. A predetermined emission factor is used to determine the emissions produced or saved.

Emission factor is a typical value that relates the amount of a pollutant released to the atmosphere with a process that gives rise to that pollutant [14]. The factor is expressed as the mass of pollutant per unit weight, volume, distance or duration of the process emitting the pollutant [14]. The equation in Figure 1.2 defines the relationship between the emissions rate (ER) of the plant in $(kg/yr)$and the emissions factor (EF). This relationship is used in the unit commitment and dispatch models, for estimating the emissions of the fossil based generators [15] [16]. AR is the activity rate of the power plant expressed as either fuel consumed (ton/yr) or electricity generated (kWh/yr). EF is the uncontrolled emission factor for the pollutant expressed in either (kg/ton) or (kg/kWh) and CE is the overall control efficiency for pollutant. CE is equal to zero if a pollution reduction system is not used for the pollutant. As illustrated in Figure 1.2, more efficient CFPPs consume less coal and subsequently have lesser emission factors than the lower efficient CFPPs.

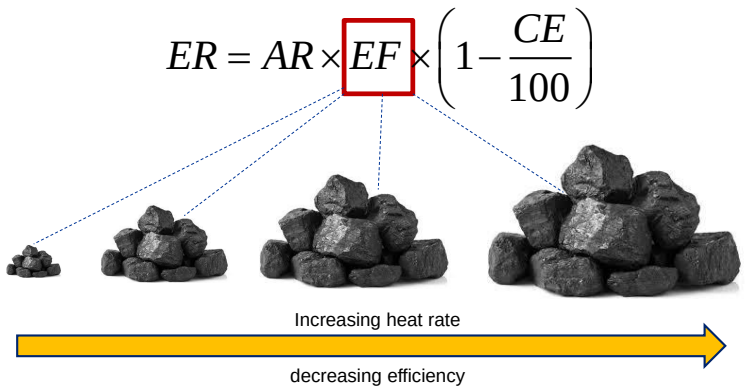

Figure 1.2 Relationship between emissions factor and coal consumption

Energy mix modellers often assume a constant emissions factor (which implies a constant heat rate to a large extent) while trying to show the emissions reduction benefits of integrating renewable power on the grid. This approach treats all the CFPPs on the network as a black box with the same heat rate characteristics at different load conditions, and sometimes the black box is considered to have the same emissions characteristics. This approach can contain significant flaws:

- Varying load operations significantly deteriorates the heat rate of CFPPs. This deterioration affects the fuel consumption which in turn affects the emissions rate [17] [18] [19] .
- It also fails to recognize the fact that the change in heat rate deterioration with load may not be the same for different CFPP architectures or configurations on a given electric power system network.

The inclusion of a variable heat rate and emissions model can be quite daunting. This is due to the fact that the evaluation of the thermal performance of each CFPP on the network must be done at various load conditions. For this to happen, a detailed knowledge of the thermodynamic steam cycle process conditions of the CFPPs at all the points, and for every generation level, is required. The studies that have tried to include a variable heat rate and/or a variable emissions factor in the Energy mix models are often limited to plant specific cases [20][21][17]. A few studies have tried to do an aggregation of the historical heat rate variation with load for the plants in the network investigated [22] [21].

This PhD study tries to move away from the black box approach, but still avoid the need for detailed cycle models. This was done by developing a simple metric that can be used to generically model the Variable Turbine Cycle Heat Rate (V-TCHR) characteristics of different Coal fired power plant configurations at different load conditions, without the need to have a detailed knowledge of the entire steam cycle parameters at various load conditions.

The output of this work presents a great potential as it provides an improved basis for predicting the Net Unit Heat Rate and CO_2 emissions of individual CFPPs, which can then be used in energy mix modelling and REPG emissions and cost impact integration studies.

1.3 Research Questions

The following research questions were posed:

a. What are the key parameters that significantly influence the heat rate and CO_2 emissions of CFPPs at varying load operations?
b. How does the factors in (a) interact at varying load conditions?
c. What are the typical architectures of coal fired power plants found in operation, and can this be described in a generic format?
d. Is it possible to categorize the various architectures such that a simplistic variable heat rate model can be developed?
e. Would it be possible to show a significant difference in predicted fleet-wide CO_2 emissions when incorporating a variable heat rate model instead of the traditional constant heat rate used in energy mix modelling?
f. What is a suitable method for selecting the CFPPs to operate at reduced generation levels for improved fleet-wide emissions reduction?

Some credible answers/explanations to the above questions will be presented in this dissertation. It is anticipated that the understanding gained could be helpful in obtaining a more precise estimate of the impacts of deploying grid connected REPG on the heat rate and emissions of CFPPs.

1.4 Hypothesis & Research Objectives

A good understanding of the nature of interaction of the key factors that significantly impact the heat rate of CFPPs of various architectures during varying load operation can provide an improved basis for quantifying the emissions reduction potential of grid-connected REPG systems. This understanding can be gained through the development of appropriate steady state models.

The aim of this research is to further the knowledge of the impact of varying/cycling load operation of various CFPP architectures on its heat rate and subsequent emissions. This is done by developing a generic model for predicting the heat rate of different Coal fired power plant configurations at

different load conditions, without the need to have a detailed knowledge of the entire steam cycle parameters at various load conditions.

The hypothesis is therefore that it may be possible to develop a simple variable heat rate model that can be used for any typical CFPP architecture without requiring detailed thermodynamic cycle parameters and models, and that such a model would produce more credible fleet-wide CO_2 emission predictions if incorporated into an energy mix model.

The research objectives to prove the above hypothesis are to:

(i) Examine the impacts of grid integrated REPG systems on the heat rate and emissions rate of CFPPs and review the research methodologies used.

(ii) Highlight the key factors that significantly affect the heat rate of CFPPs at varying load conditions.

(iii) Implement and validate a procedure for developing generic steady state CFPP process models at varying load conditions.

(iv) Propose a generic steady state model for predicting the variable heat rates of CFPPs operating at varying load conditions.

(v) Implement the generic method proposed in (iv) above in an energy mix modelling scenario and investigate the impact of its inclusion on the fleet-wide CO_2 emissions.

(vi) Propose an approach for selecting the CFPPs that should be operated at reduced loads for improved fleet-wide CO_2 emissions reduction if priority is given to emissions.

1.5 Overview of Research Methodology

Figure 1.3 highlights the five distinct phases that the PhD research was split into. These were: literature review (phase 1); Generic CFPP process model development and validation (Phase 2); V-TCHR model development and validation (Phase 3); CO_2 emissions evaluation at varying load (Phase 4); and Energy mix modelling demonstration (Phase 5). The key tasks that were completed in each phase is also highlighted on Figure 1.3 .

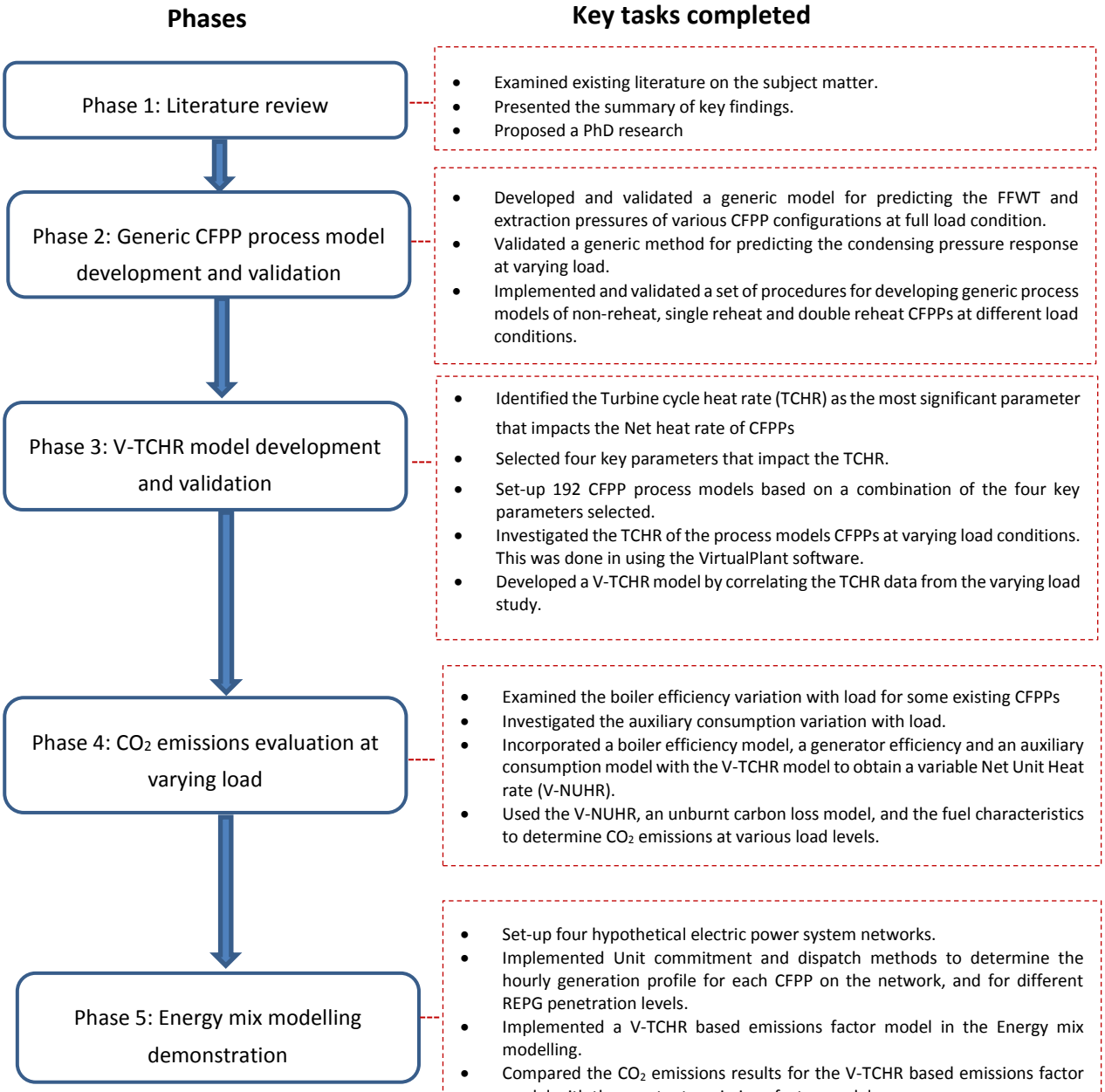

Figure 1.3 Overview of the PhD research methodology

1.6 Research Scope

The research has attempted to add to the understanding of a much broader topic on the impact of grid connected REPG System on existing CFPPs. The scope of this research is thus:

- The research focuses primarily on understanding the Turbine cycle heat rates of various CFPPs at varying load. It also goes on to include the boiler efficiency and the impact of the auxiliary consumption as well.
- It is well understood that the overall thermal performance (heat rate) of a CFPP deteriorates over time due to degradation / ageing of plant components such as turbines etc. The impact of these physical deteriorations are not captured in this study as it is a daunting task to try to model the operating and maintenance practice observed at various coal fired power stations.
- The study does not consider the system's wears and tears, and cycling costs, and issues related to the reliability and stability of the power system networks etc.
- The varying/cycling operations that require the short down and re-starting of CFPP are not considered in this study. The main type of cycling considered are part/low load operations.
- Furthermore, the study is strictly based on steady / quasi steady state operation of CFPPs. for CO_2 based emissions, which is the only gaseous emissions considered in this study, its emissions is primarily based on the quantity and property of the Coal consumed.
- The Net unit heat rate (NUHR) and Gross Unit heat rate (GUHR) results discussed in this thesis are strictly based on the high heating value (HHV) definition.
- The emissions results discussed are intended for pulverised coal (PC) plants primarily because this type of CFPP constitutes the vast majority of the existing CFPPs. However, the issues discussed around the steam cycle should also be applicable to circulating fluidised bed (CFB) CFPPs.

1.7 Thesis Contributions to Knowledge

There is one main contribution and four minor contributions from this PhD. The links between the contributions are illustrated in Figure 1.4.

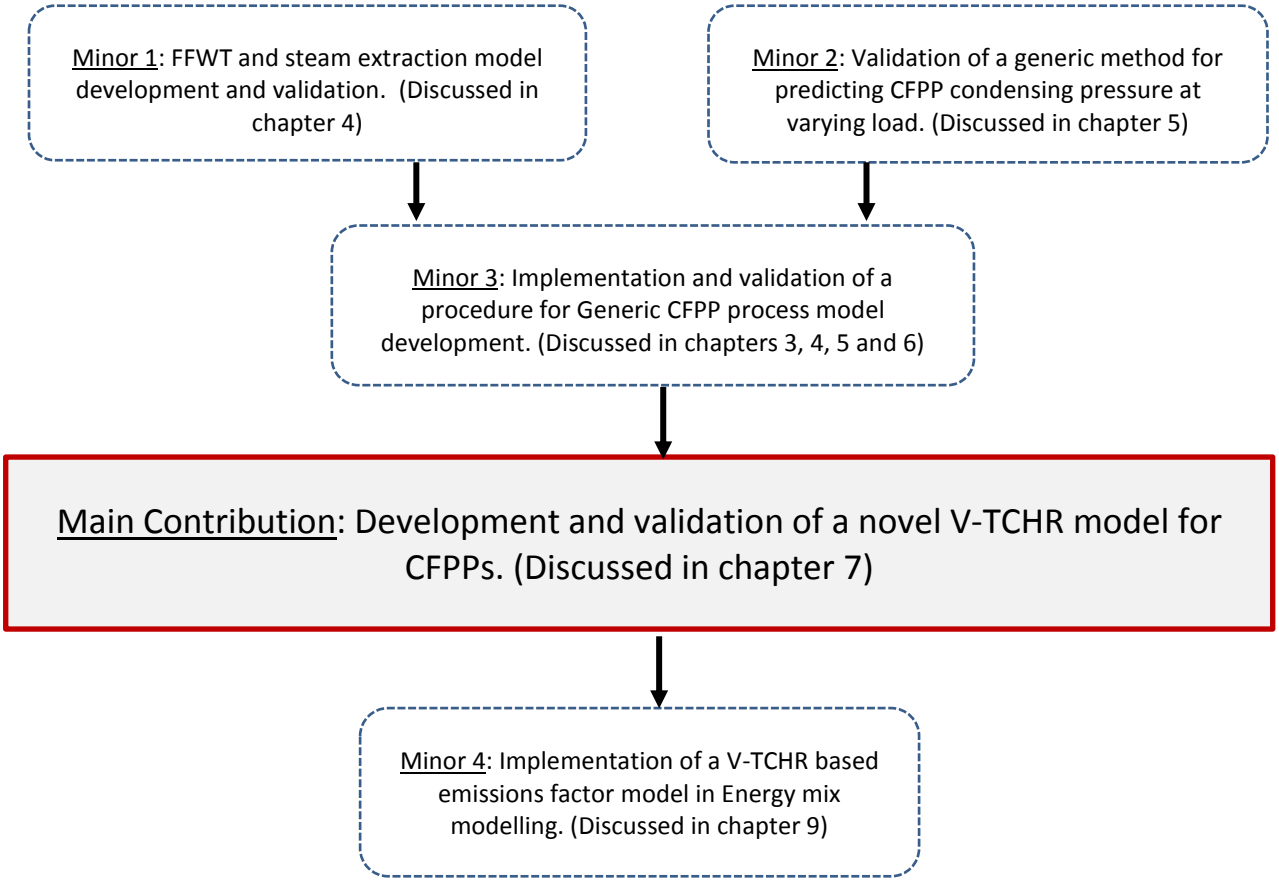

Figure 1.4 The links between the PhD Contributions.

The main contribution of this PhD research is the development and validation of a novel Variable Turbine cycle heat rate (V-TCHR) model for CFPPs. The development and validation of this V-TCHR model is discussed in Chapter 7. This model can be used to predict the Turbine Cycle Heat Rate (TCHR) characteristics of any given Coal fired power plant (CFPP) at various steady state load conditions. This model does not require a complete thermodynamic cycle modelling and performance evaluation of the CFPP. It is only dependent on the knowledge of:

- The live steam enthalpy which is easy to determine from the live steam pressure and temperature at the inlet of the high pressure (HP) turbine.

- The number of re-heat stages.
- The type of condensing cooling system.

This V-TCHR model provides a strong basis for:

- Predicting the variable Net Unit heat rate (V-NUHR) and CO_2 emissions of CFPPs at various load conditions. This is discussed in Chapter 8.
- Including a variable heat rate model in Energy mix modelling studies, and quantifying the CO_2 emissions reduction potentials in REPG emissions impact studies. This is discussed in Chapter 9.

The minor contributions made are also highlighted in Figure 1.4. These contributions are:

1. The proposition of a generic model for determining the final feed water temperature (FFWT) and steam extraction pressures of different configurations of CFPPs at full load or Turbine maximum continuous rating (MCR). The FFWT and extraction pressures for any pulverised CFPP operating at full load (design conditions) could be determined within reasonable accuracy limits by simply specifying the throttle temperature (for non-reheats), reheater inlet pressure (for reheats), condenser pressure, and the number of feed water heaters required. This model is based on a modification of an optimum cycle efficiency method (OCEM). The modification requires the determination of the FFWT before applying the equal partition of feed water temperature rise rule. The development and validation of this model is fully discussed in Chapter 4. This method was useful in the development and validation of CFPP process models in Chapters 6 and 7.
2. The validation of a simple generic methodology for predicting the condensing pressure response of steam power plant condensers at varying loads, and for cooling inlet temperatures. This method is based on a constant condenser effectiveness assumption. A full description of the model is provided in Chapter 5. This method was adopted in Chapters 6 and 7 for predicting the condensing pressure characteristics for the CFPP process models at different load conditions.
3. The implementation and validation of a procedure for developing credible CFPP process models for non-reheat, single reheat and double reheat CFPPs, with knowledge of a few

inputs. This procedure was adopted to set up all the process models that were used in this research. A full description of this procedure is presented in Chapters 3, 4 , 5 and 6.

4. The implementation of a V-TCHR based emissions factor model in the energy mix modelling of an REPG grid-integrated power system. This method was used for quantifying the CO_2 emissions reduction impact of deploying REPG system at different penetration levels. A full description of this is provided in Chapter 9.

1.8 Thesis Structure

The structure of the thesis is highlighted on Figure 1.5. It is divided into the introductory, methodology and results, and concluding sections. The introductory section is contained in Chapters 1 and 2. The methodology and results section is broadly divided into four broad sections. The first is the model development section (Chapters 3, 4, 5, and 6). The second, third and fourth sections are discussed in Chapters 7, 8, and 9 respectively. The concluding section is presented in Chapter 10.

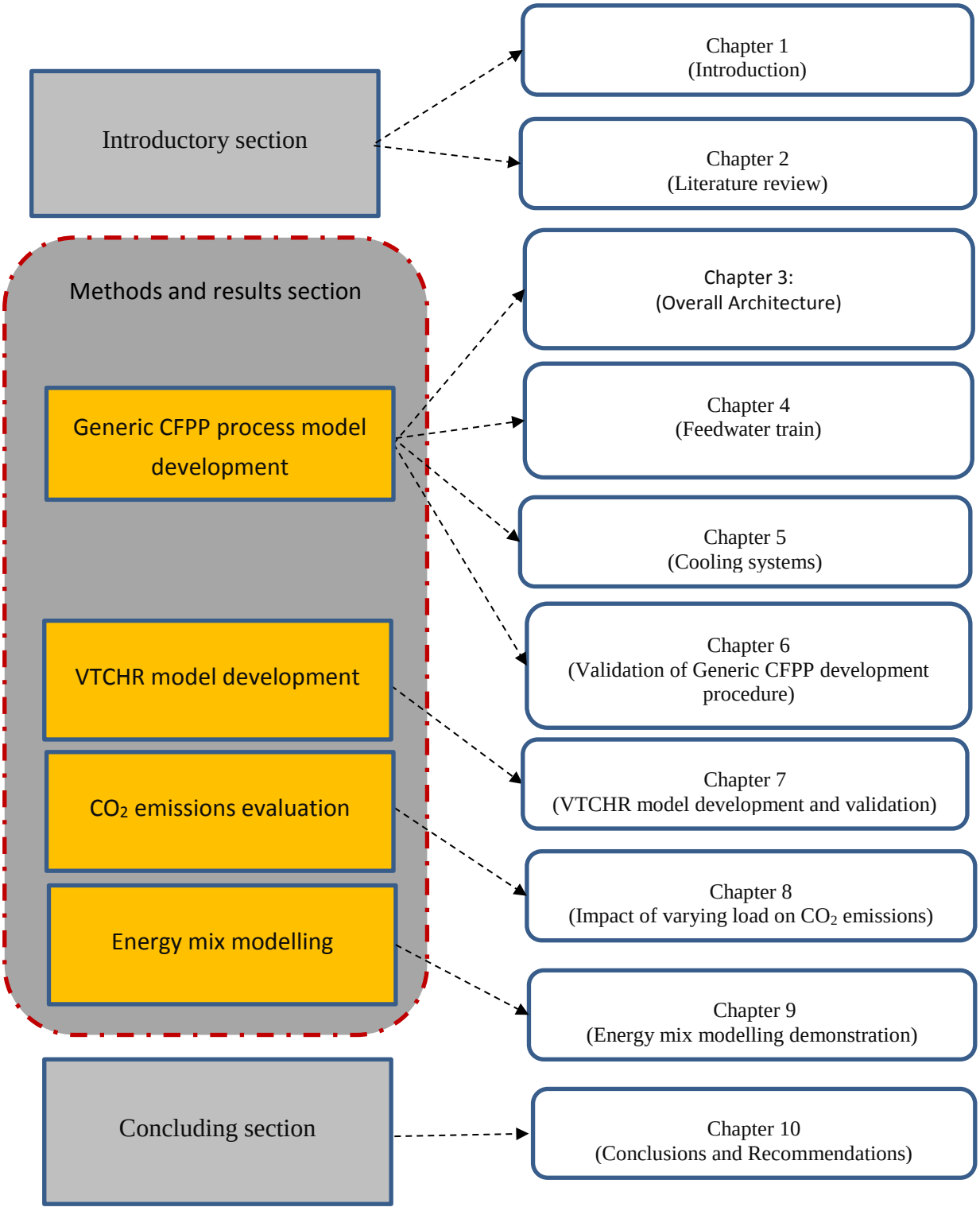

Figure 1.5 Overview of the main body of the thesis

1.9 Academic outputs

The academic outputs from this PhD research have/are been disseminated through a number of avenues. A summary of the academic outputs is presented Table 1.1.

Table 1.1 A summary of academic outputs.

a. Journal Publication	1. Akpan, P. U. and Fuls, W. F. (2019) Application and limits of a constant effectiveness model for predicting the pressure of steam condensers at varying loads. Applied Thermal Engineering 158 (2019) 113779
	2. Akpan, P. U. and Fuls, W. F. (2018) Generic method for estimating final feed water temperature and extraction pressures in coal fired power plants. Applied Thermal Engineering (141), pp. 257-268.
b. Conference Presentations	1. Akpan, P. U. and Fuls, W. F. (2018). A V-TCHR model for predicting the turbine cycle heat rate response of coal fired power plants at different loads. SAIMechE Conference Proceedings on Mechanical, Manufacturing, Materials and Biomedical Engineering. Held on 9th November, 2018. SARETEC, Cape Town, South Africa. PP. 3-4.
	2. Akpan, P. U. and Fuls, W. F. (2018). Application and limits of a constant effectiveness model for predicting the pressure of steam condensers at varying loads. SAIMechE Conference Proceedings on Mechanical, Manufacturing, Materials and Biomedical Engineering. Held on 9th November, 2018. SARETEC, Cape Town, South Africa. PP. 5-6.
	3. Akpan, P. U. and Fuls, W. F. (2017). Understanding heat rate and emissions of coal fired plants operating due to renewable energy power generation induced cycling. Sustainable Development of South Africa's Energy Sources Conference Book of abstracts. 29 – 30 Nov 2017, Glenhove Conference Centre. PP. 64-66.
	4. Akpan, P. U. and Fuls, W. F. (2017). Generic method for estimating final feed water temperature and extraction pressures in Coal fired power plants. SAIMechE Conference Proceedings on Mechanical, Manufacturing and Materials Engineering. Held on 3rd November, 2017. STIA Wallenberg Centre, Stellenbosch, South Africa. PP. 1-2
	5. Akpan, P. U. and Fuls, W. F. (2016). Impact of grid integrated renewable induced coal fired plant cycling on heat rate and emissions. SAIMechE Conference on Mechanical, Manufacturing and Materials Engineering. Held on 4th November, 2016. Cape Town, South Africa.
c. Poster presentations	Akpan, P. U. and Fuls, W. F. (2017). An Approach for estimating extraction pressures in subcritical Coal Fired Power Plants. 4th EBE Postgraduate

	Research Expo Held on 25th May, 2017. University of Cape Town South Africa
d. Manuscripts for journal publication under review/ preparation	1. Akpan, P. U. and Fuls, W. F. Methodology for developing and validating representative process models for investigating the varying load thermal performance of coal fired power plants. Status: First draft under preparation.
	2. Akpan, P. U. and Fuls, W. F. A novel V-TCHR model for predicting the turbine cycle heat rate response of coal fired power plants at different loads. Status: First draft under preparation.
	3. Akpan, P. U. and Fuls, W. F. Application of a V-TCHR model for determining the CO_2 emissions factor of Coal fired power plants (CFPPs) at varying load conditions Status: First draft under preparation.
	4. Akpan, P. U. and Fuls, W. F. Inclusion of a V-TCHR based CO_2 emissions factor model in an emissions impact study of power system networks with varying levels of renewable power penetration. Status: First draft under preparation.

2. Literature Review

2.1 Coal Fired Power Plants (CFPPs)

Coal fired power plants (CFPPs) play a significant role in the global electric power generation mix, especially when it comes to the supply of base loaded electricity generation [2][23]. It currently supplies 40% of the global electricity production [24] . The current global fleet is a mixture of non-reheat, single, reheat and double reheat units [25][26][27]. As at 2016, 75% of the global CFPPs utilize subcritical CFPP technology [24]. The average thermal efficiency of these plants is around 30-33% [24]. Supercritical plants constitute 22% of the global CFPP power fleet with thermal efficiencies of 40% [24]. The Ultra-supercritical plants currently constitute 3% of the global CFPP fleets with cycle efficiency as much as 45%. There is a further advancement in the Ultra-supercritical (USC) technology called the Advanced-ultra supercritical (AUSC) that utilize much higher steam temperatures and pressures. Demonstration plants of these are being developed in China, USA, Europe, Japan and India [24]. A closer look at the total operating fleet in the four regions/countries (see Figure 2.1) with the strictest emissions control regulations shows a combination of 54% subcritical, 30% supercritical and 16% Ultasupercritical plants - suggesting that less efficient CFPPs still form a vast majority of the CFPPs in operation. The percentage composition of the actual number of plants in these countries could be slightly different because the capacity of subcritical plants are typically smaller than the supercritical or ultracritical plants.

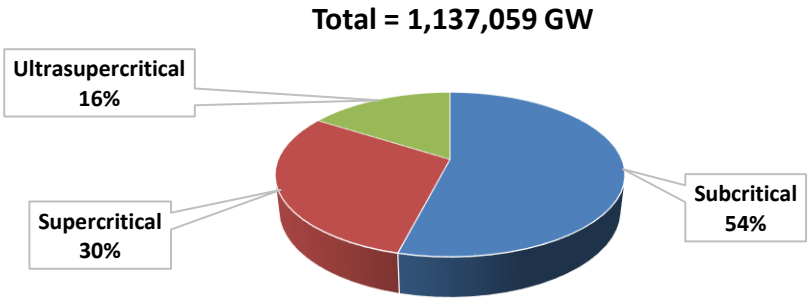

Figure 2.1 Operating CFPP fleet capacity in Japan, China, US and the EU [28].

The classification of CFPPs as subcritical, supercritical or ultracritical is primarily based on operating temperature and pressure at the exit of the boiler [29]. The most frequently used definition for subcritical, supercritical and ultracritical CFPPs is shown on Table 2.1. Generally the efficiency for most Ultasupercritical plants are higher than those of the subcritical and supercritical plants because they tend to have a higher boiler steam temperature and pressure, and they also tend to be double reheat plants as well.

Table 2.1 Key differences in subcritical, supercritical and ultra-critical CFPPs [29]

	Subcritical (conventional)	Supercritical	Ultra-supercritical
Temperature (℃)	500-600	500-600	550-600
Pressure (MPa)	16-17	24-26	27-32
Features	Drum: Single reheat	Once through: single reheat	Once through: double reheat
Cycle efficiency (%)	22-35	40-45	42-47

CFPPs are integral parts of the generation side of a power system network. These CFPPs generate power based on the demand signal from the grid control centre. The demand level of the power system can change over the course of an hour, day, week etc. CFPP operators typically operate the CFPPs under varying modes of operation to meet the demand requirements.

2.2 Varying operation of Coal fired Power Plants (CFPPs)

2.2.1 Basic definitions

It is important to understand and differentiate between the varying modes of operating a CFPP. But first, there is a need to identify the different kinds of loads that can be seen in a typical diurnal load curve and a load duration curve for a power system network. The daily load curve on Figure 2.2 shows there are usually three kinds of load within a power system network. These are the baseload, intermediate/cycling load, and peak load [30]. The baseload is the minimum amount of power that must be supplied all the time. This load requirement is mostly met by baseloaded power plants such

as CFPPs and Nuclear plants. The peak load represents as the name implies, the fraction of the load that is demanded at the peak hours. The peak load demand is usually satisfied by fast ramping power plants such as gas power plants, pumped storage hydroelectricity etc. It usually occupies a small fraction of the load duration curve. The intermediate load is sometimes referred to as the cycling or mid-merit load. This load demand is usually met by combined cycle power plants, and CFPPs occasionally.

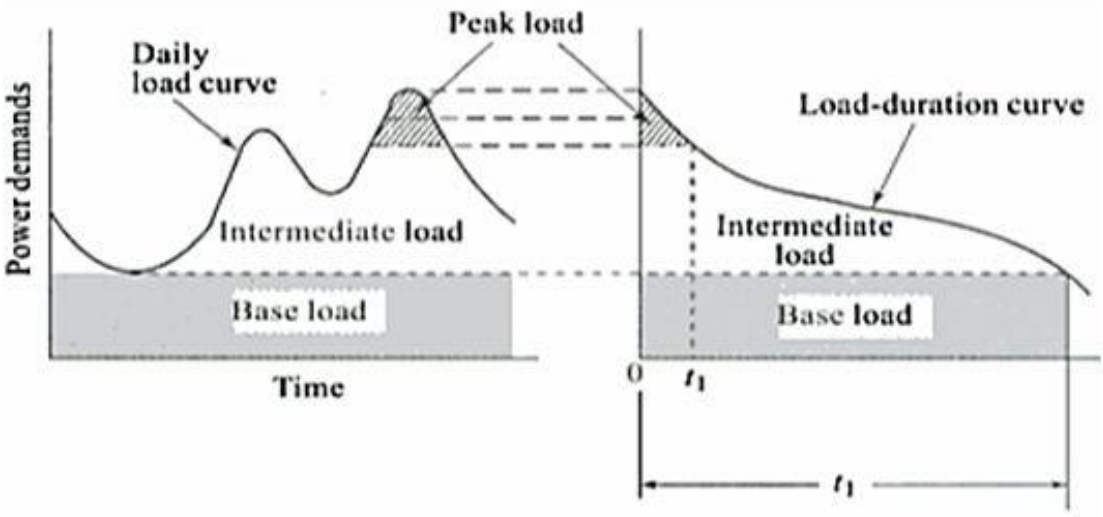

Figure 2.2 A typical daily load curve and load duration curve [30]

The two broad modes (see Figure 2.3) of operating a CFPP are baseload and cycling modes. The choice of the mode that is used depends on the market condition and other factors such as energy policy, economics, etc [31].

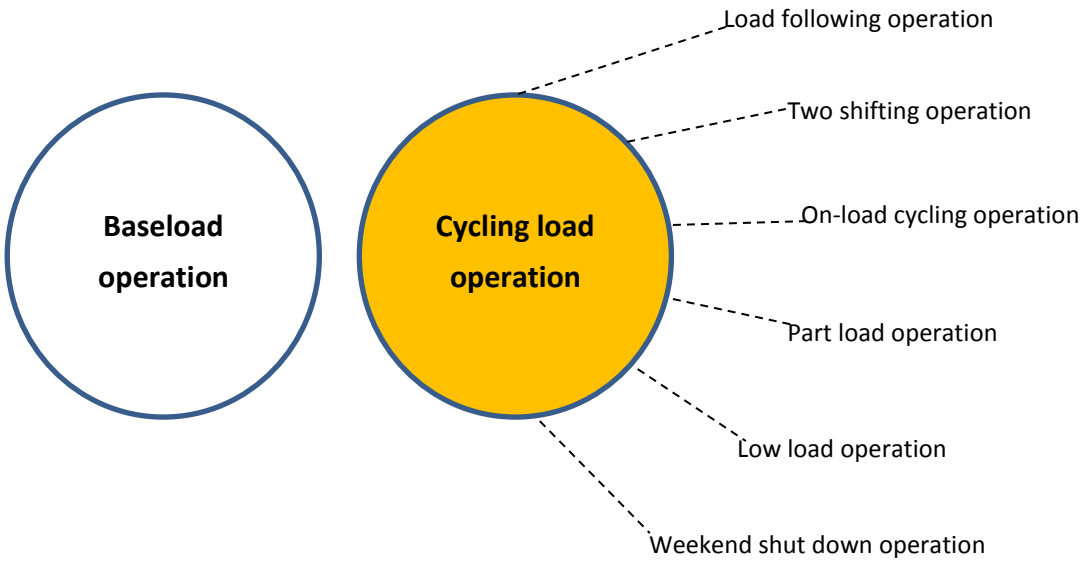

Figure 2.3 Load operations in a typical CFPP

Baseload operation: is the action of operating a CFPP at close to its maximum output on a continuous period. This is the most economic method of operating CFPPs while ***cycling load operation*** is the varying reduction or increment in power generation output. This occurs for a variety of reasons including making way for alternative generation, maintenance and/or equipment failure or sudden changes in load size [31].

The various forms of cycling a CFPP includes: load following; two-shifting; on-load cycling; part load operation; low load operation; and weekend shut downs [31]. ***Load following*** is the action of constantly following the general trending load pattern within the day [32]. The changes experienced in the load could be greater than 50% of the Turbine Maximum Continuous Rating (TMCR). TMCR is the maximum generation output from a CFPP when the high pressure (HP) turbine inlet is at a valve wide open (VWO) position. ***Two-shifting operation***: is the action of starting and shutting down the CFPP once per day. This is usually done to reduce the cost of operating the plant especially when the demand for electricity is low. This is usually not good for the overall health of the plant. ***On-load cycling***: is the action of operating the plant at base load within the day and running down the plant to minimum generation at night [33]. ***Part load operation***: is the action of running the plant continuously at a rating that is below the designed TMCR. ***Low load operation***: is the practice of

running the plant continuously at an output level that is quite close to the minimum continuous rating of the plant. The minimum continuous rating of a CFPP is the lowest possible power generation level that a CFPP is allowed to run continuously. For most CFPPs, it is usually around 30-40% TMCR. The major factors that determine the minimum continuous rating is the available turndown of pulverizers and risk of a unit trip with minimum mills in service without support fire [13]. The major problems that are experienced when a CFPP is kept online at a low load operating conditions are: an increase in heat rate, high levels of excess air, and poor control [13]. ***Weekend shut down***: is the action of shutting down the plants at weekends, and then bringing them back online during the week.

Once a CFPP is off line (shut down), there are different procedures for bringing the unit back online. These are known as hot start, warm start, or cold start. These definitions are only applicable to cycling operations that requires the shutting down of the CFPP. Figure 2.4 gives a definition of the expected cycling that the coal fired power plants could be on [12],[34], [35]. For the hot starts, the time interval between when the CFPP is off and when it is re-started is around 12 hours or less. For the warm and cold starts, the time interval is around 12-72 hours, and greater than 72 hours respectively. The level of damage that is experienced in a CFPP increases from the hot start to the cold start.

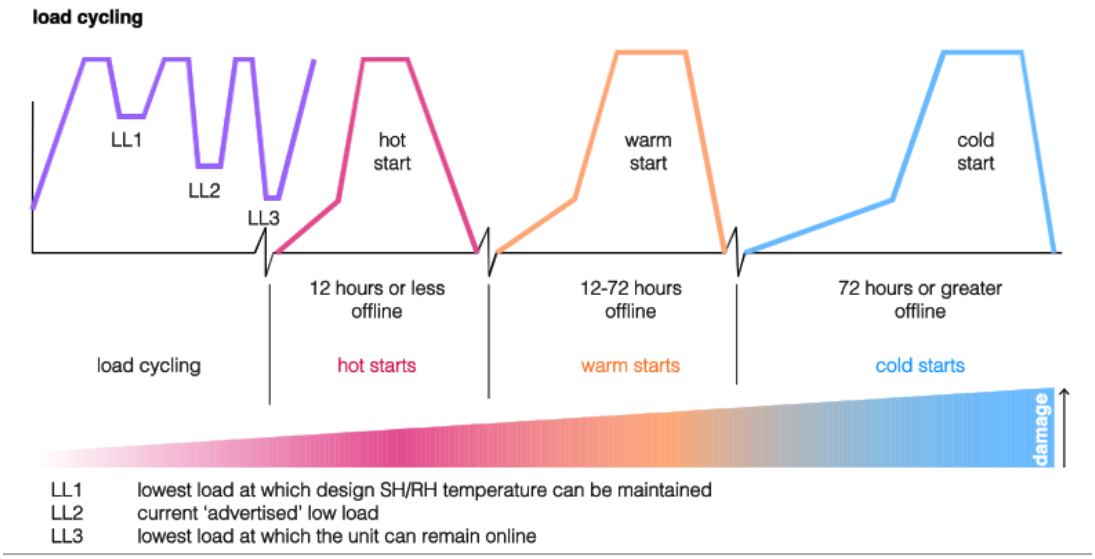

Figure 2.4 Definition for Plant generation cycling [35]

The cycling operations that require the shut down and re-starting of a CFPP are not considered in this PhD study. The main type of cycling considered are part and low load operations.

2.2.2 The need for increased CFPP cycling load operations

Cycling of Coal fired Power Plants, and indeed other type of conventional fossil based plants is not a new phenomenon. The motivation for cycling conventional power plants such as CFPPs often varies. The motivation could be economically, technically, or policy driven [36] [37]. Table 2.2 highlights in a chronological order, some of the motivations for cycling CFPP in some countries, particularly in the United States of America. It can be seen that low energy prices, inclusion of viable energy alternatives, deregulation of the electricity market, and environmental regulations are amongst the main reason for increased cycling operation of CFPPs.

Table 2.2 Motivations for Cycling of Coal fired Power Plants

Period	**Motivations**
1960-1970	• Low energy prices during periods (evenings and weekend) of low demand [38].
1970-1980	• Low energy prices during periods (evenings and weekend) of low demand [38]. • Inclusion of advanced Coal fired Power Plants. • Inclusion of large nuclear power plants that displaced old conventional fossil based generators [39].
1980-1990	• Inclusion of large nuclear power plants that displaced old conventional fossil based generators [40] [41]. • Inclusion of large sources of cheap alternatives [41]. • Low energy prices during periods (evenings and weekend) of low demand [36].
1990-2000	• Deregulation of market and competition [13]. • Low energy prices during periods (evenings and weekend) of low demand [36].
2000-2010	• Demand reduction due to economic recession [38]. • Low energy prices during periods (evenings and weekend) of low demand [38]. • Liberalization of the electricity market. • Implementation of “must take renewable energy first” policy.
2010-present	• Low energy prices during periods (evenings and weekend) of low demand [38]. • Inclusion of high levels of renewables [38]. • Lower prices of alternative fuel sources like natural gas. • Stringent environmental regulation [38]. • Implementation of “must take renewable energy first” policy.

In recent times, most governments have introduced energy policies that favour the uptake of REPG systems. This appears to be the major driver for increased cycling of CFPPs. In most cases, this decision is motivated by the notion that an increased use of renewable power generation would

drastically reduce the emissions from CFPPs. In South Africa for instance, policies like the Integrated Resource Plan (IRP) from 2010 to 2030 (Long term medium), and Renewable Energy Independent Power Producer Procurement Programme (REIPPPP) (Mid-term mechanism), have been pursued by the government, to provide legal frameworks that would guide the implementation of large scale grid-connected REPG systems [2][42]. Figure 2.5 shows the integrated Resource Plan (IRP) for capacity expansion in South Africa as from 2010. It can be seen that there is a plan to increase the installed capacity of power to 86 GW by 2030. Furthermore, an increase in the contribution of Renewable Energy Power Generation (REPG) from 5% to 14% in 2030 was proposed. The major renewables to be used are the Solar PV Systems and Wind Energy powered systems and there are plans to add a little share of concentrated solar power (CSP) systems as well.

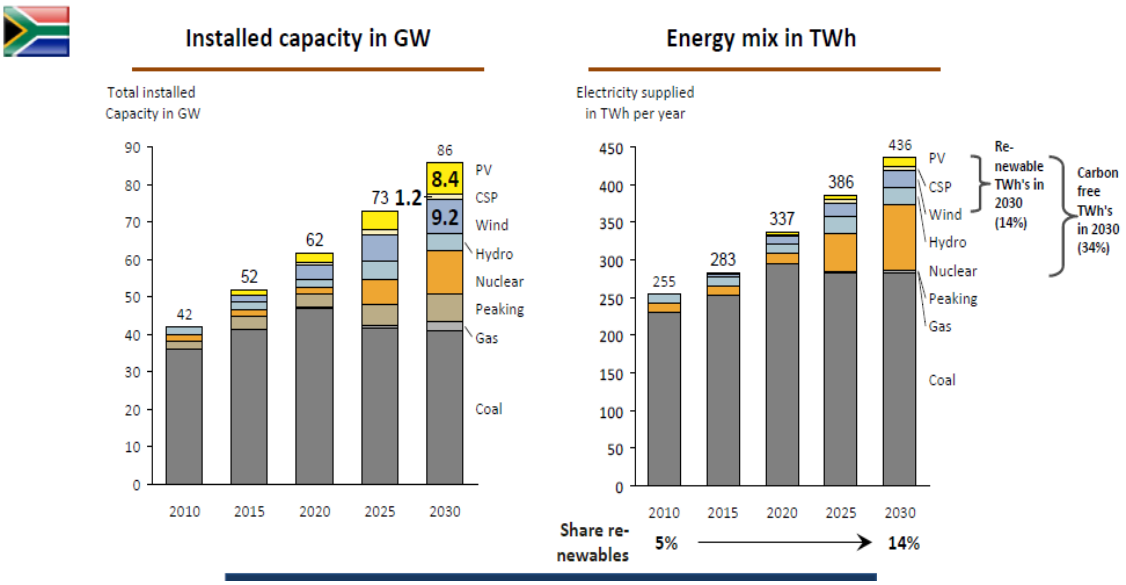

Figure 2.5 Integrated Resource Plan 2010, as promulgated in 2011 [43]

Globally, wind and solar PV are the two most common type of REPG systems that are integrated on electricity power system networks [17][44].

2.3 Impact of increased Grid Integrated REPGs on CFPPs

The large scale deployment of REPG systems in the electricity grid comes with certain operational challenges for CFPPs that are designed to operate at baseload conditions [12] [45]. The intermittent nature of REPG supply causes the CFPP to run in cycling load conditions. The degree of load changes in the CFPP is partly determined by the grid demand, the supply from the REPG systems and the relative location of REPG systems on the power system grid [46] [47]. The general effects of grid integrated REPG on CFPPs can be broadly classified under three headings: System balancing, system reliability, and system performance. These are summarized in Table 2.3. The system balancing issues are related to the capacity factor of the plant while the system reliability issues are related to the availability factor of the plant. The system performance issues are related to the thermal performance and emissions of the plant. All these issues have a combined impact on the cost of operating CFPPs under varying load conditions.

Table 2.3 Impacts of grid integrated REPG on CFPP

System Balancing	**System Reliability**	**System Performance**
Utilization of automatic controls on the output of conventional PP [48] [49].	Output may or may not be available at peak demand periods [49][50]	Decreased plant efficiencies and increased plant heat rates. [10][21][11][17][48][51] [52][53][54][31]
Requires more part loaded plant that can rapidly increase or decrease its output [17][47][48][49][51][53][54][34][55][56][57][58] It affects the way and manner in which operating reserves are allocated and deployed [32][59]	Rapid deterioration of system components due to thermal stresses. [50][51][52] [54][34]	Increased maintenance and generation cost of conventional plants due to cycling cost [51], [31] [52]
Energy spilling/curtailment [48][52][55]	Increased Forced Outages [52]	Potential for increased emissions [12][17][60][48]

Many researchers have studied various aspects of these impacts. A lot of effort has been concentrated on trying to evaluate the cost of integrating REPG [22], [37], [61]–[68], some have looked at the impact on the operation and performance of CFPPs while others have looked at the impact on the individual components of the CFPP . A summary of key findings of some case studies of real life issues that arose in power plants operated in a load following/cycling mode and strategies offered to address them, have been reported by National Energy Technology Laboratory (NETL) [12].

This research is focussed on the impact studies related to the thermal performance, heat rates and the emissions of CFPPs. It is important that a clear explanation is given on the concepts/definitions of CFPP heat rates and emissions types, and the method(s) for evaluating each parameter. Sections 2.4 and 2.5 deals with the definitions of heat rate and emissions respectively.

2.4 Heat rates: Conceptual meaning, types, factors affecting it and various methods of evaluation

2.4.1 Concept and types of heat rate

Heat rate in its basic form is defined as the quantity of fuel energy consumed (kJ) per unit of electricity (kWh) generated. It's a measure of the efficiency energy conversion of the power plant. A CFPP with a higher heat rate is less efficient than a CFPP with a lesser heat rate. The heat rate of a given CFPP depends on coal type, calorific value, boiler efficiency, and steam cycle efficiency [69]. Heat rates that are quoted in literature are either Turbine Cycle Heat Rate (TCHR), Gross Unit Heat Rate (GUHR), or Net Unit Heat Rate (NUHR). These three terminologies mean different things for plant performance assessment.

Figure 2.6 shows a graphical illustration of the three different heat rates, and the effects that are considered when defining each for a typical coal fired power plant. TCHR considers the efficiency of the Rankine cycle (steam cycle) alone i.e it assumes that the efficiency of the boiler is 100%. Typically, the TCHR for double reheat cycles are expected to be greater than those of the single reheat cycles, and the non-reheat cycles because of higher steam temperature and pressures and presence of

reheating. The inclusion of the boiler inefficiency effect to the Rankine cycle efficiency pushes the TCHR curve upward, giving rise to the GUHR. The inclusion of the auxiliary consumption pushes the curve even further upward to give the NUHR.

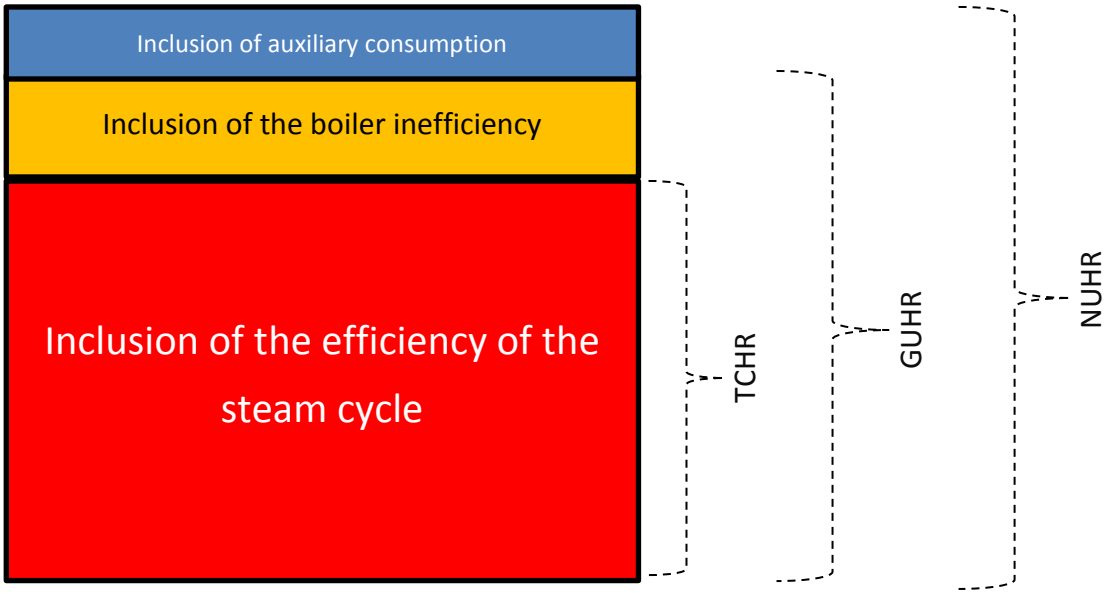

Figure 2.6 Heat rates and the major effects considered

The relationship between $NUHR$, $GUHR$ and $TCHR$ is described mathematically in the equations below:

$$TCHR = \frac{Q_{TCHI}}{W_{gross}} \tag{2.1}$$

$$GUHR = \frac{TCHR}{\eta_B \eta_G} \tag{2.2}$$

$$NUHR = \frac{GUHR}{(1 - f_{aux})} = \frac{TCHR}{(1 - f_{aux}) \cdot \eta_B \cdot \eta_G} \tag{2.3}$$

f_{aux} is the ratio of auxiliary power consumed to the total gross generation while η_B is the boiler efficiency. η_G is the generator efficiency.

The definition of GUHR and NUHR could be based on a fuel higher heating value (HHV) or a lower heating value (LHV) basis. The heat rates based on the HHV are less than those based on LHV due to the unaccounted latent heat of water in the combustion products [28]. The difference between the LHV and HHV based heat rates is even higher for high moisture coals, like many lignites [28].

From the heat rate definitions already given above, it is clear that the NUHR of a CFPP is dependent on four key parameters: (a) The efficiency of the steam cycle as captured in the TCHR; (b) the boiler efficiency; (c) the auxiliary consumption of the power plant; and (d) the generator efficiency. The factors that affect these four parameters are highlighted in sections 2.4.2, 2.4.3, 2.4.4, and 2.4.5 respectively.

2.4.2 Factors affecting the Turbine Cycle Heat Rate of CFPPs at varying loads

The factors that influence the Turbine cycle heat rate (TCHR) of a CFPP plant are highlighted on Figure 2.7. The live/main steam conditions refer to the temperature and pressure of the steam exiting the steam boiler. It is often approximately equal to the conditions (enthalpy) of the steam entering the high pressure turbine. The temperature at this point is the highest temperature within the steam cycle. Generally, CFPPs that have higher HP turbine inlet enthalpy do have lesser TCHR values than the ones with lower enthalpy. The reduction in heat rate has been the drive behind the push for the development of much higher temperature and pressures in advanced ultra-supercritical CFPPs.

The condensing pressure has a tremendous impact on the TCHR especially when compared to other parameters [70]. It determines the condensing temperature at which heat is rejected from the steam cycle. A higher condensing temperature implies more heat rejection per unit of steam flow. The impact of this on the TCHR is adverse. The condensing pressure also impacts the TCHR by affecting the low pressure (LP) turbine exhaust losses. The condensing pressure is affected by factors such as the type of cooling systems, the heat load, the fouling conditions of the condenser tube, and the prevailing environmental/ambient conditions.

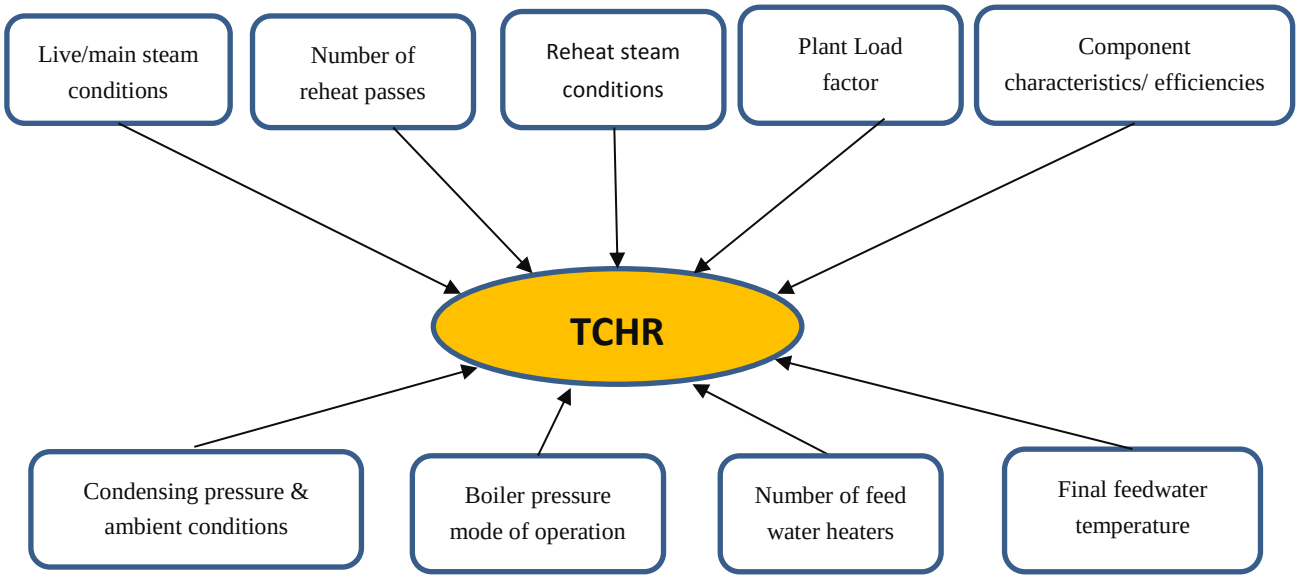

Figure 2.7 Some factors that affects TCHR

The number of reheat passes and reheat conditions of the steam cycle are also important factors that affect the TCHR of a CFPP. Currently, CFPPs exist as either Non-reheats (NRHs), single reheats (SRHs), and double reheats (DRHs). The key difference between them is the absence or presence of one or more reheater in the boiler. The NRHs don't have a reheater, while the SRHs and DRHs have one and two reheaters respectively. The benefit of the reheater is to re-energize the working fluid after the HP turbine expansion process. The re-energization improves the TCHR of the CFPP. For NRH, SRH and DRH CFPPs with the same live steam conditions and condensing pressures, the DRHs generally have lesser heat rates than SRHs, and SRHs have lesser heat rate than NRHs. Higher reheat temperatures and pressure also improve the TCHR of CFPP.

The component characteristics/efficiencies of some key components within the steam cycle also impact the TCHR. The key components include the steam turbines, and the pumps. A higher turbine isentropic efficiency means more work is extracted per unit of steam flow, thereby improving the heat rate. A higher pump efficiency implies less amount of work is done on the working fluid. This also enhances the TCHR.

The final feed water temperature (FFWT) and the number of Feedwater heaters (FWHs) also impact the TCHR of CFPPs. FFWT is the final temperature of the feed water that enters the boiler. The feed water heating is done in a series of FWHs. This temperature is dependent on the number of feedwater heaters and the conditions of the extracted steam. A higher FFWT is desirable for a decreased TCHR of the CFPP.

At varying load conditions, the plant load factor is an important factor that impacts the TCHR. Plant load factor is the ratio of the generation of a CFPP when compared to the maximum continuous rating capacity. A plant load factor of 60% implies that the CFPP is generating at 60% of its turbine maximum continuous rating. The TCHR (see Figure 2.8) of a CFPP is known to deteriorate as the plant load factor decreases. This TCHR deterioration is as a result of the throttling losses, and the operation of key components at efficiency points that are less than optimum.

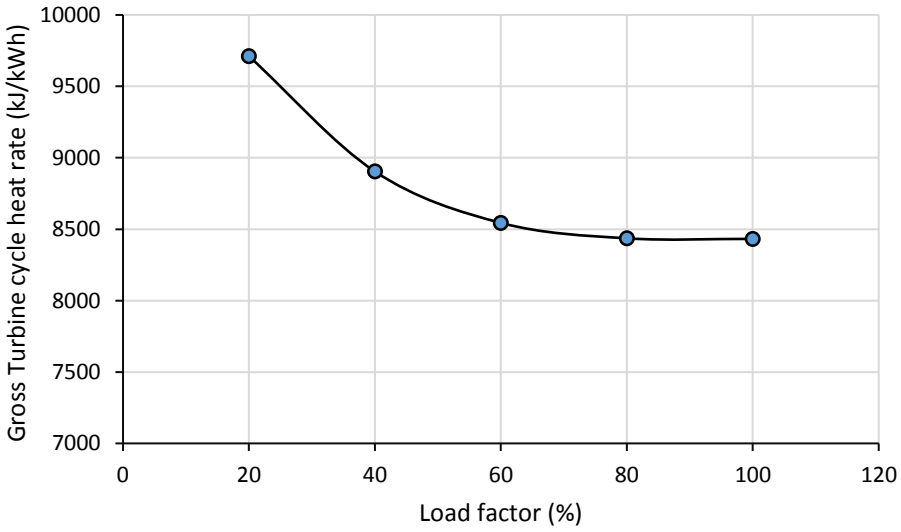

Figure 2.8 Relationship between TCHR and plant load factor for a typical CFPP: Data sourced from EPRI [71]

The cycling load operations of CFPPs is achieved primarily by reducing the energy input into the steam turbines. This can be achieved by controlling the pressure of the boiler, or throttling the inlet to the turbine:

- Fixed boiler pressure operation [38]: In this mode of operation, the pressure of the boiler remains constant. The steam flow is throttled at the HP turbine. This action impacts the TCHR adversely because of the throttling losses and the thermodynamic response of operating at

lower pressures or steam conditions. This is however the preferred method of boiler pressure control in most drum type boilers [72].

- Sliding boiler pressure operation [38]: In this mode of operation, the pressure of the boiler is adjusted or allowed to slide to a pressure that will yield the required generation level. This impacts the TCHR adversely because of the thermodynamic response of operating at a lower steam condition. The throttling losses over the valve is not present. This is the preferred method of boiler pressure control in most CFPPs that have once through boilers [72].
- Modified sliding boiler pressure operation [38]: This is a variation of the sliding boiler pressure operation. In the modified sliding boiler pressure process, the valves throttle at around 80% load. The deterioration of heat rate in this case is somewhat between that of the fixed pressure and the sliding pressure.

There is a general consensus on the merits of sliding boiler pressure operation over the fixed boiler pressure operation at low load of operations due to [71] [73]: improved efficiency of high pressure turbine, reduced auxiliary power for variable speed electrical feed pumps (EFPs), decreased throttling losses across control valves, and reduced auxiliary steam required for turbine driven pumps. The negative impact is larger cycling loads on all the pressure parts of the boiler, which in turn affects the plant life.

2.4.3 Factors affecting the boiler efficiency

There are different types of efficiencies that can be defined for a boiler namely [74]: combustion efficiency, thermal efficiency and fuel to steam efficiency:

- ***Combustion efficiency*** talks about the boiler's ability to completely combust fuel. The combustion efficiency is assessed by examining the amount of unburned fuel and excess air that is in the exhaust of a boiler. The combustion efficiency differs for different type of fuels. Generally, the combustion efficiencies of gaseous and liquid fuels tend to be higher than those of a solid fuel.
- ***Thermal efficiency:*** This is an indication of how the heat exchangers (economizer, evaporator, superheater, reheater and air heater) within the boiler transfers energy from the combustion gases to the water/steam in the boiler. The thermal efficiency does not account for the

radiative and convective losses, thus it would not properly give an account of the fuel usage [74].

- ***Fuel-to-steam efficiency***: this accounts for the heat transferred in the heat exchanger and the radiative and convective losses as well [74]. It gives a true picture of the fuel usage in the boiler. This efficiency is sometimes referred to as the ***boiler overall efficiency*** and can be used in the economic evaluation of the boiler.

This boiler overall efficiency can be determined either through the input-output (direct) method or the loss method [74] [75]. The input-output method is based on the ratio of the heat output to the heat input of the boiler. The heat loss method is based on evaluating the losses in the boiler [74] . This is the most commonly adopted method.

The losses that affects a boiler overall efficiency of a CFPP plant are highlighted on Figure 2.9.

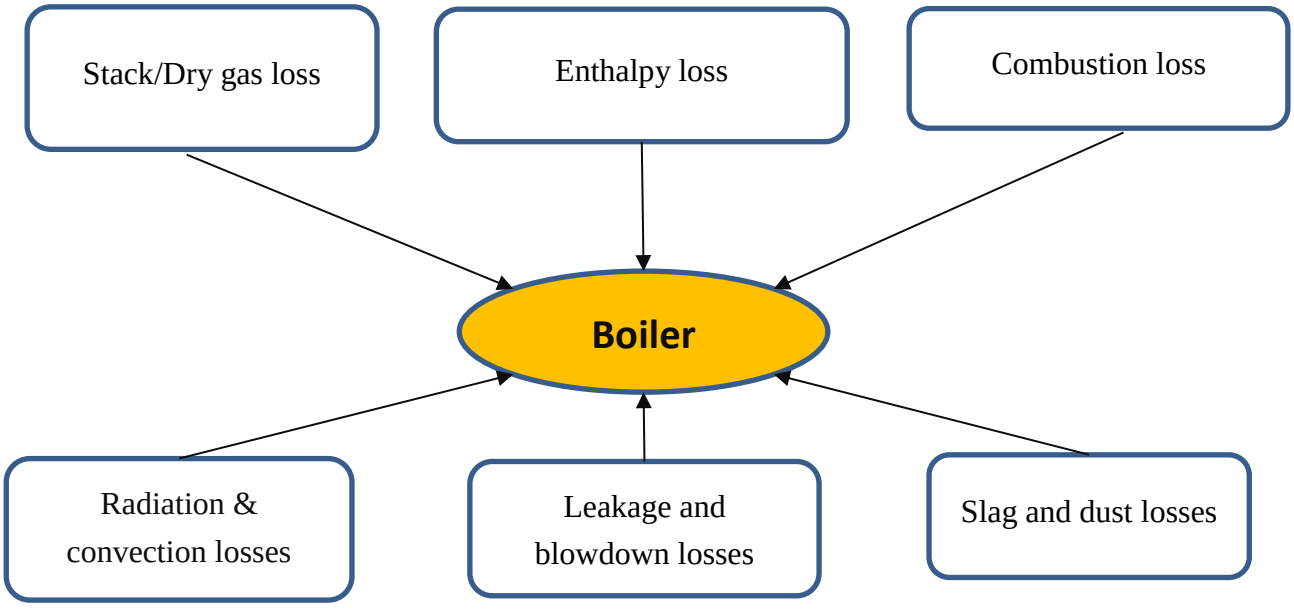

Figure 2.9 Losses affecting boiler overall efficiency

The **dry gas (stack) loss** is the energy that is carried away by the flue gases leaving the exhaust of the CFPP. The magnitude of this loss is dependent on the flue gas exit temperature, the boiler load level, and the amount of the excess air. This loss is usually the largest amongst all the heat losses

experienced in the boiler [76]. The primary purpose of the air heater is to recuperate some of the "un-used" flue gas heat and recycle it back into the air supply stream instead of discarding it to the stack. Without an air heater, the stack losses will be substantially higher. The **enthalpy loss** is made up of the heat loss from moisture in the fuel and combustion air, and the heat loss from hydrogen in the fuel. The **combustion loss** is made up of the heat loss from unburned combustible/carbon in ash, and heat loss due to CO formation. The **radiation and convection losses** are sometimes referred to as the boiler shell losses. These are the heat loss that are either radiated or convected away from the shell of the boiler to the surrounding environment. **Leakages and blowdown losses** are due to leakages caused by ruptured pipes within the steam boiler and steam loss during blowdown operations or passing valves. **Slag and dust losses** are sensible heat loss from the slag and the flue dust. **Unaccounted loss** are heat loss from the boiler that are unaccounted for.

The boiler losses is affected by the following variables which change with boiler load [77]: excess oxygen, flue gas exit temperature (FGET), main steam temperature, spray flows for reheat and superheating, reheat steam temperature, air heater exit temperature, optimum utilization of heated air from air heater, air heater leakage, fly ash unburned levels and bottom ash unburnt carbon. The others are mainly due to degradation.

The procedure for determining most of the boiler losses is well described in the ASME PTC 4 code [75].

2.4.4 Factors affecting auxiliary power consumption.

Auxiliary equipment play a very important role in the safe and successful operation of coal fired power plants [19]. Auxiliary power consumption (APC) sometimes referred to as works power or parasitic power is the power used to drive the auxiliary equipment that start and run a power plant in a power station. The APC compositions is made up of lightening, cooling system, feedwater system (boiler feed pump and the condensate extraction pump), coal handling and grinding plant, ash handling system, compressed air system, water treatment system (condensate polishing plant), draft system (ID, FD, PA, SA), others etc. The auxiliary consumption of the BFP, ID fans, and cooling pumps/ACC fans are amongst the largest contributors to the APC.

The auxiliary power consumed may be split into two components [78] [79] :

- Unit (in-house) auxiliary consumption: this consumption is by auxiliary systems that are directly linked to a single unit within the power station.
- Station (out-lying or common) auxiliary consumption: this consumption is by auxiliary systems that are commonly shared across the various units of the plant. Such systems include: Ash pump for the ash handling unit, water pumps for the central cooling systems, water treatment plant , HVAC systems, lighting etc [79]. In most practical cases, this consumption is usually divided equally across each unit within the fleet or it is divided based on the generation level of each unit [79] .

Typically, the unit auxiliary consumption far outweighs the station auxiliary consumption. For instance, in a 210 MW CFPP unit investigated by Mandi and Yaragatti [78] , the composition of the APC that is attributed to the unit auxiliary was 91% while the remaining 9% was for the station auxiliary consumption.

At full load, the APC is typically in the order of 5-15% of the full load gross generation [78] [19]. Mandi and Yaragatti [79] reported that the auxiliary consumption for a typical 30MW and 500MW plant are 12% and 7% of the respective installed gross generation capacity. It appears as though the % of the auxiliary consumption tends to decrease with the increased installed capacity of the plant [79].

The typical composition of the unit auxiliary power consumption for some CFPPS is shown on the Table 2.4. In most cases the boiler feed pump constitutes the largest portion of the auxiliary power consumption. This is usually closely followed by the draft group.

Table 2.4 Typical auxiliary consumption composition

Auxiliary type	% gross generation
Boiler feed pumps, condensate extraction pump.	2.5-4% [10], [11].
Draft group and pulverizers	ID, FD, PA fans and pulverizers take up 2-2.5% [10], [11].
ACC fans for air cooled condensers only	1.56%
Circulating water pumps for water cooled systems only	1-1.5% [11]
SOx emissions control	1.5-3% [10]
NOx emissions control	0.5-2.5 [10]
Particulate emissions control	0.5-1.5% [10]
Remaining auxiliaries (transformer losses, turbine & generator & BOP auxiliaries)	1.5% [10].

Across various CFPPs, the impact of the live steam condition on the composition of APC is shown on Figure 2.10. The auxiliary fraction required for the feed water system (BFPs, CEPs and Booster pumps) increases as the live steam conditions increase from the sub-critical CFPPs to the Ultra-supercritical type CFPPs. This is due to the need for more pumping power requirement for the CFPPs with higher steam pressure conditions. The fraction of APC required for other auxiliary systems decreases with increase in the live steam conditions.

Factors such as coal quality, type of steam cycle (subcritical, supercritical and ultasupercritical), excessive steam flow internal leakage/ingress in equipment, inefficient distribution losses, inefficient drive systems, oversizing of equipment, reduced power quality, fouling on boiler heating surfaces and ageing have all been known to impact on the auxiliary power consumption [78] [81] [81] [79]. A summary of the key factors that impact the APC of CFPPs is highlighted on Figure 2.11. These factors are broadly grouped into: plant specific factors, external factors, and grid factors. A description of the effects on the APC is presented on Table 2.5.

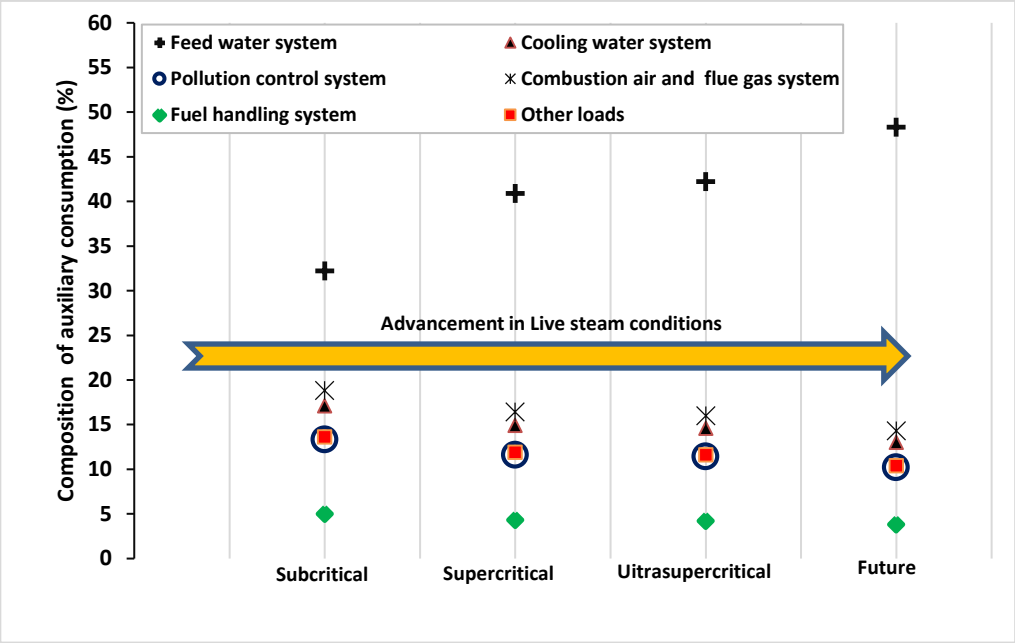

Figure 2.10 Distribution of auxiliaries' across various CFPPs : Data sourced from [80]

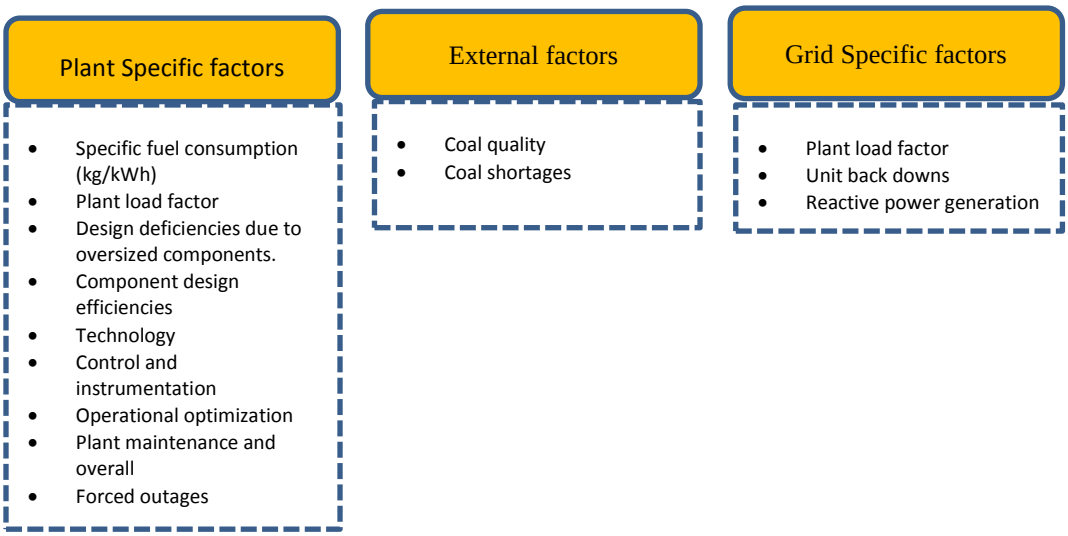

Figure 2.11 Factors that affect the auxiliary power consumption of a CFPP [79]

Table 2.5 The impact on auxiliary power consumption

S/No	Factor	Impact on Auxiliary consumption
A.	*Plant Specific factors*	
1	Specific fuel consumption (SFC) measured in kg/kWh	SFC is linked to the TCHR. A high SFC implies [82]: • Mill and coal handling equipment's power consumption increases due to increased coal flow. • Increased power consumption in the draft group (ID, FD, PA fans) is also required.
2	Plant load factor	Operating CFPPs at a lower plant factor causes throttling losses and/or shifting the operating point of most CFPP components to sub-optimal positions.
3	Design deficiency caused by oversized auxiliary equipment.	Reduced efficiency of the equipment at part load causes increased auxiliary power consumption for that component.
4	Technology (old technologies like fixed speed drives.	Reduced efficiency of the equipment at part load causes increased auxiliary power consumption for that component.
5	Control and Instrumentation	Malfunctioning instruments affects the ability to control process parameters, which in turn affects the ability to conserve resources.
6	Operational optimization.	Operator errors as far as the monitoring and control of process parameter is concerned, can also affect the auxiliary power consumption.
7	Plant maintenance and Overhaul	Poor maintenance of components may lead to efficiency degradation of various components, leakages into the boiler and air heater etc. This generally increases the power consumption.
8	Increased forced outage of units	Increases the frequency of starts (hot, warm, cold) start-ups and shut downs which means more time when auxiliary power consumption is done without power output.
B.	*External factors*	
1	Coal quality	Poor coal quality implies • Lower calorific value, and increased fuel flow for the same MW required. • Increased ash content increases the power consumption in Mills, Coal handling units and Draft groups
2	Coal shortages	Coal shortages at stations sometimes forces units to run below the maximum plant load factor, which in turn affects the APC.
C.	*Grid specific factors*	
1	Unit back downs	Reduces plant load factor
2	Reactive power generation	Grid stability requirements may warrant the grid operators to ask CFFP operators to increase the reactive power of a unit via the excitation. This reduces the generators efficiency and also increasing the auxiliary consumption due to generator losses [79].

At part load conditions, the auxiliary fraction (f_{aux}) of the gross generation increases, even though the actual MW of electricity consumed at the CFPP decreases. This is due to the fact that:

- The common (out-lying) auxiliary equipment draw the same power at partial load operations [79], and
- The power drawn by some of the in-house auxiliary equipment is not necessarily proportional to the plant load.

Mandi and Yaragatti [79] describes graphically (Figure 2.12) how the individual elements of f_{aux} changes with plant load factor for a specific 210MW CFPP. The APC increases from 8.74% at full load to 12.05% of the gross generation at 60% plant load factor. It can also be seen that the share of the individual component increases at reduced plant load factor. For instance, the fraction for the out-lying equipment increased significantly from 1.65% to 3.19%. The fraction from the in-house LT increased from 1.65 -3.19% while the one for the BFPs increased from 2.46 -2.76%.

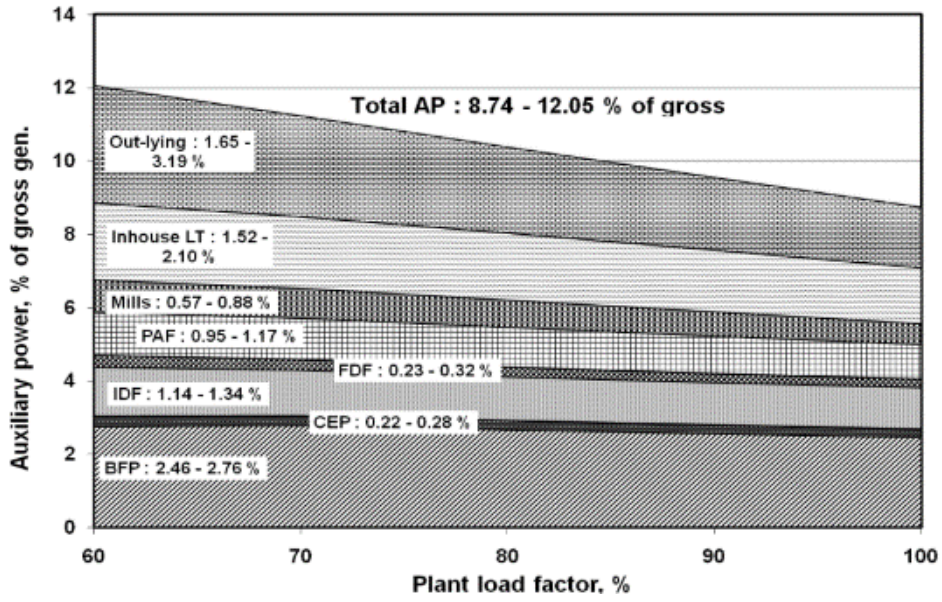

Acronyms*: *Out-lying means common/shared auxiliary equipments. (b) ***Inhouse LT*** means inhouse loads that consumes low voltages of around 0.415V. (c) ***PAF*** means primary air fan. (d) ***FDF*** means forced draft fan (e) ***IDF*** means induced draft fan. (f) ***CEP*** means Condensate extraction pump. (g) ***BFP*** means Boiler feed pump.

Figure 2.12 Auxiliary power of individual equipment [79]

2.4.5 Factors affecting electric generator efficiency

Electric generators are important equipments used in a Coal fired power plants. These equipments, when coupled to a steam turbine, converts mechanical energy to electrical energy [83]. The efficiency of generators are governed primarily by the maganitude of the mechanical and electrical losses experienced in the generator [84] [85]. The mechanical losses are caused by friction of rotating parts, and the interaction between the rotor and the air in the gap between the rotor and the stator called windage [84]. The electrical lossess include I^2R losses and the stray losses caused by eddy currents generated in the steel cores and other metallic parts of the generator [84]. These losses manifests as heat and are carried away by the coolant in the generator.

The mechanical losses and electrical losses are are dependent on [85] :

(a) The generator capability (i.e nominal capacity) in MVA: The losses increase with the generator capability.

(b) The turbine-generator configuration/arrangement and generator speed. The mechanical losses depends on weather the turbine-generator configuration is a Tandem arrangement or cross-compound arrangement; and the generator speed.

(c) The method of cooling the generator: the losses experienced in conventionally cooled generators are slightly higher the ones experienced in conductor-cooled generators.

(d) The pressure of hydrogen in the generator: higher hydrogen (rotor coolant) pressures causes the losses to increase, and vice versa.

The General Electric (GE) method [85] of calculating generator efficiency, incorporates all these factors while trying to calculate the generator efficiency. The design of most generators are optimized – giving rise to efficiencies that are close to 98 % [86] [87].

2.4.6 Impact of cycling on CFPP Heat rates and Heat rate evaluation methods

The impacts of cycling on the heat rates[1] of a CFPP can be split into two [11] [88] namely: (a) Short term (Operational) impact on heat rate are due to low load and variable load operation, and (b) Long term heat rate increases due to long term degradation of component efficiencies. A discussion of the long term effects of cycling load operation on heat rate is beyond the scope of this thesis. The short term impact of cycling load operation heat rate is discussed in the succeeding paragraphs.

Figure 2.13 illustrates how heat rates can be affected by CFPP cycling load operation. The power generation level at the pre-cycle, cyclic event, and post cycle event are shown. As CFPP generation falls, the heat rate begins to rise.

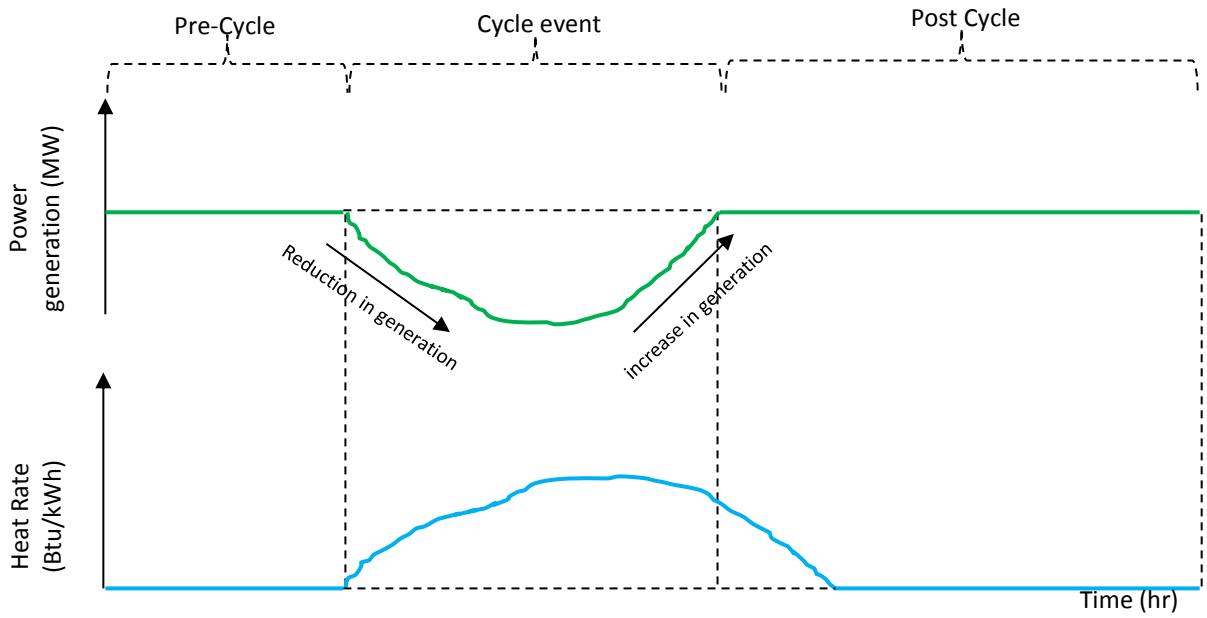

Figure 2.13 Impact of cycling on short term heat rate [89]

During the cyclic event, the heat rate increases because the generation of the plant is choked back and fewer power output is produced by the same amount of coal. Later in the cycle as generation begins to increase, the heat rate further increases because more coal is combusted in order to bring

[1] Heat rates here refers to NUHR, GUHR, TCHR

the combustion temperature back to its steady state rate value. Furthermore in some cases, it has been reported that for many hours after the load change, the heat rate remains slightly higher than its pre-cycle value [60].

Some general methods have been reported in literature for evaluating the net unit heat rate of a CFPP. The methods include: (a) The direct heat rate method; (b) the heat loss method; and (c) Parameter deviation method.

The ***direct heat rate method*** makes use of the as fired calorific value (CV) and mass flow of the fuel and the send out power of the CFPP [90]. The ***heat loss method*** utilizes the turbine cycle heat rate, the boiler efficiency determined by loss method and the auxiliary fraction to calculate the net unit heat rate [90]. The ***Parameter deviation method*** utilizes the control of process parameters to monitor heat rate deviation. This method is reported as the most suitable for plant process control, improvement in plant performance, and suggesting the type of maintenance that should be implemented for heat rate improvement [90].

A predictive heat rate model (see Equation (2.4)) was developed by using a statistical modelling technique referred to as M5P Piecewise Linear Regression Model [69]. The net unit heat rate of several CFPPs were correlated to a slope function. The slope function depends on the CFPPs unit characteristics such as the plant nameplate capacity (NPC), plant type, status of FGD, rank of coal used, and type of flue gas particle collectors. This heat rate model was used by Leidos for evaluating the heat rate improvement (HRI) potential of CFPPs in the United States of America [69]. This method however, fails to consider the mode of operation of the plant and the results that are depicted suggests that the heat rate improvement of the different classes of plant had mainly to do with the historical development of the Rankine cycle architecture of the various plants.

$$HR\left(\frac{Btu}{kWh}\right) = \begin{cases} \dfrac{10^6}{(0.262 \times NPC + 61.4)(Slopefunction)}.where\ldots NPC \leq 106MW \\ \dfrac{10^6}{(0.045 \times NPC + 90.5)(Slopefunction)}.where\ldots 181MW > NPC \leq 106MW \\ \dfrac{10^6}{(0.0071 \times NPC + 93.1)(Slopefunction)}.where\ldots NPC > 181MW \end{cases} \quad (2.4)$$

The first three methods (direct heat rate, heat loss, and parameter deviation) mentioned above require measurements at other load conditions to be able to evaluate the impact of a varying/cycling load operation on the net unit heat rate. The model of Leidos on the other hand cannot be used to evaluate the impact of cycling on the heat rate of CFPPs.

Some studies have also been reported for capturing the impact of load variation on the net unit heat rate of CFPPs with knowledge of heat rate at a few known points. Poullikkas [91] proposed a one-dimensional finite difference technique for approximating the net unit heat rate curve of CFPPs by using data obtained from the minimum and maximum operating points of a single power plant. This method is plant specific and may be grossly inaccurate when applied other CFPPs. In another work reported by EPRI, the net heat rate was predicted at various loads conditions down to 5% (with 25% air flow), with knowledge of the heat rate at loads of 90%, 50% and 25% MCR [13]. Although this approach takes in more operating data points, it does not account for the impact of the different methods of boiler pressure control.

Gutiérrez-Martín et. al. [92] investigated the impact of wind induced cyclic load on the fuel consumption in a Spanish mainland power system. The authors used a polynomial function that defines efficiency curves of two broad categories of CFPPs (below 500MW and above 500MW), at different operational load levels and two other categories of combined cycle gas turbines (single shaft and multiple shaft). This was done to capture the effect of cycling on fuel consumption and related emissions on the power system. A dimensionless excess fuel co-efficient or consumption factor (ratio of fuel consumed at part load to fuel consumed at full load) curve was created (see Figure 2.14) for the generic categories of fossil based generators that were studied. Then the CO_2 emissions were calculated by multiplying the net power output from each plant by an average base emission factors and the dimensionless coefficients for excess fuel. They concluded that wind intermittency adversely affects the expected CO_2 reduction due to degradation of efficiencies at part loads. The drawback with this approach is the presupposition that the fuel consumption factor, which is a metric representing the net heat rate, is only dependent on the size of the CFPPs instead of the thermodynamic architecture of the CFPP. If one were to adopt that approach, a NRH CFPP of 200MW capacity could be assumed to have the same heat rate as a SRH or DRH CFPP with a capacity of 499MW.

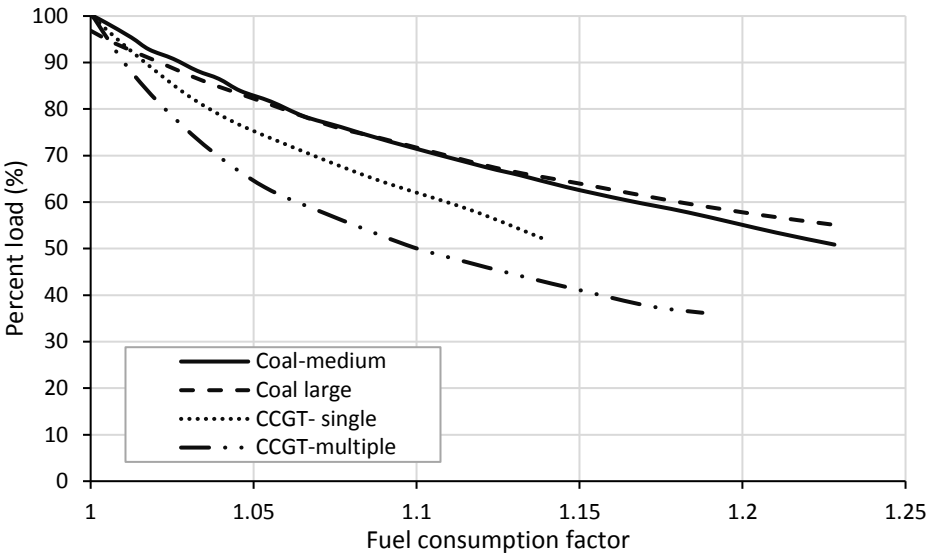

Figure 2.14 Fuel consumption curves for thermal utilities [92]

Eser et. al. also tried to represent the heat rate curves of some CFPPs as a function of the nameplate power and load condition for the various fuel type [93], while trying to quantify the impact of increased renewable generation on the cycling operation of thermal power plants.

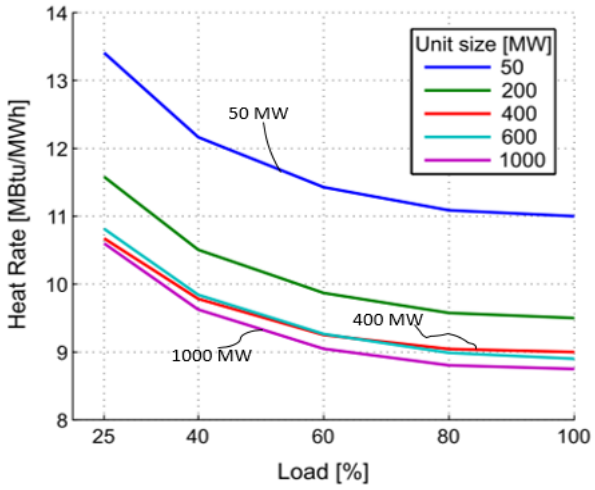

Figure 2.15 Heat rates as a function of name plate capacity and load [47]

Another interesting method that has been reported involved the use of a generation weighted average heat rate model [22]. This method was adopted in the WWSSIS study. This method is equally good except that the heat rate model would be dependent on the type of CFPPs, on the power system network investigated, and the generation profiles of the CFPP on the network.

A quantification of the impact of cyclic load operations on subcritical and supercritical CFPPs (see Figure 2.16) has been reported in [94]. The quantification was done by an examination of the rate of change of the heat rate with load. It can be seen that the heat rate increase for the sub-critical plants are almost twice the ones for the supercritical plant. Furthermore, rate of heat rate increase is much steeper in the sub-critical plants than the super-critical plant. This information is quite useful because it suggests that the steam inlet conditions can provide a great insight into how the heat rate changes with load. This information is not complete as it does not state the impact of the degree of reheat, or the method of boiler pressure operation on the heat rate increase.

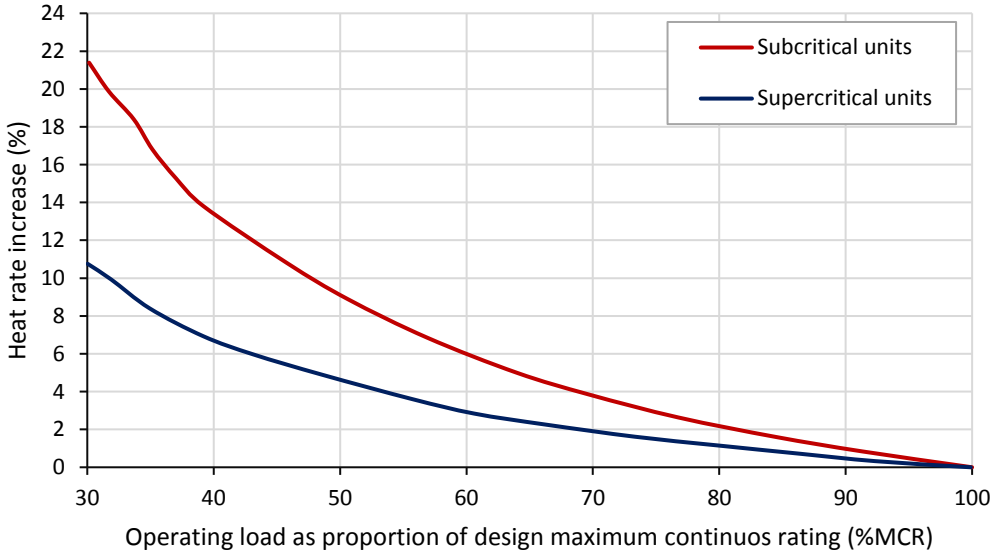

Figure 2.16 Increase in Heat rate between subcritical and supercritical plants [94]

The change in heat rate with load for both constant (fixed) pressure and sliding pressure mode of operation of an 840 MW has been quantified in [38]. In Figure 2.17, the change in the heat rate for the constant pressure is greater than the one for the sliding pressure system. The change is seen to be almost twice that of the sliding pressure. This does point to the importance to consider the boiler operating control as part of the overall heat rate model.

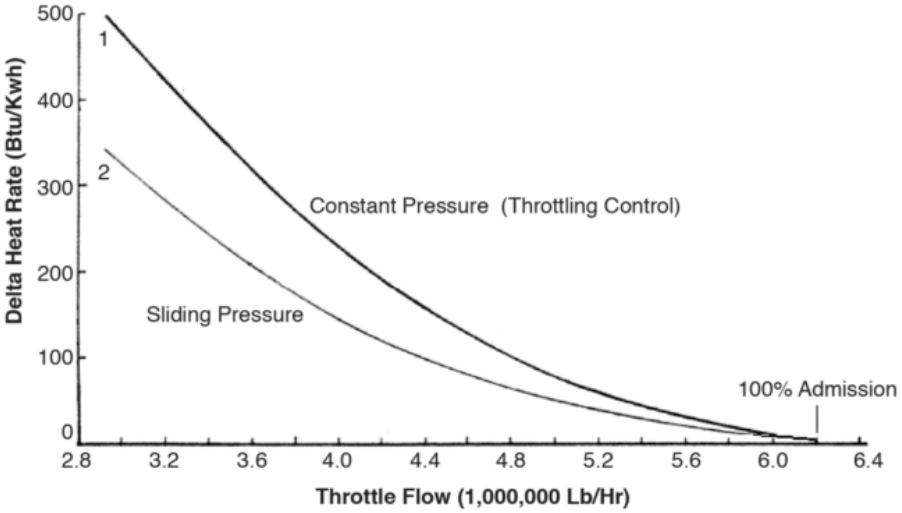

Figure 2.17: Fixed vs. Sliding pressure: relationship of flow rate (plant load) to heat rate [38]

2.5 Emissions from CFPP: types and method of evaluation

2.5.1 Gaseous Emissions from CFPPs

The gaseous emissions from Coal fired power plants can be broadly group as polluting or non-polluting (see Figure 2.18).

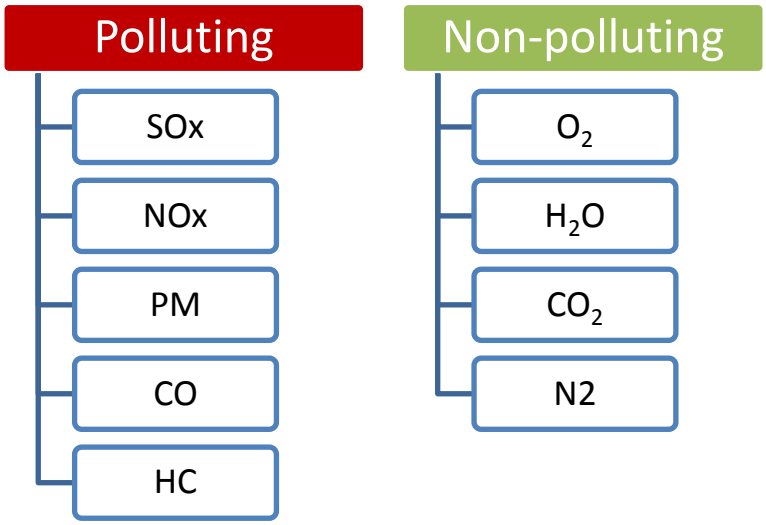

Figure 2.18 Gaseous emissions from a typical CFPP

Non-polluting gaseous emissions from CFPPs: These emissions are generally non-polluting to the environment, given the fact that they occur naturally on the earth. These include CO_2, H_2O, N_2, O_2. CO_2 and H_2O are direct products of complete combustion of Hydrocarbons. However, CO_2 is a greenhouse gas, if it is released in large quantities it can contribute significantly to global warming [6][17]. N_2 and O_2 are products of combustion because of their presence in the oxidizing agent (Air) used for combustion. Generally speaking, the amount of these emissions that is released is dependent on the coal quality, combustion efficiency, emissions control system, the generation output level etc.

Polluting gaseous emissions from CFPPs: These are emissions that are considered as generally polluting or are known to cause harmful effects to humans and the environment [95]. These emissions include CO, NOx, SO_2, HC, and Particulate Matter (PM). CO and HC are products of incomplete combustion, SO_2 originates from the quantity of sulphur present in the fuel.

The parameters that govern the emissions rate of CFPPs may be broadly grouped into the controllable and uncontrollable factors [96]. The most common uncontrollable factors are: fuel properties [94], boiler design, burner design, and mill design. The controllable factors include: operating load, excess oxygen level, burner secondary air register settings, mill operation (mills-in-service, mill-to-mill bias, primary air temperature, primary air to coal), FWHs in service, condenser cleanliness, and furnace and convective pass cleanliness [96].

2.5.2 Methods of evaluating CFPP emissions

The emissions of CFPPs can be measured directly from the CFPPs [16][97]. This can be done using continuous emissions monitoring systems (CEMS). The accuracy of this method is dependent on the accuracy of the measurement device.

An alternative approach would be to estimate the emissions from the CFPPs. There are several method for predicting the emissions of a CFPP. Emission factors still remain the most common method for estimating emissions despite its limitations [98]. Emission factors are calculated using:

(a) The EPA-4216 standard for different emission sources, and for different gaseous emission. Sometimes, the emission factors are the average of all available data of acceptable quality according to EPA. 16 [98].
(b) By other methods including material balance and modelling [16].

Emission factors specify the quantity of each constituent emissions that is released by unit of fuel that is consumed or per unit of electricity generated. Different emission factors have been reported in literature. The reason for the differences in the emission factors are due to one or more of the following [99]–[101]:

- The presence/absence of an emission control for the pollutant
- The type of CFPP from where the pollutant is taken
- The type of pollutant
- The reference temperature when the pollutant was taken
- The basis (wet or dry) that was used in the sampling process
- The generation level of the CFPP
- The sampling procedure
- The age of the CFPP

A range of some of the emission factors that have been reported for NOx, SOx, CO, and CO_2 at full load condition is shown on Figure 2.19. For the NOx emission factors, values such as 0.21 - 0.95 kg/MWh can be seen for the CFPPs while values such as 0.25 – 2.6 kg/MWh can be seen for the SOx emission factors. For the CO emission factors, values such as 0.07 – 0.18 kg/MWh is seen while the CO_2 emission factors values such as 750 – 1200 kg/MWh is seen. Some of the emission factors are also found in other publications [102] [92] [103] .

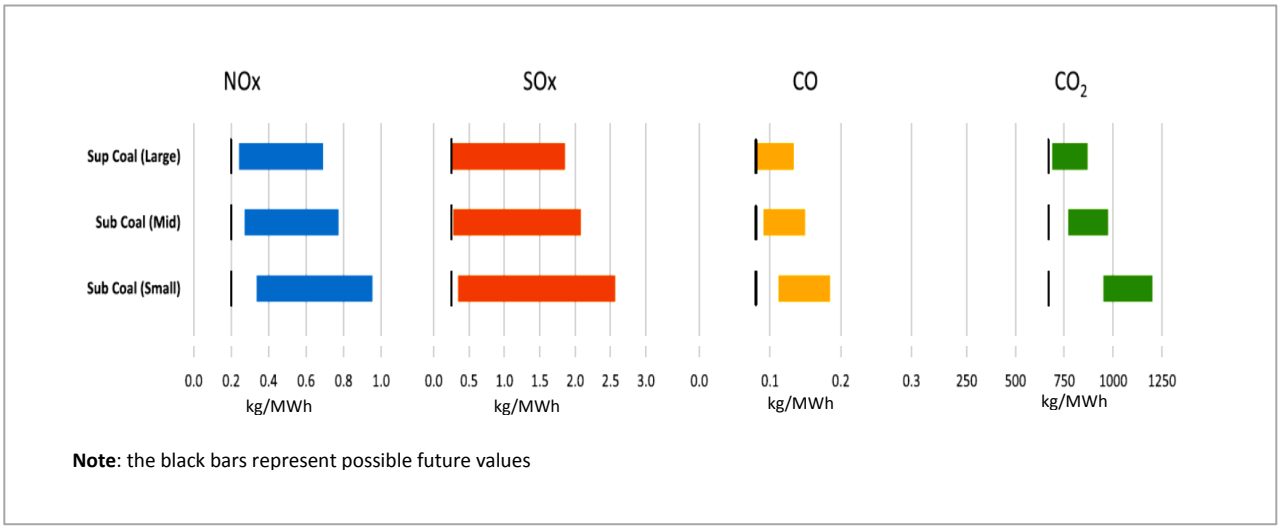

Figure 2.19 Some reported emission factors reported in literature [104]

2.5.3 Evaluating/Reporting CO_2 Emissions

The CO_2 emissions factor (intensity) of a CFPP could be reported in a number of ways [94]:

(a) **Input or output basis**: In the input basis approach (see Figure 2.20), emissions factor (intensity) are based on the quantity of the input fuel energy as expressed ($kgCO_2/kgCoal$). This method does not provide a good basis for comparing the emissions of different CFPPs, because it does not consider the effectiveness of the fuel consumed. In the output basis, the emissions intensity is based on the useful energy output - electricity. The emissions factor is expressed in $kgCO_2/kWh$. This is a more useful method of reporting emissions for a CFPP because it considers the benefits of higher efficiency, and it includes the development and implementation of cleaner, and more efficient technologies [94].

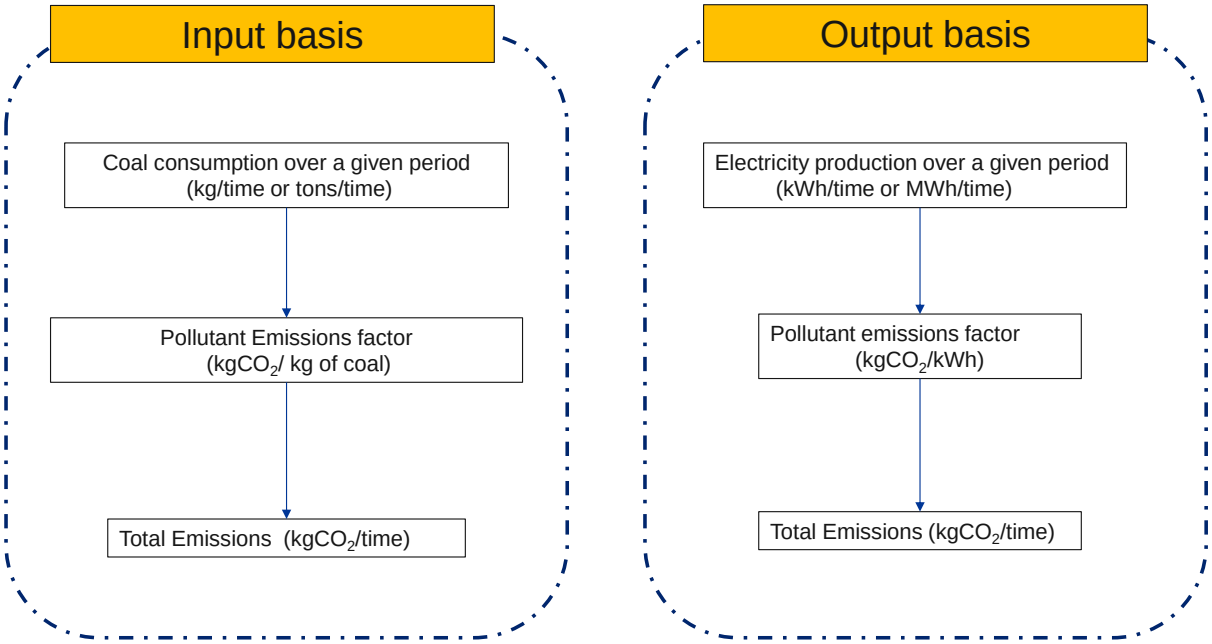

Figure 2.20 Emissions Intensity or factor: Input versus Output basis approach.

(b) **Mass or volume basis**: The emissions could be reported on a volume or a mass basis. It is a lot easier to report the emissions on a mass basis than on a volume basis. This due to the fact that emissions reporting that are based on volume basis must be linked to a reference temperature, pressure, moisture and oxygen concentration [94].

In this study, the mass based CO_2 emissions factor and the output basis of reporting CO_2 emissions will be used.

2.6 Emissions during cycling load operation

Figure 2.21 depicts the emissions that occur during cycling load operations for any given CFPP. The emissions are either due to part & low load effects, starts/shut downs, and ramping (load following) effects [22]. Emissions at part & low load is due to operations at a lower load than the rated capacity of the CFPP. This type is primarily affected by the deterioration of heat rate with the load level. Emissions during start-ups/shut downs is affected by the supplementary fuel oil consumed, number of starts/shut downs, and the type of starts (cold, warm, hot). Emissions during ramping is affected primarily by the ramp rate, and number of ramps.

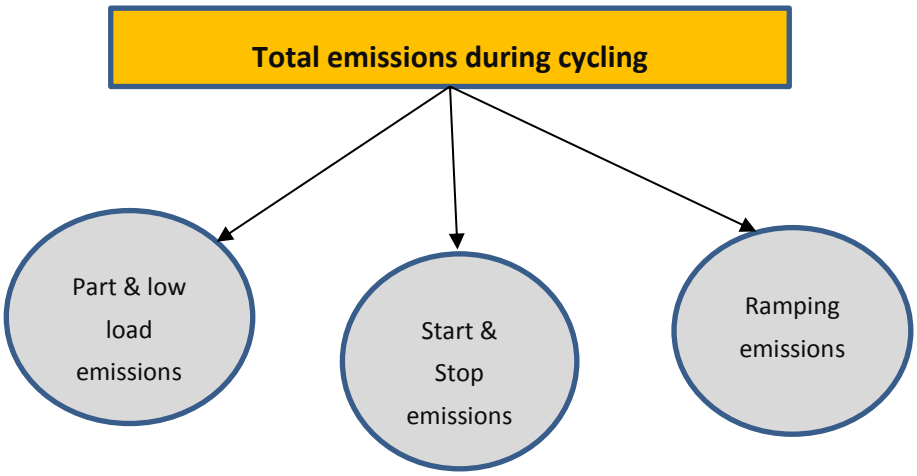

Figure 2.21 Cycling emissions type

In most cycling load operations, the part load emissions is likely to exceed the emissions from the start & stop, and the ramping emissions combined together because of the amount of time that the CFPP spends operating under part & low load conditions. The impact of the start and stop operation of a CFPP is significant as far as the cost of the cycling is concerned, because of the additional fuel costs (from fuel oil) used without any electricity generation to the grid, and the degradation impact on the CFPPs. However, the emissions that is produced in this phase of the operation does not necessarily translate to the highest amount of emissions over time.

2.7 Quantification of the emissions impact of REPG induced cycling

There are different methods in the literature for estimating the emissions impact of REPG Grid integrated systems. These models can be broadly grouped into the Economic Dispatch models and Generation (Portfolio) Dispatch models (GDM) [105] [106]. The common methods that have adopted the economic dispatch models are the static cost models, marginal cost models and econometric model, while the optimal power flow (OPF) and Energy mix model approach seems to be the most common GDM approach.

2.7.1 Economic dispatch models

The static cost approach: The most simple and common approach has been based on calculating the avoided emissions due to avoided generation (displaced by REPG Systems) from CPPFs as a product of the aggregate renewable output and the average emission rate of the dispatchable (CFPP) generation [107]. This method assumes that an equal percentage of output from each conventional technology is offset by renewable generation. This approach has been applied to different configurations of REPG and CFPP combinations.

The marginal cost approach: A second approach for evaluating the pollution avoided, identifies the change in emissions from the marginal producers that adjust output in response to renewable generation. Novan [107] has reported two methods that have been used in this approach: One method utilizes a Load Duration Curve framework to predict which power generation units are on margin at specific levels of demand while the second method uses a weighted average of the emissions rates of the load following plants as the marginal emission rate.

The Econometric Approach [95] [108] : This approach is used for evaluating the emissions offset by REPG systems. It provides an estimate of the marginal impact of REPG on the production of other fossil based generators, by observing the REPG behavior and the current market conditions.

2.7.2 Generation dispatch models

The Optimal Power Flow (OPF) approach is a Generation Dispatch Modelling (GDM) method used to first evaluate the optimum avoidable generation from the CFPP using the name plate capacity of the generators, before the ***avoided emissions*** of the plant(s) is calculated [109]. Figure 2.22 is an example of an OPF network diagram having four conventional power generation system, 1 REPG with energy storage, 3 loading points and transmission lines. This network was used by Lin et. al to investigate the impact of adding energy storage in a REPG integrated system [110]. He observed that the net impact on CO_2 emission when using energy storage in such a system varies. It could be positive, negative or even null. The key factors that affects it are generation/reserve cost, load level, reserve requirement,

the amount of energy storage-based reserve available, and transmission line constraints. The study also concluded that the notion that using energy storage for ancillary services reduces system emissions, may not hold true for all power systems. Hitaj studied the effect of the impact of the relative location of 6 CFPPs and 4 REPGs on the output and emissions in a simulation of optimal power flow in the modified IEEE 30-bus test system [46]. Different REPG capacity sizes of 10MW, 20MW, and 30MW were used to investigate different REPG penetration levels of 14%, 28%, and 42% of electricity demand. His results revealed a large variation in emission abatement by a factor of 1.7 – 7.3 across different configurations.

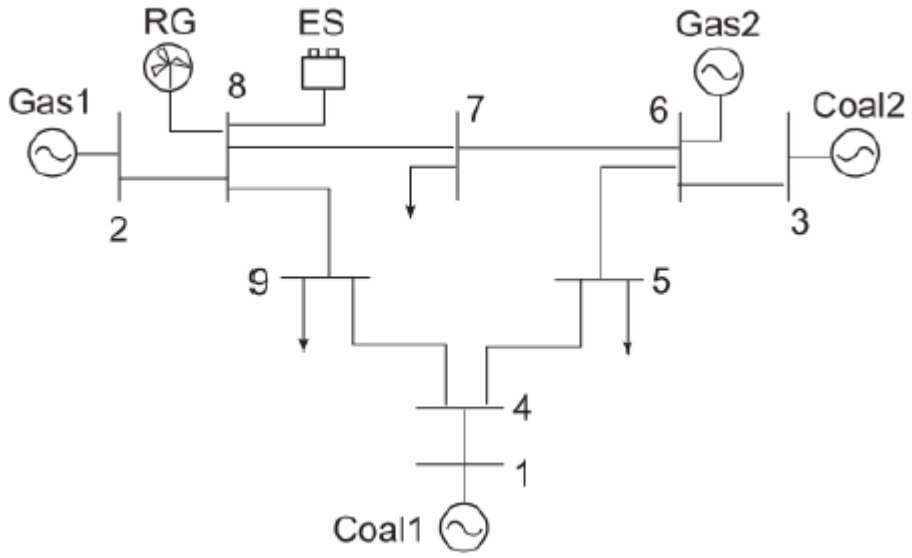

Figure 2.22 An example of an Optimal Power flow network [110].

According to [102] Energy Mix (EM) modelling/ optimization which is also referred to as generation expansion planning (GEP), is interested in the reduction of cost and emissions of producing electricity while taking into account the accessibility to fuel and the technical constraints on the power system operation. It is also a methodology that is used to provide energy and power balance in electricity generating units of a power system. It is a key aspect of energy systems modelling. This method is very useful for determining the total CO_2 emissions produced or saved from conventional fossil-based generators like CFPPs that are connected on a network of different power plants.

EM modellers typically use software to forecast the load scenarios for the individual power plants within the power system network [111]. The load scenarios are often predicted based on scheduled

outages, unit retirement, historical unscheduled frequency, projected load growths, and other factors [20][102][103]. One of the outputs of this type of tool is a histogram that illustrates the percentage of time that is spent at each load for each year projected. This data/information is usually used in conjunction with a steady state average emissions characteristic of the plants to estimate the annual emissions produced or saved.

On a power system level, the modelling tools that have been used in literature are PLEXOS [10][102], Wilmar planning tool [112] and Energy Plan. Some of these tools are able to give a number of results including generator commitment and dispatch, emissions and costs for each time step [10].

2.8 Relevant time scales for quantifying the emissions impact

On the basis of the timescale of studies, there are different approaches that have been adopted on the emissions impact studies. These range from sub-hourly, hourly, yearly and life cycle assessment approach.

a. **Sub hourly , hourly, yearly basis**: The WWIS-2 study is an example of one of the studies that was done on a sub-hourly basis [10]. Temporal resolutions of 5, 15, 30, and 60 minutes were used to investigate the effect of model resolution on the results from a power system with a significant amount of wind generation [113]. Their results suggested that an hourly or 30 min resolution is adequate for studying the impact of cycling on the system cost. They concluded that using a time resolution of 5 or 15 min in larger systems or systems with low amount of variable renewables generation may not be practicable.
b. **Yearly basis**: The temporal scale could be on a yearly basis. This type of study is usually done by carrying out an extended time simulation of the sub-hourly or hourly time scale intervals.
c. **Life cycle assessment (LCA) basis**: Turconi et. al. [17] used this LCA method to investigate, the cycling emissions of thermal power plants with high levels of wind penetration in Ireland. They found that less than 7% of the life cycle CO_2, NO_x and SO_2 emissions was due to cycling of thermal plants. They suggested that cycling emissions are not negligible, that these should be

included by using emission factors per unit of fuel input rather than per unit of power generation.

The relevant timeframes recommended for various impact of CFPP cycling operation is presented in Figure 2.23. A daily (24 hours) to monthly period is suitable for the study of thermal efficiency and the reduced emissions of a CFPP during cycling [114].

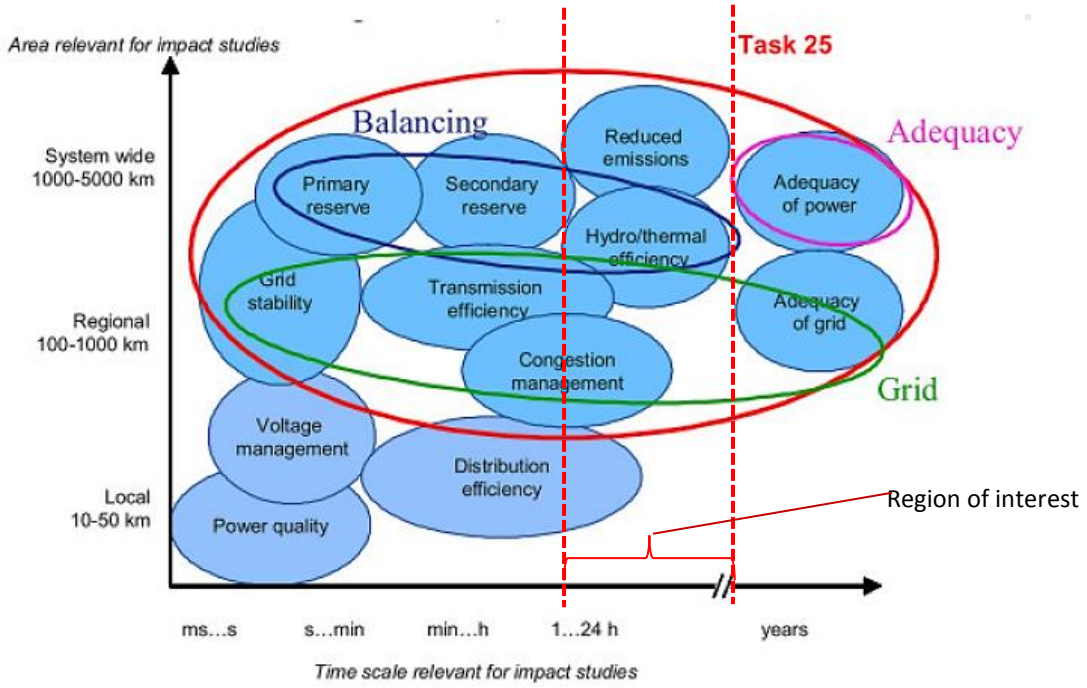

Figure 2.23 Relevant timeframes recommended for studying various impact of cycling [114]

2.9 Impact of emissions factor and heat rate assumptions on the total emissions estimated

The study of the emissions impact of integrating REPG systems on emissions begins with the inclusion of a suitable heat rate model and emissions factor model in an energy mix model of the electric power system. The use of a predetermined emission factors is the most common method used in unit commitment and economic or generation dispatch models for estimating the emissions impact of cycling fossil based plant [4][98] [17] [46] [115] [16][92] [110][106] [107][95][116][15] . Equation (2.5)

defines the emission factors that are used in the unit commitment and economic dispatch models for estimating the emissions of the fossil based generators [15] [16].

$$E_{pi,j} = AR_{pi}EF_{pi,j}\left(1 - \frac{CE_{pi,j}}{100}\right) \quad (2.5)$$

E is the Emission rate of plant (kg/yr), AR is the Fuel consumption of power plants (t/yr) ; EF is the uncontrolled emission factor for the pollutant (kg/t) ; CE is the overall control efficiency for pollutant. CE is equal to zero if a pollution reduction system is not used for the pollutant; pi is the code of power plant; j is the pollutant type.

A constant or varying heat rate model can be used, likewise a constant or varying emissions factor model can also be used. The constant heat rate assumption ignores the impact of heat rate deterioration with load. It assumes that the fuel consumed per unit of electricity produced at all load conditions is the same. The varying heat rate model tries to capture the impact of the heat deterioration with load. The constant emissions factor assumes that the emissions produced per unit of electricity produced does not change. While the varying emissions factor method tries to include the impact of the changing fuel consumption per unit electricity produced at lower loads.

The heat rate and emissions factor models that are/can be used in energy mix modelling can be grouped into four different options (see Figure 2.24). The first option which involves assuming a constant heat rate (HR) and also assuming a constant emissions factor would most likely give rise to an inaccurate total fuel consumption and inaccurate total emissions estimations. The second option which involves assuming a constant heat rate (HR) and also assuming a varying emissions factor would also most likely give rise to an inaccurate total fuel consumption and inaccurate total emissions estimations. The third option which involves assuming a varying heat rate (HR) and a constant emissions factor which is usually arbitrarily chosen would most likely give rise to an accurate total fuel consumption and inaccurate total emissions estimations. The last option is likely to be the most accurate method because it not only considers the variation of the heat rate with load, but it also ties the emissions factor directly to the variable heat rate.

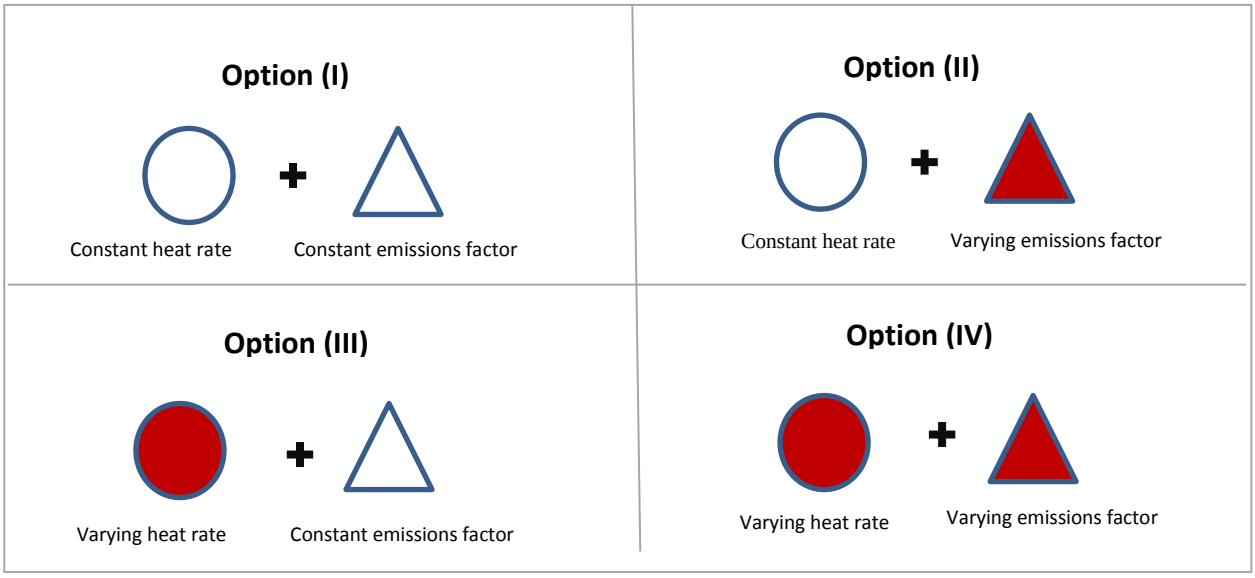

Figure 2.24 options for combining heat rate and emissions factor assumptions in energy mix studies

Figure 2.25 illustrates how the total emissions can be affected by power plant cycling and the various emissions rate approach that could be used. As CFPPs generation falls, the heat rate begins to rise. The constant emissions factor approach always predicts a reduction in total emissions. This is depicted in region PSTP of Figure 2.25. Usually, the unused fuel is used in calculating the amount of reduction. This method is potentially flawed given the fact that it underestimates the emission factor at lower load of plant operation and it also assumes a steady state of operation which is not the case in cyclic operations. Bentek Energy observed from analysing plant historical data, that the emissions rate per MW of electricity generated actually increased during and after cyclic events in the plants they studied [60]. The increased emissions is illustrated in the region bound by PQRSTP of Figure 2.25. Inefficiencies in the boiler operation and instabilities in the controls of emissions control systems have been attributed to the increase in emission rates during plant cycling [60].

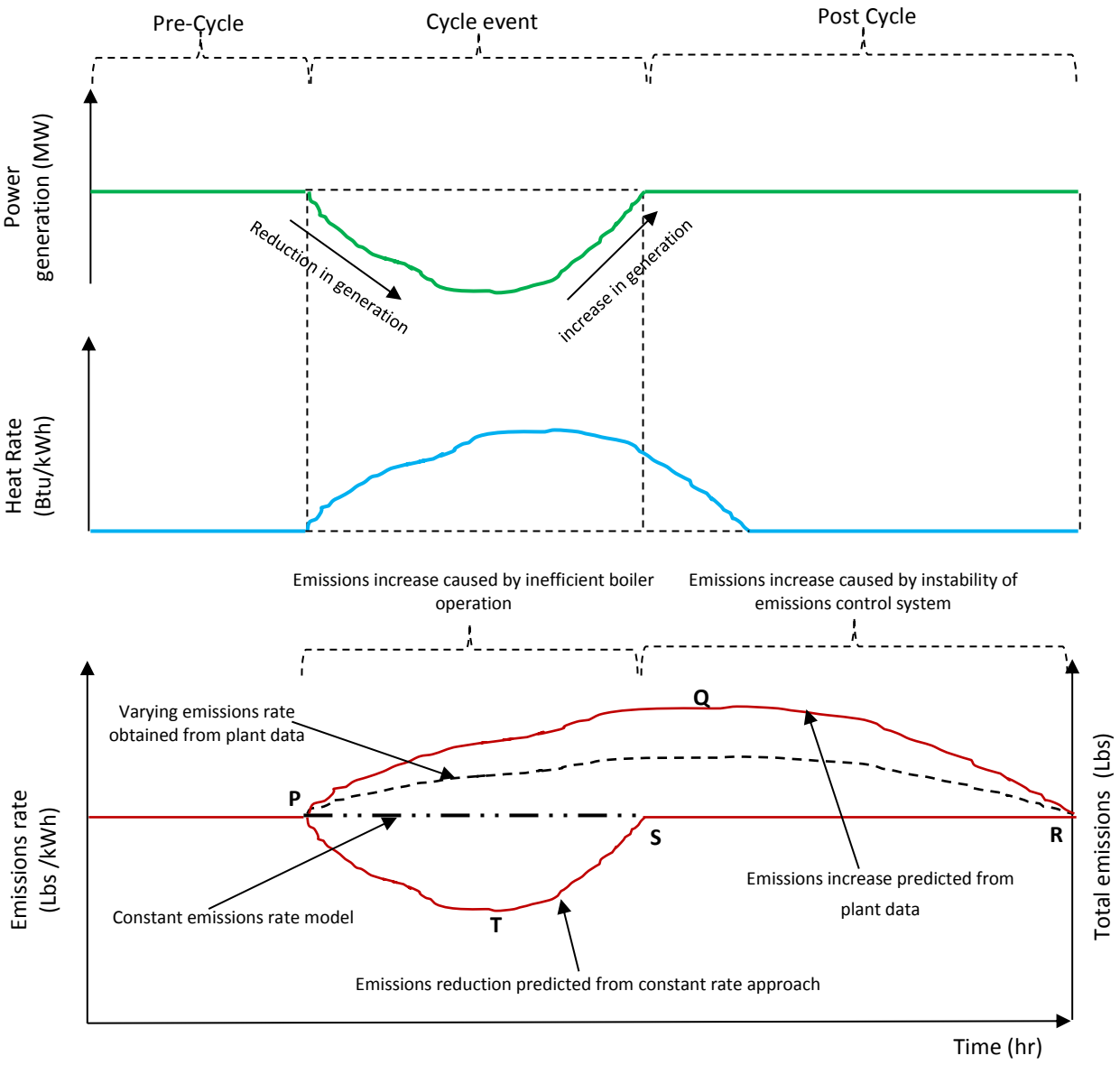

Figure 2.25 A graphical summary of the effects of cycling on Heat rates and emissions impact study approaches [89]

In most of the emission displacement studies, a constant emission factor is used in calculating the emissions that is displaced by incorporating REPG systems [106]. This factor is probably determined using a method as described in [4]. The reality is that the emission factor are underestimated for most conventional fossil based power plants which compensates for the intermittencies of REPG systems [106].

Katzenstein and Apt modelled the combination of variable renewable power at different levels of penetration, with a fast-ramping natural gas turbine to provide baseload power. This model was used to study the displaced emissions from the natural gas plant used to compensate for the intermittency of wind and solar [106]. They modelled the emissions and heat rate, using a regression analysis of measured emissions and heat rate taken from two types of gas turbines, as a function of power level and ramp rate. Their models predicted that it's only a fraction of expected emissions that was attainable. 80% of the expected CO_2, and 30-50% of the NO_x emissions were reported. Their results suggested that policy makers might be using the wrong avoided emissions for planning.

Phase 2 of the Western Wind and Solar Integration Study (WWSIS-2) is one of the largest renewable energy induced cycling emissions impact study that has been done [117], [118]. Their study simulated the operations of solar and wind in the western grid, having United States, Canada, and Mexico on a sub-hourly basis. Their results showed that although the overall emissions of the grid is reduced, a positive or negative impact on CO_2, NO_x and SO_2 emissions rates of an average fossil based generator could be seen, depending on the mix and level of penetrations of the renewables. It therefore implies there could be better ways of combining the mix at different renewable penetration rates in order to achieve maximum emissions reduction.

Some metrics have been presented in literature for quantifying different aspects of the impact of integrating renewables with conventional thermal power plants. Some of the metrics are presented in [48]. The metrics were broadly classified into: (a) net load signal metrics; (b) surplus generation metrics; (c) occurrence and duration metrics; and (d) frequency based metrics. Some have made use of a heat rate penalty [103] in trying to quantify the impact of variable REPG system on CO_2 emissions from fossil based generators [119].

Different authors have tried to study the impact of renewable power induced cycling on the emissions of different conventional thermal power plants. Their results have not yielded consistent conclusions. The reason for this may be attributed to the definition and types of emissions factor used, the type of CFPP investigated or the time resolution used in the investigation. However, Turconi et. al [17] have suggested that a more coherent assessment could be possible if the analysis is done with

emissions from specific power plants, and making comparisons with power plants/units with a similar role, i.e load following, mid-merit or baseload.

A first step in doing this would require the development of a simple metric that can be used by energy mix modellers for quantifying the impact of part and low load operation of different kinds of CFPPs. This would involve investigating the thermal performance (heat rates and the emission factors) of different configurations for CFPPs at various load conditions, and also examining how the key features of each plant affects the thermal performance at various load conditions. This type of investigation can be adequately conducted through modelling and simulation of CFPP.

2.10 Modelling and simulation of CFPP Performance

Modelling and simulation of CFPPs offers tremendous benefits and insights to understanding the response of CFPPs under various conditions. It is cost effective and reliable if the components of the CFPP are well modelled, and the right boundary conditions are applied.

Figure 2.26 gives an example of a typical process flow chart that may be implemented while modelling coal-fired power plants performance. From a thermodynamic perspective, the effort is usually focused on the steam cycle, and the air/fuel gas cycle. The complex, multivariable and non-linear nature of CFPP behaviour under various loading and operating conditions makes it practically impossible to analytically solve and predict the behaviour of CFPPs. This problem has been addressed with the development of advanced computational algorithms that have been incorporated into several computational tools. Some of the computational tools that exist include : Aspen Plus [120], EtaPRO Virtual Plant [121] [122], Flownex [123], EBSILON Professional [124], Gate Cycle [120], SteamPro [120], Modelica, gPromps [125], APROS [123], Virtual Power Plant (VPP) Software [126] [127], Cycle Tempo [120], and many more.

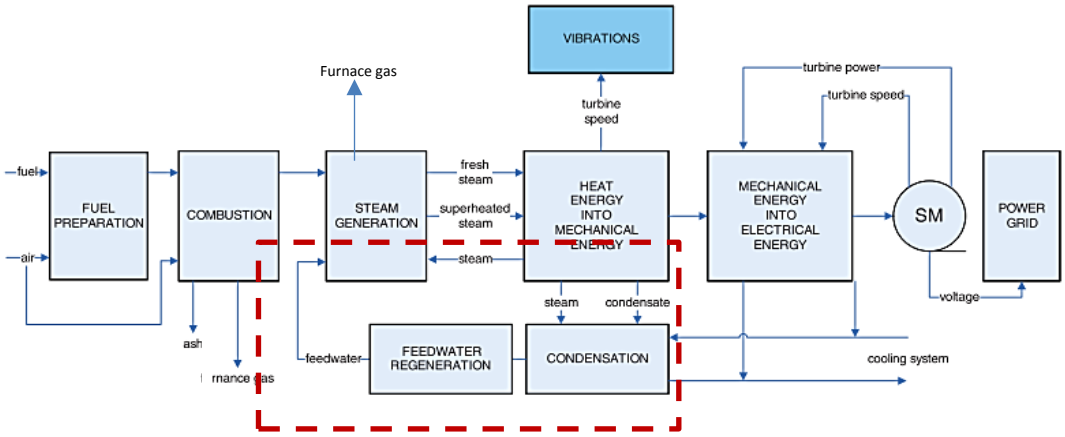

Figure 2.26 Process flowchart that are implementable in modelling coal-fired power plants [126]

The performance evaluation of CFPPs at any given operating condition is predicated using knowledge of the process parameter conditions at all the points within the cycle. But firstly, knowledge of the design conditions or physical parameters is required to be able to predict the process parameters at off-design conditions.

Several researchers have modelled the performance of CFFPs under different operations whilst considering different effects. Some of the effects that have been considered includes: effect of cycling load on the residual life of CFPP components[54]; effect of the dynamic fuel flow at the coal mill on the cycling capabilities of CFPPs [128]; effect of the coal grinding process on the cycling capabilities of a CFPP [57]; effect of the boiler dynamics on the CFPP and effects of CCS on the dynamic behaviour of CFPP [129], [120], [53]; effects of the control schemes on the dynamic behaviour of CFPPs [130]; effect of boiler-turbine unit response on the dynamic behaviour of CFPPs; and effects of load cycling on the cost of a CFPP [131] [93].

2.11 Key findings of the literature review

The key findings of the literature review can be summarized as:

A. The impact of cyclic load on CFPP operations.
   - There is an overwhelming evidence in literature that an increased penetration level of grid connected REPG systems results in increased cycling and low load operation of CFPPs.
   - The heat rate of CFPPs is an important feature that is closely linked to the efficiency, emission rates and cost of operating CFPPs.
   - The impact of CFPP cycling load operation on the heat rate of CFPPs is dependent on the live steam inlet conditions, the boiler pressure mode of operation, the plant load level and several other parameters.
   - Most of the quantitative studies that have been done to try and capture the impact of cycling load operation on heat rate of CFPPs are either component specific, or plant specific and cannot be used to predict the heat rate performance of a wide range of CFPPs.
   - There is no simple generic model that adequately describes the impact of cycling on heat rate of any CFPP – complex plant specific analyses are required. This is a major gap which this current research aims to fill.

B. On the emissions impact study of including REPG systems on the grid, the following findings were also made:
   - There are several conflicting results available about the actual emission that is "avoided" or "reduced" from CFPPs due to REPG. This is largely due to the emissions modelling/study approach that is applied to the unit commitment and economic dispatch models and the type of generators in the power system that was analysed.
   - The causes of the discrepancies also relates to the time resolution of the study, emissions factor used, size of plant study, age and status of the plant studied, modelling approach adopted, the composition/type of plants within the system, presence/absence of emissions control system etc.
   - It is inaccurate to quantify emissions rates of a CFPP undergoing cycling with a single emissions factor. This is strongly supported by the argument made in [132].

- The emissions impact study of integrating REPG systems is mostly done through the use of energy mix modelling.
- Most REPG integrated studies underestimate the emissions of CFPP when they fail to account for the efficiency reduction that occurs due to REPG induced cycling. This underestimation is done when researchers adopt constant emissions factor that are often obtained from average full load values.
- The effect of heat rate and emissions factor variation with load are yet to be captured in emissions models used in the unit commitments and economic/generation dispatch modelling used for quantifying the emissions impacts of grid connected REPG induced load cycling on CFPPs.

In concluding this literature review, it is the strong opinion of the author that a coupling of the heat rate model and the emissions factor model of CFPPs could be a means for truly capturing the impact of cycling load operation on the emissions of CFPPs.

3. Overall architecture of the generic CFPP process model

3.1 Purpose of developing generic CFPP process models

From the literature study it was concluded that most attempts to incorporate a varying heat rate into energy mix modelling was linked to location or plant specific cases. In order to develop a general model for plant heat rate, generic process models of CFPP plants are needed. These models can then be analysed at low load, and general trends can be observed which will inform the development of the varying heat rate model. The CFPP models should be representative of plant architectures found in industry, but not linked to a specific plant.

The computational tools that are used to evaluate the performance of CFPPs adopt calculation procedures that are dependent on the knowledge of the CFPP operating conditions, and the characteristics of each component of the plant at the design base. The task of setting up a representative model of the CFPPs without this information is almost impossible. Hence the need for the development of generic CFPP process models, that can be used to investigate the heat rate of different types of CFPP plant configurations at varying load conditions.

A general overview of the methodology adopted for setting up generic CFPP process models is discussed in this chapter. A description of how the selection of the key CFPP steam cycle components were made, including their characteristics, is also presented. The generic CFPP layouts selected for the non-reheat, single reheat and double reheat process models are also highlighted. The key aspects of the Generic CFPP process model development are also highlighted.

3.2 Basic CFPP Layout

Electricity from Coal Fired Power Plants (see Figure 3.1) is generated through the production of high temperature and high pressure steam from a boiler (BLR). The steam does work by expansion in a series of turbines that are connected to the shaft of an electric generator. The low pressure and temperature steam at the end of the expansion line of the LPT turbine is condensed, and then passed through a series of feed water heaters (FWHs) for recuperative heat addition. Water pumps that are along the feed water heating train raise the pressure of the steam back to the inlet pressure of the boiler, where the entire steam cycle begins again. As the operating pressure is increased, it becomes necessary in some designs (single reheat CFPPs) to re-heat the steam after an initial expansion through the high pressure turbine (HPT) to avoid excessively wet outlet conditions. Some CFPP plants (double reheat CFPPs) would even employ a double re-heat process.

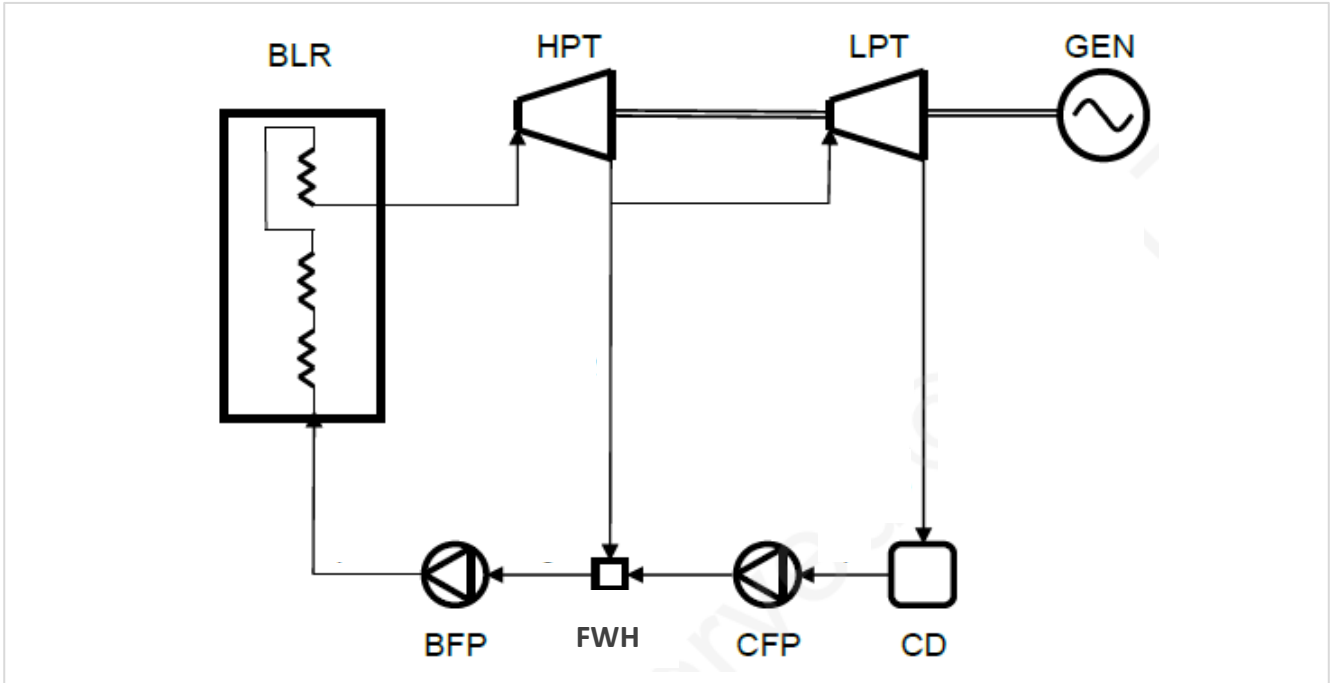

Meaning of acronyms. BLR --boiler; HPT—high pressure turbine; LPT—low pressure turbine; GEN—generator; CD—condenser; CFP—condensate feed pump; DA—dearator; BFP—boiler feed pump; FWH—Feed water heater.

Figure 3.1 Basic CFPP steam cycle layout and components [133]

It is important to understand the types, and configurations of the various key components that are typically seen in most CFPPs, before a selection of representative CFPP layouts/configurations can be made. The detailed discussion of the types and configurations for each key component, and the selections made are presented in the subsequent sections.

3.3 Boiler types and reheating

The steam generator is commonly referred to as a boiler. The following processes takes place within the boiler: (a) preheating of combustion air; (b) combustion of fuel; (c) heat addition to the working fluid. Steam boilers are the most critical component of a CFPP because the temperature, pressure and flow rate of the steam directly affects the performance of the power plant [73]. It is the location where the chemical energy inside the coal is converted to thermal energy and transferred to the working fluid (steam).

Figure 3.2 shows a typical process layout of a non-reheat drum type steam boiler. It consist of: (a) the coal and air handling equipment such as the coal bunker, mills, and etc; (b) the heat exchangers such as the economizer, superheaters; and (c) the emissions handling equipment.

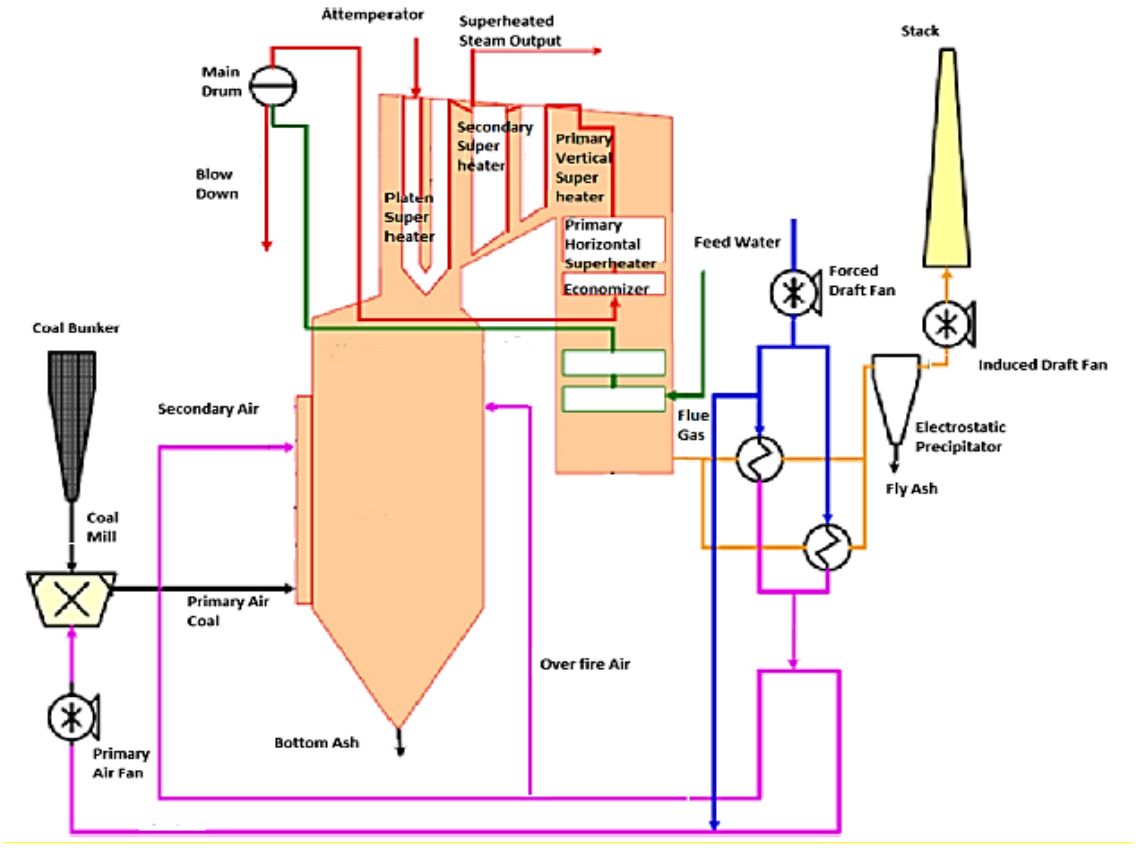

Figure 3.2 Process flow diagram of a typical drum type boiler [134]

The steam boilers that exist in CFFPs are diverse. There are some characteristics that can be used to differentiate between the various types of boilers. These include [135][136][137]: type of water

circulation, number of re-heat stages, layout of the boiler, burner configuration and number of burners, furnace wall design, mill type, arrangement of the heat exchangers, air heater type and configuration, and condition of fuel.

In terms of the ***type of circulation***, the steam boilers are mainly grouped as a drum type or a once through type [45]. In terms of ***layout***, the boilers could either be a tower type or a 2 pass layout type boiler. In terms of ***the number of re-heat stages***, the boilers could have one reheat stage, two reheat stages or no reheat stages at all. In terms of the ***live steam conditions***, there are sub-critical, supercritical, and ultra-supercritical boilers. In terms of ***burner configuration***, horizontally opposite fired burner type boilers, tangentially fired, and front wall burner type steam boilers. In terms of the ***furnace wall design***, the boilers could be single wall furnace type boilers or twin divided wall type steam boilers. In terms of the ***mill type***, there are the tube type mills and vertical spindle type mills. The ***fuel condition*** can either be pulverized or burning in a fluidized bed. This project will only consider CFPPs using pulverized fuel.

Generally, the drum type of boiler is used for non-reheat types of CFPPs while the once through type of steam boilers are typically used for single and double reheat CFPPs, mainly because the steam pressure is above the critical pressure of water. From a thermodynamic perspective when analysing the Rankine cycle, the boiler type does not matter.

Attemperator spray flows are usually present at the superheaters and reheaters of all the various types of boilers [138]. These flows are usually used for the final superheat and reheat temperature control purposes during the operation of boilers [139]. These flows are relatively small when compared to the main steam flow, and as such would be assumed to be zero in this study.

3.4 Steam turbines and generator

3.4.1 Characteristics of steam turbines

Steam turbines are at the heart of the steam cycle. It is the component that is responsible for the extraction of useful work from the working fluid and converts the thermal energy to mechanical energy. Turbines are divided into the high pressure (HP), intermediate pressure (IP) and low pressure (LP) turbines depending on the operating pressure of the steam that is expanding. Non-reheat CFPPs have been known to have only HP and LP steam turbines, while the single and double reheat type of CFPPs typically have all the three types of steam turbines.

A full description of the characteristics of the steam turbines (HP, IP, and LP) is usually necessary for preparing the heat balance diagram of a CFPP. The characteristics of the turbines are usually described by each manufacturer in the form of working curves. The categories of working curves are [140] : (a) extraction stage shell pressures; (b) expansion lines; (c) expansion line end points (ELEP); (d) packing leakages; (e) exhaust losses for LP turbines; and (f) Generator and Mechanical losses.

The nature of these working curves are usually dependent on [140]: the capacity/size of the turbine; the type of compounding (tandem vs. cross compounding); impulse or reaction type; amount of flow (single or double flow); Presence and number of governing row(s) ; Reheat or non-reheat type; Initial steam conditions; and Type of manufacturer.

Certain rules of thumb/assumptions were adopted for describing the characteristics of the steam turbines in the generic CFPP process models. These rules of thumb have been adopted due to: (a) the diverse nature of the variations that exist in steam turbine designs from various manufactures; and (b) the lack of design information that is required for fully describing the steam turbines found in existing CFPPs. The assumptions include:

(a) Extraction stage shell pressures: A full description of the procedure for determining the extraction stage shell pressures of the steam turbines is discussed in section 4.2.2.

(b) Expansion lines: different isentropic efficiencies have been assumed for the various steam turbines. Isentropic efficiencies of 86%, 92%, and 90% have been chosen for the high pressure (HP) steam turbines, intermediate pressure (IP) steam turbines, and the low pressure (LP) steam turbines respectively. These values are within the range that is typically seen in literatures [141][86] . The efficiency of the turbines are assumed to be constant throughout the various load conditions. The losses due to the throttling valve will be incorporated separately, instead of as part of the HP turbine efficiency.

(c) Expansion line end point (ELEP): The quality of the steam at the expansion line end point for the LP turbine must be greater than or equal to 0.85 [27] [142]. This is required for the protection of the turbine.

(d) Turbine Valve Stem and Shaft Packing leakages: These leakages are relatively small (0.5-1.35 %) when compared to the main steam flow [140]. The effects of the shaft packing leakage, valve-stem leakage and other leakage flows from the turbines are assumed to be too small to significantly affect the overall thermal performance of the CFPPs. For that reason, these leakages have been assumed as zero.

(e) Exhaust loss for LP turbine: A full description is given in section 3.4.2 and 3.4.3

(f) Generator & mechanical losses: In determining the generator and losses of the generic CFPP, a tandem operation of generator is assumed. The efficiency of the generators are usually quite high in most applications because of the optimized designs[143]. In this study, the generator efficiency is assumed as 98% [86]. A Power factor of 90% was selected.

3.4.2 LP turbine exhaust loss curve selection

Exhaust loss is the loss that occur between the last stage of the LP turbine and the condenser. It is a very important parameter that needs to be evaluated [144] [145], before the actual work that is extracted from a low pressure (LP) turbine is determined. It is equal to the difference between the used energy end point (UEEP) and the expansion line end Point (ELEP).

A typical exhaust loss curve is shown in Figure 3.3. It comprises of [145] [146] :

- The actual leaving loss: this loss is incurred due to the kinetic energy of the steam leaving the last stage of the LP turbine. It constitutes a substantial portion of the entire exhaust losses. It is experienced in the entire range of the annular velocity.
- The gross hood loss: This loss is due to the pressure drop that occurs when the steam is passing through the exhaust hood. This component of the exhaust loss increases when the annular velocity increases as the power plant operates close to its full load capacity.
- The annular restriction loss: This loss is experienced as the steam flow approaches the sonic velocity (choking begins to occur). The additional flow which may be caused by increased steam flow or reduction in condenser back pressure below the design is responsible for this.
- The turn up loss: These losses are experienced at low steam flow rates or high exhaust (condenser back) pressures.

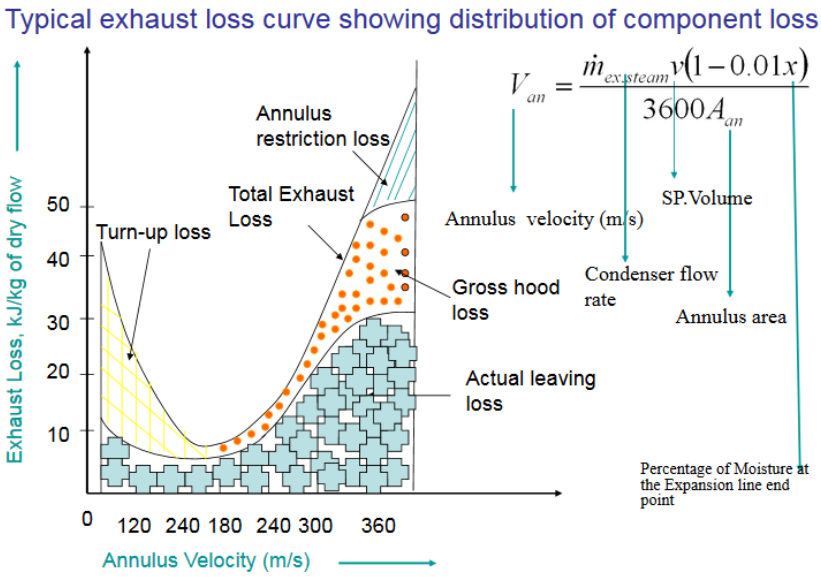

Figure 3.3 Exhaust Loss vs. Annular Velocity curve [146]

Exhaust loss curves differ from one LP turbine manufacturer to another. It is also dependent on the size of the last stage bucket (LSB) [140][85]. Some LSB sizes that have been used in the past and some of the present designs are shown on Figure 3.4. The LSB also depends on frequency of the output generator. An LP turbine operating at a 3600RPM (60Hz) would have a shorter LSB when compared with one that operates at a 3000RPM (50Hz).

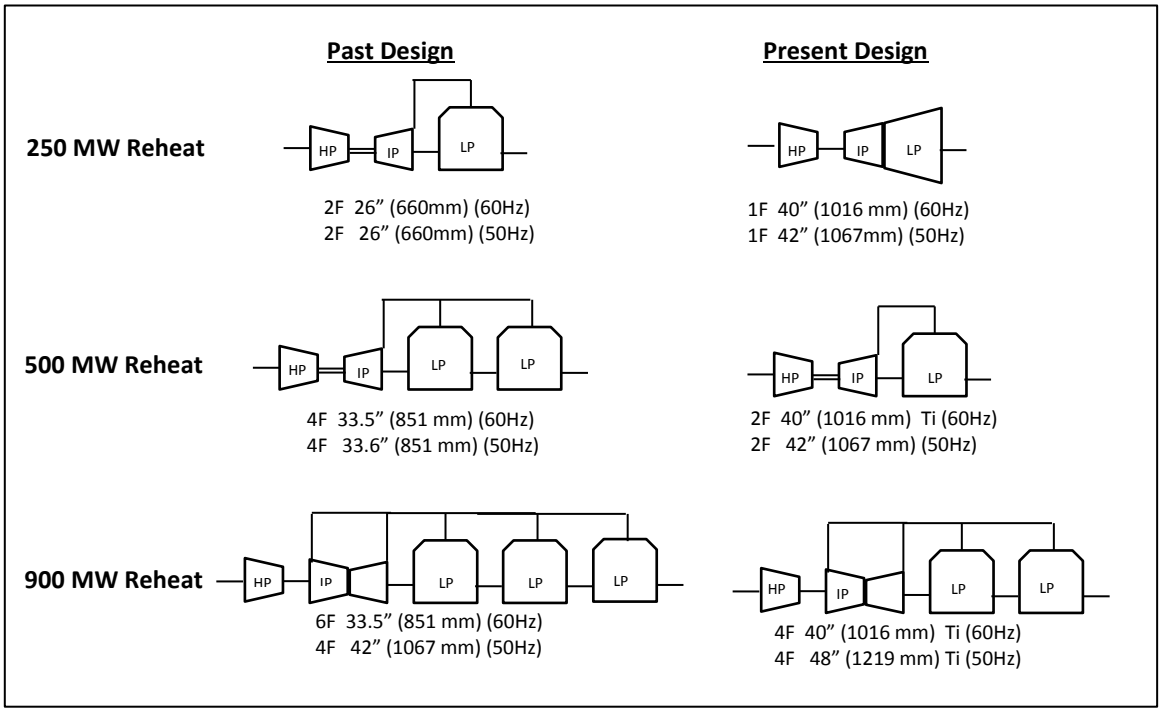

Figure 3.4 Some LSB sizes for different flow configurations [147]

Figure 3.5 shows the exhaust loss profile that was selected for the last stage blade of the LP turbine of each of the generic CFPP modelled. The profile is based on a last stage bucket (LSB) size of 0.851m, and for a turbine operating at a generator speed of 3600RPM. This profile was obtained from Spencer et. al [85] . Mathematically, the exhaust loss (kJ/kg) is given in the Equation(3.1). It is purely dependent on the annulus velocity (m/s) of the exhaust steam from the LP turbine.

$$Exh_{loss} = -(2.501 \times 10^{-11}){V_{an}}^5 + (5.539 \times 10^{-8}){V_{an}}^4 - (5.032 \times 10^{-5}){V_{an}}^3 + (2.21 \times 10^{-2}){V_{an}}^2 - 4.317V_{an} + 318.5 \quad (3.1)$$

Annulus velocity is the axial velocity of the steam through the annulus made by the last stage blades.

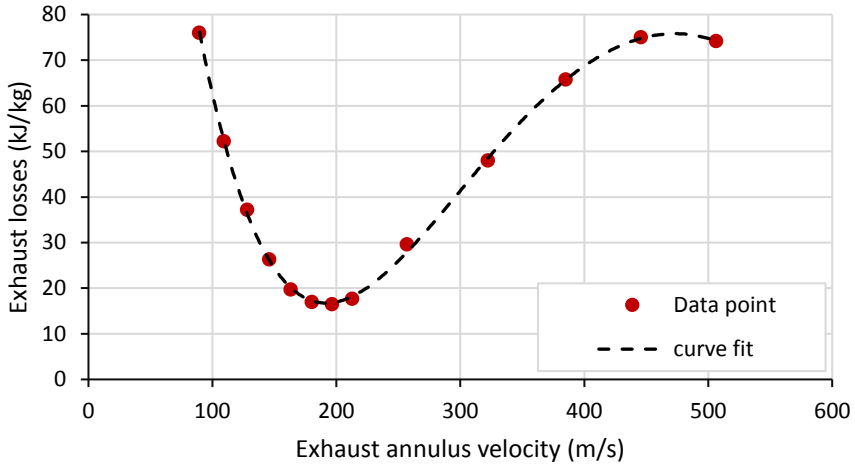

Figure 3.5 Exhaust loss curve selected for LSB=0.851m and generator speed of 3600 RPM

The annulus velocity is determined using Equation(3.2).

$$V_{an} = \frac{m_{cond} \cdot v}{A_{an}} \tag{3.2}$$

v is the specific volume of the steam, A_{an} is the annulus area of the exhaust, and m_{cond} is the condenser mass flow rate. The condenser mass flow and dryness fraction depend on the operating point of the CFPP. The annulus area is an important geometric factor that CFPP designers determine at the VWO conditions of the CFPP. A description of how the annulus area for each CFPP process was determined is presented in section 3.4.3.

3.4.3 LP Turbine exhaust annulus area determination

The main factors that influence the design of turbine exhaust and annulus area [144]:

i. Load duration Curve: Generally speaking, CFPPs that are designed to operate as base loaded plants tend to have a more liberal exhaust end area than the ones that operate more under light loads. This is due to the large steam flow that is handled at baseloaded CFPPs.

ii. Capacity of the plant (Condenser capacity): For the same system /cycle architecture, a plant with a larger MW output would have a larger total exhaust annulus area to accommodate the larger steam volume flow. This is typically subdivided into smaller areas by having multiple LP turbine flows working in parallel.
iii. Size of Last stage bucket selected: The exhaust annulus area is also a function of the LSB selected. Larger LSBs yield larger exhaust annulus areas. Turbine designers make this choice in conjunction with the previous total annulus flow required.
iv. Type of cooling system (Condenser back pressure): The cooling system determines the back pressure of a given unit. CFPPs with higher back pressures generally have lower annulus or exhaust areas. This is due to the reduction in the specific volume of the LP exhaust steam at higher condenser back pressures.

The sizing of the exhaust annulus area and exhaust hoods of an LP turbine begins with the selection of a suitable VWO operating point on the exhaust loss curve, for the given VWO design condensing pressure. Ideally, the thermodynamic optimum point (see Figure 3.6), which is the point where the minimum exhaust loss occurs, should be the best design point. However, this point is usually not the economic optimum as designers rarely design for such point. The economic optimum point is usually slightly further away from the thermodynamic optimum. This point usually corresponds to an annulus exit velocity between the range of 213 m/s to 305 m/s [146][71]. For the CFPP models built in this research, the exhaust annulus area was determined through an iterative process shown in Figure 3.7.

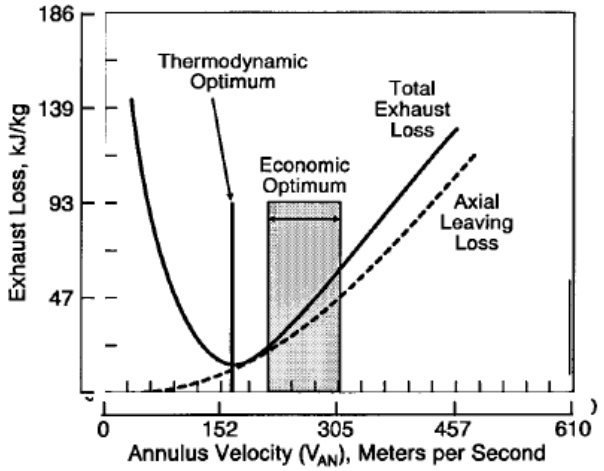

Figure 3.6 Optimum design of exhaust hood [146]

The following assumptions have been made for the sizing of the total LP turbine annulus area: (a) the exhaust loss curve is the same as the one described in Figure 3.5; (b) Annulus exit velocity of 213 m/s was selected as the VWO operating point on the selected exhaust loss curve; and (c) The CFPPs were initially designed for baseloaded operation. (d) The LP turbine has only one "large" exhaust steam flow, and subsequently one "large" annulus area to handle this volume of steam flow. In practical LP turbine designs, the number of LP turbine exhaust flows in a CFPP can range from two to six depending on the CFPP's nominal capacity and the turbine-generator configuration selected by the turbine designer[148]. The steam flow into the different exhaust flow sections are usually divided among the section, and the flow to each section is parallel to the other sections. Irrespective of the number of exhaust flows selected, the flow across each LP turbine exhaust is usually approximately equal. So therefore, for CFPPs with multiple number of LP turbine exhaust flows, the annulus area for each LP turbine exhaust flow can be obtained by simply dividing the total annulus area (A_{an}) calculated by the number of LP turbine exhaust flows available.

The total LP exhaust annulus area (A_{an}) calculation sequence shown on Figure 3.7 requires the use of a VWO heat balance (see full description how it is done in section 3.9) and the setting up of a VirtualPlant process model of the CFPP (see also described in chapter 6).

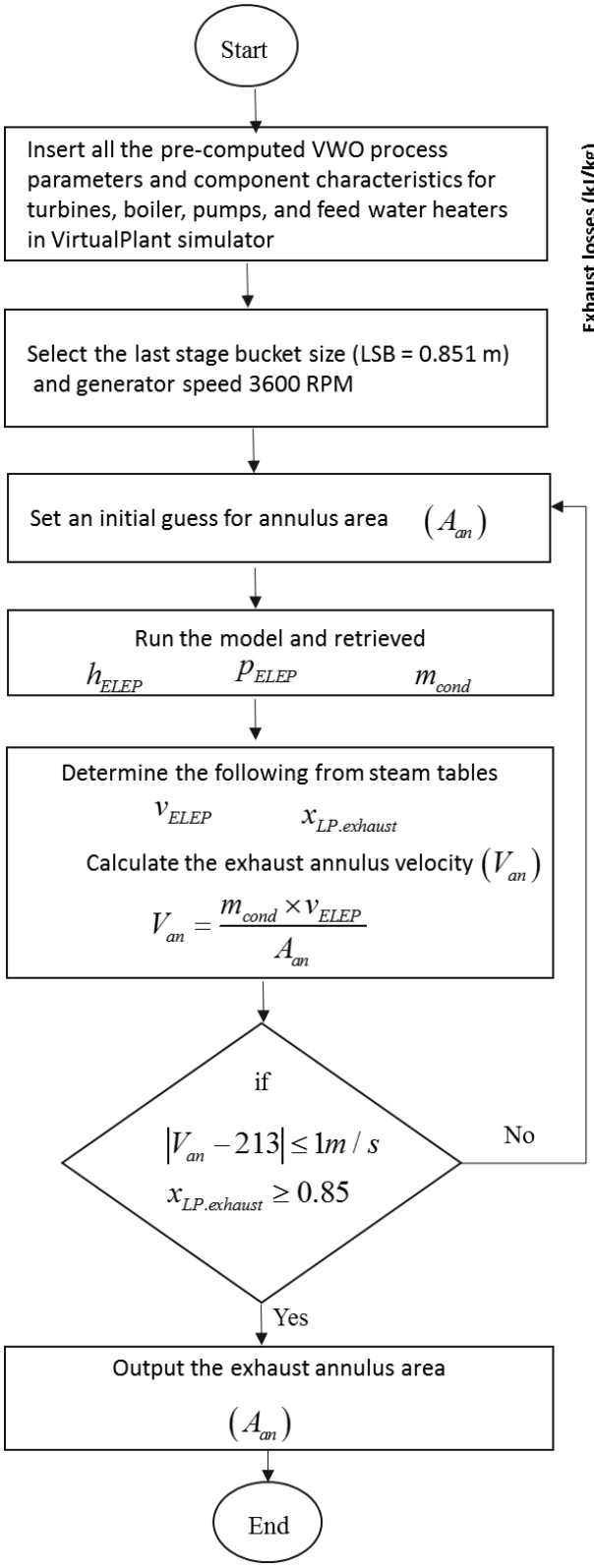

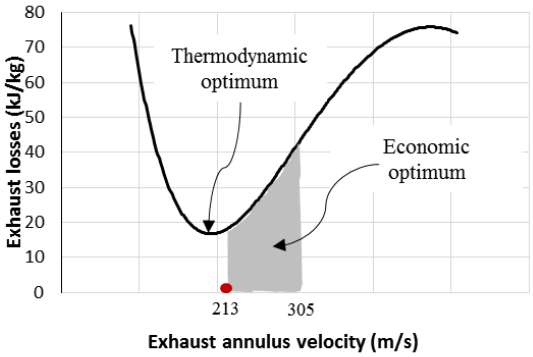

(b) Design of exhaust hood

Parameter	Description	Units
A_{an}	Exhaust annulus area [m]	[m]
h_{ELEP}	LP turbine expansion line end point (ELEP) enthalpy	[kJ/kg]
p_{ELEP}	LP turbine expansion line end point (ELEP) pressure	[kPa]
v_{ELEP}	Specific volume at ELEP	[m^3/kg]
m_{cond}	Condenser main steam mass flow rate	[kg/s]
$x_{LP.exhaust}$	Steam quality at LP turbine	[-]
A_{an}	Annulus velocity of steam at LP turbine exhaust	[m/s]

Figure 3.7 Procedure for determining the total LP turbine exhaust annular area

Once the VirtualPlant CFPP model is set-up with the VWO process parameters, an LSB of 0.851m is selected, and an initial guess is made for the annulus area, A_{an} . Then the results for the condenser mass flow (m_{cond}) , steam pressure (P_{ELEP}) and enthalpy (h_{ELEP}) at the expansion line end point (ELEP) are retrieved for determining the specific volume (v_{ELEP}) , steam quality $\left(x_{LP,exhaust}\right)$ and the annulus velocity at ELEP. Once, the conditions specified for the annulus velocity (V_{an}) and the steam quality $\left(x_{LP,exhaust}\right)$ are satisfied, then the initial guess is satisfactory, else A_{an} is adjusted and the process is repeated.

3.5 Pumps

Pumps are essential equipment in CFPPs. On the steam cycle side, they are mainly used as: boiler feed pumps (BFPs) & bolster pumps, condensate extraction pumps (CEPs), deaerator make-up pumps, heater drain pumps. They are also used as condenser circulating pumps, screen wash-water pumps and cooling tower make-up pumps [19]. Generally speaking, the boiler feed pump is known to consume the most amount of power amongst all the pumps that are used in CFPPs [19] [149]. The total power consumption by the various pumps in a power station was investigated by Wanasinghe [149], his results (Figure 3.8) show that the relative consumption contribution from the BFP, CEP, and Booster pumps were 58%, 17%, and 5% respectively.

Centrifugal pumps make up a vast majority of the pumps that are found in power stations. Typically, the design criteria for theses pumps (BFPs, Bolster, and CEPs) are for Valves wide-open (VWO) and a 5% overpressure full load condition [19] .

The power consumption of pumps at part load is dependent on a number of factors such as the flow rate, the pump efficiency and the operating drive mode of the pump. Based on the drive mode, the pumps in most CFPP are of three main types: the steam driven, motor driven variable speed, or constant-speed electric pumps [19]. A combination of these type of pumps within a CFPP is not unusual.

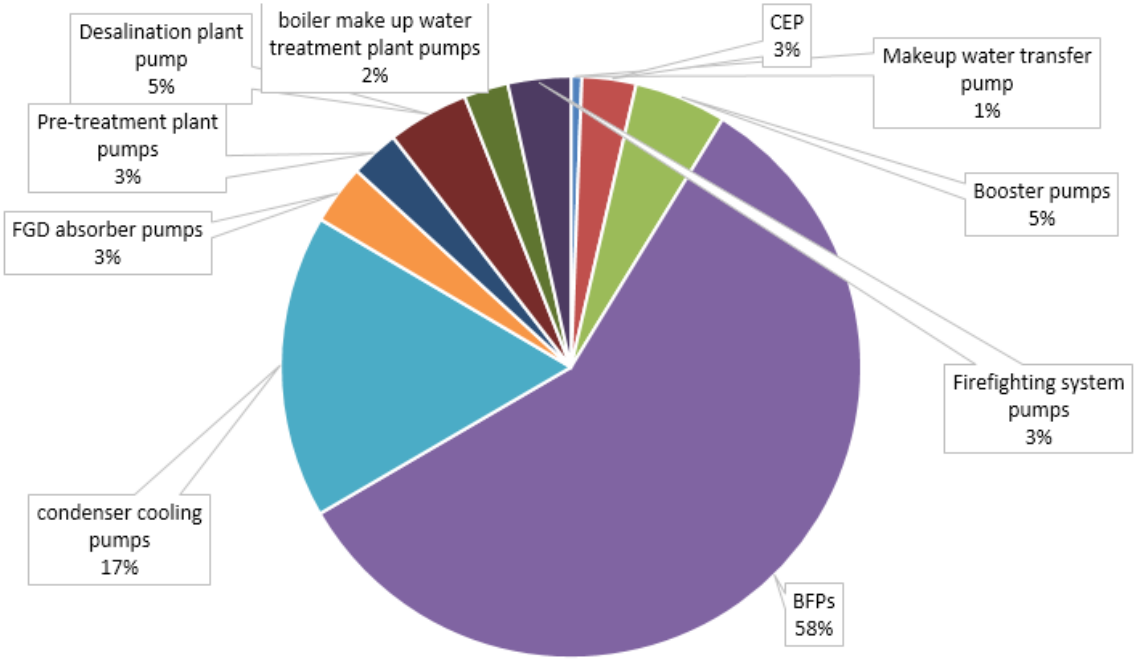

Figure 3.8 Composition of power consumption from various pumps in a CFPP station: Data sourced from Wanasinghe [149]

A comparison of the net heat consumption of three different types of boiler feed pump drive system has been investigated (see Figure 3.9) at different plant load factors for a typical CFPP. The heat consumption for all the three drive modes increases with a reduction of the plant load factor. However, the heat consumption for the steam driven boiler feed pump is lesser than the heat consumption for the electrical motor driven boiler feed pumps. Typically, some CFPPs have a steam driven pump that has a capacity to handle 100% flow requirement, and 2 standby electrically driven pumps that can each handle 50% of the flow requirement [149]. The choice of the pump that is used at any point in time can be economically or operational based.

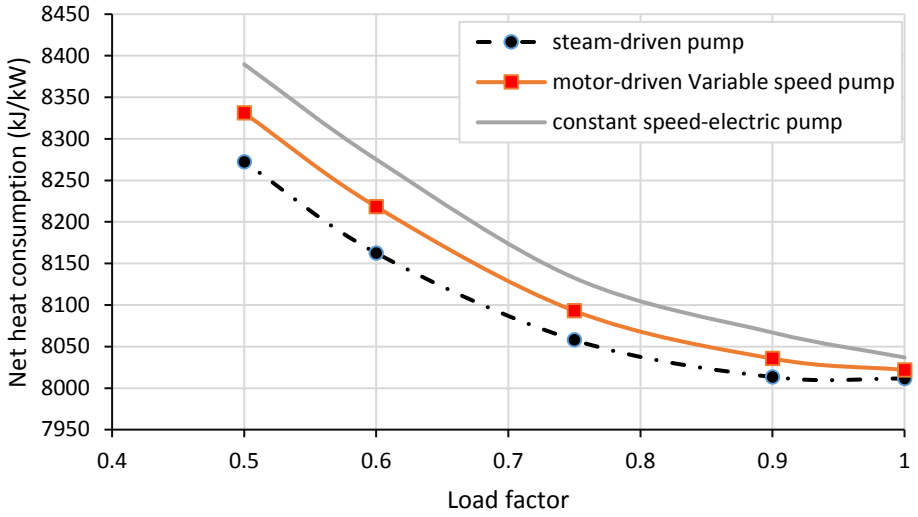

Figure 3.9 comparing different kind of pumps: Data sourced from [71]

The pump drive that has been selected for the generic CFPP process models is a constant speed electrically driven centrifugal pump, with motor efficiency of 95 % , and isentropic efficiency of 85% [150]. These efficiency values are not uncommon in open literatures.

3.6 Condensers and cooling technology

3.6.1 Overview of CFPPs Condenser and Cooling system

The waste heat of the Rankine cycle in a steam power plant is normally extracted by surface condensers [27][151]. Different cooling technologies are used to discard the heat to atmosphere once extracted by the condensers [152][153]. The performance of the condenser has a direct impact on the overall performance of the plant in terms of power output as well as thermal efficiency. Generally, the lower the condenser pressure, the better the performance would be. When a plant changes load due to operational reasons, the performance of the condenser may also be affected.

There are four main cooling technology options that could be used in steam power plants [154][151]. The four cooling technologies are shown on Figure 3.10. The ***Once through Cooled (OTC)***

system uses cooling fluid from a river, lake or sea which is passed directly through the condenser. This fluid is usually returned back to its source. A ***Wet Cooled Condenser (WCC)*** system uses water in semi-closed cycle. This circulating fluid is cooled in a cooling tower by a combination of evaporation and convection heat transfer[154]. WCC systems could exist as mechanical or natural draft cooling towers [151][155]. ***Air-Cooled Condenser (ACC)*** *systems* are often referred to as dry cooling systems because the extraction of the heat from the condensing steam is usually done by passing atmospheric air through the condensers [156]. The air flow over the condensers may be generated by either using a forced draft or an induced draft fan. Air cooled condensers have some benefits such as not requiring water consumption [3][157]. One major drawback with this type of condenser is that it consumes a lot of power [156] and is very sensitive to atmospheric day/night and seasonal changes. ***Indirect Dry Cooled (IDC)*** systems could either use a direct contact spray condenser (as shown in Figure 3.10c) or a conventional surface condenser [154]. In the former, the circulating water is cooled in a surface heat exchanger attached to the cooling tower by using atmospheric air. This circulating fluid extracts heat from the condensing steam by direct mixing in a direct contact condenser attached to the turbine exhaust. Some of the condensate is sent to the feed water system, while the rest is sent back to the cooling tower. The latter (conventional surface condenser) type of IDC are mainly used for nuclear plants, whenever dry cooling options are considered, because of the avoidance of radiation contamination [154].

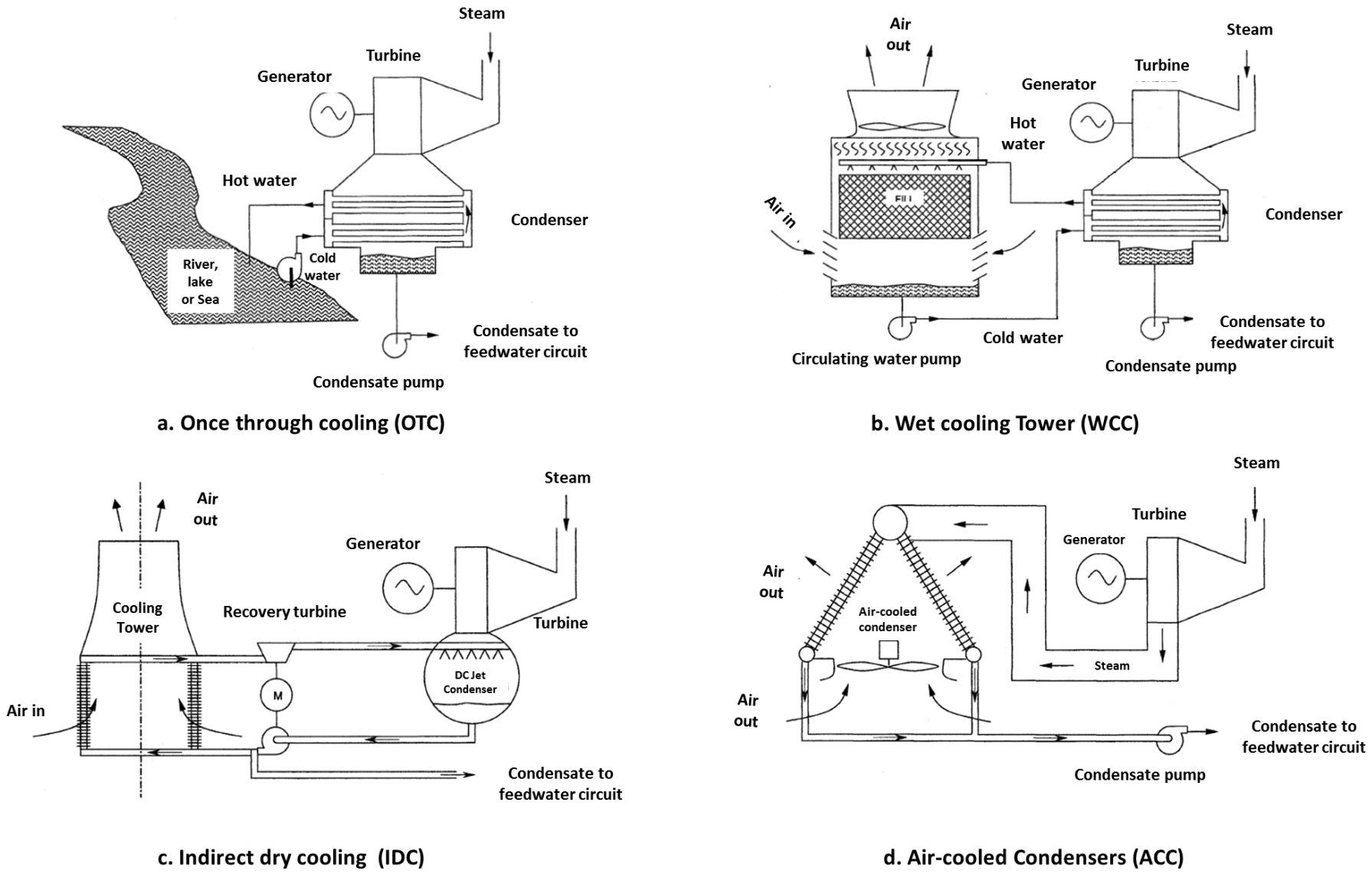

Figure 3.10 Cooling technologies for main condensers of steam power plants [154]

In some applications, there could be hybrid cooling that combines a dry cooling system and a wet cooling system to achieve the required heat removal from the condenser [158]. The wet and dry cooling system could be combined in parallel or series mode, or as one unit within a cooling tower for this kind of system [158].

Often, the design is based on the desired cooling fluid temperature rise, the turbine plant configuration, and the cooling system optimization [159]. The cooling fluid temperature rise across condensers are sometimes limited by a National Pollutant Discharge Elimination System Permit [160], especially for once through systems. The single pass, single zone condenser is the most commonly used condenser in the utility industry [159], and it may be in one, two, or three shells dependent on the number of low pressure turbines.

Figure 3.11 shows the typical performance comparison for the condensers with the various cooling system types. It is apparent that for a given dry bulb temperature, that the condenser pressures and temperatures of WCC are substantially lower than those of ACCs because WCCs achieve lower thermal equilibrium with the condensing steam than ACCs [161].

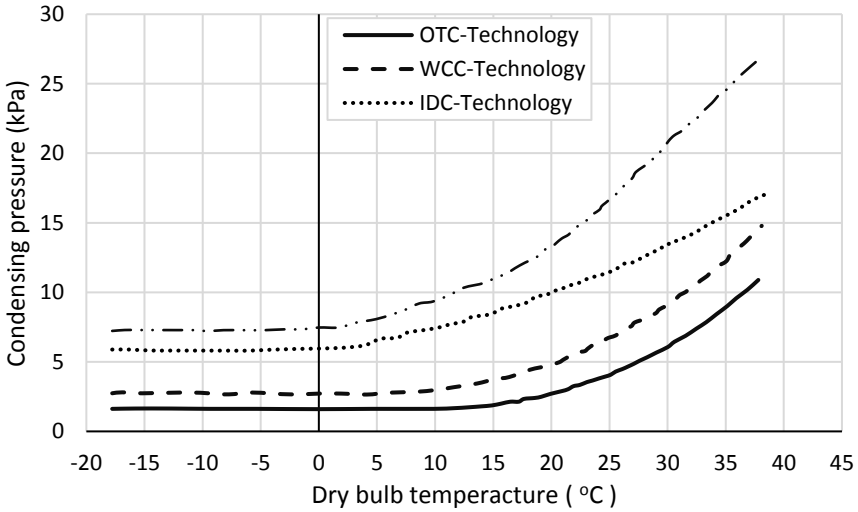

Figure 3.11 Typical condenser performance comparison [151]

The aforementioned four main types of cooling system technologies were considered in setting up the different CFPP generic models.

3.6.2 The need for predicting the main steam condensing pressure at varying load.

If the condenser pressure reduces at low load, it results in a drop in the minimum cycle temperature. This has a significant effect on the cycle efficiency, and also the steam mass flow through the turbine. There is a secondary effect on the turbine exhaust losses, which could either increase or decrease the losses. This will contribute to a change in the overall cycle performance. It is therefore important to understand how the condenser pressure changes with load for the various cooling system options, and to include this effect in the generic model.

The Heat Exchanger Institute (HEI) code provides a thorough method for determining the pressure of surface condensers under different operating conditions, including at part load operating conditions [162]. This approach is based on the general expression for heat transfer on a surface heat exchanger, $Q = U \cdot A \cdot \Delta T_{LM}$. However, this procedure requires an in-depth knowledge of the geometrical characteristics of the condenser, the design flow rate for the circulating fluid, inlet fluid conditions, and the type of material used in the condenser, in order to calculate the UA value – which is an indication of the condenser effectiveness. Some of the information are proprietary in nature, and may be difficult to access.

Laskowski [163] proposed a method for determining the performance of a steam power plant condenser at off-design conditions. The author proposed two different equations for determining the cooling water outlet temperature based on inlet and reference parameters such as cooling water inlet temperature, cooling water mass flow rate, and steam temperature. However, his study only considered a single wet cooled condenser. Therefore, the model results may be dependent on the specific case study. Furthermore, it does not predict the pressure response - it only determines the cooling fluid outlet temperature.

Some mathematical algorithms have also been used to predict the performance of condensers at various operating and load conditions. Algorithms such as data mining techniques, artificial intelligence, evolutionary algorithms, and grey relational degrees have been used to investigate the relationship between desired outputs and input variables from historical data sets [164]–[166]. These techniques are indeed very useful as they provide data for online condition monitoring of condensers. However, these techniques are heavily reliant on the availability of a significant amount of historical data for training and testing the models for each condenser that is analysed.

A more simplistic procedure has been described by Gill [167] for determining the pressure response of a condenser considering the effect of variation of the heat rejected at the condenser. The method requires three main inputs at the turbine maximum continuous rated condition (TMCR):

i. The cooling fluid inlet temperature;
ii. The cooling fluid outlet temperature, and
iii. The condensing temperature/pressure of the steam.

These parameters are needed to calculate the log-mean temperature difference $(LMTD)$ required for evaluating the actual condenser pressure response at part load.

The procedure uses two simple linear relations. The first one is the relationship between the $LMTD$ and the heat rejected at the condenser, and the second one is the relationship between the condenser cooling fluid temperature rise and the heat rejected at the condenser. It assumes a reduction in the condenser heat load at part load operation causes a proportional drop in the cooling fluid temperature rise across the condenser, and a corresponding change in the $LMTD$. It will be shown later that this approach actually assumes that a constant condenser effectiveness value is applicable throughout the operating range of the plant. This assumption may appear crude and oversimplified. However, it proved to be a useful assumption if the limits of its application are well known and thus formed the basis for predicting the condensing pressure of the main steam condensers at part load conditions. A full discussion of the theory behind the constant effectiveness assumption, its implementation and validation is discussed in chapter 5.

3.7 Feedwater train

3.7.1 Feed water heater types, characteristics & layout

The feed water train of a CFPP is a network of feed water heaters (FWHs) from the exit of the main steam condenser to the inlet of the steam boiler. The sole purpose of this train is to pre-heat the feedwater with steam extracted from the steam turbines, so that the required energy input into the boiler is reduced [168]. It has the additional effect of reducing the heat load on the condenser. This has the net effect of increasing the thermal efficiency of the cycle, hence the reason for installing such heaters. The feed water heaters used in coal fired plants are the open type (contact FWH) and the closed feed water heaters. The heat transferred in a closed feed water is via a surface that separates the extracted steam and the feed water. The different drain types that can be seen in closed feed waters are shown in Figure 3.12. The drains are either flashed drain, drain cooled or pumped drain. The open feed water heater provides feed water heating by direct mixing of the extracted steam and the feed water. It also provides the correct conditions for extraction of non-condensable gasses (such as air), hence is normally called the de-aerator.

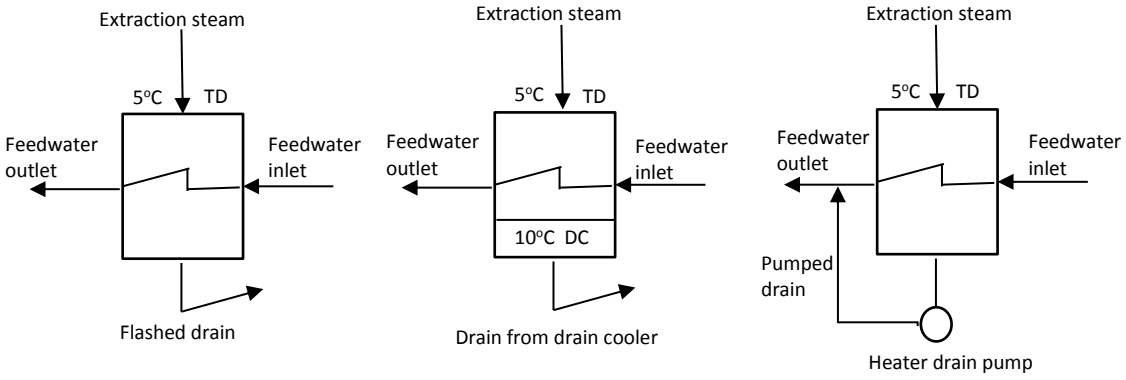

(a) Flashed heater (b) Drain cooler heater (c) Pumped heater

Figure 3.12 Schematic diagrams for different drain types in closed FWHs [169]

The number of feed water heaters used in a particular power plant is dependent on a number of factors such as: the diminishing performance gains, cost of extra heaters, limitations in the turbine design, the space limit in the turbine room, the size of the power plant etc [170]. Based on economic

appraisal, the practice in the industry as per the number of feed water heaters is depicted on Table 3.1. Irrespective of the number of FWHs in a CFPP, there is usually only one open feed water heater in-between the low pressure and high pressure feed water heaters.

Table 3.1 Number of FWH and plant capacity [71] [170]

Plant Capacity (MW)	Typical No of Feed water heaters
20-50	4 - 5
50-100	5 - 6
100-200	5 - 7
200 and above	6 - 10

The operating thermal performance of FWHs is often examined by looking at the terminal temperature difference (*TTD*) and drain cooler approach (DCA) [122]. *TTD* (see Figure 3.13) is the difference between the saturation temperature (T_{sat}) of the extracted steam and the feed water outlet temperature (T_{c2}). *TTD* values of between -2 to 3 $^{\circ}C$ are commonly seen in high pressure and low pressure feed water heaters [140][150].

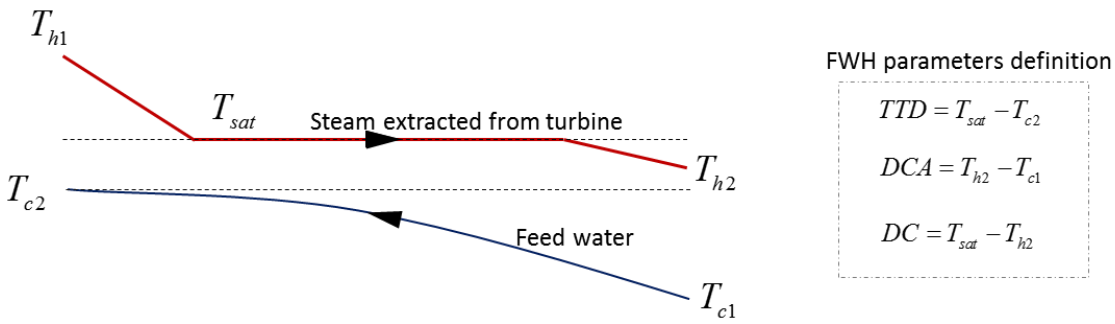

Figure 3.13 Process flows in a typical FWH and parameters

The drain cooler approach (DCA) on the other hand helps to determine the water levels on the feed water heater. It is evaluated as the difference between the drain cooler outlet temperature (T_{h2}) and the feed water inlet temperature(T_{c2}). The problem of using DCA as a design parameters is that it is a direct function of the FWH water inlet temperature - which cannot be controlled by the

FWH. A more useful design parameter to use is the Drain sub-cooling (DC) value. The sub-cooling value is the difference between the saturation temperature (T_{sat}) and the outlet temperature(T_{h2})

The number of feed water heaters that have been specified for the generic CFPP models and the performance indicators assumed are presented on Table 3.2. The total number of feed water heaters (FWHs) specified for the NRH & SRH is 6. This assumption is motivated by the general industry practice and by the analysis shown by Nag [27] on why most power plant designers prefer to stick to six FWHs in their architectural design. According to Nag [27], the additional efficiency gain after the sixth FWH begins to drop with each additional FWH added to the cycle. For the double reheat CFPPs, a total number of FWHs selected was 8. A higher number of FWHs was selected for this kind of CFPPs because DRHs generally tend to be designed for much higher generation output and are expected to attain higher final feed water temperatures (FFWT) than the NRHs and SRHs. The consequence of this is that more feed water heaters is required to heat the increased mass flow, and to achieve the higher FFWT.

Table 3.2 Number of FWH and performance of FWH used in the generic CFPP models

Degree of reheat	Total No. of FWHs	Low pressure closed FWHs	High pressure closed FWHs	Open FWH
Non-reheat (NRH)	6	3	2	1
Single-reheat (SRH)	6	3	2	1
Double reheat (DRH)	8	5	2	1

At VWO conditions, a zero TTD and zero sub-cooling (SC) have been applied for all the FWHs for the generic CFPP process models. These same values have been assumed at varying load conditions.

3.7.2 Importance of a generic FFWT and extraction pressure method for VWO heat balance development

Once the number of FWHs in a CFPP has been selected, the next two important steps are to determine: (a) The selection of VWO final feed water temperature (FFWT), and (b) the economic placement of feed water heaters. These two steps are very important in the development of the VWO heat balance [168].

FFWT is the temperature of the feed water entering the boiler (and thus the economiser inlet). This temperature is achieved after the water has passed through the bank of feed water heaters arranged from the low pressure (LP) FWHs to the final high pressure (HP) FWHs. It plays a key role in the overall performance of the plant [171]. A 0.15% gain in efficiency of a plant has been reported for a 20 ℃ increase in FFWT [171]. Typical values of FFWT at maximum continuous rating (MCR) are 230 – 260 ℃ for subcritical plants [125][172] [173] [174] and 280 - 300℃ for a supercritical plant [171] [175]. The value of the final feed water temperature has an impact on the possible boiling conditions within the economizer, the exhaust conditions of air heaters, and the boiler efficiency.

The optimal placement of feed water heaters is dependent on the turbine design, the number of heaters to be placed, and the optimization criteria selected [176]. In the industry, the number of feed water heaters found in CFPPs vary from 4-10 [177] [178] [170]. The number and placement of feed water heaters within a CFPP unit affects the cycle efficiency and performance of the steam turbine [178].

There are some natural (or default) turbine extraction points for feed water heaters such as at turbine cross overs or before reheat [176]. There may be situations that could warrant the placement of a FWH above reheat points. These type of heaters are sometimes referred to as heaters above reheat point (HARP) [179].

After the power plant designer has chosen the number of feedwater heaters, the optimum turbine extraction pressures must be determined. Different methods have been reported in literature for

estimating the extraction pressures at plant full load [179]. The optimal cycle efficiency method (OCEM) appears to be the most common approach [179] [176]. This approach adopts an equal partitioning of feed water temperature (enthalpy) rise across all FWHs, including the economizer, as is illustrated in Figure 3.14.

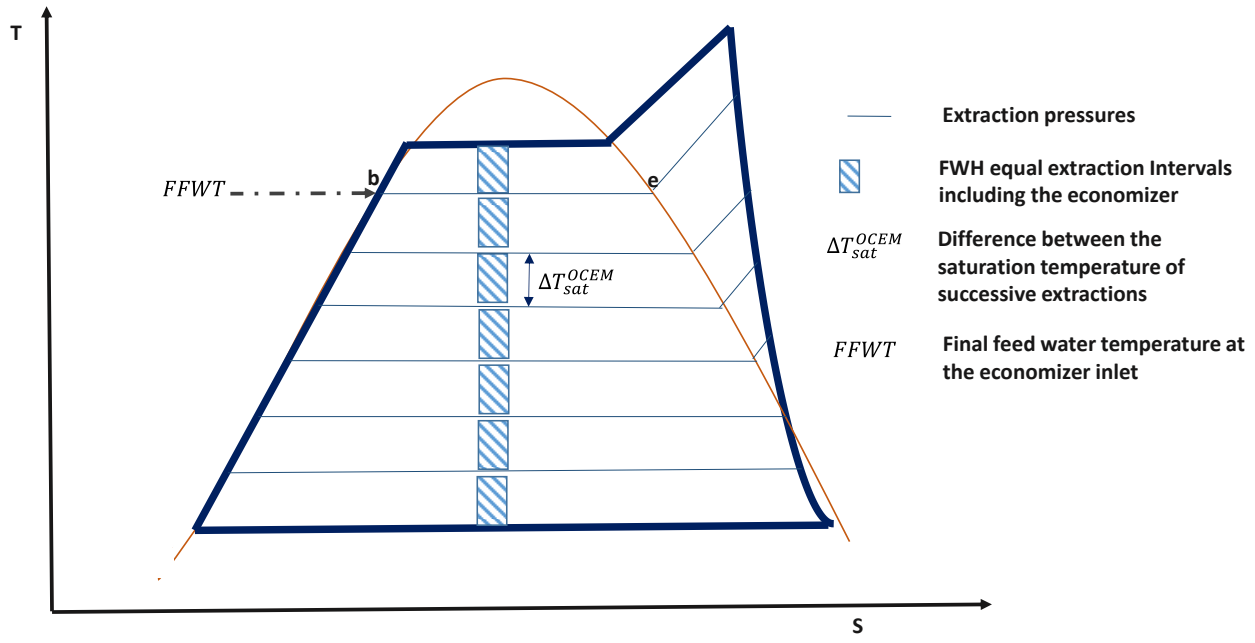

Figure 3.14 Graphical representation of OCEM method for a typical non-reheat CFPP with six FWHs

Edelioglu and Aybar [178] stated that this method is not suitable because it does not consider specific plant issues such as the effect of terminal temperatures differences (TTD), extraction line pressure drops, impact of turbine internal efficiency changes, non-utilization of leakage and gland steams. They proposed an iterative approach for optimizing the cycle efficiency of a non-reheat 60 MWe oil fired power plant by varying the five steam extraction pressures.

Other cycle optimization attempts have also been reported in literature. In Weir's study [178], an algorithm was used to calculate the difference between the extraction enthalpy and the saturated liquid enthalpy at each extraction point. The algorithm assumed that this difference was the same for all the FWHs along the expansion line for the non-reheat systems, and FWHs below reheat points for single and double reheat systems.

Sanaye et. al [177] estimated the extraction pressures by optimizing the cycle efficiency whilst varying the extraction pressures. This was done using three different non-gradient based optimization methods (Hook-Jeeves, full search and Nedler-Mead algorithms). They reported that the extraction pressures predicted compared favourably with plant data from Karaj and Wisconsin steam power plants.

A non-linear sequential quadratic programming (SQP) technique was adopted by Espatolero et. al [175] for estimating extraction pressures of a nine FWH single reheat supercritical CFPP. The cycle efficiency was set as the objective function whilst varying the extraction pressures. The objective function is subject to constraints imposed by the energy and mass balance and the pressure variation intervals specified.

The problem with the approach adopted by Sanaye et. al [177] and Espatolero et. al [175], is that the results predicted are highly dependent on the choice of the initial guess and the range of constraints that is placed on the objective function. This implies that expert knowledge of the various typical values of extraction pressures is required to achieve an accurate result.

The reasons given by Egelioglu and Aybar [178], for the inapplicability of the OCEM method in real plants may appear plausible. However, economics, steam turbine characteristics and operational concerns such as avoiding non-steaming conditions in the economizer and protecting the last stage blade of LP exhaust remain important factors that determine the extraction pressures of FWHs and the FFWT. The maximum temperatures which the air heater can accommodate is also a factor.

The problem with all the aforementioned methods used in determining extraction pressures and FFWT at full load conditions is that they are purely based on the thermodynamic optimization of the cycle efficiency. Little or no attention is given to the economic or practical design implications of having such kind of process conditions. On the other hand, thermo-economic based optimization methods for predicting extraction pressures are rarely reported in literature because these kind of studies are usually performed by OEMs with actual cost and plant performance data.

The absence of a suitable generic method for determining the VWO FFWT and the extraction pressures motivated a further investigation of the feed water heating train of some existing CFPPs within and outside Eskom's fleet. The outcome of this investigation led to the development of a generic method for predicting the FFWT and extraction pressures of FWHs which closely represents what is actually observed in current power plants. A full description of the study is presented in chapter 4.

3.8 Generic CFPP layouts selected and component characteristics

Having selected the key components required for setting up a generic CFPP process model, it was important to select representative layouts for the different categories of CFPPs.

The design of the Valve wide open (VWO) Rankine cycle heat balance diagram is dependent on the CFPP layout selected. There are many variations in the steam cycle layouts of CFPPs that exist around the world, but some typical CFPP layouts have been reported in literature for non-reheat, single reheats, and double reheat plants. The variations seen in each type are usually based on the choice of CFPP designers and utility owners. The major difference between the various CFPP layouts could be:

- The type of boiler (drum vs. once through) used
- The number of FWHs, the deaerator position and the drain flow directions.
- The availability of secondary turbine utilization for boiler feed pump
- The number of condenser zones (hot or cold) present
- The number of LP exhaust flows, and extractions per turbine
- The presence/absence of gland steam condensers (GSC), Air ejector condenser etc.
- Cross-compound vs. tandem turbine generator combination.

The intention of this PhD research is not to study all the possible layouts but to simply select layouts that is typical for CFPPs. No gland steam or valve stem losses are considered. The layouts that have

been selected for the non-reheat, single reheat and double reheat units are shown in Figure 3.15, Figure 3.16, and Figure 3.17 respectively. The typical non-reheat layout consists of six feedwater heaters (FWHs) in its feed water heating train; one high pressure (HP) turbine with three steam extraction points fed to two HP FWHs and a deaerator; and a low pressure (LP) double flow turbine with three steam extraction points fed to the three LP FWHs. The typical single reheat layout also has six FWHs in its feed water heating train, one HP turbine with one steam extraction at the exhaust for the last HP FWH, one intermediate turbine (IP) with two extractions for one HP FWH and a deaerator, and one double flow LP turbine with three steam extraction for heating the three LP FWHs. The typical double reheat layout selected has eight FWHs [26]; one HP turbine with one steam extraction port for heating the last HP FWH; two intermediate turbines both having two steam extraction points; and one double flow LP turbine with three extraction points for the last three LP FWHs. All the FWH drains (except the 1st LP FWH) are cascaded downward. The convention for numbering the FWHs here begins with the last high pressure (HP) feed water heater.

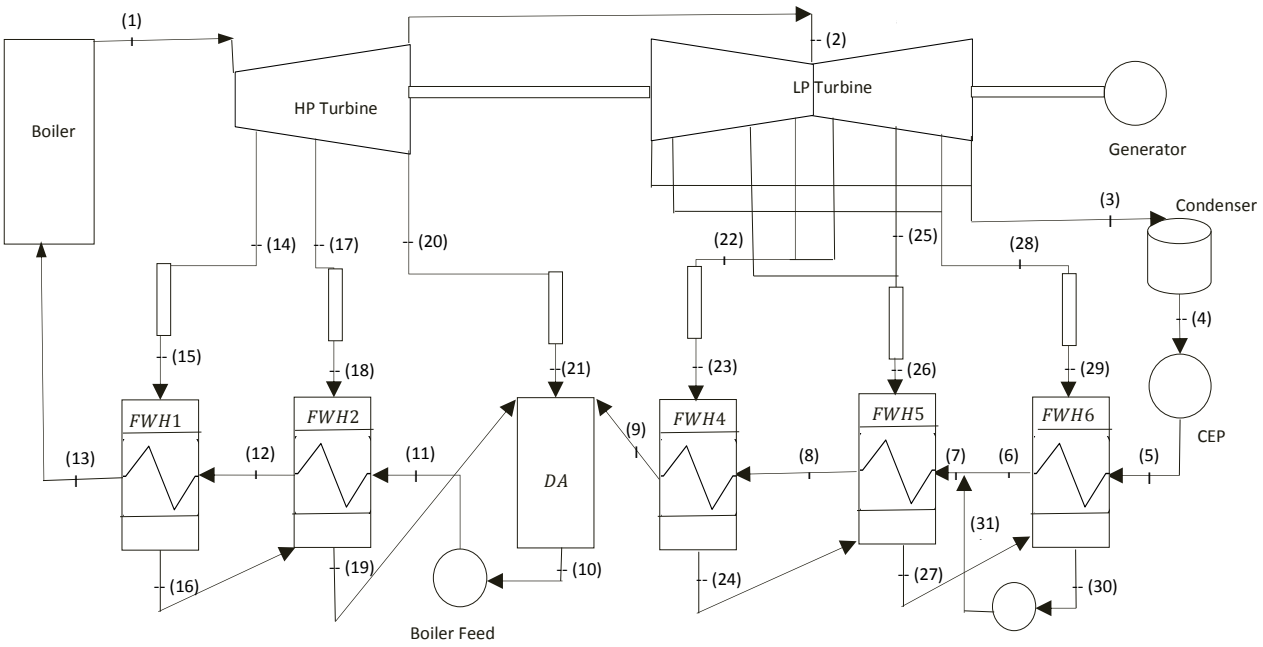

Figure 3.15 Layout selected for the generic non-reheat CFPP process models

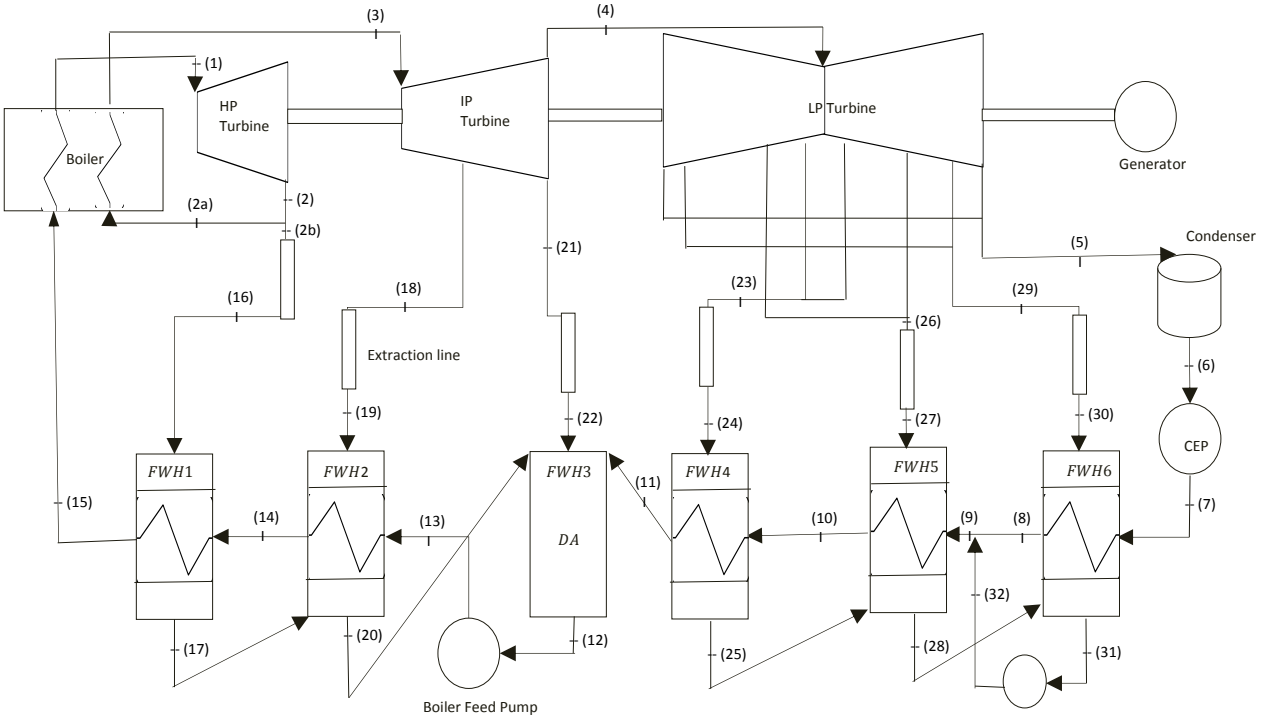

Figure 3.16 layout selected for the generic single-reheat CFPP process models

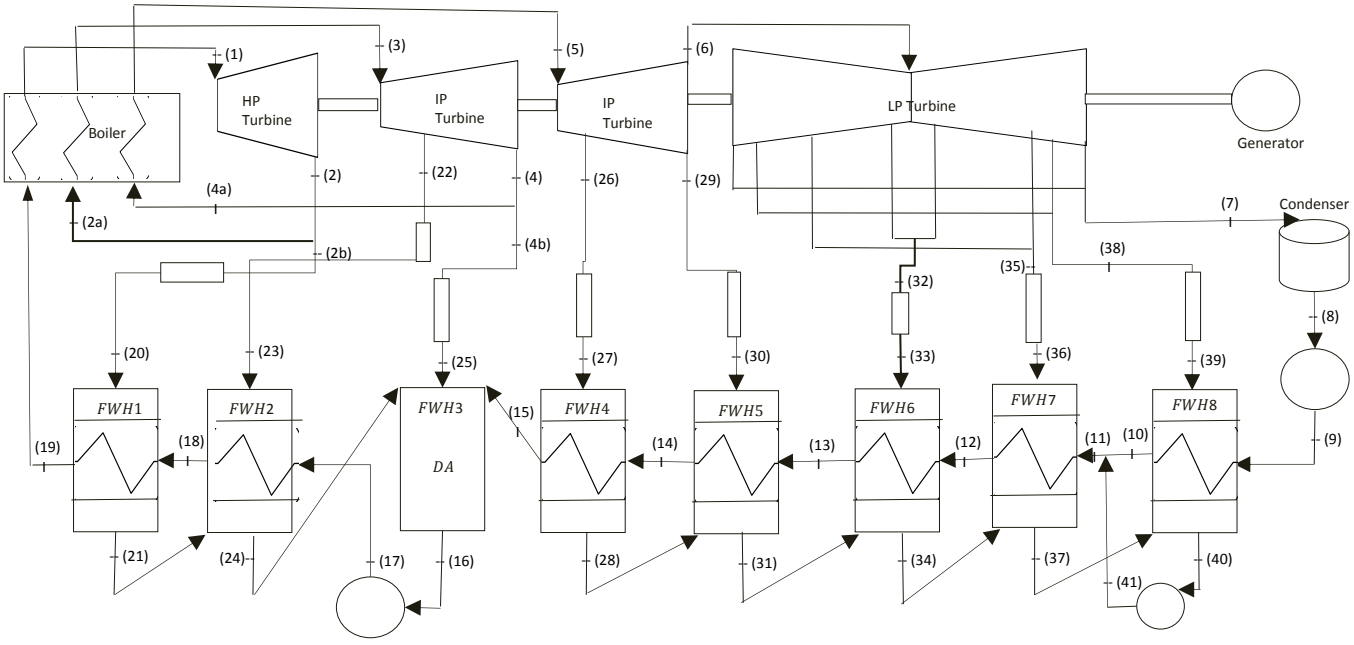

Figure 3.17 layout selected for the generic double-reheat CFPP process models

In setting up the generic CFPP process models, it is equally important to select the characteristics of key components in the CFPP cycle.

Table 3.3 Selected parameters of the model Plant

S/N	item	Non-reheat	Single reheat (once through)	Double reheat (once through)
1	SH Pressure drop (%)	19[a]	15 [a]	15 [a]
2	RH Pressure drop (%)	N/A	7	7
3	2nd RH Pressure drop (%)	N/A	N/A	7
4	Boiler fuel Efficiency (%) HHV	100 [b]	100 [b]	100 [b]
5	HP Efficiency (%)	86	86	86
6	IP Efficiency (%)	N/A	92	92
7	LP Efficiency (%)	85	90	90
9	Design VWO 1st stage Press. [c]	$(0.8 \times P_{thr})$ [d]	$(0.9 \times P_{thr})$ [d]	$(0.9 \times P_{thr})$ [d]
12	Low pressure turbine Crossover valve pressure drop (%)	1%	1%	1%
13	Design Intercept valve pressure drop [e] (%)	N/A	2.5	2.5
14	Extraction line press drop (%)	5	5	5
15	FWH Pressure drop (MPa)	0.24	0.24	0.24
16	Pump motor efficiency (%)	95	95	95
17	Pump Isentropic efficiency (%)	85	85	85
18	FWH TTD (°C)	0	0	0
19	FWH sub-cooling (°C)	0	0	0

Note:

[a] The pressure drop for the drum type boilers are generally higher than the once through boilers

[b] A 100% boiler efficiency is used at this stage because TCHR calculations do not really need this input.

[c] This input is required by the VirtualPlant software used in this study.

[d] P_{thr} is the throttle steam pressure

[e] Intercept valve is located between the hot reheater and the Intermediate pressure turbine.

The component characteristics include pressure drops in boiler components, the efficiencies of the high pressure, intermediate pressure and low pressure turbines, the pump efficiencies, extraction line pressure drops etc. The numerical value of these component characteristics change from CFPPs

to CFPPs. Table 3.3 shows a summary of the component characteristics that were selected for the generic CFPP process models. These values were drawn from typical values that are seen in Eskom's CFPP fleets. For the Double reheat CFPPs, the values for the single reheat CFPPs were also assumed for it.

3.9 VWO heat balance development for Generic CFPP Process models

The development of a valve wide open (VWO) heat balance diagram is an important first step in the development of any steam power plant [168]. This process involves numerous calculations that produces the required thermodynamic state and mass flow requirements at all locations of the cycle [180]. The process information on a VWO heat balance diagram are useful to determine the plant performance at other operating conditions including varying load operation.

In recent times, research focus has shifted away from the VWO heat balance diagram development aspect of CFPP performance evaluation because most researchers, in evaluating the performance of specific plants just use the VWO heat balance diagram information supplied by OEMs/vendors [71]. This is the sensible thing to do under normal circumstances when there is access to such proprietary information. However, in the larger scheme of things, if one needs to perform a renewable energy integration impact study on multiple CFPPs connected to a power system network for instance, then one may be expected to get all the VWO heat balance diagrams for the affected CFPPs on the network - this can be a tough mission. In the absence of a vendor supplied VWO heat balance diagram, a credible VWO heat balance diagram can still be developed and used in place of the OEM supplied one.

3.9.1 Overall heat balance

A general overview of the computational steps/procedure for the VWO heat balance development adopted in this work is shown in Figure 3.18.

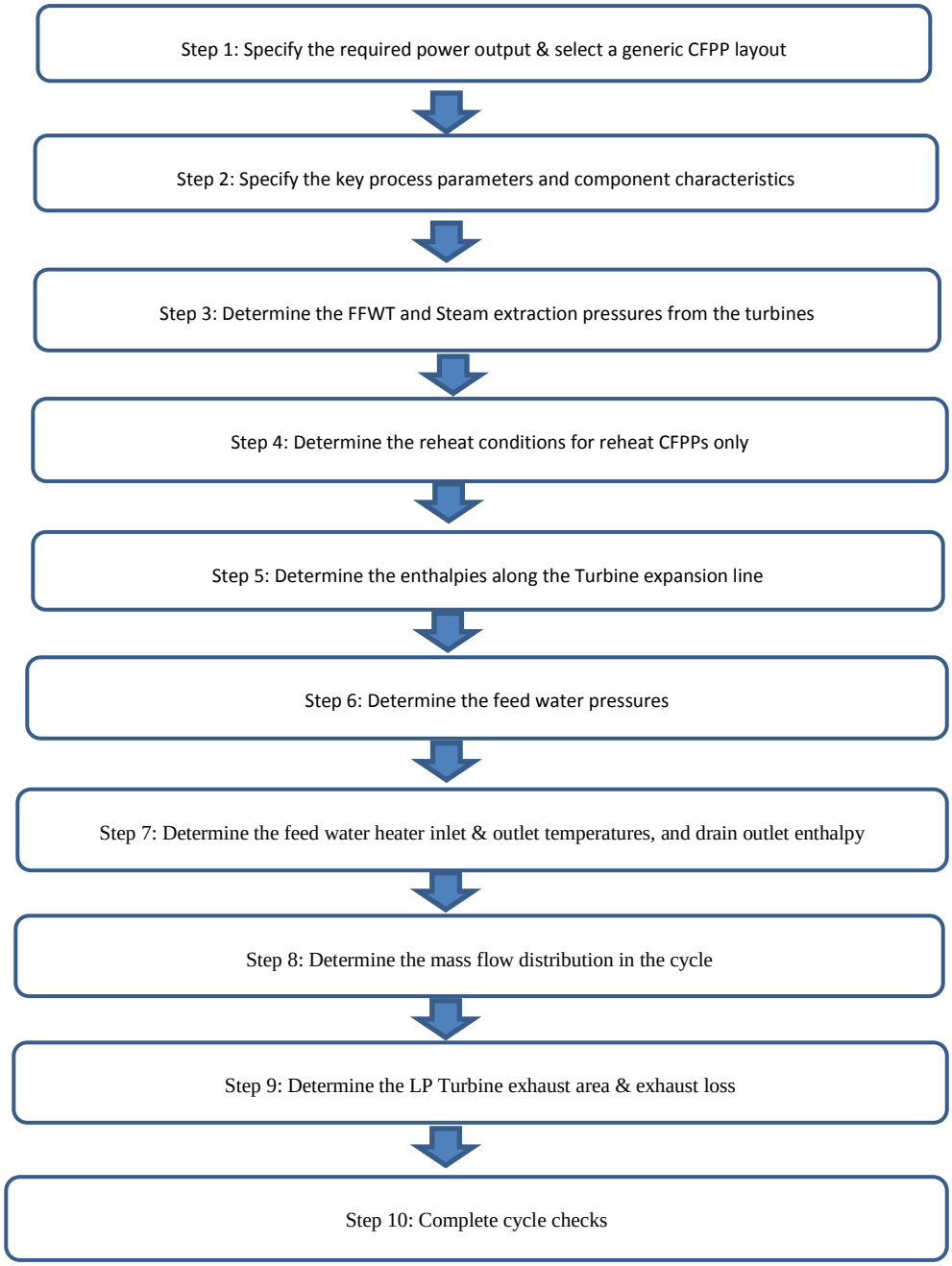

Figure 3.18 Computational steps required for setting up a VWO heat balance

This procedure was adapted from Bartlett [180]. The procedure is sub-divided into ten key steps. Once the required power output is known, the first step is to select a given generic CFPP layout. The second step would be to specify the key process parameters (such as the initial/live steam temperatures and pressure and condensing pressure) and the characteristics of key components (such as the turbines, pumps) in the steam cycle. The third step involves determining the final feed water temperature and the steam extraction pressures from the turbines. The determination of the reheat conditions (for reheat units only), the enthalpies along the expansion line, and the feed water pressures along the feed water train are the 4th, 5th, and 6th steps respectively. The 7th step involves determining the feed water heater inlet & outlet temperatures, and drain outlet enthalpy. Once this is done, then the mass flow distribution in the cycle can be determined in the 8th step. The 9th step involves the determination of the exhaust losses for the LP turbine. The final step is taken to check that the turbine cycle heat balance diagram is completely balanced.

Discussions of the aforementioned steps 1 & 2 have been done in section 3.8. The discussions on step 3 and 4 are given in chapter 4 and section 3.9.2 respectively. The discussions on step 5 & 9 are given in sections 3.4.2, while the discussions for step 6 & 7 are given in section 3.9.3. The discussion of step 8 is given in section 3.9.4.

Once the complete process conditions have been determined, then the complete VWO heat balance cycle checks (step 10) is done to ensure that there is an energy and mass balance in the cycle. This is done by checking that the energy input to the cycle $\left(Q_{in.cycle}\right)$ is equal to the energy output from the cycle$\left(Q_{out.cycle}\right)$. The cycle energy input and output are determined from Equations (3.3) and (3.4) respectively.

$$Q_{in.cycle} = Q_{TCHI} + W_{pumps} \tag{3.3}$$

$$Q_{out.cycle} = W_{turbines} + Q_{condenser} \tag{3.4}$$

Q_{TCHI} is the turbine cycle heat input, and W_{pumps} is the total pump work . $Q_{condenser}$ is the heat rejected from the cycle , and $W_{turbines}$ is the total turbine work . All the terms are positive defined, which is different to many traditional thermodynamic text book which defines heat input as positive, but work input as negative.

The total work input for the pumps (W_{pumps}) is calculated thus as:

$$W_{pumps} = W_{BFP} + W_{CEP} + W_{CDP} \tag{3.5}$$

W_{BFP}, W_{CEP}, and W_{CDP} are the work done by the boiler feed pump, condensate extraction pump, and the condensate pump respectively.

For each pump, the pump work is determined as:

$$W_P = \frac{m(h_{ex} - h_{in})}{\eta_{mech}} \tag{3.6}$$

h_{ex}, h_{in}, η_{mech} are the exit and inlet enthalpies, and the mechanical efficiency of the pump respectively. m is the fluid mass flow rate through the pump.

For the turbines, the work is:

$$W_{turbines} = W_{HP} + W_{IP} + W_{LP} \tag{3.7}$$

For each turbine, the work is determined as:

$$W_T = m_{in}h_{in} - m_{ex}h_{ex} - \sum_{i}^{n} m_{ext_i}h_{ext_i} \tag{3.8}$$

m_{in}, m_{ex} are the inet and exit mass flows of the turbine. m_{ext} is the extraction mass flow from the turbine. h_{in}, h_{ex} are the inet and exit enthalpy of the turbine. h_{ext} is the enthalpy of the extraction mass flow from the turbine.

The condenser heat rejected is described as:

$$Q_{condenser} = m_{cond} \cdot (h_{ex} - h_{in}) \tag{3.9}$$

The VWO heat balance is accepted as "balanced" provided the condition in Equation (3.10) is satisfied [140]:

$$\left| \frac{Q_{in.cycle} - Q_{out.cycle}}{W_{gross}} \right| \leq 0.5275 \frac{kJ}{kWh} \tag{3.10}$$

The gross generation W_{gross} is defined as:

$$W_{gross} = W_{turbines} \tag{3.11}$$

3.9.2 Reheating Condition

Reheating is a very useful way of improving the thermal performance of a steam cycle[27]. The thermodynamic optimum reheat pressure for CFPPs is dependent on the throttle conditions (temperature and pressure), reheat temperature and the LP turbine exhaust conditions [181] [182] [143]. The ratio of the reheat pressure (P_{rh}) to the throttle pressure (P_{thr}) is sometimes defined as the reheat pressure ratio(P_{rat}). For single reheat cycles, typical optimal reheat pressure ratio values that have been used are 0.15 - 0.25 [183] [184]. For Double reheat cycles, 0.2 - 0.30 have been reported for the first Reheat pressure ratio $\left(P_{rat1} = \frac{P_{rh1}}{P_{thr}}\right)$ while 0.15 - 0.30 have been reported for the second reheat pressure ratio $\left(P_{rat2} = \frac{P_{rh2}}{P_{rh1}}\right)$ [183]. P_{rh1} and P_{rh2} are the 1st and 2nd reheat pressures for a double reheat cycle.

An optimum cycle efficiency approach was used to determine the reheat pressure(s) for the single and double reheat CFPPs. The following assumptions were made:

- The reheat temperature (s) are equal to the main steam temperature.
- There is no sub-cooling in the condenser
- The expansion processes in the turbine is isentropic.
- The pump work is also isentropic.
- No steam extraction from the turbines.
- No pressure drops in the superheaters or reheater.

The cycle used for evaluating the thermodynamic efficiency of the single and non-reheat cycles are shown in Figure 3.19(a) and (b). The reheat pressure(s) that yields the optimum thermodynamic cycle efficiency.

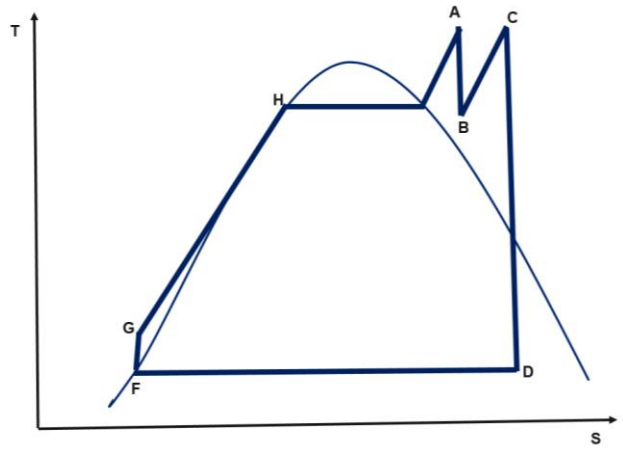

(a) Single reheat Temperature-enthropy diagram

Process Points Description: *On the single reheat T-S diagram in Figure (a), the points A, B, C, D, F, G, and H represents the throttle inlet (live steam), cold reheat, hot reheat, LP turbine exhaust outlet, condenser outlet, pump outlet, and boiler evaporator inlet conditions respectively.*

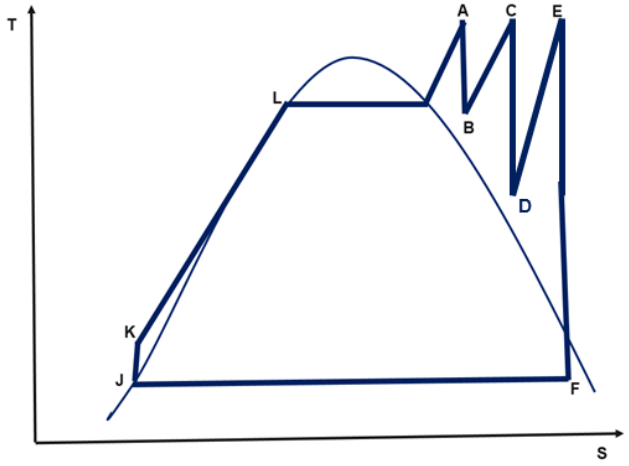

(b) Double reheat Temperature-enthropy diagram

Process Points Description: *On the double reheat T-S diagram in Figure (b), the points A, B, C, D, E, F, J, K, and L represents the throttle inlet (live steam), cold inlet for 1st reheater, hot outlet for 1st reheater, cold inlet for 2nd reheater, hot outlet for 2nd reheater, LP turbine exhaust outlet, condenser outlet, pump outlet, and boiler evaporator inlet conditions respectively.*

Figure 3.19 Temperature-enthropy diagram of single and double reheat steam cycles used for determining the optimum reheat pressure ratio(s)

Figure 3.20 describes the computational sequence that was used for determining the reheat pressure of the single and double reheat CFPPs. The definition for each of the points is already given in Figure 3.18. The process simply involves the systematic determination of the specific enthalpy and entropy at all the points, beginning from the known conditions to the unknown conditions. In both cases, the reheat conditions that corresponds the maximum cycle efficiency is selected.

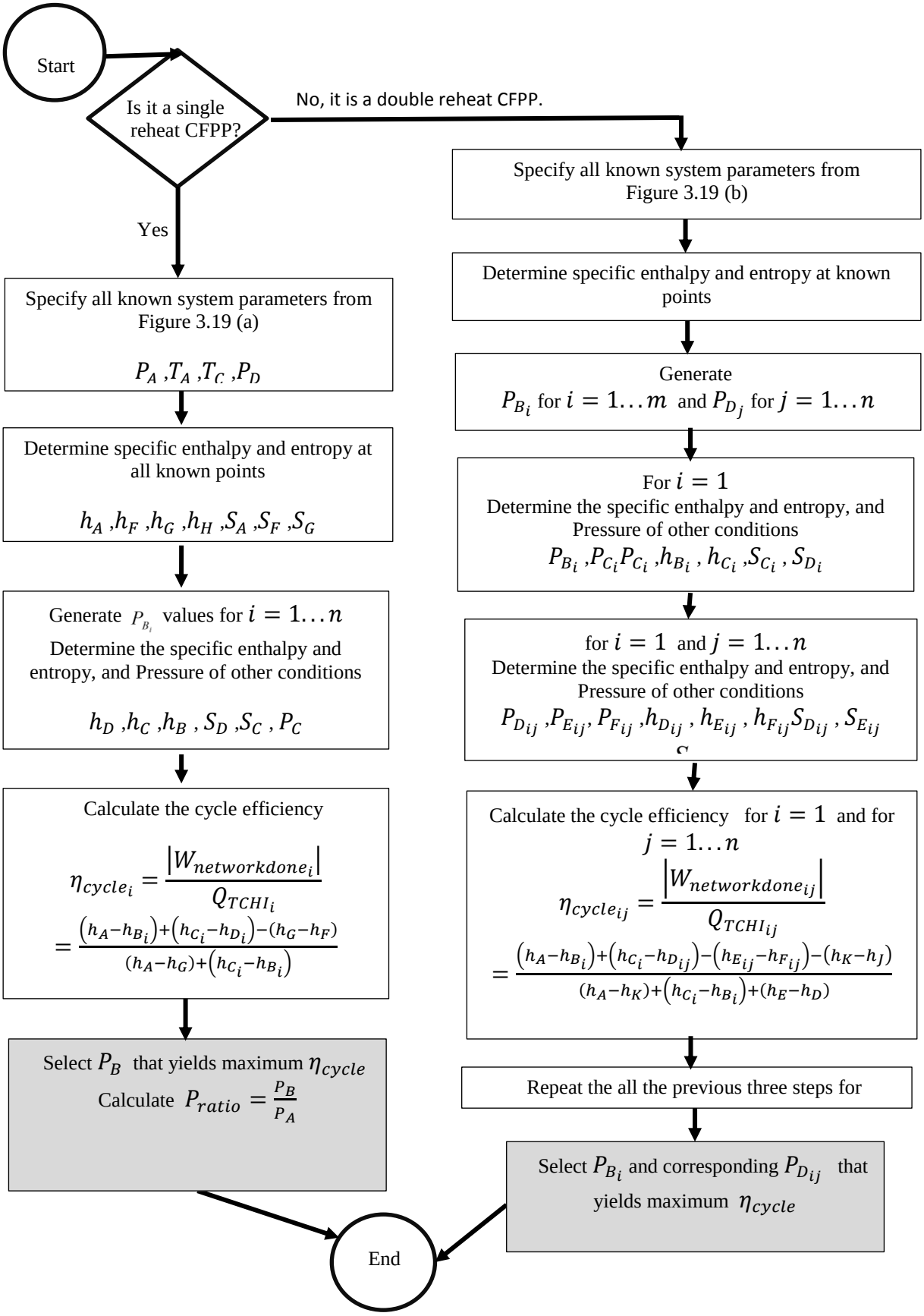

Figure 3.20 Reheat temperature determination calculation sequence

Figure 3.21 shows an example of the cycle efficiency and reheat pressure ratio $\left(P_{rat} = \frac{P_{rh1}}{P_{thr}}\right)$ calculated for a single reheat CFPP with the following conditions. $P_{thr} = 17MPa$, $T_{thr} = 565℃$, and $P_{cond} = 12kPa$. At the optimum cycle efficiency of 44.18%, the reheat pressure is $P_{rat} = 0.2236$ and the reheat pressure is$P_{rh1} = 3.8MPa$.

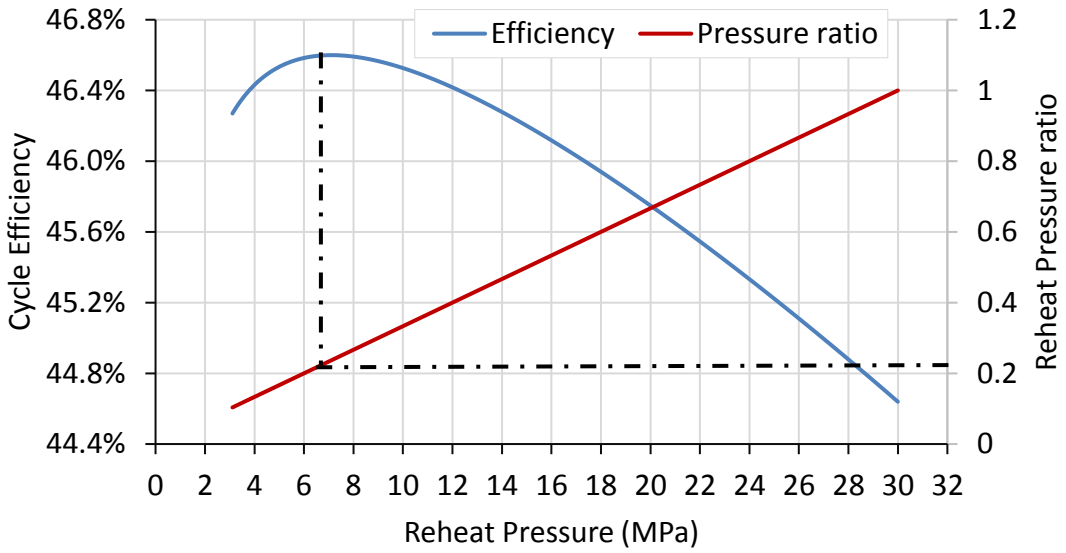

Figure 3.21 Relationship of reheat pressure for a model CFPP

3.9.3 Feedwater inlet & outlet temperatures and pressures determination

The final feed water temperature (FFWT) and the steam extraction pressure (P_{ext}) for each FWH must be determined first, before calculating feedwater inlet & outlet temperatures and pressures. The method of achieving this is described in chapter 4.

Once the FFWT and the steam extraction pressures are known, the feedwater inlet & outlet temperatures and pressures are systematically determined from the exit conditions of the final HP feed water heater i.e point A on Figure 3.22, to point G, the inlet to the first LP feed water heater. The key assumptions made for each feed water train is summarized on Figure 3.22. At point A, the final feed water pressure (FFWP) was determined from Equation(3.12).

$$FFWP = \frac{P_{thr}}{(1 - \Delta P_{boiler})} \tag{3.12}$$

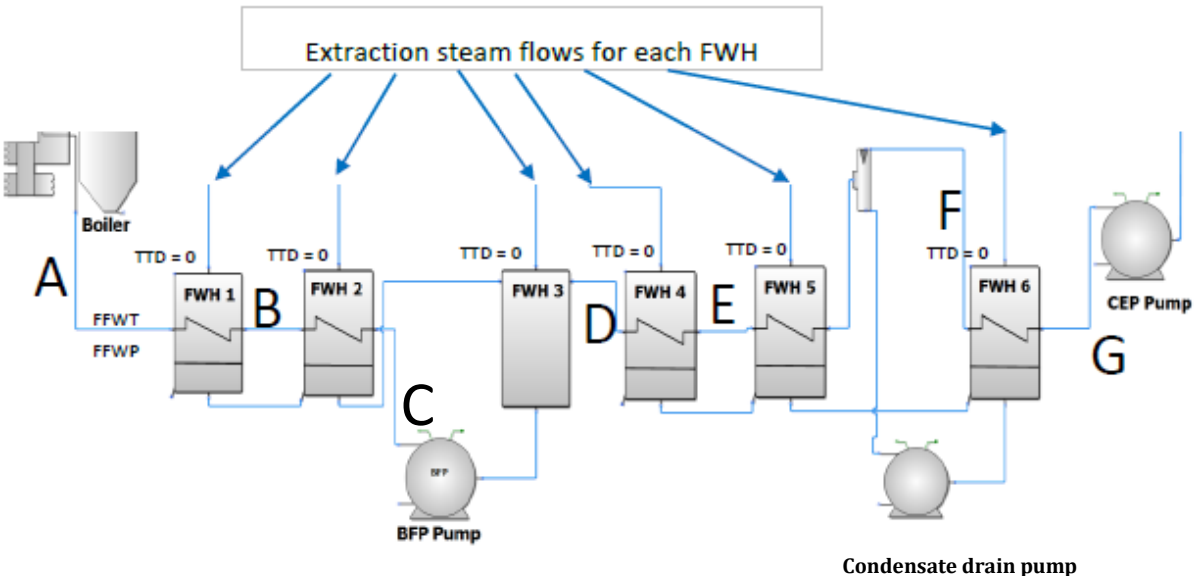

Figure 3.22 Feed water heat train modelling for non-reheat and single reheat CFPPs

P_{thr} is the throttle or superheater steam outlet pressure. This parameter is usually specified for each CFPP. ΔP_{boiler} is the pressure drop percentage between the boiler inlet and the final superheater outlet. The pressure drop due to elevation is typically included into this term. ΔP_{boiler} has been specified on Table 3.3 for each type of CFPP.

The zero drain sub cooling (DC) assumption for the FWH implies that the extraction steam temperatures at the inlet and the exit of each FWH is equal to the saturation temperature that corresponds to the extraction steam pressure entering each FWH. The condition of the hot fluid leaving each FWH is saturated liquid. Similarly, the no pressure drop assumption on the steam side of the FWH, implies that the inlet and outlet extraction steam flow pressure ($P_{FWH,ext}$) for a given FWH is equal, and can be calculated from Equation (3.13)

$$P_{FWH,ext} = P_{ext} \times \left(1 - \Delta P_{ext-pipe}\right) \tag{3.13}$$

$\Delta P_{ext-pipe}$ is the VWO pressure drop percentage on the steam extraction lines from the steam turbines and entering each FWH. It was assumed to be equal to 8% of the steam extraction pressure at the flange of each extraction stage.

The feed water pressure at points B (exit of FWH 2) and C (discharge of boiler feed pump) can be determined from Equations (3.14) and (3.15) respectively. ΔP_{FWH} is the pressure drop on the feed water side. It was assume to be 0.24 MPa for each FWH.

$$P_{FW-B} = FFWP + \Delta P_{FWH} \tag{3.14}$$

$$P_{FW-C} = P_{FW-B} + \Delta P_{FWH} \tag{3.15}$$

The feed water pressure at point D is equal to the $P_{FWH,ext}$ entering FWH 3. Once the feed water pressure at point D is known, then the feed water pressures at points E, F and G can be determined in a similar manner as points B and C. The pressure at the discharge of the condnsate drain pump is equal to the feed water pressure at point F.

The assumption of a zero TTD for each FWH implies that the feed water outlet temperature from a given feed water heater is equal to the saturation temperature that corresponds to $P_{FWH,ext}$ for that FWH.

3.9.4 Distribution of mass flows

The mass flows within the cycle is determined once the enthalpies for all the process points within the cycle is known. The mass flows across the FWHs and condenser and the throttle steam flow is calculated through an iterative process described in Figure 3.23. It all begins by assuming a steam mass fraction for the deaerator (f_{dea}^{as}) and the condenser (f_{cond}^{as}). Steam mass fraction in this case refers to the ratio of the steam mass flow through a component to the boiler main steam flow (throttle steam flow through the HP turbine). An energy and mass balance calculation is done on each of the FWHs to determine the extraction mass fraction for each of the FWHs. The energy and mass balance is done for the last high pressure feedwater heater first, and then for each successive FWH along the train to the condenser. The equation for calculating the extracted steam mass flow depends on the flow configuration/type of FWH. A summary of the equations for calculating the extraction steam mass flow for each FWH type is shown on Figure 3.24. The mass fraction through the condenser is calculated. A comparison is made between the assumed mass fractions (in steps 1 and 2) and the calculated mass fractions (in steps 3 and 4). Once the difference between the assumed and calculated values is less than or equal to 10^{-5} absolute, the calculated mass fractions is deemed accepted. The throttle steam mass flow (m_{thr}) is then determined to achieve the desired plant output power. Once this is determined, then the mass flows through the feedwater heaters, condenser and the remaining components is determined.

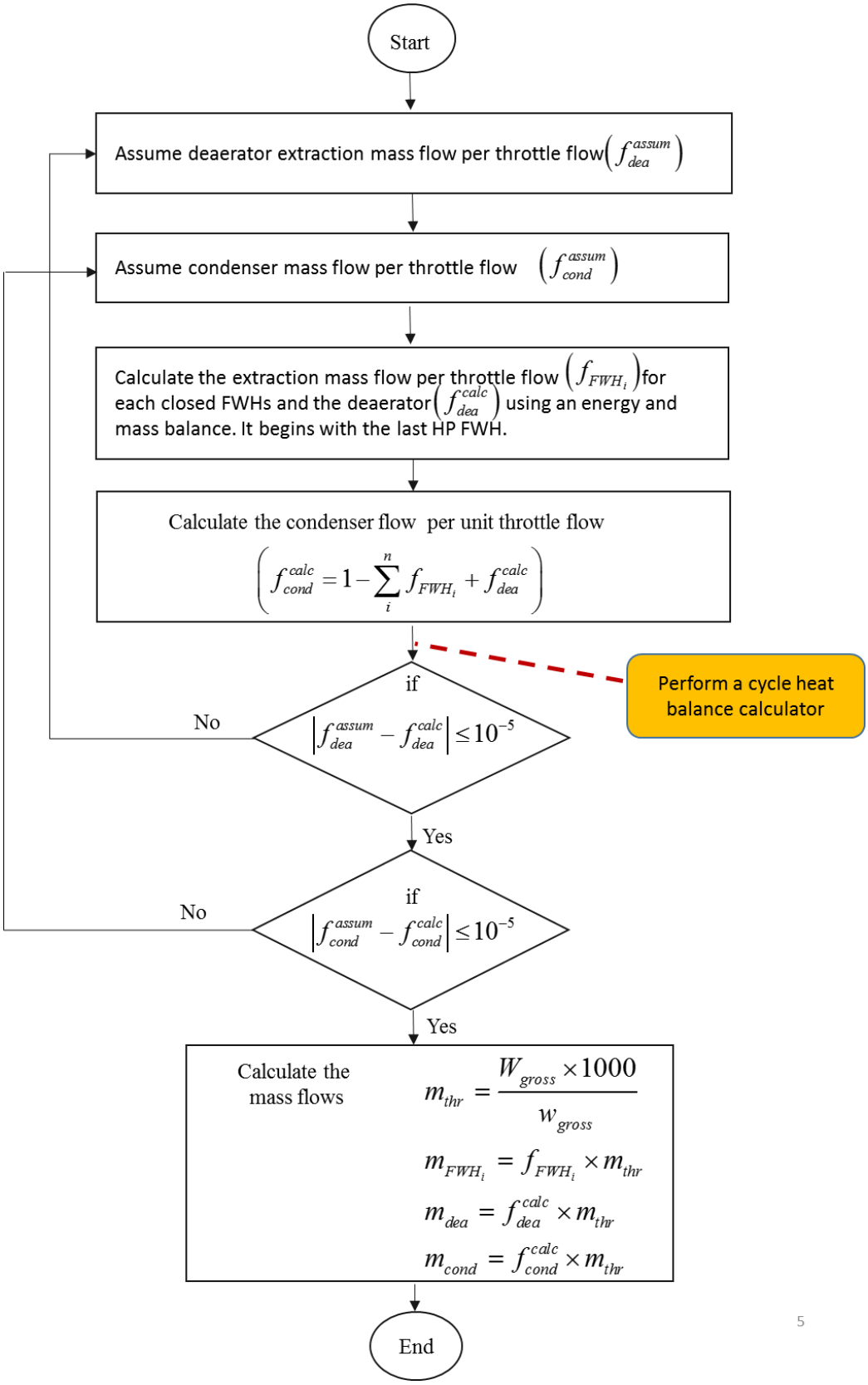

Figure 3.23 Procedure for determining the mass flows

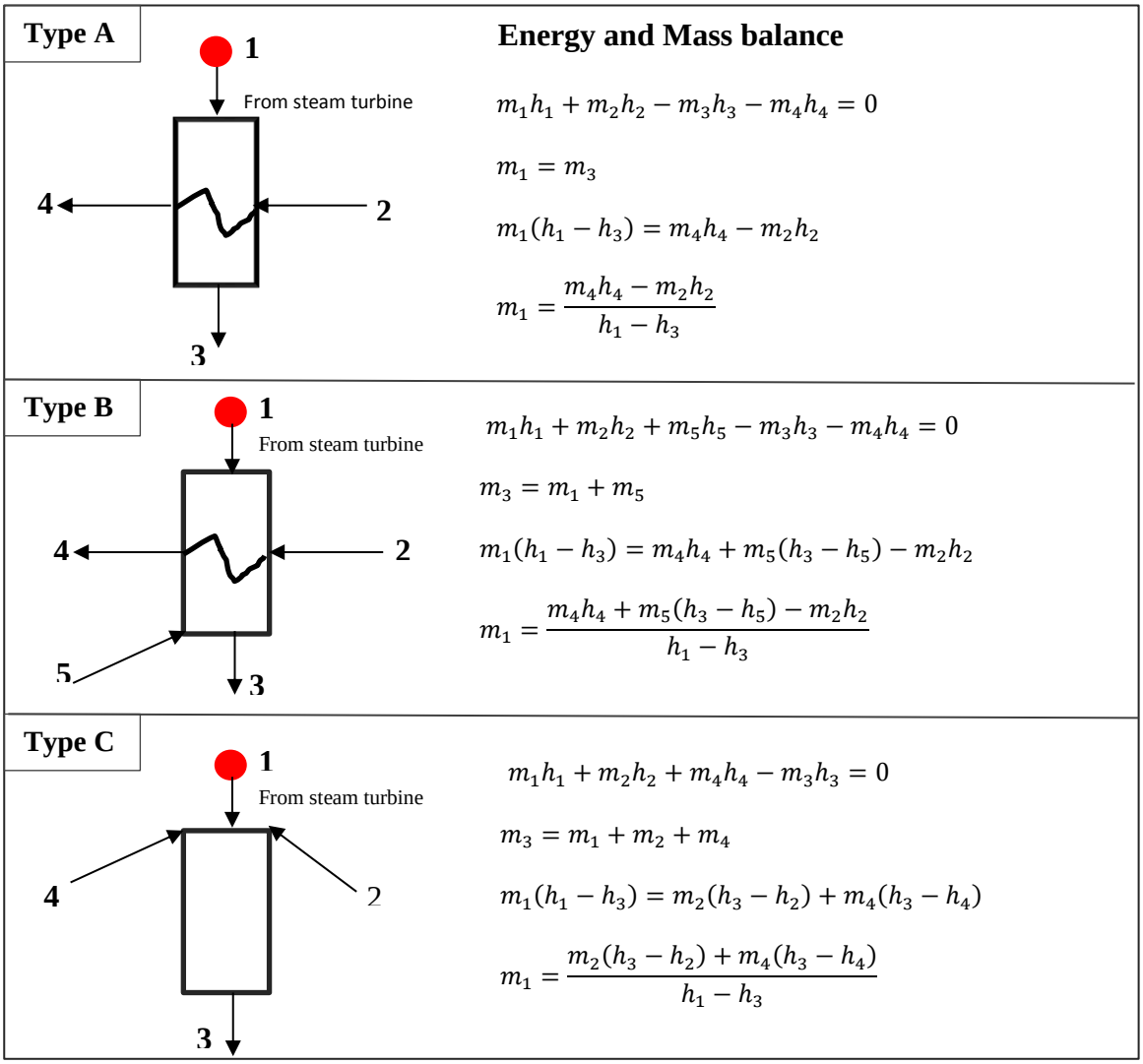

Figure 3.24 FWHs Extraction mass flow calculation procedure

3.9.5 Implementation of the VWO heat balance computation steps

The implementation of the computational steps described in Figure 3.18 were done using Microsoft Excel Spreadsheets. A different spreadsheet template was set up for each of the three different the CFPP layouts. These spreadsheets are macro-enabled with IAPWS IF97 Steam Tables incorporated by Magnus Holmgren, called XSteam [185]. Once the computational steps for a CFPP is completed, a summary of the process conditions (mass flow, temperature, pressure, enthalpy and entropy) at all the points on the CFPP layout is collated in a format that is similar to Table 3.4 which is for a non-reheat plant. This information is then transferred to the VirtualPlant software to set up the various

generic CFPP models. A sample of the calculated process conditions and a description of the points for the single reheat and double reheat CFPP is shown in Appendix A.

Table 3.4 A sample of the calculated process conditions for a non-reheat VWO heat balance

Point	Description	Mass Flow rate (kg/s)	Mass fraction	Temperature (C)	Pressure (MPa)	Enthalpy (kJ/kg)	Enthropy (kJ/kgK)
1	Throttle Conditions	191.1585	1	510	12	3376.812	6.524698
2	HP Turbine Outlet (LP Turbine Inlet)	161.5986	0.8453642	145.6551165	0.423186	2702.952	6.786624
3	LP Exhaust (Condenser inlet)	135.3429	0.708014	28.9615038	0.004	2142.919	7.113754
4	Condenser outlet	135.3429	0.708014	28.9615038	0.004	121.4036	0.42275
5	Condensate Extration Pump outlet Pressure	135.3429	0.708014	29.06893525	1.003034	122.6818	0.423638
6	Feed water outlet from FWH # 6	135.3429	0.708014	57.69241983	0.803034	242.1646	0.801801
7	Feed water inlet to FWH # 5	161.5965	0.8453534	57.69713372	0.803034	242.1646	0.801801
8	Feed water outlet from FWH # 5	161.5965	0.8453534	86.42333586	0.603034	362.3514	1.150663
9	Feed water outlet from FWH #4	161.5965	0.8453534	115.1542519	0.403034	483.3738	1.475106
10	Feed water outlet from Deaerator (FWH #3)	191.1585	1	143.8851679	0.403034	605.8963	1.779616
11	BFP Discharge	191.1585	1	146.1011017	15.21481	624.8217	1.786496
12	Feed water outlet from FWH #2 (inlet to FWH No 1)	191.1585	1	172.616084	15.01481	738.4542	2.049862
13	Final feed water condition	191.1585	1	201.347	14.81481	863.9957	2.323185
14	Extraction #1 exit from HP Turbine	11.01729	0.0576343	254.1847503	1.678907	2926.854	6.66766
15	Extraction #1 inlet to FWH	11.01729	0.0576343	252.8688319	1.598959	2926.854	6.688835
16	Drains outlet from FWH #1	11.01729	0.0576343	176.616084	1.598959	748.6117	2.105967
17	Extraction #2 exit from HP Turbine	9.270275	0.0484952	192.7535226	0.885569	2817.698	6.72597
18	Extraction #2 inlet to FWH	9.270275	0.0484952	191.6586595	0.843399	2817.698	6.747314
19	Drains outlet from FWH #2	20.28757	0.1061296	147.8851679	0.843399	623.371	1.820184
20	Extraction #3 exit from HP Turbine	9.27238	0.0485062	145.6551165	0.423186	2702.952	6.786624
21	Extraction #3 inlet to (Deaerator)	9.27238	0.0485062	143.8851679	0.403034	2702.952	6.807888
22	Extraction #4 exit from LP Turbine	8.900737	0.0465621	116.6584929	0.178531	2576.036	6.84408
23	Extraction #4 inlet to FWH	8.900737	0.0465621	115.1542519	0.17003	2576.036	6.864869
24	Drains outlet from FWH #4	8.900737	0.0465621	90.42333586	0.17003	378.8259	1.197476
25	Extraction #5 exit from LP Turbine	9.623666	0.0503439	87.68419601	0.064232	2441.563	6.914459
26	Extraction #5 inlet to FWH	9.623666	0.0503439	86.42333586	0.061173	2441.563	6.934652
27	Drains outlet from FWH #5	18.5244	0.096906	61.69713372	0.061173	258.2885	0.852497
28	Extraction #6 exit from LP Turbine	7.708692	0.0403262	58.73369833	0.018806	2298.943	7.001445
29	Extraction #6 inlet to FWH	7.708692	0.0403262	57.69241983	0.01791	2298.943	7.02094
30	Drains outlet from FWH #6	26.2331	0.1372322	57.69241983	0.01791	241.5013	0.802218
31	FWH #6 Drain Pump Discharge	26.2331	0.1372322	57.76563501	0.803034	242.4511	0.802666

3.10 Conclusion of the chapter

The development of a model that would predict the heat rate of various types of CFPPs begins with the setting up of generic CFPP process models at VWO conditions. This chapter presented an overview of the procedure adopted in setting up the generic CFPP process models.

The various types of the components that make up the Rankine cycle were briefly reviewed. A selection of the unique features/characteristics of the main components that constitute the CFPP turbine cycles was done. Three layouts were selected, one for each type of reheating.

Finally, the procedure for developing the VWO heat balance for the generic CFPP process models was discussed. The methodologies include a procedure for:

- Specifying the key process parameters and component characteristics of the CFPPs
- Determining the reheat temperatures and pressures
- Determining the enthalpies along the expansion lines
- Determining the feed water pressures and temperatures
- Mass flow distributions
- LP turbine exhaust area and exhaust loss

4. Feedwater train of the generic CFPP process model

The need for a generic method for predicting the final feed water temperature (FFWT) and extraction pressures of the FWHs on the feed water train of CFPPs have been highlighted in section 3.7.2. This chapter describes the development and validation of such a generic method. It gives a description of an extensive study of the feed water heating trains of existing CFPPs. It is intended that the generic approach developed would indirectly encapsulate the economics and operational based concerns that OEMs adopt when placing FWHs in CFPPs.

The outcome of this research was used for the determining extraction pressures of FWHs in different CFPP process models. A significant portion of this chapter has already been published in reference [168].

4.1 Methodology

4.1.1 Data Collection

An extensive analysis of the full load feed water temperature and enthalpy rise across the FWHs and economizers of sixteen (16) pulverised CFPPs. These plants comprised of 5 non-reheat, 10 single reheat (9 subcritical and 1 supercritical), and 1 double reheat supercritical unit. An additional 20 single reheat plants were included in a study of the final feedwater temperature.

There are some slight differences between the architecture of the CFPPs examined. These variations exist because different designers have developed certain in-house techniques or rules of thumb on how their designs should be. The key aspects that differs between the various architectures are: The FWH layout (the number of FWHs and the operating extraction pressures, the position of the deaerator within the FWH train, the direction of drain flow from each FWH); the presence or

absence of secondary turbines with steam extractions; the number of zones within the condenser; the number of flows within each turbine; the presence or absence of gland steam condensers (GSC), Air ejector condenser etc.

An example of one of such plant architecture is shown in Figure 4.1. This layout is for a single reheat unit having all its FWH drains (except number 6) cascaded backward. The convention for numbering the FWHs here begins with the last high pressure (HP) feed water heater.

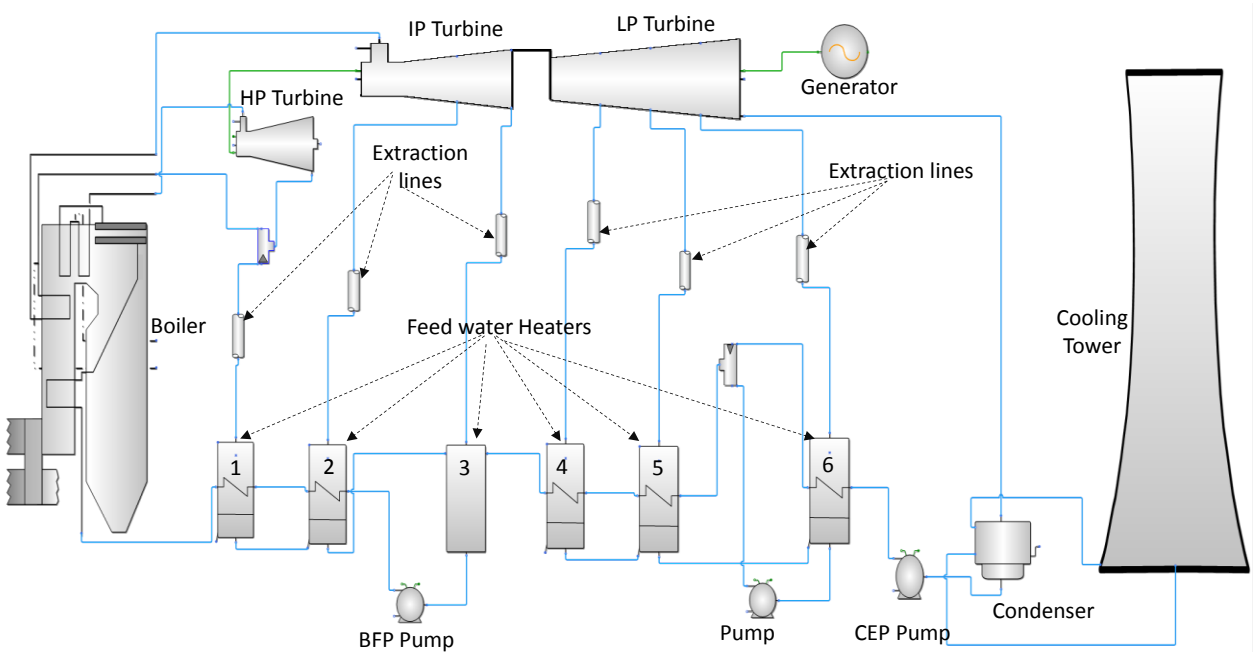

Figure 4.1 Architecture of one of the single reheat units

The CFPPs examined have been represented using generic names for confidentiality purposes. The design process parameters for the selected CFPPs are shown on Table 4.1 and Table 4.2 . The capacity of the non-reheat systems are between 100MW-200MW while the capacity of the reheat systems are between 127 MW- 800MW. It should be noted that these plants have different OEMs and different FWH drain flow configurations. These were built between 1962 and 2001. By selecting such a range of plants, it is expected that the trends observed are independent of OEMs suppliers, and are not limited by the kind of technologies available when these designs were made. The feed water temperature rise across each feedwater heater is shown in Table 4.3. Observations made from this analysis have led to the proposition of an approach for modelling the final feed water temperature, and an approach for predicting the extraction pressures of FWHs in CFPPs.

Table 4.1 List of the non-reheat units and main process parameters used

Plant Name	Capacity (MW)	Boiler Pressure (MPa)	Throttle Steam conditions		Condenser Saturation Temperature (℃)	No of Feed Water Heaters	Position of Deaerator (counting from FWH1)
			Pressure (MPa)	Temp (℃)			
A	200	11.49	10.44	538	43.8	6	3
B	200	12.32	10.44	538	38.7	6	3
C	200	11.57	10.44	538	39	6	3
D	150	9.73	8.44	509	38.8	7	4
E	100	10.80	8.38	494	32.9	6	3

Table 4.2 List of the single & double reheat units, and their main process parameters

Plant Name	Capacity (MW)	Boiler Pressure (MPa)	Throttle Steam conditions		Reheat Steam parameters		Condenser Saturation Temperature (℃)	No of Feed Water Heaters	Position of Deaerator (counting from FWH1)
			Pressure (MPa)	Temp (℃)	Pressure (MPa)	Temp (℃)			
F	400	18.71	15.42	510	3.83	505	44.6	6	2
G	578	16.90	16.10	535	3.60	534	43.3	6	4
H	500	20.96	16.85	512.7	3.08	513.1	42.9	7	5
I	618	19.77	16.03	535	3.65	535	34.3	6	4
J	600	18.81	16.01	528.1	3.66	524	43.4	6	4
K	655	19.98	16.10	535	3.70	533.8	55.5	6	4
L	580	18.72	15.08	535.5	2.79	534.8	45	6	4
M	656	17.71	16.10	535	3.64	535	62.1	6	4
N	520	16.78	15.98	531.1	3.12	527.7	45.5	6	4
O*	800	30	24.10	560	5.03	570	42.6	6	3
P**	127	35	31.02	621	7.88	565	26.1	7	3

* Plant O is a supercritical single reheat unit.

** Plant P is a supercritical double reheat unit. The second reheat temperature and pressure are 533℃ and 1.323 MPa respectively.

Table 4.3 Feed water temperature rise across each feed water heater

Plant	Feed water temperature rise across each feedwater heater (FWH)						
	FWH 1 (℃)	FWH 2 (℃)	FWH 3 (℃)	FWH 4 (℃)	FWH 5 (℃)	FWH 6 (℃)	FWH 7 (℃)
A	32.1	26.4	24.3	37.8	26.8	21.7	--
B	24.8	30.7	32.6	30.8	29.6	27.1	--
C	27.4	26	38.5	45.3	24.6	17.4	--
D	24.1	25.5	27.1	24.9	23.6	24.2	13.1
E	24.5	31.1	23.2	25	27.4	15	--
F	34.2	42.9	25.2	20.8	33.2	41	--
G	61.6	43.7	40.3	19.1	25.9	11.4	--
H	31.5	27.5	31.6	27.3	29	17.1	23.3
I	35.1	46.6	32.2	25	36.1	39.4	--
J	36.9	29.9	29.1	36.1	35.8	30.4	--
K	56	45.1	21.7	5.1	22	26.6	--
L	48.7	46.4	22.8	35	19.6	14.8	--
M	42.6	31.7	30.1	29.6	23.9	22	--
N	24.8	42.8	39.9	18.3	25.3	7.4	--
O	38.8	40.4	29	28.8	36.3	45	--
P	30.4	36.4	47.37	28.17	23.96	31.09	31.81

4.1.2 Data Processing and Interpretation

In order to evaluate the results of all plants, the normalized feed water temperature rise across the components along the feed water heating cycle and the economizer was calculated. The normalized feed water temperature rise $\overline{T}_{N,i}$ for a component i, is defined as: the ratio of feed water temperature rise in that component (ΔT_{FWi}) to the total feed water temperature rise between the condenser exit and the economizer exit ($\Delta T_{FWtotal}$):

$$\overline{T}_{N,i} = \frac{\Delta T_{FWi}}{\Delta T_{FWtotal}} \tag{4.1}$$

Figure 4.2 and Figure 4.3 shows the normalized feed water temperature rise for the non-reheat and single reheat units investigated. For the non-reheat units, the average normalized feed water total temperature rise experienced across the pumps (including the gland steam condensers) is 2 %, over the economizer it is 39 % and over all the FWHs 59 %. For the single-reheat units, the distribution is 2 %, 38 % and 60 %. The normalized feed water temperature rise for the two supercritical units were not done. This is because the boilers of these units do not have a steam drum - hence there is no saturation temperature. So it would be difficult to normalize the feed water temperature rise using the same benchmark as the sub-critical units.

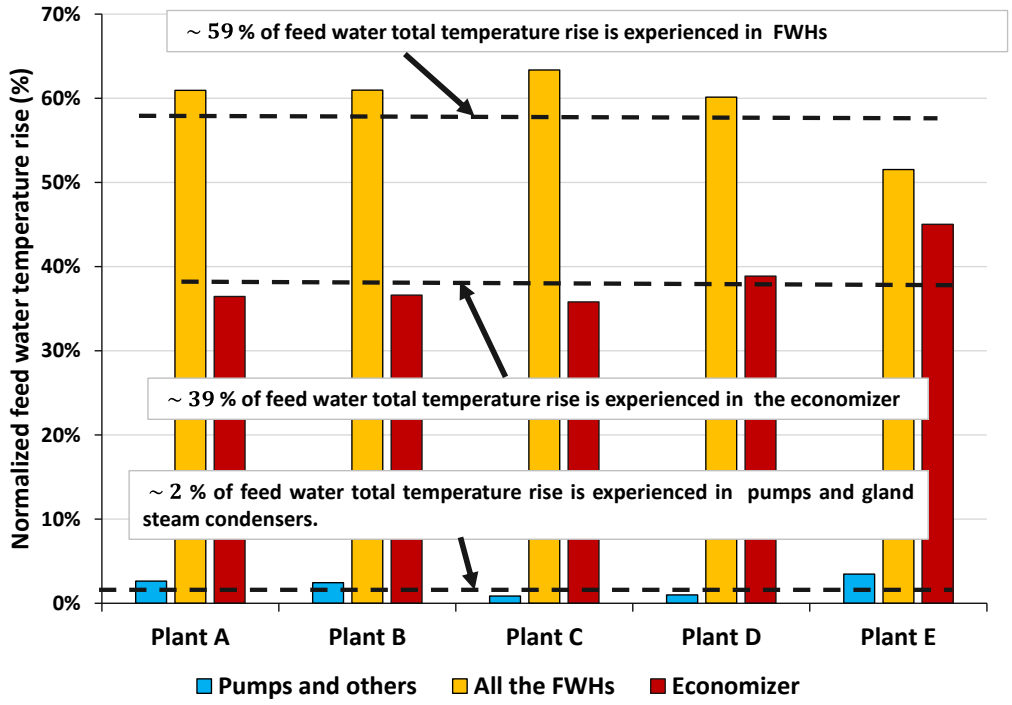

Figure 4.2 Normalized feed water temperature rise: non-reheat

Looking at the individual FWHs (See

Figure 4.4 and Figure 4.5), there are variations in the normalized feed water temperature rise across each. It appears that the normalized feed water temperature across most of the FWHs is about 10%. This trend is more pronounced in the non-reheat units. Furthermore, the normalized feed water temperature rise in the economizer for both categories of plant is typically three times more than the average normalized feed water temperature rise. This is in clear contradiction to the OCEM method that proposes an equal temperature rise for FWHs and economiser.

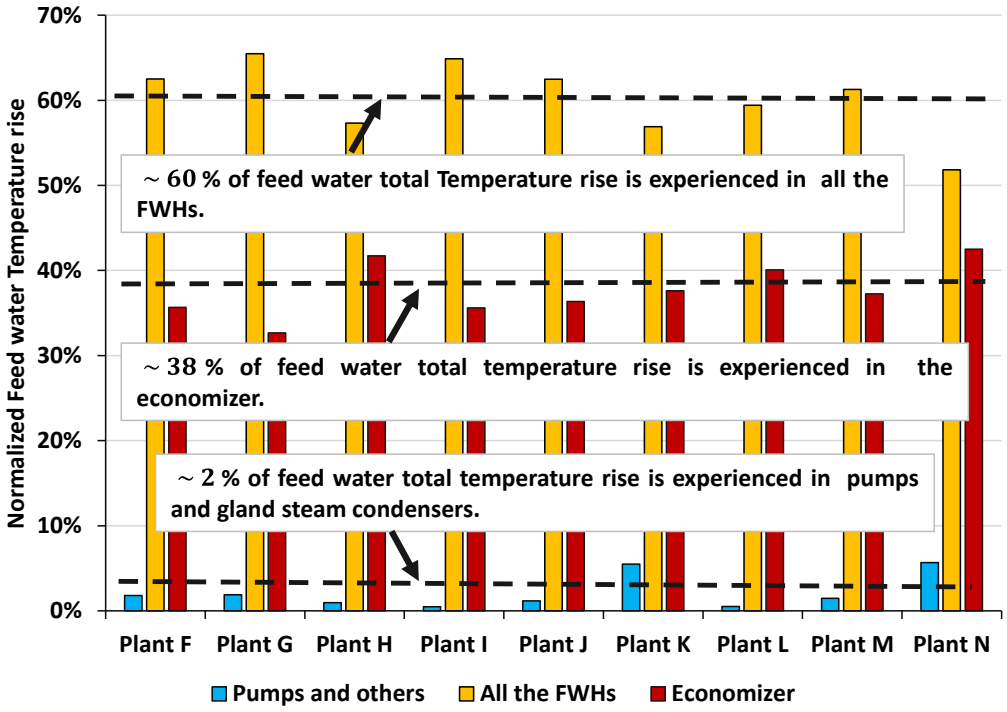

Figure 4.3 Normalized feed water temperature rise: subcritical reheat units

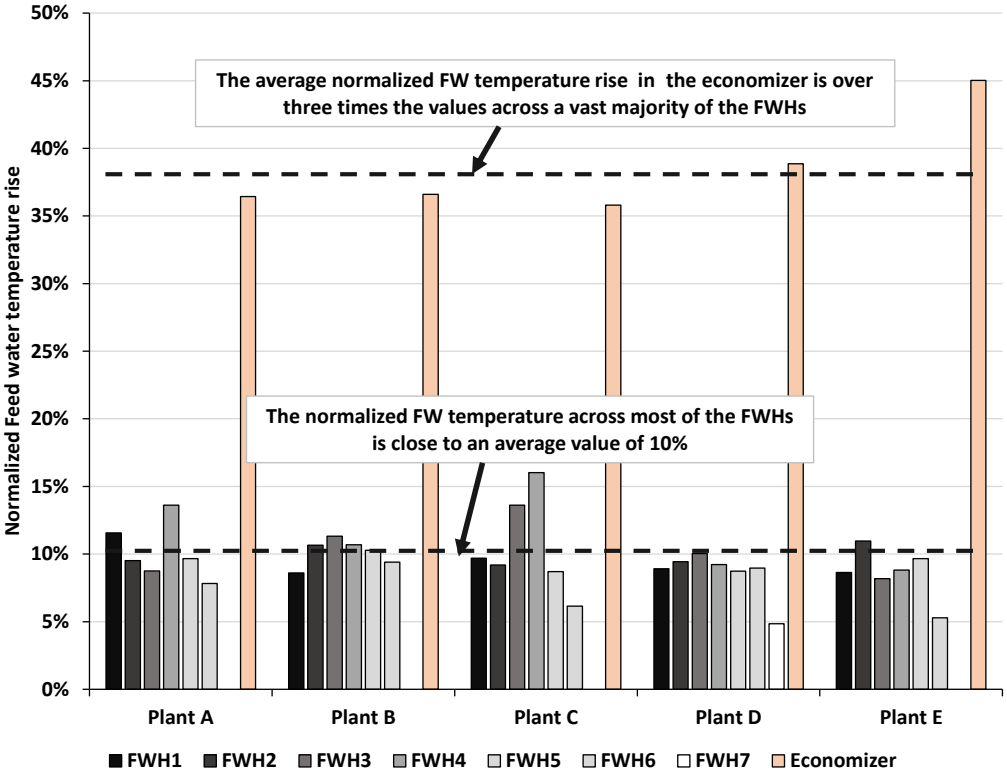

Figure 4.4 Normalized feed water temperature rise for each component: Non-reheat units

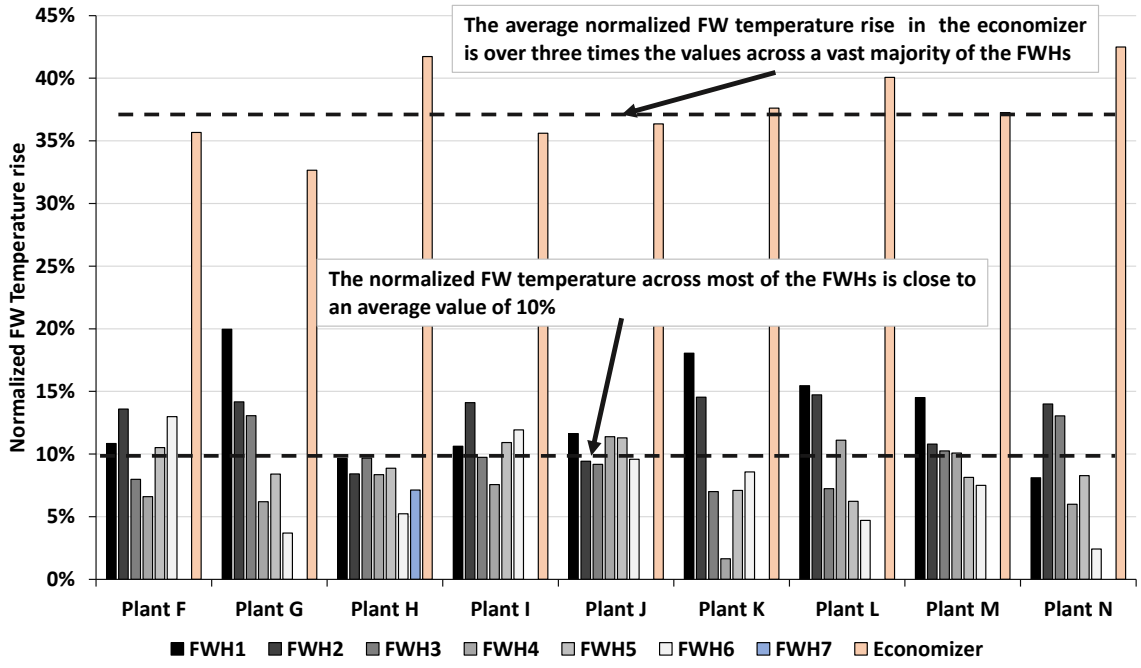

Figure 4.5 Normalized feed water temperature rise for each component: single-reheat units

These observations are very useful as it indicates the common practice amongst OEMs. It suggests that a practical model should account for the extra feed water temperature rise in the economizers by specifying a FFWT that is reflective of the types found in existing CFPPs.

4.2 Model development

4.2.1 Final Feed Water Temperature (FFWT) prediction method

The thermodynamic optimum FFWT obtained using the OCEM method, should ordinarily be the best option for the performance of CFPPs. However, this choice would lead to a reduction in the size of the economizer area. This would imply that a larger and more expensive air heater would be used to reduce the stack losses. Most OEMs prefer to use FFWT that is less than the thermodynamic optimum for economic reasons. The true reason for the deviation is unknown, hence this section will attempt to present a trend based on the available information, and speculate on possible

reasons. There seems to be a definite separation between non-reheat and reheat plants, hence the trends will be generated separately.

4.2.1.1 Non-Reheat Units

A look at the data gathered showed that there is a strong correlation between the throttle temperature and the final feed water temperature (FFWT) (see
Figure 4.6). Plants with higher throttle temperatures (in most cases with higher power output, and smaller age) tend to have a higher FFWT. The higher throttle temperatures seen were typically made possible because of advancement in boiler materials and manufacturing process. It appears as-if this gradual improvement in materials also lead to an increase in the FFWT.

Note that the flue gas inlet temperature of the air heater is directly linked to the economizer's minimum temperature. Hence, in order to increase the FFWT, one needs to also increase the thermal limits of the air heater. It is possible that this limit was the main reason for determining the FFWT, and its increase as technology advanced.

The linear correlation shown Equation (4.2) fits the available data reasonably well, and can be used as a method for predicting the FFWT of non-reheat units.

$$FFWT = -122.86 + 0.6357 \times T_{thr} \tag{4.2}$$

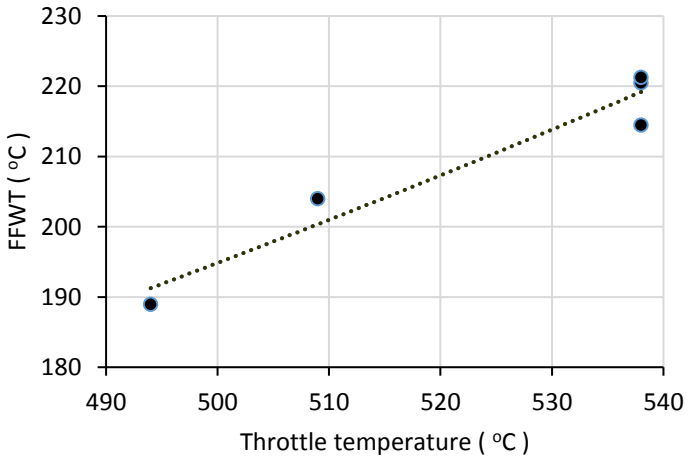

Figure 4.6 FFWT correlation for non-reheats

4.2.1.2 Reheat Units

For reheat units, there is a convenient location for the extraction of the last HP FWH: at the outlet of the HP turbine, just before the steam is returned to the boiler for reheating. Because a FWH functions primarily as a condensing heater, the exit temperature is very much linked to the saturation temperature corresponding to the steam pressure. For many HP FWHs, the terminal temperature difference (TTD) is either zero or slightly below zero. If the steam extraction of the last FHW is at the reheat pressure, one could deduce that the FFWT might be related to the saturation temperature at the reheat pressure minus the TTD.

Additional data was obtained for 20 extra CFPPs operating in the United States of America, to be able correlate a trend. Figure 4.7 shows that there is in fact a relationship between the saturation temperature at the reheat pressure and the FFWT for most of the reheat units examined. There are a few outliers which might be due to other architecture decisions not visible from the data obtained.

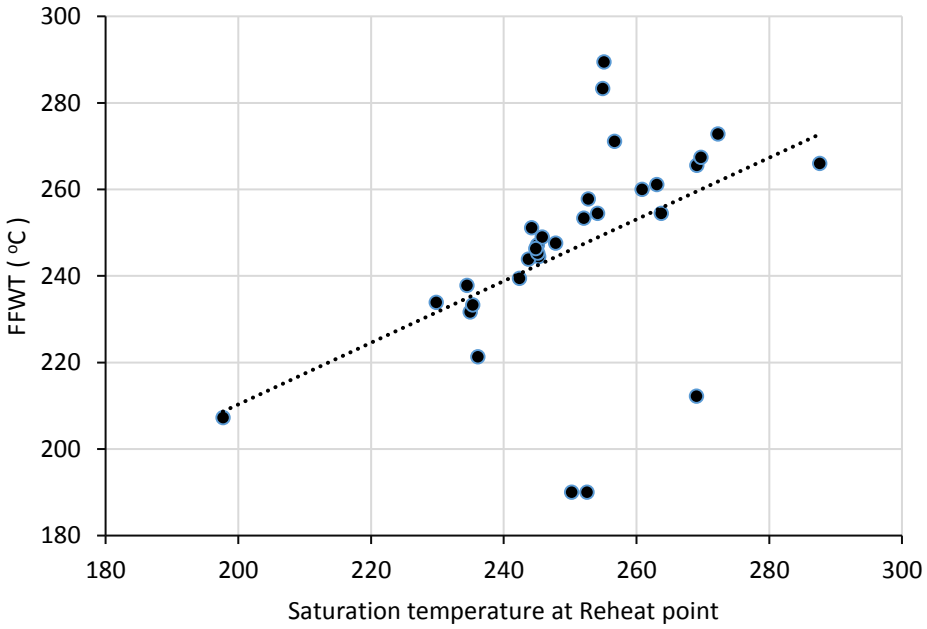

Figure 4.7 Relationship between FFWT and reheater inlet pressure

The reheat pressure is easily determined from thermodynamic principles, with the aim to maintain the steam quality of the LP turbine exhaust at a value that is greater than 85% [27] [142]. One can therefore easily determine the FFWT of a reheat plant if the reheat pressure is known. An

assumption on the pressure drop from the turbine to the FWH can be added for increased accuracy, as well as the inclusion of a TTD that is not equal to zero.

4.2.2 Extraction Pressure Prediction Method

Looking at the individual FWHs (See
Figure 4.4 and Figure 4.5), there are variations in the normalized temperature rise across each. These variations are often based on a number of optimization reasons, which are likely driven by plant economics and operation. The temperature rise between FWHs does seem to be somewhat equal, though bigger variations exist at the re-heat plants. It also seems that the lower pressure FWHs typically experience a lower temperature rise. This may be due to the fact that OEMs traditionally give special considerations to the design of the last low pressure FWH. This is due to the enormous amount of volumetric extraction flow that would be required for this heater [176].

In formulating a generic approach for predicting the extraction pressure, a modified version of the OCEM was adopted. The modification was made by selecting a FFWT that is reflective of what is usually available in most CFFPs. This implies shifting line b-e (FWH extraction saturation temperature for the last HP based on OCEM approach) in Figure 4.8 down to line c-d. Doing this automatically nullifies the OCEM assumption that the feed water temperature rise in the economizer is the same as the feed heaters. Furthermore, the feed water temperature rise between the condenser exit and the FFWT is equally partitioned across all the feed heaters excluding the economizer. From an entropy generation point of view, it also results in a more efficient cycle if the water heating is done in equally small increments.

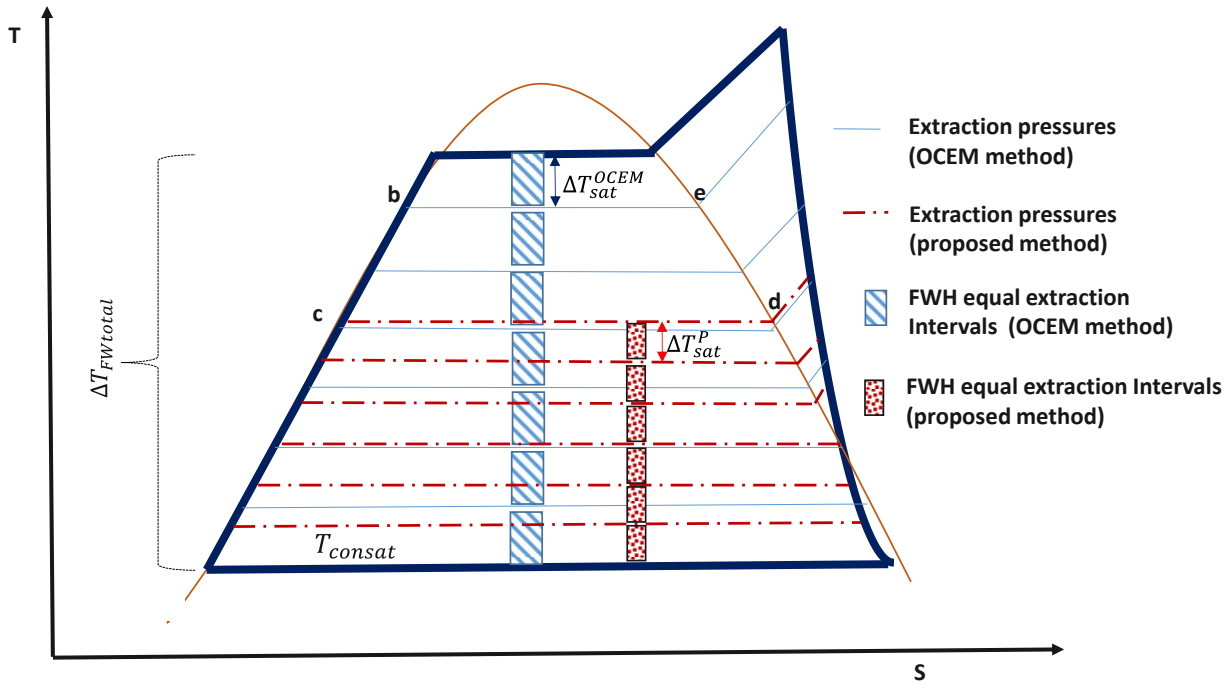

Figure 4.8 OCEM vs. proposed method for a typical non-reheat CFPP with six FWHs

The main assumptions in this model are: There is no sub-cooling in the condensers; there is equal feed water temperature rise across all the feed water heaters excluding the economizers; the pressure drop for each extraction line is the same.

A summary of the extraction pressures calculation sequence is shown on Figure 4.9. Once the FFWT for the CFPP is known based on the procedure described in section 4.2.1, then the saturation temperatures ($T_{sat,i}$) of the extraction steam at all the extraction points can be determined by using the equal temperature partition (ΔT_{sat}^{p}) between successive extractions lines from the last HP FWH to the condenser. The FWH shell extraction pressure ($P_{FWH,i}$) is evaluated by looking up the saturation pressure that correspond to each saturation temperature. Once this is done, the extraction pressure at the turbine ($P_{ext,i}$) for each FWH can be calculated by factoring in the pressure drop in the extraction lines.

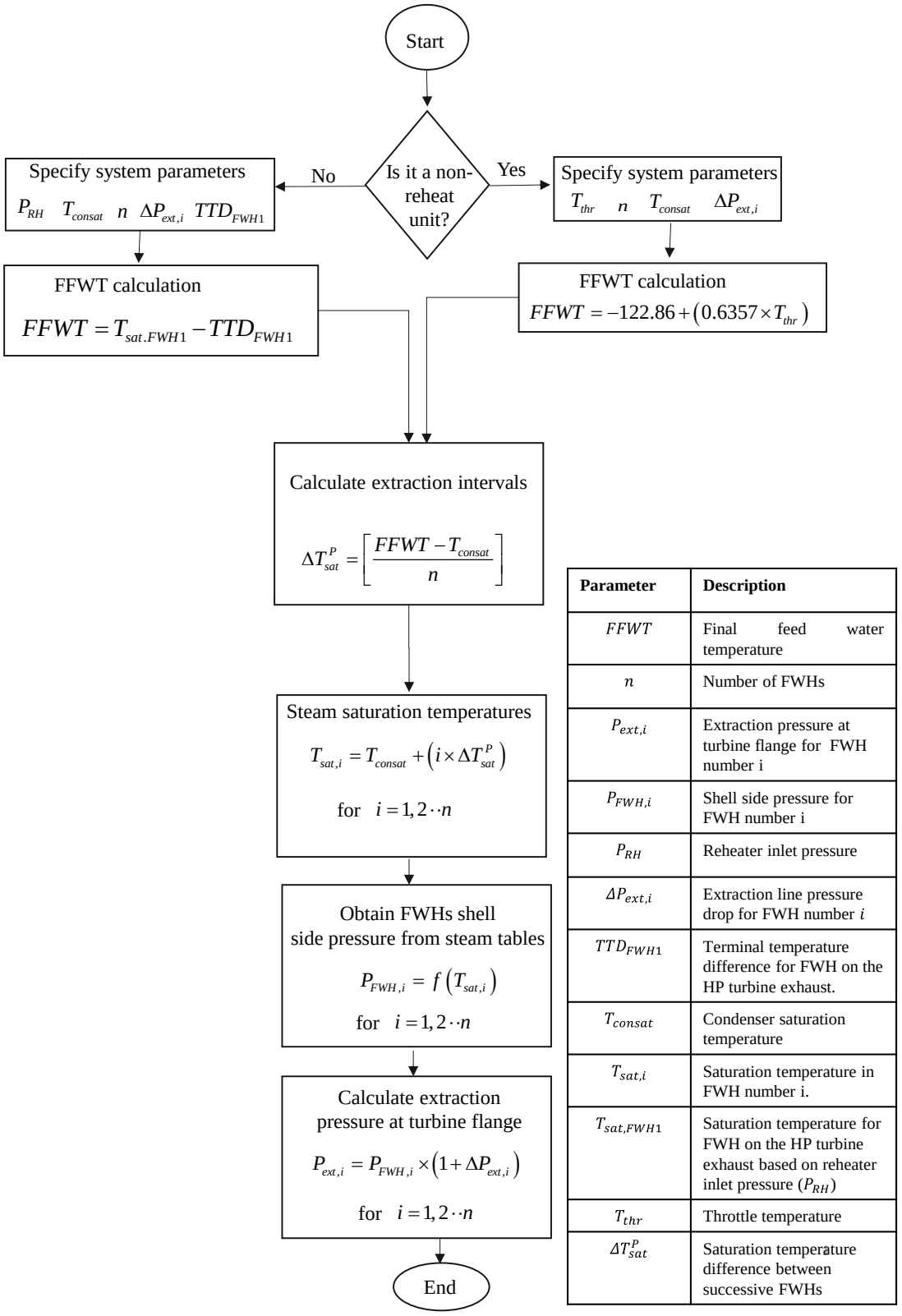

Parameter	Description
$FFWT$	Final feed water temperature
n	Number of FWHs
$P_{ext,i}$	Extraction pressure at turbine flange for FWH number i
$P_{FWH,i}$	Shell side pressure for FWH number i
P_{RH}	Reheater inlet pressure
$\Delta P_{ext,i}$	Extraction line pressure drop for FWH number i
TTD_{FWH1}	Terminal temperature difference for FWH on the HP turbine exhaust.
T_{consat}	Condenser saturation temperature
$T_{sat,i}$	Saturation temperature in FWH number i.
$T_{sat,FWH1}$	Saturation temperature for FWH on the HP turbine exhaust based on reheater inlet pressure (P_{RH})
T_{thr}	Throttle temperature
ΔT_{sat}^{P}	Saturation temperature difference between successive FWHs

Figure 4.9 Extraction pressures calculation sequence

4.2.3 A note on the extraction line pressure drop

The total pressure drop in an extraction line is typically 8% from the steam pressure at the turbine stage. This is comprised of a 3% drop from turbine stage to turbine flange, and 5 % pressure drop from turbine flange to the heater [140]. To verify this statement, the actual extraction line pressure drops from turbine flange to the heater observed for the FWHs of the plants studied were collected. Figure 4.9 shows some statistics that was obtained. The typical minimum value found was around 2% while the maximum value ranged from 5% to 16%. Line 4 is typically where the de-aerator is located, which tend to be a much longer pipe since the de-aerator is usually at an elevated level relative to the turbine and other FWHs.

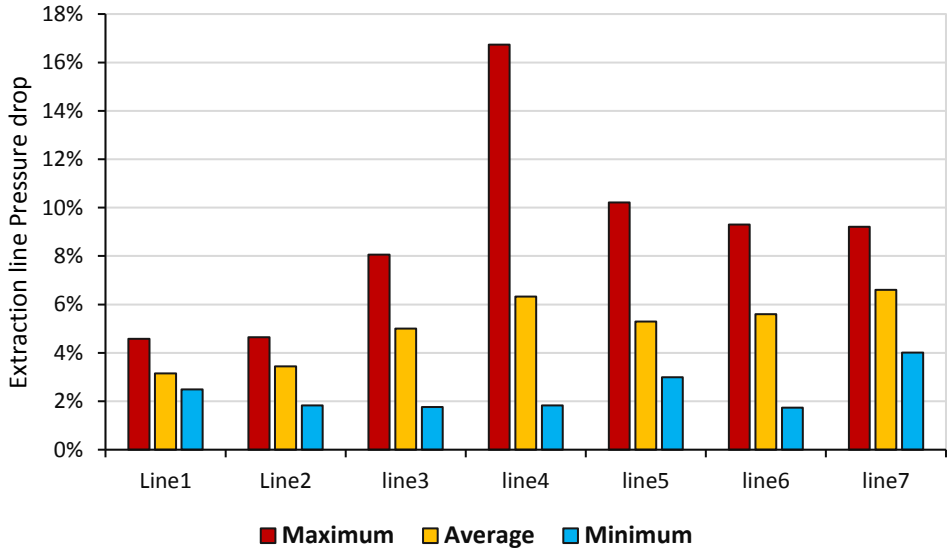

Figure 4.10 Typical values for extraction line Pressure drops seen in the Plants

4.3 Results, Discussions and Validation

4.3.1 Final feed water Temperature (FFWT)

The described above was used to predict the FFWT for the sixteen plants that were investigated. This is shown on Figure 4.11. Plants A-E, F-O, and P represents the non-reheat units, single reheat units and double reheat unit respectively. There is a good correlation between the actual and predicted FFWT results. A maximum deviation of $\pm 1.6\%$ was seen for the non-reheat units while a maximum deviation of $\pm 7.7\%$ was seen for the reheat units. The reason for the higher deviations experienced with the reheat units may have to do with the fact that no extraction line pressure drop assumption was made in this case. The extraction line pressure drops varies for each plant.

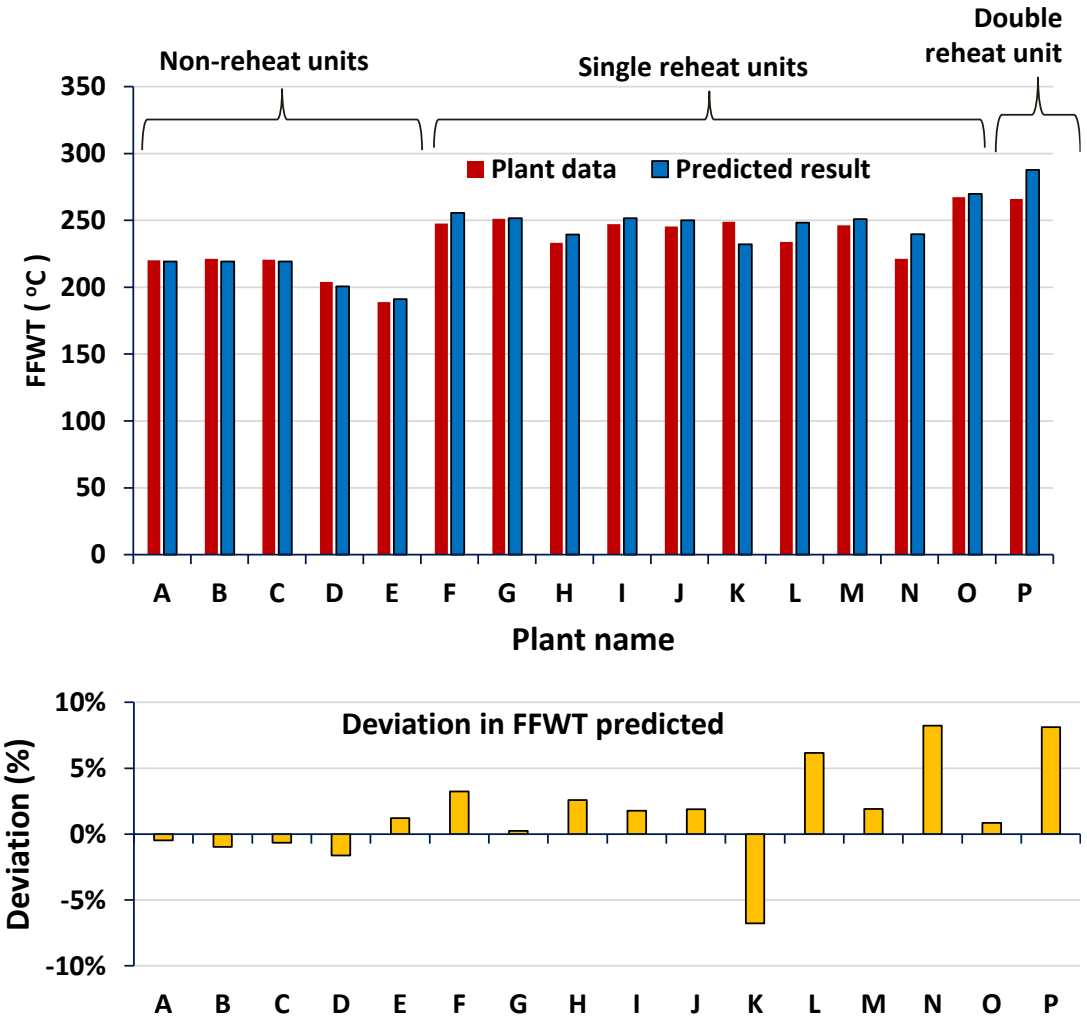

Figure 4.11 Comparing predicted and final feed water temperature: Single reheat

4.3.2 Predicting extraction pressures

A comparison of the extraction pressures predicted for the non-reheat and single reheat systems is shown in Figure 4.12(a) – (d). Three different predicted results were compared against the plant data for each extraction line. The OCEM method, the proposed method with an extraction line pressure drop of 2% and the proposed method with an extraction line pressure drop of 10%. As expected, the proposed method predicted better results than the OCEM method when compared with the available plant data.

The proposed method predicts extraction pressures that are generally less than the plant data for the non-reheat systems (Plants A & B), and predicts extraction pressures that are slightly higher for the reheat plants. It is worth noting that Plants D and H have seven FWHs and the model still predicts a reasonably accurate result like it did for the plants having six FWHs. This suggests that this model is independent of the number of FWHs available in the CFPPs. The effect of typical extraction line pressure drop values limit of between 2% and 10% examined shows very minimal impact on the models results. The trends described were seen in all the plants examined.

Because of the logarithmic nature of saturation pressure vs temperature, it is not very useful to look at the deviation of pressures. Instead, the enthalpy associated with the extraction pressure is used. After all, it is the energy content (enthalpy) of the steam which causes the feedwater heating. Figure 4.13 shows the deviations of the dry saturated vapor enthalpies predicted versus the ones obtained using the plant data. An absolute maximum of 2.2 % deviation was seen.

It can also be seen that the deviations tend to increase from the high pressure FWHs to the last low pressure FWH for most of the systems. This may be due to the fact that OEMs traditionally give special considerations to the design of the last low pressure FWH. This is due to the enormous amount of volumetric extraction flow that would be required for this heater. If an equal FW temperature rise approach is used, the flow becomes quite difficult to extract from the turbine stage [176]. This special consideration was not factored in the proposed approach.

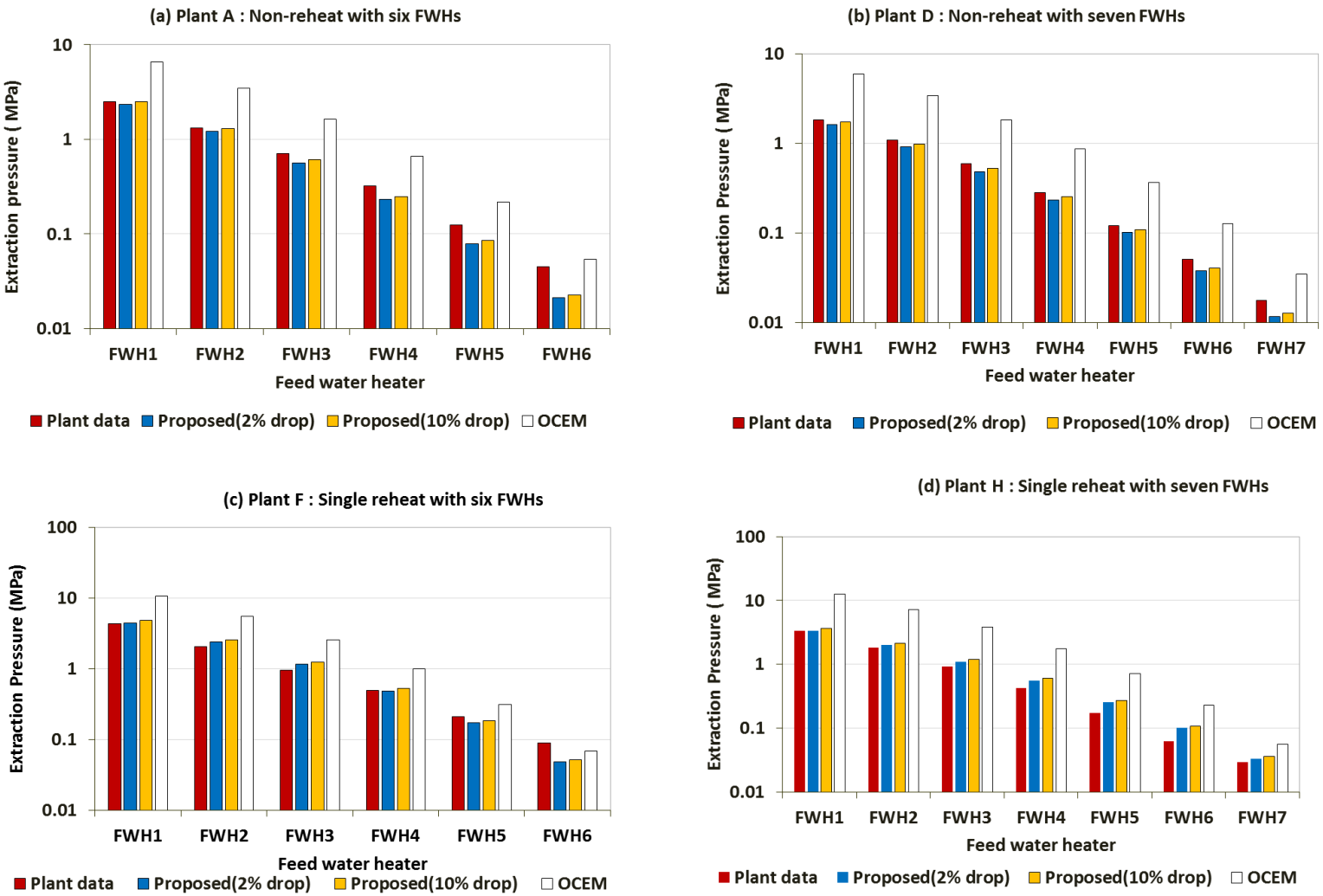

Figure 4.12 Comparison of extraction pressures predicted for some of the plants

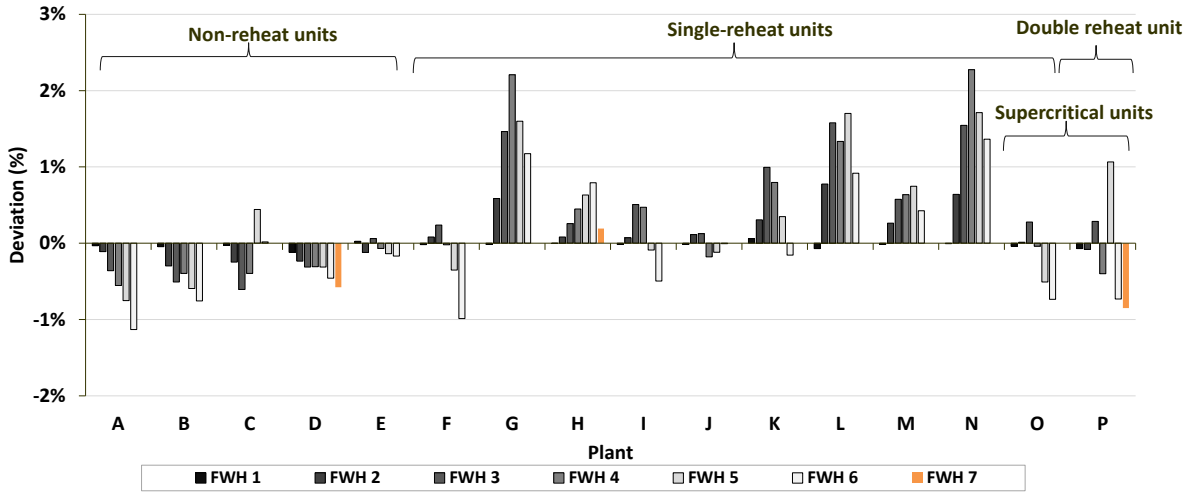

Figure 4.13 Deviation of vapour saturation enthalpy at extraction pressures

In summary, the OCEM method could be modified to predict FWH design extractions pressures that are comparable to the ones used by most OEMs if:

- The economizer is not included in the equal temperature rise of the FWHs.
- The FFWT entering the boiler is determined using the methods described in sections 4.3.1 .
- The feed water temperature rise from the condenser saturation temperature to the FFWT is equally divided across the feed water heaters.

4.4 Conclusions of the Chapter

The proposition of: (i) A generic approach for estimating the FFWT of CFPPs, and (ii) A generic approach for modelling the extraction pressures of FWHs of CFPPs is presented in this paper. The FFWT and extraction pressures for any pulverised CFPP operating at full load (design conditions) could be determined within reasonable accuracy limits by simply specifying the throttle temperature (for non-reheats), reheater inlet pressure (for reheats), condenser pressure, and the number of feed water heaters required. These are independent of the number of FWHs, the drain outlet flow configurations, or the position of the deaerator. The method is suitable for non-reheat and single reheat units, would probably also be suitable for double reheat systems. The proposed method does not consider specific plant issues such as effect of terminal temperatures differences (TTD), drain outlet flow, extraction line pressure drops, and impact of turbine internal efficiency changes, or non-utilization of leakage and gland steams.

The method proposed may not yield the optimum cycle efficiency, however it predicts extraction pressures and FFWT that are reflective of practical values found in the CFPPs examined. For that reason, it can be used for the generic modelling of extraction pressures and final feed water temperatures in FWH cycle of CFPPs at full load.

This method was used for setting up the VWO heat balance of all the VirtualPlant CFPP process models that were investigated in Chapters 6 and 7.

5. Cooling systems of the generic CFPP process model

The need for a method to predict the condensing pressure of CFPPs at varying load has already been highlighted in section 3.6.2. This chapter describes the validation of a constant effectiveness assumption method for predicting the main steam condenser pressure response of steam power plants operating at various heat rejection loads, and/or for different cooling fluid inlet temperature conditions. A description of the constant effectiveness theory is given. The results predicted from this approach were compared with performance data from 2 Air-cooled condensers (ACC), and 1 Wet cooled condenser (WCC).

The knowledge gained from this chapter is required for determining the variation in condensing pressure of CFPPs with load, for all the model CFPPs investigated in Chapter 6 and 7. A significant portion of this chapter has already been published in reference [186].

5.1 Constant effectiveness theory

5.1.1 Determination of condenser effectiveness from LMTD characteristics

The log mean temperature difference (ΔT_{LM}) definition for a heat exchanger shown in Figure 5.1, is given in Equation(5.1). Note that for a condensing heat exchanger, T_{hi} and T_{ho} is the same and equal to the saturation temperature at the condenser pressure (assuming no air ingress).

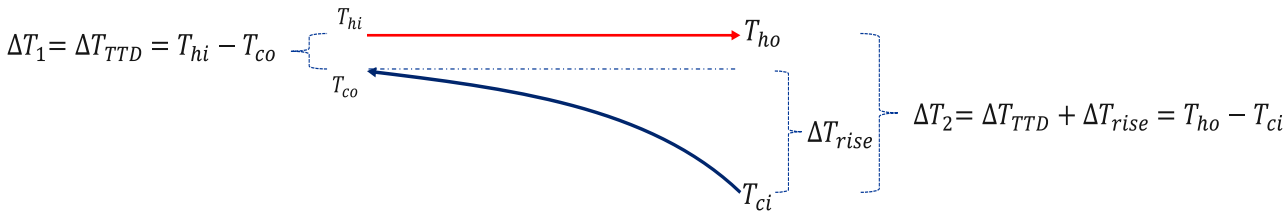

Figure 5.1 Process conditions for a typical condenser

$$\Delta T_{LM} = \frac{\Delta T_2 - \Delta T_1}{ln\left(\frac{\Delta T_2}{\Delta T_1}\right)} = \frac{\Delta T_{rise}}{ln\left(\frac{\Delta T_{rise}+\Delta T_{TTD}}{\Delta T_{TTD}}\right)} \quad (5.1)$$

This can be rewritten in the following form:

$$T_{hi} = \frac{T_{ci} - T_{co} \cdot e^{\left(\frac{\Delta T_{rise}}{\Delta T_{LM}}\right)}}{1 - e^{\left(\frac{\Delta T_{rise}}{\Delta T_{LM}}\right)}} \quad (5.2)$$

The standard definition for effectiveness for a heat exchanger is given as:

$$\varepsilon = \frac{q_{actual}}{q_{max}} = \frac{C_c(T_{co} - T_{ci})}{C_{min}(T_{hi} - T_{ci})} \quad (5.3)$$

For condensers $C_c = C_{min}$, therefore it can also be expressed as:

$$\varepsilon = \frac{(T_{co} - T_{ci})}{(T_{hi} - T_{ci})} \quad (5.4)$$

The effectiveness of a condenser is also expressed as:

$$\varepsilon = 1 - e^{-NTU} \quad (5.5)$$

The condensing temperature (T_{hi}) can be obtained from combining Equations (5.4) and(5.5), giving:

$$T_{hi} = \frac{T_{ci} - T_{co} \cdot e^{(NTU)}}{1 - e^{(NTU)}} \quad (5.6)$$

Comparing Equations (5.2) and (5.6) the number of transfer units (NTU) of a condenser equates to:

$$NTU = \frac{\Delta T_{rise}}{\Delta T_{LM}} = \frac{UA}{C_{min}} \quad (5.7)$$

The ratio $\left(\frac{\Delta T_{LM}}{\Delta T_{rise}}\right)$ can be defined as the **normalized $\boldsymbol{LMTD}$** of the condenser. This means that the effectiveness of a condenser at any operating condition can theoretically be determined without

the knowledge of the UA or C_{min} values of the condenser, provided the condensing temperature, inlet and outlet cooling fluid temperatures are known.

The effectiveness of a condenser as defined in Equation (5.5) can thus be re-written as:

$$\varepsilon = 1 - e^{-\left(\frac{\Delta T_{rise}}{\Delta T_{LM}}\right)} \tag{5.8}$$

5.1.2 Predicting the condenser pressure response at varying conditions

Gills' model [167] assumes that the ΔT_{LM} and ΔT_{rise} of the condenser is proportional to the heat load rejected or load factor X. This implies:

$$\Delta T_{LM} = X \cdot \Delta T_{LM_D} \tag{5.9}$$

$$\Delta T_{rise} = X \cdot \Delta T_{rise_D} \tag{5.10}$$

ΔT_{LM}, ΔT_{LM_D} are the Log mean temperature difference at any steady state and TMCR/design state respectively. ΔT_{rise}, ΔT_{rise_D} are the cooling fluid temperature rise corresponding to the aforementioned states. X is the heat load factor, which is a ratio of the heat rejected by the condenser at any steady state Q , to the heat rejected by the condenser at the TMCR, Q_D. For normal operation, this is very much the same as the plant load factor. X can be greater than 1 for abnormal operations of the power plant (such as emergency shut down, turbine bypass operations etc.). In these situations, the condenser is expected to accommodate additional heat that ought to have been extracted by the turbines. This fact is usually taken into consideration by most condenser designers.

Equation (5.9) divided by Equation (5.10) gives:

$$\frac{\Delta T_{LM}}{\Delta T_{rise}} = \frac{\Delta T_{LM_D}}{\Delta T_{rise_D}} \tag{5.11}$$

Equation (5.11) is describing the normalized LMTD, which can be seen to be the same for any load. Recalling Equation(5.8), this implies that the effectiveness of a condenser is constant throughout the load range, and process conditions. It therefore means that the condensing temperature of the condenser at any load can be determined from Equation (5.2) giving:

$$T_{hi} = \frac{T_{ci} - T_{co} \cdot e^{\left(\frac{\Delta T_{rise_D}}{\Delta T_{LM_D}}\right)}}{1 - e^{\left(\frac{\Delta T_{rise_D}}{\Delta T_{LM_D}}\right)}} \tag{5.12}$$

From Equation (5.10) we have:

$$T_{co} = T_{ci} + X \cdot \Delta T_{rise_D} \tag{5.13}$$

Giving the condenser temperature T_{hi} only as a function of the variable cooling fluid inlet T_{ci} and load factor, X:

$$T_{hi} = \frac{T_{ci} - \left(T_{ci} + X \cdot \Delta T_{rise_D}\right) \cdot e^{\left(\frac{\Delta T_{rise_D}}{\Delta T_{LM_D}}\right)}}{1 - e^{\left(\frac{\Delta T_{rise_D}}{\Delta T_{LM_D}}\right)}} \tag{5.14}$$

5.2 Condensers Investigated

5.2.1 Source Data

In this study, three different main steam condensers were investigated. The nominal parameters of the condensers (ACC-1, ACC-2, and WCC-1) are presented on Table 5.1. The pseudo-names are used for the condensers for confidentiality purpose. Two of these condensers (ACC-1 & WCC-1) were obtained from stations in the UK while ACC-2 is a condenser that is part of Eskom's current operating fleet. Additional data was obtained to be able to give a general perception of what the effectiveness of WCC-systems are like. The additional data used were for WCC-2, WCC-3, and WCC-4.

Table 5.1 Design process parameters of the main steam condensers examined

S/ No	Pseudo name & Source		Cooling technology	Condensing temperature (°C)	Cooling fluid inlet Temperature (°C)	Cooling fluid outlet Temperature (°C)
1	ACC-1* (UK)		Air cooled condenser (ACC)	49.42	15.00	45.12
2	ACC-2* (ESKOM)		Air cooled condenser (ACC)	52.69	23.70	46.01
3	WCC-1* (UK)		Wet cooled condenser (WCC)	27.06	13.00	23.17
4	WCC-2** (ESKOM)	Hot zone WCC-2H	Wet cooled condenser (WCC)	38.68	26.85	34.70
5		Cold zone WCC-2C		32.04	19	26.85
6	WCC-3 [187]		Wet cooled condenser (WCC)	40.00	31	37.30
7	WCC-4 [163]		Wet cooled condenser (WCC)	29.56	17	25.36

Note:

* Performance data was available for these condensers

**WCC-2 is a two zone condenser. The hot zone has a higher condensing temperature than the cold zone.

5.2.2 Key modelling assumptions

The following assumptions were made in the data analysis:

- The cooling fluid inlet temperature to the condenser does not change while considering the effects of changing heat load.
- There is no trapped incondensables in the condenser.
- The pressure drop (exhaust resistance) on the steam side of the condenser is zero.
- There is no sub-cooling in the condensers.
- The effect of fouling has already been captured in the performance curves used for the model validation. However, while considering any single condenser, it is believed that this

effect would give rise to approximately the same effect across the entire load range, and cooling fluid inlet temperature [188] .

- The relationship between the generated load and the condenser heat load is directly proportional.

5.3 Results and Discussions

The relationship between effectiveness and the normalized $LMTD$ for a typical condenser is shown on Figure 5.2. A normalized $LMTD$ that is greater than 1 would yield an effectiveness that is less than 0.632. This normalized $LMTD$ parameter is a useful indicator of the effectiveness of the condenser. It therefore means that the effectiveness of the condenser can be determined with only three non-geometrical parameters namely: cooling fluid inlet and outlet temperatures, and the condensing temperature.

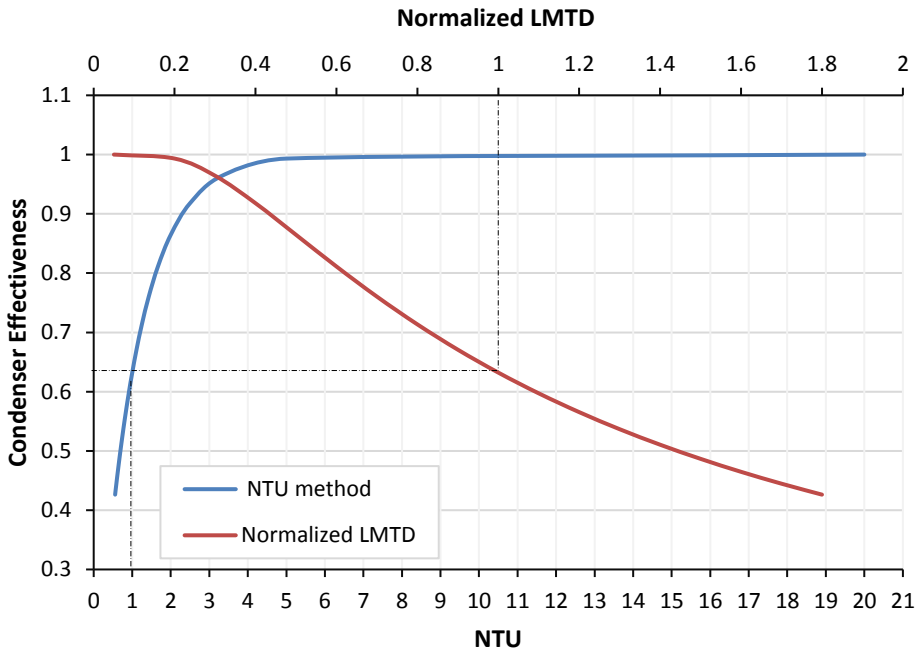

Figure 5.2 Effectiveness profile of condensers

The effectiveness of the condensers evaluated is shown in Figure 5.3. It appears that the air cooled condensers (ACC) have a higher effectiveness than the wet-cooled condensers (WCC). The probable reason for this may be found on Figure 5.4. A larger cooling temperature rise of between 20 - 30 °C is seen for the ACC systems while around 6 – 10 °C is seen for WCC systems.

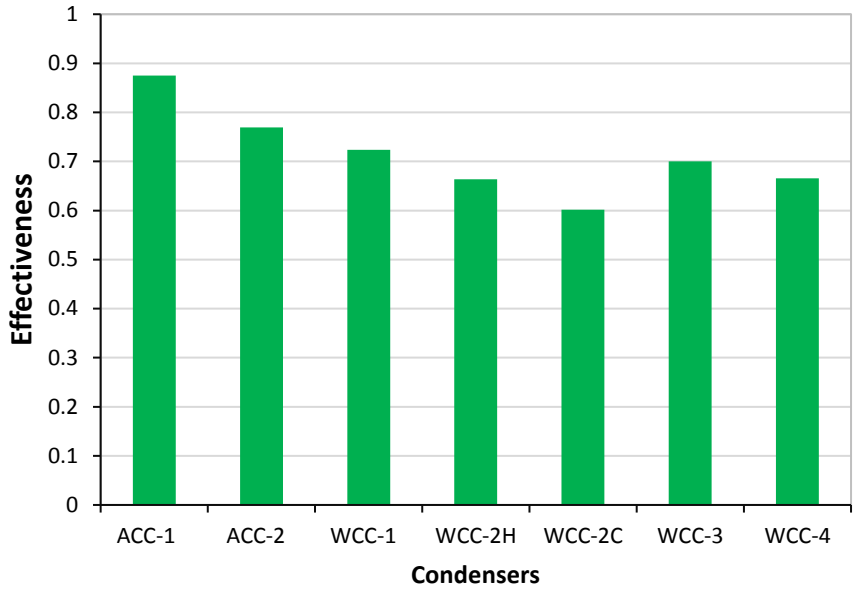

Figure 5.3 The calculated effectiveness of the condensers

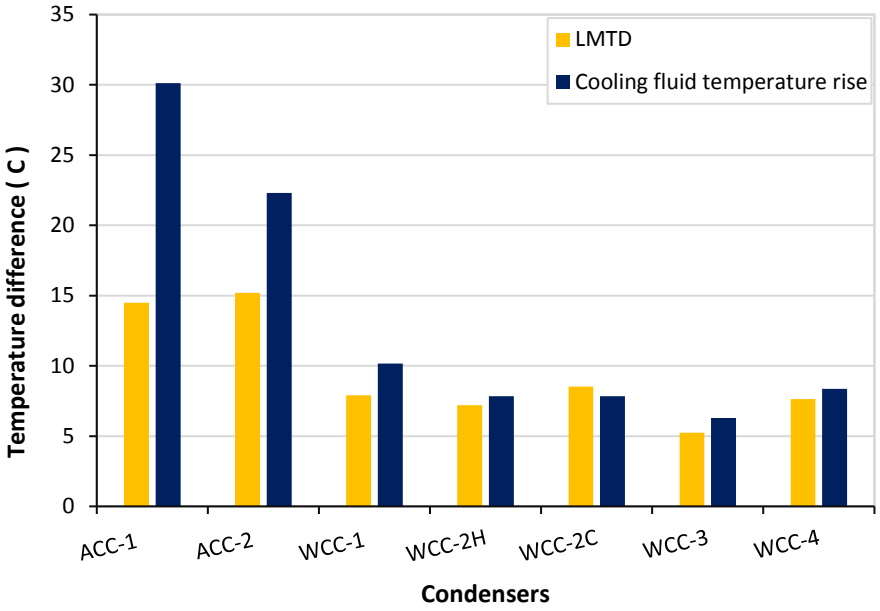

Figure 5.4 LMTD and cooling fluid temperature rise for some condensers

Figure 5.5 and Figure 5.6 shows a comparison of the predicted and actual performance data pressure response of the condensers examined at the design cooling inlet temperature. The deviations in the pressure is also shown. It can be seen that for all the three condensers examined, the predicted response is quite close to the performance curve data. The model slightly under-predicts the pressure response at load factors less than 0.6 for the WCC system, and it also slightly

over-predicts the response at loads above 1.2 for the WCC system. The probable reasons for the deviation may be better explained by looking at the key variables that affects the condenser effectiveness in Equations (5.7) and (5.8). A constant effectiveness assumption implies that $\frac{C_{min}}{UA}$ is assumed to be constant throughout the entire load range. This assumption may not be completely true as changes in the temperature dependent thermophysical properties such as density, viscosity and specific heat capacity impact the heat transfer properties of the cooling fluid. Furthermore, the mass flows of the cooling fluid at different loads are not exactly the same, especially in the case of air-cooled systems. This may also affect the heat transfer co-efficient, and the C_{min} value at different loads. However, most cooling systems in operation do not reduce the cooling fluid circulation rate. Only in some energy optimized ACCs would some of the fans be switched off as the load reduces. In such a case, the constant effectiveness assumption would not hold.

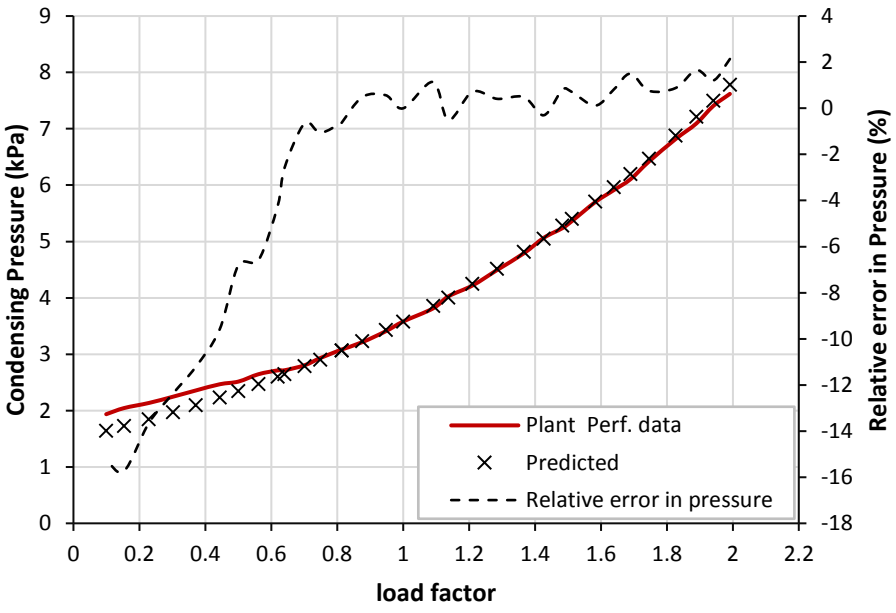

Figure 5.5 Predicted results and plant performance data for WCC-1 at design cooling inlet temperature of 13°C

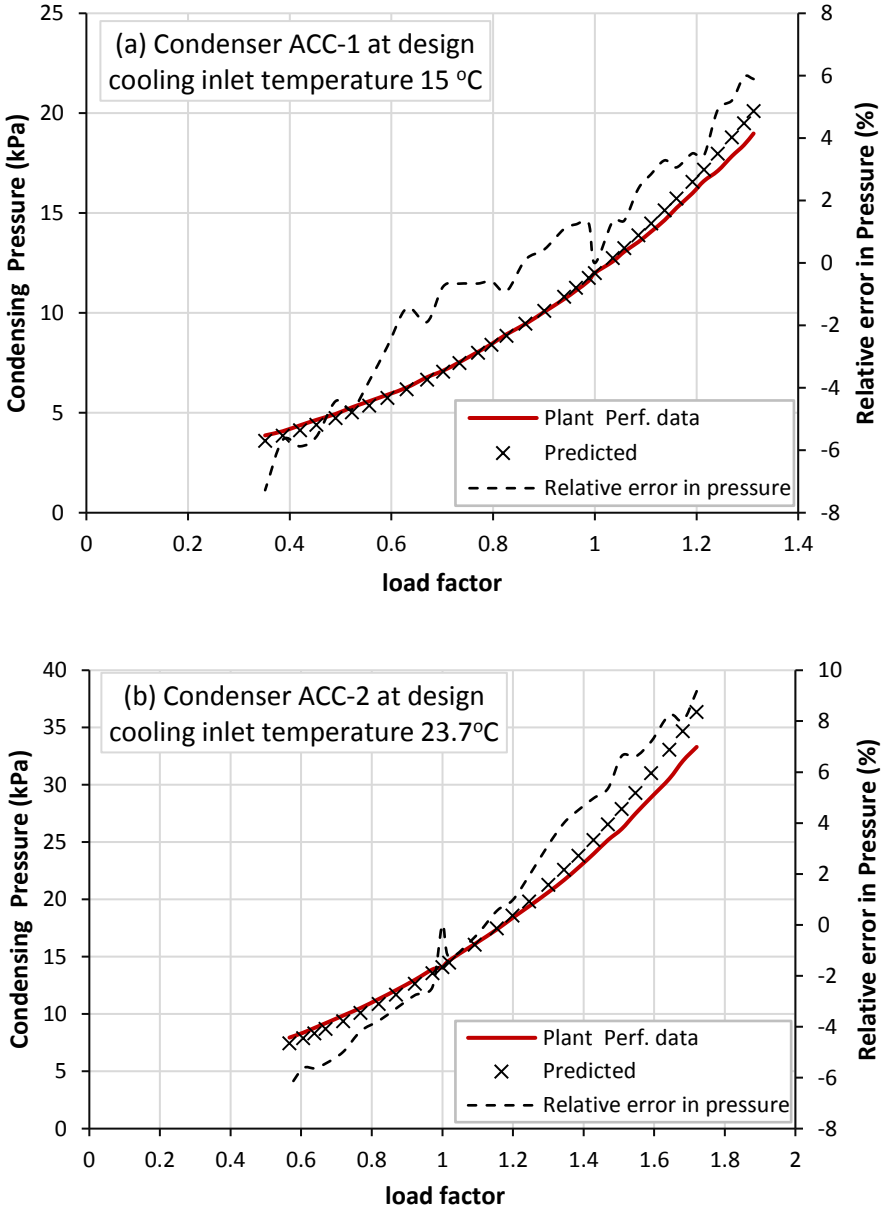

Figure 5.6 Predicted results and plant performance data for ACC-1 and ACC-2

At different cooling inlet temperatures $T_{ci_{off-D}}$, the model results for WCC-1 still compares favorably with the plant performance curve data (see Figure 5.7 (a) – (f)). For temperatures below the design cooling inlet temperature (see Figure 5.7 (a) –(c)), the trends observed are similar to the ones observed for the design inlet cooling condition. Hence, the same explanation is applicable. Furthermore, it can be seen that the deviations at inlet conditions below the design tend to be higher than those with inlet conditions above the design. Similar trends were also observed for ACC-1 and ACC-2.

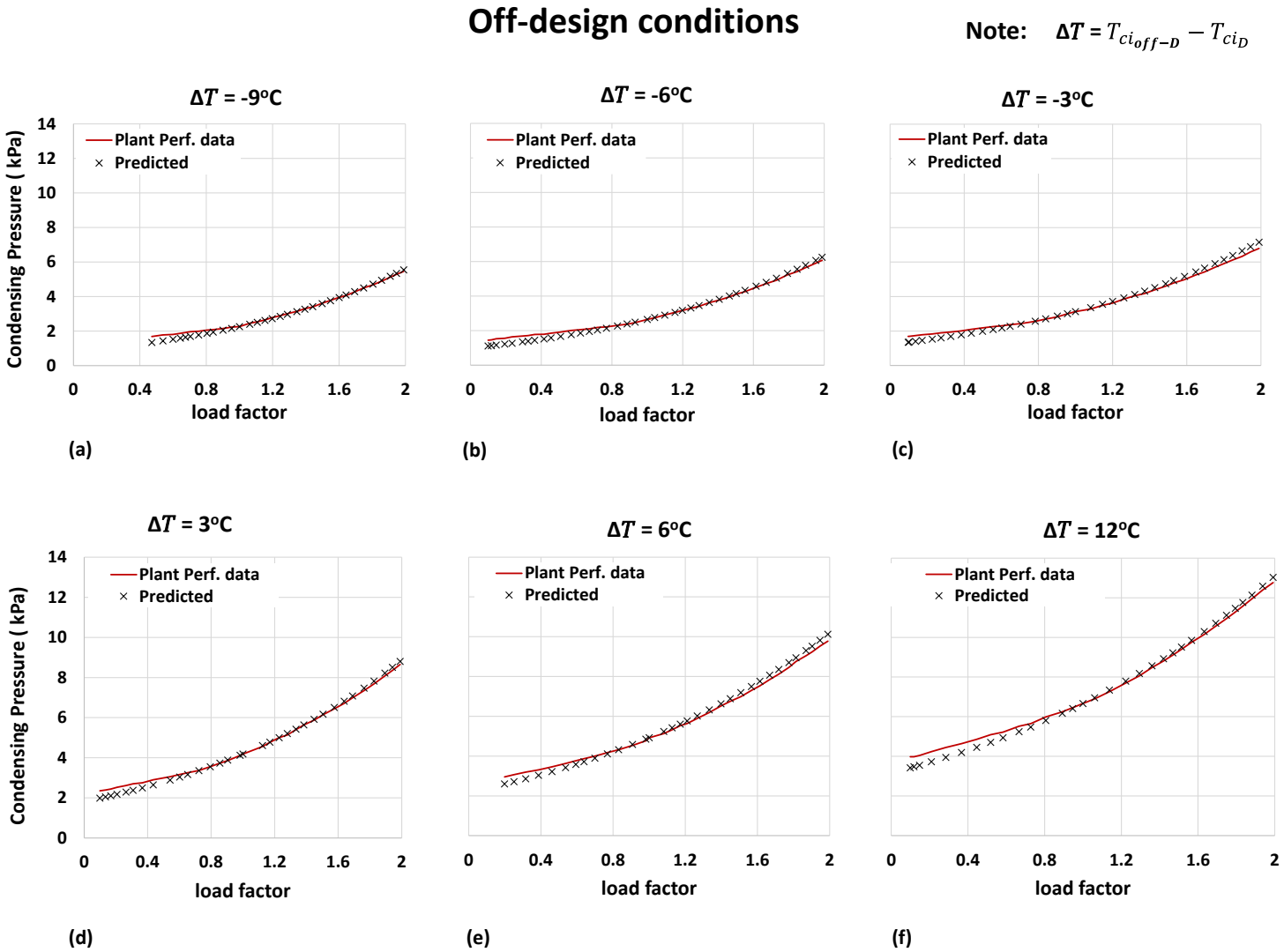

Figure 5.7 Predicted and actual condenser pressures for WCC-1 with inlet temperatures at various degrees away from the design point

The relative error (deviation) of the pressure response calculated for the WCC and the ACCs are shown in Figure 5.8 and Figure 5.9 respectively. It can be seen that the deviations for the WCC-1 is around 5% for most of the inlet conditions, and for load factors greater than 1. The deviations tend to be much higher at cooling inlet temperatures below the design inlet cooling temperature. The relative error is slightly worse for the ACCs. This may be related to the specific heat capacity of air at low temperatures and the increased performance of the fans at higher densities. These observations indicate that the assumption of a constant effectiveness might be too coarse for inlet cooling temperatures that are far away from the design inlet cooling temperature in the case of ACCs.

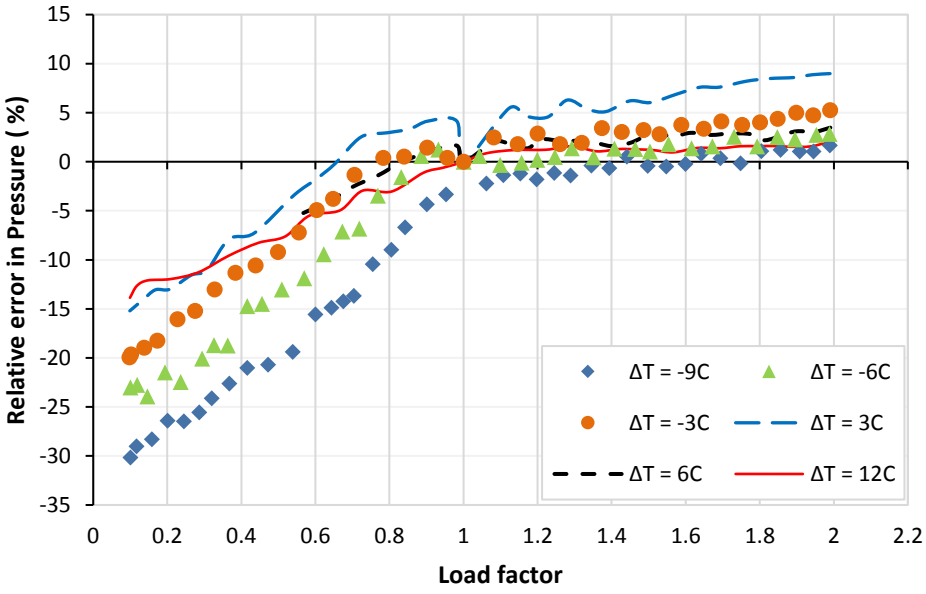

Figure 5.8 Differences in pressure predicted for WCC-1

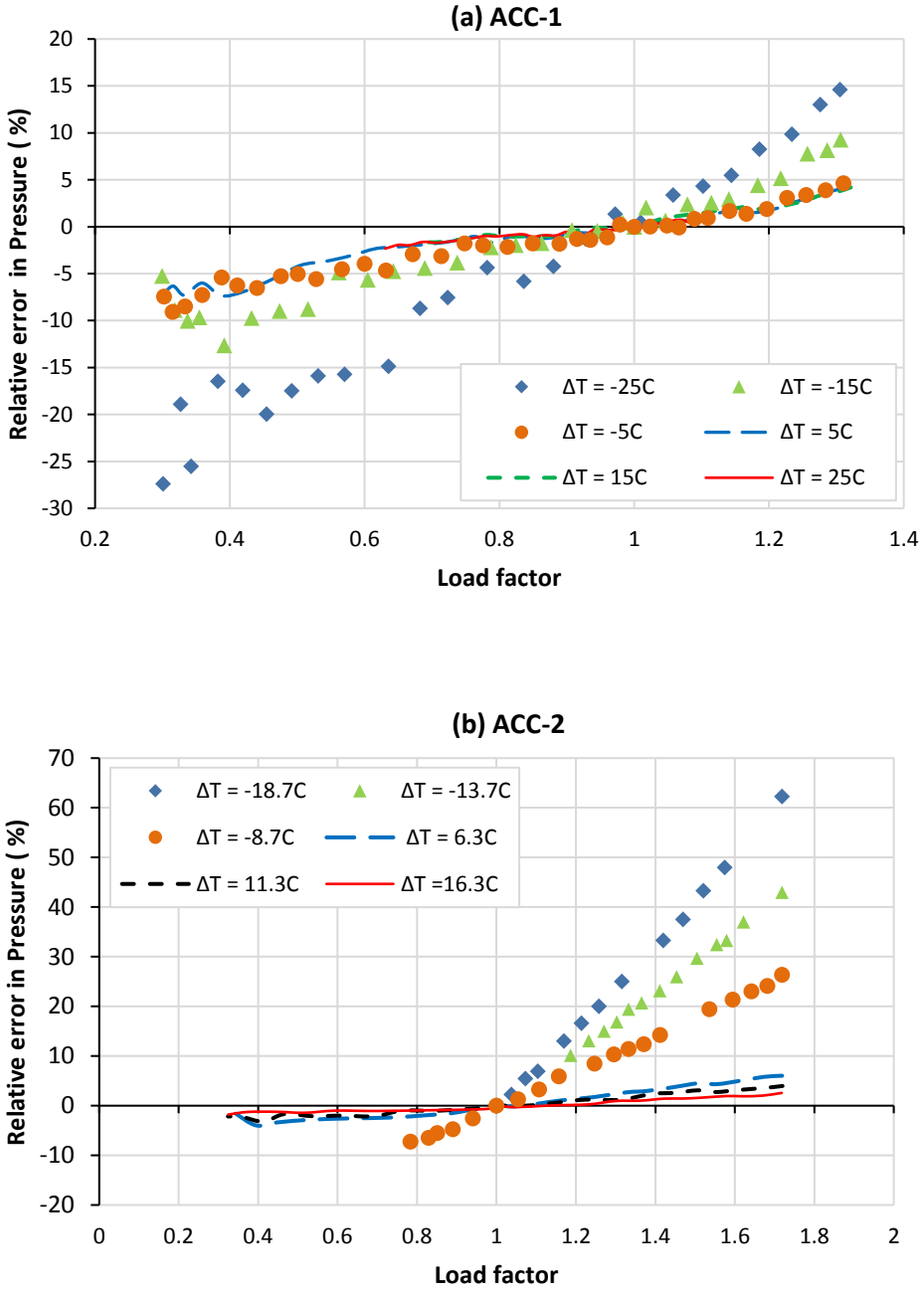

Figure 5.9 Differences in condenser pressure predicted for the ACCs

Adjustments can be made to reduce the deviations observed for varying load, and for different cooling fluid inlet temperatures. This is achieved by performing an error analysis on deviation of the condensing temperatures predicted. The adjusted condensing temperature (T_{hi}^{*}) at different load can be evaluated using Equation (5.15).

$$T_{hi}^{*} = T_{hi} - Err_{T_{ci}}(X) \tag{5.15}$$

$Err_{T_{ci}}(X)$ is the correction function for the effect of varying load at various cooling fluid inlet temperatures.

The deviations of the condensing temperature predicted for the three condensers are displayed on Figure 5.10. The deviations in the ACC systems appear to be linear for the full load factor range. For the WCC system, the deviation is almost insignificant at above full load, but approximately linear at low load. The slope for each line is displayed on the graph given they cross the zero point.

Because of the linear nature, one can easily obtain the slope for any plant, by having one additional low load dataset for the condensing temperature. The adjustment slope is then defined for an additional load point A as:

$$C_{adj} = \frac{T_{h,pred.A} - T_{h,known.A}}{X_A - 1} \tag{5.16}$$

$T_{h,known.A}$ and X_A are the known condensing temperature and the load factor respectively at point A. $T_{h,pred.A}$ is the condensing temperature predicted at load point A using the constant effectiveness approach.

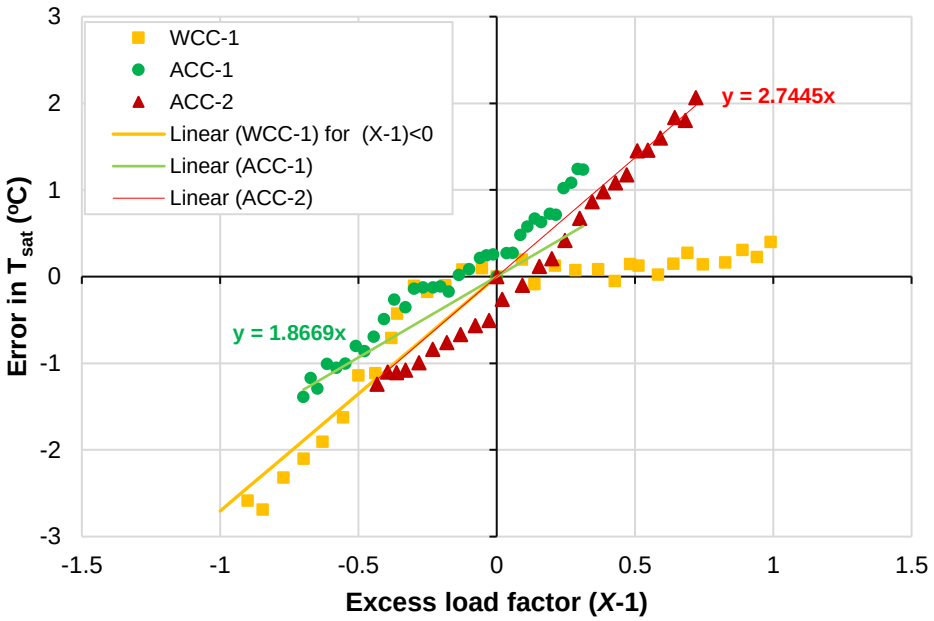

Figure 5.10 Error Analysis of condensing temperature at design cooling inlet temperature

The adjusted condenser temperature is thus defined by:

$$T_{hi} = \frac{T_{ci} - \left(T_{ci} + X \cdot \Delta T_{rise_D}\right) \cdot e^{\left(\frac{\Delta T_{rise_D}}{\Delta T_{LM_D}}\right)}}{1 - e^{\left(\frac{\Delta T_{rise_D}}{\Delta T_{LM_D}}\right)}} - C_{adj} \cdot (X - 1) \qquad (5.17)$$

A plot of the adjusted condenser pressure response at the design inlet cooling fluid temperature is shown in Figure 5.11 (a) –(c). For all the three systems investigated, the relative error is now within a very small margin of $\pm 4\%$.

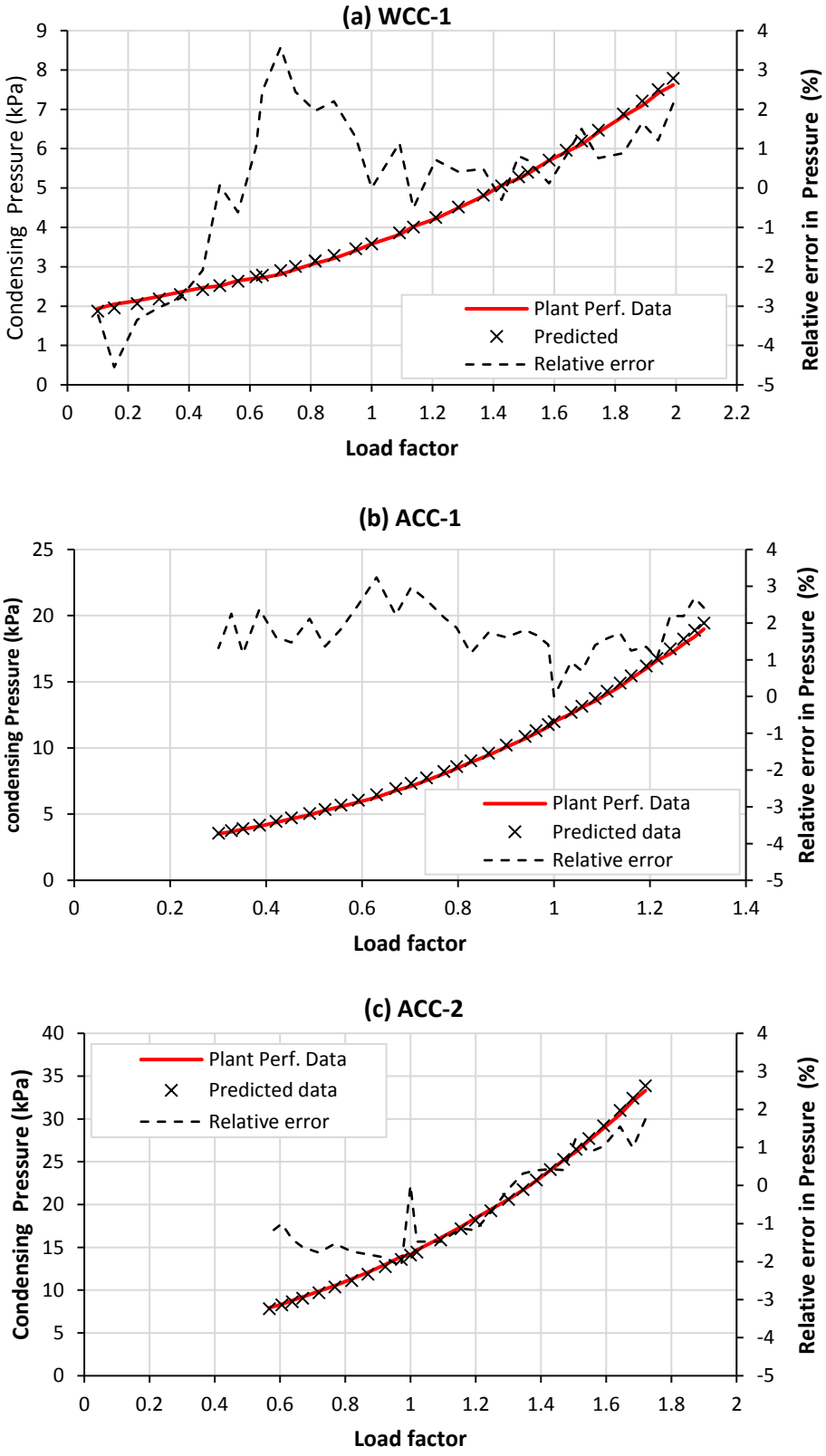

Figure 5.11 Adjusted Condenser pressures at design cooling inlet fluid temperature

In a similar manner, the adjustment coefficients for the error function at different cooling inlet temperatures is shown on Figure 5.12. The value of the coefficient differs for different inlet cooling temperatures. It is generally higher for cooling inlet fluid temperatures that are less than the design inlet condition. It therefore implies that for each inlet cooling temperature, the adjustment coefficient of the error function can also be determined by knowledge of an additional load point.

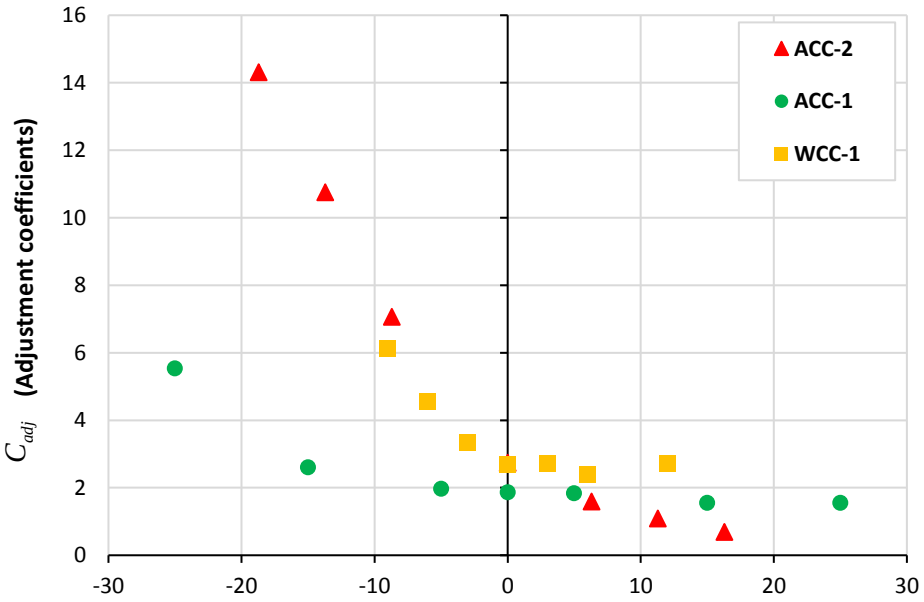

Figure 5.12 Adjustment coefficients for other cooling fluid inlet temperatures

5.4 Conclusions of the chapter

The main argument put forward in this chapter is that the constant condenser effectiveness assumption is an adequate model for predicting the pressure response of the main steam condensers of steam power plants operating at various heat rejection loads, and/or for different cooling fluid inlet temperature conditions. This model assumed the effects of air moisture content, wind speed and direction for ACC systems is insignificant.

The pressure response of three existing steam power plant main condensers (2 Air-cooled condensers and 1 Wet cooled condenser) were predicted at different loads, and for different cooling fluid inlet temperatures using the proposed method. The model results were validated by the performance data from these condensers.

At design and operating inlet temperature conditions, the model appears to work within a reasonable accuracy limit, while the accuracy of the model is poor at extreme cooling inlet temperatures and very low loads. The accuracy of the model can be improved by including an adjustment coefficient for each cooling fluid inlet temperature. The adjustment coefficient can be determined with the knowledge of one other load point.

The benefit of using this method despite the crude assumptions made, is that the performance of an existing main steam condenser can be quickly determined without knowledge of the condenser's geometrical parameter information such as number of tubes, water passes, diameter of tubes etc. It only requires knowledge of the condensing temperature, cooling fluid inlet and outlet temperatures at the steady state full load condition of the plant. The results predicted in this model may not be as accurate as the HEI Code, however, this approach is particular helpful in the absence of proprietary information, and will allow easy modelling of complete power plant systems with minimal design information.

This approach was adopted in Chapter 6, for predicting the condensing pressure of all the model CFPPs at varying load condition, with the exception that the additional adjustment has not been done because there is not an actual low load data point available.

6. Generic CFPP process model set-up, simulation and validation

This chapter presents the final aspect of the generic CFPP model development methodology, which involves setting up process models for CFPPs using the VirtualPlant software, simulating the models at various low load conditions, and the validation of the results from the models. A full description of each procedure is presented in this chapter.

6.1 Description of the VirtualPlant Software Used

EtaPRO Virtual Plant is the computational tool that was used in this research for investigating the variation of TCHR with load for each CFPP investigated. The tool was developed by General Physics Strategies [189]. VirtualPlant^{TM} is a commercially available tool for modelling the steady state thermodynamic behaviour of Rankine (Steam) and gas powered cycles [122] [189]. It forms part of the online EtaPRO Power Plant condition monitoring system, where VirtualPlant models are used to predict the performance at a specific operating condition, and compare this with the measured values from the plant [122] [189]. It includes more than 500 calculations for different components of steam, gas, nuclear, and combined cycle power plants [122]. VirtualPlant^{TM} applies thermodynamic first principles of energy and mass balance, ASME Performance test codes (PTC) and Heat Exchanger Institute (HEI) codes for relevant key components such as steam turbines, feed water heaters, and condensers to predict the overall performance of CFPPs for different operation conditions and environments.

The VirtualPlant software has a parametric study add-in feature in Microsoft Excel. This feature enables one to carry out different kinds of parametric studies. A sample display of the excel parametric study is shown on Figure 6.1. The impact of changing various system variables such as the power generation and the condensing pressure of the CFPP on other process and performance parameters such as the TCHR, can easily be investigated using this parametric study feature. The procedure for performing a parametric study is fully described in [190].

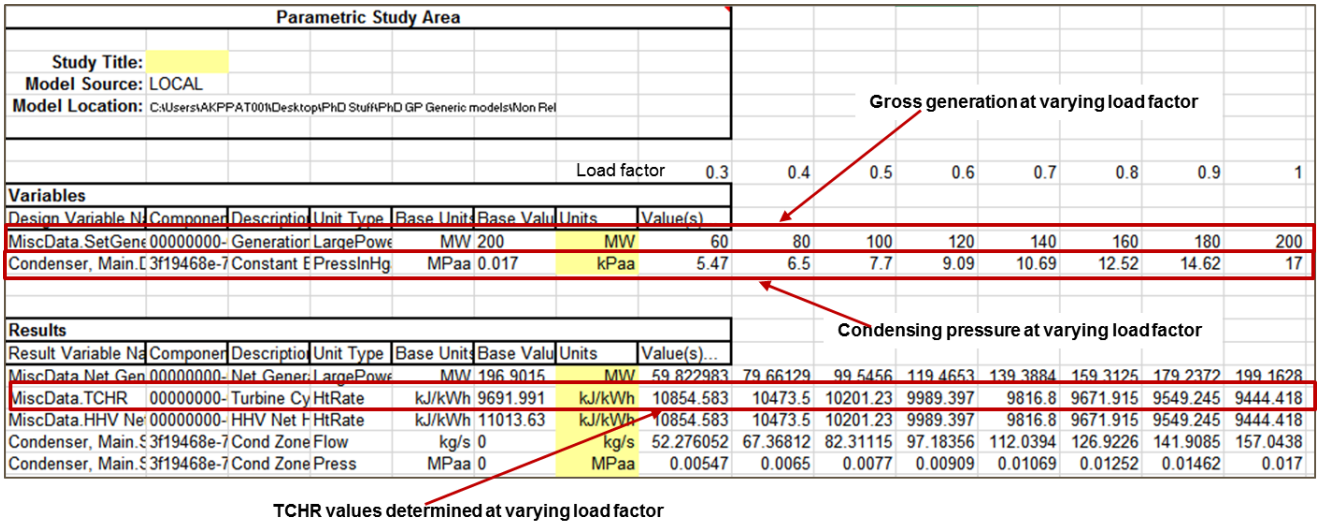

Parametric Study Area

Study Title:
Model Source: LOCAL
Model Location: C:\Users\AKPPAT001\Desktop\PhD Stuff\PhD GP Generic models\Non Rel

Gross generation at varying load factor

	Load factor	0.3	0.4	0.5	0.6	0.7	0.8	0.9	1
Variables									
Design Variable Na	Componen	Descriptio	Unit Type	Base Units	Base Valu	Units	Value(s)		
MiscData.SetGene	00000000-	Generatior	LargePowe	MW	200	MW	60	80	100	120	140	160	180	200
Condenser, Main.D	3f19468e-7	Constant E	PressInHg	MPaa	0.017	kPaa	5.47	6.5	7.7	9.09	10.69	12.52	14.62	17
Results														
Result Variable Na	Componen	Descriptio	Unit Type	Base Units	Base Valu	Units	Value(s)...							
MiscData.Net Gen	00000000-	Net Gener	LargePowe	MW	196.9015	MW	59.822983	79.66129	99.5456	119.4653	139.3884	159.3125	179.2372	199.1628
MiscData.TCHR	00000000-	Turbine Cy	HtRate	kJ/kWh	9691.991	kJ/kWh	10854.583	10473.5	10201.23	9989.397	9816.8	9671.915	9549.245	9444.418
MiscData.HHV Ne	00000000-	HHV Net H	HtRate	kJ/kWh	11013.63	kJ/kWh	10854.583	10473.5	10201.23	9989.397	9816.8	9671.915	9549.245	9444.418
Condenser, Main.S	3f19468e-7	Cond Zone	Flow	kg/s	0	kg/s	52.276052	67.36812	82.31115	97.18356	112.0394	126.9226	141.9085	157.0438
Condenser, Main.S	3f19468e-7	Cond Zone	Press	MPaa	0	MPaa	0.00547	0.0065	0.0077	0.00909	0.01069	0.01252	0.01462	0.017

Condensing pressure at varying load factor

TCHR values determined at varying load factor

Figure 6.1 Parametric study features of VirtualPlant software

The EtaPRO platform is currently used for the condition monitoring of all Eskom's conventional fossil based power plants in South Africa.

6.2 Setting up the CFPP Steam cycle Process models in VirtualPlant™

Figure 6.2 highlights the steps that were undertaken before any of CFPP steam cycle process models were built in VirtualPlant.

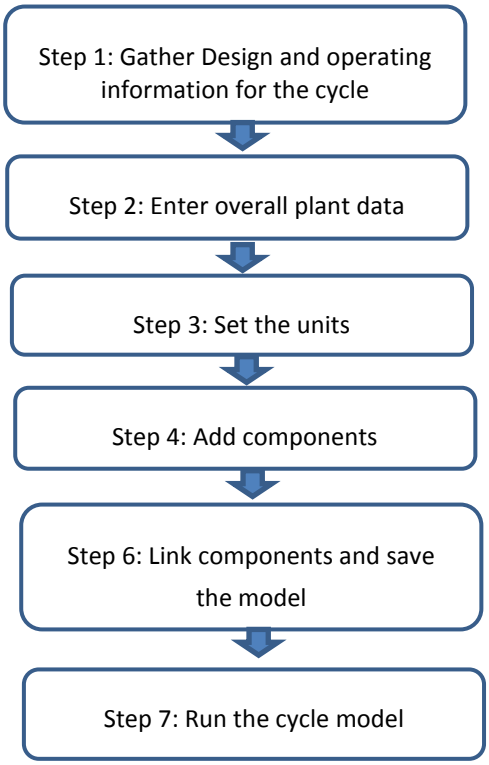

Figure 6.2 Major steps to building a CFPP steam cycle model in VirtualPlant™

The first step involved gathering design and operating information for the steam cycle. One of the most important information required for the CFPP steam cycle process model development is the VWO heat balance diagram. The process conditions for this diagram was obtained for each process model through the procedure described in section 3.9. The other information required include the characteristics of components such as boiler, pump, condenser, cooling systems etc. The typical values chosen for the process models have already been highlighted in Table 3.3. The exhaust loss curve shown on Figure 3.5 was used. Once a new model file is created, the overall plant data (see Figure 6.3), and the appropriate SI unit set and IF97 Steam Properties formulation were selected in steps 2 and 3 respectively.

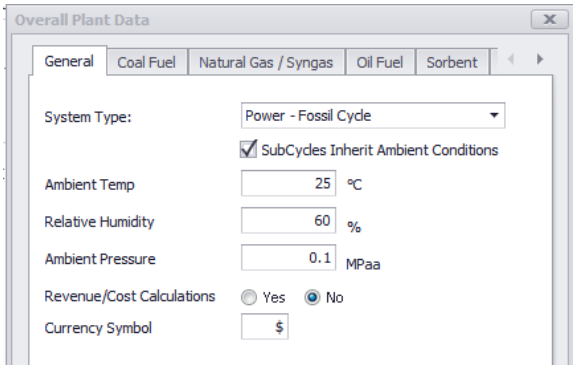

Figure 6.3 Overall plant data selected

The components required for setting up the process models of the NRH, SRH, and DRH CFPPs were then added, and linked in a logical manner from one component outlet to the appropriate inlet of another component. Figure 6.4, Figure 6.5, and Figure 6.6 shows the process model layout for the NRH, SRH, and DRH CFPPs respectively. The VirtualPlant process model for the NRH CFPP (see Figure 6.4) has a non-reheat drum type boiler, a control valve, a non-reheat steam turbine for modelling the HP and LP turbines, a generator, condenser, 3 pumps, 6 FWHs and 6 steam extraction pipes, and mixer. The VirtualPlant process model for the SRH CFPPs (see Figure 6.5) has a once-through type single reheat boiler, a control valve, an HP turbine , an IP-LP turbine model, a generator, condenser, 3 pumps, 6 FWHs and 6 steam extraction pipes, a mixer, and a splitter. The VirtualPlant process model for the DRH CFPPs (see Figure 6.6) has a once-through double reheat type boiler, a control valve, a HP turbine, a generic turbine for modelling the 1st IP turbine, an IP-LP turbine for modelling the second IP turbine and the LP turbine, a generator, condenser, 3 pumps, 8 FWHs and 8 steam extraction pipes, a mixer, and 2 splitters.

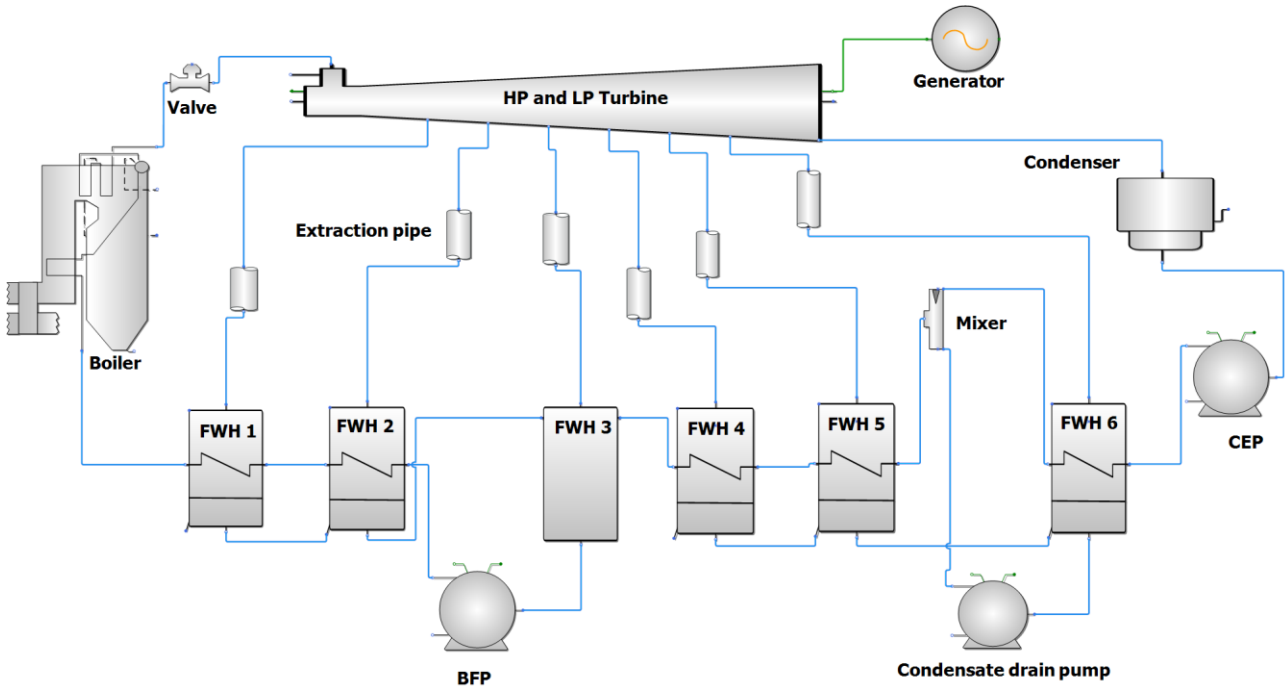

Figure 6.4 Non-reheat CFPP model in VirtualPlant

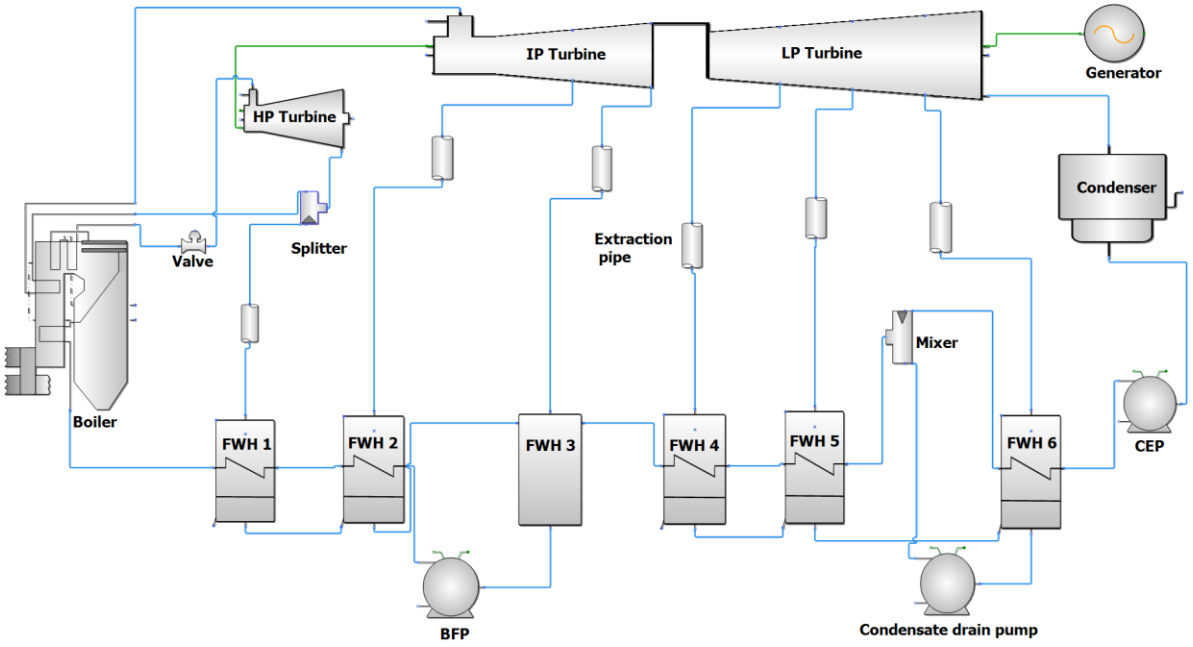

Figure 6.5 Single reheat CFPP model in VirtualPlant

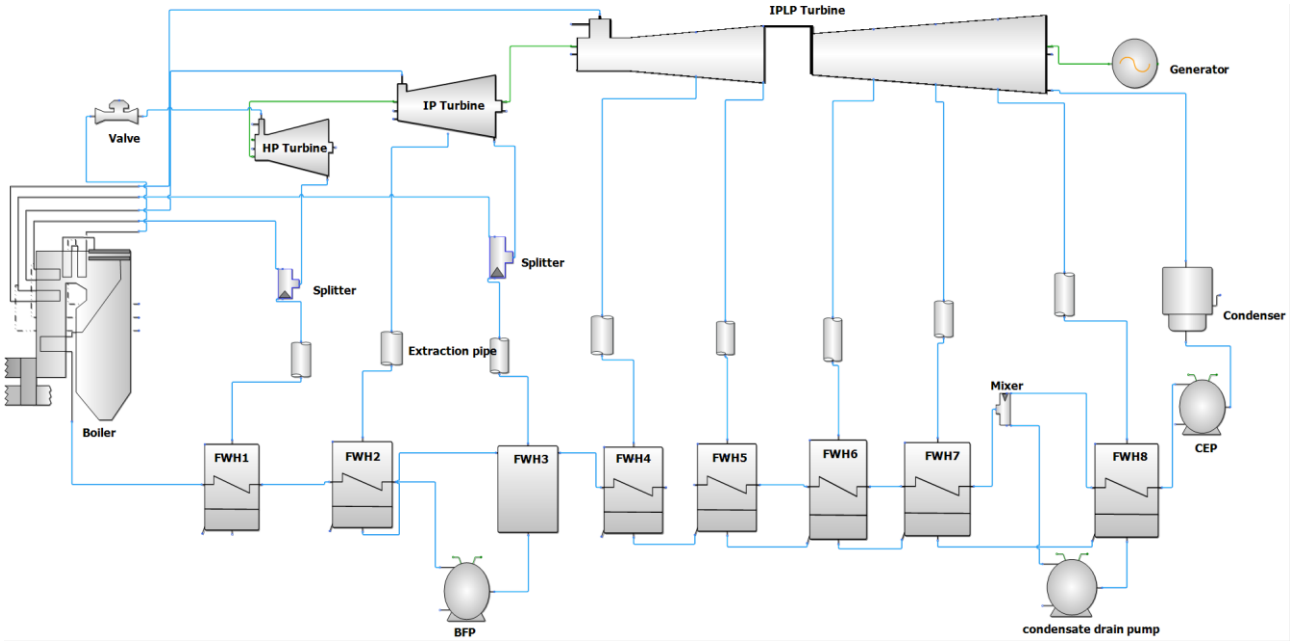

Figure 6.6 Double reheat layout CFPP model in VirtualPlant

The description of each of the aforementioned components and how they were configured is given in section 6.3.

Once all the components were properly linked and configured on the VirtualPlant process flowsheet, then it was run to ensure that convergence is achieved. The results was examined for consistency with the input heat balance diagram data. The dialogue box showing the set-up for calculating the gross generation is shown on Figure 6.7. VirtualPlant does this calculation by varying the mass flow through the system. The maximum number of iterations specified for each calculation was 100. The maximum convergence tolerance limit set was 0.01%. This value represents the percent difference between the heat input to the cycle and the heat output to the cycle. A tolerance limit of 0.01% is reasonable and typical for most steam power calculations [190].

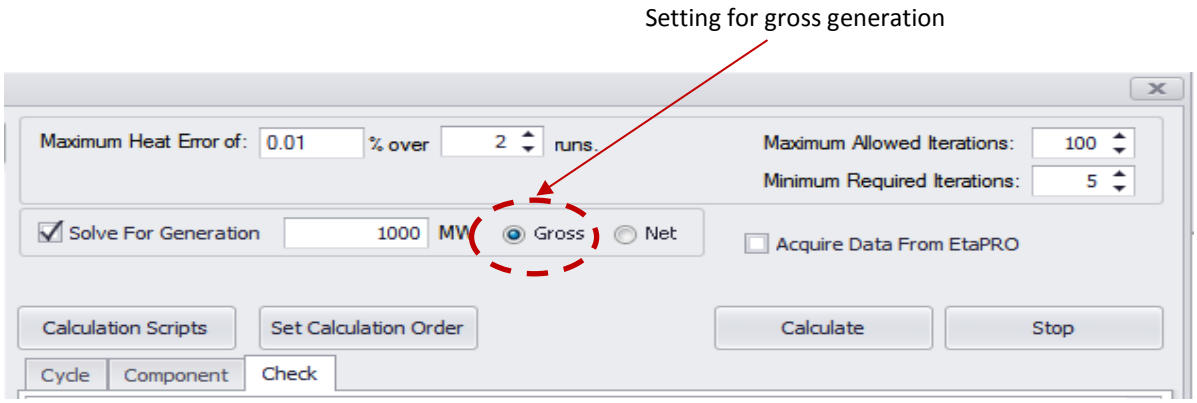

Figure 6.7 Dialog box showing set-up for gross generation

6.3 Configuration of VirtualPlant process model components

6.3.1 Steam boilers

The three different types of steam boiler types were used in the VirtualPlant CFPP process model development as shown in Figure 6.8. The fundamental difference between the types of boilers are the number of re-heat stages. All the boiler models can be calculated using two different modes: Heat transfer and the Simple boiler mode.

The heat transfer mode of these boilers use standard heat transfer correlations to model conditions of the steam and flue gas across the different sections of the boiler [190]. The sections of the boiler are the furnace, convective surfaces, and the air heater. This model allows the impact of changes in fuel, excess air, and heat transfer surfaces cleanliness factor to be passed to the turbine cycle model. It requires the specification of various geometrical and design parameters that are often linked to specific boilers. For this reason it was not used, as the actual heat profile inside the boiler is not significant for the Rankine cycle calculations.

The simple boiler mode requires much less detail, such as the design or VWO superheater and reheater(s) outlet steam conditions, and the spray conditions as fixed values (see Figure 6.9.). The model is basically a "black box" for setting inputs to the turbine cycle model.

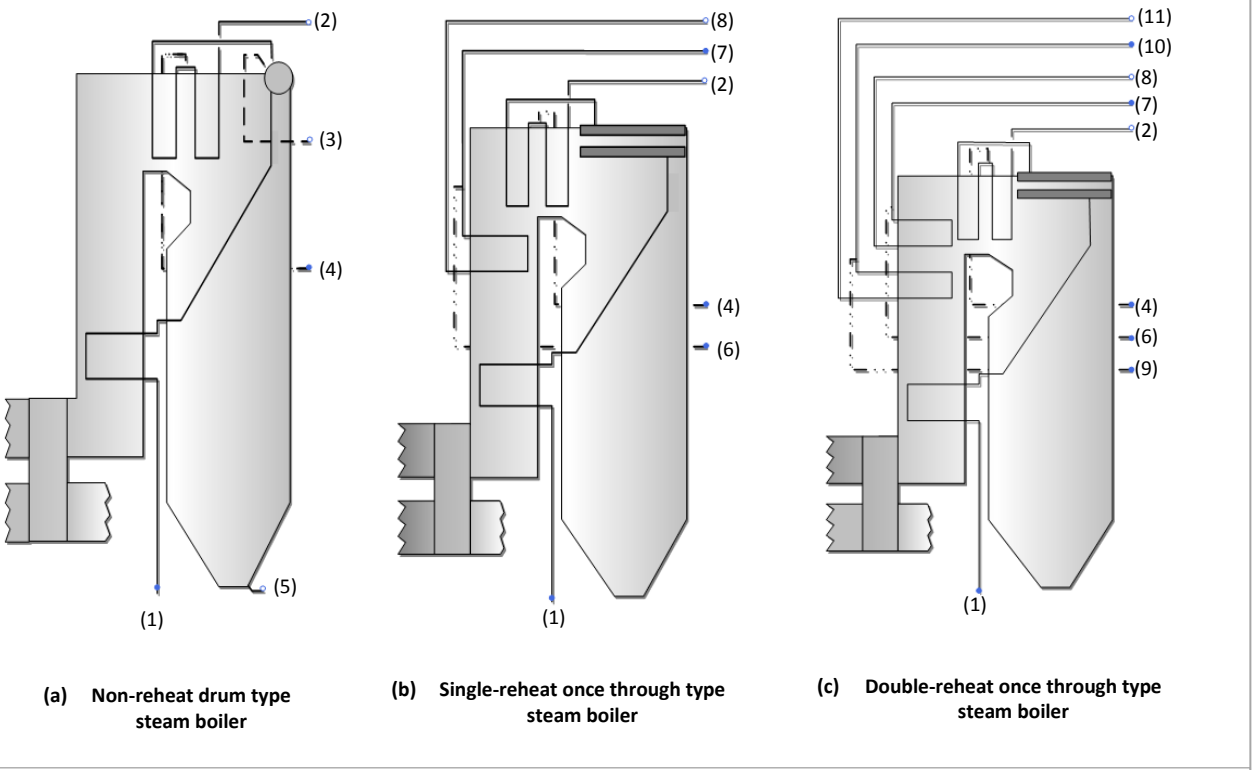

For the numberings on the boilers. (1). Feed water inlet (2). Superheater steam outlet (3). Auxiliary steam taken from steam drum (4) Superheat spray (5) Boiler blow down. (6) Reheater spray (7) Reheater steam inlet (8) Reheater steam outlet (9) Low pressure reheater spray (10). Low pressure reheater steam inlet (11) low pressure reheater steam outlet.

Figure 6.8 Steam boiler models that were used in the VirtualPlant process models

It is very useful in setting up turbine cycle heat balance diagrams at various load conditions, as well as evaluating performance test data [190]. Depending on the type of boiler, this simple model requires the specification of additional information as shown in Figure 6.9. Some of the information are not applicable to non-reheat CFPPs and single reheat CFPPs. The numerical value of the boiler efficiency specified (100%) in the boiler input panel, is irrelevant to the turbine cycle heat rate evaluation. The boiler efficiency only comes into play when considering the fuel consumption and NUHR, but this will be evaluated differently in this study. This also means that the coal definition is not important in setting up the VirtualPlant models.

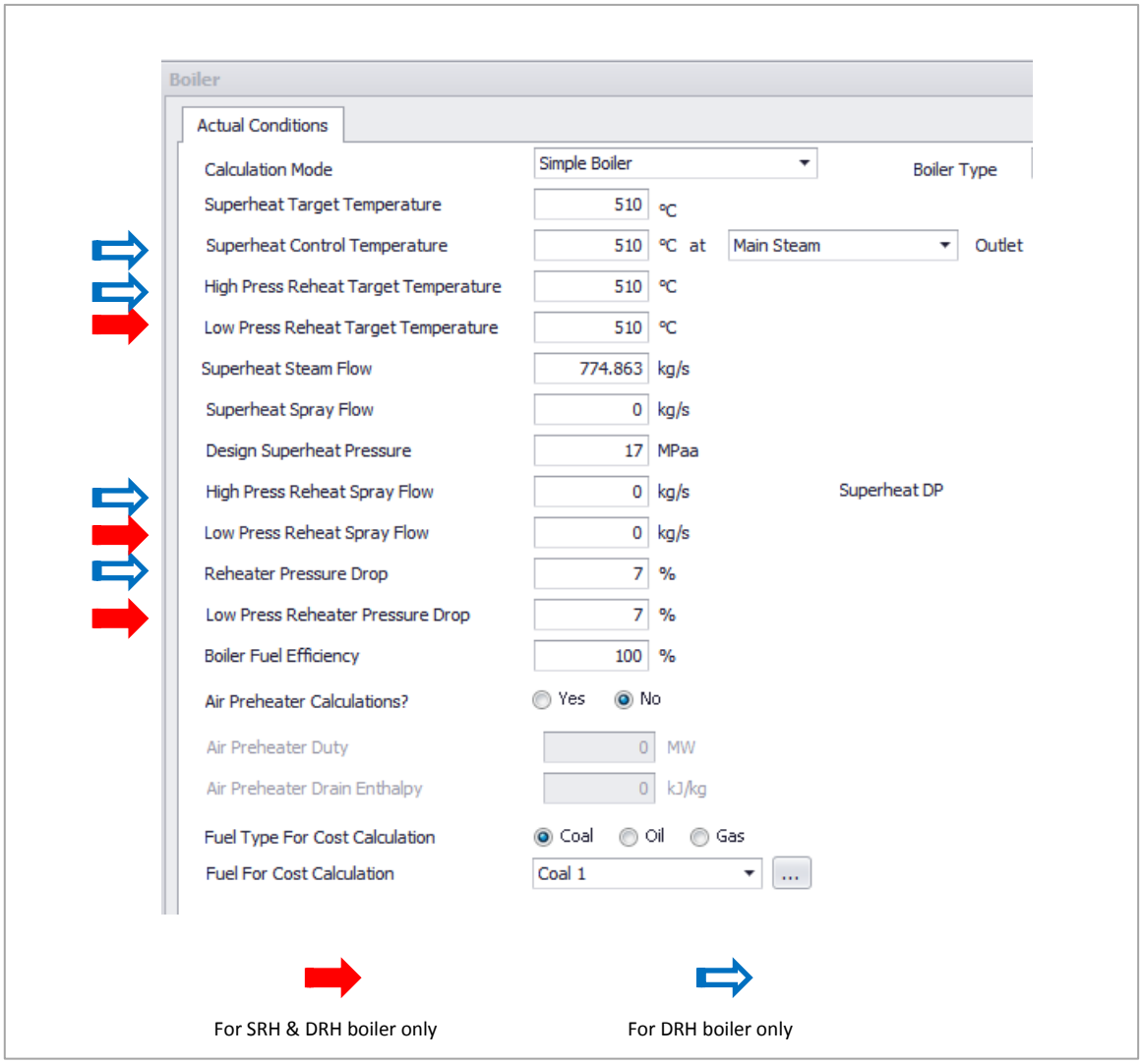

Figure 6.9 Simple boiler model Inputs required to configure the different steam boilers

6.3.2 Steam turbines & generator

The four different VirtualPlant steam turbine models that were used are shown on Figure 6.10. The first turbine model (see Figure 6.10a) was used for modelling the high pressure turbine for the single and double reheat CFPPs. The IP-LP turbine model (see Figure 6.10b), was used to model the IP and LP turbines for the single and double reheat CFPPs. The non-reheat turbine model (see Figure 6.10c) was used to model the HP and LP turbines of the non-reheat CFPPs only while the double reheat turbine model in (see Figure 6.10d) was used to model the second IP turbine of the double reheat CFPPs.

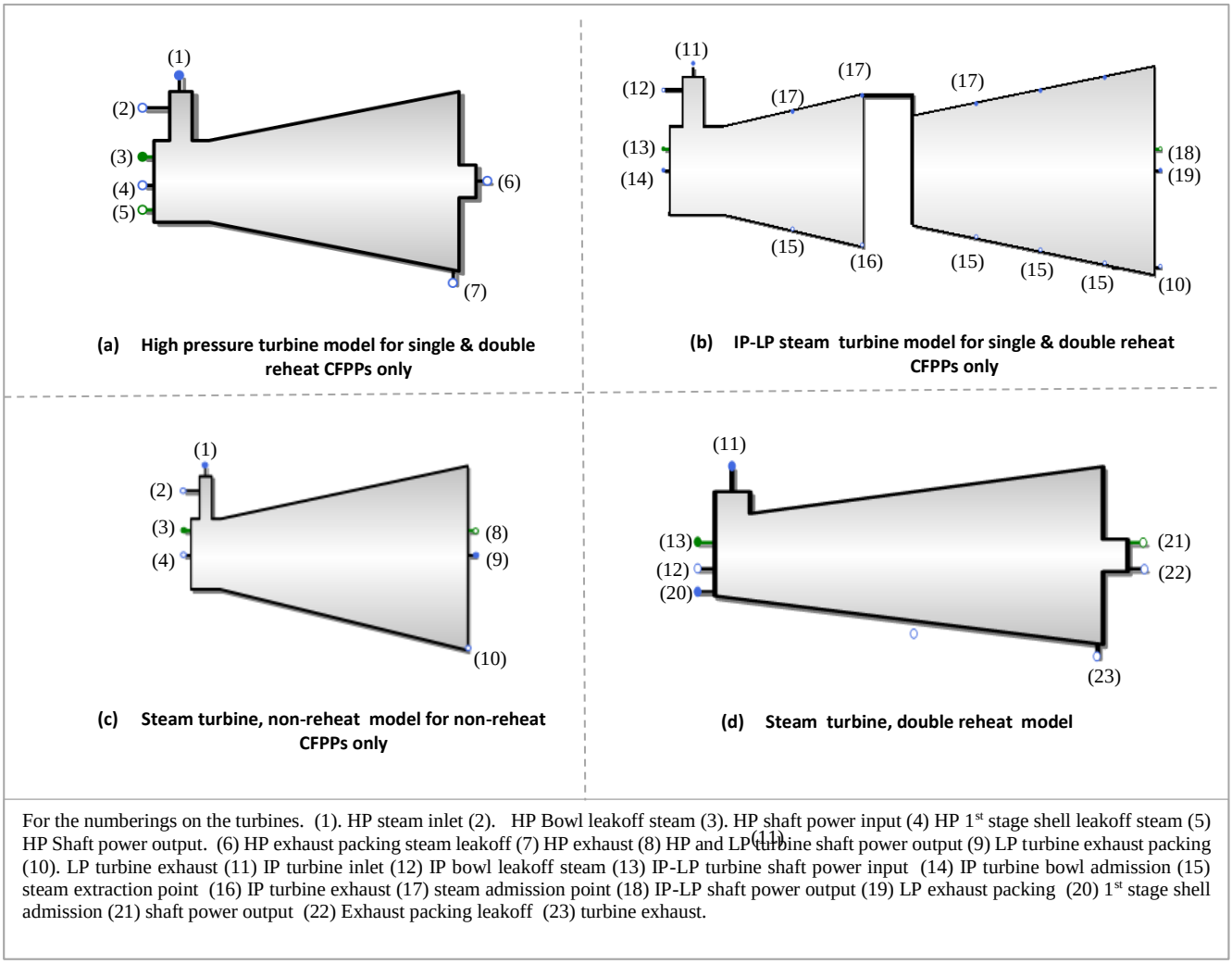

For the numberings on the turbines. (1). HP steam inlet (2). HP Bowl leakoff steam (3). HP shaft power input (4) HP 1st stage shell leakoff steam (5) HP Shaft power output. (6) HP exhaust packing steam leakoff (7) HP exhaust (8) HP and LP turbine shaft power output (9) LP turbine exhaust packing (10). LP turbine exhaust (11) IP turbine inlet (12) IP bowl leakoff steam (13) IP-LP turbine shaft power input (14) IP turbine bowl admission (15) steam extraction point (16) IP turbine exhaust (17) steam admission point (18) IP-LP shaft power output (19) LP exhaust packing (20) 1st stage shell admission (21) shaft power output (22) Exhaust packing leakoff (23) turbine exhaust.

Figure 6.10 the steam turbine models used

On the HP turbine model, it is very important to specify the right method for determining the operating pressure conditions at the inlet of this turbine. This is done by selecting the variable pressure (Constant: flow sqrt (P/v)) option on the configuration panel for steam turbine operating conditions (see Figure 6.11). The importance of this setting together with the control valve setting on Figure 6.12 is critical to ensure the constant turbine efficiency assumption is valid.

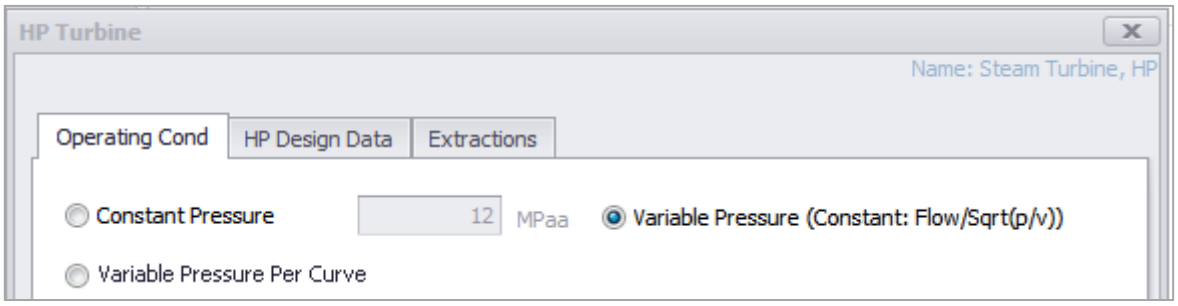

Figure 6.11 configuration panel for steam turbine operating conditions

The control valve shown on Figure 6.12, was used to control the live steam pressure. The control valve and its configuration panel is shown on Table 3.3. There is no flow and temperature control. However, there is need to control the inlet pressure. The method of pressure control selected was dependent on the mode of boiler pressure control. For the fixed boiler pressure calculations, the pressure control of the valve setting was used to control the valve inlet pressure (or boiler superheater pressure) to the specified live steam pressure at full load. For the sliding boiler pressure mode calculations, the "no pressure control (in =out)" method was selected.

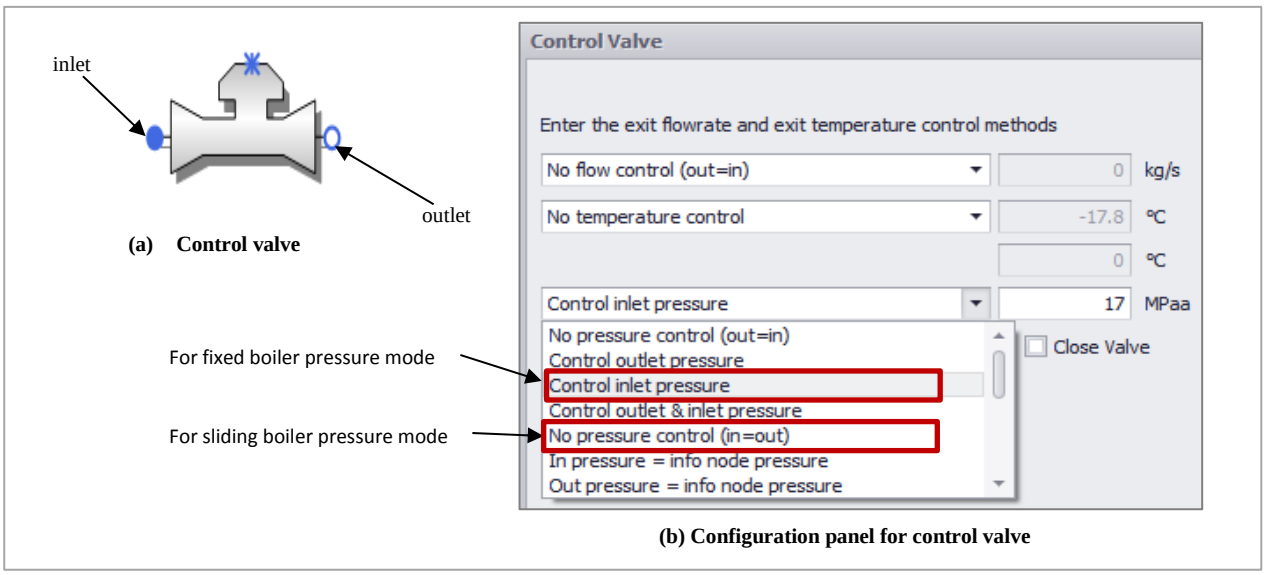

Figure 6.12 Control valve and configuration panel

The configuration panel for the HP turbine design information is shown on Figure 6.13. The configuration panel for specifying the design information of the other types of turbine is quite similar to this, except that reference is made to the relevant turbine efficiencies. A constant efficiency calculation model was selected for determining the HP, LP, and IP section efficiency of the different models. The design VWO flow is the main steam flow. The design VWO throttle temperature and pressure are the live steam pressure and temperatures respectively. Design VWO 1st stage shell pressure was determined in accordance with Table 3.3. The design VWO 1st stage shell enthalpy is the enthalpy that corresponds to the Design VWO 1st stage shell pressure and temperature. The design VWO 2nd stage flow was assumed to be equal to the design VWO flow. This implies that there are no leakages, extractions or steam admission between the 1st and second stage of the HP turbine. The first stage shell pressure calculation is done by using a constant flow coefficient relation (see Equation (6.1)). This same equation was used to determine the off-design pressures and/or flows in the turbines, steam extraction pipes, and other necessary points. It is defined as $C = W/sqrt(P/v)$ on the configuration panel of most VirtualPlant components. The mass flow in off design conditions is then calculated as:

$$m_{off-design} = m_{design} \times \sqrt{\frac{\left(\frac{P}{v}\right)_{off-design}}{\left(\frac{P}{v}\right)_{design}}} \tag{6.1}$$

m , P , and v are the mass flow, pressure and specific volume respectively.

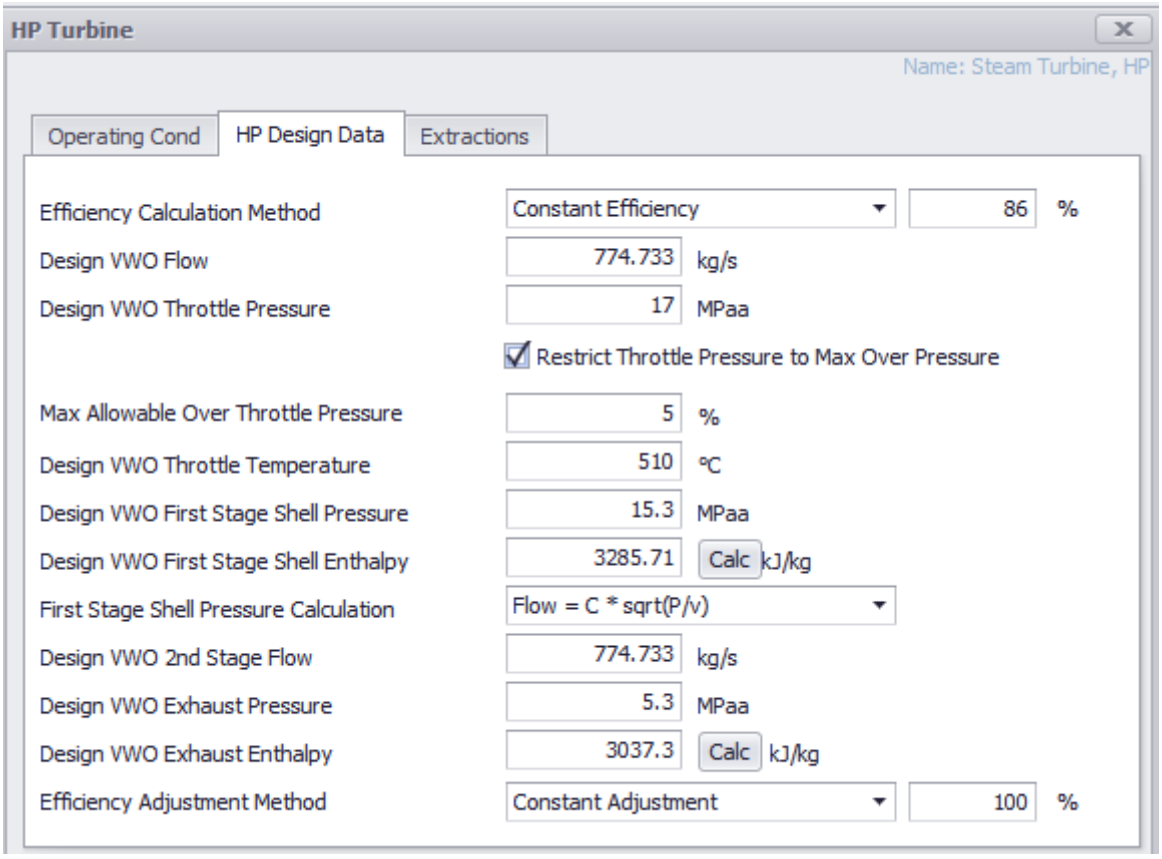

Figure 6.13 Turbine design data configuration panel

In configuring the extraction flows (see Figure 6.14) for each of the steam turbine types used, the flow coefficient equation was used to calculate the extraction pressures from the turbine. The design stage pressure, enthalpy and flow to the next stage were also specified on the extraction/admissions configuration panel. For the IP-LP turbine model the IP exhaust extraction number is specified, for the non-reheat turbine model, the HP turbine exhaust extraction number is also specified.

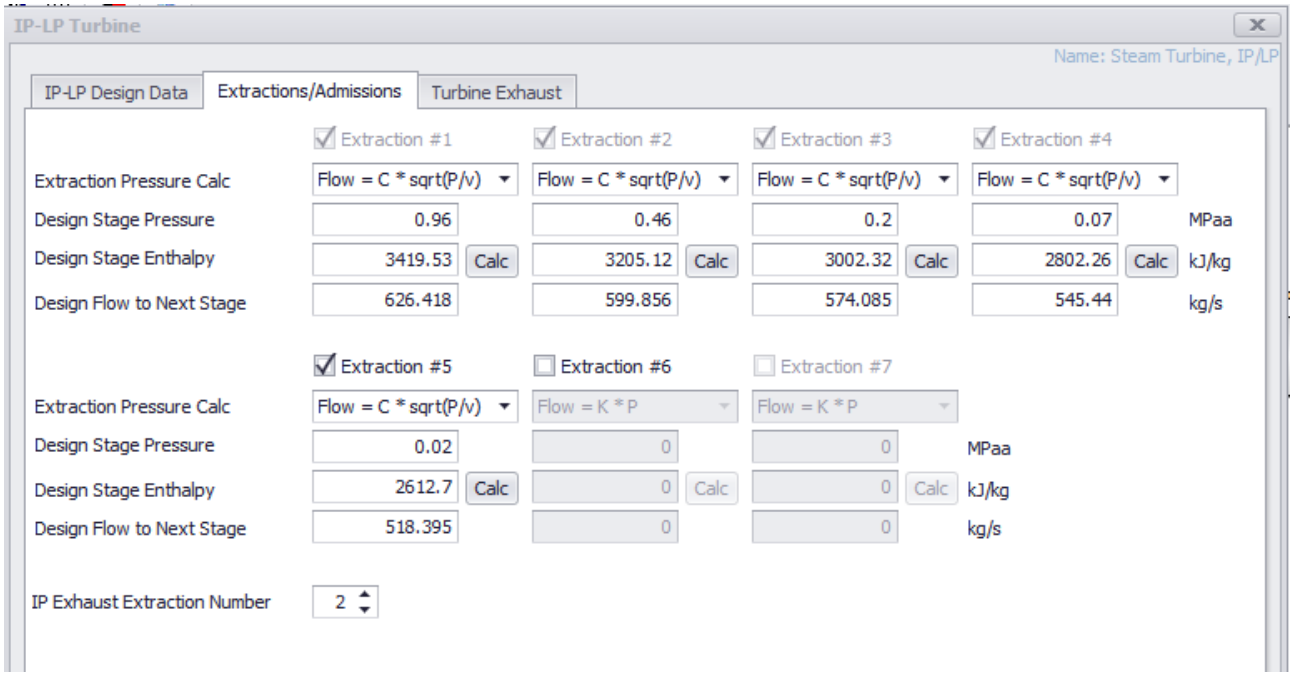

Figure 6.14 Turbine extraction configuration panel for an IP-LP turbine

The LP exhaust configuration panel for the non-reheat and IP-LP turbine models is shown on Figure 6.15. The “GE published curves exhaust calculation” method was used for all the VirtualPlant CFPP process models. This method is based on exhaust loss curves that were published by General Electric [85]. The number of exhaust ends and condenser zones specified was 1. The exhaust loss curve is a function of the last stage bucket (LSB) selected. An exhaust loss curve (see Figure 6.15b) that is based on LSB size of 0.851 m and generator speed of 3600RPM was selected. The last stage flow area per end can also be referred to as the exhaust annulus area for a single end turbine flow. It was specified for each VirtualPlant CFPP process model. This value was obtained through the process described in section 3.4.3.

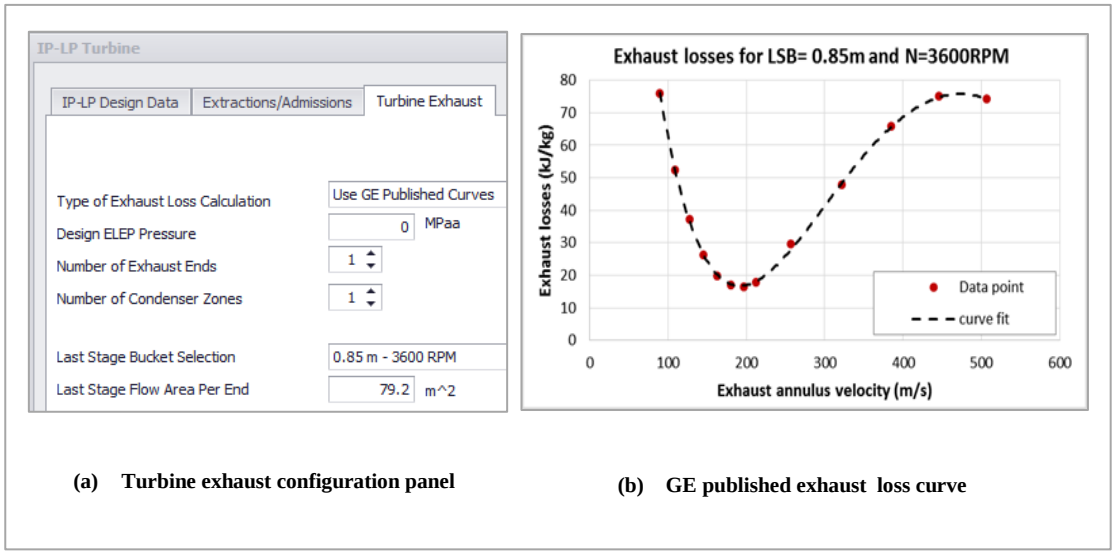

(a) Turbine exhaust configuration panel **(b) GE published exhaust loss curve**

Figure 6.15 LP turbine exhaust configuration panel

The generator model and its configuration panel is shown on Figure 6.16. This component enables the modelling of an electrical generator by using the GE 1962 method, which uses a design generator loss curve. The generator loss curves are published in [85]. The assumptions made for the generator model were: (a) All the turbines and generator were connected in tandem (b) the conventional cooling method was assumed, (c) a power factor of 90% was assumed, (d) A generator fixed losses of 1 kW/ 200kVA is assumed [85].

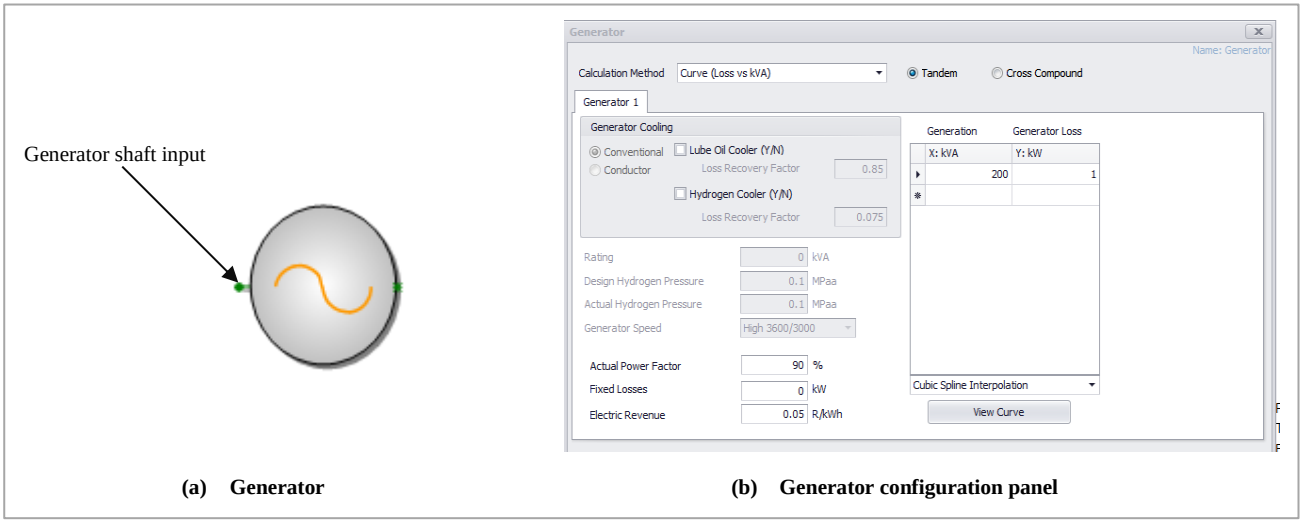

(a) Generator **(b) Generator configuration panel**

Figure 6.16 Generator model and configuration panel

6.3.3 Feed water heaters and condenser

The closed FWH model and the settings on its configuration panel are shown on Figure 6.17. The constant TTD/DCA calculation method with no drain cooler was used. This implies that the TTD is constant at all load conditions. The terminal temperature difference (TTD) and drain sub-cooling were set to zero for all the feed water heaters. The feed water inlet pressure and temperature of each FWH at VWO conditions were also specified. The calculation of the mass flow extracted by the FWH is done using an energy and balance calculation similar to type A FWH on Figure 3.24.

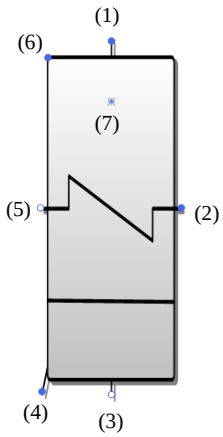

(a) **Closed FWH**

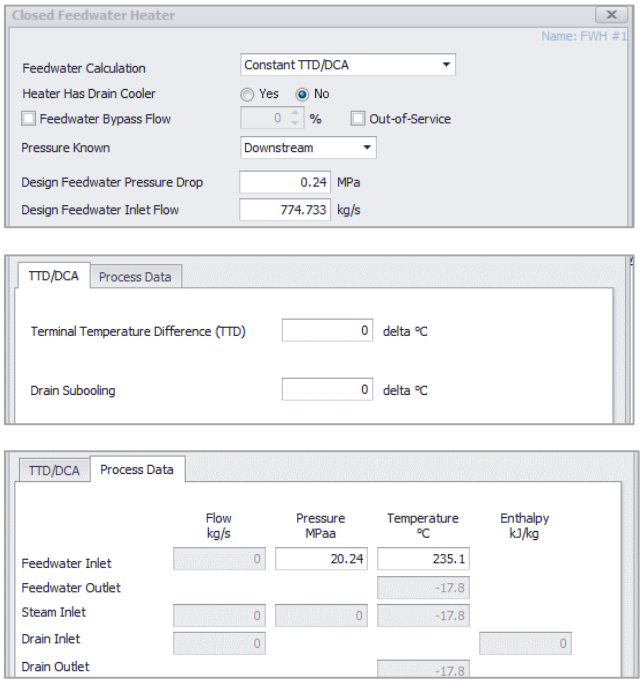

(b) **Configuration panel for a closed FWH**

For the numberings on the FWH. (1). Extraction steam inlet (2). Feed water inlet (3). Drain outlet (4) Drain inlet (5) Feed water outlet (6) special moisture removal extraction (7) extraction information.

Figure 6.17 Closed FWH model and configuration panel

The open FWH model and the settings on its configuration panel are shown on Figure 6.18. This component was used to model the deaerator in the steam cycle. The assumption used in this model is that the extraction steam pressure at node #1 is known from extraction pipe. An energy and mass balance calculation (similar to type C FWH on Figure 3.24) was done around the FWH inorder to

determine the extraction steam flow. The sub-cooling is assumed as zero while the FWH elevation is also assumed as zero.

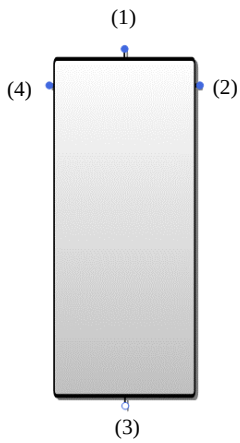

(a) Open FWH

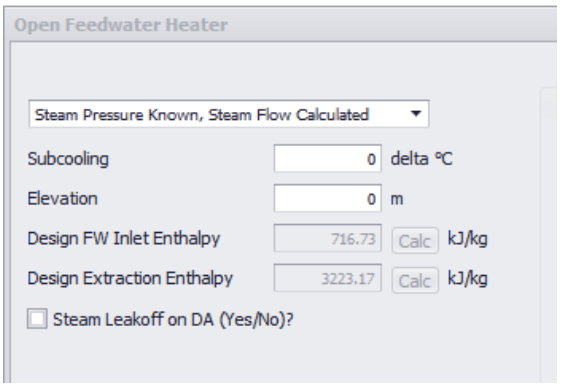

(b) Configuration panel for Open FWH

For the numberings on the FWH. (1). Extraction steam inlet (2). Feed water inlet (3). Feed water outlet (4) Drain inlet

Figure 6.18 Open FWH model and configuration panel

There are several options for modelling the main steam condenser component (see Figure 6.19) in VirtualPlant. The options include: (a) once-through condensing; (b) mechanical draft cooling-tower; (c) air-cooled condenser; and (d) constant backpressure. The first three options (a-c) adopt the 9th edition HEI code to determine the expected turbine backpressure (or condensing pressure) of different types of cooling systems. These options provide a basis for capturing the impact of changes in cooling fluid inlet condition, plugging of condenser tubes, etc. on the performance of the condenser. These options can only be used if the manufacturer's cooling tower curves and condenser geometrical specifications are available. The fourth option (the constant back pressure model) was adopted in this study. This option allows the user to specify the value of the condensing pressure and a sub-cooling (see Figure 6.19b) which will remain constant during the calculations [190]. For the varying load parametric studies carried out, the condensing back pressure specified at each load condition, and for each cooling system technology type was evaluated through the method that is described in chapter 5.

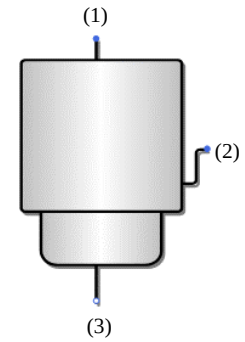

(a) Condenser

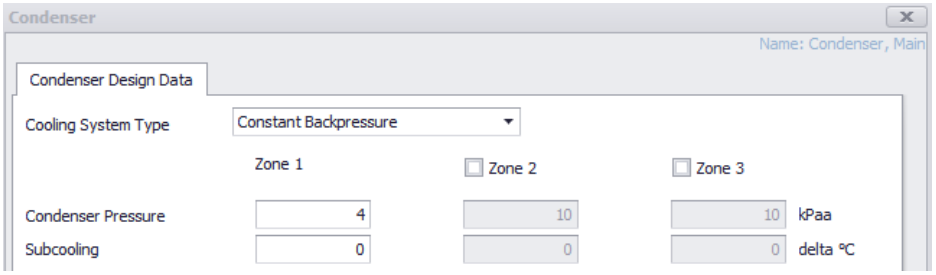

(b) Condenser configuration panel

For the numberings on the condenser. (1). Condensing steam inlet (2). Drains inlet (3). Condenser hotwell outlet

Figure 6.19 condenser model and configuration panel

6.3.4 Pumps

There are two main pump model types in VirtualPlant. The complex pump and a simple pump. The complex pump model gives a detailed model of the pump, provided that one can specify the design pump curve characteristics etc. The simple pump models the pump by a specification of a constant pump efficiency and the inlet and outlet flow conditions. The latter method was used to model the CEP, condensate drain pump, and BFP pumps. This pump model and the settings on its configuration panel is shown on Figure 6.20. A motor efficiency of 95% and an isentropic efficiency of 85% were specified. The pump was configured to always calculate the discharge flow from a known suction flow emanating from the extracted steam from the steam turbines. The suction and discharge pressures are assumed to be known from upstream and downstream components. A specification of the VWO conditions is also specified.

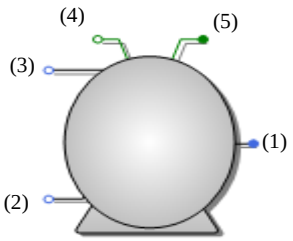

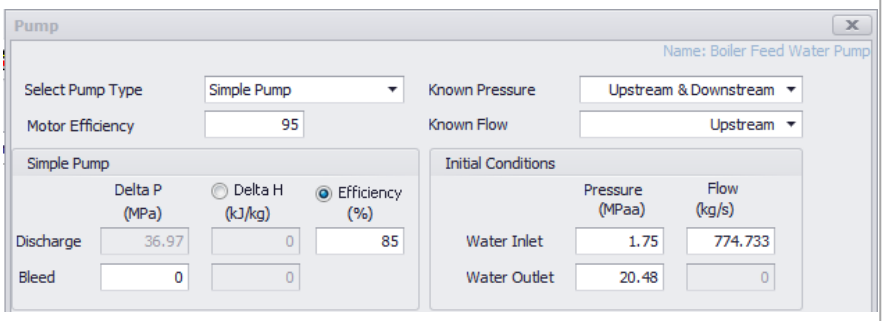

(a) Pump **(b) Configuration panel for a simple pump model**

For the numberings on the pump. (1). Pump suction (2). Interstage bleed (3). Pump discharge (4). Pump power output (5) Pump power input

Figure 6.20 Pump model and the configuration panel a simple pump model

6.3.5 Extraction pipes, splitters, and mixers

The steam extraction pipe model and the settings on the configuration panel is shown on Figure 6.21.

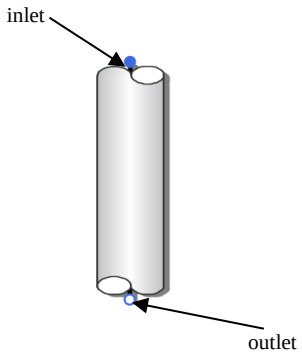

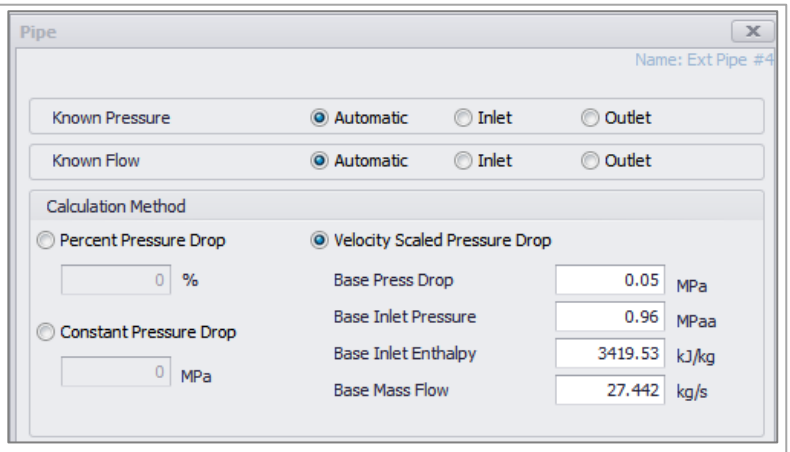

(a) steam extraction pipe **(b) Configuration panel for steam extraction pipes**

Figure 6.21 Steam extraction pipe and configuration panel

The velocity scale pressure drop calculation method was selected because the pressure drop at part and low conditions in the extraction pipe is dependent on the velocity of the steam flow. This

method accounts for the influence of the reduced steam extraction flow at low load conditions when determining the pressure drop from the steam extraction pipe. The relevant base (design) pressure drop, inlet pressure, inlet enthalpy and extraction mass flow are also specified for each pipe. The design pressure drop was calculated applying a 8% pressure drop to the VWO/full load extraction pressures determined using the method described in chapter 4.

The splitter component can be used for splitting steam and water flows to different number of outlets depending on the settings on the configuration panel shown on Figure 6.22. This component was specifically used to model the splitting of the steam from the exhaust of the HP turbine in the single and double reheat CFPPs, into the flows going to the reheater, and the final feed water heater. The calculation method for the pressure and flow is as shown on Figure 6.22. This calculation method for the flow assumes that all nodes (#1 and #3) except node #2 are connected to known flows either upstream or downstream [190], implying that the outlet pressure of node #2 is known while the second outlet pressure at node #1 and the inlet node will be set to the known outlet pressure at node #2.

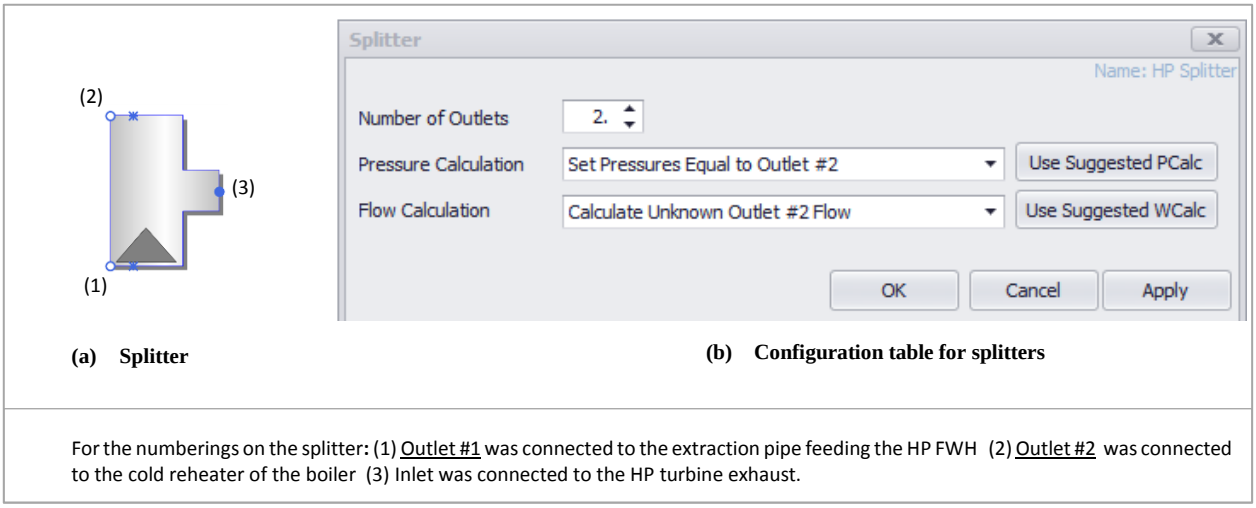

(a) Splitter **(b) Configuration table for splitters**

For the numberings on the splitter: (1) Outlet #1 was connected to the extraction pipe feeding the HP FWH (2) Outlet #2 was connected to the cold reheater of the boiler (3) Inlet was connected to the HP turbine exhaust.

Figure 6.22 Splitter and its configuration panel

The mixer component can be used for mixing steam and water flows from different number of outlets depending on the settings on the configuration panel shown on Figure 6.23. This component was specifically used to model the mixing of the feed water from lowest pressure FWH and extracted steam pump through the feed water heater condensate pump of all the CFPP process

models, into the flow going to next low pressure feed water heater. The calculation method for the pressure and flow is as shown on Figure 6.23. This calculation method for the flow assumes that the flows to the inlet nodes (#1 and #2) is known upstream [190], implying that the outlet pressure of node #3 is known while the inlet pressure at node #1 and #2 is equal to the known outlet pressure at node #3.

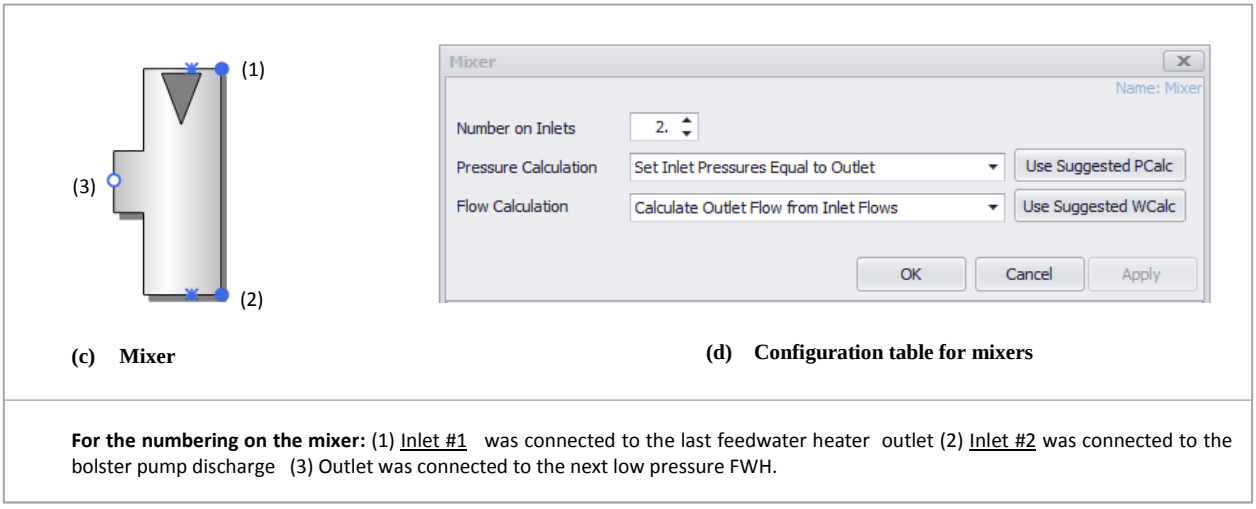

(c) Mixer

(d) Configuration table for mixers

For the numbering on the mixer: (1) Inlet #1 was connected to the last feedwater heater outlet (2) Inlet #2 was connected to the bolster pump discharge (3) Outlet was connected to the next low pressure FWH.

Figure 6.23 Mixer and its configuration panel

6.4 Source data for the model validation

The validation of the generic CFPP model development procedure was done by setting up models for actual plants whose process data is known. A total of 11 CFPPs models (2 NRH's, 8 SRH's and 1 DRH) mostly from the Eskom fleet was developed. The input data of the CFPPs considered is shown on Table 6.1

Table 6.1 Eleven CFPPs used in validating the generic CFPP model development procedure

S/No	Plant	Reheat	Full load (MW)	P_{thr} (MPa)	T_{thr} (°C)	Pcond (kPa)	Cooling system	Boiler pressure control	Presence of BFPT	Condenser pressure
1	Plant B	NRH	200	10.78	538	11.6	IDC	fixed pressure	yes	Varying
2	Plant C	NRH	200	10.79	538	7.0	WCC	fixed pressure	yes	Varying
3	Plant O	SRH	793	24.1	560	14.1	ACC	sliding pressure	No	Varying
4	Plant F	SRH	352	15.8	510	7.2	WCC	fixed pressure	Yes	Varying
5	Plant H	SRH	504	16.1	510	7.7	WCC	fixed pressure	No	Varying
6	Plant I	SRH	619	16.1	535	5.5	WCC	fixed pressure	Yes	Varying
7	Plant J	SRH	600	16.1	535	7.0	WCC	fixed pressure	Yes	Varying
8	Plant U	SRH	686	16.1	535	13.6	ACC	modified sliding	No	Varying
9	Plant K	SRH	657	16.1	535	16.1	ACC	sliding pressure	No	constant
10	Plant L	SRH	714	16.1	535	5.5	WCC	sliding pressure	Yes	constant
11	Plant P	DRH	127.6	31.0	621	3.4	OTC	**	No	
** No Plant data for studying the CFPP process model at part load.										

Only some critical process and performance parameters were selected for the validation exercise. These are:

- The LP turbine exhaust condition
- Main steam flow entering the HP turbine
- Condenser steam flow
- Final feed water temperature (FFWT)
- Live steam pressure (for varying load operation alone)
- Reheat steam temperature
- Reheat steam pressure
- Turbine cycle heat rate (TCHR)

The validation of the models was done in two stages. The first stage (see discussion in section 6.5) was done at the VWO (100% MCR) condition, and for all the CFPPs listed on Table 6.1. The objective of this stage of the validation was to show how a model developed using the rules of the generic CFPP model procedure is able to accurately represent the actual performance of a given CFPP. This should provide confidence that the procedure does produce credible real-life power plant architectures.

The second stage (see discussion in section 6.6) of the validation was carried out at three lower load conditions (80%, 60%, and 40%) for most of the CFPPs considered with the exception of the double reheat CFPP (Plant P) due to unavailability of data at the lower loads. This should provide confidence that the processes which change at low load has been correctly captured by the models.

6.5 Model validation results at full load

6.5.1 LP Turbine exhaust condition

The LP turbine exhaust steam quality is an important parameter that is usually monitored for the protection of the last stage blades against erosion damages. A comparison of the plant and the predicted VWO/full load turbine exhaust steam quality for the CFPPs are shown on Figure 6.24.

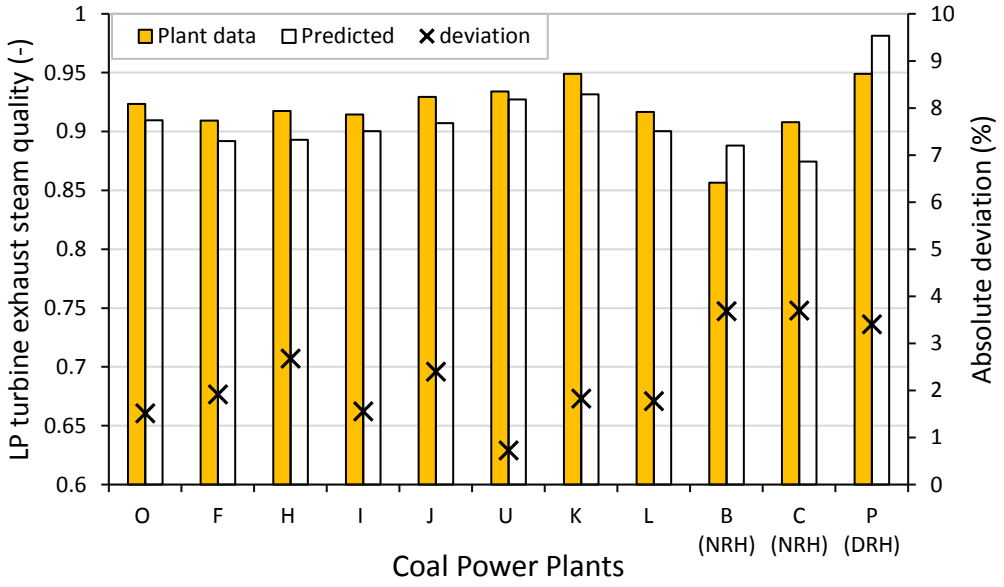

Figure 6.24 Full load validation of Generic CFPP Process models: LP turbine exhaust steam quality

It can be seen that the predicted LP turbine exhaust steam quality for the all the cases studied is above the 0.85 threshold, satisfying the minimum requirement for setting up a CFPP steam cycle process model. It can also be seen that the predicted steam quality is lesser than the plant data obtained, for most of the CFPPs with the exception of plants B & P. The reason for this trend may

be due to the value of LP turbine efficiency that was assumed. The assumption of a higher LP turbine efficiency would imply that more work is extracted at the LP turbine per unit of steam flow. The minimum and maximum absolute deviations from the plant data were 0.724% and 3.68% respectively. This can be considered as quite small.

6.5.2 Main steam flow

The main steam mass flow is an important parameter that affects the mass flow across the various components in the CFPP. A comparison of the plant and the predicted VWO/full load main steam mass flow for the CFPPs are shown on Figure 6.25. It can also be seen that the predicted main steam mass flow is higher than the plant data in some cases (Plants O, H, U, K, L & C), while it is lesser at other cases. The absolute deviation for most (except Plants O, C, and P) of the plants was less than 6%. The minimum and maximum absolute deviations seen were 0.15% and 9.37% respectively.

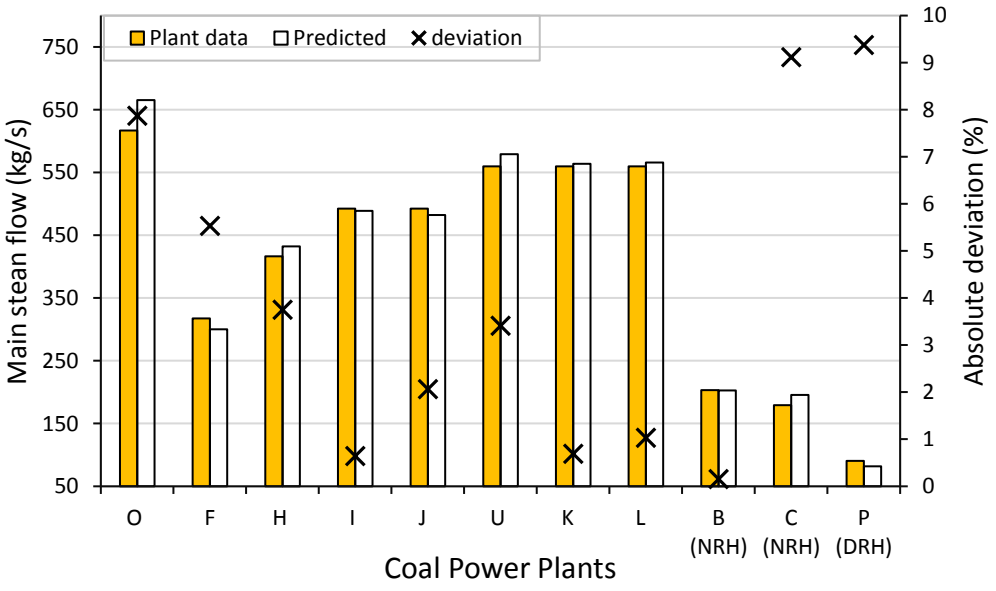

Figure 6.25 Full load validation of Generic CFPP Process models: main steam flow

6.5.3 Condenser flow

The condenser mass flow is an important parameter that affects the heat rejection from the steam cycle, and the sizing of the LP turbine exhaust annulus area. A comparison of the plant and the predicted VWO/full load condenser steam mass flow for the CFPPs are shown on Figure 6.26. It can be seen that the predicted condenser steam mass flow is higher than the plant data in some cases (Plants O, H, I, U, B & C), while it is lesser at other cases. The reason for the trend in Plants O, H, I, U, B & C may be due to one or both of the following reasons:

(a) Nock-on effect from the main steam flow predicted: The main steam mass flow has a direct influence on the mass flows across various components in the steam cycle. It appears that some CFPPs whose predicted main steam mass flows (see Figure 6.25) were greater than the plant data, also had a corresponding effect on the condensing steam mass flow.

(b) Lower steam extraction mass flows for FWHs. This is a consequence of having higher FWH extraction pressures on the steam turbines.

The absolute deviation for most of the plants (except Plants B, C, and P) was less than 6%. The minimum and maximum absolute deviations seen were 0.39% and 14.83% respectively.

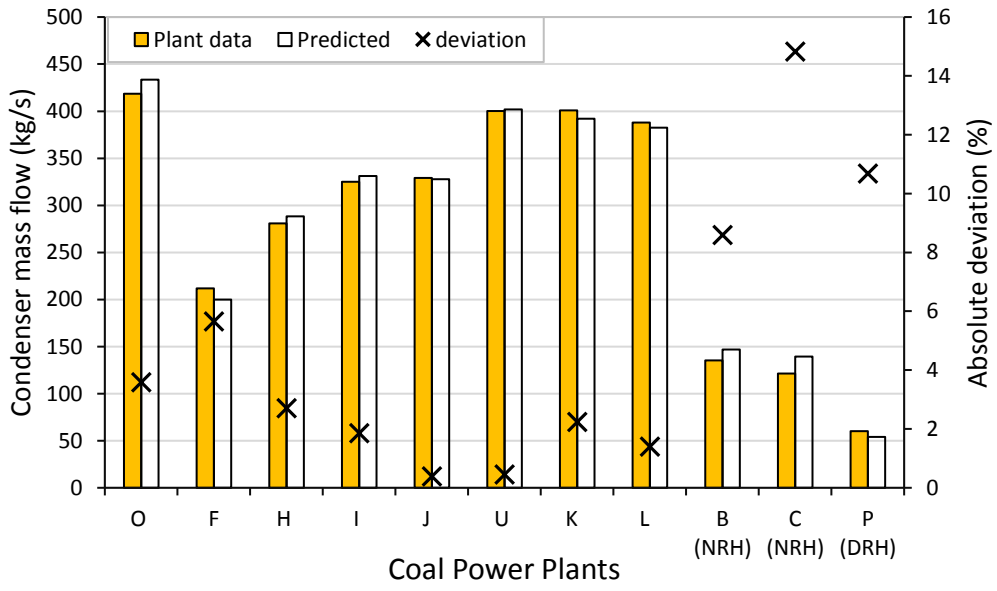

Figure 6.26 Full load validation of Generic CFPP Process models: condenser steam flow

6.5.4 Final feed water temperature

A comparison of the plant and the predicted VWO/full load FFWT for the CFPPs are shown on Figure 6.27. It can be seen that the predicted FFWT is greater than the plant data obtained, for most of the CFPPs with the exception of plants B & C. The reason for this trend could be due to the reheat pressure that was selected. The absolute deviation for most of the plants (except Plant H) was less than 6%. The minimum and maximum absolute deviations seen were 0.48% and 8% respectively.

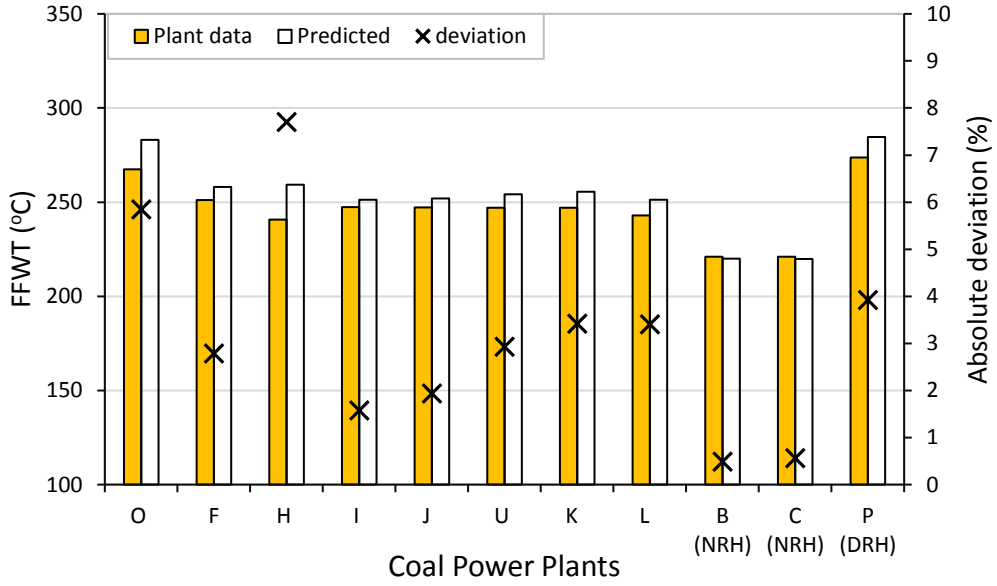

Figure 6.27 Full load validation of Generic CFPP Process models: FFWT

6.5.5 Reheat temperature and pressure

One of the key modelling assumptions that was made was that the reheat temperature is equal to the superheat or live steam temperature. This assumption was required to determine the reheat pressure in the cycle. So, a quick comparison of the plant and the assumed VWO/full load reheat temperature for the CFPPs shown in Figure 6.28, suggests that this assumption holds true for most of the CFPPs except Plants O & P. The absolute deviation for plants O & P are 1.8% and 9.8% respectively.

A comparison of the plant and the predicted VWO/full load reheat pressures for the CFPPs are shown on Figure 6.29. It can be seen that the predicted reheat pressure is greater than the plant

data, for most of the CFPPs with the exception of Plant P. The probable reasons for this deviations could be that economic based decisions made by OEM's do not often require the selection of the most efficient point; or OEM's do not assume isentropic conditions in determining the optimum reheat pressure. The absolute deviation for most of the plants (except Plant O & H) was less than 12%. The minimum and maximum absolute deviations seen were 0.48% and 8% respectively.

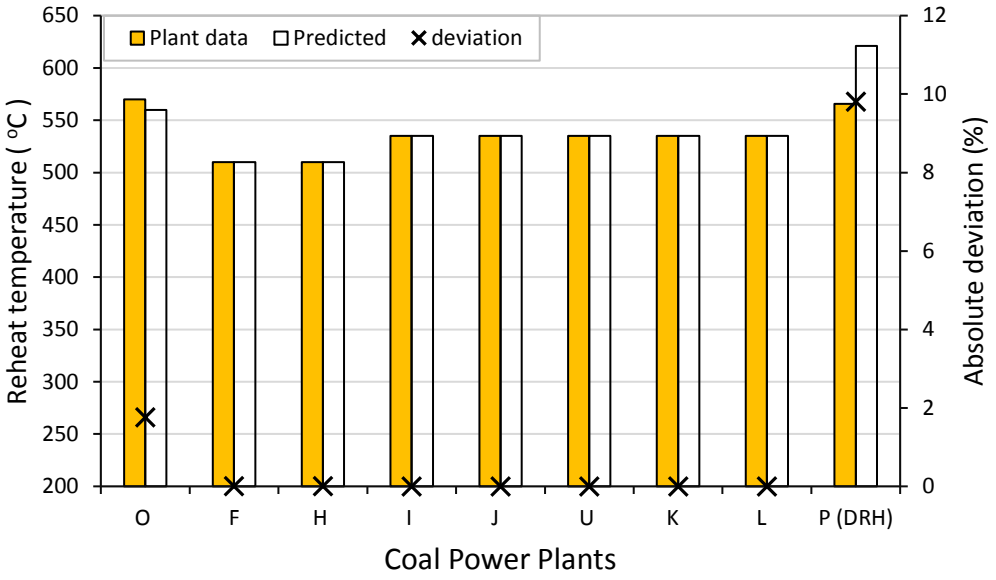

Figure 6.28 Full load validation of Generic CFPP Process models: Reheat temperature

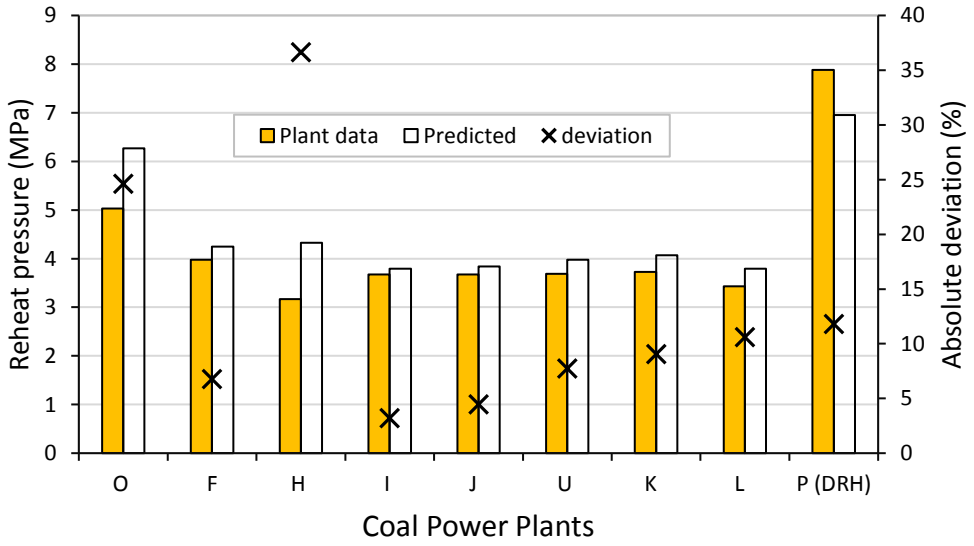

Figure 6.29 Full load validation of Generic CFPP Process models: Reheat pressure

6.5.6 TCHR

A comparison of the plant and the predicted VWO/full TCHR for the CFPPs are shown on Figure 6.30. It can be seen that the predicted TCHR is lesser than the plant data, for most of the CFPPs with the exception of Plants O, U and B. The absolute deviations seen for the non-reheat (NRH) coal fired power plants were less than 1 %, while the absolute deviations in the TCHR seen for the single reheats and double reheats are less than 8%.

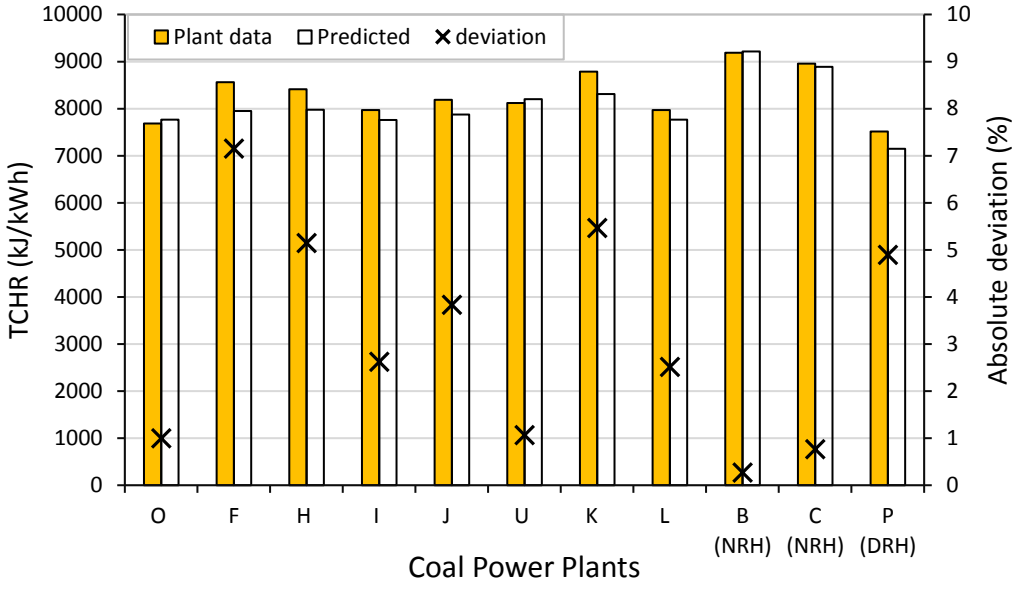

Figure 6.30 Full load validation of Generic CFPP Process models: TCHR

6.6 Model validation at part load conditions

Having completed the validation of the generic CFPP process model at VWO/full load conditions, it is important to examine the suitability of the model for predicting the performance parameters at various part load conditions. This is in fact the most important element to get correct in this research, as the change in TCHR will be used to develop the simple V-TCHR model. The part load validations were only done for the non-reheat and single reheat CFPPs. The validation could not be done for the DRHs because part load validation data for DRH was not available. However, given the

fact that the DRHs uses the same part load loss models as for SRH, one may also extend the conclusions drawn from the SRH to the DRH plants.

6.6.1 LP Turbine Exhaust steam quality

Figure 6.31 (a) and (b) shows the results of the LP turbine exhaust steam quality predicted and the plant data for Plants C and O respectively.

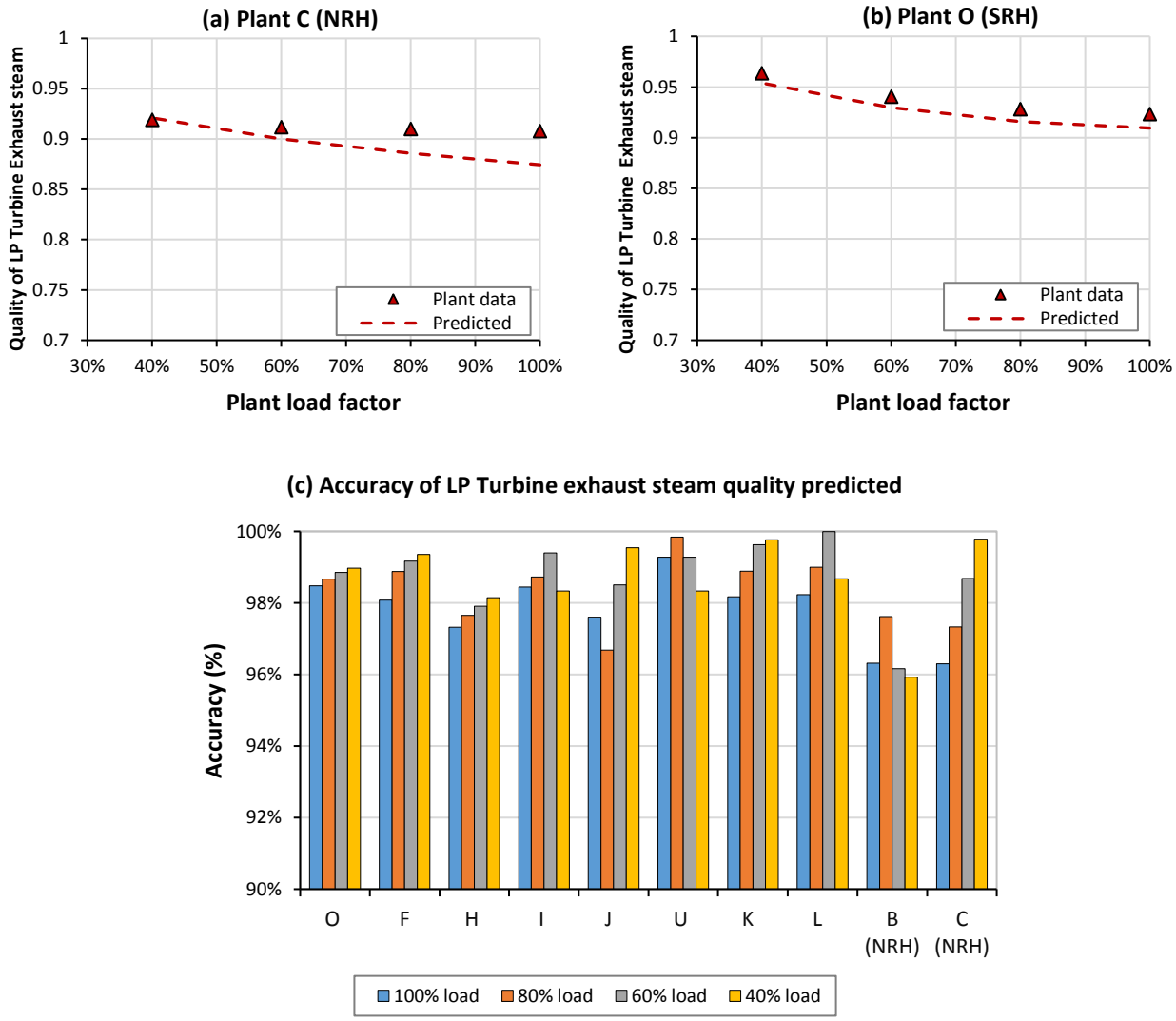

Figure 6.31 Comparing the LP Turbine exhaust steam quality for the NRHs and SRHs

Plants C and O is a non-reheat (NRH) and single reheat (SRH) CFPP respectively. It can be seen in both cases that the predicted LP turbine exhaust steam quality increases (i.e the steam becomes dryer) as plant load factor decreases. This observation is corroborated by evidence from the plant

data. It must be stated that this observation was also seen for all the other cases studied. An examination of the model accuracy[2] at part load condition is shown on Figure 6.31 (c). The least accuracy seen across the loads investigated was 95.9%. It does seem to appear that the accuracy of the LP turbine exhaust steam quality predicted increases at lower part load.

6.6.2 Main Steam flow

Figure 6.32 (a) and (b) shows the results of the main steam flow predicted and the plant data for Plants C and O respectively.

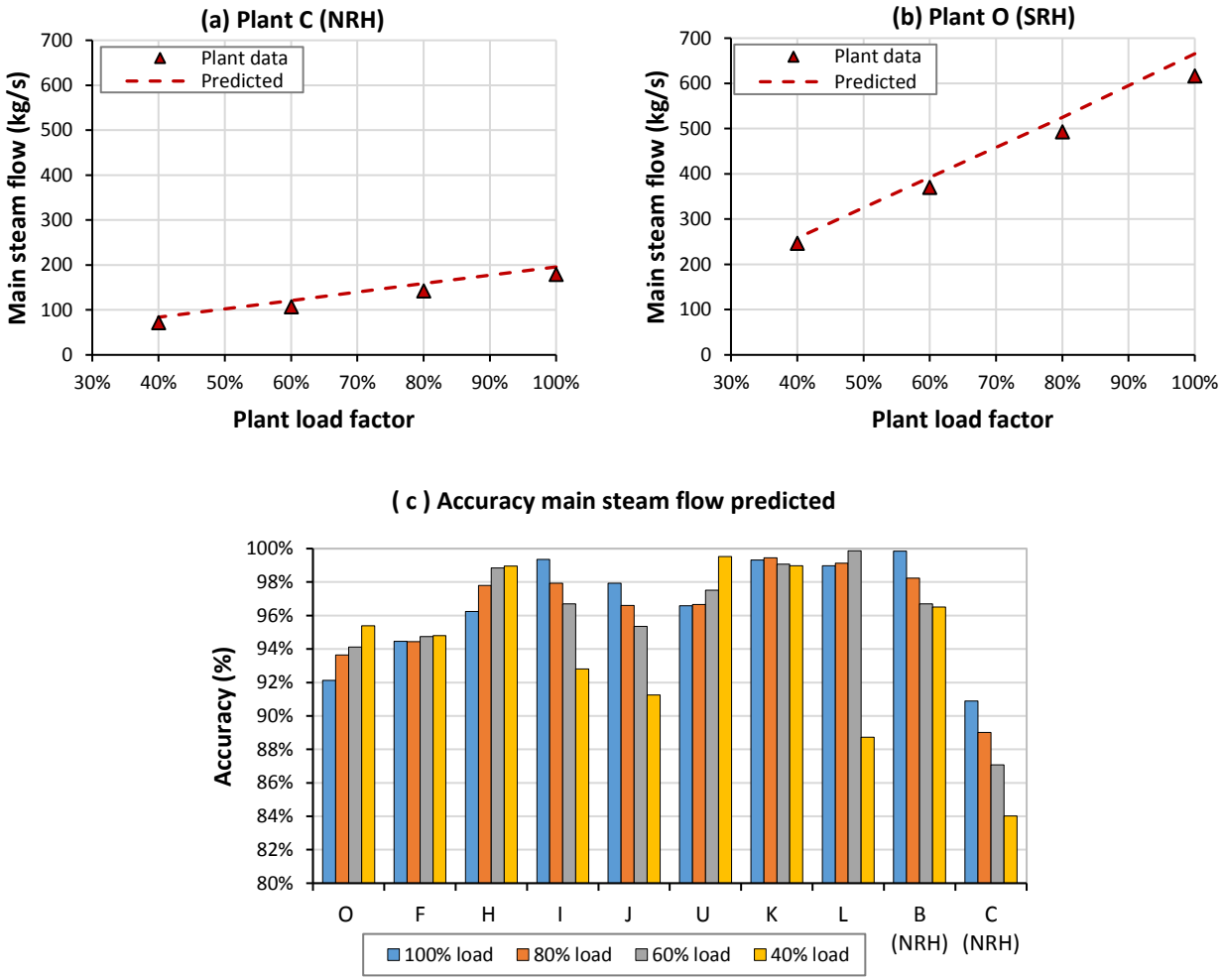

Figure 6.32 Comparing the main steam flow for the NRHs and SRHs

[2] Model accuracy is defined as 100% minus the absolute deviation.

The installed capacity for Plant O is larger than Plant C hence the reason why its steam mass flow is higher than that of Plant C. Irrespective of the capacity or type of CFPP, it can be seen that the model predicts a decreased mass flow at lower plant load factor. This is expected, and it is also corroborated by the evidence from the plant data. This same observation was also seen for all the other cases studied. An examination of the model accuracy at part load condition is shown on Figure 6.32 (c). The least accuracy seen across the loads investigated was 95.9%. The accuracy of the main steam flow predicted increased at lower plant load factors for some CFPPs (Plants O, F, H, U, L), and increased at lower plant load for the others.

6.6.3 Condenser flow

Figure 6.33 (a) and (b) shows the results of the condensing steam flow predicted and the plant data for Plants C and O respectively. It can be seen that the model predicts a decreased mass flow at lower plant load factor. This is expected, and it is also corroborated by the evidence from the plant data. This same observation was also seen for all the other cases studied. An examination of the model accuracy at part load condition is shown on Figure 6.33 (a). The accuracy of the condensing flow predicted decreased at lower plant load factors for most of the CFPPs.

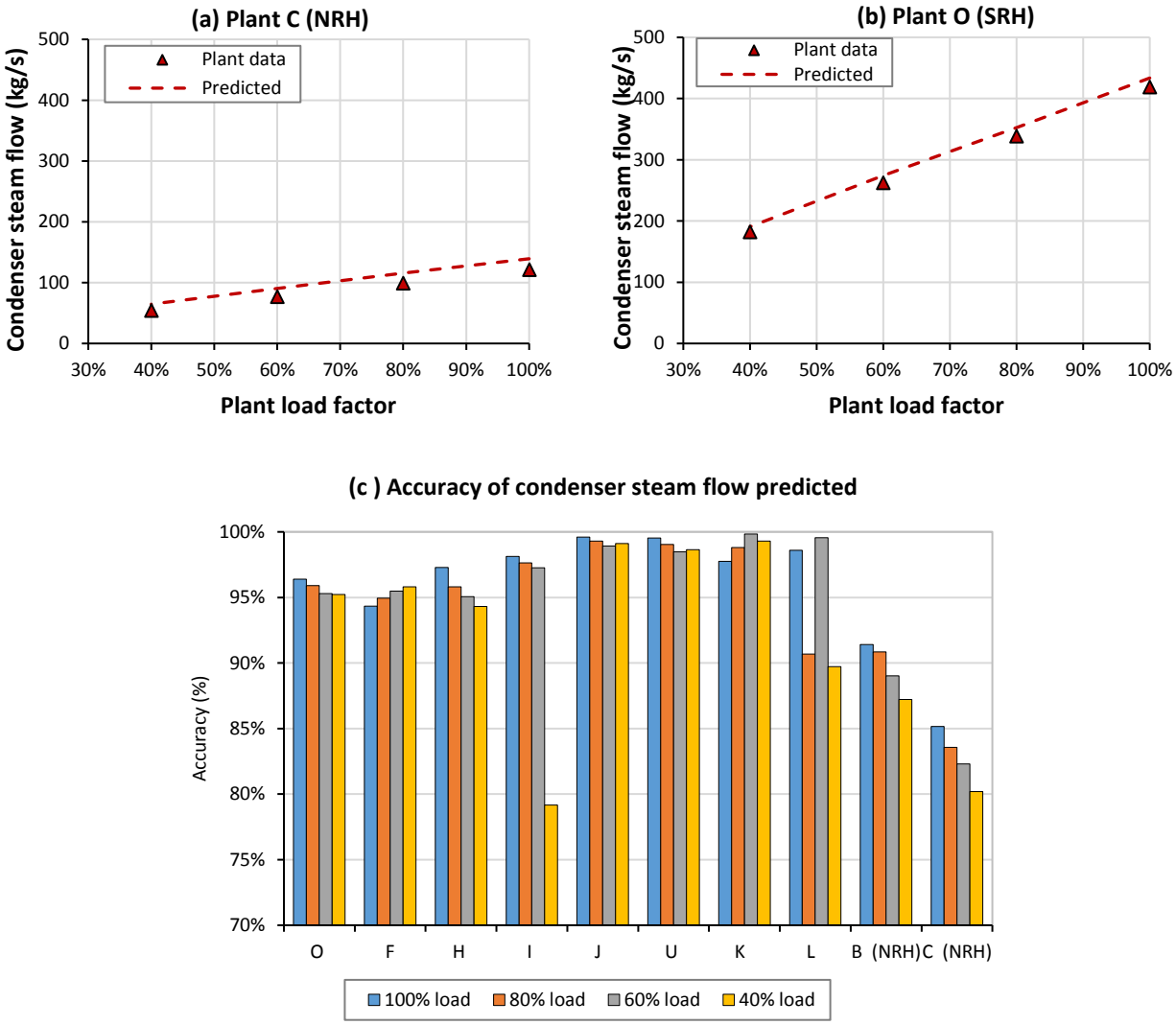

Figure 6.33 comparing the condenser steam flow for the NRHs and SRHs

6.6.4 Final feed water temperature (FFWT)

Figure 6.34 (a) and (b) shows the results of the final feed water temperature predicted and the plant data for Plants C and O respectively. It can be seen in both cases, that the model predicts a decreased FFWT at lower plant load factors. This is expected, and it is also corroborated by the evidence from the plant data. The FFWT decreases with load because of its link to the reheat pressure. The reheat pressure drops at part load either due to valve throttling or boiler pressure drop in sliding pressure mode. This drop affects how much heat that can be extracted by the HP FWH positioned before the boiler. This same observation was also seen for all the other cases studied. An examination of the model accuracy at part load condition is shown on Figure 6.34 (c). The accuracy of the FFWT

predicted for most of the single reheat CFPP process models is seen to increase at lower plant load factors while the one for the non-reheat is seen to decrease at lower plant load factors.

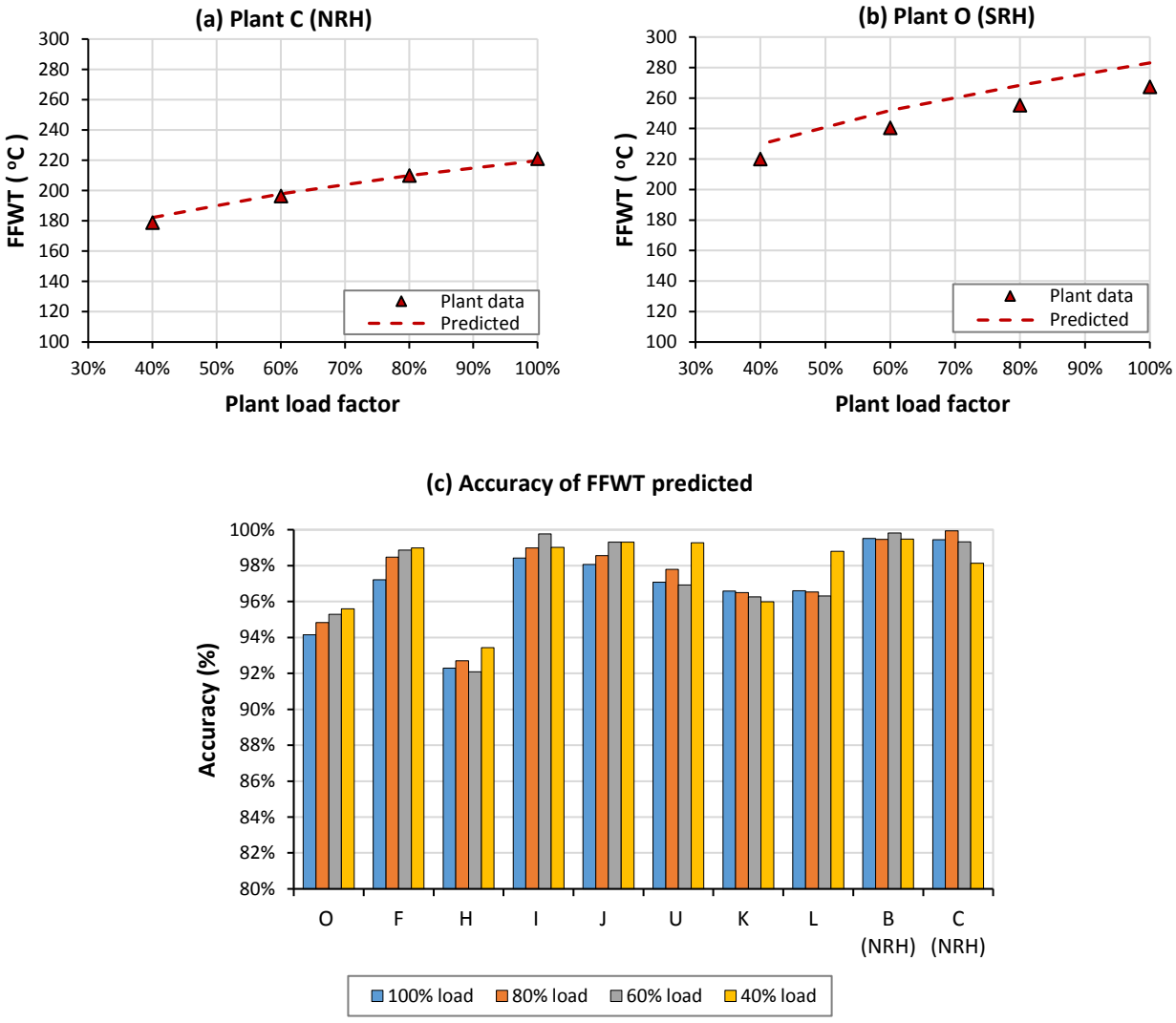

Figure 6.34 Comparing the final feed water temperature (FFWT) for the NRHs and SRHs

6.6.5 Live steam Pressure (HP Turbine inlet Pressure)

Figure 6.35(a) and (b) shows the results of the live steam pressure predicted and the plant data for Plants C and O respectively. The part load investigation for Plants C and O were done by simulating their CFPP process models at fixed and sliding boiler pressures respectively. The results and accuracy for the fixed boiler pressure operated CFPPs (Plants C, F, H, I, J & B) in Figure 6.35 (a) & (c) is expected to be 100% as the data is an input to the model. On the other hand, the results predicted for the

sliding pressure mode cases is a bit more interesting. The Plant O results predicted on Figure 6.35(c) shows a decrease in the live steam pressure with plant load factor. This is expected, and it is also corroborated by the evidence from the plant data. An examination of the model accuracy for all the sliding boiler pressure cases (Plants O, U, K, L) shows that the accuracy of the model tends to decrease at lower load for most of the CFPPs except plant K. The minimum accuracy level seen was 85%.

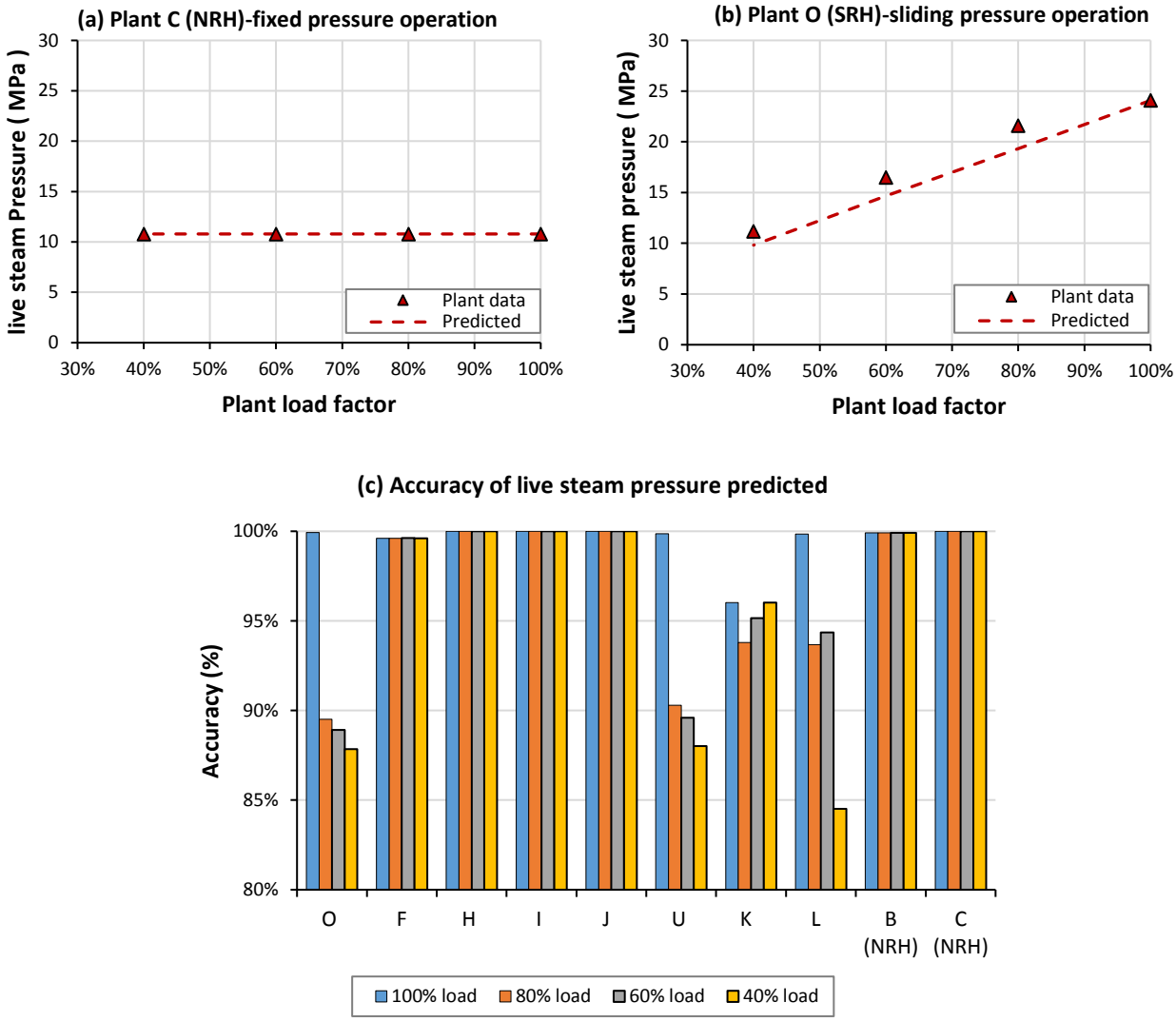

Figure 6.35 Comparing the live steam pressure for the NRHs and SRHs

6.6.6 Reheat steam pressure

The predicted results for the reheat pressure of Plant O and the accuracy for the reheat pressure predicted for other CFPPs at varying load conditions are presented on Figure 6.36. At lower plant load factors, the reheat pressures predicted decreases. This is expected and is also corroborated by the plant data. However, the reheat pressure predicted for Plant O was higher than the plant data at all the load conditions. This kind of trend was also seen in most of the CFPPs investigated. The probable reason for this deviation in Plant O has to do with the fact that the full load reheat pressure calculated for this plant was too high, thus all other pressures will be too high as the pressure is driven by the turbine characteristics for a given mass flow. An examination of the model accuracy for all the CFPPs at part load condition shows the accuracy of the reheat pressure predicted appears to decrease at lower plant load factors for most of the CFPPs.

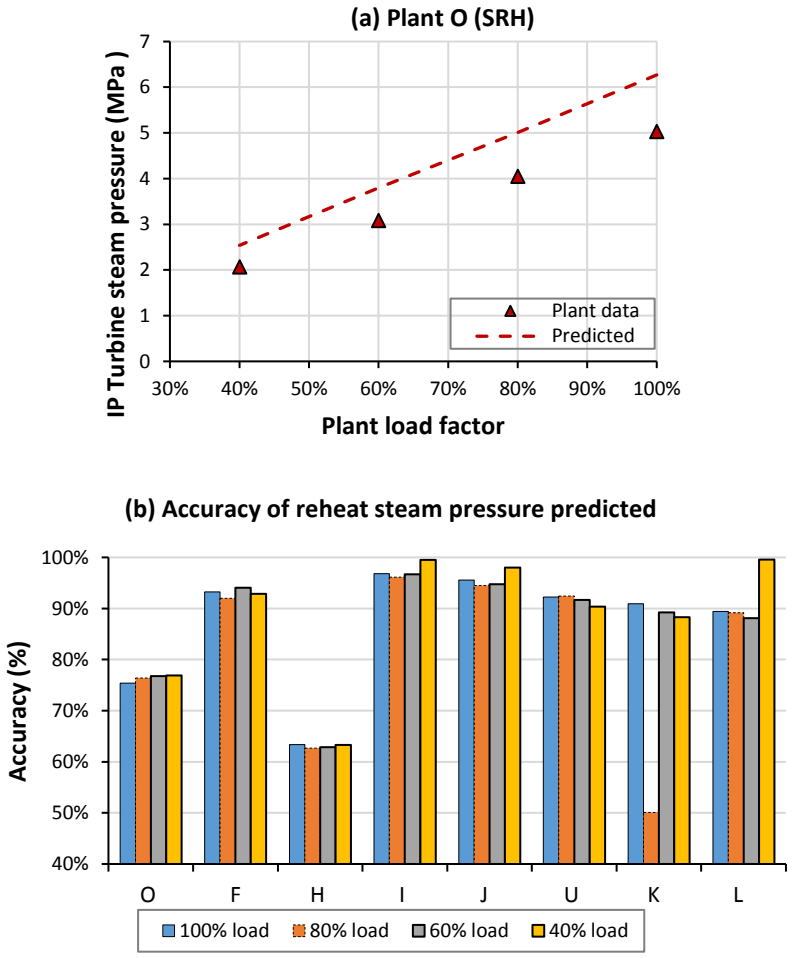

Figure 6.36 Comparing the intermediate turbine inlet steam pressure

6.6.7 TCHR

Figure 6.37 (a) and (b) shows the results of the Turbine cycle heat rate (TCHR) predicted and the plant data for Plants C and O respectively. It can be seen in both cases, that the model predicts an increased TCHR at lower plant load factors, and that the results predicted were higher than the plant data. This increased TCHR causes a deterioration of the performance of the CFPPs at lower loads. This trend is expected, and it is also corroborated by the evidence from the plant data. This same observation was also seen for all the other cases studied.

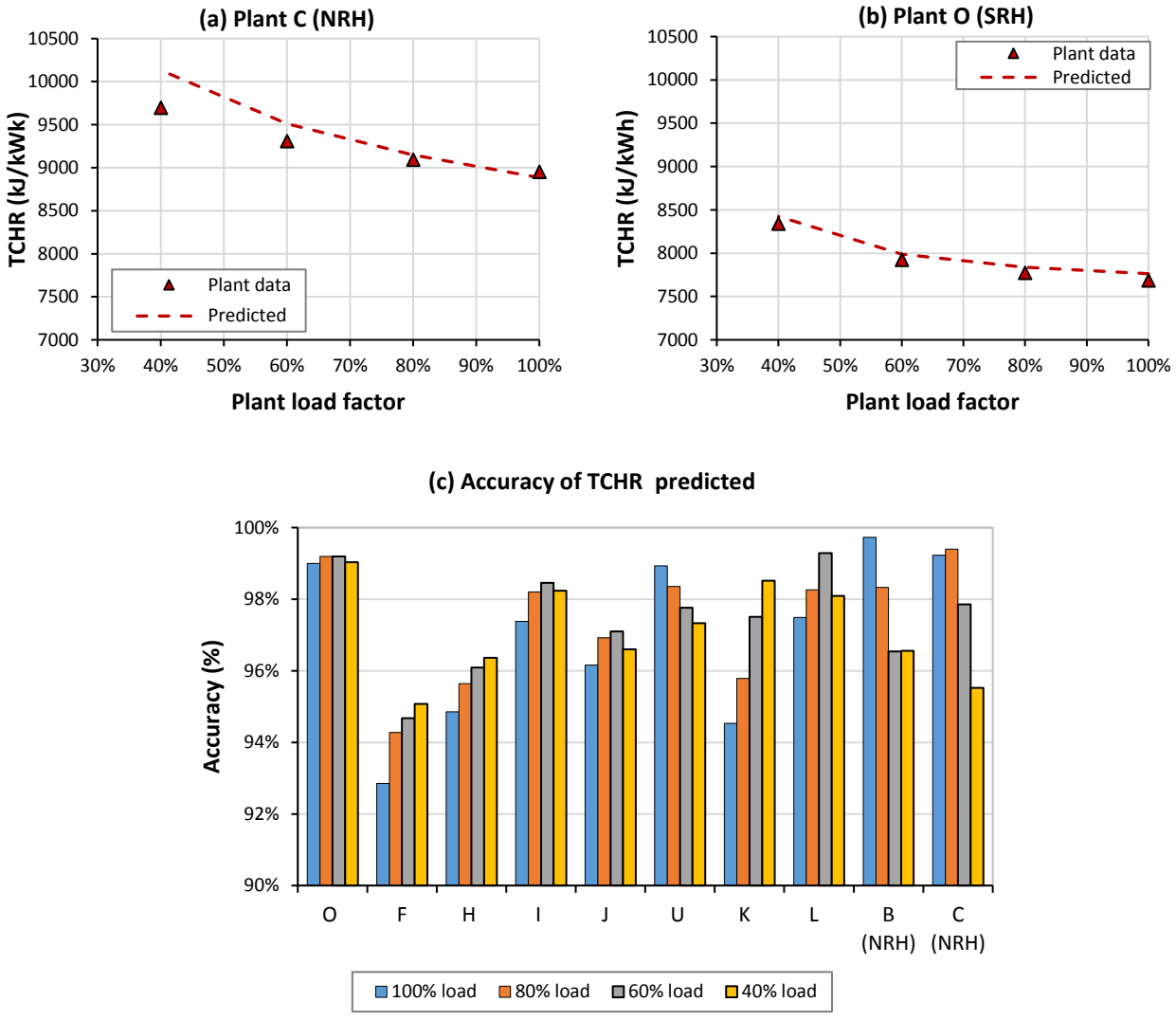

Figure 6.37 Comparing the Turbine cycle heat rate (TCHR) for the NRHs and SRHs

An examination of the model accuracy at part load condition is shown on Figure 6.37 (c). The accuracy of the TCHR predicted for most of the non-reheat CFPP process models for Plants B & C is seen to decrease at lower plant load factors. The accuracy of the model results for most of the single-reheat CFPPs is seen to increase at lower plant load factors. The minimum accuracy seen was around 92.8%.

The probable reasons for the deviations in the TCHR predicted may include:

- The differences in the architectures/layout of the real CFFPs and the model CFPPs which include the presence of auxiliary steam turbine for boiler feed pump power input, and the presence of additional feedwater heaters that were not included in the generic CFPPprocess models.
- Turbine efficiencies assumed in the models may be lesser: the efficiencies of the steam turbines have a significant impact on TCHR [122]. For instance, a 1% decrease in the HP and LP efficiencies produces an approximately 0.17% and 0.5% increase respectively in TCHR [122]. The impact for an IP Turbine is slightly less than that of the HP Turbine. The turbine efficiency also do not remain perfectly constant as is assumed in the models.
- The assumption of reheat temperatures that are of the same value as the superheat temperature. In reality, the reheat temperatures are mostly higher than the superheated steam temperature.

6.7 Independence of TCHR on Plant Size

A demonstration study was done to check the dependence of the predicted TCHR on the VWO generation capacity used to set up the CFPPs investigated. This study was done by setting up 2 additional VirtualPlant CFPP process models for each Plant C, O, and P cases. The VWO generation capacity of the six additional CFPPs, which are listed under the hypothetical size A & B headings, are shown on Table 6.2. The hypothetically sized plants A and B under each category represent CFPPs with lower and higher VWO generation capacity respectively for each case studied. The 6 additional CFPPs were set up using the same procedures described in previous chapters. In setting up the hypothetically sized plants for each case study, the thermodynamic properties of the steam (temperatures, pressures, and enthalpies) of both hypothetical plants at all the process point were

the same with the baseline case. However, the mass flows were different and the exhaust annulus area determined for each hypothetical case were also different from the baseline case because of the change in the condenser mass flow.

Table 6.2 List of additional hypothetical cases

Category of CFPP	Case study	Hypothetical size A (MW)	Baseline case (MW)	Hypothetical size B (MW)
NRH	Plant C	102	200	295
SRH	Plant O	400	647	741
DRH	Plant P	80	127	780

The results of the TCHR demonstration study are shown on Figure 6.38 (a) –(c) for the non-reheat, single reheat, double reheat CFPPs. It can be seen that for all the three cases studied, the TCHR predicted at all the load conditions are approximately the same for the hypothetical cases and the baseline case. This suggests that the predicted TCHR of the VirtualPlant CFPP process models are independent of the VWO generation capacity used to set-up the VirtualPlant process models. This ought to be the expected outcome as the performance of the steam cycle (excluding the boiler and auxiliary effects) at various load levels, is solely based on thermodynamic state of the steam at all the points on the cycle.

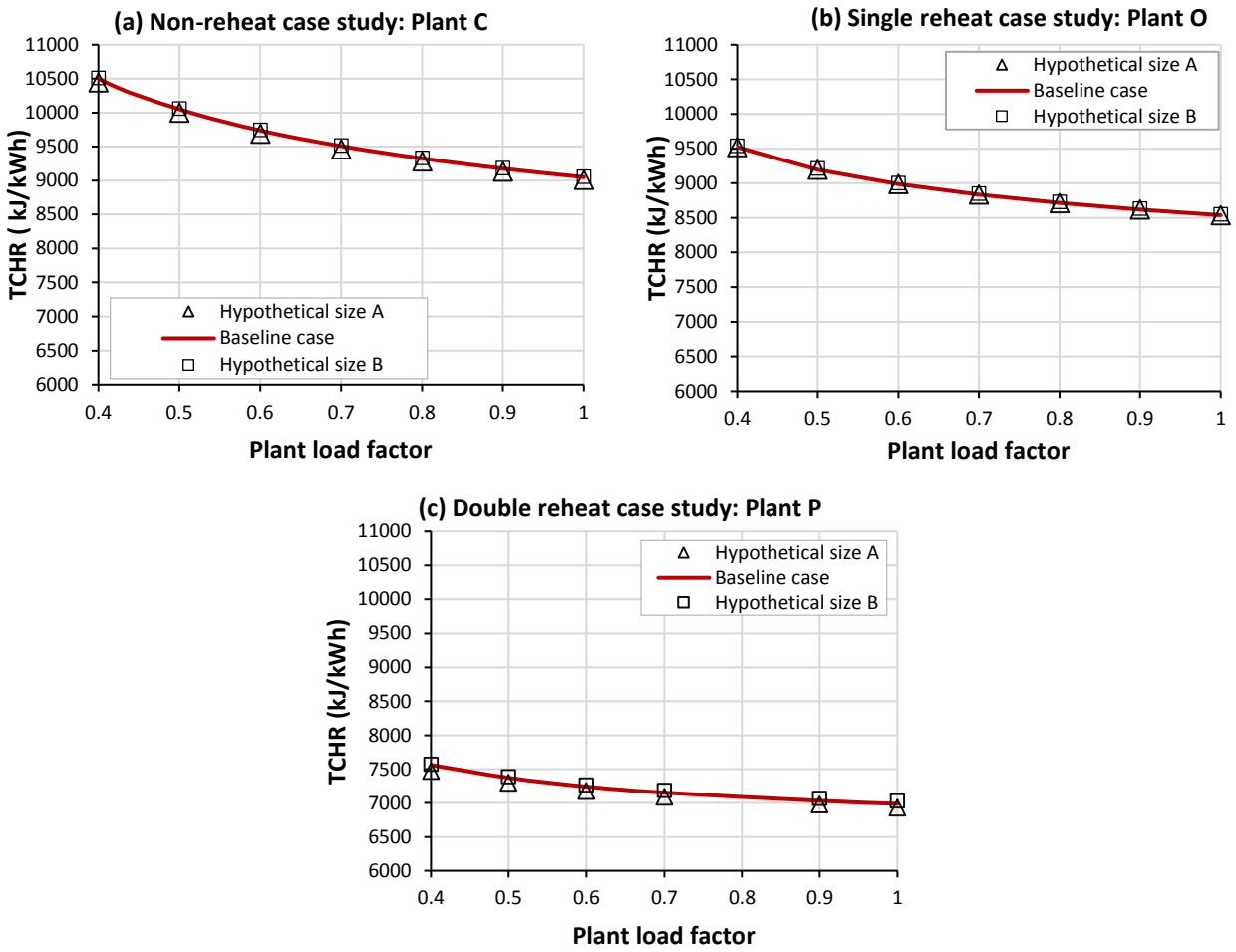

Figure 6.38 Investigating the dependence of TCHR on Plant VWO capacity

6.8 Conclusion of the chapter

The procedure for setting up the generic process models in VirtualPlant using the methodology described in previous chapters has been presented. Sample CFPP process models of actual plants were set up and simulated in order to validate the generic model development method. The validation of the sample models was done at the VWO (100% MCR) condition as well as at low load conditions.

A summary of the deviations predicted for some of the important process parameters and the TCHR, from the VirtualPlant CFPP process models across all the four load scenarios, is shown in Figure 6.39. The absolute deviations from the plant data for the predicted LP exhaust, main steam flow, final feed water temperature, live steam pressure, and turbine cycle heat rate (TCHR) were below 5% for 75% of the load scenarios investigated. However, the deviations for the predicted condenser flow and reheat pressure predicted were higher. Absolute deviation values less than 8% for the condenser steam flow and 22.5 % for the reheat pressure, were seen for 75% of the model results predicted. Although the deviation in the reheat pressure predicted appears to look high. Evidence from literature shows that a deviation of 15% from the reheat pressure typically yields a change in heat rate of approximately 0.05 % [181].

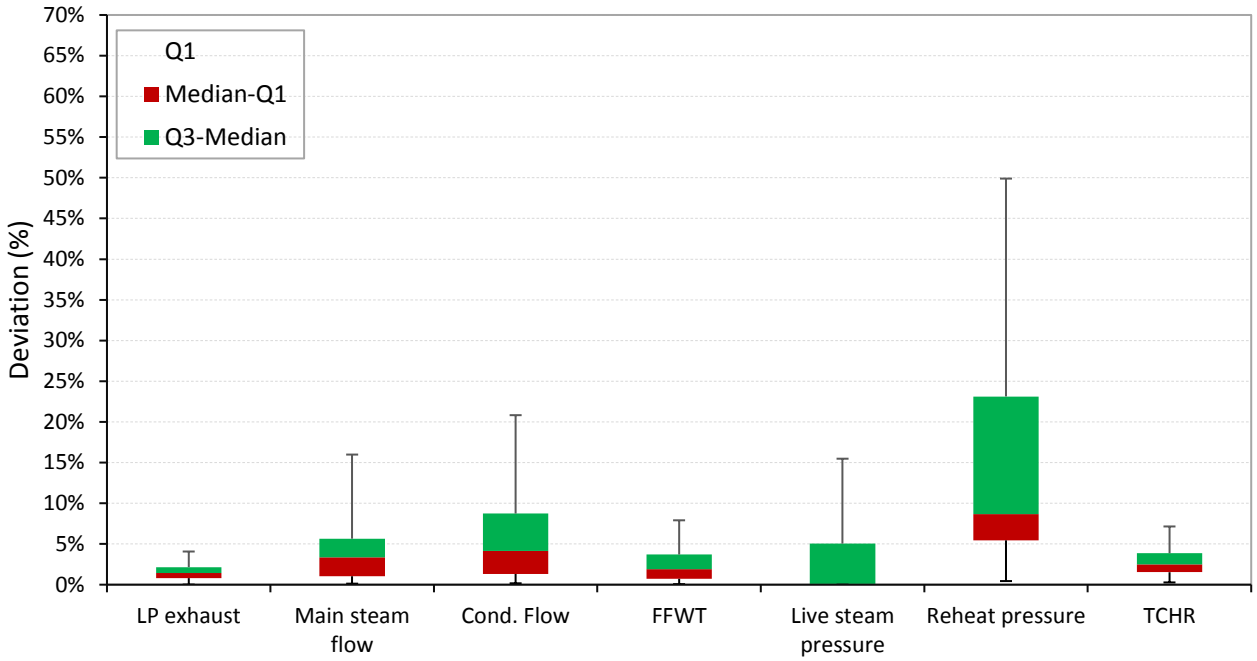

Figure 6.39 A summary of deviations for the VirtualPlant CFPP process model results predicted across all loads

There are sufficient probable reasons for the deviations, which mostly relates to specific differences seen in actual plants. Although the part load validation data for DRH was not available, but given the fact that it uses the same part load loss models as for SRH, one may assume the trends seen in the SRH models could be replicated in the DRH process models.

The results analysed from this chapter, has demonstrated the suitability of using the generic CFPP model development methodology for: (a) Setting up steam cycle process models for CFPPs of different architectures at full load, and (b) for investigating the overall thermal performance of the CFPP via TCHR, at various load conditions.

Finally, it was demonstrated that the TCHR of CFPPs with similar layouts, and with steam at similar thermodynamic state at corresponding points, is independent of the capacity of the plant. It therefore means that the choice of the VWO capacity selected for the process model has little or no effect on the overall thermal performance of the regenerative Rankine cycle, except the steam mass flows at various points in the cycle.

7. V-TCHR model development and validation

The development and validation of a novel variable turbine cycle heat rate (V-TCHR) model, for predicting the turbine cycle heat rate (TCHR) characteristics of CFPPs at various load conditions is presented in this chapter. A description of the characteristics of the various CFPPs that were investigated, and the data analysis method used are also discussed. The sensitivity analysis and validation are also presented herein.

The V-TCHR model was developed by setting up VirtualPlant process models for 192 hypothetical model CFPPs, and then investigating the varying load TCHR characteristics thereof. The methodology described in chapter 6 was adopted in setting up the process models. The critical process parameters of each model CFPP was selected from a combination of typical values of four selected key parameters that significantly affect the TCHR of CFPPs at various load conditions.

7.1 Selection of representative process conditions for setting up hypothetical CFPPs

7.1.1 Overview of the parameters considered

The various parameters that affect the TCHR of a CFPP at varying load conditions have already been highlighted in section 2.4.2. The four most important parameters identified are: (a) the steam throttle pressure, (b) steam throttle temperature, (c) the condensing pressure, and (d) the number of reheat stages.

The steam throttle temperature (T_{thr}) and pressure (P_{thr}) are two very important parameters that affect the energy content of the steam entering the high pressure turbine. These values are approximately the same as those coming out of the exit of the boiler's superheater. At full load conditions, it is well understood that a CFPP with a higher steam throttle temperature and pressure would have a lesser heat rate than a CFPP with a smaller value. The condensing pressure (P_{cond}) determines the back pressure of the LP turbine. It is strongly linked to the cooling technology and

the ambient conditions around the CFPP. A lower condensing pressure means a lesser TCHR. CFPPs exist as either Non-Reheat (NRH), single reheats (SRH), and double reheats (DRH). For different CFPPs with the same(T_{thr}),(P_{thr}), (P_{cond}) values, the heat rate of a DRH CFPP is lesser than the one for a SRH, which is also less than the one for a NRH.

7.1.2 Typical live steam temperature and pressures selected

A vast majority of CFPPs that have ever been built (both existing and decommissioned) all over the world, have throttle/live steam enthalpy that fall within the region ABCD depicted in Figure 7.1. This region covers live steam temperatures between $510℃$ and$600℃$; and live steam pressures between $10MPa$ and$30MPa$. Therefore, in this study, some representative values of live steam temperatures and pressures are selected in this region only.

Selection of four Live Steam Temperatures: The four typical live steam temperatures that were selected are $510℃$, $535℃$, $565℃$, and $600℃$. These temperatures cover a wide range of current exiting plants. For simplicity purposes, the reheat temperatures was taken to be the same as the live steam conditions. There are CFPPs that may have live steam temperatures beyond $600℃$ or lesser than $510℃$, these plants do not however constitute a majority of CFPPs that exist. For that reason it is believed that the values selected are a good representation of the current fleet of CFPPs globally.

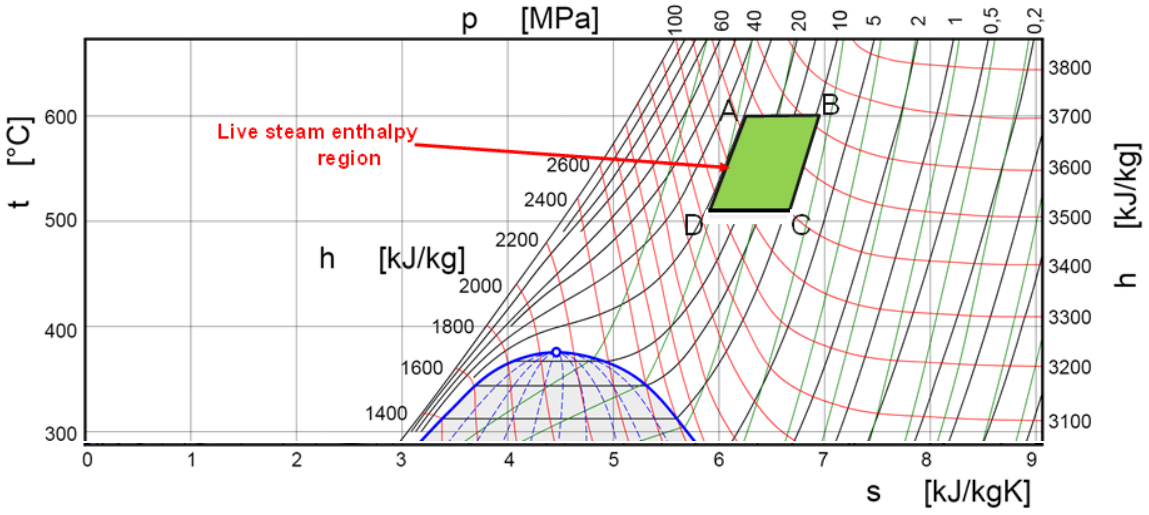

Figure 7.1 Current region of interest for live steam enthalpy of existing CFPPs

Selection of four live Steam Pressures: A total of four pressures have been selected to cover the different range of live steam pressures that could be found in existing CFPPs. These are:

- $12MPa$ was selected for the low subcritical pressure range ($5MPa – 12MPa$) [69] CFPPs.
- $17MPa$ was selected for the high subcritical pressure range ($13MPa – 18MPa$) CFPPs [69]
- $24MPa$ was selected for the supercritical pressure range ($22.9MPa – 25MPa$) CFPPs
- $30MPa$ was selected for the ultra-supercritical range [29] CFPPs.

7.1.3 Selection of typical condensing pressures for the different cooling technologies

The condenser pressure of a typical CFPP is dependent primarily on the environmental conditions, and the type and capacity of the cooling system that is used. In this study, the choice of an environment with RH of 60% and dry bulb temperature of $25℃$ was selected for all the CFPPs studied. In reality, CFPPs usually operate under different environmental conditions. Since the objectives of this study is not to consider the effects of the weather conditions, one can still use these values as it is.

For the cooling system types, it is generally understood that CFPPs with once through cooling (OTC) systems, generally have lower back pressure than the other types.

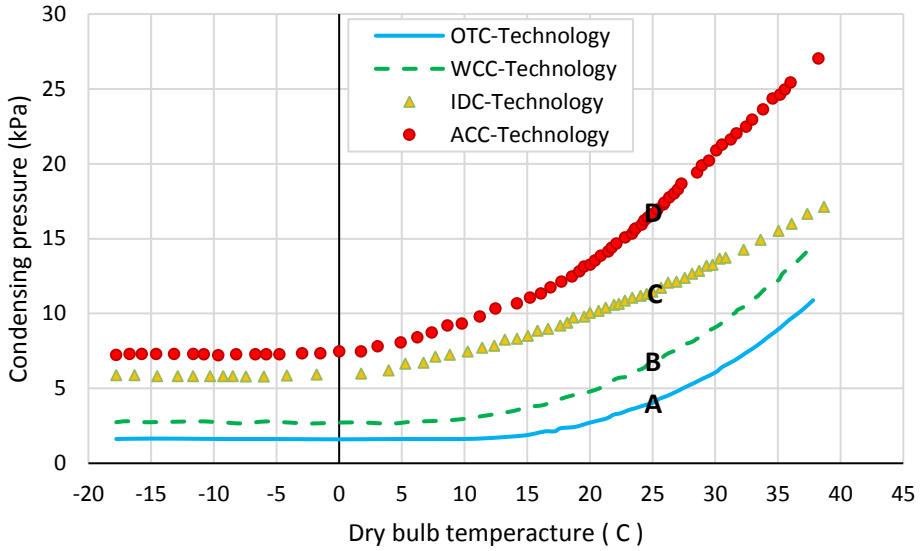

Note: Points A, B, C, D are the selected full load condensing pressures for OTC, WCC, IDC, and ACC technology respectively.

Figure 7.2 Typical condenser performance comparison: Data sourced from [151]

Figure 7.2 shows a typical condenser performance comparison for different condenser cooling systems that exist. The typical condensing pressures seen in the once through surface condensers is the least value while those of the indirect or direct air cooled condensers is the highest for all the various dry bulb temperature. At full load conditions, typical condensing pressures at points A, B, C, and D were assumed as the full load condensing pressure for the various cooling technologies. These points are at a dry bulb temperature condition of $25℃$. The values are summarized on Table 7.1.

Table 7.1 Typical CFPP condenser back pressures for a 25^{o}C and 60% RH environment

S/No	Type of Cooling system	Typical condenser pressure (kPa)
1	Once through condensers (OTC)	4
2	Evaporative cooling Tower or Wet cooled towers (WCC)	7
3	Wet surface or Indirect air cooled (IDC)	12
4	Direct or indirect air cooled (ACC)	17

In practice, there are situations where the condenser configurations in CFPPs might have two zones (hot and cold) i.e the hot zone having a higher condensing pressure than the cold zone. In such cases, it is sufficient to use the average pressure of the two values. The values in Table 7.1 would therefore represent the average condensing pressure in such cases.

7.1.4 Determination of the condenser effectiveness and pressure response at varying load conditions for each cooling technology

Once the condensing pressure is selected for the condenser, the next important parameter that was selected is the condenser effectiveness for the various cooling systems. This parameter is important for predicting the typical response of the condensing pressure at various load conditions.

Figure 7.3 shows the key temperature parameters that were used to determine the effectiveness of the main steam condenser for each of the various technologies.

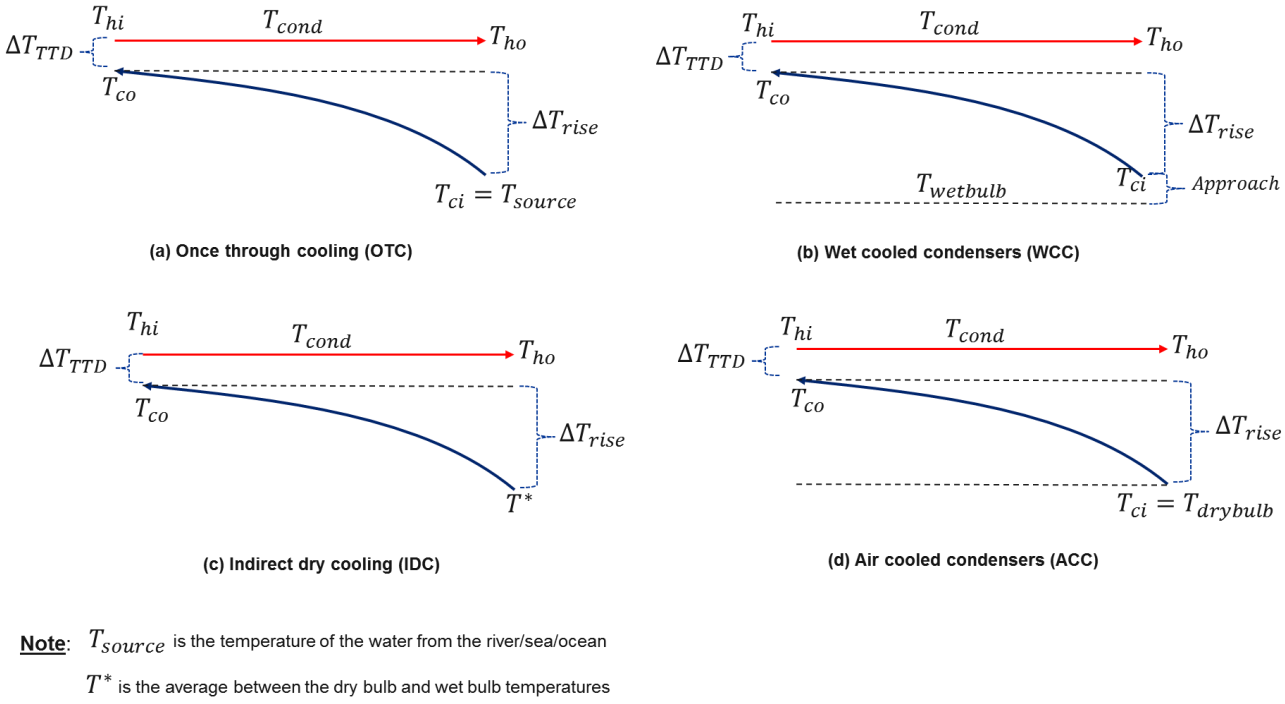

Note: T_{source} is the temperature of the water from the river/sea/ocean

T^* is the average between the dry bulb and wet bulb temperatures

Figure 7.3 important condenser temperatures for the different cooling systems

The condensing temperature (and corresponding pressures) for the various cooling technologies can be determined in Equations (7.1) –(7.4):

OTC systems:

$$T_{cond} = T_{source} + \Delta T_{rise} + \Delta T_{TTD} \tag{7.1}$$

WCC systems:

$$T_{cond} = T_{wetbulb} + Approach + \Delta T_{rise} + \Delta T_{TTD} \tag{7.2}$$

IDC systems:

$$T_{cond} = T^* + Approach + \Delta T_{rise} + \Delta T_{TTD} \tag{7.3}$$

ACC systems:

$$T_{cond} = T_{drybulb} + \Delta T_{rise} + \Delta T_{TTD} \tag{7.4}$$

Once the key parameters in Equations (7.1) –(7.4) are known, then the effectiveness of the condenser can be determined using $\varepsilon = 1 - e^{-\left(\frac{\Delta T_{rise}}{\Delta T_{LM}}\right)}$. The explanation for this has already been given in chapter 5.

The relevant values from Table 7.2 were used in to determine a typical effectiveness for each cooling technology. The values of $5℃$ and $2℃$ were assumed for ΔT_{TTD} and approach for each of the cooling systems. The values of $10℃$,$12.5℃$, $20.2℃$ and $26.6℃$ were used as the cooling fluid temperature rise ΔT_{Trise} for the OTC, WCC, IDC, and ACC systems respectively. These ΔT_{Trise} values were taken from some sample CFPP plants on the Eskom fleet. The wet bulb temperature is determined from psychrometric chart at dry bulb temperature of $25℃$ and relative humidity of 60%.

Table 7.2 selection of typical ΔT_{Trise}, ΔT_{TTD} and approach of the different technologies

	OTC	*WCC*	*IDC*	*ACC*
ΔT_{TTD} $(℃)$	5	5	5	
Approach $(℃)$	2	2	2	2
ΔT_{Trise} $(℃)$	10	12.5	20.2	26.6
T_{source} $(℃)$	14	N/A	N/A	N/A
$T_{wetbulb}$ $(℃)$	19.47			

The calculated condenser effectiveness for each cooling technology is presented on Figure 7.4. The condenser effectiveness for each OTC, WCC, IDC, and ACC system is 0.667, 0.714, 0.801, and 0.842 respectively. By this evaluation, it can be demonstrated that the condenser effectiveness of the ACC-cooled system is higher than those of the other systems. This trend is consistent with the cases studied in section 5.3.

Once, the condenser effectiveness was determined, the characteristic response of the condensers at various load conditions are predicted using the constant effectiveness assumption approach in chapter 5.

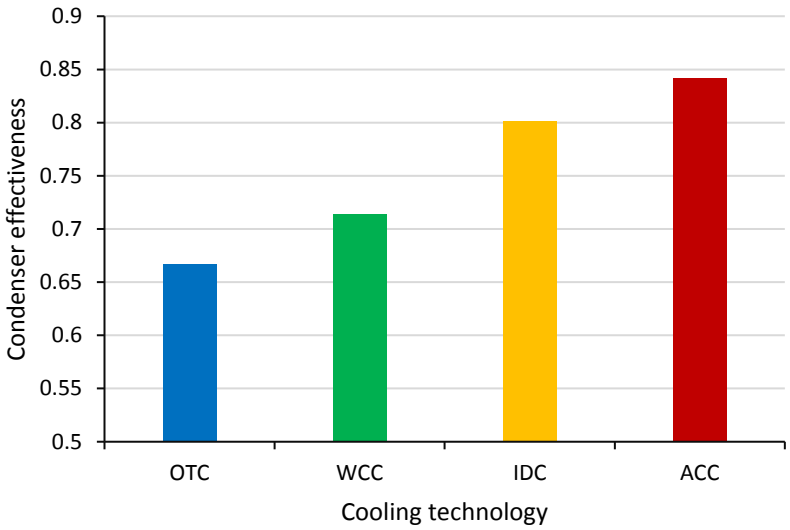

Figure 7.4 Effectiveness of cooling technology selected

Figure 7.5 describes the condensing pressure response characteristics for each of the cooling systems type at varying load conditions. This profile described for each system was used to investigate the part load behaviour of the CFPPs.

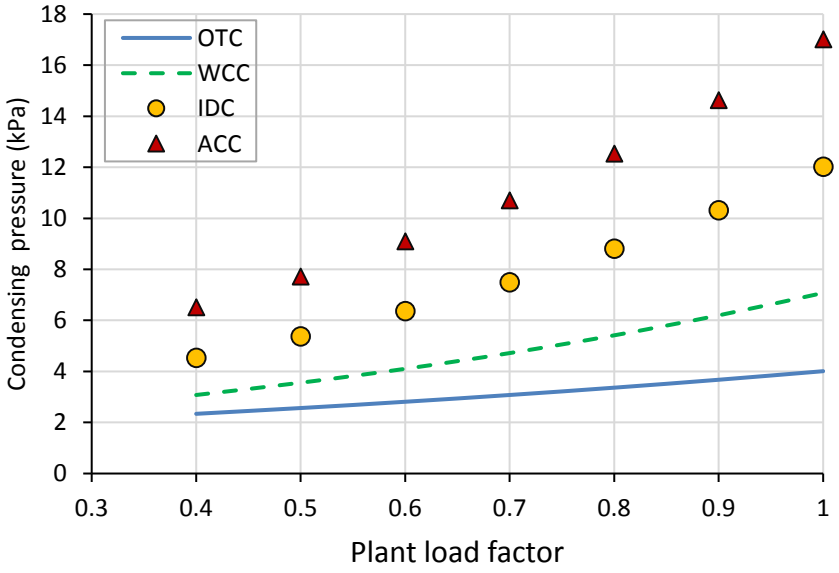

Figure 7.5 The pressure characteristics of the different cooling technologies at part load

7.2 Description of model CFPPs Investigated

The VirtualPlant process model layouts in Figure 6.4, Figure 6.5, and Figure 6.6 were used to set up the hypothetical non-reheat, single reheat, and double reheat CFPPs. With a possible 4 live steam temperatures, 4 pressures, 4 condenser types and 3 reheat options, there is a total combination of 192 power plants. The 192 CFPPs comprises of 64 NRHs, 64 SRHs, and 64 DRHs.

A 12 character naming pattern, that is similar to the one shown in Figure 7.6, was adopted for identifying the key features of each model CFPP. For instance, a CFPP that is identified as R0P12T535C12 (see Figure 7.6), is a non-reheat plant with live steam pressure of 12MPa, temperature of 535℃ and condenser pressure of 12kPa. A single and double reheat type of plant having the same live steam pressure, temperature and condenser back pressure conditions would be represented as R1P12T535C12 and R2P12T535C12 respectively.

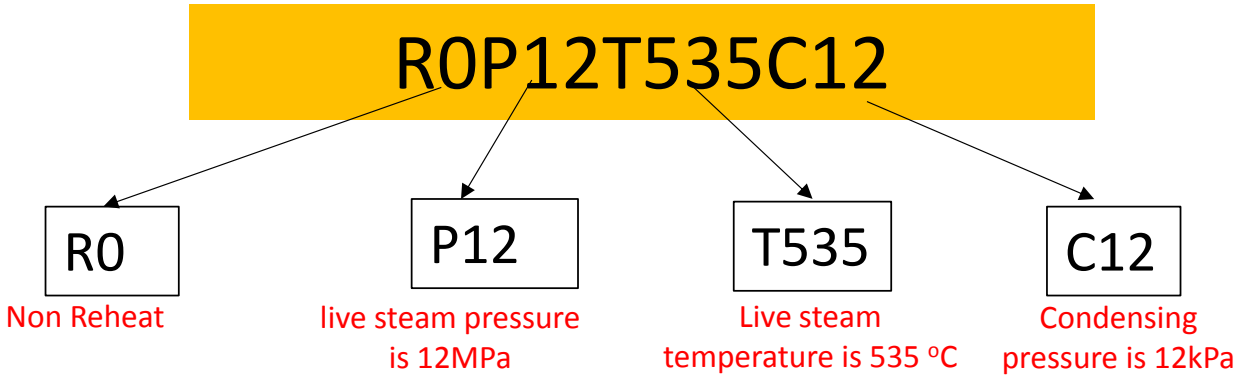

Figure 7.6 Nomenclature for each model plant.

Table 7.3 shows an abridged list of non-reheat, single reheat and double reheat CFPPs that were considered. The key features of each model CFPP is also highlighted. The comprehensive list of all the 192 model CFPP combinations is presented in Appendix B. Plants 001-064 are non-reheats, plants 065-128 are single reheats, while plants 129-192 are double reheats.

Table 7.3 Abridged list of model CFPPs set-up

Plant Name	Plant Description	Degree of Reheat	Throttle Pressure (MPa)	Throttle Temperature (C)	Condensing Pressure (kPa)	1st Reheat Temperature (C)	1st Reheat Pressure (MPa)	2nd Reheat Temperature (C)	2nd Reheat Pressure (MPa)
A.	**Non-reheat CFPPs**								
Plant 001	ROP12T510C4	Non	12	510	4	N/A	N/A	N/A	N/A
Plant 002	ROP12T510C7	Non	12	510	7	N/A	N/A	N/A	N/A
Plant 003	ROP12T510C12	Non	12	510	12	N/A	N/A	N/A	N/A
Plant 004	ROP12T510C17	Non	12	510	17	N/A	N/A	N/A	N/A
B.	Single reheat CFPPs								
Plant 065	RIP12T510C4	Single	12	510	4	510	2.85	N/A	N/A
Plant 066	RIP12T510C7	Single	12	510	7	510	2.91	N/A	N/A
Plant 067	RIP12T510C12	Single	12	510	12	510	3.02	N/A	N/A
Plant 068	RIP12T510C17	Single	12	510	17	510	3.08	N/A	N/A
C.	Double reheat CFPPs								
Plant 129	R2'P12T510C4	Double	12	510	4	510	3.12	510	0.67
Plant 130	R2'P12T510C7	Double	12	510	7	510	3.12	510	0.67
Plant 131	R2'P12T510C12	Double	12	510	12	510	3.48	510	0.95
Plant 132	R2'P12T510C17	Double	12	510	17	510	3.48	510	0.95

Table 7.4 shows a matrix of the possible/practical CFPPs that may exist from the 192 model. There are some combinations that are not practically useful. For instance, it is highly unlikely to find a supercritical or ultra-supercritical CFPP that does not have reheat. Similarly, it is rare to find a double reheat CFPP with a low throttle pressure of 12 MPa. However, these non-practicable CFPPs were still included in the analysis to better understand the trends of the data gathered from the models.

Table 7.4 Combination matrix of typical existing CFPPs

Type of CFPP	Subcritical (Both low and high Subcritical Pressure)	Supercritical	Ultra-critical
NRH	Yes	No	No
SRH	Yes	Yes	Maybe
DRH	Maybe	Yes	Yes

Sizing the model CFPP full load generation capacity: It is common knowledge that large CFPPs tend to be more efficient than the smaller CFPPs. The improvement in the efficiency of the larger CFPPs has little to do with the size of the CFPPs, rather it has to do with the type of steam cycle that the CFPP is operating at. In practice, existing large/big sized CFPP plants tend to have higher cycle efficiencies than the smaller ones due to the following reasons:

- Technological advancements in process equipment material types, process equipment design and manufacture meant that newer plants (and often larger ones) seem to have higher live steam temperature and pressure parameters.
- The smaller sized plants (and usually older ones) tend be non-reheat in nature, unlike the larger CFPP plants which are newer, and tend to have reheats (either single or double reheats).

From the arguments presented in section 6.7, it was shown that the TCHR of CFPPs with similar layouts, and with similar thermodynamic state at corresponding points, is independent of the capacity of the plant. It therefore means that the choice of the capacity has little or no effect on the overall thermal performance of the regenerative Rankine cycle. Any reasonable value could be used for the modelling exercise. Therefore, full load capacity of 200MW, 500MW, and 1000MW were selected as the Turbine Cycle Maximum Continuous Rating (TMCR) gross output for each of the NRHs, SRHs, and DRHs respectively.

7.3 Investigation of TCHR at various load conditions

Each of the 192 model CFPP was set-up at full load conditions by using a similar procedure described in chapter 6. Once, this model setup was completed in the VirtualPlant software, the TCHR at load conditions from 40% to 100% MCR was investigated for each CFPP using the Excel Parametric study feature of VirtualPlant. These load conditions were selected since most CFPPs that run below 40% MCR often require the use of oil support for flame stability. This additional support causes additional emissions that are not from Coal.

In this study, all the CFPPs were investigated using a fixed pressure mode, and then the effect of the sliding boiler pressure operation mode was considered for only the single and double reheats only. There was no need to simulate the modified sliding pressure mode because the fixed and sliding pressure values form the upper and lower limits of the modelling result.

The TCHR data generated from simulating the models at various load conditions were then processed and analysed in a procedure that is described in the next sub-sections.

7.3.1 Data generated and processing

The TCHR characteristics for some of the model CFPPs examined is shown on Figure 7.7. This data was obtained for a fixed boiler pressure operation mode of load control. The general trend is that the heat rate increases with load. However, the information is not very useful in its current form. Therefore, a better way of visualizing the data would be to define a curve fit that has coefficients that bear some physical meaning with the characteristics of each CFPP.

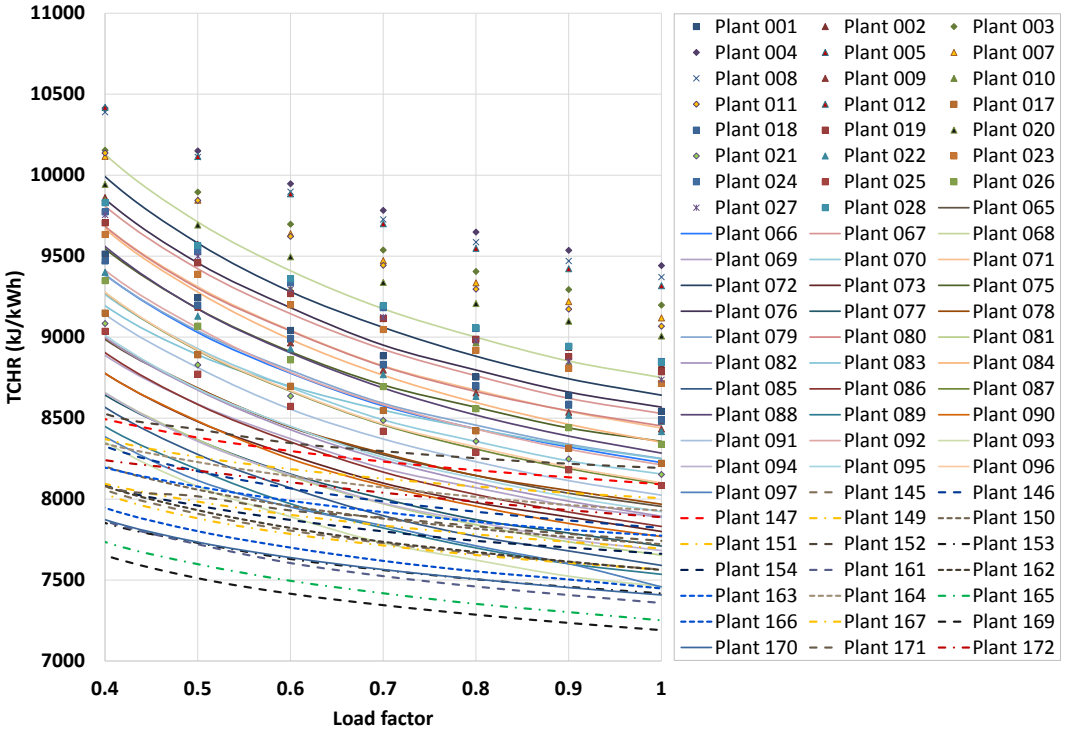

Figure 7.7 TCHR for some of the model CFPPs Investigated at fixed boiler pressure operation mode

The data points obtained from the varying load study were fitted with a power curve as shown in Figure 7.8. The two key parameters (A and $\Re$) of the function tend to have some physical meaning. At $x = 1$, $A = TCHR$. This simply implies that the coefficient A is equal to the TCHR at the turbine maximum continuous rating. The symbol A can be replaced as $TCHR_{FL}$. This value is easily obtained from the full load or valve wide open heat balance diagram.

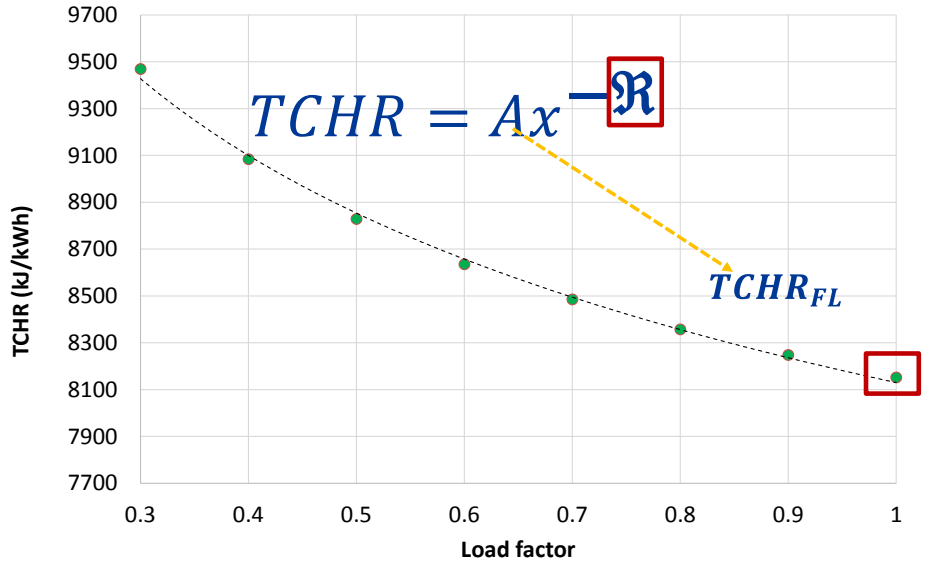

Figure 7.8 Curve fitting the data for one of the CFPPs investigated

In the case where that information is not available, $TCHR_{FL}$ may be estimated using either of the following approaches:

From the **overall plant efficiency data** at full load, it can be written as:

$$TCHR_{FL} = \frac{\eta_{B\cdot FL}}{\eta_{plant_{FL}} \times (1 + f_{aux\cdot FL})} \times 3600 \left(\frac{kJ}{kWh}\right) \tag{7.5}$$

From the **net unit heat rate data**, it can be written as:

$$TCHR_{FL} = NUHR_{FL} \cdot (1 - f_{aux\cdot FL}) \cdot \eta_{B\cdot FL} \cdot \eta_G \tag{7.6}$$

From the **thermal cycle efficiency** at full load, this can be expressed as:

$$TCHR = \frac{1}{\eta_{cycle}} \times 3600 \left(\frac{kJ}{kWh}\right) \tag{7.7}$$

$\eta_{B \cdot FL}$, $\eta_{plant_{FL}}$, $f_{aux \cdot FL}$, $NUHR_{FL}$, η_{cycle}, η_G are the boiler efficiency, power plant efficiency, auxiliary fraction, net unit heat rate, thermal cycle efficiency, and generator efficiency evaluated at the full load conditions.

$\Re$ Is the second coefficient of the curve fit on Figure 7.8. It could be described as the rate of deterioration of TCHR with load. A higher $\Re$ signifies a higher degradation/deterioration of TCHR with load. This is the coefficient that is really unknown and not described in literature. The major output of this work is to offer a simple method to determine $\Re$.

All the subsequent results from the 192 model CFPPs are discussed in terms of the $TCHR_{FL}$ and $\Re$ coefficients generated from the TCHR data produced from the VirtualPlant models.

7.3.2 General Overview of $TCHR_{FL}$ and $\Re$ Values

An overview of the $TCHR_{FL}$ is shown on Figure 7.9. It can be seen that the $TCHR_{FL}$ for the double reheats are generally less than those of single and non-reheats. There is a substantial overlap. This simply indicates that at full load, some single reheat CFPP could actually be more efficient that some double reheats depending on the operating temperatures and pressures at the inlet of the HP turbines, and the condensing pressures.

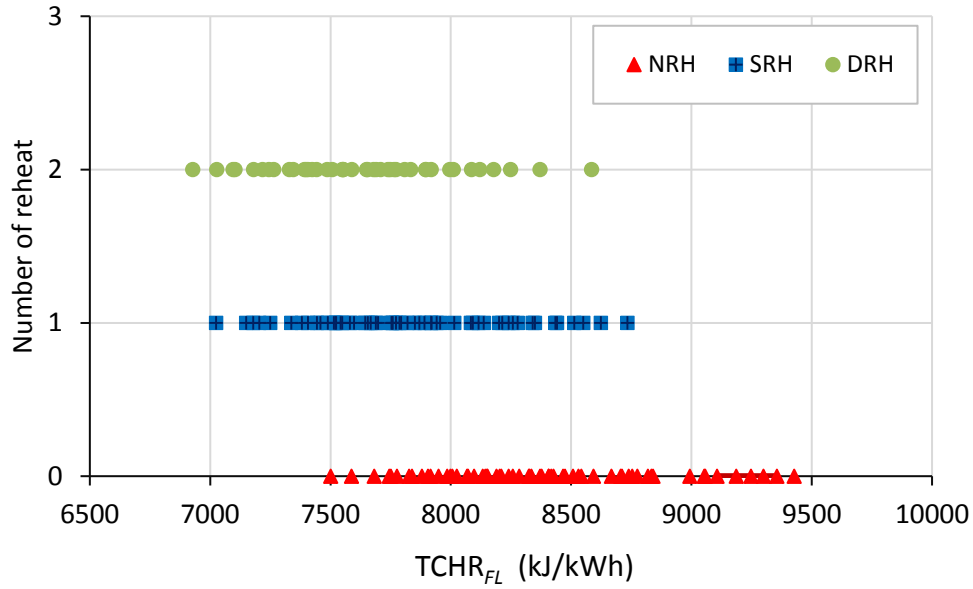

Figure 7.9 Comparing $TCHR_{FL}$ from the simulator

The deviations of the curve-fitted a value compared to the actual heat rate at full load is shown on Figure 7.10. It shows an absolute maximum deviation of 0.2% for most of the units investigated. This therefore confirms that $TCHR_{FL}$ can be used to represent the the A coefficient in the V-TCHR model.

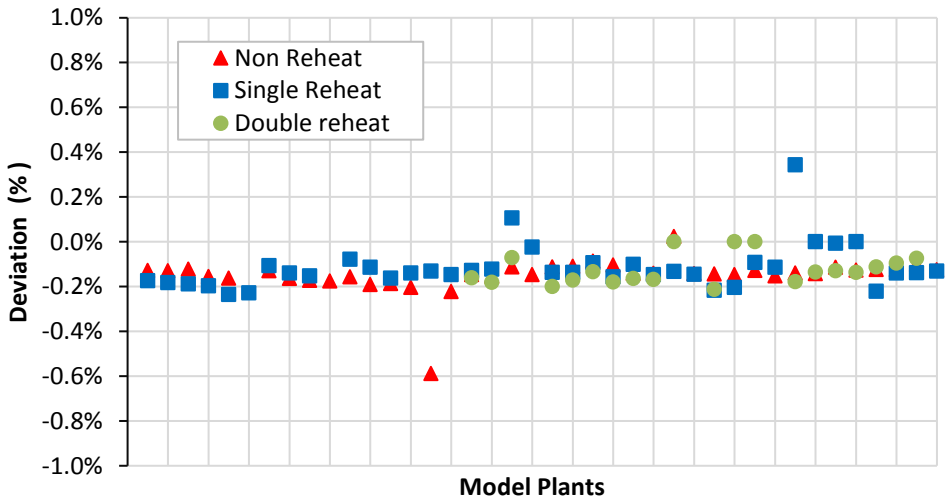

Figure 7.10 Deviations in A-value from the full load TCHR from the simulator

The relationship between $TCHR_{FL}$ and $\Re$ for the various CFPPs is given in Figure 7.11. The first thing that is obvious is that on average, the rate of TCHR deterioration ($\Re$) of the non-reheats

appears to be almost twice the value for the single and double reheats. As a coarse assumption, $\mathfrak{R}$ could be taken as 0.12 for the non-reheats, 0.06 for the single and 0.05 for double reheats. This could serve as a first rough estimate of the rate of TCHR deterioration. It therefore means that the degree of reheat plays a strong role in the rate of TCHR deterioration for the non-reheat and reheat cycles. The range of $\mathfrak{R}$ values seen for each degree of Reheat is displayed in Table 7.5.

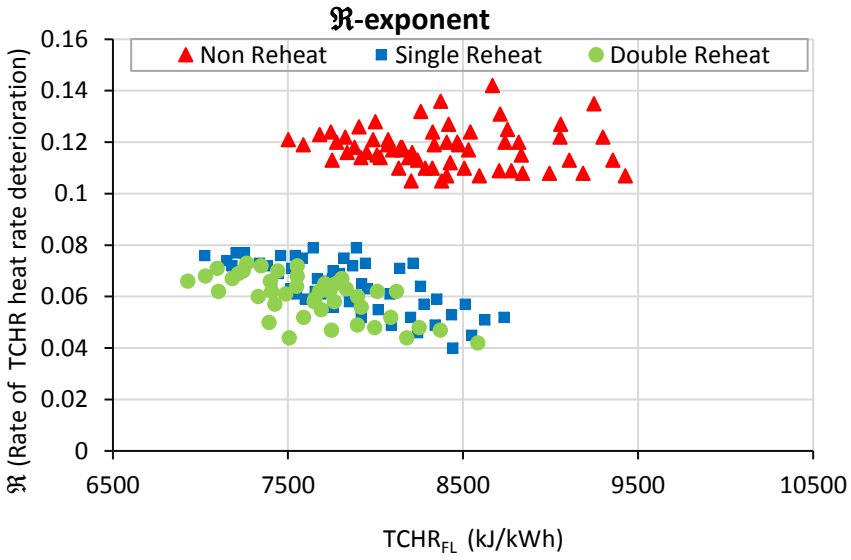

Figure 7.11 Relationship between $\mathfrak{R}$ and $TCHR_{FL}$

Table 7.5 Rate of deterioration of TCHR ($\mathfrak{R}$)

	Range
NRHs	0.109 – 0.142
SRHs	0.046 – 0.079
DRHs	0.047 – 0.072

7.4 V-TCHR Generic Model Description

The high level analysis of the data in section 7.3.2 already suggests that there is a relationship between the degree of reheat and the rate of TCHR deterioration at varying load conditions. The impact of the interaction between the key parameters (see Figure 7.12) on the TCHR rate of deterioration ($\mathfrak{R}$) at varying load conditions is further investigated.

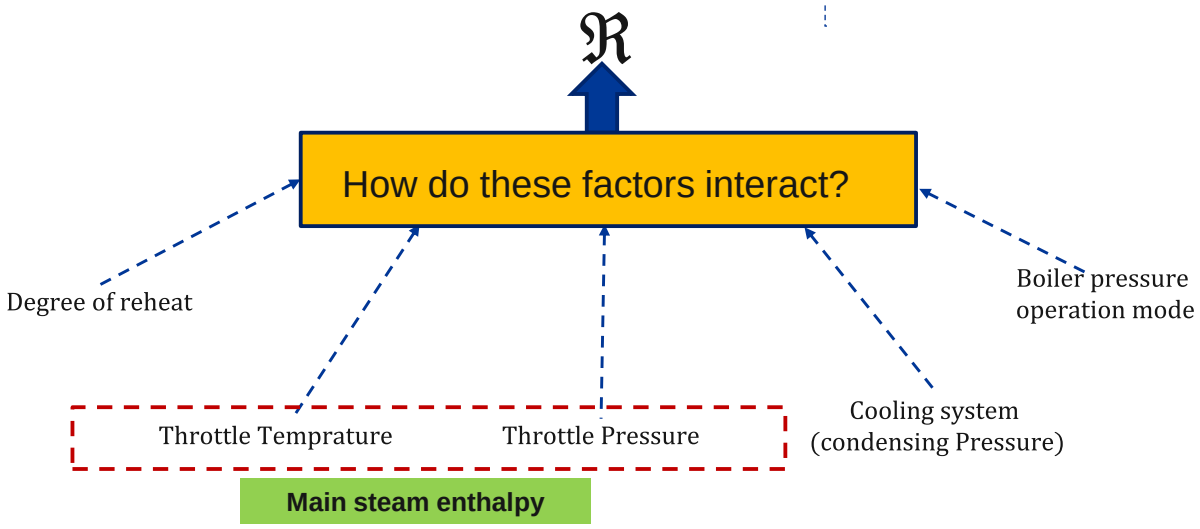

Figure 7.12 Key parameters that could have an impact on $\mathfrak{R}$

The combined effects of live steam temperature and pressure for the different cooling technologies is investigated by examining the impact of the live/main steam enthalpy on $\mathfrak{R}$ for the model CFPPs. This effect is shown on Figure 7.13, Figure 7.14, and Figure 7.15 for the non-reheat, single reheat and double reheat CFPPs respectively.

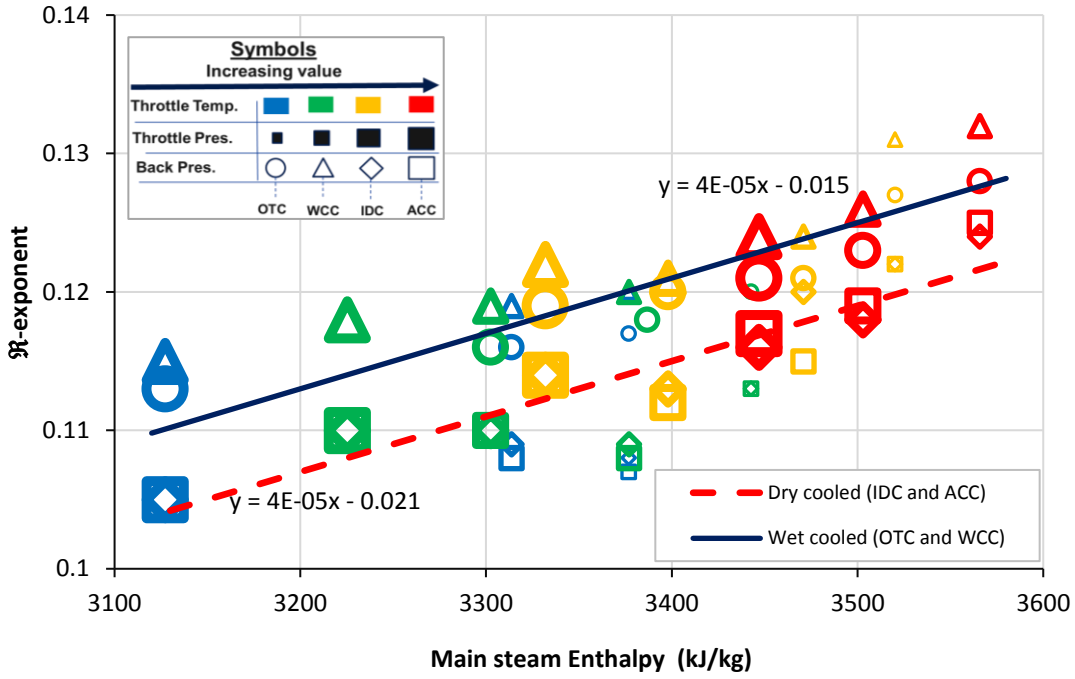

Figure 7.13 Profile for ℜ –exponent: Non reheat (fixed boiler pressure operation mode)

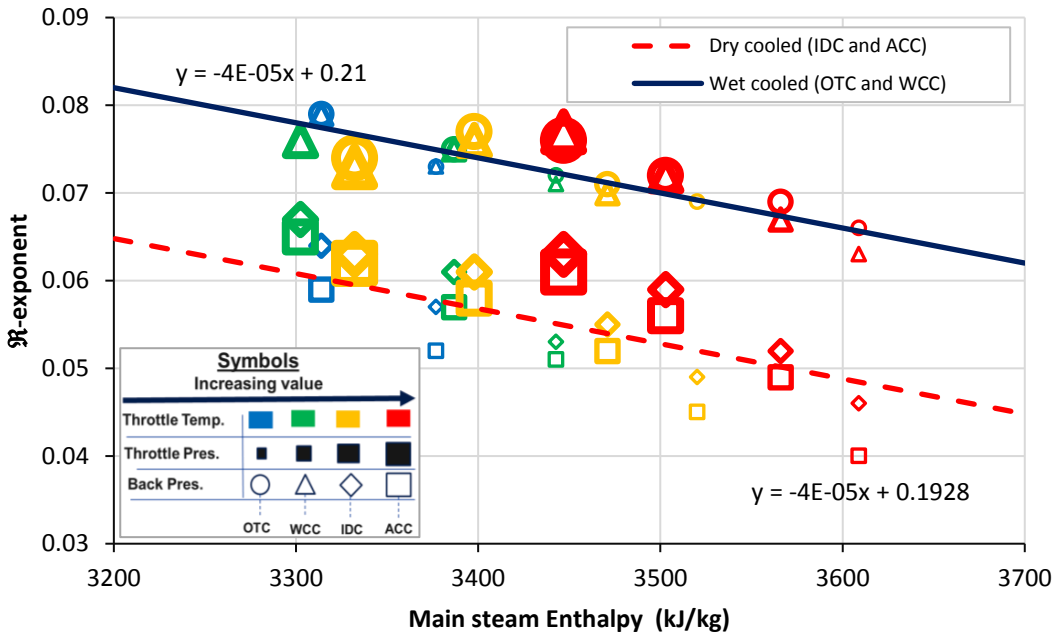

Figure 7.14 Profile for ℜ –exponent: Single reheat (fixed boiler operation mode)

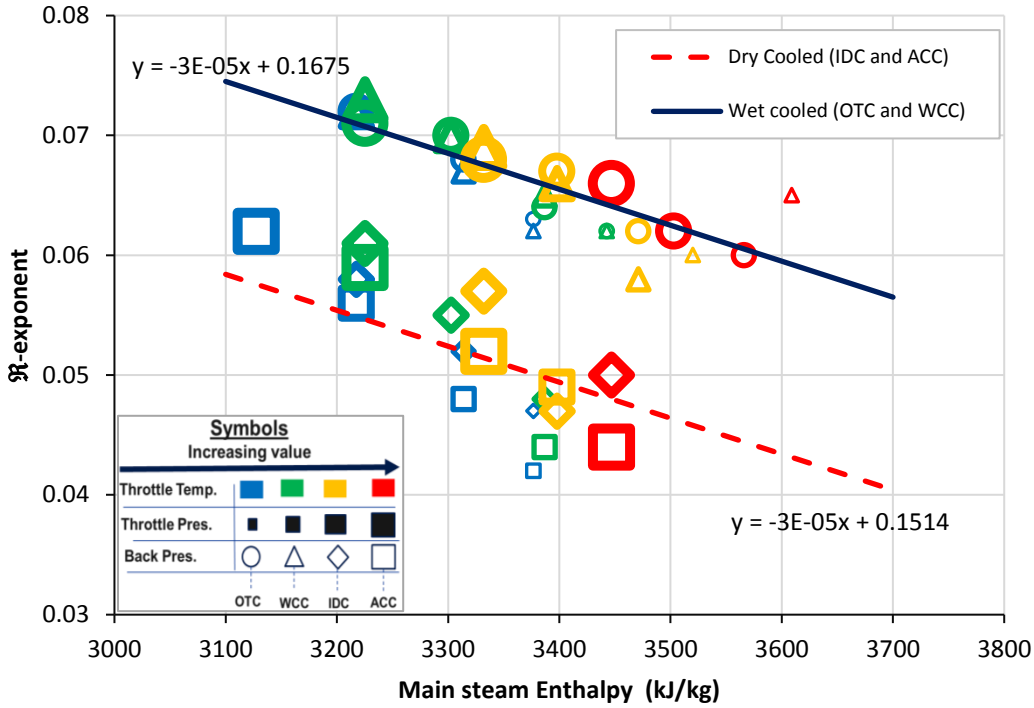

Figure 7.15 Profile for $\Re$ –exponent: Double reheat (fixed boiler pressure Operation mode)

The live/main steam enthalpy (h_{main}) is the steam enthalpy at the inlet of the high pressure turbine. It is a function of the live steam temperature and pressure. For the NRH CFPPs (see Figure 7.13), it can be seen that the rate of TCHR deterioration ($\Re$) is directly proportional to the live steam enthalpy. It can also be seen that $\Re$ for the wet-cooled systems (OTC & WCC) appear to be larger than those of the dry cooled systems (IDC & ACC). For the SRH CFPPs (see Figure 7.14) and DRH CFPPs (Figure 7.15), the rate of TCHR deterioration ($\Re$) is inversely proportional to the live/main steam enthalpy. This is likely due to the presence of a reheat point. Similar to the NRH CFPPs, the rate of TCHR deterioration ($\Re$) for the wet-cooled systems (OTC & WCC) appear to be more than those of the dry cooled systems (IDC & ACC).

It might appear that the higher condenser pressures (12kPa & 17kPa selected for the dry cooled systems) yields a lower rate of TCHR deterioration. However, it is the change in the condenser pressure response at low load rather than full load condenser pressure that affects the rate of TCHR deterioration. This change in the condenser pressure response at varying load is strongly linked to the effectiveness of the main steam condenser of the CFPP. A condenser with a higher effectiveness

such as is generally present in the dry cooled systems would cause a higher/greater change in the back pressure response at part load, than the condensers of wet-cooled systems (WCCs and OTCs) that have a slightly lower effectiveness. This is demonstrated in Figure 7.16 (a) where the same plant was analyzed with a constant and varying condenser pressure. It can be seen in Figure 7.16 (b), that the $\mathfrak{R}$-value for a constant condenser pressure scenario, which depicts a situation where the condenser effectiveness is much lower than the typical condenser effectiveness, is higher than the varying condenser pressure scenario.

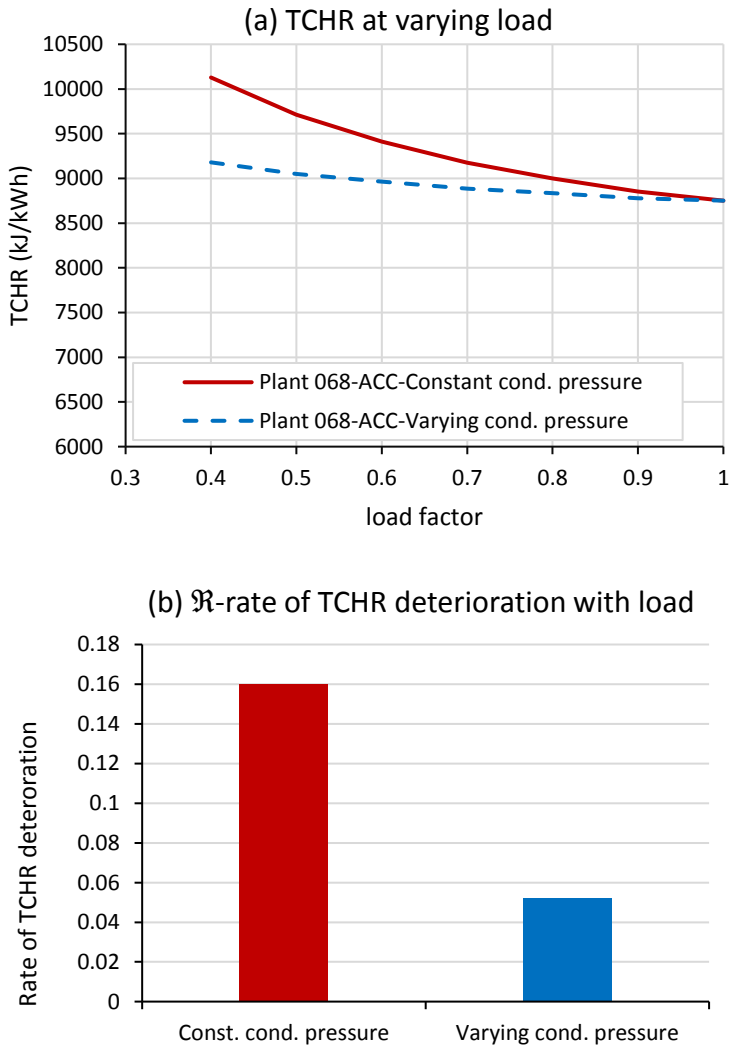

Figure 7.16 Demonstrating the impact of effectiveness on $\mathfrak{R}$: Model CFPP Plant No. 068

The key finding here is that, CFPPs that have higher main steam condenser effectiveness, would experience a smaller deterioration in the TCHR, and hence would/should have a lesser adverse impact on the heat rate deterioration at part load.

The expression for the $\Re$ –exponent of the V-TCHR model can be defined by a simple linear model for the non-reheats, single reheats, and double reheats in Equation (7.8). h_{main} is the live/main steam enthalpy in (kJ/kg), at the inlet of the high pressure turbine. $S_{\Re}$ and $C_{\Re}$ are the slope and the intercept of the $\Re$ vs. h_{main} plot. The values for $S_{\Re}$ and $C_{\Re}$ are presented in Table 7.6. $C_{\Re}$ appears to be linked to the kind of condenser cooling system technology used while considering the same category of reheats.

$$\Re = S_{\Re} h_{main} + C_{\Re} \tag{7.8}$$

Table 7.6 Values for $S_{\Re}$ and $C_{\Re}$ for fixed boiler pressure operation

Number of Reheat stages	$S_{\Re}$	$C_{\Re}$	
		OTC & WCC	IDC & ACC
NRH	$+4x10^{-5}$	-0.015	-0.021
SRH	$-4x10^{-5}$	0.210	0.1928
DRH	$-3x10^{-5}$	0.1625	0.1514

7.5 Sensitivity Analysis

7.5.1 Dependence of $\Re$ on Pressure and/or Cooling Technology

The sensitivity of $\Re$ to the condensing pressure selected for each cooling technology is presented here. This was done by selecting two additional ambient scenarios (see Table 7.7). The low ambient condition has a dry bulb temperature and relative humidity lower than the reference ambient, while the high ambient conditions has a dry bulb temperature that is greater than the reference condition.

The selection of these two additional ambient conditions would impact the cooling fluid inlet temperature into the condenser, and consequently affect the condensing pressure.

Table 7.7 Reference ambient conditions considered.

Ambient conditions	Dry Bulb Temperature $(°C)$	Wet bulb Temperature $(°C)$	Relative Humidity (%)
Low	15	7.36	30
Reference	25	18	60
High	40	32.68	60

The condenser effectiveness, the approach, TTD value, and the cooling fluid temperature rise assumed for the different cooling systems, in the high and low ambient condition, is similar to the ones used under the reference conditions. The same method was used to obtain the condensing pressure at the various load conditions.

The condensing pressure profiles for each cooling technology at different ambient conditions is shown on Figure 7.17. These additional condensing pressure profiles were used in investigating the sensitivity of $\mathfrak{R}$ to the selected pressure response.

A total of 24 additional process CFPP models were built by altering the design condenser pressures for each cooling technology. The plant description for the reference cases for each technology and the altered cases (high and low) are presented on Table 7.8. For the non-reheat CFPPs, Plants 1, 22, 43, and 64 were selected as the reference cases for the OTC, WCC, IDC, and ACC cooling technologies. These model CFPPs are represented as Plants 1ref, 22ref, 43ref, and 64 ref respectively on Table 7.8. For instance, Plants 1ref, 1low, & 1high are once through cooled (OTC) non-reheat CFPPs with the same live steam temperature and pressure, same condenser effectiveness but with condensing pressures of 2.81 kPa, 4 kPa, and 7 kPa respectively. Plants 65, 86, 107, and 138 were selected as the reference CFPPs for the single reheat while Plants 129, 150, 167 and 192 were selected as the reference CFPPs for the double reheats. The effectiveness of the condensers selected for each cooling technology are the same for the low, reference and high ambient conditions selected.

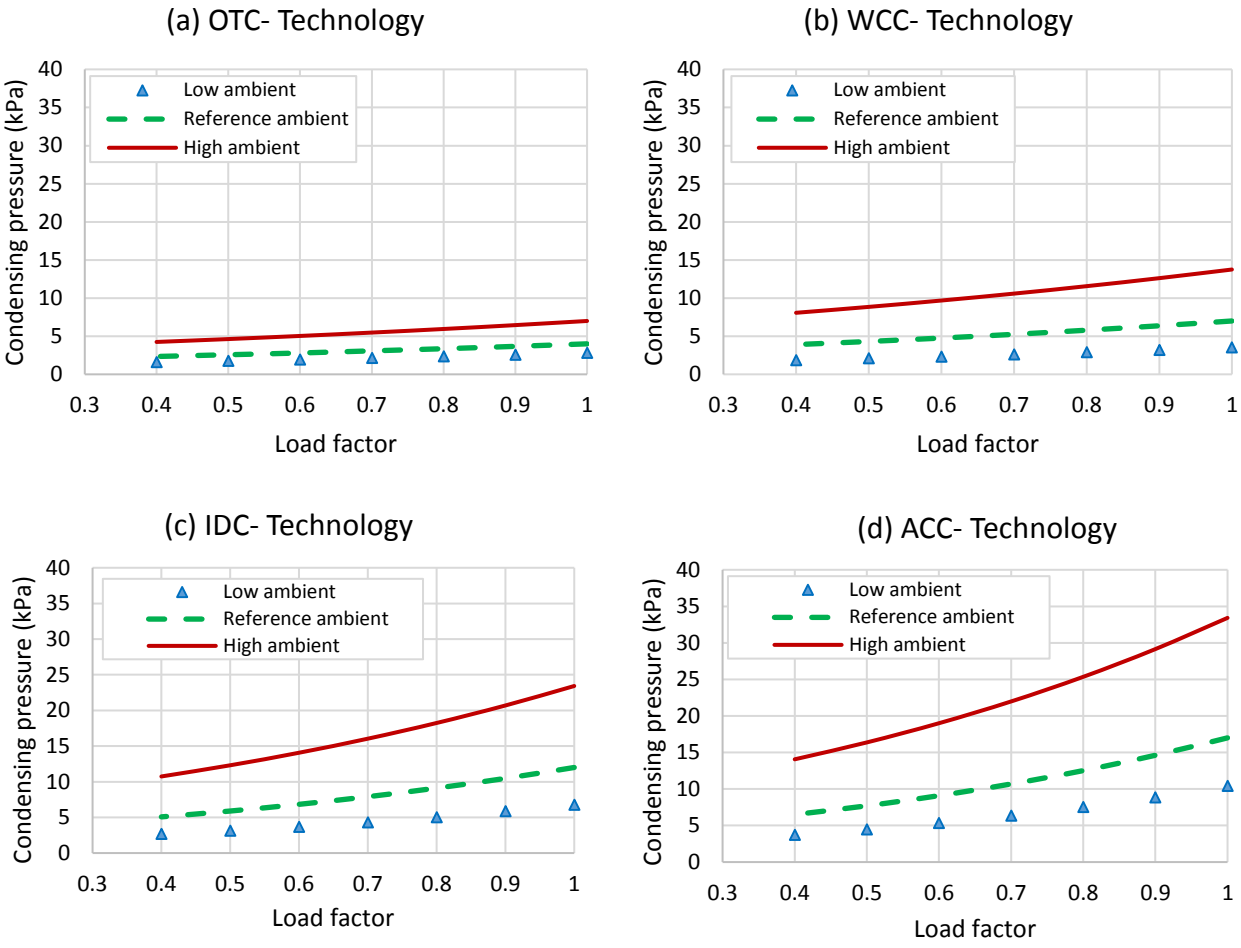

Figure 7.17 condensing pressure profiles for each cooling technology at different ambient conditions

Table 7.8 24 Additional model CFPPs with different ambient conditions

	NRH CFPPs		SRH CFPPs		DRH CFPPs	
	Plant name	Plant description	Plant name	Plant description	Plant name	Plant description
OTC	Plant 1low	ROP12T510C2.81	Plant 065low	RIP12T510C2.81	Plant 129low	R2'P12T510C2.81
	Plant 1ref	ROP12T510C4	Plant 065ref	RIP12T510C4	Plant 129ref	R2'P12T510C4
	Plant 1high	ROP12T510C7	Plant 065high	RIP12T510C7	Plant 129high	R2'P12T510C7
WCC	Plant 22low	ROP17T535C3.54	Plant 086low	RIP17T535C3.54	Plant 150low	R2'P17T535C3.54
	Plant 22ref	ROP17T535C7	Plant 086ref	RIP17T535C7	Plant 150ref	R2'P17T535C7
	Plant 22high	ROP17T535C13.75	Plant 086high	RIP17T535C13.75	Plant 150high	R2'P17T535C13.75
IDC	Plant 43low	ROP24T565C6.76	Plant 107low	RIP24T565C6.76	Plant 167low	R2'P24T535C6.76
	Plant 43ref	ROP24T565C12	Plant 107ref	RIP24T565C12	Plant 167ref	R2'P24T535C12
	Plant 43high	ROP24T565C23.42	Plant 107high	RIP24T565C23.42	Plant 167high	R2'P24T535C23.42
ACC	Plant 64low	ROP30T600C10.41	Plant 128low	RIP30T600C10.41	Plant 192low	R2'P30T600C10.41
	Plant 64ref	ROP30T600C17	Plant 128ref	RIP30T600C17	Plant 192ref	R2'P30T600C17
	Plant 64high	ROP30T600C33.42	Plant 128high	RIP30T600C33.42	Plant 192high	R2'P30T600C33.42

In all the 24 cases examined, it is evident on Figure 7.18, Figure 7.19, and Figure 7.20 that $\mathfrak{R}$ is directly proportional to the condenser pressure selected. It is also interesting to note that the $\mathfrak{R}$ -value for the wet-cooled (OTC & WCC) still tends to be higher than the values for the dry-cooled systems (IDC & ACC). The magnitude of this effect appears to reduce with the degree of reheat. Similarly, while considering how the specific cooling technologies impact the $\mathfrak{R}$ values. It appears that for all the non-reheats, single reheats and double reheats, the $\mathfrak{R}$ values can be grouped into the wet cooled systems (OTC, and WCC) and the dry cooled systems (IDC & ACC). This implies that the cooling technology effectiveness (type) has a stronger influence on the $\mathfrak{R}$ exponent than the actual pressure of the condenser selected.

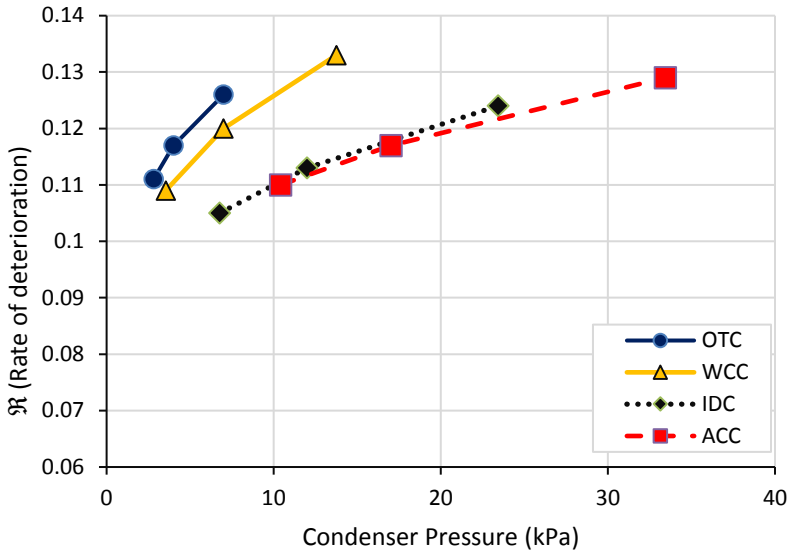

Figure 7.18 Impact of selecting a different design condenser pressure at full load: Non reheats

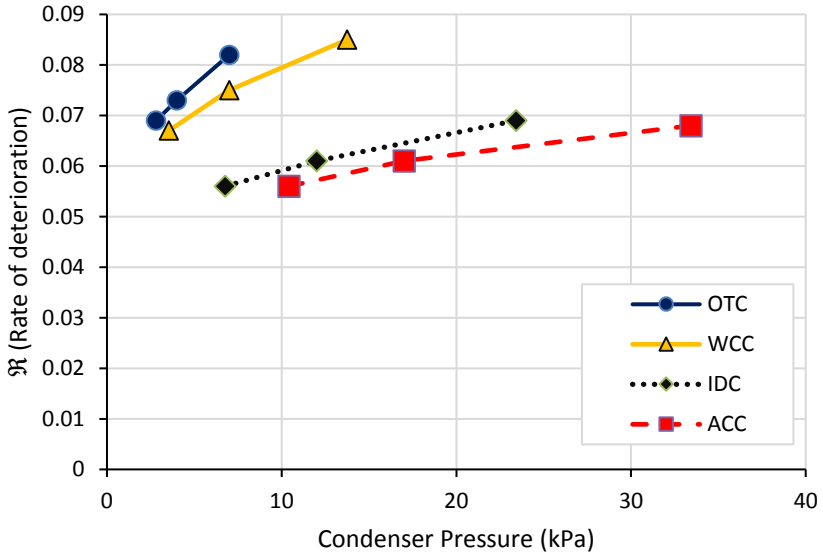

Figure 7.19 Impact of selecting a different design condenser pressure at full load: Single reheats

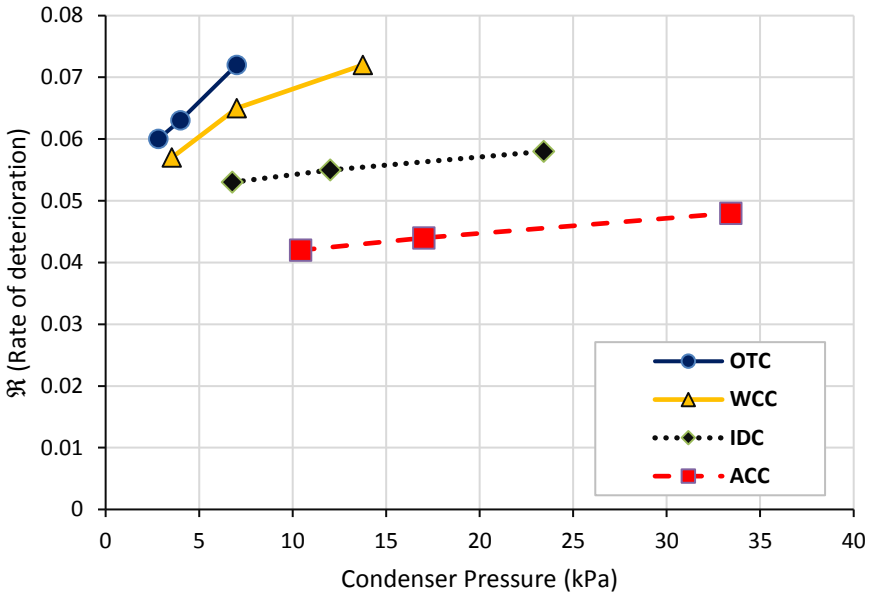

Figure 7.20 Impact of selecting a different design condenser pressure at full load: Double reheats

The V-TCHR model can still be used if the VWO condenser pressure is different from the references values (see Table 7.1) used to develop the model. The rate of TCHR deterioration with load can be adjusted for a different condenser back pressure by using the equation below:

$$\Re = \Re_{ref}(1 + \theta_{\Re}) \tag{7.9}$$

$\Re_{ref}$ is the rate of TCHR deterioration with load at the relevant reference condensing pressure (Table 7.1). This is determined using the relevant V-TCHR model already described. $\theta_{\Re}$ is the condenser pressure based $\Re$ adjustment coefficient for VWO condenser pressure. $\theta_{\Re}$ is evaluated from any of the relevant curves presented in Figure 7.21, Figure 7.22, Figure 7.23. These figures represent the $\Re$ adjustment curves for non-reheat, single reheat and double reheat CFPPs respectively. The data for these curves were derived from Figure 7.18, Figure 7.19, and Figure 7.20 respectively.

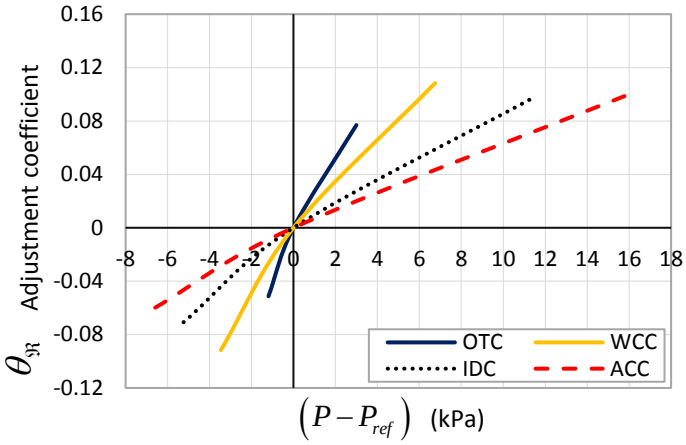

Figure 7.21 $\Re$ adjustment curves for different VWO condenser pressure: Non reheat CFPPs

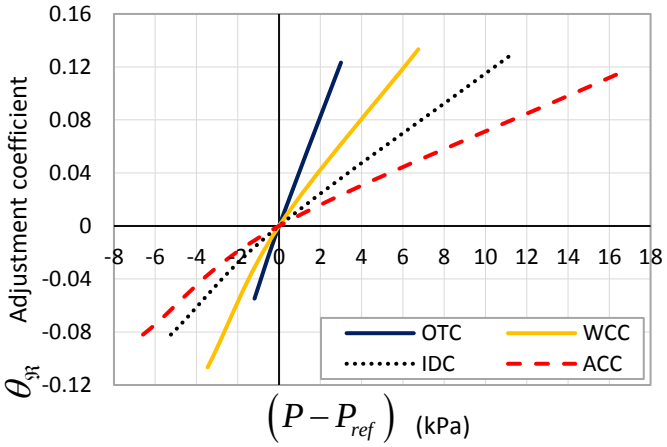

Figure 7.22 $\Re$ adjustment curves for different VWO condenser pressure: Single reheat CFPPs

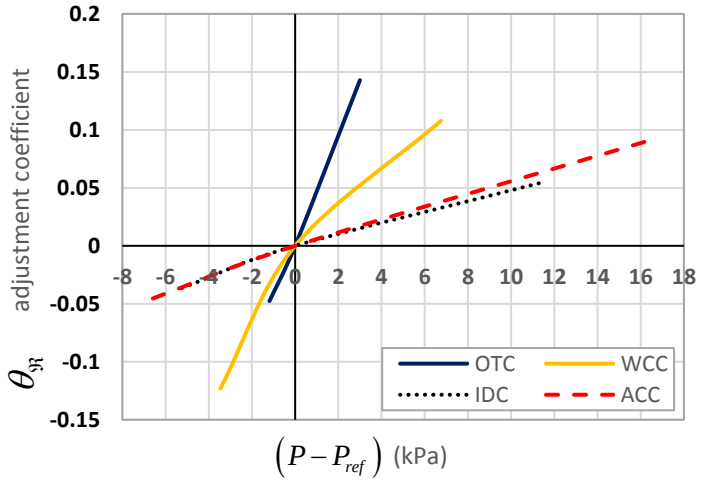

Figure 7.23 $\Re$ adjustment curves for different VWO condenser pressure: Double reheat CFPPs

7.5.2 Dependence of $\mathfrak{R}$ on Boiler pressure operation mode

The dependence of $\mathfrak{R}$ on the boiler pressure mode of operation at part load is presented here. Fixed pressure operation is the common method of operation for most non-reheats plants. This is because these are drum type boilers, and these types of boilers are best controlled using the fixed pressure operation. Since some single and double reheat CFPPs either use the fixed boiler pressure operation or the sliding boiler pressure method to attain a low load generation level, it therefore becomes important to examine the sensitivity of $\mathfrak{R}$ to the type of boiler pressure mode of operation.

A simulation of all the single reheats and double reheat CFPPs was carried out under the sliding boiler pressure mode of operation. The relationship between the $\mathfrak{R}$ -value and the live steam enthalpy is shown on Figure 7.24 and Figure 7.25 respectively. It can be seen that the same trends discussed for the fixed boiler pressure operation mode were seen. However, the rate of TCHR deterioration ($\mathfrak{R}$) for the sliding pressure mode of operation appears to be lesser than the one for the fixed pressure mode of operation. This is evidence in the $S_{\mathfrak{R}}$ and $C_{\mathfrak{R}}$ values presented on Table 7.9. This observation is expected as it has been reported in [38] that the heat rate at low load for the sliding boiler pressure mode of operation is less than the one for the fixed boiler pressure mode of operation.

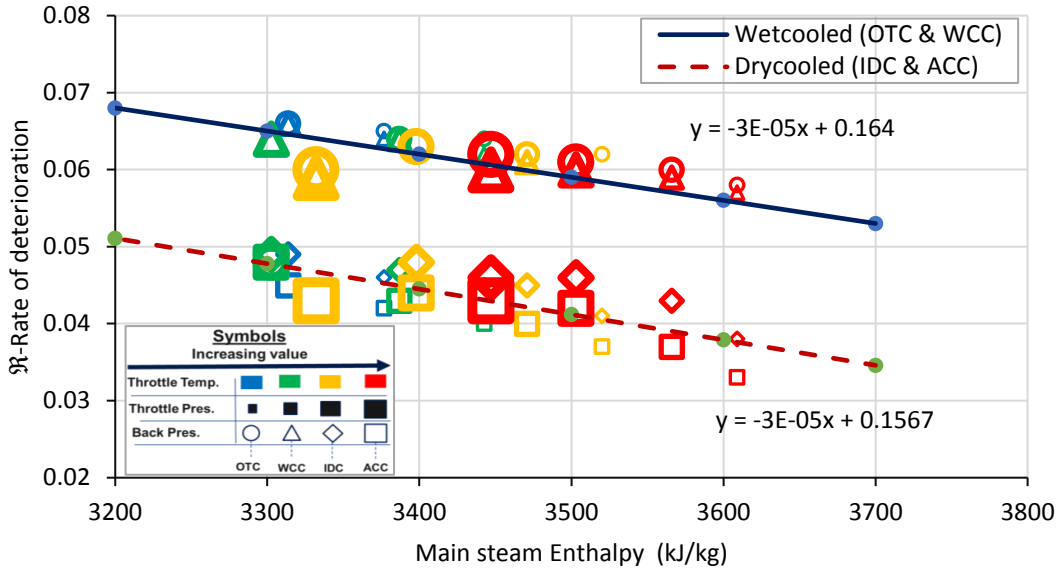

Figure 7.24 Profile for $\Re$ –exponent for single reheat: Sliding boiler pressure mode

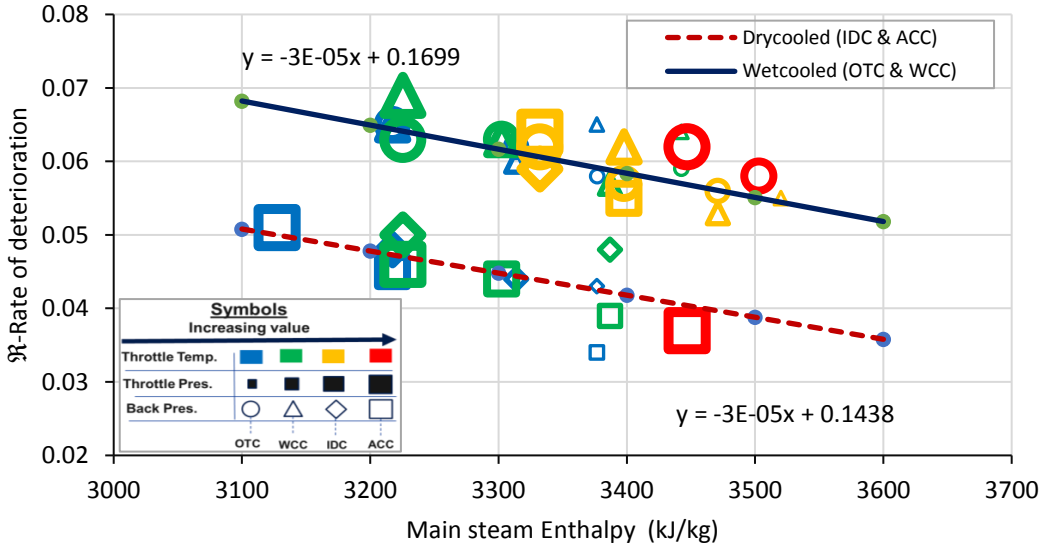

Figure 7.25 Profile for $\Re$ –exponent for double reheat: sliding boiler pressure mode

Table 7.9 values for $S_{\Re}$ and $C_{\Re}$ for sliding boiler pressure operation

Number of Reheat stages	$S_{\Re}$	$C_{\Re}$	
		OTC & WCC	IDC & ACC
SRH	-3×10^{-5}	0.164	0.1567
DRH	-3×10^{-5}	0.1699	0.1438

7.6 Validation of the V-TCHR Model

The validation of the V-TCHR was done for five different case study categories (discussed in sections 7.6.1 and 7.6.2) with data drawn from 9 CFPPs (2 non-reheats, and 7 SRHs) listed on Table 6.2. There are a few variations in the case study categories. The variation is either due to cooling technologies, or number of reheat stages or the mode of boiler pressure operation of the CFPPs at part load conditions.

7.6.1 Non-Reheats

The validation of the V-TCHR model for non-reheat CFPPs was done using two different non-reheat CFPPs (Plants B and C).

- Plant B is an indirect dry cooled (IDC) type non-reheat CFPP operated under fixed boiler pressure mode. This plant represents case study category 1.
- Plant C is a wet cooled condenser (WCC) type non-reheat CFPP operated under fixed boiler pressure mode. This plant represents case study category 2.

A comparison of the V-TCHR model results with the plant performance data of case study category 1 & 2 is shown on Figure 7.26 and Figure 7.27 respectively. It can be seen that the model result compares favourably well with the performance data. The model slightly over-predicts the TCHR at lower loads. The mean and maximum absolute deviation seen for Plant B are 2.7% and 4.3% while those of Plant C are 1.2% and 2.9% respectively. One of the possible reason for the discrepancy could be due to the presence of a steam driven boiler feed pump in the real CFPP. CFPPS with steam driven BFPs usually have lesser heat rates than ones with electrically driven motor.

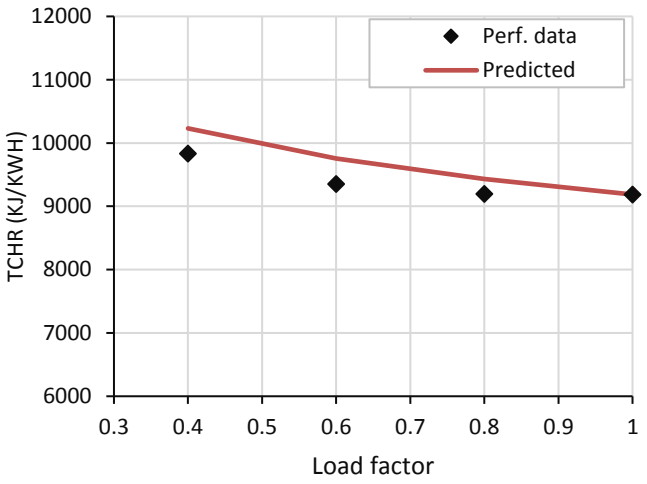

Figure 7.26 V-TCHR model validation for case study category 1: Plant B

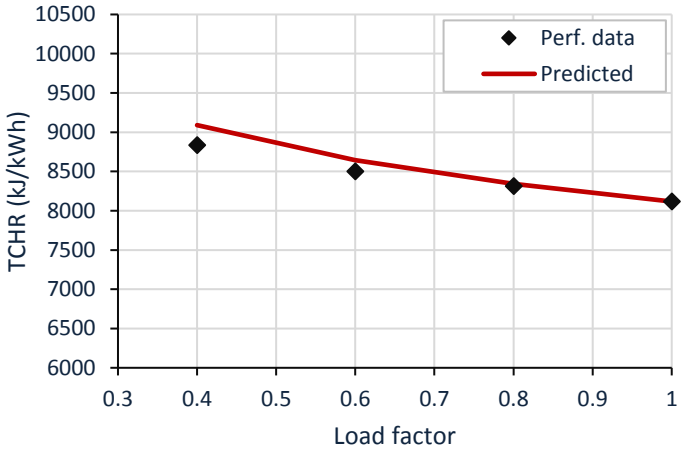

Figure 7.27 V-TCHR model validation for case study category 2: Plant C

7.6.2 Single Reheats

The validation of the V-TCHR model for single-reheat CFPPs was done using seven different single reheat CFPPs (Plants U, O, K, J, F, H, and I).

- Plant U is an indirect dry cooled condenser (IDC) type single-reheat CFPP operated under sliding boiler pressure mode. This plant represents case study category 3.
- Plant O and K are Air-cooled condenser (ACC) type single-reheat CFPP operated under sliding boiler pressure mode. These plants represents case study category 4.

- Plant J, F, H, and I are wet cooled condenser (WCC) type single-reheat CFPPs operated under fixed boiler pressure mode. These plants represent case study category 5.

A comparison of the V-TCHR model results with the plant performance data of case study category 3, 4, and 5 is shown on Figure 7.28, Figure 7.29, and Figure 7.30 respectively. It can be seen that the model results also compares favourably well with the performance data. For case study category 3 (see Figure 7.28), at 80% and 60% MCR, the absolute maximum deviation at these two load points were within 2%. However, at 37% MCR load condition, the absolute deviation was 6.9% - this margin is higher than the ones that have been seen in the previous models. The main reason for this is because the condenser pressure at all the load conditions in the performance data is reported as constant. The V-TCHR model fundamentally assumes that the condensing pressure of the CFPPs reduces at lower load. This assumption is consistent with what is seen in most plants that operate at lower load conditions. The constant condenser pressure in this case study category adds an additional effect on the TCHR, which the V-TCHR model does not capture. For case study category 4 (Figure 7.29), It can be seen that the model result also compares favourably well with the plant performance data at 80% and 60% MCR. The absolute maximum at these two load points were within 0.5%. However, at 40% MCR (for plant O) and 45.6% MCR (for plant K), the absolute deviation were slightly higher, a margin of 3.2% and 2.1% respectively. For case study Category 5 (Figure 7.30), it is interesting to note for Plant J, that the model still predicts a reasonably accurate result below 40% MCR. Furthermore, there was a steam driven feed pump in the four plants in this category that were not modelled. In plant H there was an extra FWH that was not included in the VirtualPlant process models. Despite of these additional components, the maximum absolute deviation seen in the model results for Plants J, F, H & I were 1.9%, 1.7%, 1.3%, and 1% respectively.

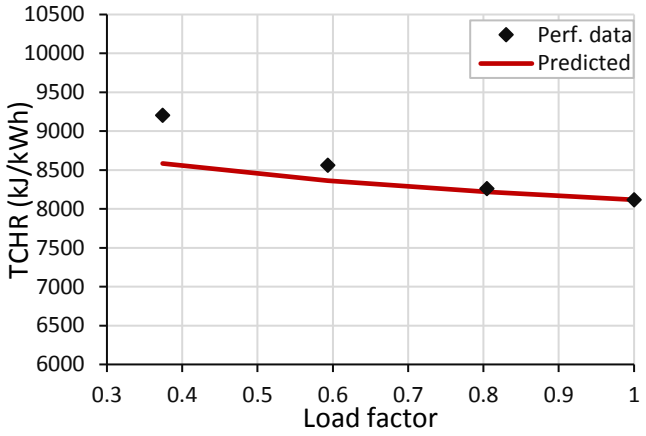

Figure 7.28 V-TCHR model validation for case study category 3: Plant U

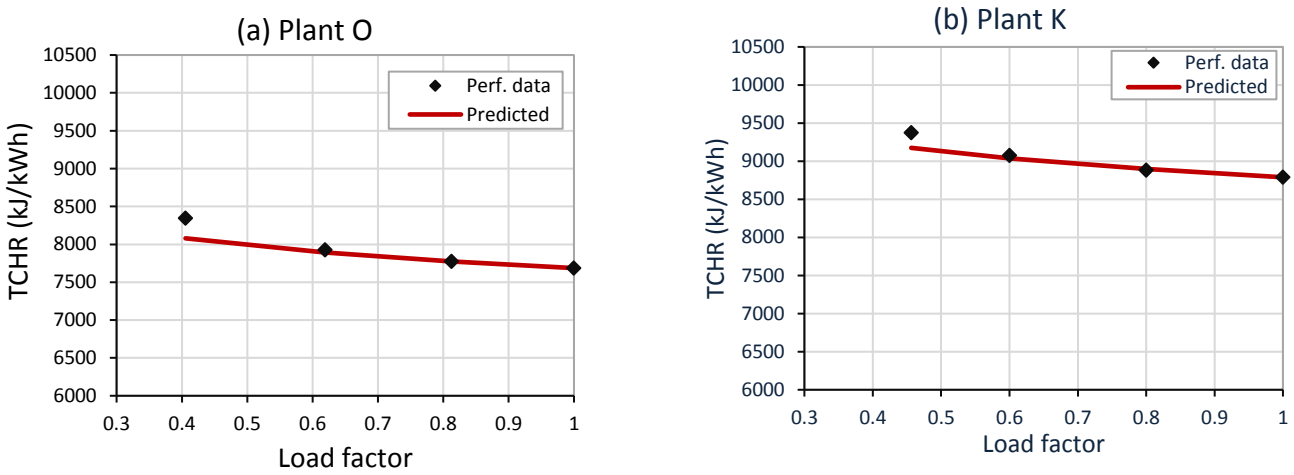

Figure 7.29 V-TCHR model validation for case study category 4: Plant O & K

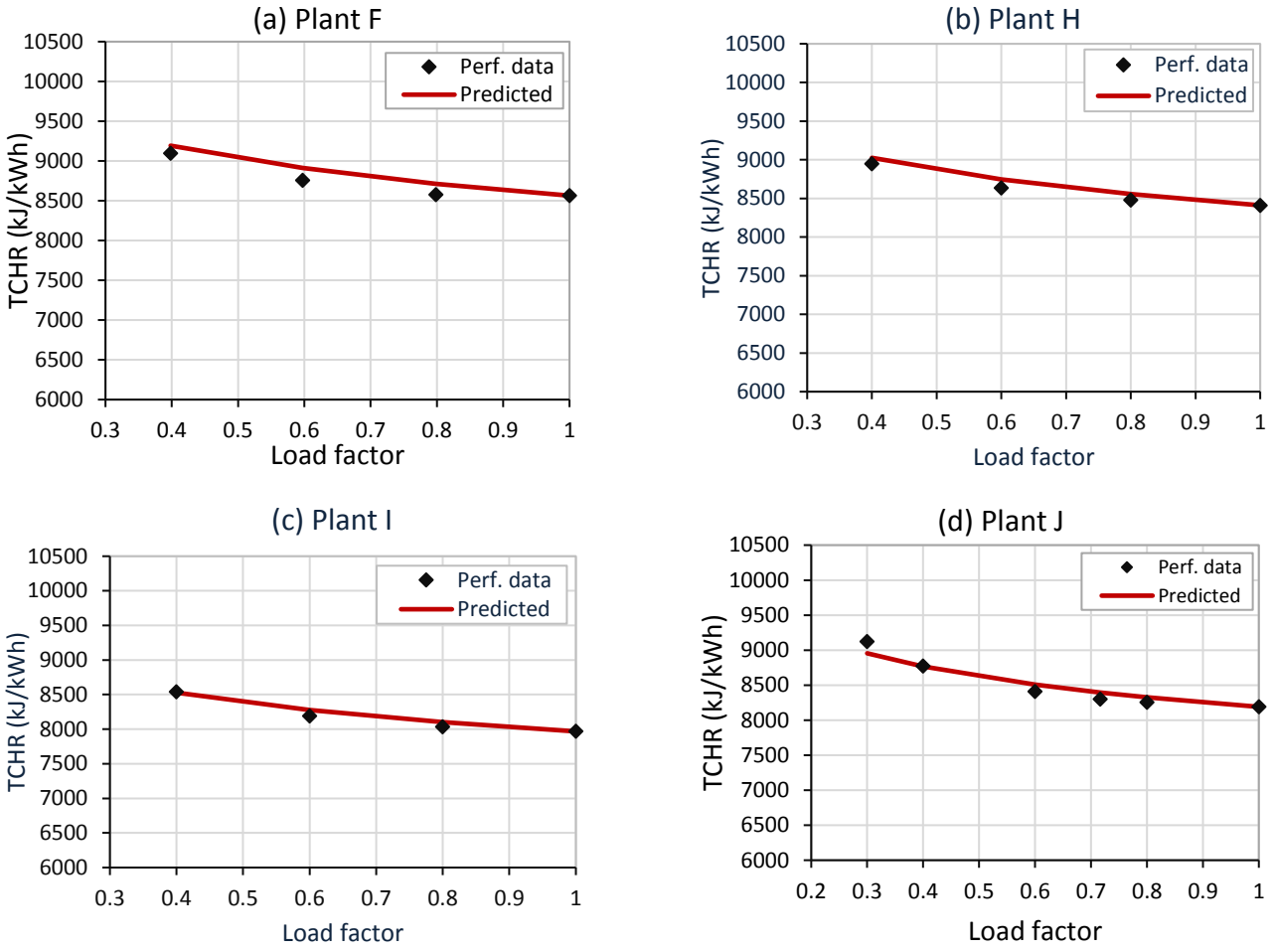

Figure 7.30 V-TCHR model validation for case study category 5: Plant F, H, I, J

7.6.3 Summary of validation results

A summary of the deviations of the V-TCHR model results for all the cases investigated is presented on Figure 7.31 and Figure 7.32. Across the various load conditions, the maximum absolute deviation seen for most of the CFPPs at plant load factors of 30-45%, 60%, 80% load conditions were 3.03%, 1.74%, 1.13% respectively. From these observations, it can be seen that the accuracy of the model decreases with load. Despite of this, the accuracy of the V-TCHR model is still commendable considering the level of simplification done from a very detailed actual plant to a generic CFPP model, to a heat rate model, to a grouping of heat rate responses and then to this simplistic V-TCHR model. Across the various CFPP types, the accuracy of the V-TCHR model (see Figure 7.32) appears

to be higher in the single reheat cases that the non-reheat systems. The maximum absolute deviation seen in non-reheats and single reheats were 2.24% and 1.71% respectively.

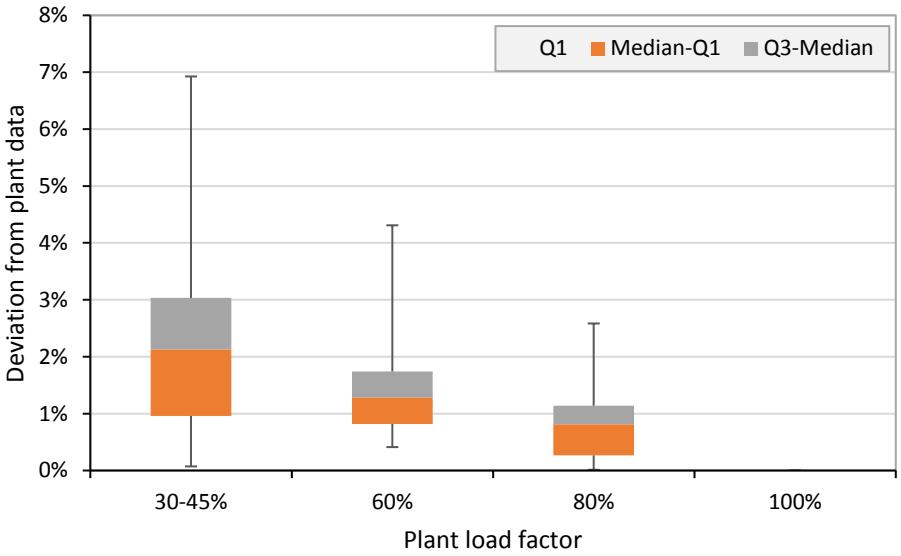

Figure 7.31 Summary of deviations from across load factors

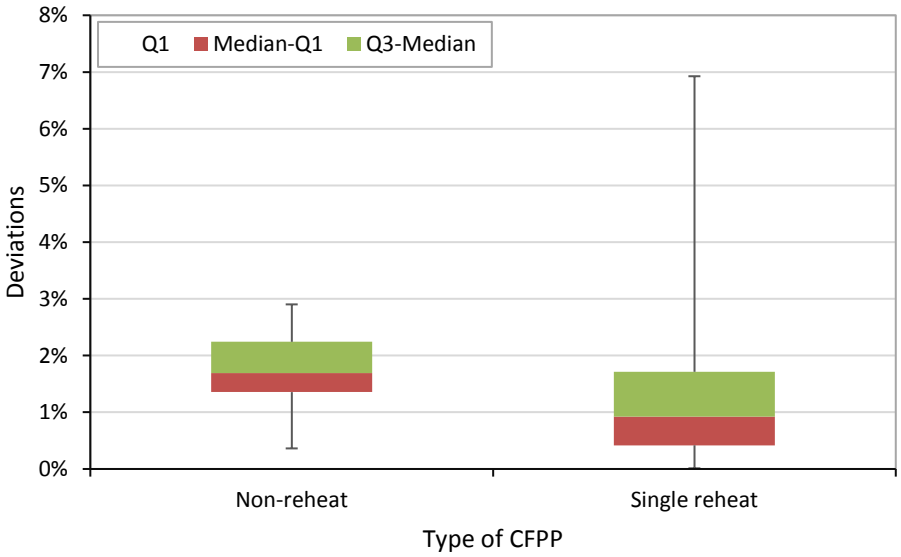

Figure 7.32 Summary of deviations different CFPP types

The reasons for the deviations seen may be connected to the following:

i The presence of additional feedwater heaters (FWHs) more than the number of FWHs used in the model CFPPs developed in VirtualPlant. Additional FWHs reduces the heat rate by a small margin.

ii The presence of an auxiliary turbine for a steam driven BFP pump in the real plants. The CFPP model that were investigated included an electrically driven BFP pump which consumes more energy than the steam driven BFPs at part load operations. The reason for the high energy consumption (hence higher heat rate) is because steam turbine driven BFPs have the advantage of variable speed operation that regulates flow more efficiently [71]. In situations like this, CFPPs coupled with steam driven BFPs have a lower heat rate than the ones with electric boiler feed pumps.

iii The assumption of a constant pump efficiency at part load operation which may not be accurate. At lower loads, the pump (BFPs and CEPs) efficiency drops slightly into a less efficient range [71].

iv The assumption of a constant turbine efficiency at part load operation which may not be accurate. The efficiency of HP turbine has the most direct correlation with load than the IP and LP turbines [71]. This is due to the variable-pressure ratio (for fixed pressure operations), and variable efficiency of the first stage of HP turbines, and the throttling effects at the inlet valves [71]. The efficiency drop of LP turbines is mainly due to the increase of the exhaust losses at lower loads [71].

v The condensing pressure of the data used for validating the model results.

7.7 Conclusion of the Chapter

In this chapter, a novel variable turbine cycle heat rate (V-TCHR) model was proposed for predicting the part load turbine cycle heat rate response of various CFPP configurations, without detail knowledge of the entire steam cycle parameters. This was developed by analysing 192 CFPP architectures of typical plants found in industry, using the generic modelling method developed in chapters 3, 4, 5, and 6.

The method shows that using a power law function in the form $TCHR = TCHR_{FL}X^{-\Re}$, with X being the part load fraction (0.4-1), best describes the response for different CFPP architectures. The coefficient $TCHR_{FL}$ is simply the heat rate at full load, and the exponent $\Re$ can be determined from simple correlations ($C_{\Re}$ and $S_{\Re}$) which considers the degree of reheat, cooling technology, main/live steam enthalpy (h_{main}) and the boiler pressure mode of operation. Using this methodology, the TCHR at part load can be adequately predicted without the need for any thermodynamic cycle model. A summary of the model and the correlation coefficients are presented on Figure 7.33.

(a) ***V-TCHR*** **model equations**

$$TCHR = TCHR_{FL} \times X^{-\Re}$$

$$\Re = S_{\Re} h_{main} + C_{\Re}$$

$$h_{main} = f(P_{thr}, T_{thr})$$

(b) $\Re$ **Correlation coefficients: Fixed boiler pressure operation**

Degree of Reheat	$S_{\Re}$	$C_{\Re}$	
		Wet cooled condensers (OTC & WCC)	Dry cooled condensers (IDC & ACC)
NRH	0.00004	-0.0150	-0.0210
SRH	-0.00004	0.2100	0.1928
DRH	-0.00003	0.1625	0.1514

(c) $\Re$ **Correlation coefficients: Sliding boiler pressure operation**

Degree of Reheat	$S_{\Re}$	$C_{\Re}$	
		Wet cooled condensers (OTC & WCC)	Dry cooled condensers (IDC & ACC)
SRH	-0.00003	0.1640	0.1567
DRH	-0.00003	0.1699	0.1438

(d) Rough estimates for $\Re$ **based on fixed boiler pressure operation mode**

CFPP Type	$\Re$-value
NRH	0.118
SRH	0.064
DRH	0.060

Figure 7.33 A summary of the V-TCHR model and the correlation coefficients for determining $\Re$

The model was validated with data from 9 CFPPs (2 NRHs and 7 SRHs) and the maximum absolute error that was seen was 7 %. The reason(s) for the discrepancies differ from one CFPP to another. In some cases, it could be due to the presence of components (e.g. additional FWH, auxiliary

turbines for steam driven feed pumps) in the real plants that were not included in the generic CFPP configuration selected, in other cases it could be due to the assumptions made in the model development.

The sensitivity of the V-TCHR model to the reference condenser back pressure selected for each cooling technology can be addressed with a set of adjustment coefficient curves that were recommended in section 7.5.1. The correction factors were determined by performing a sensitivity study on the impact of the condenser back pressure.

The outcome of this chapter will be used in Chapters 8 and 9, for determining the variable net unit heat rate (V-NUHR) used for calculating the fuel consumption and subsequent CO_2 emissions at various load levels.

8. Impact of varying load on CO_2 emissions factor

The combustion of solid fuels such as coal involves a complex set of processes that includes heat transfer, chemical reactions, and thermodynamic. Furthermore, the formation of some gaseous products such as NOx are complex to predict. The detailed modelling of coal combustion is not the focus of this study. However, attention is given to predicting the emissions and emissions factor of CO_2 for a number of reasons. Firstly, the formation and quantification of CO_2 from CFPPs is fairly straightforward and easy to determine once the heat rate, fuel characteristics, and the fuel mass flow are known [22]. Secondly, CO_2 is often referred to as the chief cause of global warming. Thirdly, the control of CO_2 emissions from CFPPs has not been implemented on large scale CFPPs yet thus implying that the CO_2 produced from combusting fuel will be the emissions from the plant.

This chapter is focused on the application of the V-TCHR model to determine the CO_2 emissions factor of CFPPs at varying load conditions. A description of how the Net Unit Heat Rate (NUHR) of a CFPP is determined from the generic V-TCHR model is given by incorporating boiler efficiency and auxiliary consumption, and generator models.

8.1 Overview of the CO_2 emissions factor and total emissions computation procedure.

Figure 8.1 shows an overview of the computational steps that were used to determine the CO_2 emissions factor and the total CO_2 emissions predicted at varying load levels. The procedure begins with the turbine cycle heat rate as determined from the V-TCHR model, a suitable boiler efficiency model, an auxiliary consumption, and a generator model at varying load conditions. These are combined to determine the NUHR as described in section 2.4.6. A combustion analysis of the fuel is then carried out to determine the concentration of the CO_2 per unit fuel flow. Once this is done, the emissions factor (kg/kWh) of the CFPP is determined at the various load levels.

The detailed description of the mathematical derivations/models for the NUHR, boiler efficiency, auxiliary consumption, generator and CO_2 emission factor are presented in sections 8.2, 8.3, 8.4, 8.5 and 8.6 respectively.

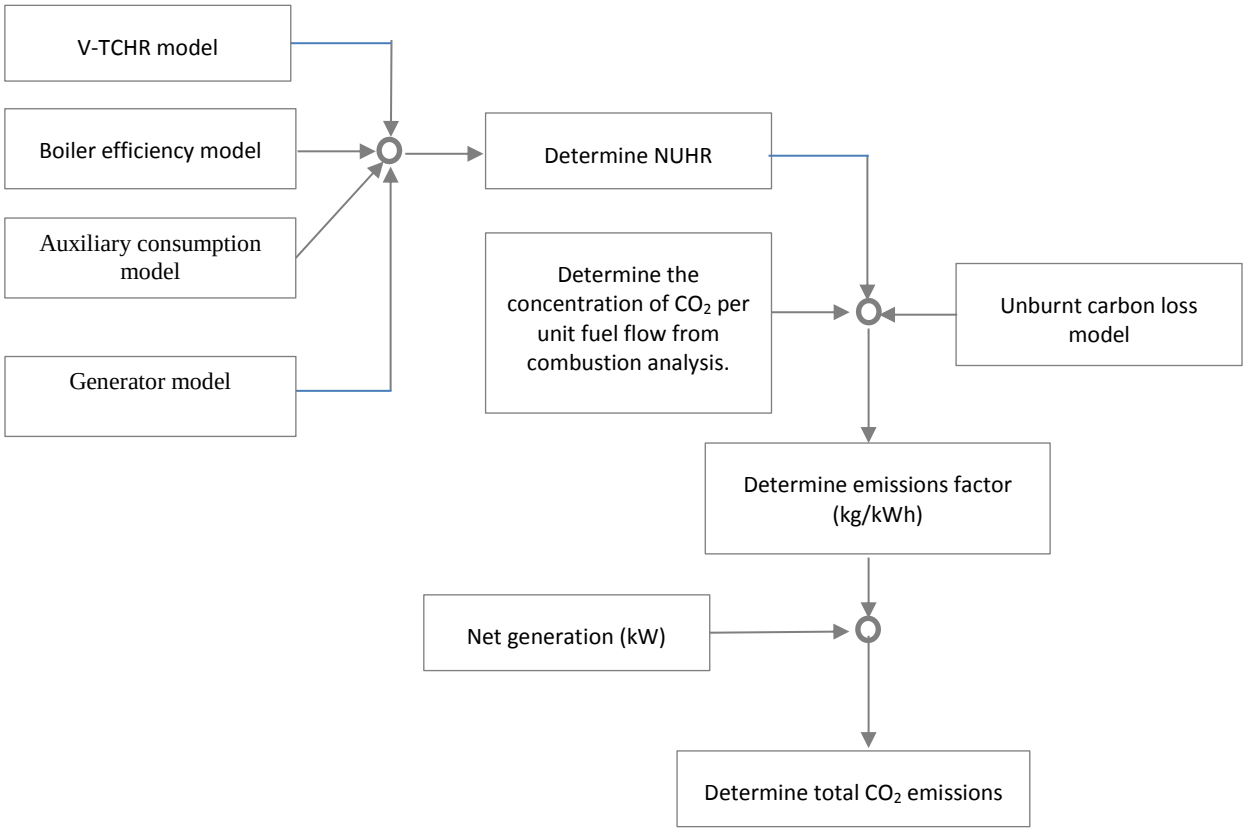

Figure 8.1 Computation procedure for determining CO_2 emissions factor and total CO_2 emissions produced

8.2 Determination of the V-NUHR

The V-TCHR model defines the turbine cycle heat rate response at varying load as:

$$TCHR = TCHR_{FL}X^{-\Re} = \frac{Q_{TCHI}}{W_{gross}} \tag{8.1}$$

Where $TCHR_{FL}$ is the turbine cycle heat rate at full load or maximum continuous rating (MCR), X is the gross generation load factor, $\Re$ is the exponential coefficient of the V-TCHR model. Q_{TCHI} and

W_{gross} are the turbine cycle heat input and gross power generation respectively. Both are determined at X load factor. X is defined mathematically as:

$$X = \frac{W_{gross}}{W_{gross.FL}} \tag{8.2}$$

Where $W_{gross.FL}$ the gross power is generated at full load and W_{gross} is the gross power generation evaluated at gross load factor X.

Substituting the V-TCHR model into Equation (2.3) gives

$$NUHR = \frac{TCHR_{FL} \cdot X^{-\Re}}{\eta_G \cdot \eta_B \cdot (1 - f_{aux})} \tag{8.3}$$

f_{aux} is the ratio of the auxillary power consumption to the gross power i.e $f_{aux} = \frac{W_{aux}}{W_{gross}}$.

Equation (8.3) shows the relationship between NUHR, TCHR, plant gross load factor, the boiler efficiency, generator efficiency and the auxillary power fraction. The numerator of that equation is the V-TCHR model. The terms at the denominator - the boiler efficiency (η_B), the auxillary fraction (f_{aux}), and the generator efficiency are important terms that must be properly modelled at varying load conditions.

Note: Equation (8.3) has been defined based on the gross load factor(X). It can also be defined based on the net load factor (X_{net}). X_{net} is defined mathematically as:

$$X_{net} = \frac{W_{net}}{W_{net.FL}} = \frac{W_{gross} - W_{aux}}{W_{gross.FL} - W_{aux.FL}} \tag{8.4}$$

8.3 The Boiler efficiency model for varying load operation

The factors that affect the efficiency of a steam boiler have already been highlighted in section 2.4.3 . Since the loss method of defining the efficiency of a boiler relies on the knowledge of the losses profile variation with load of the boiler, it therefore becomes important to consider how the losses in a boiler changes with load for some typical CFPP steam boilers.

$$\eta_B = 100 - Loss_{boiler} \tag{8.5}$$

It is difficult, if not impossible to quantitatively describe how the losses in different steam boilers vary with load considering the different design configurations, sizes and types of steam boilers that exist in CFPPs. One plausible way of solving this problem would be to take a statistical average of some steam boilers that exist. This is the approach that was adopted in this research.

Data for three different boiler load points were collected from 10 steam boilers (4 NRHs and 6 SRHs) currently in the Eskom fleet. There were 6 drum type and 4 once through type boilers. Five of the boilers are of the tower type while the others are of the 2 pass layout type boilers. There were 6 horizontally opposite fired burner type boilers, 2 tangentially fired burners, and 2 front wall burner type steam boilers. There were 6 single wall furnace type boilers, and 4 twin divided furnace wall type steam boilers. There were six tube type mills, and 4 vertical spindle type mills. The steam boilers were drawn from CFPPs whose TMCR is between 100 MW and 700 MW. It is believed that the characteristics of the boiler types considered covers the various steam boiler design types found in a coal fired power plants with the exception of a double reheat steam boiler. The information should still be applicable to the double reheat boilers though.

The boiler load points (see Figure 8.2) were 100%, 97.5%, and 68%. The 100% boiler heat load corresponds to the boiler's maximum continuous rating (BMCR) which is usually about 105% TMCR. The 97.5% boiler heat load corresponds to the 100% TMCR, while the 68.7% corresponds to 70% TMCR.

Figure 8.2 shows the contribution of the losses at various loads. The major losses to the boiler system are the dry flue gas losses, wet losses and combustible (unburnt carbon) losses. At part load, the percentage dry flue gas losses (Figure 8.2 a) decreased slightly. This usually occurs because of

reduced flue gas outlet temperature and the lesser flue gas mass flows which in turn increases the air heater effectiveness. The wet losses (Figure 8.2 b) which is made up of the moisture and fuel hydrogen losses are almost constant at lower loads. This is mainly because the fuel hydrogen is dependent on the coal quality only and the boiler load level does not affect it. The combustible losses which is made up of the unburnt carbon & hopper losses (see Figure 8.2 c) increases at part load because of the increase in unburnt carbon. This increase is caused by a drop in the efficiency of the classifier resulting in larger coal particles in the furnace which does not completely combust by the time it reaches the colder parts of the boiler. The other boiler losses (radiation and convection losses, and unaccounted losses) do not change significantly at lower loads.

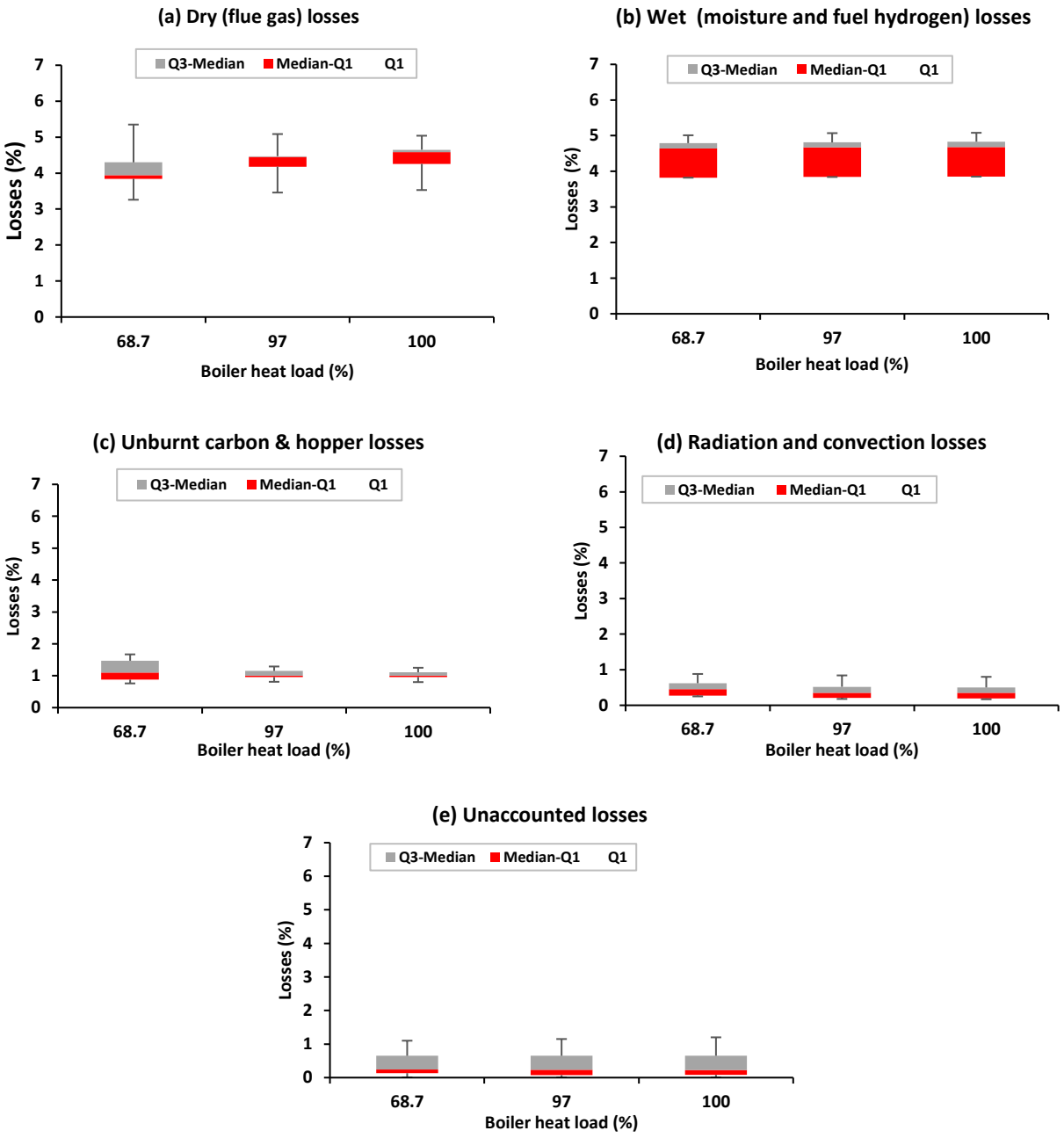

Figure 8.2 Boiler losses from 10 CFPP steam boilers: Data sourced from Eskom Power Generation

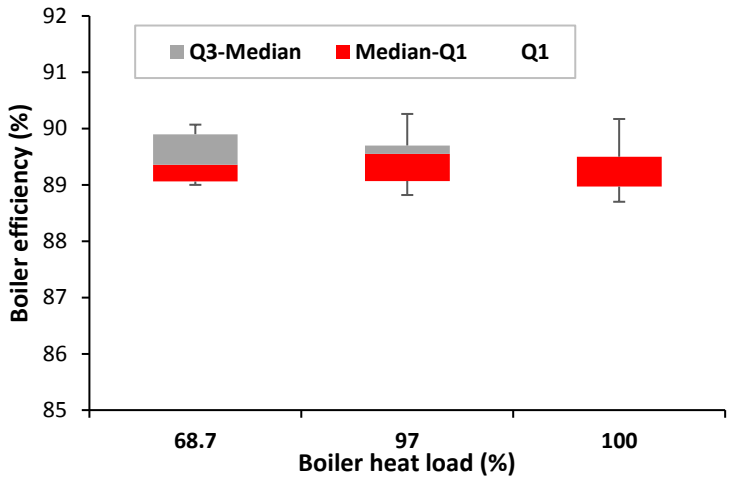

Figure 8.3 Boiler efficiency from the 10 steam boilers considered

An assessment of the effect of low load operations on the efficiency of most utility boilers only show a slight drop of between 0.5% -1.5% between 100-68.7% boiler heat load. This slight drop in efficiency is caused primarily by the counteracting effects of reduced dry flue gas losses and increased combustion losses experienced at lower load operations (see Figure 8.2). A statistical presentation of the boiler efficiency of the steam boilers is presented on Figure 8.3. The boiler efficiency appears to be between 89 and 90% over the entire load range. Although there is a slight change in the boiler efficiency, this change is quite small. Therefore, an average boiler efficiency (η_B) of 89.3% was selected. This efficiency is assumed to be constant over the entire load range of (40% - 100% TMCR). The boiler efficiency for these plants were also looked at based on the HHV of the fuel.

$$\eta_B = 89.3\% \tag{8.6}$$

8.4 Auxiliary consumption model for varying Load conditions

As already discussed in section 2.4.4, there are many factors that affects the auxiliary power consumption (APC) at full load and part load. There appears to be no generic way of describing this APC. Mandi and Yaragatti [79] used a simple power law model to describe the relationship between auxiliary consumption of a 210MW plant and its plant load factor. The expression is given in

Equation 8.13. f_{aux} is the percentage of gross generation consumed by the auxiliaries while X is the plant load factor expressed in %.

$$f_{aux} = 45.909 \cdot X^{-0.3626} \tag{8.7}$$

This model is simple and easy to implement for the particular plant studied. It may not be a suitable representation of the relationship between f_{aux} and X for any CFPP because of the sensitive nature of the coefficients. For this reason, a more generic model is required. The approach adopted in this study was to examine the fixed and variable auxiliary consumption of different CFPPs.

At full load or VWO condition, the auxiliary consumption expressed in % of the gross generation at full load $(f_{aux.FL})$ is defined by Equation(8.8). This equation was derived from correlating the auxiliary fraction of over 85 CFPPs drawn from India and South Africa with their full load gross generation. The source of the data for the India CFPPs was from this report [82]. $W_{gross.FL}$ is defined in MW.

$$f_{aux.FL} = 41.945 \times W_{gross.FL}^{-0.277} \tag{8.8}$$

A plot of the correlated data is shown on Figure 8.4. As can be seen, it appears that the auxiliary consumption fraction of gross generation at full load tends to decrease with the increased installed generation capacity of the plant. One plausible explanation for this trend could be that designers of larger plants (which are often more modern) tend to adopt newer and more efficient technologies in the design of auxiliary systems. This often results in reduced auxiliary power consumption fraction and reduced specific steam consumption [79]. There could also be the effect of economy of scale present.

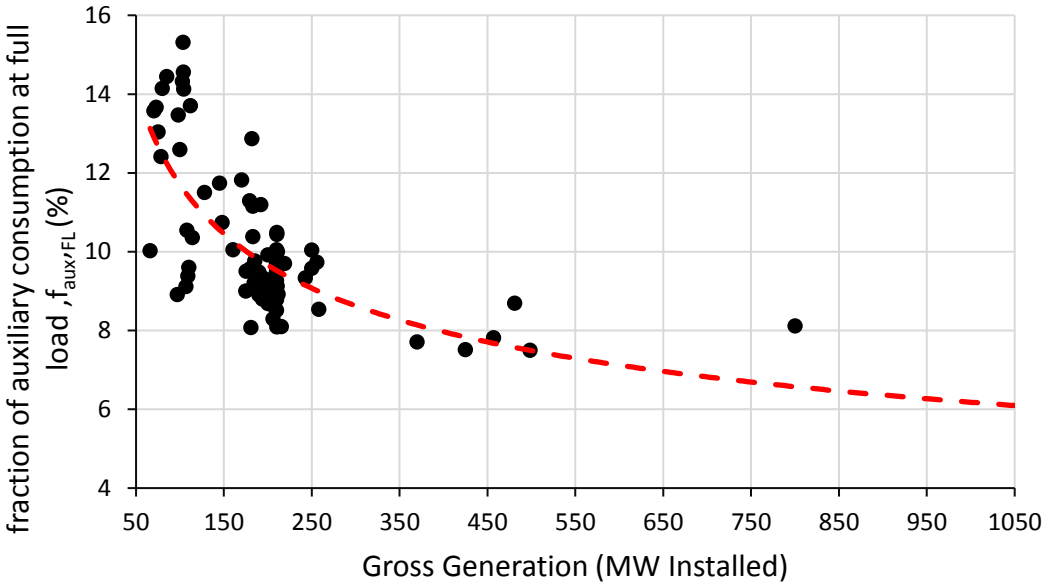

Figure 8.4 Correlating the auxiliary fraction of gross generation at full load using data from over 85 CFPPs : Data sourced from EESI [82] and Eskom

Once the fraction of the auxiliary consumption is determined at full load, the next thing to do is to determine its composition at part/low load. The auxiliary consumption power (W_{aux}) of a CFPP is assumed to comprise of a fixed auxiliary ($W_{aux.fix}$) and a variable ($W_{aux.var}$) component (see Figure 8.5). The fixed consumptions does not change with operating load point of the plant, while the varying consumption is dependent on the operating load condition of the plant, and assumed to be linear.

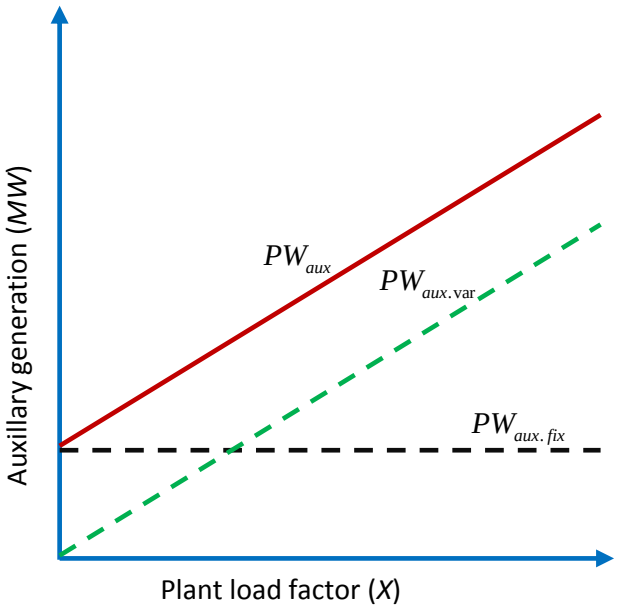

Figure 8.5 Fixed and variable components of auxiliary power

The auxiliary power consumption (APC) at any load can be mathematically expressed as:

$$W_{aux} = W_{aux.fix} + W_{aux.var} \tag{8.9}$$

The variable and the fixed components of APC can be defined as Equations (8.10) and (8.11) respectively.

$$W_{aux.var} = W_{aux.var.FL}.X \tag{8.10}$$

$$W_{aux.fix} = W_{aux.fix.FL} \tag{8.11}$$

Let's define the fraction of APC that is fixed at full load with a β parameter. Mathematically, this is given as

$$\beta = \frac{W_{aux.fix.FL}}{W_{aux.FL}} \tag{8.12}$$

The variable component of APC at full load can then be expressed as $W_{aux.var.FL} = (1-\beta) \cdot W_{aux.FL}$. It therefore means that the auxillary power at any load factor can be expressed as

$$W_{aux} = [\beta + (1-\beta) \cdot X] \cdot W_{aux.FL} \tag{8.13}$$

From the empirical data correlation given in Equation(8.8), the auxillary fraction at full load ($f_{aux.FL}$) can also be written as:

$$f_{aux.FL} = \frac{W_{aux.FL}}{W_{gross.FL}} = 41.945 \cdot W_{gross.FL}^{-0.277} \tag{8.14}$$

At varying load condition the auxillary power could be defined as

$$f_{aux} = [\beta + (1-\beta) \cdot X] \cdot f_{aux.FL} \tag{8.15}$$

The substitution of $f_{aux.FL}$ from Equation (8.14) into Equation (8.15) Gives

$$f_{aux} = [\beta + (1-\beta) \cdot X] \cdot 41.945 \cdot W_{gross.FL}^{-0.277} \tag{8.16}$$

Equation (8.16) defines the variation of the auxillary power consumption at various plant load factors.

8.5 Generator efficiency

As already discussed in section 2.4.5, there are many factors that affects the efficiency of an electrical generator. At lower loads, most of the losses experienced decreases slightly. These decreases only have a minute effect on the generator efficiency. Since the efficiencies of generators are already quite high in the first place, i.e 98%, and the efficiency changes experienced at lower loads are not quite significant, it therefore means that an assumption of a constant generator efficiency of 98% at all the load conditions is still valid. This assumption was applied to all the model CFPPs investigated.

8.6 CO_2 emissions determination at varying loads

8.6.1 Combustion analysis

CO_2 is a gaseous product of the complete combustion of carbon present in solid and liquid fuels. A combustion analysis is required to be able to determine the quantity of CO_2 emitted per unit flow of the fuel. This ratio is dependent on the characteristics of the fuel being combusted and the combustion efficiency.

A simple (but less accurate) method of predicting the CO_2 emissions per unit fuel consumed from a plant at varying loads, would be to assume the complete combustion of all carbon at any load. However, it is well understood that for solid fuel combustion, like the type that occurs in a pulverized coal plant, there are some unburnt carbon in the discard products. For an improved CO_2 emissions prediction model, it is important to understand how the unburnt carbon changes with load in typical CFPPs.

In this study, the fraction of carbon that is combusted, is analyzed as a complete combustion process. The fraction of carbon that is not combusted is determined through an unburnt carbon loss model discussed in section 8.6.2.

The combustion analysis begins with a look at the characteristics of the fuel to be analysed. The chemical composition of coal may be represented as [191]:

$$C_{(n_C)}H_{(n_H)}O_{(n_O)}N_{(n_H)}S_{(n_S)} \tag{8.17}$$

n_C, n_H, n_O, n_N, n_S is the number of moles of each of the respective element in the fuel. For a given element i, n_i is normalized with respect to carbon and expressed as:

$$n_i = \frac{\frac{x_i}{M_i}}{\frac{x_C}{M_C}} \tag{8.18}$$

x_i, M_i represents the mass fraction and molar mass for element i. Note that $n_C = 1$ due to the normalization. The mass fractions are obtained from the ultimate analysis of the coal.

The general combustion equation for the solid fuel $C_{(n_C)}H_{(n_H)}O_{(n_O)}N_{(n_H)}S_{(n_S)}$ may be written as:

$$\begin{aligned} C_{(n_C)}H_{(n_H)}O_{(n_O)}N_{(n_H)}S_{(n_S)} + \left(n_C + \frac{1}{4}n_H - \frac{1}{2}n_O + f_{NOx}\frac{1}{2}n_N + n_S\right)O_2 \\ \rightarrow n_C CO_2 + \frac{1}{2}n_H H_2O + n_S SO_2 + f_{NOx}n_N NO \\ + (1 - f_{NOx})\frac{1}{2}n_N N_2 \end{aligned} \tag{8.19}$$

From the equation above, the theoretical air ratio (TAR) required for complete combustion is given below in kg air / kg fuel after substituting the definition of equation (8.18) for all the elements:

$$TAR = \left(\frac{x_C}{M_C} + \frac{1}{4}\frac{x_H}{M_H} - \frac{1}{2}\frac{x_O}{M_O} + \frac{f_{NOx}}{2}\frac{x_N}{M_N} + \frac{x_S}{M_S}\right)\frac{M_{air}}{y_{O2/air}} \tag{8.20}$$

f_{NOx} is the fraction of fuel NOx formed, and it could be assumed as 30% for most coal fired burners [191]. $y_{O2/air}$ is the mole fraction of oxygen in air and is equal to 0.2096. M_{air} is the molar mass of air, equal to $28.958\ \ kg/kmol$.

The mass flow of CO_2 is simply given as:

$$m_{CO_2} = \frac{M_{CO_2}}{M_C}x_C m_{coal} \tag{8.21}$$

Note that equation (8.21) assumes that all the carbon in the fuel reacts with oxygen to form CO_2. However, this is not the case in most coal fired steam boiler systems. It is important to determine the actual faction of carbon that is combusted (x_{BC}). This can be determined by subtracting the unburnt carbon mass fraction (x_{UC}) from the total carbon mass fraction x_C in the fuel. The unburnt carbon mass fraction (x_{UC}) can be determined from a suitable unburnt carbon loss model described in section 8.6.2. The actual mass flow for CO_2 is now given as:

$$m_{CO_2}^{act} = \frac{M_{CO_2}}{M_C}(x_C - x_{UC})m_{coal} \tag{8.22}$$

8.6.2 Unburnt carbon loss model and V-TCHR based CO_2 emissions factor model

The unburnt carbon loss ($Loss_{uc}$) of a boiler represents the fraction of carbon that is unburnt. It can be represented as:

$$Loss_{uc} = \frac{E_{UC}}{HHV} \tag{8.23}$$

E_{UC} is the unburnt carbon energy loss while HHV is the high heating value of fuel. The high heating value of the fuel can be calculated from Dulong's expression given in equation(8.24). x_C , x_H, x_O, and x_S represents the mass fraction of carbon, hydrogen, oxygen and sulphur in the fuel respectively.

$$HHV = [33.83x_C + 144.25x_H - 18.04x_O + 9.42x_S]\frac{MJ}{kg} \tag{8.24}$$

Given the Dulong's definition of HHV, If x_{UC} represents the fraction of carbon that is not burnt in the fuel, it therefore implies that the energy loss associated with this fraction can be represented as:

$$Loss_{UC} = \frac{33.83 \cdot x_{UC}}{HHV} \tag{8.25}$$

Then the unburnt carbon mass fraction can be calculated thus as:

$$x_{UC} = \frac{HHV \cdot Loss_{UC}}{33.83} \tag{8.26}$$

$Loss_{UC}$ can be derived from empirical correlations drawn from typical CFPPs data. Figure 8.6 shows the range of unburnt carbon losses of the non-reheat and single reheat steam boilers examined in section 8.3. It can be seen that the unburnt carbon losses increase for the plants examined. The model for predicting the unburnt carbon losses ($Loss_{uc}$), is based on the average calculated from

the plants examined. It is represented in Equation 8.2. In this case X is the boiler load fraction, but it will be approximated as the gross load factor to be consistent with the V-TCHR model.

$$Loss_{uc} = -0.0881 \cdot X + 1.2746 \tag{8.27}$$

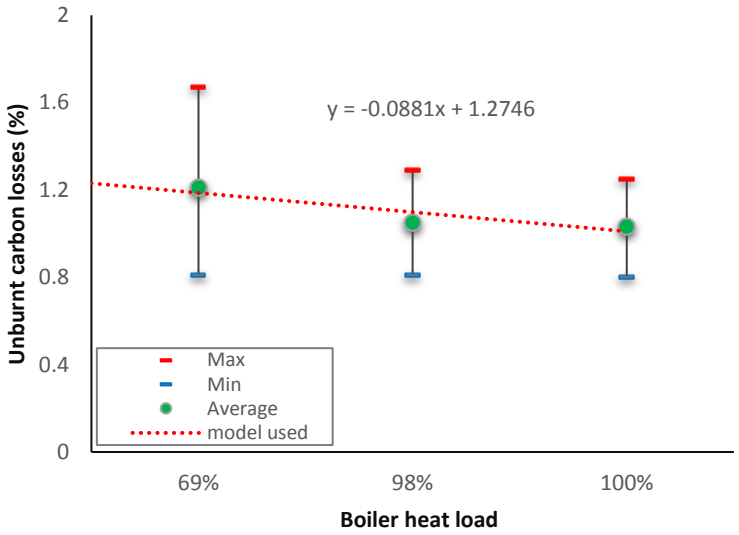

Figure 8.6 Unburnt Carbon loss model used: Data sourced from Eskom

The mass flow of the coal is determined from:

$$m_{coal} = \frac{NUHR \times W_{net}}{HHV \times (1 - Loss_{uc})} \tag{8.28}$$

HHV is the higher heating value of the coal in (kJ/kg), W_{net} is net power generated in kW at the plant load factor. $NUHR$ is the net unit heat rate (kJ/kWh). It is defined in Equation (8.27)

The CO_2 emissions factor (EF) in *kg/kWh* is given as

$$EF = \frac{m_{CO_2}^{act}}{W_{net}} \tag{8.29}$$

The substitution of the definition for $m_{CO_2}^{act}$ into Equation (8.29) gives

$$EF = \left[\frac{M_{CO_2}}{M_C} \times (x_C - x_{UC})\right] \cdot \left[\frac{NUHR}{HHV \times (1 - Loss_{uc})}\right] \tag{8.30}$$

A substitution of the definition of $NUHR$ at different load factors from Equation (8.3) into Equation (8.30) gives

$$EF = \left[\frac{M_{CO_2}}{M_C} \times (x_C - x_{UC})\right] \cdot \left[\frac{TCHR_{FL} \cdot X^{-\Re}}{HHV \times (1 - Loss_{uc}) \times \eta_B \times \eta_G \times (1 - f_{aux})}\right] \tag{8.31}$$

This definition of the CO_2 emissions factor provides an opportunity for capturing the impact of three key effects that are usually associated with the part and low load operations of CFPPs. The effects are:

(a) Increased turbine cycle heat rate at part and low load conditions.
(b) Increased combustion losses at lower loads.
(c) Increased auxiliary fraction at lower loads.

8.7 Verification/validation procedure explained

A validation of the CO_2 emissions factor would be a difficult tasks considering the fact that: (a) it is dependent on a number of factors (see section 2.5.2) that may be difficult to fully integrate into one single model, and (b) it is difficult to get the emissions data of some plants. Instead of validating the model results, a verification was done. This verification was done by comparing the emission factors predicted with some benchmarks / emission factor ranges that have been published in literature. Figure 8.7 shows a range of emission factors of different categories of CFPPs that have been published by the World Energy Council (WEC) [24]. This is the benchmarking tool that was used to verify the CO_2 emissions factor that was predicted.

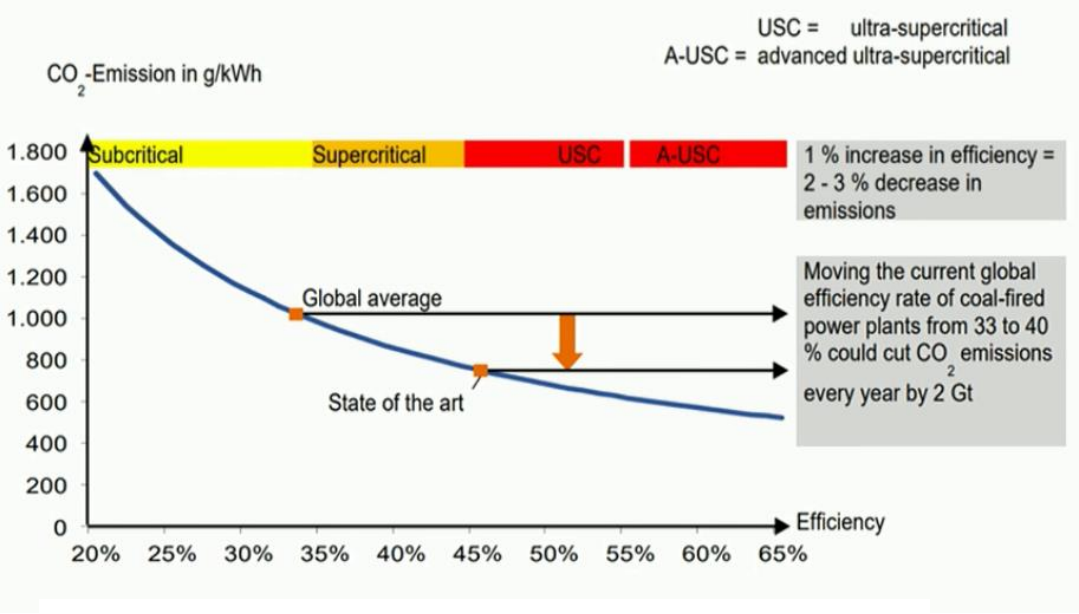

Note: The efficiency described is based on the net unit heat rate.

Figure 8.7 Current global plant efficieincy and emissions [24]

The CO_2 emissions factor model verification was carried out through a demonstration study on six hypothetical CFPPs drawn from the list of 192 CFPP models built in chapter 7 (see Table 8.1). The six CFPPs is made up of two NRHs (NRH-1, and NRH-2), two SRHs (SRH-1, and SRH-2), and two DRHs (DRH-1, and DRH-2). The $TCHR_{FL}$and $\Re$ -values determined are also shown on Table 8.1. The CFPPs have been selected to represent various $TCHR_{FL}$and $\Re$ -values based on the cooling systems, degree of reheats, and live steam conditions.

Table 8.1 Six selected Coal fired Power Plants

Type	Capacity (MW)	P_{thr} (MPa)	T_{thr} $(℃)$	T_{rh1} $(℃)$	P_{rh1} (MPa)	T_{rh2} $(℃)$	P_{rh2} (MPa)	P_{cond} (kPa)	Cooling Technology	$TCHR_{FL}$ (kJ/kWh)	$\Re$
NRH-1 (Plant 004)	200	12	510	N/A	N/A	N/A	N/A	17	Dry cooled	9426.7	0.1141
NRH-2 (Plant 006)	200	12	535	N/A	N/A	N/A	N/A	4	Wet cooled	8466.4	0.1227
SRH-1 (Plant 087)	500	17	535	535	4.33	N/A	N/A	12	Dry cooled	8083.5	0.0573
SRH-2 (Plant 106)	500	24	565	565	5.88	N/A	N/A	7	Wet cooled	7457.9	0.0741
DRH-1 (Plant 187)	1000	30	565	565	9.60	565	2.364	12	Dry cooled	7423.9	0.0514
DRH-2 (Plant 189)	1000	30	600	600	7.80	600	1.515	4	Wet cooled	8927.1	0.0591

The characteristics of the two fuels that were used for the emissions verification study is shown on Table 8.2. The "best coal" used here was a subbituminous coal, while the "worst coal" used here was a lignite coal. The carbon content of the best coal is approximately twice of the one from the worst coal. The worst coal has a lot more water content than the best coal. Despite of this, the lignite coal was used as the reference coal for the study.

Table 8.2 Fuel characteristics [192]

	Best Coal	Worst Coal
Calorific Value of Coal (HHV) kJ/kg	23150	10597
Carbon content, fuel (by mass)	0.59780	0.29060
Hydrogen content, fuel (by mass)	0.03610	0.02590
Sulphur content, fuel (by mass)	0.00740	0.01690
Oxygen content, fuel (by mass)	0.05110	0.06210
Nitrogen content, fuel (by mass)	0.01240	0.00270
Ash content, fuel (by mass)	0.16030	0.07800
Water content, fuel (by mass)	0.13490	0.52380
Bottom Ash Collection (efficiency)	0.39000	0.05300
Calorific value of unburned combustibles, Ash & Slag	33000.00	27200.00
Volatile matter content, ash	0.05	0.05

The validation of the auxiliary model was done using auxiliary consumption data for Plant O. The plant is an ACC-cooled condenser CFPP with a single reheat boiler. The critical process parameters for this CFPP is shown on Table 6.1.

8.8 Results and Discussions

8.8.1 Auxiliary fraction, net, and gross load factor results

Comparison of the model results with the data from Plant O is shown on Figure 8.8. There are two different model types that were validated. The first type (type 1), is based on using a known auxiliary consumption fraction at full load was $f_{aux\cdot FL} = 9\%$. Based on an assumption of $\beta = 30\%$, a comparison of this model with the plant data shows a very accurate model with little deviation for this plant. The type 2 method determines the auxiliary consumption fraction at full load $(f_{aux\cdot FL})$ through Equation (8.8) . Using this type at various values of β, it can be seen that $f_{aux\cdot FL}$ was predicted around 2.7 percentage points lower than the plant data. Although the $f_{aux\cdot FL}$ value predicted in Type 2 is lesser than the plant data, the important observations to note here are:

(1) The auxiliary fraction $f_{aux}$for CFPPs increases at lower loads.

(2) If the correct $f_{aux\cdot FL}$ is selected, one may successfully model the auxiliary fraction of a CFPP at lower loads by splitting the auxiliary power consumption (APC) into a fixed and varying component. The fixed component (β) of the APC, at different load conditions could be between 25-30%.

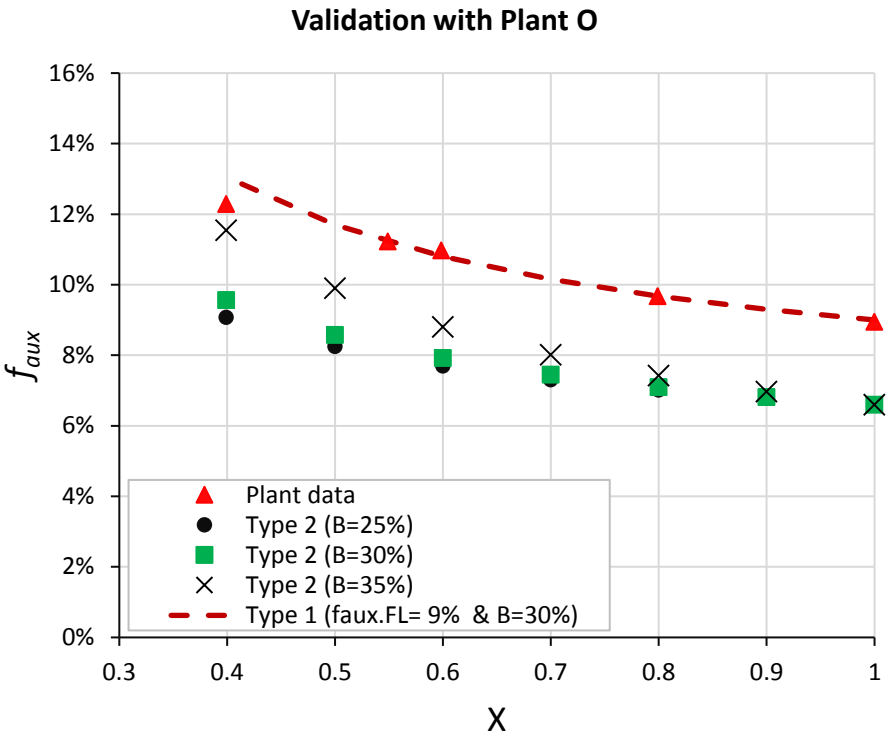

Figure 8.8 Auxiliary fraction relationship with gross load factor

The relationship between the net load factor and the gross load factor is shown in Figure 8.9. It can be seen that for the various β cases (25%, 30%, and 35%) and the plant data examined, the relationship between Plant O's net load plant factor (X_{net}) and the plant's gross load factor (X) is quite similar, so that it does not matter which case is being investigated. The mathematical expression for the trendline is displayed on Figure 8.9. The expression shows that the net load factor is approximately 98.9% of the gross load factor. Given that this is the case, then one may still assume $X_{net} \approx X$ i.e that the net load factor of a CFPP is approximately equal to the gross load factor at all plant load factors.

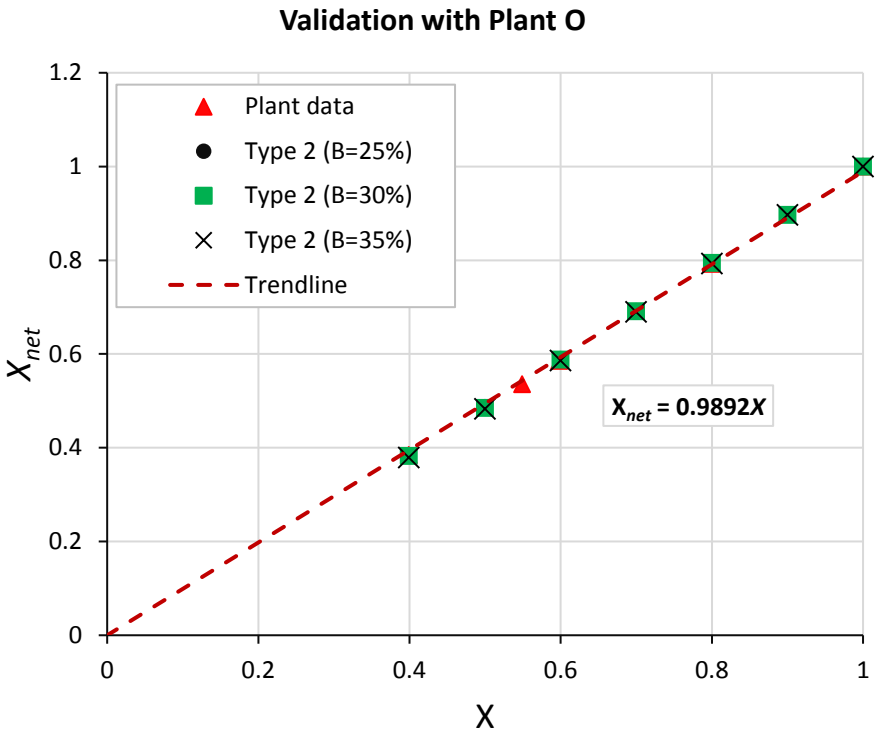

Figure 8.9 Relationship between X_{net} and X

8.8.2 CO_2 emissions factor predicted at full load conditions

A comparison of the full load/VWO emissions factor predicted versus the global industry benchmark emissions factor, for the six unique CFPPs described on Table 8.1 is shown on Figure 8.10. It can be seen that the full load emissions factor predicted for the non-reheats, single reheats, and double reheats are slightly greater than the benchmark values. The results is fairly close considering that the benchmark data probably did not consider the various factors that was considered in this study. The deviation ranged from 2.1% to 5.7% when the sub-bituminous fuel was used. However, if the reference fuel (lignite) is used, the deviations increased to between 8.6% and 12.2%. It is expected that the emissions for bad coal will be more than for good coal, and the emissions model confirms this.

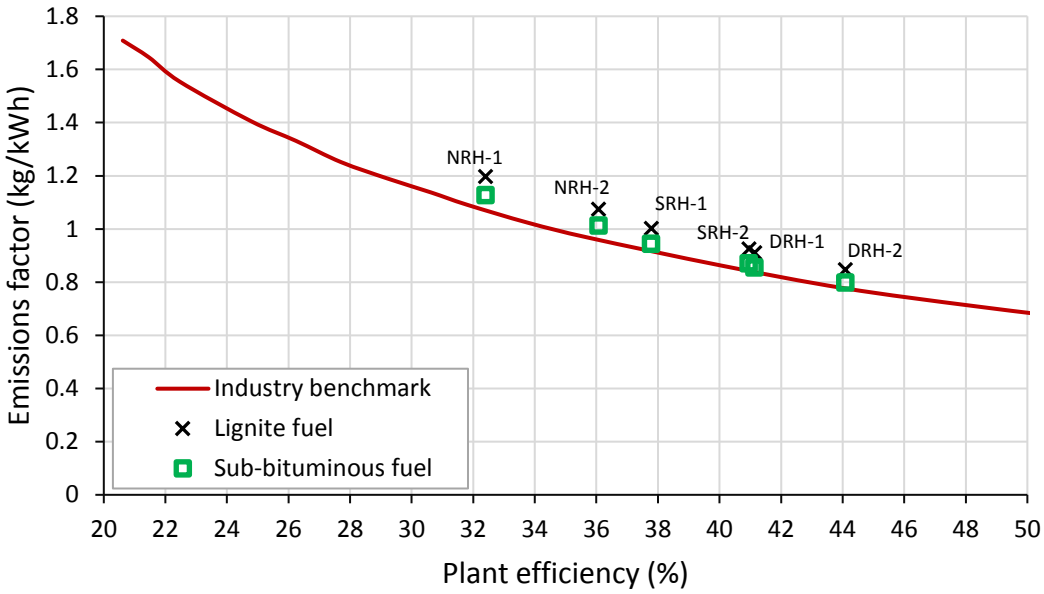

Figure 8.10 Comparing V-TCHR based emissions factors with industry benchmarks using a boiler efficiency of 89.3%

The impact of the boiler efficiency on the emissions factor calculated is shown on Figure 8.11.

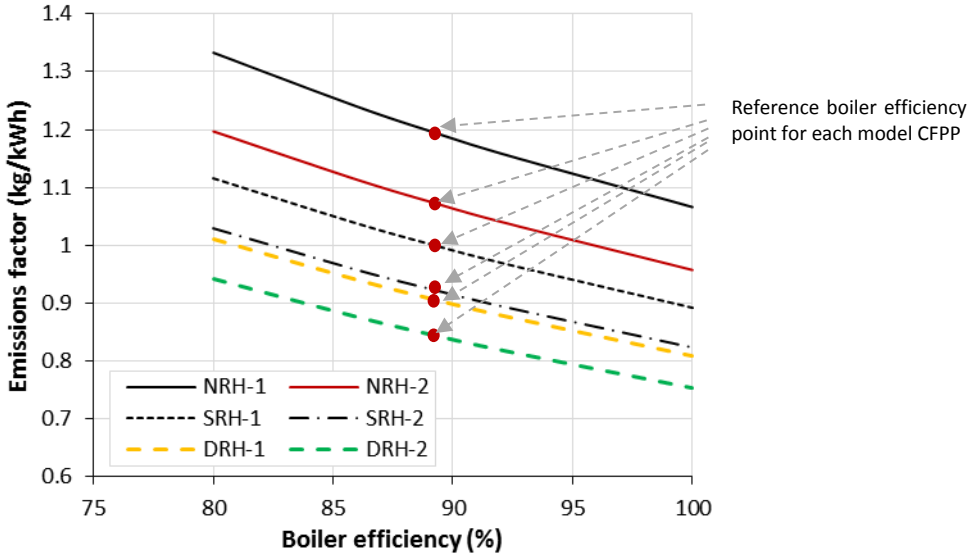

Figure 8.11 The impact of boiler efficiency on emissions factor at full load condition

It can be seen the emissions factor is inversely proportional to the boiler efficiency. At boiler efficiencies above and below the reference boiler efficiency (89.3%), it can be seen that the changes in the emissions factors is linear.

8.8.3 CO_2 emissions factor predicted at different load conditions

A comparison of the emissions factor predicted at various load conditions (100% MCR – 40% MCR) versus the global industry benchmark emissions factors, for the six CFPPs is shown on Figure 8.12 (a) – (f). These profiles are based on the specified sub-bituminous fuel. It can be seen that the emissions factor for all the six unique CFPPs increased at lower plant load factors – this trend is expected. It can also be seen that the rate of change of the emissions factor with load factor for the NRHs is higher than the ones for single reheats and double reheats. This observation has to do with the fact that the rate of TCHR change with load is higher for the NRHs than the other CFPPs.

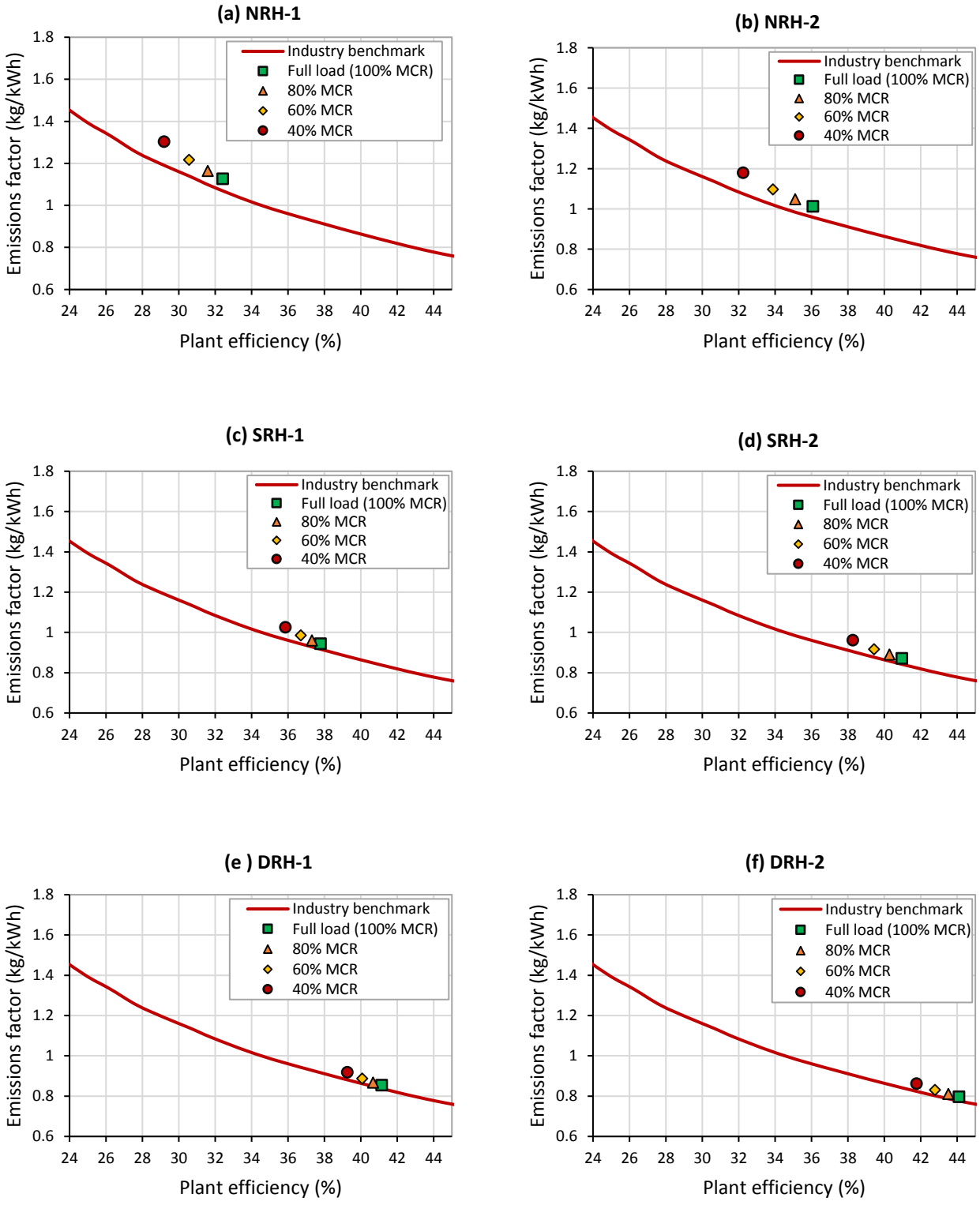

Figure 8.12 validating the emissions factor at varying load conditions

A graphical illustration of the difference between the emissions factor at full load and the value at 40% MCR is shown on Figure 8.13. It can also been seen that the part load effects on the emissions factor, over the load range (40% - 100% MCR) considered, is more significant for the CFPPs with fewer reheat stages.

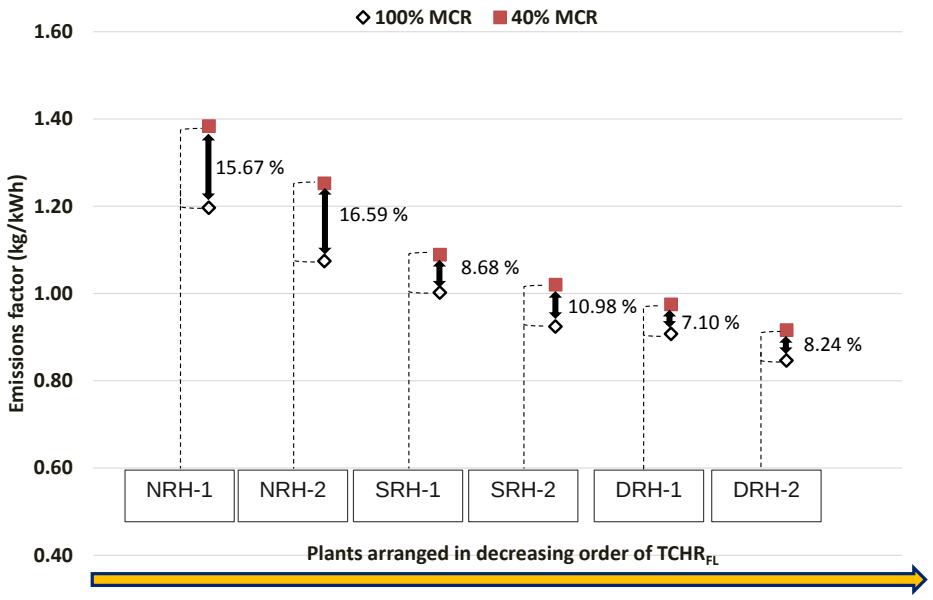

Figure 8.13 Impact of part load on the emissions factor (lignite coal)

8.8.4 Total CO_2 emissions predicted

A plot of the hourly CO_2 emissions for each load factor investigated is shown on Figure 8.14. It can be seen that the hourly emissions for each CFPP drops with load - this is the natural consequence of generating less electricity. It can also be seen that the hourly CO_2 emissions for the DRHs are higher than the ones from the SRHs and NRHs at each plant factor level, even though the emission factors for the DRHs are less than the ones for the NRHs and SRHs. This is because the chosen plant size is 200MW for NRH, 500MW for SRH and 1000MW for DRH – hence the total emissions for any given load factor for the larger sized CFPPs will be more due to the fact that more electricity is generated at that load factor.

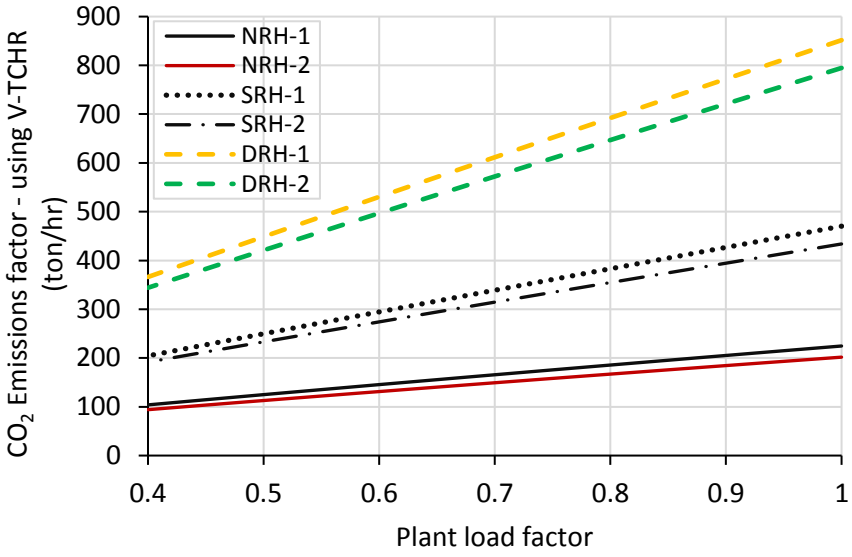

Figure 8.14 V-TCHR model hourly CO_2 emissions from different CFPPs

The impact of including a V-TCHR model on the total CO_2 emissions from individual CFPPs is better seen by looking at a CO_2 emissions penalty. It compares the adverse effect of not including the impact of the heat rate deterioration with load, while accounting for the total CO_2 emissions produced at lower loads. The CO_2 emissions emission penalty for each CFPP is determined from the equation below.

$$CO2_{penalty} = \frac{CO2_{V-TCHR} - CO2_{conv}}{CO2_{V-TCHR}} \tag{8.32}$$

The CO_2 emissions penalty of the six model CFPPs, is shown on Figure 8.15. This indicates that there is an additional amount of emissions that may be unaccounted for by the constant heat rate emissions factor model. As could be expected, the plant with a larger change in heat rate at low load i.e. the NRH, exhibits the largest emissions penalty, meaning one would make a large under-estimation of the actual total emission when assuming a constant heat rate.

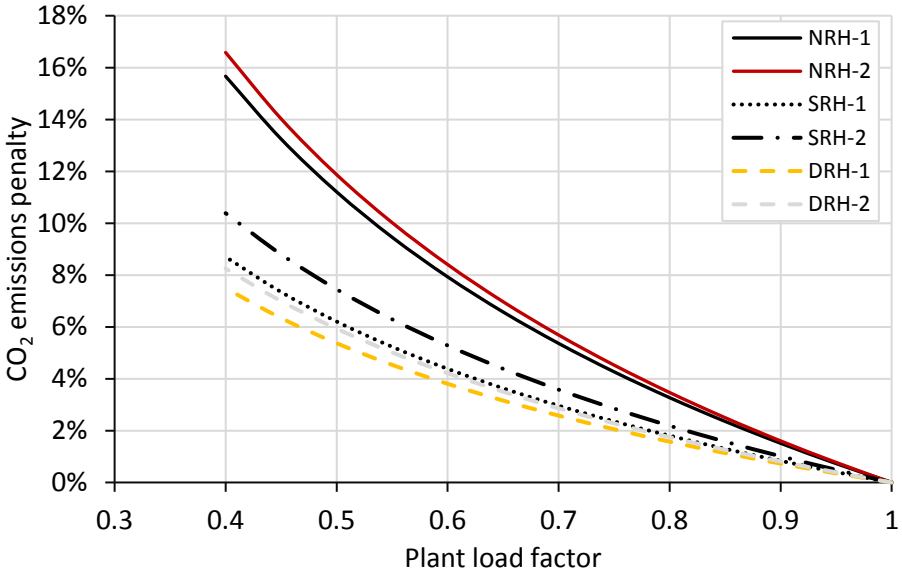

Figure 8.15 Impact of not including a V-TCHR based emissions factor

8.9 Conclusions of the Chapter

This chapter demonstrates how the V-TCHR model proposed in chapter 7 can be applied for predicting the CO_2 emissions characteristics of different types of CFPPs at different part/low load conditions.

A demonstration study was conducted on six model CFPPs and the predicted emissions factor results where compared against industry benchmark. The impacts of the boiler efficiency, coal quality and load factors were considered. A comparison of the emissions predicted by using the constant emissions factor model versus using the V-TCHR based emissions factor was also done by looking at the CO_2 emissions penalty.

The results of the study show that:

- The full load/VWO emissions factor predicted are reasonably accurate and the deviations are within 3 – 13 % of the global industry benchmark. This deviation is dependent on the type of fuel and the boiler efficiency used.
- The emissions factor of a CFPP increases at lower plant load factor levels. The rate of increase of the emissions factor is more severe for the non-reheats than the reheat systems.
- One would under-estimate the total CO_2 emissions whenever a constant heat rate based emissions factor model is used to quantify the CO_2 emissions at lower loads.
- The magnitude of the additional CO_2 emissions is dependent on:
    - The cycle effects: This is related to the $\Re$ value of the specific plant's V-TCHR model, as well as the duration at low load.
    - The capacity effects: This is related to the quantity of electricity generated, or rather the plant's rated capacity.

Using the V-TCHR based emissions factor model, one could adequately capture the impact of three key effects that are usually associated with the part and low load operations of CFPPs. The effects are: (a) Increased turbine cycle heat rate at part and low load conditions; (b) Increased combustion losses at lower loads; and (c) increased auxiliary fraction at lower loads.

9. Energy mix modelling demonstration

Energy mix modelling is a common method used whenever the emissions impact of integrating different power generation systems within an electric power system network is investigated. In this chapter, the V-TCHR based emissions factor model developed in chapter 8 will be implemented in an energy mix modelling demonstration of four different hypothetical electrical power system networks. The objectives of this exercise were to:

- Demonstrate how the inclusion of a V-TCHR based emission factor model can impact the fleet-wide CO_2 emissions in a power system network integrated with different levels of REPG penetration, and to compare the model results with the traditional method.
- Suggest a method for selecting which CFPPs to cycle and at what level in order to achieve an improved fleet-wide CO_2 emissions reduction on the grid.

The study will not attempt to make any conclusion or verification of published energy mix models or energy policy documents. The power system networks chosen are also not related to any specific site or country, however the selection was done to represent some extreme but plausible networks. The energy model will also not contain all the various complex nuances that are often found in detail energy mix models, but will rather contain specific simplification assumptions.

The chapter gives a description of the how four hypothetical electrical power system networks were set up. The networks have renewable energy resources that were obtained from South African sources, but could easily be applicable in other regions. A discussion of the emissions impact of including various levels of grid integrated REPG system under different merit order scenarios is also presented. The daily fleet-wide CO_2 emissions predicted for the traditional emission factor model will be compared with the one predicted using the V-TCHR based emissions factor model. Finally, a possible method for dispatching the CFPPs for a reduced fleet-wide CO_2 emissions is discussed.

9.1 Overview of the energy mix modelling methodology

In setting up an electrical power system network for energy mix modelling, one needs to consider the aspects displayed on Figure 9.1. It often begins with a forecast of the power system load. An understanding of the characteristics of the generators (power plants) in the network is also required. The structure of the transmission network and its constraints, and the maintenance schedule which relates to the availability of certain aspects of the network also needs to be understood properly. The unit commitment model (UCM) and the generation dispatch (GDM) model also needs to be defined. A discussion of these aspects is presented in the following sections.

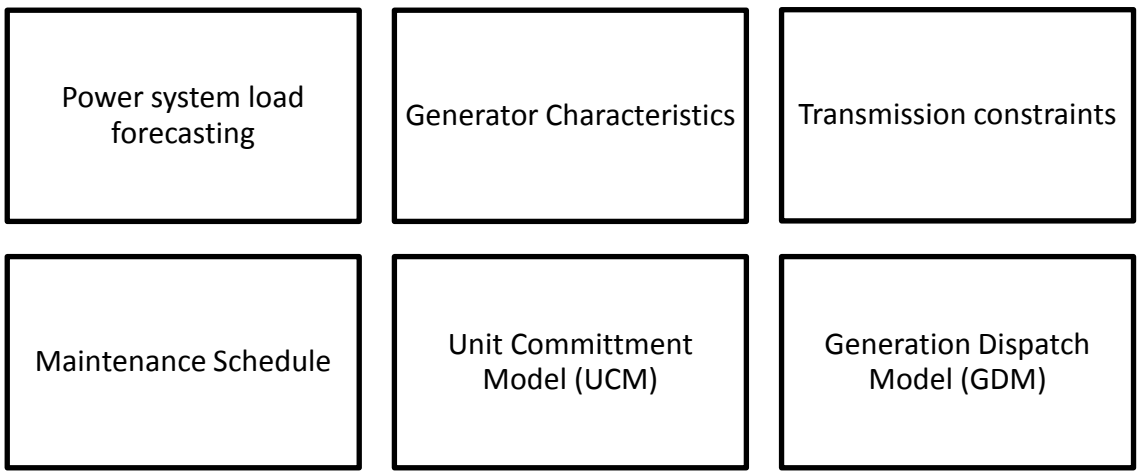

Figure 9.1 Factors to consider in an electrical Power System network setup.

9.2 Power system network load forecasting

The system load for a typical electrical power system networks varies over time. The variation can be on an hourly, daily, weekly, and even seasonal basis. In this study, an average diurnal system load of South Africa, for the 31 days of December 2014 was used for the power system networks (see Figure 9.2). The system load curve was obtained from a CSIR report presented in [43]. The shape of the load curve is not uncommon for most countries during summer period. It shows the typical morning and evening peak, with a dip during the night. This shape was deemed suitable to represent a generic network load.

The curve was normalized by dividing it by the maximum system load. The solid line on the chart represents a curve fit used to approximate the data. This curve fit can be represented mathematically as:

$$\overline{L_{sys}}(t) = 8.1132 \times 10^{-8}t^6 - 8.2798 \times 10^{-6}t^5 + 3.0956 \times 10^{-4}t^4 - 5.3817 \times 10^{-3}t^3 + 4.3 \times 10^{-2}t^2 - 1.1361t + 0.8673 \quad (9.1)$$

t is time expressed in hour.

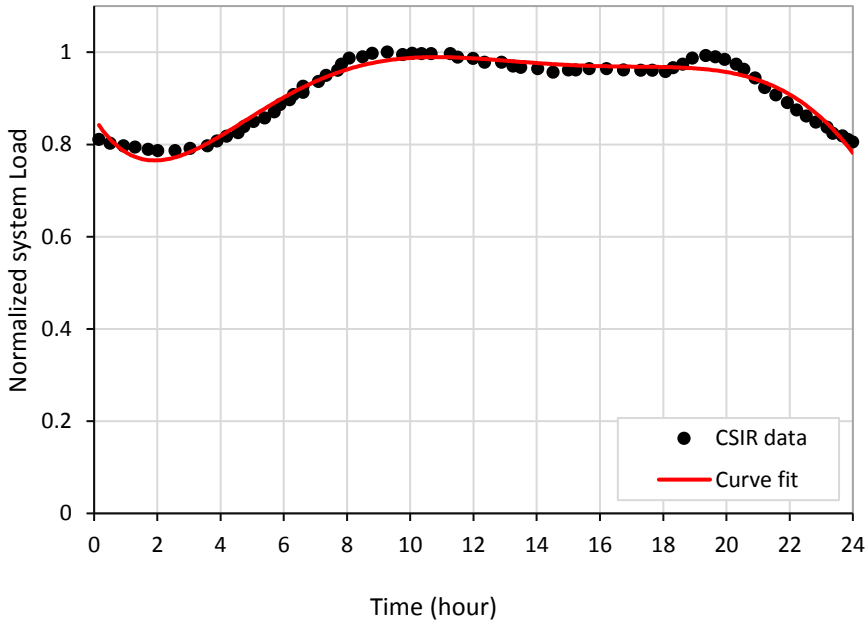

Figure 9.2 Normalized power system load curve

For an arbitrary sized network, the instantaneous system load ($L_{sys}(t)$) is then

$$L_{sys}(t) = \overline{L_{sys}}(t) \cdot L_{sys.max} \quad (9.2)$$

$L_{sys.max}$ is the maximum power system load, and $\overline{L_{sys}}(t)$ is the normalized daily system load.

9.3 Characteristics of different power generators and supply

Power system networks are generally known to have base-loaded plants, mid-merit plants, and peaking plants for meeting the baseloads, cycling loads, and peaking loads respectively. In this study, the total load in the power system network considered will be satisfied by only renewable systems (REPG) and coal fired power plants. The REPG systems are made up of solar photo voltaic (PV) and wind generation. One important assumption is that the REPG systems are always given dispatch priority over the CFPPs.

9.3.1 REPG generation, mix and penetration levels on the networks

The minimum average hourly solar PV and wind production profiles is shown on Figure 9.3 and Figure 9.4 respectively. The markers on the plots represent data from [43], while the solid line represents the curve fit.

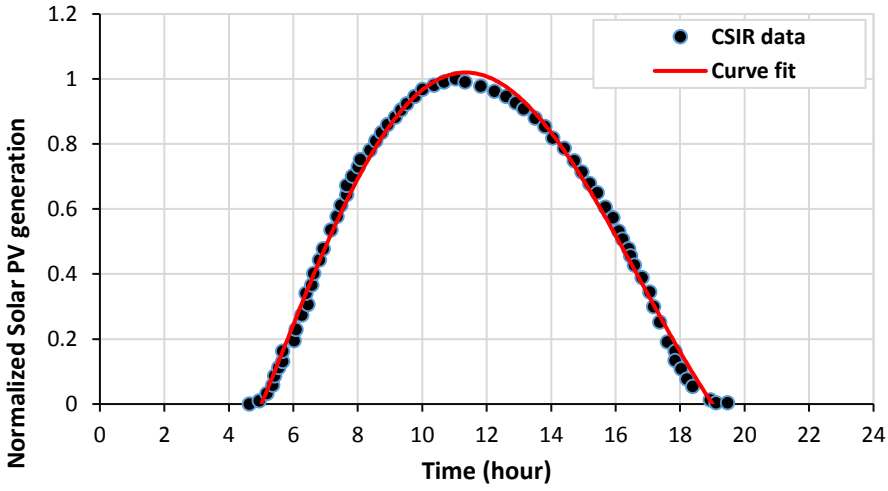

Figure 9.3 Normalized solar PV generation profile

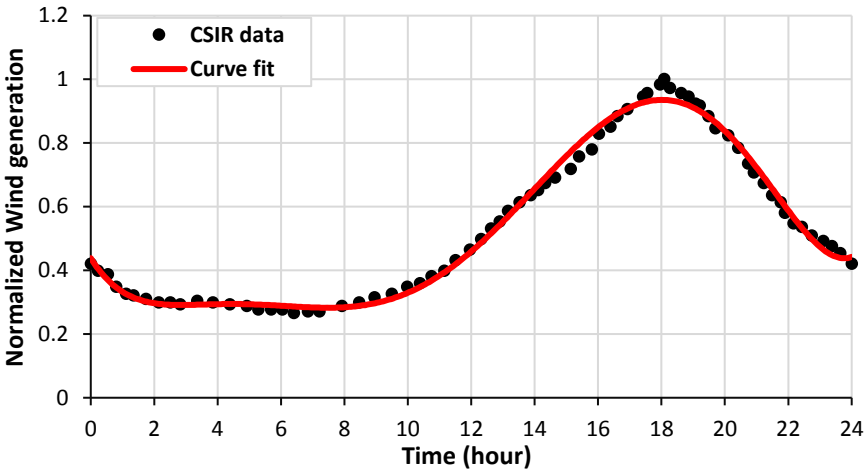

Figure 9.4 Normalized Wind power generation profile

The normalized solar power generation curve fit is mathematically defined as:

$$\overline{W_{solar}}(t) = \begin{cases} -2.2234 \times 10^{-2}t^2 + 0.5208t - 2.0642 & if \quad 5h < t \leq 19h \\ 0 \quad otherwise \end{cases} \tag{9.3}$$

For an arbitrary sized network, the instantaneous solar PV generation ($W_{solar}(t)$) is then

$$W_{solar}(t) = \overline{W_{solar}}(t) \cdot W_{solar.max} \tag{9.4}$$

$W_{solar.max}$ is the maximum solar PV power generation, and $\overline{W_{solar}}(t)$ is the normalized daily solar PV generation.

The normalized wind power generation curve fit is mathematically defined as:

$$\begin{aligned} \overline{W_{wind}}(t) = {} & 6.461 \times 10^{-7}t^6 - 4.3866 \times 10^{-5}t^5 + 1.0795 \times 10^{-3}t^4 \\ & - 1.1953 \times 10^{-2}t^3 + 6.3723 \times 10^{-2}t^2 - 0.1582t + 0.4380 \end{aligned} \tag{9.5}$$

For an arbitrary sized network, the instantaneous wind power generation ($W_{wind}(t)$) is defined as:

$$W_{wind}(t) = \overline{W_{wind}}(t) \cdot W_{wind,max} \tag{9.6}$$

$W_{wind,max}$ is the maximum wind power generation, and $\overline{W_{wind}}(t)$ is the normalized daily wind power generation.

There are two different methods for describing the penetration level of REPG systems. The power-based definition and the energy-based definition [193]. In the power-based definition, the penetration level is evaluated by dividing the total name plate installed REPG capacity by the peak load demand on the network. Although this method is very useful for understanding the impact of REPG integration on the electrical circuitry of the network [193], it does not provide a direct relationship to the fossil based generation that is displaced. The energy-based definition considers the amount of energy (electricity) supplied by the REPG system relative to the total electricity required by the power system over a given period. This method directly relates the displaced fossil based generation and the subsequent fuel/emissions reduction to the REPG penetration level [193]. It is also the preferred method in many Renewable Portfolio standards. For these reasons, the energy-based definition was selected as the basis for defining the REPG penetration levels.

This study considered REPG penetration levels ranging from 0% up to 70%, in 10% increments. Three REPG mix scenarios were also considered. On Table 9.1 the Reference scenario depicts a situation where the electricity generated from wind and solar PV is equal over a 24 hour interval. The High Wind scenario depicts a case where the electricity generated from wind is four times the amount generated from solar PV over a 24 hour period. Conversely, the High Solar scenario depicts a situation where the contribution from solar PV is four times the amount from wind.

Table 9.1 REPG mix scenarios investigated

Scenario	% REPG from Wind ($f_{wind/REPG}$)	% REPG from Solar PV ($f_{solar/REPG}$)
Reference	50%	50%
High Wind	80%	20%
High Solar	20%	80%

9.3.2 Determination of residual load, maximum solar and wind generation

Residual load is sometimes referred to as the net load. It is the total system load demand minus the total REPG generation supply [48]. This load is often used to determine the dispatch generation for the fossil-based generators. It is mathematically represented as:

$$L_{residual}(t) = L_{sys}(t) - W_{solar}(t) - W_{wind}(t) \quad (9.7)$$

The residual load calculation is done on an hourly time scale, for a 24 hour cycle. The sequence for determining the residual load involves the following calculation steps:

a) Total CFPP net generation capacity (MW) available on the network
b) Total system hourly electricity demand / load (MWh) from the network
c) Solar PV hourly generation (MW) supplied
d) Wind hourly generation (MW) supplied
e) Residual hourly load demand (MW)

The process starts by determining the total CFPP net generation capacity available $(W_{CFPP.avail})$ at any point in time. This is expressed as:

$$W_{CFPP.avail} = C_{reserve} \times W_{CFPP.total} \quad (9.8)$$

$W_{CFPP.total}$ is the total installed CFPP net generation capacity. It is the sum of the full load net generation capacity of all the CFPPs on the network. For this study, it is made up of various combinations of CFPPs as described in section 9.3.5. $C_{reserve}$ is the reserve generation capacity. This reserve takes care of the spinning and maintenance reserve that may be required at any point in time. Typical values found in literature for a power system network is between 10 - 12% [2]. For grid stability, the maximum load that a network may demand from the CFPP generators may not exceed the net generation capacity available. The maximum load is thus simply:

$$L_{sys.max} = W_{CFPP.avail} \quad (9.9)$$

The system load curve can now be defined using equation(9.2).

Because the REPG penetration definition is energy-based, the second step involves determining the total energy demand (MWh) on the network over a 24 hour period. The load curve is approximated as 24 hourly steps, with the assumption that the load remains constant during the hour. The total system energy can then be written as:

$$E_{sys} = \int_{t=0}^{24h} L_{sys}(t)dt \approx \sum_{i=0}^{23} L_{sys}(t_i) \cdot 1h \quad with \quad t_0 = 0 \tag{9.10}$$

Now the total REPG energy (E_{REPG}) can be calculated based on the chosen REPG penetration level (f_{REPG}):

$$E_{REPG} = f_{REPG} \times E_{sys} \tag{9.11}$$

This is made up of the solar energy contribution (E_{solar}) and the wind energy (E_{wind}) given their chosen relative contributions $f_{solar/REPG}$ and $f_{wind/REPG}$ as listed in Table 9.1.

$$E_{solar} = f_{solar/REPG} \times E_{REPG} \tag{9.12}$$

$$E_{wind} = f_{wind/REPG} \times E_{REPG} \tag{9.13}$$

The maximum solar PV (see Equations (9.14) and wind power (see Equations (9.15) generation can now be determined by integrating the respective normalised generation curve to obtain a normalized energy, and scale it using the previously calculated energy contribution.

$$W_{solar,max} = \frac{E_{wind}}{\int_{t=0}^{24} \overline{W_{solar}}(t)dt} \tag{9.14}$$

$$W_{wind,max} = \frac{E_{wind}}{\int_{t=0}^{24} \overline{W_{solar}}(t)dt} \tag{9.15}$$

The profile for the solar PV ($W_{solar}(t)$) and wind power ($W_{wind}(t)$) generation can be determined through Equations (9.4) and (9.6) respectively. Finally the residual load is then evaluated using Equation(9.7).

9.3.3 Modelling assumptions & constraints

There are some technical limitations that constrain the varying load operation of CFPPs. Some of the constraints are based on dynamic or steady operations. The dynamic constraints are usually ramping rates, start-up and shut down times [194]. The steady state constraints include the minimum and maximum operating load [195] [194]. The steady state constraint at the minimum condition is necessary to maintain flame stability without oil support while the maximum operating constraint is due to the fan and mill capacity limits of the draught group and the boiler.

Steady state operation limits set for this study are:

- Each CFPP model operates between a 40% minimum load and a maximum power output.
- The maximum net output for the non-reheats, single reheats and double reheats are 200MW, 500MW, and 1000MW respectively.
- A 10% reserve capacity margin is adopted in this study. It is consistent with what is seen in literature [2].
- Renewable curtailment is only done when the total supply from the REPG supply is greater than the total system load demand with no CFPP in operation.
- There are no de-rated units within the network. De-rating of units is a phenomenon which describes a reduced maximum generation capacity below the installed capacity. This is usually due to ageing and component degradation of the power plant component. All the plants maintain their original installed capacity.
- The reliability factor (loss of load probability) of each CFPP on the network is the same, and it is assumed to be equal to 1 – implying that all installed plants are assumed to be able to supply whenever required.
- The amount of transmissions losses within a power system network generally increases if there are significant distances between different unit locations. Sometimes losses

(technical and theft based) in a network is typically between 4-15% of the total power delivered on the network [196]. Power losses on the network could be seen as an additional load on the network and may be shared equally among the generators. For this study, the load is actually determined from the installed capacity instead of the actual power consumed by users and the distribution losses, hence it does not feature in the analysis.

- There are no congestion in the grid i.e the power flow within the network is unrestricted.

9.3.4 CFPP characteristics and generation capacity planning in the networks investigated

Generally, electric power system networks across the world typically have a varying number of CFPPs within them. South Africa for instance has over 77 CFPPs on its network. Some of the CFPPs are of the same configurations and design, even though they may have different operating process parameters. There is also a large variation in plant age and technology. In this study, six unique CFPP characteristics (same as the ones selected in chapter 8) have been selected to represent the different types of CFPPs that are in the networks considered.

The specific details of the CFPPs are presented on Table 9.2. These CFPPs were selected from the 192 VirtualPlant model CFPPs built in chapter 7. There are two NRHs (NRH-1 and NRH-2), two SRHs (SRH-1 and SRH-2), and two DRHs (DRH-1 and DRH-2). NRH-1, SRH-1, and DRH-1 represents dry-cooled NRH, SRH, and DRH CFPPs respectively while NRH-2, SRH-2, and DRH-2represents wet-cooled NRH, SRH, and DRH CFPPs respectively. The Turbine cycle heat rate at full load ($TCHR_{FL}$), that was already determined for each of the model CFPPs in chapter 7, were used. The rate of TCHR deterioration with load ($\Re$) was determined using the *V-TCHR* model proposed in chapter 7. These six unique CFPPs were selected by considering their $TCHR_{FL}$ and $\Re$ values, which makes them quite different from each-other. The net generation capacity for the NRHs, SRHs, and DRHs are 200MW, 500MW, and 1000MW respectively. Note that in developing the V-TCHR model, the gross generation was used as the focus was on the turbine cycle only. Since it was already demonstrated

that the actual plant output does not affect the heat rate, the plant sizes where chosen to be the net generation to be more compatible with how energy mix models are defined.

Table 9.2 Characteristics of the selected six CFPPs for Energy mix demonstration

Plant Name	**Process parameter description**								**Cooling technology**	$TCHR_{FL}$ (kJ/kWh)	$\Re$
	P_{thr} (MPa)	T_{thr} (℃)	T_{rh1} (℃)	P_{rh1} (MPa)	T_{rh2} (℃)	P_{rh2} (MPa)	P_{cond} (kPa)	Live steam enthalpy			
NRH-1 (Plant 004*)	12	510	N/A	N/A	N/A	N/A	17	3376.8	Dry-cooled (ACC)	9426.7	0.1141
NRH-2 (Plant 006*)	12	535	N/A	N/A	N/A	N/A	4	3442.8	Wet-cooled (OTC)	8466.4	0.1227
SRH-1 (Plant 087*)	17	535	535	4.33	N/A	N/A	12	3386.64	Dry-cooled (IDC)	8083.5	0.0573
SRH-2 (Plant 106*)	24	565	565	5.88	N/A	N/A	7	3397.83	Wet-cooled (WCC)	7457.9	0.0741
DRH-1 (Plant 187*)	30	565	565	9.60	565	2.364	12	3331.9	Dry-cooled (IDC)	7423.9	0.0514
DRH-2 (Plant 189*)	30	600	600	7.80	600	1.515	4	3446.87	Wet-cooled (OTC)	6927.1	0.0591

Note:
* The model CFPP plant number from chapter 7. For instance, NRH-1 is the model CFPP Plant number 004.
P_{thr} & T_{thr} – The steam throttle pressure and temperature respectively.
P_{rh1} & T_{rh1} – The 1st reheat pressure and temperature respectively.
P_{rh2} & T_{rh2} – The 2nd reheat pressure and temperature respectively.

V-TCHR based CO_2 emissions factor curves for the six unique model CFPPs under consideration were generated from the part load emissions factor presented in Figure 8.12. This was done to simplify the energy mix modelling. The emissions factor curve for each of the six CFPPs can be defined with a generic profile in Equation(9.16). EF_{FL} is the emissions factor at full load and the exponent b represents the rate of change of the emission factor with load. The coefficients for the six CFPPs are presented on

Table 9.3. The reference fuel characteristics used in this study is the same as the one used in chapter 8

$$EF(X) = EF_{FL}.X^{-b} \tag{9.16}$$

Table 9.3 Coefficients for the emissions factor profile

Type	EF_{FL} (kg/kWh) (Lignite Coal)	EF_{FL} (kg/kWh) (Sub-bituminous coal)	b
NRH-1 (Plant 004)	1.1939	1.1242	0.1576
NRH-2 (Plant 006)	1.0722	1.0097	0.1662
SRH-1 (Plant 087)	1.0004	0.9420	0.0901
SRH-2 (Plant 106)	0.9229	0.8691	0.1069
DRH-1 (Plant 187)	0.9062	0.8533	0.0781
DRH-2 (Plant 189)	0.8456	0.7962	0.0858

9.3.5 CFPP composition in the four power system networks considered

The composition of the different CFPPs within the electric power system networks differs from countries to countries around the world. In this study, four different hypothetical networks have been considered. A summary of the composition of each network is presented on Figure 9.5. Network 1 is a balanced network that contains an equal total installed capacity for the NRHs, SRHs and DRHs. This does not necessarily translate to equal number of CFPPs in each category because of the choice that NRH capacity is less than SRH and also DRH. It just means that if the total generation installed capacity for the NRHs is 2000 MW for instance, then the total installed generation capacity for the SRHs category is 2000 MW and for the DRHs is 2000 MW as well. Network 2 is largely dominated by NRHs. This type of network depicts the scenario of a country that would have mostly old CFPPs. Network 3 is largely dominated by SRHs. This type of network appears to be a good representation of the typical network seen across the world. Network 4 is dominated by modern technology DRH CFPPs. This represents the power system of the future for countries who plan to use more efficient CFPP in their generation mix.

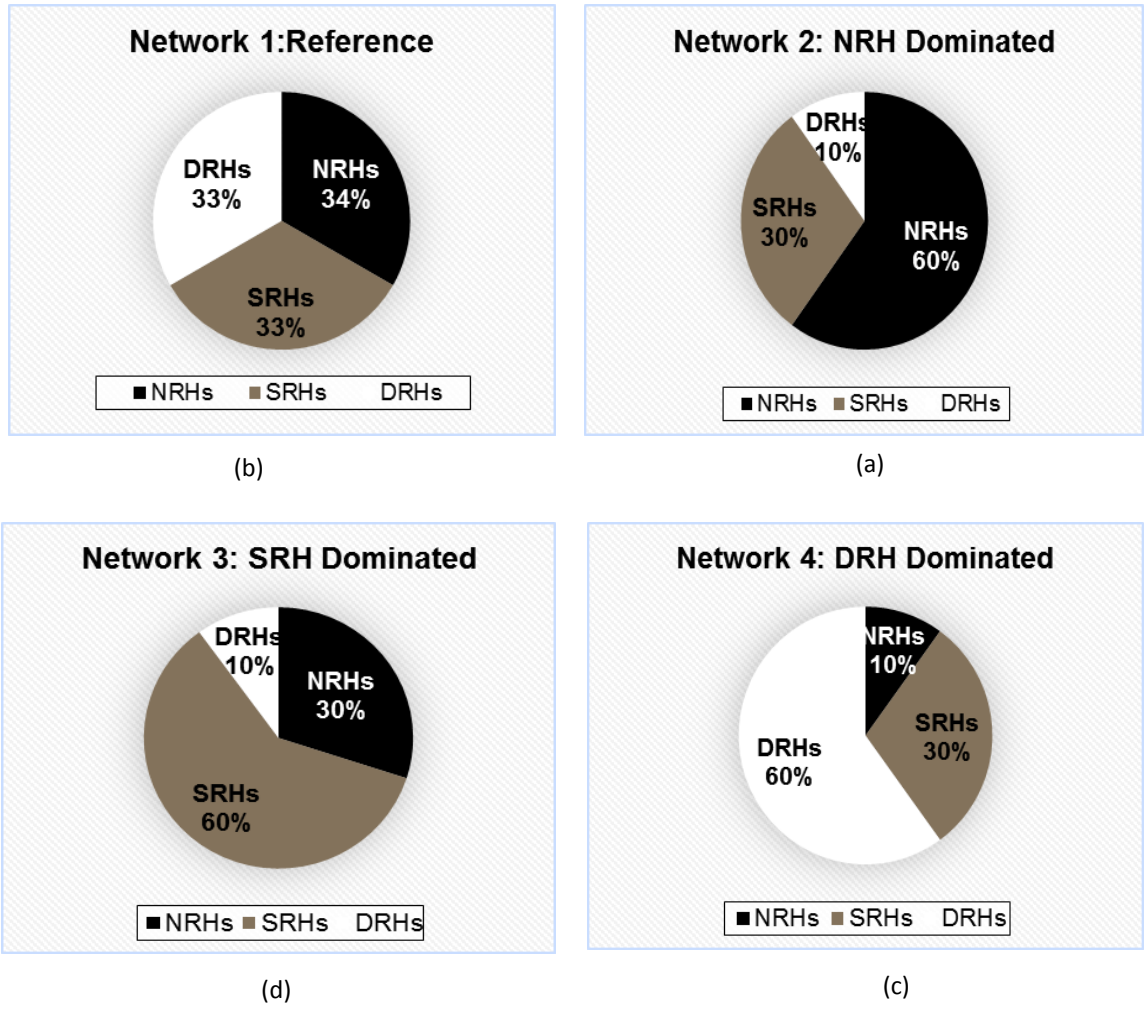

Figure 9.5 Composition of the CFPPs of the four Networks considered

Each of the power system networks considered contains one or more units of each of the chosen six unique CFPP plants. Take Network 1 (see Table 9.4) for instance, there are a total of 16 CFPPs on this network. It contains 10 units of NRHs (5 X NRH-1 & 5 X NRH-2), 4 units of SRHs (2 X SRH-1 & 2 X SRH-2), and 2 units of DRH (1 X DRH-1 & 1 X DRH-2). A numbering system is used to identify the different CFPPs on a given network. NRH-1.1, NRH-1.2, and NRH-1.n is used to distinguish between the 1st, 2nd and the nth NRH-1 plant on a network.

Table 9.4 Composition of the different CFPPs in the different Networks

Name of network	**Net Generation installed capacity**	**Number of NRH units**	**Number of SRH units**	**Number of DRH units**	**Total number of CFPPs**
Network 1[3]	6,000 MW	10 units (5 X NRH-1) (5 X NRH-2)	4 units (2 X SRH-1) (2 X SRH-2)	2 units (1 X DRH-1) (1 X SRH-2)	16
Network 2	10,000 MW	30 units (15 X NRH-1) (15 X NRH-2)	6 units (3 X SRH-1) (3 X SRH-2)	1 units (1 X DRH-1)	37
Network 3	10,000 MW	15 units (7 X NRH-1) (8 X NRH-2)	12 units (6 X SRH-1) (6 X SRH-2)	1 units (1 X DRH-1)	28
Network 4	10,000 MW	5 units (2 X NRH-1) (3 X NRH-2)	6 units (3 X SRH-1) (3 X SRH-2)	6 units (3 X SRH-1) (3 X SRH-2)	17
Note: The net generation installed capacity for each NRH, SRH, and DRH is 200MW, 500MW, and 1000MW respectively.					

9.4 Transmission Network

The transmission and distribution network was not modelled in detail. Instead, a single node approach was adopted. This approach is similar to the method adopted by Sklar-Chik [197]. Using Network 1 as illustration (see Figure 9.6.), the system load is aggregated at a single node with all 16 CFPPs, solar and wind generators supplying to the single node.

[3] Ideally the size of Network 1 should also be 10,000MW like the others. Unfortunately, the nominal sizes of the CFPPs selected made it difficult to get a combination of NRHs, SRHs, and DRHs that would ensure that one third of the total CFPP installed capacity is contributed by each category of CFPPs. Hence the value of 6000 MW was selected for this network. However, for effective comparison of the total CO_2 emissions from the four Networks, the total daily CO_2 emissions presented for Network 1 in the result and discussion section was scaled up by a factor of 10/6.

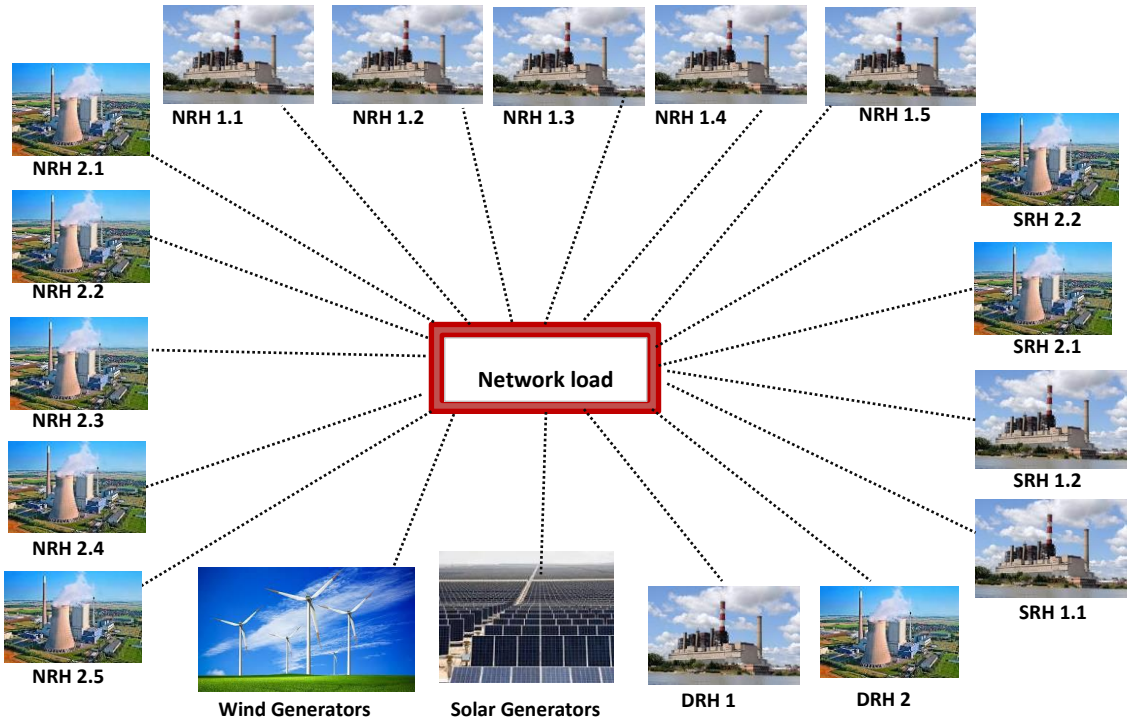

Figure 9.6 Power System transmission model for Network 1 comprising 10 NRHs, 4 SRHs & 2 DRHs and REPG systems

The following assumptions are made for the single node approach.

- The voltage and current on all the equipment are maintained within the regulatory limits, and at all points within each power system network.
- There are no transmission & technical losses in the grid and there are no transmission constraints on the grid. This kind of assumption is not unusual as it is commonly used for simplification [98] [103][197] [198].
- Ramp rate effects are usually too small to have impact on CO_2 emissions calculations that are done on an hourly time step basis [103]. Therefore, there was no need to consider the effects of ramp rates in this study.

9.5 Unit commitment and generation dispatch methods

Traditionally, the main factors that determine which CFPP is dispatched is based on : (a) the rapid frequency (load demand) response needed to satisfy the electricity grid requirements [128] [199]; and (b) The cost of generating electricity from a specific unit [199].

Method A

Priority	CFPP
6th	NRH-1
5th	NRH-2
4th	SRH-1
3rd	SRH-2
2nd	DRH-1
1st	DRH-2

Method B

Priority	CFPP
6th	DRH-2
5th	DRH-1
4th	SRH-2
3rd	SRH-1
2nd	NRH-2
1st	NRH-1

Method C

Priority	CFPP
6th	NRH-2
5th	NRH-1
4th	SRH-2
3rd	DRH-2
2nd	SRH-1
1st	DRH-1

Method D

Priority	CFPP
6th	DRH-1
5th	SRH-1
4th	DRH-2
3rd	SRH-2
2nd	NRH-1
1st	NRH-2

Method E

Priority	CFPP
6th	NRH-1
5th	NRH-2
4th	SRH-1
3rd	SRH-2
2nd	DRH-1
1st	DRH-2

(a) Overview of the merit order systems considered

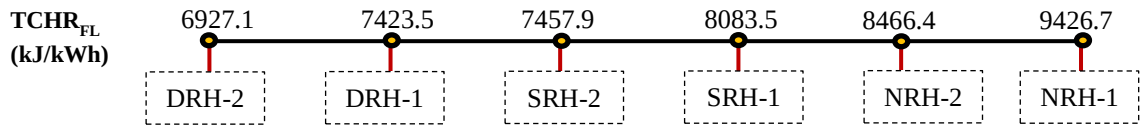

(b) Criteria for merit orders A and B is based on the $TCHR_{FL}$ value at full load.

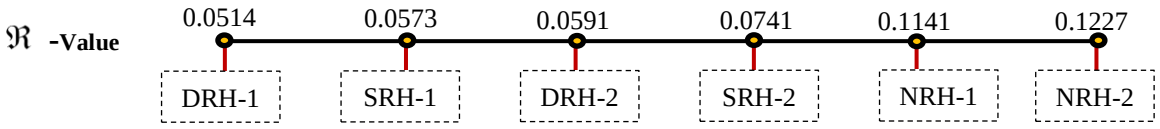

(c) Criteria for merit orders C and D is based on the $\Im$ Value

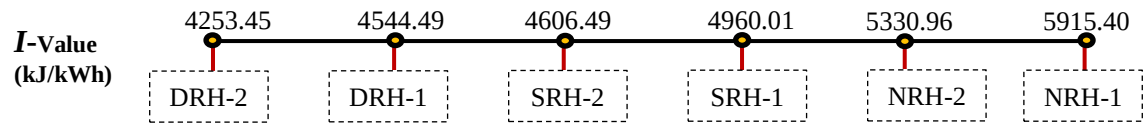

(d) Criteria for merit order E is based on the I-value

Figure 9.7 Merit order system and criteria for ranking the CFPPs

The generation/production profile for the different CFPP systems is dependent on the merit order system that is used in the unit commitment and generation dispatch model (UCGDM). Five different

merit order systems were considered in the generation dispatch model. The description of the five merit order systems and the criteria for the ranking the CFPPs on those merit order systems is summarized on Figure 9.7.

The dispatch priority for **Method A** considers the most efficient to least efficient CFPP. i.e the CFPPs are dispatched based on their full load turbine cycle heat rate value ($TCHR_{FL}$). The most efficient plants are operated as the base loaded plants or dispatched first. If there is a need for cycling load operation at any time interval, the least efficient CFFPs are the first to be cycled. Dispatch **Method B** is the reverse of Method A, i.e. the least efficient plants are used for base load, and the most efficient plants are cycled first. Dispatch **Method C** only considers the rate of TCHR deterioration ($\Re$) with load as the primary criteria for ranking the CFPPs. The plant with the least $\Re$ value is dispatched first, followed by the plant with next closest $\Re$ -value. If there is a need for cycling at any time interval, the CFPP with the largest $\Re$ is the first to be cycled. Dispatch **Method D** is again the reverse of Method C. In dispatch Method E, the combined effects of $TCHR_{FL}$ and $\Re$ from the V-TCHR model is used as the criteria for ranking the CFPPs. The combined effect is captured in a I parameter. This parameter is evaluated by integrating the V-TCHR model over the entire load range from 40% to 100% maximum continuous rating. Recall that the V-TCHR model definition is given as:

$$TCHR = TCHR_{FL} \cdot X^{-\Re} \tag{9.17}$$

The integral of this function with respect to *X*, and over the load range considered yields

$$I = \int_{0.4}^{1} TCHR_{FL} X^{-\Re} dX = TCHR_{FL} \frac{X^{-\Re+1}}{-\Re+1}\Bigg|_{0.4}^{1} = \frac{TCHR_{FL}}{1-\Re}\left(1 - 0.4^{1-\Re}\right) \tag{9.18}$$

From the I -value calculated for each CFPP (see Figure 9.7 (d)), it can be seen that the dispatch priority for Method E is the same as Method A. This similarity suggests that the effect of $TCHR_{FL}$ could be much greater than the effect of $\Re$. Because of this similarity, there is no need to include Method E into further analyses, as it will produce the same results as Method A. It is worth noting that if there were two CFPPs with the same $TCHR_{FL}$ value and boiler efficiency, then the one with the least $\Re$ value would be given the highest dispatch priority using the integral method.

The generation/production schedules for the dispatched CFPPs were done in a spreadsheet calculation implemented in Microsoft Excel. A simple stack-overflow method was used to distribute the residual loads amongst the dispatched CFPPs. This simply means that at every time step, the residual load is shared among the CFPPs based on the priority already discussed for each dispatch method. For each CFPP that is committed & dispatched, the minimum generation is 40% MCR and the maximum generation 100% MCR.

9.6 Results and Discussion

9.6.1 System and residual load with various REPG generation penetration levels

The system load, residual load, and the generation from the wind and solar PV systems for Network 1 are presented on Figure 9.8. The minimum and maximum system load is 3853 MW and 4980 MW respectively. The supply from the wind and solar PV system appears to be the same around the 6th and 16th hour for all the levels of REPG penetration considered. At 0% REPG penetration (see Figure 9.8a), the residual load is equal to the total power system load for the 24 hour time interval. At 20% REPG penetration, the residual load decreased until it reached a minimum load of about 3000 MW between the 13th and 14th hour. The decrease in the residual load continues at a REPG penetration of 30% until the power supplied by the REPG systems exceed the residual load between the 13th and 14th hour. The minimum residual load dropped to around 2500MW. At 60% and 70% REPG penetration level, the REPG supply exceeds the power system load demand (see coloured region on Figure 9.8 (e) and (f)). In order to ensure that the grid stability criteria is maintained, there was need for curtailment of the REPG supply. The excess REPG that is supplied beyond the power system load is curtailed plus an additional REPG generation that is equivalent to 40% MCR of the CFPP that is ranked no 1 on the dispatch order. This additional REPG generation that is curtailed was done to ensure that at least one CFPP is always available to supply electricity in the event of a failure of the REPG systems.

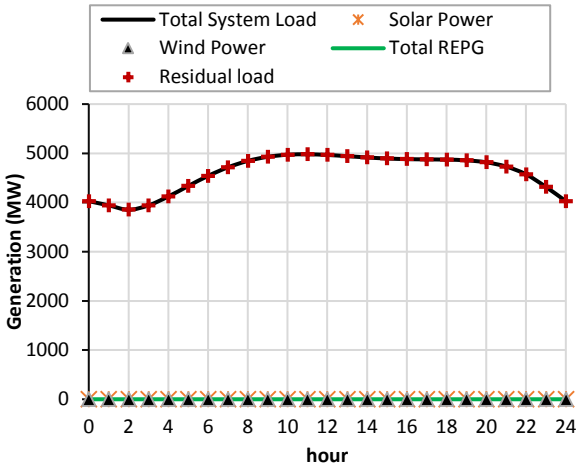

(a) 0% REPG Penetration level

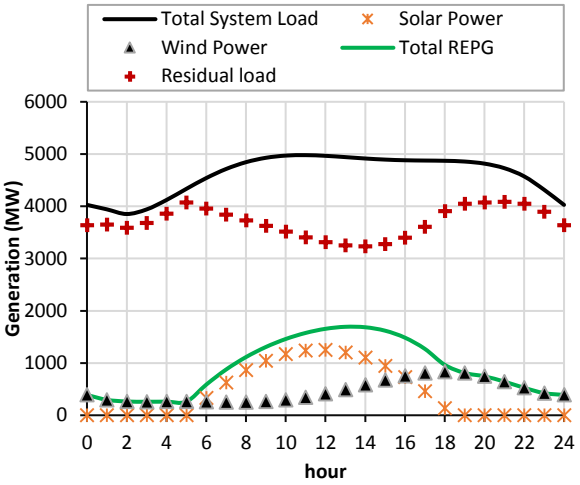

(b) 20% REPG Penetration level

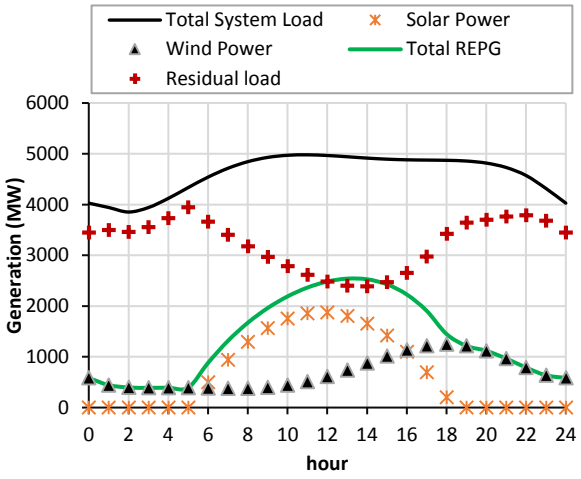

(c) 30% REPG Penetration level

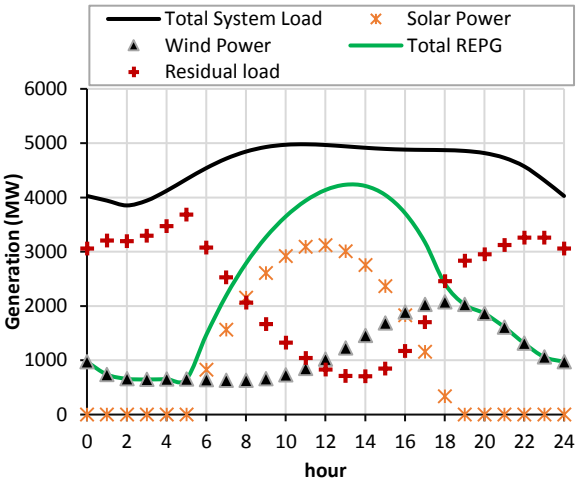

(d) 50% REPG Penetration level

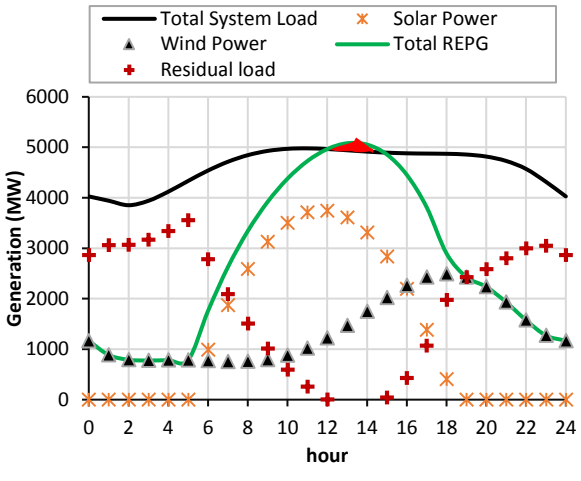

(e) 60% REPG Penetration level

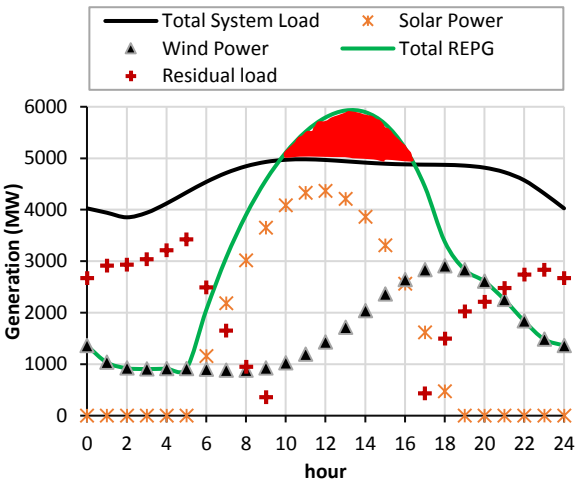

(f) 70% REPG Penetration level

Figure 9.8 Residual load, Solar and Wind generation at various REPG penetration levels for the reference REPG mix for Network 1.

The impact of the REGP mix on the predicted residual load is shown on Figure 9.9(a) – (f). The residual load for the reference REPG mix appears to be an average of the high solar and high wind REPG mix scenarios at all the REPG penetration levels. The residual load from the three REPG mix scenarios appear to be equal at the 6^{th} and 16^{th} hour. This is because the generation/supply from the wind and solar PV systems are approximately equal at the 6^{th} and 16^{th} hour for all the levels of REPG penetration considered. At REPG penetration level of 50% and above, there is need for curtailing the REPG supply from the high solar REPG mix scenario. The curtailment of the REPG supply for the reference scenario only begins at 60% REPG penetration while the curtailment of the REPG supply from the high wind scenario only begins from the 70% REPG penetration level.

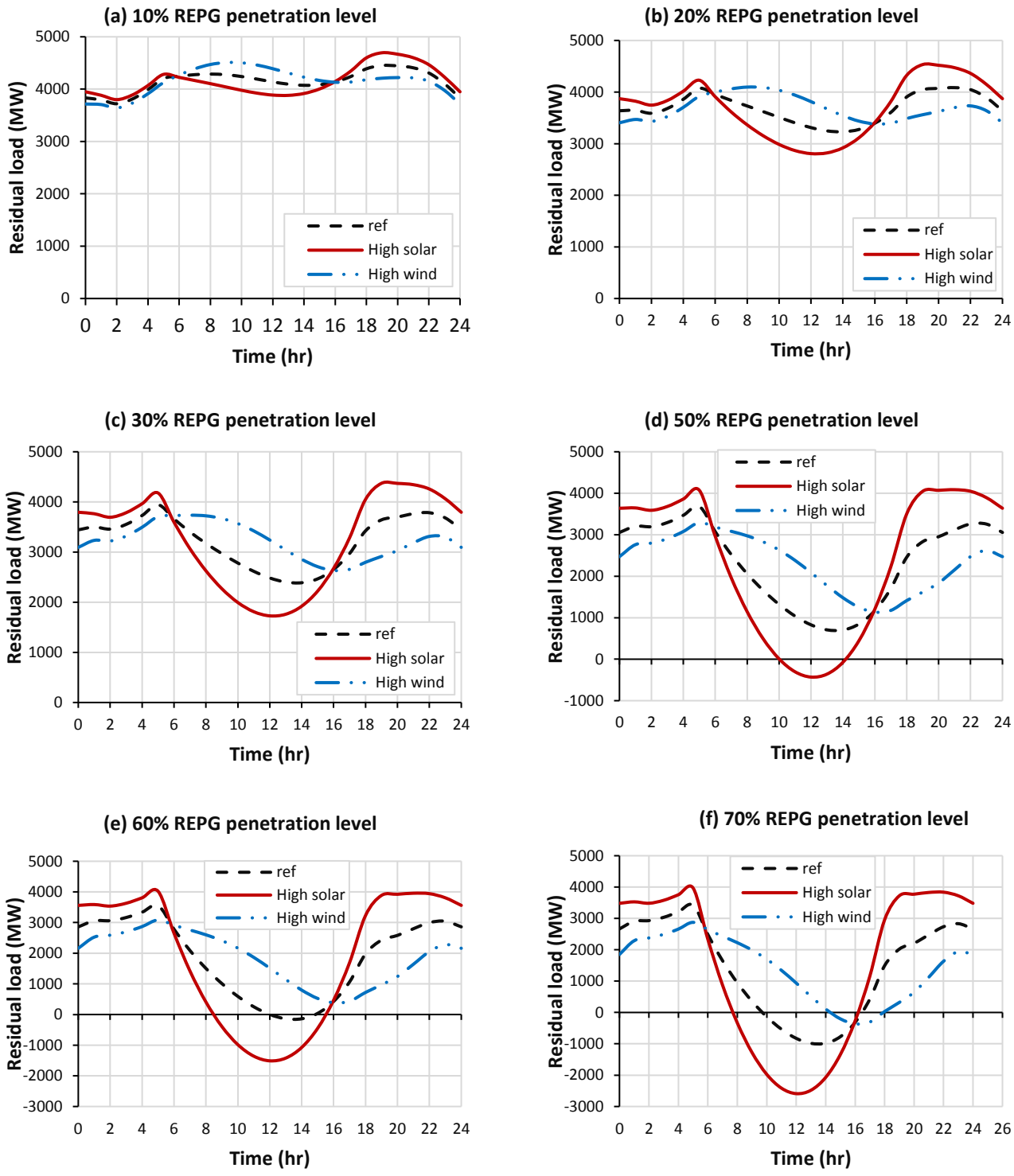

Figure 9.9 Impact of REGP mix on Residual load at various REPG penetration levels for Network 1

9.6.2 CFPP production scheduling profiles for the reference REPG mix

The hourly production scheduling profiles for some of the REPG penetration levels for Network 1, using dispatch method A, is shown on the

Figure 9.10 (a) – (f). At 0% REPG, DRH-2, DRH-1, SRH-2.1, SRH-2.2 were the only CFPPs that were dispatched at full load conditions (base loaded) throughout the 24 hours period simulated. The remaining CFPPs were dispatched at varying load conditions within the 24 hour period. At other REPG penetration levels (20%-70%), it can be seen that the amount of cycling (part load operation) done by the CFPPs increases as the REPG penetration level increases. At REPG penetration levels of 50% and above, all the CFPPs were dispatched at part load generation levels within the 24 hour period. Furthermore, between the 12^{th} and 14^{th} hour, the residual load demand on the power system network was so low that the operation of only DRH-2 was sufficient to satisfy the system load demand. The curtailment of the REPG supply for REPG penetration level of 60% occurs between the 11^{th} and 16^{th} hour, while the REPG curtailment for penetration level of 7 occurs between the 9^{th} and 17^{th} hour.

The hourly production profiles using dispatch method B for Network 1 is shown in Figure 9.11 (a) – (f). At 0% REPG, all the CFPPs except DRH-2, DRH-1, SRH-2.2 and SRH-2.1 were dispatched at full load conditions throughout the 24 hours period simulated. At REPG level of 60% and above, DRH-2 was not dispatched because the residual load requirements had dropped to the point where the minimum load (40% MCR) condition imposed could not be satisfied for DRH-2. Just like the dispatch method A, the curtailment of the REPG supply begins from REPG penetration level of 60% and above. This REPG curtailment for REPG penetration level of 60% occurs between the 12^{th} and 15^{th} hour, while the REPG curtailment for penetration level of 7 occurs between the 10^{th} and 16^{th} hour.

Sample hourly production profiles for the remaining two dispatch methods (C and D) for Network 1, and for Networks 2, 3, and 4 are shown in Appendix C. The trends are not too different from what has been discussed above.

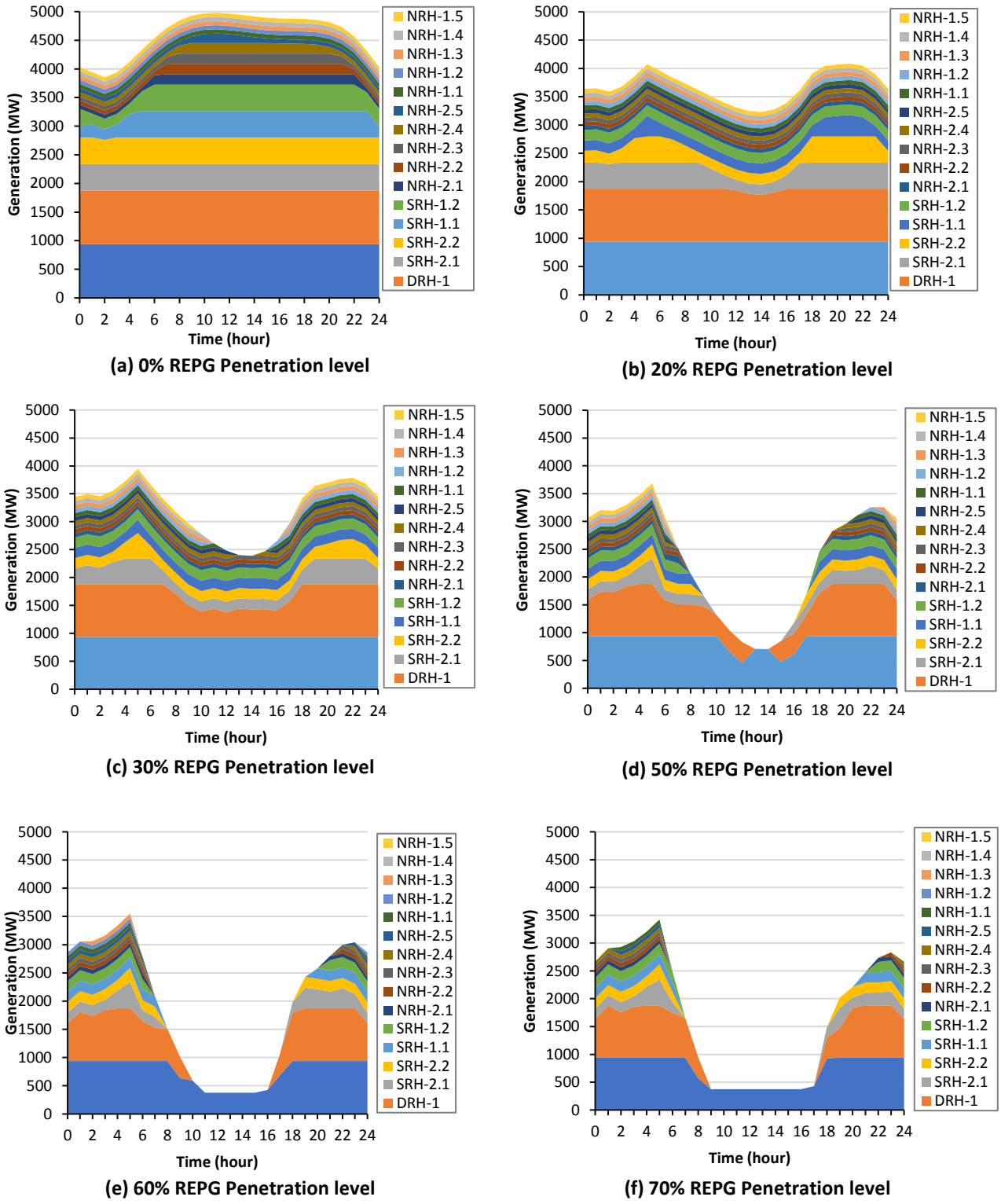

Figure 9.10 Hourly Production profiles for different REPG penetration: Network 1 (dispatch method A)

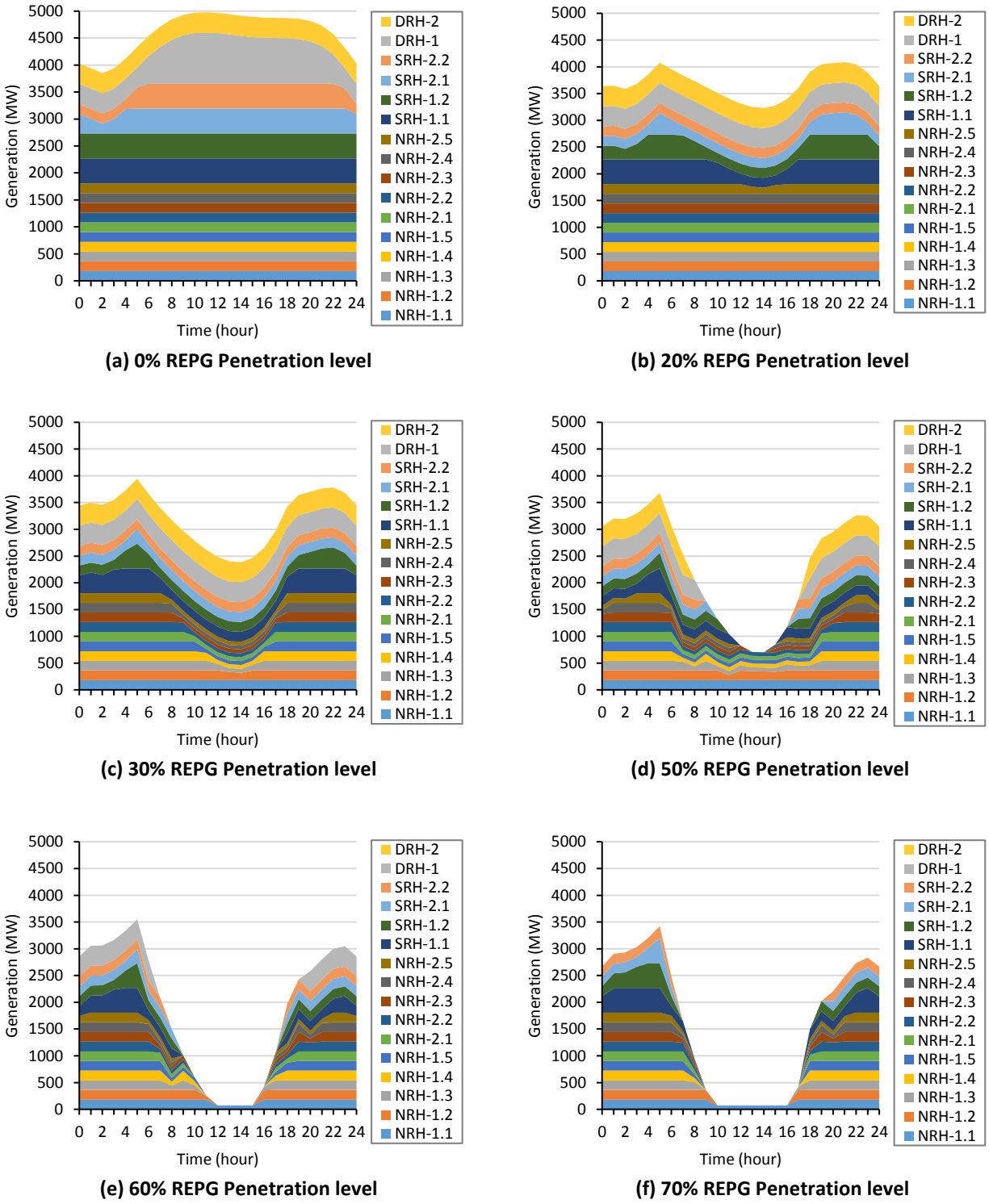

Figure 9.11 Hourly Production profiles for different REPG penetration: Network 1 (dispatch method B)

9.6.3 Hourly CO_2 emissions and description of emissions indicators

A sample of the hourly CO_2 emissions profile predicted using the V-TCHR model, and the total CFPP generation (residual load) for Network 1 is shown Figure 9.12.

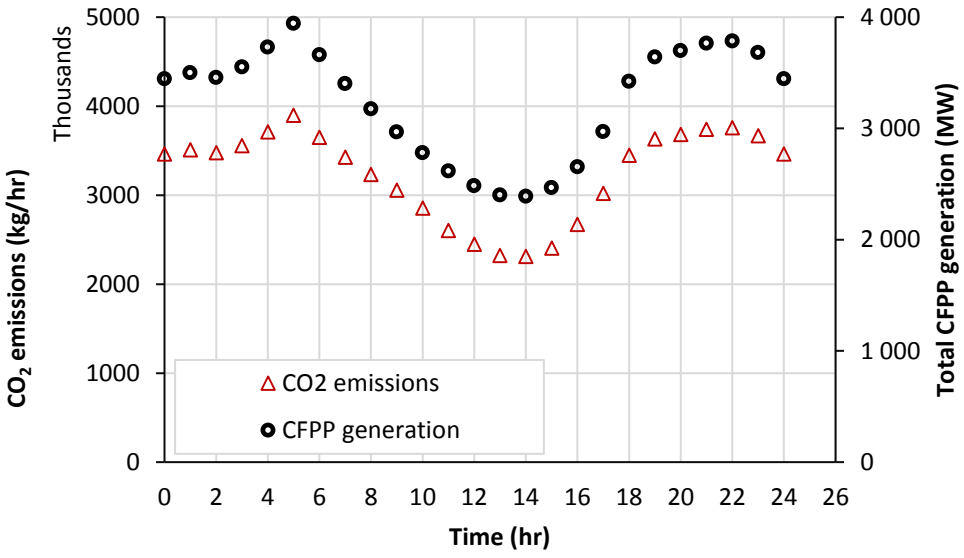

Figure 9.12 CO_2 emissions based on the V-TCHR model for a 30% REPG penetration level

The CO_2 emissions profile is almost similar to that of the CFPP generation (residual load) profile. This is because the CO_2 emissions from CFPPs is mainly dependent on the generation level / fuel consumption of the CFPPs used to meet the residual load. This relationship between CFPP generation level and CO_2 production is well known in literature, so it is not discussed further. The subsequent discussions around the predicted CO_2 emissions will rather be done with the aid of three emissions indicators defined below:

i ***The total daily fleet wide CO_2 emissions*** $\left(CO2_{tot-daily-fleet}\right)$ in tons/day. This is defined as the sum of the CO_2 emitted from all the dispatched CFPPs in 24 hours. For instance, if the total hourly CO_2 emissions produced by all the dispatched CFPP is shown on Figure 9.12, then the area under the curve would yield the total daily fleet wide CO_2 emissions.

The area under the curve can be approximated by numerical integration as:

$$CO2_{tot-daily-fleet} = \sum_{i=0}^{23} CO2_{tot,i} \cdot 1h \tag{9.19}$$

$CO2_{tot,i}$ is the sum of the CO_2 emission rate from all the CFPPs dispatched at time t_i with $t_0 = 0$, and assumed to be constant for the hour.

ii ***The unaccounted daily fleet wide CO_2 emissions*** $(CO2_{unacct})$ in tons/day.

A sample profile showing a comparison of the hourly fleet wide CO_2 emissions from the V-TCHR based emission factor model and the conventional constant emissions factor model is shown on Figure 9.13. The conventional method refers to the use of a constant emissions factor obtained at 100% MCR for each CFPP. The CO_2 emissions predicted using the V-TCHR method is higher than that of the conventional method because of the inclusion of the effect of heat rate deterioration with load. Therefore, an unaccounted daily fleet wide CO_2 emissions ($CO2_{unacct}$) parameter is defined as the emissions that would be unaccounted for if the V-TCHR model is not implemented in the energy mix modelling. It is represented by the green-coloured area on Figure 9.13. $CO2_{unacct}$ is evaluated using the equation below.

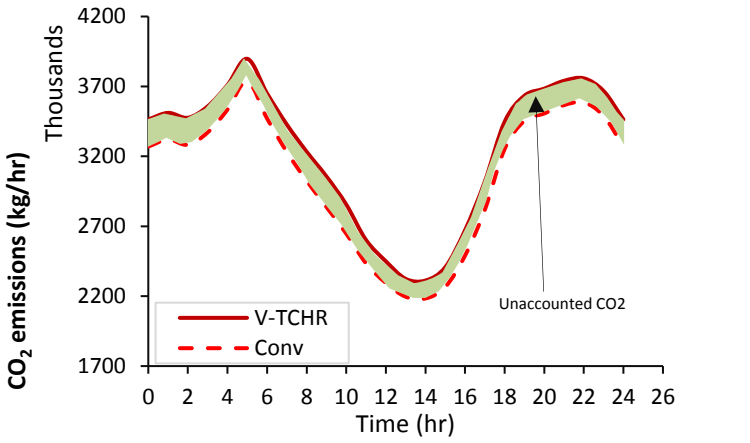

Figure 9.13 Sample comparison for CO_2 emissions from V-TCHR and the conventional method

$$CO2_{unacct} = \left(CO2_{tot-daily-fleet}\right)_{V-TCHR} - \left(CO2_{tot-daily-fleet}\right)_{conv} \tag{9.20}$$

$\left(CO2_{tot-daily-fleet}\right)_{conv}$, $\left(CO2_{tot-daily-fleet}\right)_{V-TCHR}$ is the total daily fleet-wide CO_2 emissions evaluated based on the conventional and V-TCHR model respectively.

iii ***Fleet-wide CO_2 emissions penalty*** predicted $\left(CO2_{fleet-penalty}\right)$ in %. This is expressed mathematically as:

$$CO2_{fleet-penalty} = \frac{CO2_{unacct}}{\left(CO2_{tot-daily-fleet}\right)_{V-TCHR}} \times 100 \quad (9.21)$$

This parameter depicts the margin of the deviation in the total fleet wide CO_2 emission of the conventional method from the V-TCHR method. It can also be considered the underestimation error made by the conventional method.

9.6.4 Fleet wide CO_2 emissions for Network 1

The total daily fleet-wide CO_2 emissions and unaccounted fleet wide CO_2 emissions for Network 1 are presented on Figure 9.14 (a). As expected, the total CO_2 emissions decreases with the penetration level of REPG. At 0% REPG penetration level, the unaccounted CO_2 emissions is 4.2 tons/day (see Figure 9.14 (a)). This constitutes ~2.5% of the total fleet-wide CO_2 emissions. The reason why there is an unaccounted emissions at 0% REPG is because some of the CFPPs are on part load operations during some hours, therefore assuming a constant full load emissions factor for those CFPPs imply that the emissions of those plants are potentially underestimated when the conventional emissions factor method is used. The unaccounted emissions grows from 4.2 tons/day at 0% REPG penetration level to 7.2 tons/day at 30% REPG penetration level. A turning point is reached between 30%-40% REPG penetration level. Beyond this point, the unaccounted CO_2 emission begins to reduce with REPG penetration level. The unaccounted CO_2 emission profile in Figure 9.14 (a) shows that at all the REPG levels of penetrations investigated, the total fleet-wide CO_2 emissions is underestimated, because the impact of the heat rate deterioration with load as captured by the V-TCHR based emission factor model is ignored.

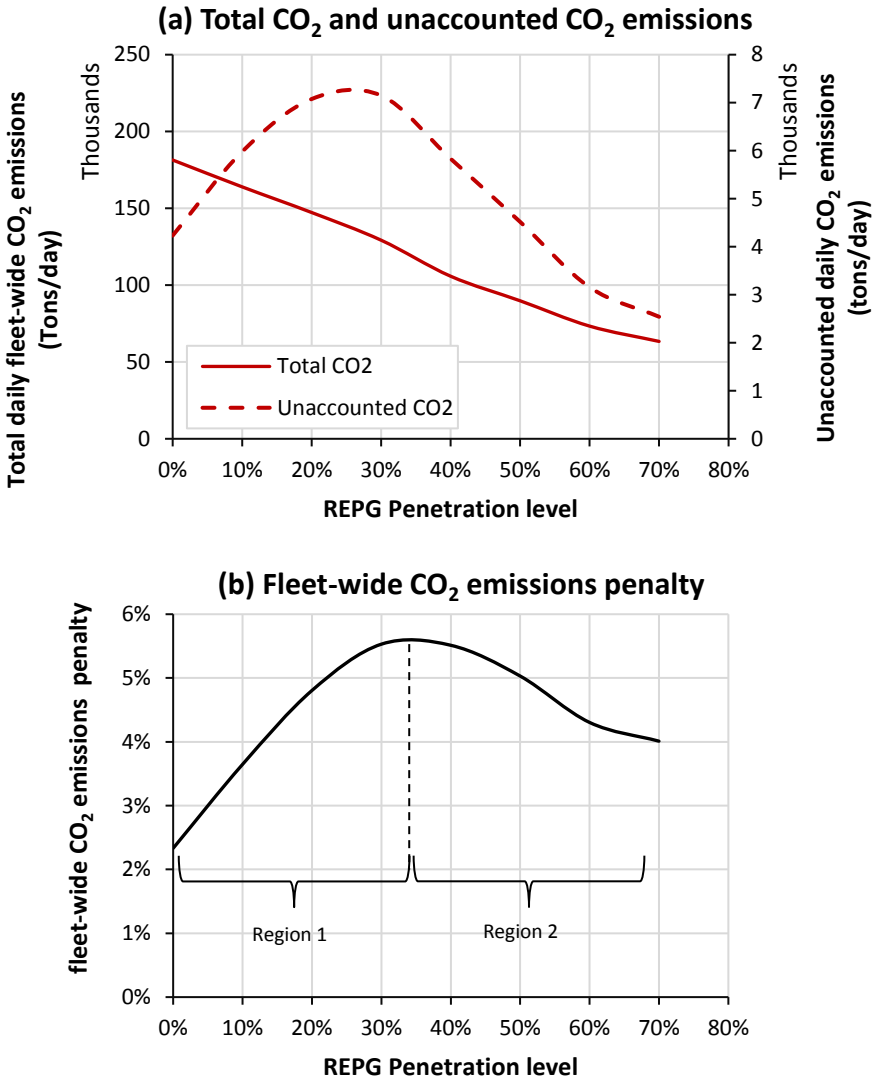

Figure 9.14 Fleet wide CO_2 emissions based on V-TCHR model for Network 1, reference REPG mix and dispatch method A

The profile of the fleet-wide CO_2 emissions penalty associated with using the conventional method is shown on Figure 9.14 (b). It can be seen that the relative error profile is quite similar to the profile of the unaccounted CO_2 emissions in Figure 9.14 (a). There are two distinct regions (1 & 2) that are visible. In region 1 (REPG penetration below 30%), there is an increase in the fleet-wide CO_2 emissions penalty while there is a decrease in the fleet-wide CO_2 emissions penalty in region 2. The changing profile in both regions is caused by the interaction between the unaccounted CO_2 emissions and the total fleet wide CO_2 emissions in both regions. In both regions 1 and 2, there is a reduction in the total fleetwide CO_2 emissions. In region 1, there is an increase in the unaccounted

CO_2 emissions caused by the impact of running the CFPPs at lower loads, while the decrease in the unaccounted CO_2 emissions in region 2 is caused by the fact that fewer number of CFPPs are dispatched, albeit at much lesser plant load factors

9.6.5 Fleet wide CO_2 emissions: Impact of dispatch method

The impact of the dispatch method on the energy mix modelling results were investigated. The total daily fleet-wide CO_2 emissions, unaccounted fleet wide CO_2 emissions, and fleet-wide CO_2 emissions penalty for the four different dispatch method are presented on Figure 9.15.

The total daily fleet wide CO_2 emissions predicted is seen to decrease for all the dispatch methods as the REPG penetration level increases. The total daily fleet wide CO_2 emissions predicted for the dispatch method A is the least at all the REPG penetration levels. This is closely followed by the emissions from dispatch method C, then methods D and B. This results suggests that using the dispatch method A, which considers the least turbine cycle full load heat rate as the criteria for ranking the CFPP with the highest dispatch priority yields the least amount of daily fleet wide CO_2 emissions at all the REPG penetration levels considered. Dispatch method C which considers the least $\mathfrak{R}$ value as the criteria for ranking the CFPP with the highest dispatch priority yields the next lowest amount of daily fleetwide emissions. This can be explained when looking at Table 9.2 which shows that picking the lowest $\mathfrak{R}$ values also tend to favour the lower heat rate plants (SRH and DRH).

The profiles for the unaccounted CO_2 emissions in Figure 9.15 (b) and the fleet wide CO_2 emissions penalty in Figure 9.15 (c) for the four dispatch methods appear to be similar. The fleet wide CO_2 emissions penalty increases steadily from 2.2% at 0% REPG penetration level to approximately 5.5% at 30% REPG penetration level, for dispatch methods A and C. One can see a turning point in the fleet wide emissions penalty for all four methods in the region of 30-50% REPG penetration. The seemingly outlier at 50% REPG penetration for Method D in the unaccounted emissions curve is possibly due to an incidental combination of active plants at this level. If a dispatch method D is used, the fleet wide emissions penalty is potentially lesser than for the others.

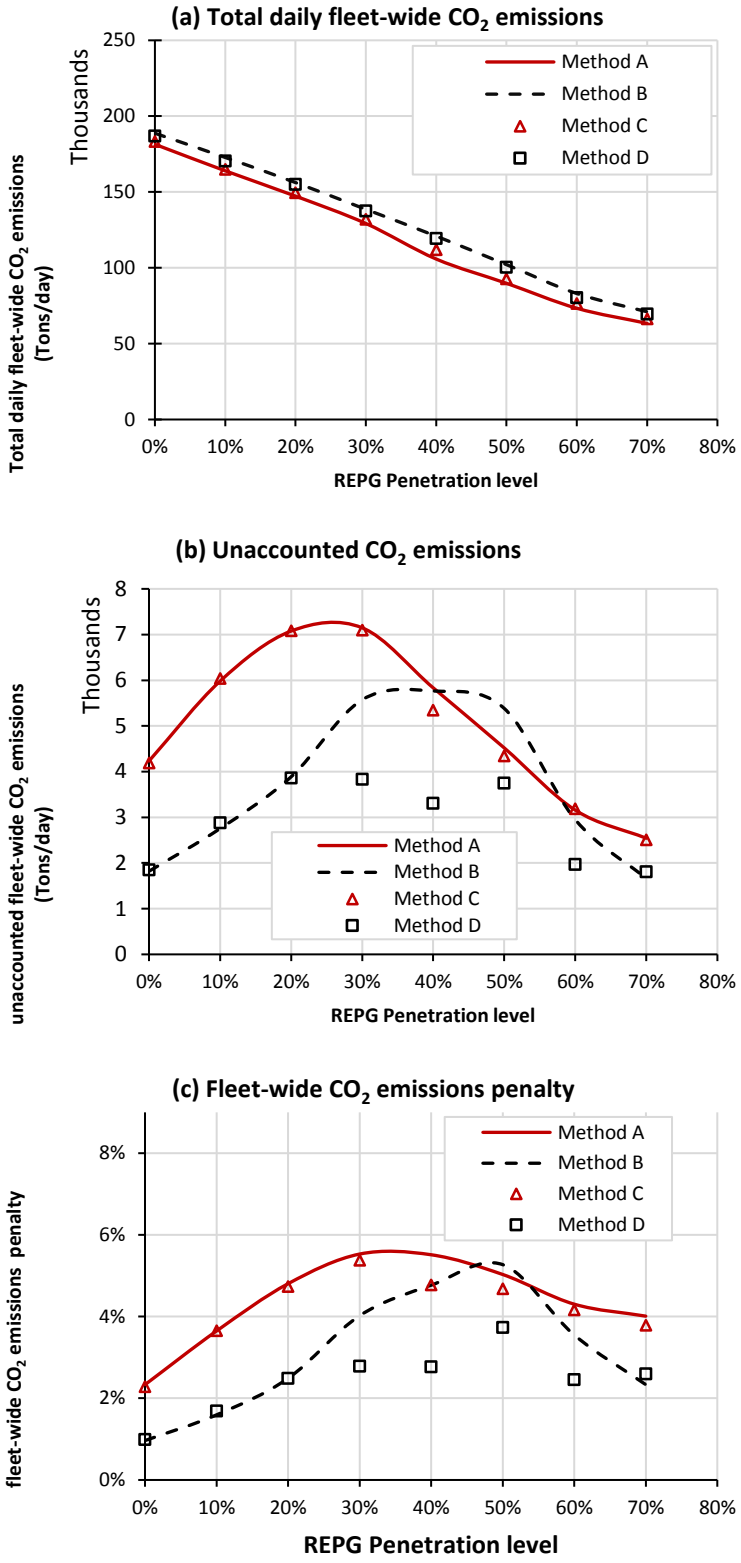

Figure 9.15 Impact of dispatch method on fleet wide CO_2 emissions for Network 1: Reference REPG mix scenario

9.6.6 Fleet wide CO_2 emissions: Impact of network composition

One can expect that the types of CFPPs that are on the power network could affect the quantity of the CO_2 emissions and the relative error in the CO_2 emissions predicted. Figure 9.16 shows the impact of the REPG penetration level on the total daily fleet-wide CO_2 emissions for the four networks considered. The daily fleet-wide CO_2 emissions in all four networks decreased with REPG Penetration level. At all REPG penetration level, the fleet-wide CO_2 emissions for Network 2 (NRH dominated) is higher than the value for Networks 1,3 and 4. This is primarily due to the impact of the poor TCHR effects at full load condition, and the higher impact of the rate of heat rate deterioration with load seen in NRH CFPPs.

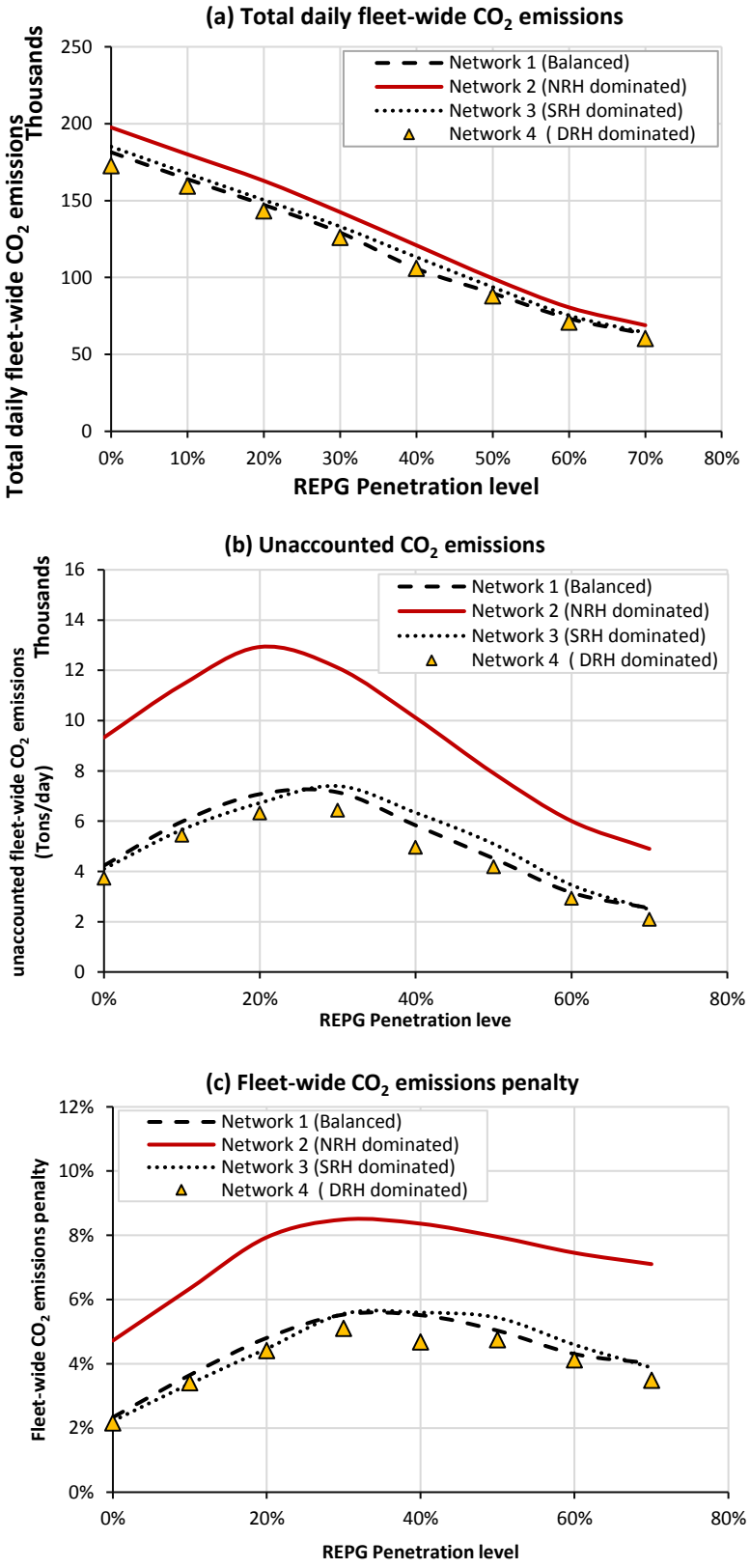

Figure 9.16 Fleet wide CO_2 emissions for dispatch method A: Impact of Network composition

The fleet wide CO_2 emissions penalty predicted for the four networks, using dispatch method A is shown on Figure 9.16 (c). It can be seen that the fleet wide CO_2 emissions penalty for Network 1, 3, and 4 rises from 2% to around 5.5% between 0% REPG and 30% REPG penetration level. The primary reason why the fleet wide CO_2 emissions penalty between Networks 1, 3 and 4 are quite similar is due to the similarity of the emissions factor of both categories of CFPPs at full load conditions. Given that the power system network for most countries are typically of Networks 1, 3 and 4, the fleet wide CO_2 emissions penalty seen in these cases are likely to be representative of what could be seen in reality. This means that having considered all those networks, the fleet wide CO_2 emissions penalty in the CO_2 predicted could potentially be the same if the network is not NRH-dominated.

The total daily fleet wide CO_2 emissions and the fleet wide CO_2 emissions penalty predicted for the four networks, and using dispatch methods B, C, and D are shown on Figure 9.17. The trends which were discussed in the previous paragraphs are also seen. However, the difference between fleet wide CO_2 emissions penalty of the four networks, when the dispatch method D is used is not so significant.

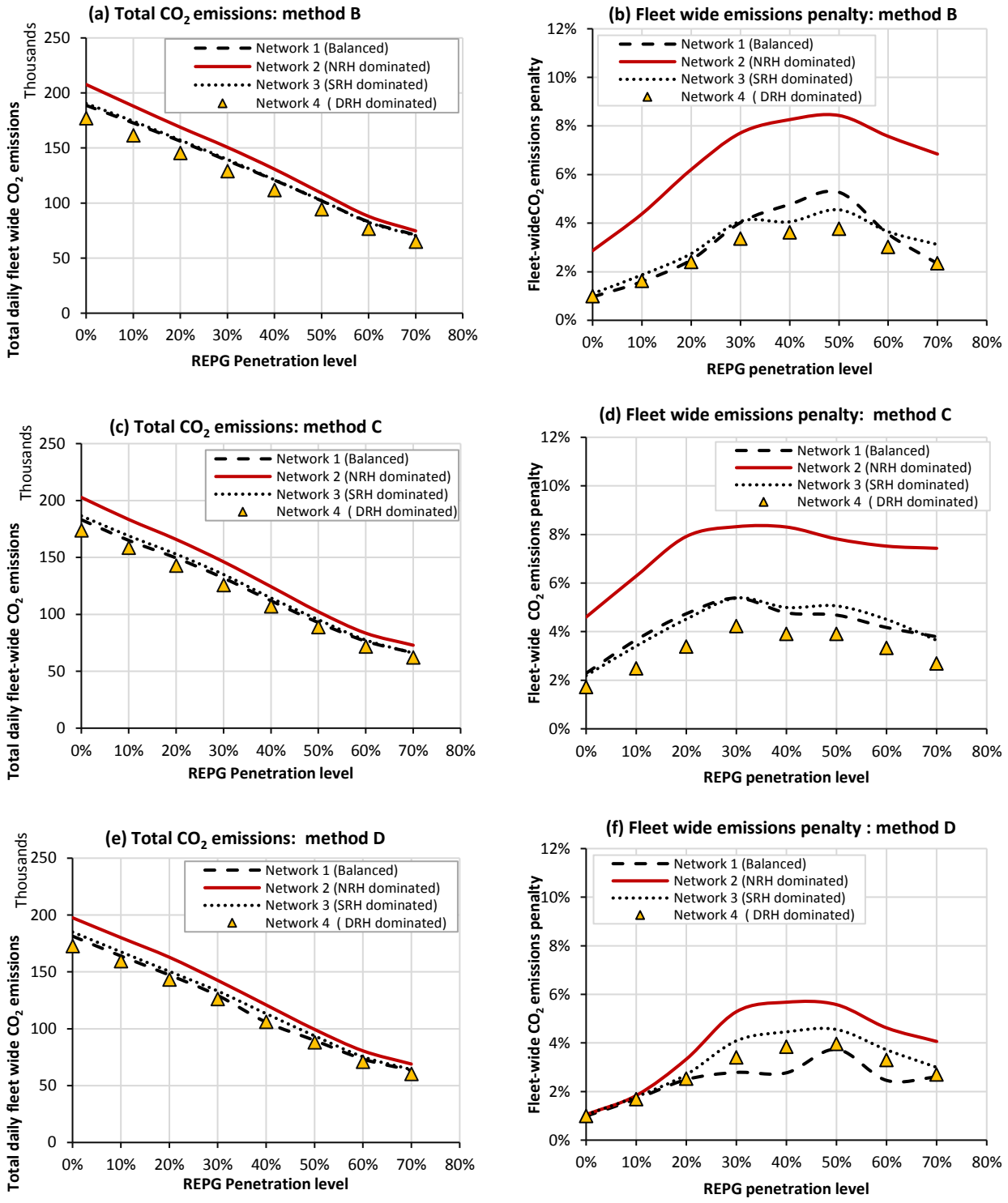

Figure 9.17 Fleet wide CO_2 emissions for dispatch methods B, C, & D: Impact of Network composition

9.6.7 Fleet wide CO_2 emissions: Impact of mix scenario

A sensitivity study was also carried out to check the impact of the REPG mix scenario on the fleet-wide CO_2 emissions. The total daily fleet-wide CO_2 emissions (see Figure 9.18) predicted from V-TCHR based emissions factor for all the four networks were approximately the same up to REPG penetration levels of 40%. From REPG penetration level of 50% and above, the total fleet-wide CO_2 emissions for the high solar REPG mix scenario is higher than the reference case, while the one for the high wind case is lower than the reference case.

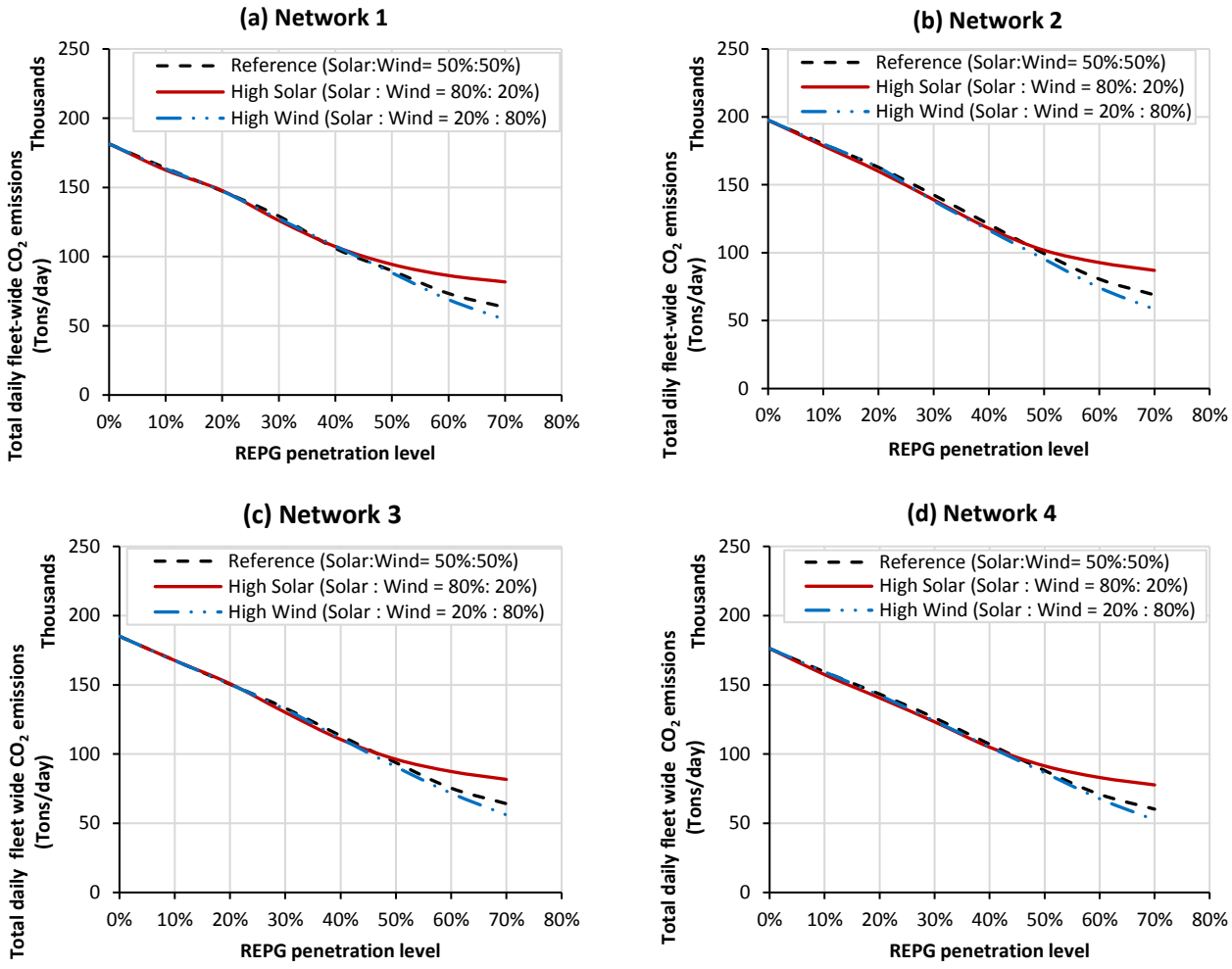

Figure 9.18 Fleet wide CO_2 emissions for different Networks: Impact of REPG mix scenario

The fleet-wide CO_2 emissions penalty for the different networks is shown in Figure 9.19. It can be seen that the magnitude of the fleet-wide CO_2 emissions penalty is dependent on the REPG mix

scenario. The penalty for the high solar scenario is smaller than the high wind scenario which is in turn smaller than the reference scenario.

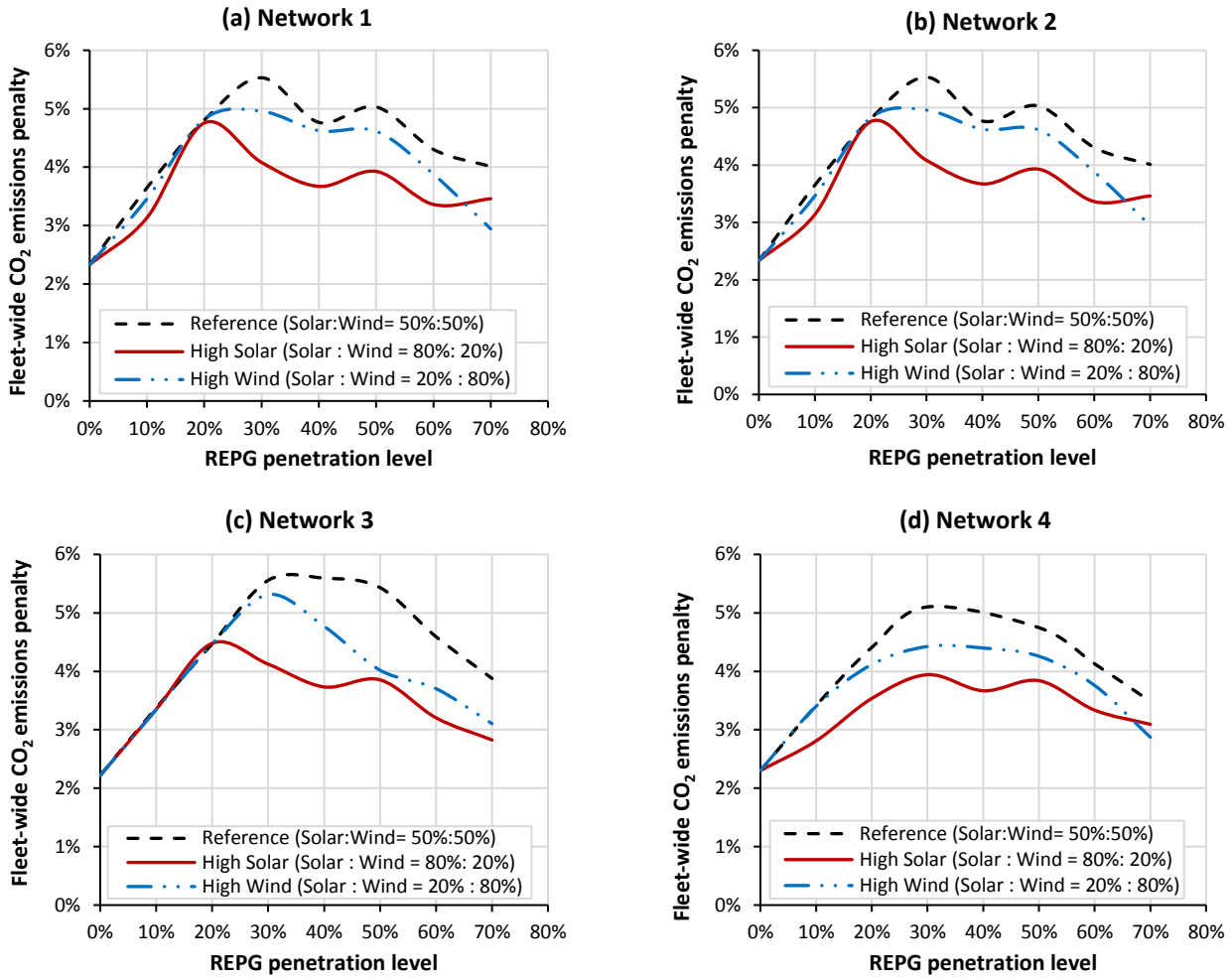

Figure 9.19 Fleet wide CO_2 emissions penalty for different networks: Impact of REPG mix scenario

9.6.8 Fleet wide CO_2 emissions: Impact of coal quality

A sensitivity study was also carried out to check the impact of the coal quality on the results. Figure 9.20 shows the total daily fleet-wide CO_2 emissions results for the sub-bituminous coal and the lignite coal, for Network 1 using dispatch method A. It can be seen that the total daily fleet-wide CO_2 emissions for the sub-bituminous coal is lower than the one for the lignite coal. This is expected because the lower heating value for the lignite coal means that more coal mass flow is required for

the same boiler heat input. The amount of CO_2 emitted at a given load level is primarily driven by the carbon content and the heating value of the fuel consumed. Even though the mass fraction of carbon in the sub-bituminous is higher than the one for the lignite fuel, the impact of the increased coal mass flow in the lignite case causes the predicted CO_2 emissions to be higher. This same trend is seen for cases studied in Networks 2, 3, and 4 (see Appendix D).

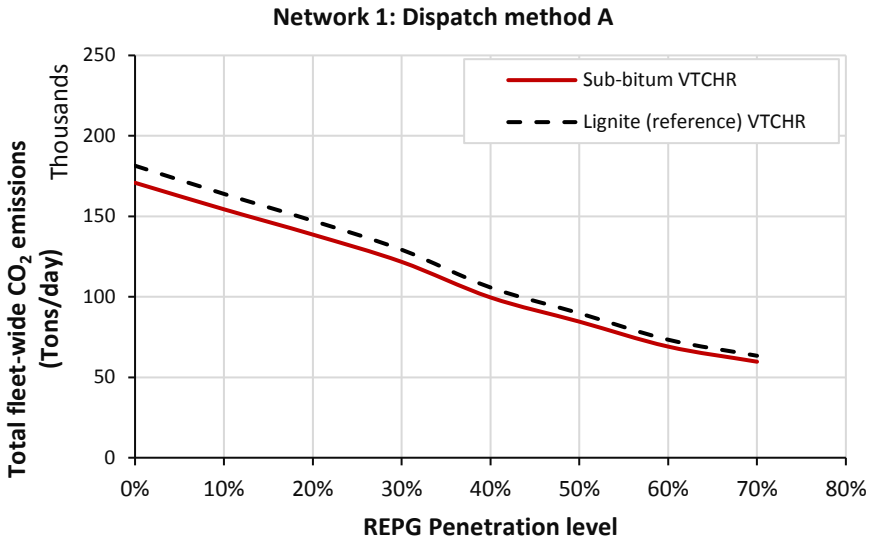

Figure 9.20 Fleet-wide CO_2 emissions: Impact of fuel quality

A comparison of the fleet-wide CO_2 emissions penalty predicted for both lignite and sub-bituminous coal is shown on Figure 9.21. It can be seen that the results for both type of fuel is similar. This suggests that although the fuel type affects the total CO_2 emissions predicted, however the fleet-wide CO_2 emissions penalty (% unaccounted CO_2 emissions) in the CO_2 emissions predicted is independent of the fuel type. This trend is depicted for Networks 2, 3, and 4 shown in Figure 9.22, Figure 9.23, and Figure 9.24 respectively.

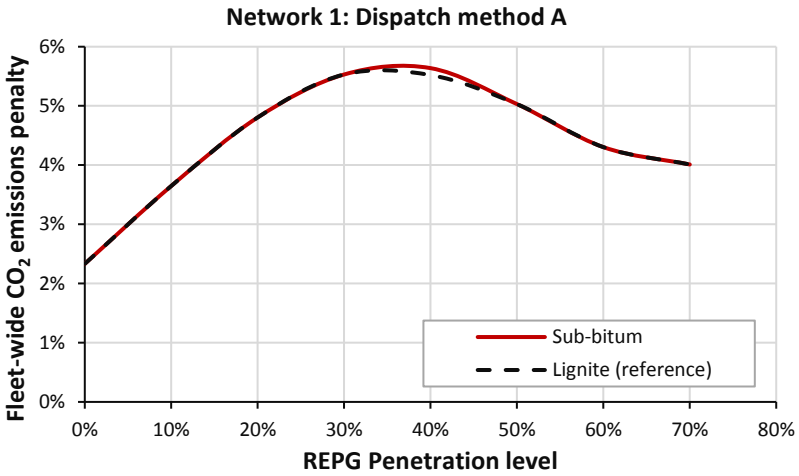

Figure 9.21 Fleet wide CO_2 emissions penalty for Network 1: Impact of coal quality

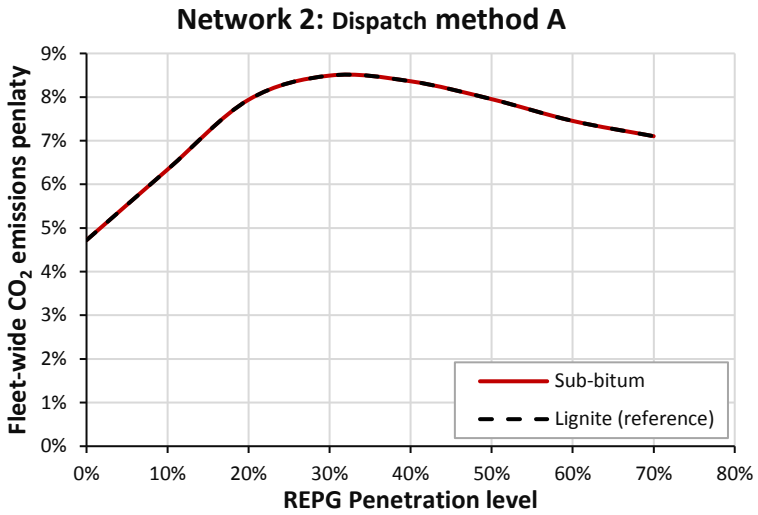

Figure 9.22 Fleet wide CO_2 emissions penalty for Network 21: Impact of coal quality

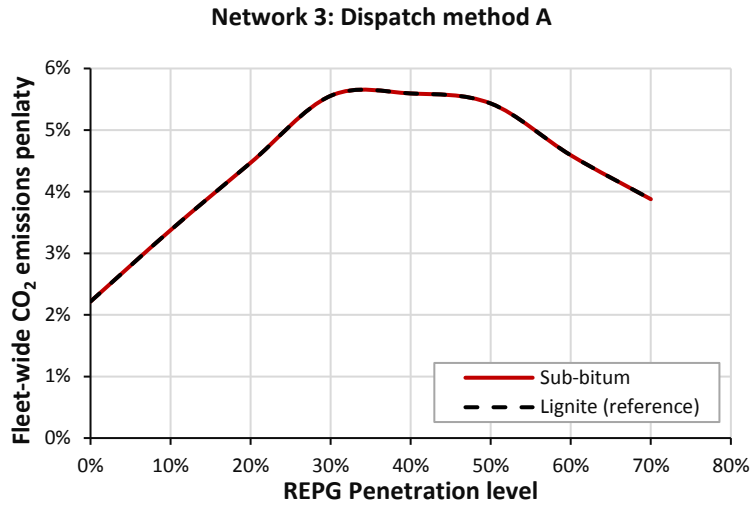

Figure 9.23 Fleet wide CO_2 emissions penalty for Network 3: Impact of coal quality

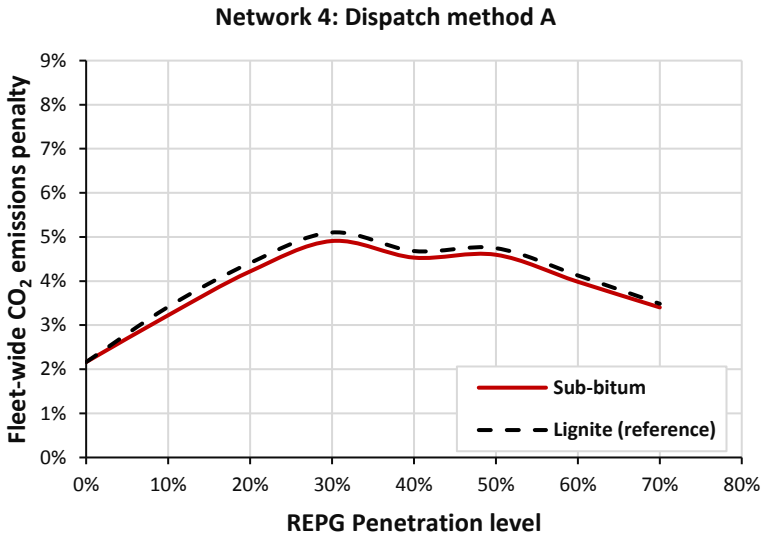

Figure 9.24 Fleet wide CO_2 emissions penalty for Network 4: Impact of coal quality

9.7 Conclusions of the chapter

The implementation of a V-TCHR based emissions factor in an energy mix demonstration study was presented in this chapter. The primary objective of this exercise was to demonstrate the impact of including a variable heat rate / emissions factor model on the CO_2 emissions reduction potential of grid connected REPG systems at various levels of REPG penetration.

The inclusion of a V-TCHR based emissions factor model shows that there are additional CO_2 emissions which is not captured if the conventional method of a constant emissions factor is used. This is due to the inability of the conventional method to adequately include the effect of heat rate deterioration with load for each individual CFPP that is on the power system network.

The inclusion of the V-TCHR model also shows that the fleet wide CO_2 emissions penalty predicted when the conventional method is used is dependent on:

- The amount of REPG penetration level within the system
- The varying load emissions characteristics (and thus varying load heat rate) of the individual CFPPs on the network.
- The contributions from each CFPP (based on the merit order of dispatch) on the network.

The fleet wide CO_2 emissions penalty for the power system networks investigated increased with the level of REPG. However, there is a turning point in which the fleet-wide CO_2 penalty begins to reduce until it reaches a quasi-stable value. This turning point appears to be dependent on the residual load profile of the power system network, but appears to be around 30-50%. The maximum penalty calculated for all the scenarios studied was 9%, while the average was about 4%. The typical Fleet wide CO_2 emissions penalty predicted for the different power system networks investigated shows:

- For SRH and DRH CFPP dominated networks: values ranging from 2-6% less than the V-TCHR predicted values were seen.
- For NRH CFPPs dominated networks: Values ranging from 5-9% less than the V-TCHR predicted values were seen.

The impact of four different dispatch methods on the CO_2 emissions was also investigated. The results suggests that using the dispatch Method A, which considers the least turbine cycle full load heat rate as the criteria for ranking the CFPP with the highest dispatch priority yields the least amount of daily fleet wide CO_2 emissions at all the REPG penetration levels considered. Dispatch Method C which considers the least $\mathfrak{R}$ value as the criteria for ranking the CFPP with the highest dispatch priority yields the next lowest amount of daily fleetwide emissions. Dispatch Method D which gives priority to the highest $\mathfrak{R}$ value results in the least emissions penalty, i.e. a constant heat rate model would not underestimate the emissions by a substantial amount as compared to the other methods. However, the total emissions for Method D is still larger than Method A.

Irrespective of the configuration of the power system network, there is always a fleet wide CO_2 emissions penalty that is predicted if a V-TCHR based emissions factormodel is not included in similar power networks. For accurate emissions predictions, it is therefore important to always include a V-TCHR based emissions factor model in the calculations.

10. Conclusions and Recommendations

10.1 Summary of the research conducted

The inclusion of a variable heat rate and emissions factor model for individual CFPPs in grid integrated REPG emissions impact studies can be a daunting task. This is because the evaluation of the thermal performance (heat rate and emissions) of each CFPP on the network must be known at various load conditions. For this to happen, a detailed knowledge of the thermodynamic steam cycle process conditions of the CFPPs at all the process points, and for every generation level, is required.

This PhD research sought to address the aforementioned problem by furthering the knowledge of the impact of varying/cycling load operation of various CFPPs architectures on its heat rate and subsequent emissions. In pursuant of this aim, six cardinal objectives were set out in section 1.4. Below is a summary of this research work in relation to the set objectives.

Objective (i): The impacts of grid integrated REPG systems on the heat rate and CO_2 emissions of CFPPs, and the research methodologies used to investigate these impacts were examined. Some of the key findings have been:

- There are several of conflicting results available in literature about the actual emissions that is “avoided” or “reduced” from CFPPs due to REPG grid integration. This is largely due to the emissions factor model that is applied to the unit commitment and economic/generation dispatch models, and the type of generators in the power system that is analysed.
- A coupling of the emissions factor model to the net unit heat rate model of CFPPs was suggested as a means of truly capturing the impact of cycling load operation on the emissions of CFPPs.

Objective (ii): The key factors that significantly affect the net unit heat rate (NUHR) of CFPPs at varying load conditions were highlighted in this research. The TCHR, boiler efficiency and the auxiliary consumption and generator efficiency are the four broad factors that were identified. The TCHR was identified as the most significant of all the effects at all load conditions, and for all CFPP architectures. The key factors that also impact the TCHR at varying load conditions were highlighted.

The understanding obtained provided a basis for the further investigation of the TCHR of various CFPPs at various load conditions.

Objective (iii): A set of generic procedures were developed in order to set up arbitrary but representative CFPP process models which can be used for investigating the impact of cyclic load operation on the turbine cycle heat rate. These procedures can be sub-divided into:

(a) A generic model for determining the final feed water temperature (FFWT) of different Coal fired power plants (CFPPs)
(b) A generic model for determining the steam extraction pressures of FWHs of different Coal fired power plants (CFPPs)
(c) The implementation and validation of a simple generic methodology for predicting the condensing pressure response of coal fired power plant main steam condensers at varying loads.
(d) Overall procedure for developing credible CFPP process models for non-reheat, single reheat and double reheat CFPPs, with knowledge of only a few input parameters.

The FFWT and extraction pressures for any pulverised CFPP operating at full load (design conditions) could be determined within reasonable accuracy limits by simply specifying the throttle temperature (for non-reheats), reheater inlet pressure (for reheats), condenser pressure, and the number of feed water heaters required. This model is based on a modification of an optimum cycle efficiency method (OCEM). The modification requires the determination of the FFWT before applying the equal partition of feed water temperature rise rule.

The condenser pressure response method is based on a constant condenser effectiveness assumption. At design and off-design inlet temperature conditions, the model appears to work within a reasonable accuracy limit, while the accuracy of the model is poor at extreme cooling inlet temperatures, and at very low loads. The accuracy of the model can be improved by including an adjustment coefficient for each cooling fluid inlet temperature. The adjustment coefficient can be determined with the knowledge of one other load point.

The overall procedure was validated at four different load conditions (40%, 60%, 80%, and 100% MCR), with data from 10 CFPPs. The absolute deviations of the model results predicted for most of the critical process parameters, and the TCHR were within 5%.

Objective (iv) was accomplished with the development and validation of a novel V-TCHR model. This model can be used for investigating the TCHR characteristics of any given CFPP at various steady state load conditions, irrespective of the CFPP design configurations. This model does not require a complete thermodynamic cycle model or performance evaluation of the CFPP. It is only dependent on the knowledge of: (a) The live steam enthalpy which is easy to determine from the live steam pressure and temperature at the inlet of the high pressure (HP) turbine; (b) the number of reheat stages; (c) the type of condensing cooling system; and (d) the boiler pressure mode of operation. The model was validated with data from 2 NRHs, and 7 SRHs, and the results obtained were within 3% accuracy for a vaste majority of the plants investigated. The model could still be applied to double reheat CFPPs because it uses the same part load loss models similar to the SRH CFPP.

Objective (v): The V-TCHR model provided the basis for investigating impact of cycling load operation on the CO_2 emissions factor and total CO_2 emissions of some model CFPPs. The key findings from this investigation were:

- The inclusion of the V-TCHR model shows that the magnitude of the CO_2 emissions not accounted for when the constant emissions factor model is used range from 0 - 14% , over the entire load range considered.
- The magnitude of the unaccounted CO_2 emissions is dependent on:
  - The plant load factor: The additional emissions increases with decrease in load factor.
  - The number of reheat stages : The impact of not considering a variable heat rate model is most significant for the non-reheat CFPPs, which not only generally have the worst heat rates at full load conditions, but they also experience the greatest amount of heat rate deterioration with load.

The Implementation of the novel V-TCHR model in an energy mix demonstration study was also carried out. This was done to investigate: (a) the impact of including a variable heat rate model and emissions factor model on the fleet-wide CO_2 emissions reduction potentials of grid integrated REPGs systems; and (b) investigate a suitable method for selecting the CFPPs that should be operated at reduced loads for improved fleet-wide CO_2 emissions reduction in support of **Objective (vi)**. The key findings were as follows:

- The inclusion of a V-TCHR model shows that there is an additional CO_2 emissions which is not captured if the conventional method is used.
- The inclusion of the V-TCHR model also shows that the fleet-wide CO_2 penalty emissions predicted when the conventional method is used is dependent on:

  - The amount of REPG penetration level within the system
  - The varying load emissions characteristics (and thus varying load heat rate) of the individual CFPPs on the network.
  - The contributions from each CFPP (based on the merit order of dispatch) on the network.
- Using the dispatch Method A, which considers the least turbine cycle full load heat rate as the criteria for ranking the CFPP with the highest dispatch priority yields the least amount of daily fleet wide CO_2 emissions at all the REPG penetration levels considered. Dispatch Method C which considers the least $\mathfrak{R}$ value as the criteria for ranking the CFPP with the highest dispatch priority yields the next lowest amount of daily fleetwide emissions. Dispatch Method D which gives priority to the highest $\mathfrak{R}$ value results in the least emissions penalty, i.e. a constant heat rate model would not underestimate the emissions by a substantial amount as compared to the other methods. However, the total emissions for Method D is still larger than Method A.

10.2 Recommendations for further study

Research in this field is not complete, and some further study considerations are:

- Energy Mix modellers that adopt optimal Unit commitment model (UCM) and Generation dispatch model (GDM) approaches are encouraged to include the variable heat rate response of CFPPs for specific plants, while undertaking the emissions impact of including REPG systems at various penetration levels.
- A proper understanding of NOx formation mechanism at varying load conditions is required for the V-TCHR to be used alongside for its emissions prediction. This could be further extended to include the performance of emissions reduction technology at varying load.
- The study could be extended for dynamic load variations, where the ramp rates and other dynamic constraints are considered.
- A generic method for evaluating the start up emissions from Coal Fired Power Plants can also be done.

10.3 Concluding remarks

This PhD dissertation brings two things to the energy mix modelling and renewable integration impacts studies. Firstly, the possibility for the inclusion of a variable heat rate model with little effort. Secondly, it gives one the added information of knowing the CFPPs that have the least CO_2 emissions penalty at low and part load operations. These are the type of CFPPs that should be cycled more frequently, for an improved fleet-wide CO_2 emissions reduction.

For the broader CFPP modelling research fraternity, the methods developed to create a representative CPFF process model with limited input can be useful for various other studies. This is because most process studies require a consistent heat balance diagram as primary input, which can often be hard to obtain. The proposed methods overcomes this problem.

The outcomes of this research can be a useful tool in:

- Providing guidance on improved control strategies for gaseous emissions control systems and heat rate improvement strategies of CFPPs operating at various cyclic load conditions such as part load and low load conditions.
- Influencing policy regarding existing and near future coal power plant operations.
- Developing emissions models used for energy mix optimization modelling.
- Determining heat rate degradation related cost used for production cost simulation during transient operations of CFPPs.
- Identifying the CFPPs that are potentially less polluting at low loads, or would have a better marginal CO_2 reduction benefit at low loads.

Finally, this study is potentially useful to countries such as China, India, Australia, Indonesia, South Africa, and Poland which are still heavily dependent on the use of coal to supply baseload electricity, and plan to deploy grid connected REPG systems on a large scale in future.

11. List of References

[1] LX Innovations, “Intelligence Embedded Power Grids,” *PRLOG Press Release Distribution*, 2011. [Online]. Available: https://www.prlog.org/11243229-intelligence-embedded-power-grids.html. [Accessed: 24-Jan-2019].

[2] S. Giglmayr, A. C. Brent, P. Gauché, and H. Fechner, “Utility-scale PV power and energy supply outlook for South Africa in 2015,” *Renew. Energy*, vol. 83, pp. 779–785, 2015.

[3] K. B. Porate, K. L. Thakre, and G. L. Bodhe, “Impact of wind power on generation economy and emission from coal based thermal power plant,” *Int. J. Electr. Power Energy Syst.*, vol. 44, no. 1, pp. 889–896, 2013.

[4] N. Chakraborty *et al.*, “Measurement of CO2, CO, SO2, and NO emissions from coal-based thermal power plants in India,” *Atmos. Environ.*, vol. 42, no. 5, pp. 1073–1082, 2008.

[5] A. Pegels, “Renewable energy in South Africa: Potentials, barriers and options for support,” *Energy Policy*, vol. 38, no. 9, pp. 4945–4954, 2010.

[6] M. Ozcan, “Estimation of Turkey×s GHG emissions from electricity generation by fuel types,” *Renew. Sustain. Energy Rev.*, vol. 53, pp. 832–840, 2016.

[7] I. A. Urzúa, J. C. Olmedo, and E. E. Sauma, “Impact of intermittent non-conventional renewable generation in the costs of the Chilean main power system,” *Renew. Sustain. Energy Rev.*, vol. 60, pp. 810–821, 2016.

[8] J. Qin and E. Hu, “Technical assessment of a renewable aided power plant for different operational load,” *Energy Procedia*, vol. 61, pp. 1505–1510, 2014.

[9] Y. Zhu, R. Zhai, M. Zhao, and Y. Yang, “Analysis of solar contribution evaluation method in solar aided coal-fired power plants,” in *Energy Procedia*, 2014, vol. 61, pp. 1610–1613.

[10] D. Lew *et al.*, “The Western Wind and Solar Integration Study Phase 2,” 2013.

[11] N. Kumar, P. Besuner, S. Lefton, D. Agan, and D. Hilleman, “Power Plant Cycling Costs,” *NREL Tech. Rep.*, no. July, pp. 1–46, 2012.

[12] N. E. T. L. (NETL), “Impact of Load Following on Power Plant Cost and Performance : Literature

Review and Industry Interviews," 2012.

[13] Electric Power Research Institute (EPRI), "Low Load / Low Air Flow Optimum Control Applications," *EPRI*, p. TR-111541, 1998.

[14] Environmental Protection Agency (EPA), "Emission Factors (AP-42)." pp. 1–10, 1990.

[15] E. Corporation, "Eastern Wind Integration and Transmission Study," *NREL Tech. Rep.*, no. NREL/SR-5500-47078, pp. 1–241, 2011.

[16] S. Nazari, O. Shahhoseini, A. Sohrabi-Kashani, S. Davari, R. Paydar, and Z. Delavar-Moghadam, "Experimental determination and analysis of CO2, SO2 and NOx emission factors in Iran's thermal power plants," *Energy*, vol. 35, no. 7, pp. 2992–2998, 2010.

[17] R. Turconi, C. O'Dwyer, D. Flynn, and T. Astrup, "Emissions from cycling of thermal power plants in electricity systems with high penetration of wind power: Life cycle assessment for Ireland," *Appl. Energy*, vol. 131, pp. 1–8, 2014.

[18] V. I. Kouprianov and W. Kaewboonsong, "Assessment of Annual rate of gaseous pollutants from variable load fuel oil fired boiler," in *Proceedings of the Third Asia-Pasific Conference on Sustainable Energy and Environmental Technologies*, 2001, pp. 503–507.

[19] ABB Energy Efficiency, *Power Generation Energy Efficient Design of Auxiliary Systems in Fossil-Fuel Power Plants*. Zurich: ABB, 2009.

[20] D. Lew and G. Brinkman, "Western Wind and Solar Integration Study Phase 2: Executive Summary," *Nrel*, 2013.

[21] D. Lew, G. Brinkman, N. Kumar, P. Besuner, D. Agan, and S. Lefton, "Impacts of Wind and Solar on Fossil-Fueled Generators," *Proc. IEEE PES Gen. Meet. 2012*, no. August, pp. 1–10, 2012.

[22] G. Brinkman, D. Lew, and P. Denholm, "Impacts of renewable generation on fossil-fuel unit cycling: Costs and emissions," in *Clean Energy Regulatory Forum: Prelimnary Background Paper*, 2012, pp. 1–42.

[23] US Energy Information Admininstration, *International Energy Outlook 2016*, vol. 0484, no. May. 2016.

[24] World Energy Council, "World Energy Resources Coal," 2016.

[25] G. Xu, L. Zhou, S. Zhao, F. Liang, C. Xu, and Y. Yang, "Optimum superheat utilization of

extraction steam in double reheat ultra-supercritical power plants," *Appl. Energy*, vol. 160, pp. 863–872, 2015.

[26] Y. Li, L. Zhou, G. Xu, Y. Fang, S. Zhao, and Y. Yang, "Thermodynamic analysis and optimization of a double reheat system in an ultra-supercritical power plant," *Energy*, vol. 74, pp. 202–214, 2014.

[27] P. K. Nag, *Power Plant Engineering*, Third Edit. New Delhi: McGraw Hill, 2008.

[28] M. Wiatros-Motyka, *An overview of HELE technology deployment in the coal power plant fleets of China, EU, Japan and USA*, no. December. London: IEA Clean Coal Centre, 2016.

[29] J. Wang, J. D. Wojcik, and Y. Xue, "Study of Supercritical Coal Fired Power Plant Dynamic Responses and Control for Grid Code Compliance," in *Mathematical Modelling and Simulation of Power Plants and CO2 Capture Workshop*, 2012, no. March, p. 2014.

[30] P. K. Nag, "Introduction: Economics of Power Generation," in *Power Plant Engineering*, New Delhi: Tata McGraw-Hill Publishing Company limited, 2008, pp. 1–40.

[31] S. J. Mills, *Integrating intermittent renewable energy technologies with coal-fired power plant*. iEA Clean Coal Centre, 2011.

[32] E. Ela, M. Milligan, and B. Kirby, "Operating Reserves and Variable Generation," *NREL Tech. Rep.*, no. NREL/TP-5500-51978, pp. 1–92, 2011.

[33] Electrical Power Research Institute (EPRI), "Electric Power System Flexibility: Challenges and Opportunities," *Tech. Rep.*, pp. 1–43, 2016.

[34] P. Keatley, A. Shibli, and N. J. Hewitt, "Estimating power plant start costs in cyclic operation," *Appl. Energy*, vol. 111, pp. 550–557, 2013.

[35] Colin Henderson, "Increasing the flexibility of coal fired power plants," 2014.

[36] R. Fernando *et al.*, *Non-baseload operation of coal-fired power plant*. London: iEA Clean Coal Research, 2000.

[37] P. Keatley, *Cost modelling of coal power plant start-up in cyclical operation*. Elsevier, 2014.

[38] Electric Power Research Institute (EPRI), "Impact of Minimum Load Operation on Steam Turbines," *EPRI Tech. Rep.*, no. 3002001263, pp. 1.1-8.8, 2013.

[39] Electrical Power Research Institute (EPRI), “Determining the Cost of Cycling and Varied Load Operations : Methodology,” *EPRI Tech. Rep.*, no. 1004412, pp. 1.1-7.8, 2002.

[40] J. Cochran, D. Lew, and N. Kumar, “Flexible Coal: Evolution from Baseload to Peaking Plant,” *NREL Rep.*, pp. 1–10, 2013.

[41] Electric Power Research Institute (EPRI), “Cycling of Fossil-Fueled Power Plants Volume 6 : Evaluation and Strategy,” *EPRI Tech. Rep.*, no. GS-7219, 1993.

[42] A. Nakumuryango and R. Inglesi-Lotz, “South Africa’s performance on renewable energy and its relative position against the OECD countries and the rest of Africa,” *Renew. Sustain. Energy Rev.*, vol. 56, pp. 999–1007, 2016.

[43] T. Bischof-Niemz, “Financial benefits of renewables in South Africa in 2014,” in *Round Table on Energy Choice*, 2015, no. January.

[44] K. Van Den Bergh, E. Delarue, and W. D’Haeseleer, “The impact of renewable injections on cycling of conventional power plants,” *Int. Conf. Eur. Energy Mark. EEM*, 2013.

[45] J. Lindsay and K. Dragoon, “Summary Report on Coal Plant Dynamic Performance Capability.” Unpublished, pp. 1–17, 2010.

[46] C. Hitaj, “Location matters: The impact of renewable power on transmission congestion and emissions,” *Energy Policy*, vol. 86, pp. 1–16, 2015.

[47] P. Eser, A. Singh, N. Chokani, and R. S. Abhari, “Effect of increased renewables generation on operation of thermal power plants,” *Appl. Energy*, vol. 164, pp. 723–732, 2016.

[48] B. Tarroja, F. Mueller, J. D. Eichman, and S. Samuelsen, “Metrics for evaluating the impacts of intermittent renewable generation on utility load-balancing,” *Energy*, vol. 42, no. 1, pp. 546–562, 2012.

[49] R. Gross, P. Heptonstall, M. Leach, J. Skea, D. Anderson, and T. Green, “The UK energy research centre review of the costs and impacts of intermittency,” in *Renewable Electricity and the Grid: The Challenge of Variability*, vol. 9781849772, G. Boyle, Ed. Taylor and Francis, 2012, pp. 73–94.

[50] A. S. Brouwer, M. van den Broek, W. Zappa, W. C. Turkenburg, and A. Faaij, “Least-cost options for integrating intermittent renewables in low-carbon power systems,” *Appl. Energy*,

vol. 161, pp. 48–74, 2016.

[51] P. Schierhorn, T. Brown, and E. Tröster, “Cycling Requirements for Conventional Power Plants at High Shares of Renewable Energy,” *13th Wind Integration Workshop*. 2012.

[52] F. Starr, “Flexibility of fossil fuel plant in a renewable energy scenario: Possible implications for the UK,” in *Renewable Electricity and the Grid: The Challenge of Variability*, vol. 9781849772, G. Boyle, Ed. Taylor and Francis, 2012, pp. 121–142.

[53] V. Roeder and A. Kather, “Part load behaviour of power plants with a retrofitted post-combustion CO2 capture process,” in *Energy Procedia*, 2013, vol. 51, pp. 207–216.

[54] A. Benato, S. Bracco, A. Stoppato, and A. Mirandola, “LTE: A procedure to predict power plants dynamic behaviour and components lifetime reduction during transient operation,” *Appl. Energy*, vol. 162, pp. 880–891, 2016.

[55] H. Shaker, H. Zareipour, and D. Wood, “Impacts of large-scale wind and solar power integration on California’s net electrical load,” *Renew. Sustain. Energy Rev.*, vol. 58, pp. 761–774, 2016.

[56] C. Ziems and H. Weber, “Integration of large-scale renewable energy sources: Challenges to thermal generation in Germany BT - 18th IFAC World Congress, August 28, 2011 - September 2, 2011,” in *18th IFAC World Congress*, 2011, vol. 18, no. PART 1, pp. 12845–12851.

[57] P. Niemczyk, “Model-based fuel flow control for fossil-fired power plants,” Aalborg University, 2010.

[58] A. Benato, A. Stoppato, and A. Mirandola, “Dynamic behaviour analysis of a three pressure level heat recovery steam generator during transient operation,” *Energy*, vol. 90, pp. 1595–1605, 2015.

[59] D. A. Halamay, T. K. A. Brekken, A. Simmons, and S. McArthur, “Reserve requirement impacts of large-scale integration of wind, solar, and ocean wave power generation,” *IEEE Trans. Sustain. Energy*, vol. 2, no. 3, pp. 321–328, 2011.

[60] Bentek Energy, “How Less Became More... Wind , Power and Unintended Consequences in the Colorado Energy Market,” Evergreen, Colorado, 2010.

[61] M. Milligan and N. R. Energy, “Costs of Integration for Wind and and Solar Energy : Large-

scale studies and implications." NREL, 2011.

[62] T. Niamh, "Generator Cycling due to High Penetrations of Wind Power," no. August, p. 188, 2011.

[63] APTECH & XcelEnergy, "Integrating Wind : Cost of cycling Analysis for Harrington Station Unit 3 Phase 1: Top-Down Analysis."

[64] S. Babrowski, P. Jochem, and W. Fichtner, "How to model the cycling ability of thermal units in power systems," *Energy*, vol. 103, pp. 397–409, 2016.

[65] W.-P. Schill, "On Start-up Costs of Thermal Power Plants in Markets with Increasing Shares of Fluctuating Renewables," *Dtsch. Inst. für Wirtschaftsforsch.*, 2016.

[66] N. Kumar, P. Besuner, S. Lefton, D. Agan, and D. Hilleman, "Power Plant Cycling Costs," no. July, 2012.

[67] L. Dale, D. Milborrow, R. Slark, and G. Strbac, "Quantifying the system cost of additional renewables in 2020," *Energy Policy*, no. 17, pp. 1949–1956, 2004.

[68] National Energy Technology Laboratory, "Impact of Load Following on Power Plant Cost and Performance : Literature Review and Industry Interviews," p. 49, 2012.

[69] U.S. Energy Information Administration (EIA), "Analysis of Heat Rate Improvement Potential at Coal- Fired Power Plants," Washington, 2015.

[70] Electric Power Research Institute (EPRI), "Condenser Performance Improvement : Evaluating Measurements," *EPRI Tech. Rep.*, no. 3002003455, 2014.

[71] Electric Power Research Institute (EPRI), "Effects of Flexible Operation on Turbines and Generators," *EPRI Tech. Rep.*, no. 1008351, pp. 1.1-8.3, 2004.

[72] Daedalus Associates, "Cycling of Fossil-Fueled of Fossil-Fueled : Evaluation and Strategy," California, 1993.

[73] S. Aliakbari, M. Ayati, J. H. S. Osman, and Y. Md Sam, "Second-order sliding mode fault-tolerant control of heat recovery steam generator boiler in combined cycle power plants," *Appl. Therm. Eng.*, vol. 50, no. 1, pp. 1326–1338, 2013.

[74] CleaverBrooks, "Boiler Efficirncy Guide: facts about firetube boilers and boiler efficiency," *Boiler efficiency guiide*. Thomasville,GA, pp. 1–22, 2010.

[75] American Society of Mechanical Engineers (ASME), *ASME PTC 4: Fired Steam Generators Performance Test Codes*, vol. 2008. USA: ASME, 2009.

[76] D. Eoff, "Understanding Fuel Savings in the boiler room," *ASHRAE J.*, no. December, pp. 38–43, 2008.

[77] C. Henderson, *Improving efficiencies of coal-fired power plants in developing countries*, no. CCC/70. London: IEA Clean Coal Centre, 2003.

[78] M. S. Bhatt and R. P. Mandi, "Performance Enhancement in Coal-fired Thermal Power Plants . Part III : Auxillary Power," *Int. J. Energy Res.*, vol. 804, no. October 1998, pp. 779–804, 1999.

[79] R. P. Mandi and U. R. Yaragatti, "Energy audit of auxiliary power in a coal fired thermal power energy audit of auxiliary power in a coal fired," in *Technological Advances for New Power Generating Units and for Performance Enhancement of Present Plants*, 2010, no. November, pp. II-1-II–11.

[80] Steag Energy, "Auxiliary Power measurement, optiization and analysis," 2013. [Online]. Available: https://www.eecpowerindia.com/codelibrary/ckeditor/ckfinder/userfiles/files/APC-EEC workshop.pdf. [Accessed: 07-May-2019].

[81] Steag Energy, "Auxillary Power Measurement, Optimization & Analysis," 2013. [Online]. Available: https://www.eecpowerindia.com/codelibrary/ckeditor/ckfinder/userfiles/files/APC-EEC workshop.pdf. [Accessed: 17-Oct-2018].

[82] Evonik Energy Services India (EESI), "Mapping of 85 pulverized coal fired therml power generating units in different states," India, 2007.

[83] I. Boldea, "Electric Energy and Electric Generators," in *The electric generators handbook : Volume I-Synchronous generators*, Taylor and Francis, 2006, pp. 1–13.

[84] K. D. A.J. Pansini and Smalling., "Generators," in *Guide to electric power generation*, 2nd ed., lilburn: Fairmont Press., 2002, p. 27.

[85] R. C. Spencer, K. C. Cotton, and C. N. Cannon, "A Method for Predicting Performance of Steam Turbine Generators 16500 KW and Larger," in *ASME Conference*, 1974, no. 249–298, pp. 1–

62.

[86] A. K. Olaleye, M. Wang, and G. Kelsall, “Steady state simulation and exergy analysis of supercritical coal-fired power plant with CO2capture,” *Fuel*, vol. 151, pp. 57–72, 2015.

[87] D. P. Hanak, C. Biliyok, and V. Manovic, “Evaluation and modeling of part-load performance of coal-fired power plant with postcombustion CO<inf>2</inf> capture,” *Energy and Fuels*, vol. 29, no. 6, pp. 3833–3844, 2015.

[88] Electric Power Research Institute (EPRI), “Cycling and Load-Following Effects on Heat Rate,” Palo Alto, CA, 2011.

[89] P. U. Akpan and W. Fuls, “Understanding heat rate and emissions of coal fired plants operating due to renewable energy power generation induced cycling,” in *Sustainable Development of South Africa’s Energy Sources Conference proceedings*, 2017, pp. 64–66.

[90] P. K. Prasad, P. and Rao, “Heat Rate-The Pulse Rate of Power Plants,” *Linkeldin Slideshare*, 2013. [Online]. Available: https://www.slideshare.net/porhalakrao/heat-rate-pulse-rate-of-power-plant. [Accessed: 17-Sep-2018].

[91] A. Poullikkas, “Heat rate curve approximation for power plants without data measuring devices,” *Int. J. Energy Environ.*, vol. 3, no. 5, pp. 651–658, 2011.

[92] F. Gutiérrez-Martín, R. A. Da Silva-Álvarez, and P. Montoro-Pintado, “Effects of wind intermittency on reduction of CO2 emissions: The case of the Spanish power system,” *Energy*, vol. 61, pp. 108–117, 2013.

[93] S. Lefton, “Power Plant Asset Management: Cost Analysis and Cost-Based Power Plant Asset Management – Thermal Power Plant Cycling Costs,” *Intertek APTECH*. pp. 1–57.

[94] International Energy Agency, “Generation from Coal Generation from Coal: Measuring and Reporting Efficiency Performance and CO2 Emissions,” *IEA Publ.*, pp. 1–111, 2010.

[95] J. Cullen, “Measuring the Environmental Benefits of Wind-Generated Electricity,” *Am. Econ. J. Econ. Policy*, vol. 5, no. 4, pp. 107–133, 2013.

[96] D. Kanary and L. Smith, “EPRI 1990 report Effects of Boiler Cycling on NOx Emissions,” in *Proceedings: 1990 Fossil plant cycling conference proceedings*, 1991, pp. 26.1-26.17.

[97] L. L. Sloss, *Continuous emissions mo itoring for coal-fired power stations*. London, UK.: IEA

Clean Coal Centre, 1997.

[98] L. Valentino, V. Valenzuela, A. Botterud, Z. Zhou, and G. Conzelmann, "System-wide emissions implications of increased wind power penetration," *Environ. Sci. Technol.*, vol. 46, no. 7, pp. 4200–4206, 2012.

[99] Acurex Environ. Corp., Edward Aul & Assoc., and E. H. Pechan and Assoc., "Emission factor documentation for AP-42 Section 1.1: Bituminous and Subbituminous coal combustion," North Carolina, 1993.

[100] E. A. & Assoc. and E. H. P. and Assoc., "Emission factor documentation for AP-42 section 1.2: Anthracite coal combustion," North Carolina, 1993.

[101] E. H. Pechan and Assoc., Edward Aul & Assoc., and E. H. Pechan and Assoc., "Emission factor documentation for AP-42 section 1.7: lignite combustion," North Carolina, 1993.

[102] M. Wierzbowski, W. Lyzwa, and I. Musial, "MILP model for long-term energy mix planning with consideration of power system reserves," *Appl. Energy*, vol. 169, pp. 93–111, 2016.

[103] D. L. Oates and P. Jaramillo, "Production cost and air emissions impacts of coal cycling in power systems with large-scale wind penetration," *Environ. Res. Lett.*, vol. 8, no. 2, 2013.

[104] M. A. Gonzalez-salazar, T. Kirsten, and L. Prchlik, "Review of the operational flexibility and emissions of gas- and coal- fired power plants in a future with growing renewables," *Renew. Sustain. Energy Rev.*, vol. 82, no. July 2017, pp. 1497–1513, 2018.

[105] L. L. Sloss, *Levelling the intermittency of renewables with coal*, no. CCC/268. London, UK.: IEA Clean Coal Centre, 2016.

[106] W. Katzenstein and J. Apt, "Air emissions due to wind and solar power," *Environ. Sci. Technol.*, vol. 43, no. 2, pp. 253–258, 2009.

[107] K. Novan, "Valuing the Wind : Renewable Energy Policies and Air Pollution Avoided," *Am. Econ. J. Econ. Policy*, vol. 7, no. 3, pp. 291–326, 2014.

[108] M. Jaforullah and A. King, "Does the use of renewable energy sources mitigate CO2emissions? A reassessment of the US evidence," *Energy Econ.*, vol. 49, pp. 711–717, 2015.

[109] H. Hou, J. Wu, Y. Yang, E. Hu, and S. Chen, "Performance of a solar aided power plant in fuel saving mode," *Appl. Energy*, vol. 160, pp. 873–881, 2014.

[110] Y. Lin, J. X. Johnson, and J. L. Mathieu, “Emissions impacts of using energy storage for power system reserves,” *Appl. Energy*, vol. 168, no. 784, pp. 444–456, 2016.

[111] S. Pfenninger, A. Hawkes, and J. Keirstead, “Energy systems modeling for twenty- fi rst century energy challenges,” *Renew. Sustain. Energy Rev.*, vol. 33, pp. 74–86, 2014.

[112] N. Troy, E. Denny, and M. O’Malley, “Base-load cycling on a system with significant wind penetration,” *IEEE Trans. Power Syst.*, vol. 25, no. 2, pp. 1088–1097, 2010.

[113] J. P. Deane, G. Drayton, and B. P. Ó Gallachóir, “The impact of sub-hourly modelling in power systems with significant levels of renewable generation,” *Appl. Energy*, vol. 113, pp. 152–158, 2014.

[114] H. Holttinen *et al.*, “Impacts of large amounts of wind power on design and operation of power systems , results of IEA collaboration,” in *8th International Workshop on Large-Scale Integration of Wind Power into Power Systems as well as on Transmission Networks of Offshore Wind Farms*, 2009.

[115] N. Vardar and Z. Yumurtaci, “Emissions estimation for lignite-fired power plants in Turkey,” *Energy Policy*, vol. 38, no. 1, pp. 243–252, 2010.

[116] M. Jaforullah and A. King, “Does the use of renewable energy sources mitigate CO2 emissions? A reassessment of the US evidence,” *Energy Econ.*, vol. 49, pp. 711–717, 2015.

[117] D. Lew, G. Brinkman, N. Kumar, P. Besuner, D. Agan, and S. Lefton, “Impacts of wind and solar on emissions and wear and tear of fossil-fueled generators,” *IEEE Power Energy Soc. Gen. Meet.*, pp. 1–8, 2012.

[118] NREL, “The Western Wind and Solar Integration Study Phase 2,” 2013.

[119] K. Hawkins, “Wind Integration: Incremental Emissions from Back-Up Generation Cycling (Part V: Calculator Update),” 2010. [Online]. Available: https://www.masterresource.org/wind-power/wind-integration-incremental-emissions-from-back-up-generation-cycling-part-v-calculator-update/. [Accessed: 07-May-2016].

[120] D. P. Hanak, C. Biliyok, and V. Manovic, “Evaluation and Modeling of Part-Load Performance of Coal-Fired Power Plant with Postcombustion CO2 Capture,” *Energy and Fuels*, vol. 29, no. 6, pp. 3833–3844, 2015.

[121] General Physics Corporation, “EtaPRO VirtualPlant User Guide.” Amherst , New York, pp. 1–107, 2011.

[122] Electric Power Research Institute (EPRI), “Turbine Cycle Heat Rate Monitoring : Technology and Application,” Palo Alto, USA, 2006.

[123] MTech Industrial, “Flownex Simulation Environment.” South Africa.

[124] V. Roeder, C. Hasenbein, and A. Kather, “Evaluation and comparison of the part load behaviour of the CO2 capture technologies oxyfuel and post-combustion,” *Energy Procedia*, vol. 37, pp. 2420–2431, 2013.

[125] E. Oko and M. Wang, “Dynamic modelling, validation and analysis of coal-fired subcritical power plant,” *Fuel*, vol. 135, pp. 292–300, 2014.

[126] T. Barszcz and P. Czop, “Presentation of a virtual power plant environment and its application with combined first-principle and data-driven models intended for the diagnostics of a power plant – Part 1,” *Simul. Trans. Soc. Model. Simul. Int.*, vol. 0, no. 00, pp. 1–28, 2011.

[127] T. Barszcz and P. Czop, “Presentation of a virtual power plant environment and its application with combined first-principle and data-driven models intended for the diagnostics of a power plant – Part 2,” *Simulation*, vol. 88, no. 2, pp. 167–179, 2012.

[128] O. R. I. Mohamed, “Study of Energy Efficient Supercritical Coal-Fired Power Plant Dynamic Responses and Control Strategies,” University of Birmingham, 2012.

[129] K. Goto, K. Yogo, and T. Higashii, “A review of efficiency penalty in a coal-fired power plant with post-combustion CO2capture,” *Appl. Energy*, vol. 111, pp. 710–720, 2013.

[130] M. Ataei, R. A. Hooshmand, and S. G. Samani, “A coordinated MIMO control design for a power plant using improved sliding mode controller,” *ISA Trans.*, vol. 53, no. 2, pp. 415–422, 2014.

[131] Electrical Power Research Institute (EPRI), “Correlating Cycle Duty With Cost at Fossil Fuel Power Plants,” *EPRI Tech. Rep.*, no. 1004010, pp. 1.1-7.1, 2001.

[132] D. White, “Reduction in Carbon Dioxide Emissions: Estimating the Potential Contribution From Wind-Power,” *Renew. Energy Found.*, no. December, pp. 1–38, 2004.

[133] P. Rousseau and W. Fuls, “Power plant cycle analysis,” in *Power Plant Systems Analysis*, Cape

Town: University of Cape Town, 2017, pp. 160–202.

[134] S. S. Daood, G. Ord, T. Wilkinson, and W. Nimmo, "Fuel additive technology - NOx reduction, combustion efficiency and fly ash improvement for coal fired power stations," *Fuel*, vol. 134, no. 1308472, pp. 293–306, 2014.

[135] S. Kakac, *Boilers, Evaporators & Condensers*. John Wiley & Sons, Inc, 1991.

[136] P. Basu, C. Kefa, and L. Jestin, *Boilers and Burners: Design and Theory*, 1st ed. New York: Springer-Verlag, 2000.

[137] J. B. Kitto and S. C. Stultz, *Steam its generation and use*, 41st ed. Ohio: The Babcock & Wilcox company, 2005.

[138] W. Zima, "Simulation of dynamics of a boiler steam superheater with an attemperator," *Proc. Inst. Mech. Eng. Part A J. Power Energy*, vol. 220, no. 7, pp. 793–801, 2006.

[139] Y. Uruno, G. Choi, M. Sung, J. Chung, H. Kim, and K. Lee, "Transient analysis of attemperator enthalpy balance based on the commissioning data of a coal-fired steam power plant," *Appl. Therm. Eng.*, vol. 150, no. December 2018, pp. 1141–1158, 2019.

[140] R. L. Bartlett, J. E. Mulder, and R. C. Sheldon, "The Turbine Heat Balance," in *Steam Turbine Performance and Economics*, New York, 1958, pp. 37–69.

[141] R. L. Bartlett, J. E. Mulder, and R. C. Sheldon, "Turbine Efficiency," in *Steam Turbine Performance and Economics*, 1958, pp. 70–109.

[142] Aleksandr Shaulovich Leĭzerovich, "Last stages and exhaust hoods of LP cylinders," in *Steam turbines for modern fossil-fuel power plants*, Indian Trail: The fairmont press, Inc, 2008, pp. 135–168.

[143] L. Zhou, G. Xu, S. Zhao, C. Xu, and Y. Yang, "Parametric analysis and process optimization of steam cycle in double reheat ultra-supercritical power plants," *Appl. Therm. Eng.*, vol. 99, pp. 652–660, 2016.

[144] E. E. Robinson and N. N. Schenectady, "L eaving-Velocity and Exhaust Loss in Steam Turbines," *Trans. ASME*, no. FSP-56-10, pp. 515–526, 1933.

[145] R. E. Willis, "Reduction of turbine exhaust losses by optimizing the cooling tower operation." pp. 3.1-3.15.

[146] P. M. V Subbarao, “Irreversibilities : Turbine to Condenser-II.” Delhi.

[147] J. Reinker and P. Mason, “Steam Turbines for Large Power Applications,” 1996.

[148] M. M. El-Wakil, “Turbines,” in *PowerPlant Technology*, New York: McGraw-Hill, 1984, pp. 173–211.

[149] B. H. Wanasinghe, “Steam driven boiler feed pumps for Lakvijaya Power Station, Sri Lanka,” KTH University, 2016.

[150] D. P. Hanak, C. Biliyok, and V. Manovic, “Evaluation and modeling of part-load performance of coal-fired power plant with postcombustion CO2 capture,” *Energy and Fuels*, vol. 29, no. 6, pp. 3833–3844, 2015.

[151] H. van Ballegooyen and P. Durkin, “Condenser applications,” *Gryphon Reports*. [Online]. Available: http://www.gryphoneng.com/papers/. [Accessed: 08-Jul-2018].

[152] W. Wróblewski, S. Dykas, and S. Rulik, “Selection of the cooling system configuration for an ultra-critical coal-fired power plant,” *Energy Convers. Manag.*, vol. 76, pp. 554–560, 2013.

[153] J. Li, Z. Zhai, J. Wang, and S. Huang, “On-line fouling monitoring model of condenser in coal-fired power plants,” *Appl. Therm. Eng.*, vol. 104, pp. 628–635, 2016.

[154] H. Reuter, “Air-Cooled Condensers.” 2001.

[155] J. M. Burns *et al.*, “ASME PTC 23-2003: The new alternative for accurate cooling tower performance testing,” in *Cooling Tower Technology Conference*, 2003, pp. 2.1-2.11.

[156] J. G. Bustamante, A. S. Rattner, and S. Garimella, “Achieving near-water-cooled power plant performance with air-cooled condensers,” *Appl. Therm. Eng.*, vol. 105, pp. 362–371, 2016.

[157] A. R. V Ramani, B. A. Paul, and D. A. D. Saparia, “Performance characteristics of an Air-Cooled condenser under ambient conditions,” in *International conference on Current trends in Technology.*, 2011, pp. 1–6.

[158] Electric Power Research Institute (EPRI), “Power Plant Cooling System Overview for Researchers and Technology Developers,” Palo Alto, 2013.

[159] R. J. Bell, “An Introduction to condenser design philosophy,” in *Seminar Proceedings: Prevention of condenser failures-The state of the Art*, Palo Alto: Electric Power Research Institute (EPRI), 1985, pp. 2.1-2.5.

[160] B. Monteleone *et al.*, "Life cycle analysis of small scale pellet boilers characterized by high efficiency and low emissions," *Appl. Energy*, vol. 155, pp. 160–170, 2015.

[161] Electric Power Research Institute (EPRI), "Condensers for Combined-Cycle Plants: Air-Cooled and Water-Cooled Condensers Design Best Practices and Procurement Specifications," Palo Alto, 2010.

[162] Heat Exchanger Institute, "Condenser Performance," in *Standards for Surface Steam Condensers*, 11th ed., Cleveland: Heat Exchanger Institute (HEI), 2012, pp. 6–25.

[163] R. Laskowski, "Relations for steam power plant condenser performance in off-design conditions in the function of inlet parameters and those relevant in reference conditions," *Appl. Therm. Eng.*, vol. 103, pp. 528–536, 2016.

[164] X. Li, N. Wang, L. Wang, Y. Yang, and F. Maréchal, "Identification of optimal operating strategy of direct air-cooling condenser for Rankine cycle based power plants," *Appl. Energy*, vol. 209, no. November 2017, pp. 153–166, 2018.

[165] X. Du *et al.*, "Back pressure prediction of the direct air cooled power generating unit using the arti fi cial neural network model," *Appl. Therm. Eng.*, vol. 31, pp. 3009–3014, 2011.

[166] X. Li, N. Wang, L. Wang, I. Kantor, J. Robineau, and Y. Yang, "A data-driven model for the air-cooling condenser of thermal power plants based on data reconciliation and support vector regression," *Appl. Therm. Eng.*, vol. 129, pp. 1496–1507, 2018.

[167] A. B. Gill, "Condensers and Back Pressure," in *Power Plant Performance*, London: Butterworths and Co, 1984, pp. 492–526.

[168] P. U. Akpan and W. F. Fuls, "Generic approach for estimating final feed water temperature and extraction pressures in pulverised coal power plants," *Appl. Therm. Eng.*, vol. 141, 2018.

[169] R. L. Bartlett, J. E. Mulder, and R. C. Sheldon, "Thermodynamics of Turbine Performance," in *Steam Turbine Performance and Economics*, 1958, pp. 15–35.

[170] R. L. Bartlett, J. E. Mulder, and R. C. Sheldon, "The Feedwater heating cycle," in *Steam Turbine Performance and Economics*, 1958, pp. 133–159.

[171] C. Henderson, *Understanding coal-fired power plant cycles*, no. CCC/91. Palo Alto, CA, USA: IEA Clean Coal Centre, 2004.

[172] C. Bhattacharya and N. Banerjee, "Optimizing Boiler Feed Water Inlet Temperature to Maximize Efficiency of Steam Power Plant," in *1st International Conference on Advances in Energy Conversion Technologies*, 2010, pp. 1–5.

[173] H. Huseyin *et al.*, "Comparative energetic and exergetic performance analyses for coal-fired thermal power plants in Turkey," *Int. J. Therm. Sci.*, vol. 48, no. 11, pp. 2179–2186, 2009.

[174] G. Tzolakis, P. Papanikolaou, D. Kolokotronis, N. Samaras, A. Tourlidakis, and A. Tomboulides, "Simulation of a coal-fired power plant using mathematical programming algorithms in order to optimize its efficiency," *Appl. Therm. Eng.*, vol. 48, pp. 256–267, 2012.

[175] S. Espatolero, L. M. Romeo, and C. Cortes, "Efficiency improvement strategies for the feedwater heaters network designing in supercritical coal- fired power plants," *Appl. Therm. Eng.*, vol. 73, pp. 449–460, 2014.

[176] R. L. Bartlett, J. E. Mulder, and R. C. Sheldon, "The feedwater heating cycle," in *Steam Turbine Performance and Economics*, New York: McGraw Hill, 1958, pp. 133–158.

[177] S. Sanaye, B. Farshi, and H. Turk, "Optimum Turbine Extraction Pressures For Maximum Efficiency in Steam Power Plant Cycle," in *Proceedings of IJPGC03 2003 International Joint Power Generation Conference*, 2003, pp. 1–8.

[178] F. Egelioglu and H. S. Aybar, "Optimization of steam turbine extraction pressures," in *ASME Proceedings of IJPGC2003*, 2003, pp. 1–6.

[179] P. M. V Subbarao, "Analysis of Rankine Cycle with FWHs." [Online]. Available: https://vdocuments.mx/analysis-of-rankine-cycle-with-fwhs.html. [Accessed: 06-Apr-2017].

[180] R. L. Bartlett, J. E. Mulder, and R. C. Sheldon, "The Turbine Heat Balance," in *Steam Turbine Performance and Economics*, London: McGraw-Hill Book Company, 1958, pp. 37–69.

[181] R. L. Bartlett, J. E. Mulder, and R. C. Sheldon, "The Effect of Steam conditions on Performance," in *Steam Turbine Performance and Economics*, New York: McGraw Hill, 1958, pp. 110–132.

[182] Y. Ust, G. Gonca, and H. K. Kayadelen, "Determination of optimum reheat pressures for single and double reheat irreversible Rankine cycle," *J. Energy Inst.*, vol. 84, no. 4, pp. 215–219, 2011.

[183] L. Wang, Y. Yang, C. Dong, T. Morosuk, and G. Tsatsaronis, "Parametric optimization of supercritical coal-fired power plants by MINLP and differential evolution," *Energy Convers. Manag.*, vol. 85, pp. 828–838, 2014.

[184] T. K. Gogoi, M. Pandey, and R. Das, "Estimation of operating parameters of a reheat regenerative power cycle using simplex search and differential evolution based inverse methods," *Energy Convers. Manag.*, vol. 91, pp. 204–218, 2015.

[185] M. Holmgren, "X Steam Tables: Excel Macros, IF-97 Steam Tables." [Online]. Available: www.x-eng.com.

[186] P. U. Akpan and W. F. Fuls, "Application and limits of a constant effectiveness model for predicting the pressure of steam condensers at off-design loads and cooling fluid temperatures," *Appl. Therm. Eng.*, vol. 158, no. 2019, p. 113779, 2019.

[187] A. Bolatturk, A. Coskun, and C. Geredelioglu, "Thermodynamic and exergoeconomic analysis of Çayırhan thermal power plant," *Energy Convers. Manag.*, vol. 101, pp. 371–378, 2015.

[188] J. Pretorius, "Eskom perspective on specifications for large ACC ' s," in *ACC user's group meeting*, 2012.

[189] GP Strategies, *EtaPRO Performance and Condition Monitoring Calculation Templates*. New York, 2012.

[190] GP Strategies, "EtaPRO VirtualPlant User Guide." GP Strategies Corporation, New York, 2011.

[191] P. G. Rousseau and W. F. Fuls, "Air and Flue gas cycle analysis," in *Power Plant Systems Analysis*, Rev 1.0., Cape Town, 2017, pp. 209–234.

[192] A. Senegac, I. Kuštrin, and M. Sekavc, "Accuracy Improvement Analysis of the Standard Indirect Method for Determining a Steam Boiler ' s Efficiency," in *VGB Power Tech*, 2008, pp. 100–106.

[193] J. Bebic, "Power System Planning : Emerging Practices Suitable for Evaluating the Impact of High-Penetration Photovoltaics," 2008.

[194] K. Van Den Bergh and E. Delarue, "Facilitating variable generation of renewables by conventional power plant cycling : costs and benefits," *KU Leuven Energy Inst. Work. Pap. EN2014-9*, no. WP EN2014-9, pp. 1–8, 2014.

[195] K. Van Den Bergh and E. Delarue, “Cycling of conventional power plants: Technical limits and actual costs,” *Energy Convers. Manag.*, vol. 97, no. March, pp. 70–77, 2015.

[196] K. Sadovskaia, D. Bogdanov, S. Honkapuro, and C. Breyer, “Electrical Power and Energy Systems Power transmission and distribution losses – A model based on available empirical data and future trends for all countries globally,” *Electr. Power Energy Syst.*, vol. 107, no. November 2018, pp. 98–109, 2019.

[197] M. D. Sklar-chik, “System Cost of Energy Generation Scenarios for South Africa : Understanding the real cost of integrating energy generation technologies,” University of Stellenbosch, 2017.

[198] B. Nyamdash, E. Denny, and M. O. Malley, “The viability of balancing wind generation with large scale energy storage $,” *Energy Policy*, vol. 38, no. 11, pp. 7200–7208, 2010.

[199] D. Lindsley, *Power Plant Control and Instrumentation the control of boilers and HRSG systems*. .

Appendix A. Sample process conditions for SRH and DRH CFPPs

A.1 Sample VWO heat balance process conditions generated for a single reheat CFPP

Point	Description	Mass Flow rate (kg/s)	Mass fraction	Temperature (C)	Pressure (MPa)	Enthalpy (kJ/kg)	Enthropy (kJ/kgK)
1	Throttle Conditions	407.1294	1	510	12	3376.812	6.524698
2	HP Outlet condition	407.1294	1	323.3024383	3.091	3049.848	6.623351
2a	Inlet to Reheater	378.3997	0.9294335	323.3024383	3.091	3049.848	6.623351
2b	inlet to FWH Pipe #1	28.72968	0.0705665	323.3024383	3.091	3049.848	6.623351
3	Inlet to IP Turbine	378.3997	0.9294335	510	2.81	3481.553	7.296635
4	Exhaust of IP Turbine	337.9819	0.8301585	320.9025458	0.732127	3102.513	7.352858
5	LP Exhaust (Condenser inlet)	279.7729	0.6871841	28.9615038	0.004	2303.891	7.646578
6	Condenser Outlet	279.7729	0.6871841	28.9615038	0.004	121.4036	0.42275
7	FWH #6 Drain Pump Discharge	279.7729	0.6871841	29.08807471	1.310803	123.0451	0.423811
8	Feed water outlet from FWH # 6	279.7729	0.6871841	63.11398486	1.110803	264.1847	0.866867
9	Feed water inlet to FWH # 5	337.9793	0.830152	62.89935634	1.110803	264.1847	0.866867
10	Feed water outlet from FWH # 5	337.9793	0.830152	97.26646592	0.910803	407.5703	1.273729
11	Feed water outlet from FWH #4	337.9793	0.830152	131.418947	0.710803	552.4493	1.648634
12	Feed water outlet from Deaerator (FWH #3)	407.1294	1	165.571428	0.710803	699.8432	1.998445
13	BFP Discharge	407.1294	1	168.0213276	15.01481	718.5442	2.004961
14	Feed water outlet from FWH #2 (inlet to FWH No 1)	407.1294	1	199.7239091	15.01481	856.9031	2.307736
15	Final feed water condition	407.1294	1	233.8763902	14.81481	1010.747	2.622096
16	Extraction #1 inlet to FWH	28.72968	0.0705665	322.3271903	3.000971	3049.848	6.636064
17	Drains outlet from FWH #1	28.72968	0.0705665	203.7239091	3.000971	869.7186	2.363792
18	Extraction #2 exit from HP Turbine	20.26755	0.0497816	424.2559031	1.592085	3307.519	7.318431
19	Extraction #2 inlet to FWH	20.26755	0.0497816	423.9436213	1.545714	3307.519	7.331826
20	Drains outlet from FWH #2	48.99723	0.120348	172.0213276	1.545714	728.4511	2.061059
21	Extraction #3 exit from HP Turbine	20.15024	0.0494934	320.9025458	0.732127	3102.513	7.352858
22	Extraction #3 inlet to (Deaerator)	20.15024	0.0494934	320.6692248	0.710803	3102.513	7.366291
23	Extraction #4 exit from LP Turbine	19.77878	0.0485811	216.5551189	0.290386	2900.264	7.399284
24	Extraction #4 inlet to FWH	19.77878	0.0485811	216.3783222	0.281928	2900.264	7.412749
25	Drains outlet from FWH #4	19.77878	0.0485811	101.2664659	0.281928	424.5755	1.321183
26	Extraction #5 exit from LP Turbine	21.15542	0.0519624	115.153148	0.094674	2707.401	7.468988
27	Extraction #5 inlet to FWH	21.15542	0.0519624	115.0038288	0.091916	2707.401	7.482473
28	Drains outlet from FWH #5	40.9342	0.1005435	66.89935634	0.091916	280.0847	0.91697
29	Extraction #6 exit from LP Turbine	17.26387	0.0424039	63.7678532	0.023693	2513.749	7.547025
30	Extraction #6 inlet to FWH	17.26387	0.0424039	63.11398486	0.023003	2513.749	7.560003
31	Drains outlet from FWH #6	58.19807	0.1429474	63.11398486	0.023003	264.1847	0.870177
32	Condensate Extration Pump outlet Pressure	58.19807	0.1429474	63.21163063	1.110803	265.4912	0.870751

A.2 Sample process conditions for a double reheat VWO heat balance diagram

Point	Description	Mass Flow rate (kg/s)	Mass fraction	Temperature (C)	Pressure (MPa)	Enthalpy (kJ/kg)	Enthropy (kJ/kgK)
1	Throttle Conditions	761.8654	1	510	12	3376.812	6.524698
2	HP Outlet condition	761.8654	1	331.5526746	3.354839	3063.274	6.610554
2a	Inlet to Reheater #1	718.7132	0.9433598	331.5526746	3.354839	3063.274	6.610554
2b	inlet to FWH Pipe #1	43.1522	0.0566402	331.5526746	3.354839	3063.274	6.610554
3	Inlet to First IP Turbine	718.7132	0.9433598	510	3.12	3478.229	7.245143
4	Exhaust of first IP Turbine	662.3155	0.8693341	369.0616364	1.186697	3195.208	7.283801
4a	Inlet to Reheater #2	633.8769	0.8320064	369.0616364	1.186697	3195.208	7.283801
4b	inlet to FWH Pipe #3	28.43864	0.0373276	369.0616364	1.186697	3195.208	7.283801
5	Inlet to Second IP Turbine	662.3155	0.8693341	510	0.67	3504.16	7.979979
6	Exhaust of second IP Turbine	615.0884	0.8073452	397.9727812	0.311729	3271.022	8.010426
7	LP Exhaust (Condenser inlet)	541.5088	0.710767	28.9615038	0.004	2499.534	8.294166
8	Condenser Outlet	541.5088	0.710767	28.9615038	0.004	121.4036	0.42275
9	CEP Discharge	541.5088	0.710767	28.49612696	2.330188	121.5112	0.415325
10	Feed water outlet from FWH # 8	541.5088	0.710767	55.01355417	2.090188	232.0625	0.767177
11	Feed water inlet to FWH # 7	619.1688	0.812701	55.01355417	2.090188	232.0625	0.767177
12	Feed water inlet to FWH #6	619.1688	0.812701	81.06560455	1.850188	340.8507	1.086799
13	Feed water inlet to FWH #5	619.1688	0.812701	107.1176549	1.610188	450.2538	1.385559
14	Feed water inlet to FWH #4	619.1688	0.812701	133.1697053	1.370188	560.651	1.667123
15	Feed water inlet to FWH #3	619.1688	0.812701	159.2217557	1.130188	672.4997	1.934601
16	Feed water outlet from Deaerator (FWH #3)	761.8654	1	185.2738061	1.130188	786.5395	2.19062
17	BFP Discharge	761.8654	1	187.873555	14.59765	804.5193	2.196597
18	Feed water outlet from FWH #2 (inlet to FWH No 1)	761.8654	1	211.3258564	14.35765	903.7815	2.407304
19	Final feed water condition	761.8654	1	237.3779068	14.11765	1025.039	2.651826
20	Extraction #1 inlet to FWH	43.1522	0.0566402	329.8949946	3.195084	3063.274	6.631503
21	Drains outlet from FWH #1	43.1522	0.0566402	215.3258564	3.195084	922.4347	2.472454
22	Extraction #2 exit from first IP Turbine	27.95902	0.0366981	450.2674744	2.11514	3357.12	7.259738
23	Extraction #2 inlet to FWH	27.95902	0.0366981	449.3200569	1.958463	3357.12	7.29453
24	Drains outlet from FWH #2	71.11122	0.0933383	191.873555	1.958463	816.22	2.252821
25	Extraction #3 inlet to (Deaerator)	28.43864	0.0373276	368.5746222	1.130188	3195.208	7.305906
26	Extraction #4 exit from secon IP Turbine	23.79888	0.0312376	501.9605087	0.636301	3487.176	7.981883
27	Extraction #4 inlet to FWH	23.79888	0.0312376	501.8098434	0.606001	3487.176	8.004295
28	Drains outlet from FWH #4	23.79888	0.0312376	137.1697053	0.606001	577.239	1.709785
29	Extraction #5 exit from second IP Turbine	23.42826	0.0307512	397.9727812	0.311729	3271.022	8.010426
30	Extraction #5 inlet to FWH #5	23.42826	0.0307512	397.8605867	0.296885	3271.022	8.032854
31	Drains outlet from FWH #5	47.22714	0.0619888	111.1176549	0.296885	466.2036	1.430927
32	Extraction #6 exit from LP Turbine	23.06146	0.0302697	297.4891552	0.140439	3068.487	8.050254
33	Extraction #6 inlet to FWH	23.06146	0.0302697	297.3607534	0.130036	3068.487	8.085656
34	Drains outlet from FWH #6	70.2886	0.0922586	85.06560455	0.130036	3068.487	8.085656
35	Extraction #7 exit from LP Turbine	26.41177	0.0346672	195.2694718	0.053458	2868.355	8.108353
36	Extraction #7 inlet to FWH	26.41177	0.0346672	195.1733519	0.049498	2868.355	8.143774
37	Drains outlet from FWH #7	47.22714	0.0619888	59.01355417	0.049498	247.0532	0.81886
38	Extraction #8 exit from LP Turbine	24.11313	0.0316501	96.6148038	0.01656	2680.133	8.196771
39	Extraction #8 inlet to FWH	24.11313	0.0316501	96.56154992	0.015772	2680.133	8.219234
40	Drains outlet from FWH #8	71.34027	0.0936389	55.01355417	0.015772	230.2977	0.768241
41	Condensate Extration Pump outlet Pressure	71.34027	0.0936389	55.19247166	2.090188	232.7912	0.769395

Appendix B. List of the Model CFPPs Investigated

Plant Name	Plant Description	Degree of Reheat	Throttle Pressure (MPa)	Throttle Temperature (C)	Condensing Pressure (kPa)	1st Reheat Temperature (C)	1st Reheat Pressure (MPa)	2nd Reheat Temperature (C)	2nd Reheat Pressure (MPa)
A.	**Non-Reheats**								
Plant 001	ROP12T510C4	Non	12	510	4	N/A	N/A	N/A	N/A
Plant 002	ROP12T510C7	Non	12	510	7	N/A	N/A	N/A	N/A
Plant 003	ROP12T510C12	Non	12	510	12	N/A	N/A	N/A	N/A
Plant 004	ROP12T510C17	Non	12	510	17	N/A	N/A	N/A	N/A
Plant 005	ROP12T535C4	Non	12	535	4	N/A	N/A	N/A	N/A
Plant 006	ROP12T535C7	Non	12	535	7	N/A	N/A	N/A	N/A
Plant 007	ROP12T535C12	Non	12	535	12	N/A	N/A	N/A	N/A
Plant 008	ROP12T535C17	Non	12	535	17	N/A	N/A	N/A	N/A
Plant 009	ROP12T565C4	Non	12	565	4	N/A	N/A	N/A	N/A
Plant 010	ROP12T565C7	Non	12	565	7	N/A	N/A	N/A	N/A
Plant 011	ROP12T565C12	Non	12	565	12	N/A	N/A	N/A	N/A
Plant 012	ROP12T565C17	Non	12	565	17	N/A	N/A	N/A	N/A
Plant 013	ROP12T600C4	Non	12	600	4	N/A	N/A	N/A	N/A
Plant 014	ROP12T600C7	Non	12	600	7	N/A	N/A	N/A	N/A
Plant 015	ROP12T600C12	Non	12	600	12	N/A	N/A	N/A	N/A
Plant 016	ROP12T600C17	Non	12	600	17	N/A	N/A	N/A	N/A
Plant 017	ROP17T510C4	Non	17	510	4	N/A	N/A	N/A	N/A
Plant 018	ROP17T510C7	Non	17	510	7	N/A	N/A	N/A	N/A
Plant 019	ROP17T510C12	Non	17	510	12	N/A	N/A	N/A	N/A
Plant 020	ROP17T510C17	Non	17	510	17	N/A	N/A	N/A	N/A
Plant 021	ROP17T535C4	Non	17	535	4	N/A	N/A	N/A	N/A
Plant 022	ROP17T535C7	Non	17	535	7	N/A	N/A	N/A	N/A
Plant 023	ROP17T535C12	Non	17	535	12	N/A	N/A	N/A	N/A
Plant 024	ROP17T535C17	Non	17	535	17	N/A	N/A	N/A	N/A
Plant 025	ROP17T565C4	Non	17	565	4	N/A	N/A	N/A	N/A
Plant 026	ROP17T565C7	Non	17	565	7	N/A	N/A	N/A	N/A
Plant 027	ROP17T565C12	Non	17	565	12	N/A	N/A	N/A	N/A
Plant 028	ROP17T565C17	Non	17	565	17	N/A	N/A	N/A	N/A
Plant 029	ROP17T600C4	Non	17	600	4	N/A	N/A	N/A	N/A
Plant 030	ROP17T600C7	Non	17	600	7	N/A	N/A	N/A	N/A
Plant 031	ROP17T600C12	Non	17	600	12	N/A	N/A	N/A	N/A
Plant 032	ROP17T600C17	Non	17	600	17	N/A	N/A	N/A	N/A
Plant 033	ROP24T510C4	Non	24	510	4	N/A	N/A	N/A	N/A

Plant Name	Plant Description	Degree of Reheat	Throttle Pressure (MPa)	Throttle Temperature (C)	Condensing Pressure (kPa)	1st Reheat Temperature (C)	1st Reheat Pressure (MPa)	2nd Reheat Temperature (C)	2nd Reheat Pressure (MPa)
Plant 034	ROP24T510C7	Non	24	510	7	N/A	N/A	N/A	N/A
Plant 035	ROP24T510C12	Non	24	510	12	N/A	N/A	N/A	N/A
Plant 036	ROP24T510C17	Non	24	510	17	N/A	N/A	N/A	N/A
Plant 037	ROP24T535C4	Non	24	535	4	N/A	N/A	N/A	N/A
Plant 038	ROP24T535C7	Non	24	535	7	N/A	N/A	N/A	N/A
Plant 039	ROP24T535C12	Non	24	535	12	N/A	N/A	N/A	N/A
Plant 040	ROP24T535C17	Non	24	535	17	N/A	N/A	N/A	N/A
Plant 041	ROP24T565C4	Non	24	565	4	N/A	N/A	N/A	N/A
Plant 042	ROP24T565C7	Non	24	565	7	N/A	N/A	N/A	N/A
Plant 043	ROP24T565C12	Non	24	565	12	N/A	N/A	N/A	N/A
Plant 044	ROP24T565C17	Non	24	565	17	N/A	N/A	N/A	N/A
Plant 045	ROP24T600C4	Non	24	600	4	N/A	N/A	N/A	N/A
Plant 046	ROP24T600C7	Non	24	600	7	N/A	N/A	N/A	N/A
Plant 047	ROP24T600C12	Non	24	600	12	N/A	N/A	N/A	N/A
Plant 048	ROP24T600C17	Non	24	600	17	N/A	N/A	N/A	N/A
Plant 049	ROP30T510C4	Non	30	510	4	N/A	N/A	N/A	N/A
Plant 050	ROP30T510C7	Non	30	510	7	N/A	N/A	N/A	N/A
Plant 051	ROP30T510C12	Non	30	510	12	N/A	N/A	N/A	N/A
Plant 052	ROP30T510C17	Non	30	510	17	N/A	N/A	N/A	N/A
Plant 053	ROP30T535C4	Non	30	535	4	N/A	N/A	N/A	N/A
Plant 054	ROP30T535C7	Non	30	535	7	N/A	N/A	N/A	N/A
Plant 055	ROP30T535C12	Non	30	535	12	N/A	N/A	N/A	N/A
Plant 056	ROP30T535C17	Non	30	535	17	N/A	N/A	N/A	N/A
Plant 057	ROP30T565C4	Non	30	565	4	N/A	N/A	N/A	N/A
Plant 058	ROP30T565C7	Non	30	565	7	N/A	N/A	N/A	N/A
Plant 059	ROP30T565C12	Non	30	565	12	N/A	N/A	N/A	N/A
Plant 060	ROP30T565C17	Non	30	565	17	N/A	N/A	N/A	N/A
Plant 061	ROP30T600C4	Non	30	600	4	N/A	N/A	N/A	N/A
Plant 062	ROP30T600C7	Non	30	600	7	N/A	N/A	N/A	N/A
Plant 063	ROP30T600C12	Non	30	600	12	N/A	N/A	N/A	N/A
Plant 064	ROP30T600C17	Non	30	600	17	N/A	N/A	N/A	N/A
B. Single Reheats									
Plant 065	RIP12T510C4	Single	12	510	4	510	2.85	N/A	N/A
Plant 066	RIP12T510C7	Single	12	510	7	510	2.91	N/A	N/A
Plant 067	RIP12T510C12	Single	12	510	12	510	3.02	N/A	N/A
Plant 068	RIP12T510C17	Single	12	510	17	510	3.08	N/A	N/A
Plant 069	RIP12T535C4	Single	12	535	4	535	2.55	N/A	N/A

Plant Name	Plant Description	Degree of Reheat	Throttle Pressure (MPa)	Throttle Temperature (C)	Condensing Pressure (kPa)	1st Reheat Temperature (C)	1st Reheat Pressure (MPa)	2nd Reheat Temperature (C)	2nd Reheat Pressure (MPa)
Plant 070	RIP12T535C7	Single	12	535	7	535	2.61	N/A	N/A
Plant 071	RIP12T535C12	Single	12	535	12	535	2.7	N/A	N/A
Plant 072	RIP12T535C17	Single	12	535	17	535	2.77	N/A	N/A
Plant 073	RIP12T565C4	Single	12	565	4	565	2.25	N/A	N/A
Plant 074	RIP12T565C7	Single	12	565	7	565	2.29	N/A	N/A
Plant 075	RIP12T565C12	Single	12	565	12	565	2.38	N/A	N/A
Plant 076	RIP12T565C17	Single	12	565	17	565	2.43	N/A	N/A
Plant 077	RIP12T600C4	Single	12	600	4	600	1.94	N/A	N/A
Plant 078	RIP12T600C7	Single	12	600	7	600	1.99	N/A	N/A
Plant 079	RIP12T600C12	Single	12	600	12	600	2.06	N/A	N/A
Plant 080	RIP12T600C17	Single	12	600	17	600	2.11	N/A	N/A
Plant 081	RIP17T510C4	Single	17	510	4	510	4.56	N/A	N/A
Plant 082	RIP17T510C7	Single	17	510	7	510	4.66	N/A	N/A
Plant 083	RIP17T510C12	Single	17	510	12	510	4.83	N/A	N/A
Plant 084	RIP17T510C17	Single	17	510	17	510	4.94	N/A	N/A
Plant 085	RIP17T535C4	Single	17	535	4	535	4.09	N/A	N/A
Plant 086	RIP17T535C7	Single	17	535	7	535	4.17	N/A	N/A
Plant 087	RIP17T535C12	Single	17	535	12	535	4.33	N/A	N/A
Plant 088	RIP17T535C17	Single	17	535	17	535	4.43	N/A	N/A
Plant 089	RIP17T565C4	Single	17	565	4	565	3.59	N/A	N/A
Plant 090	RIP17T565C7	Single	17	565	7	565	3.67	N/A	N/A
Plant 091	RIP17T565C12	Single	17	565	12	565	3.8	N/A	N/A
Plant 092	RIP17T565C17	Single	17	565	17	565	3.89	N/A	N/A
Plant 093	RIP17T600C4	Single	17	600	4	600	3.11	N/A	N/A
Plant 094	RIP17T600C7	Single	17	600	7	600	3.18	N/A	N/A
Plant 095	RIP17T600C12	Single	17	600	12	600	3.29	N/A	N/A
Plant 096	RIP17T600C17	Single	17	600	17	600	3.38	N/A	N/A
Plant 097	RIP24T510C4	Single	24	510	4	510	7.29	N/A	N/A
Plant 098	RIP24T510C7	Single	24	510	7	510	7.44	N/A	N/A
Plant 099	RIP24T510C12	Single	24	510	12	510	7.7	N/A	N/A
Plant 100	RIP24T510C17	Single	24	510	17	510	7.88	N/A	N/A
Plant 101	RIP24T535C4	Single	24	535	4	535	6.54	N/A	N/A
Plant 102	RIP24T535C7	Single	24	535	7	535	6.68	N/A	N/A
Plant 103	RIP24T535C12	Single	24	535	12	535	6.92	N/A	N/A
Plant 104	RIP24T535C17	Single	24	535	17	535	7.08	N/A	N/A
Plant 105	RIP24T565C4	Single	24	565	4	565	5.76	N/A	N/A
Plant 106	RIP24T565C7	Single	24	565	7	565	5.88	N/A	N/A
Plant 107	RIP24T565C12	Single	24	565	12	565	6.09	N/A	N/A

Plant Name	Plant Description	Degree of Reheat	Throttle Pressure (MPa)	Throttle Temperature (C)	Condensing Pressure (kPa)	1st Reheat Temperature (C)	1st Reheat Pressure (MPa)	2nd Reheat Temperature (C)	2nd Reheat Pressure (MPa)
Plant 108	RIP24T565C17	Single	24	565	17	565	6.24	N/A	N/A
Plant 109	RIP24T600C4	Single	24	600	4	600	4.98	N/A	N/A
Plant 110	RIP24T600C7	Single	24	600	7	600	5.1	N/A	N/A
Plant 111	RIP24T600C12	Single	24	600	12	600	5.28	N/A	N/A
Plant 112	RIP24T600C17	Single	24	600	17	600	5.42	N/A	N/A
Plant 113	RIP30T510C4	Single	30	510	4	510	9.72	N/A	N/A
Plant 114	RIP30T510C7	Single	30	510	7	510	10.05	N/A	N/A
Plant 115	RIP30T510C12	Single	30	510	12	510	10.38	N/A	N/A
Plant 116	RIP30T510C17	Single	30	510	17	510	10.61	N/A	N/A
Plant 117	RIP30T535C4	Single	30	535	4	535	8.75	N/A	N/A
Plant 118	RIP30T535C7	Single	30	535	7	535	9.06	N/A	N/A
Plant 119	RIP30T535C12	Single	30	535	12	535	9.37	N/A	N/A
Plant 120	RIP30T535C17	Single	30	535	17	535	9.59	N/A	N/A
Plant 121	RIP30T565C4	Single	30	565	4	565	7.71	N/A	N/A
Plant 122	RIP30T565C7	Single	30	565	7	565	7.99	N/A	N/A
Plant 123	RIP30T565C12	Single	30	565	12	565	8.29	N/A	N/A
Plant 124	RIP30T565C17	Single	30	565	17	565	8.49	N/A	N/A
Plant 125	RIP30T600C4	Single	30	600	4	600	6.67	N/A	N/A
Plant 126	RIP30T600C7	Single	30	600	7	600	6.93	N/A	N/A
Plant 127	RIP30T600C12	Single	30	600	12	600	7.18	N/A	N/A
Plant 128	RIP30T600C17	Single	30	600	17	600	7.36	N/A	N/A
C. Double Reheat									
Plant 129	R2'P12T510C4	Double	12	510	4	510	3.12	510	0.67
Plant 130	R2'P12T510C7	Double	12	510	7	510	3.12	510	0.67
Plant 131	R2'P12T510C12	Double	12	510	12	510	3.48	510	0.95
Plant 132	R2'P12T510C17	Double	12	510	17	510	3.48	510	0.95
Plant 133	R2'P12T535C4	Double	12	535	4	535	3.12	535	0.67
Plant 134	R2'P12T535C7	Double	12	535	7	535	3.12	535	0.67
Plant 135	R2'P12T535C12	Double	12	535	12	535	3.12	535	0.67
Plant 136	R2'P12T535C17	Double	12	535	17	535	3.12	535	0.67
Plant 137	R2'P12T565C4	Double	12	565	4	565	2.4	565	0.38
Plant 138	R2'P12T565C7	Double	12	565	7	565	3.12	565	0.67
Plant 139	R2'P12T565C12	Double	12	565	12	565	3.12	565	0.67
Plant 140	R2'P12T565C17	Double	12	565	17	565	3.48	565	0.95
Plant 141	R2'P12T600C4	Double	12	600	4	600	2.4	600	0.38
Plant 142	R2'P12T600C7	Double	12	600	7	600	3.12	600	0.67
Plant 143	R2'P12T600C12	Double	12	600	12	600	3.12	600	0.67

Plant Name	Plant Description	Degree of Reheat	Throttle Pressure (MPa)	Throttle Temperature (C)	Condensing Pressure (kPa)	1st Reheat Temperature (C)	1st Reheat Pressure (MPa)	2nd Reheat Temperature (C)	2nd Reheat Pressure (MPa)
Plant 144	R2'P12T600C17	Double	12	600	17	600	3.48	600	0.95
Plant 145	R2'P17T510C4	Double	17	510	4	510	4.93	510	1.232
Plant 146	R2'P17T510C7	Double	17	510	7	510	4.93	510	1.232
Plant 147	R2'P17T510C12	Double	17	510	12	510	5.44	510	1.515
Plant 148	R2'P17T510C17	Double	17	510	17	510	5.4	510	1.515
Plant 149	R2'P17T535C4	Double	17	535	4	535	4.42	535	0.95
Plant 150	R2'P17T535C7	Double	17	535	7	535	4.93	535	1.232
Plant 151	R2'P17T535C12	Double	17	535	12	535	4.93	535	1.232
Plant 152	R2'P17T535C17	Double	17	535	17	535	4.93	535	1.232
Plant 153	R2'P17T565C4	Double	17	565	4	565	4.42	565	0.95
Plant 154	R2'P17T565C7	Double	17	565	7	565	4.42	565	0.95
Plant 155	R2'P17T565C12	Double	17	565	12	565	4.42	565	0.95
Plant 156	R2'P17T565C17	Double	17	565	17	565	4.42	565	0.95
Plant 157	R2'P17T600C4	Double	17	600	4	600	3.4	600	0.67
Plant 158	R2'P17T600C7	Double	17	600	7	600	3.4	600	0.67
Plant 159	R2'P17T600C12	Double	17	600	12	600	4.42	600	0.95
Plant 160	R2'P17T600C17	Double	17	600	17	600	4.42	600	0.95
Plant 161	R2'P24T510C4	Double	24	510	4	510	8.4	510	2.36
Plant 162	R2'P24T510C7	Double	24	510	7	510	8.4	510	2.36
Plant 163	R2'P24T510C12	Double	24	510	12	510	8.4	510	2.36
Plant 164	R2'P24T510C17	Double	24	510	17	510	9.12	510	2.65
Plant 165	R2'P24T535C4	Double	24	535	4	535	6.96	535	1.8
Plant 166	R2'P24T535C7	Double	24	535	7	535	7.68	535	2.08
Plant 167	R2'P24T535C12	Double	24	535	12	535	7.68	535	2.08
Plant 168	R2'P24T535C17	Double	24	535	17	535	7.68	535	2.08
Plant 169	R2'P24T565C4	Double	24	565	4	565	6.96	565	1.515
Plant 170	R2'P24T565C7	Double	24	565	7	565	6.96	565	1.515
Plant 171	R2'P24T565C12	Double	24	565	12	565	6.96	565	1.515
Plant 172	R2'P24T565C17	Double	24	565	17	565	6.96	565	1.798
Plant 173	R2'P24T600C4	Double	24	600	4	600	6.24	600	1.232
Plant 174	R2'P24T600C7	Double	24	600	7	600	6.24	600	1.232
Plant 175	R2'P24T600C12	Double	24	600	12	600	6.24	600	1.232
Plant 176	R2'P24T600C17	Double	24	600	17	600	6.24	600	1.232
Plant 177	R2'P30T510C4	Double	30	510	4	510	11.4	510	3.213
Plant 178	R2'P30T510C7	Double	30	510	7	510	11.4	510	3.496
Plant 179	R2'P30T510C12	Double	30	510	12	510	11.4	510	3.496
Plant 180	R2'P30T510C17	Double	30	510	17	510	12.3	510	4.062
Plant 181	R2'P30T535C4	Double	30	535	4	535	10.5	535	2.647

Plant Name	Plant Description	Degree of Reheat	Throttle Pressure (MPa)	Throttle Temperature (C)	Condensing Pressure (kPa)	1st Reheat Temperature (C)	1st Reheat Pressure (MPa)	2nd Reheat Temperature (C)	2nd Reheat Pressure (MPa)
Plant 182	R2'P30T535C7	Double	30	535	7	535	10.5	535	2.93
Plant 183	R2'P30T535C12	Double	30	535	12	535	10.5	535	2.93
Plant 184	R2'P30T535C17	Double	30	535	17	535	10.5	535	2.93
Plant 185	R2'P30T565C4	Double	30	565	4	565	8.7	565	2.081
Plant 186	R2'P30T565C7	Double	30	565	7	565	8.7	565	2.081
Plant 187	R2'P30T565C12	Double	30	565	12	565	9.6	565	2.364
Plant 188	R2'P30T565C17	Double	30	565	17	565	9.6	565	2.364
Plant 189	R2'P30T600C4	Double	30	600	4	600	7.8	600	1.515
Plant 190	R2'P30T600C7	Double	30	600	7	600	7.8	600	1.515
Plant 191	R2'P30T600C12	Double	30	600	12	600	7.8	600	1.798
Plant 192	R2'P30T600C17	Double	30	600	17	600	8.7	600	2.081

Appendix C. CFPP Profiles from Energy mix Study

C.1 Hourly Production profiles for Network 1 : Dispatch method C

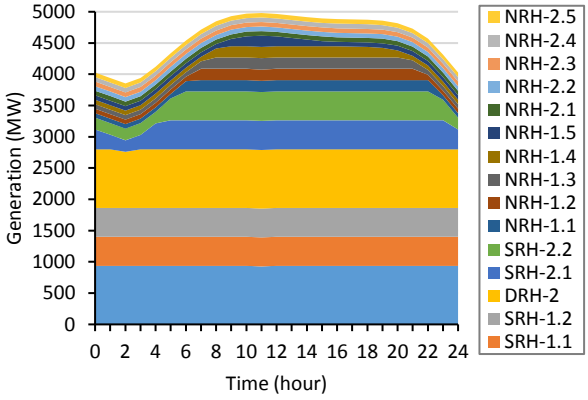

(a) 0% REPG Penetration level

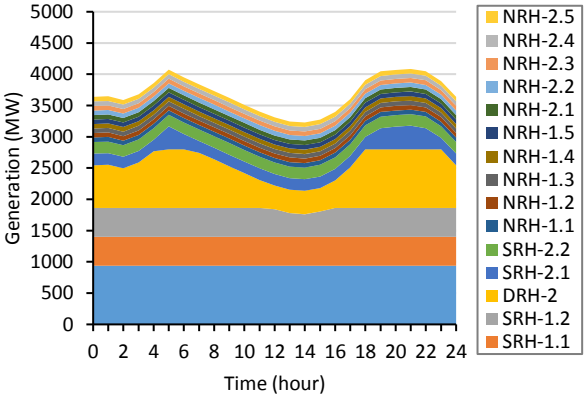

(b) 20% REPG Penetration level

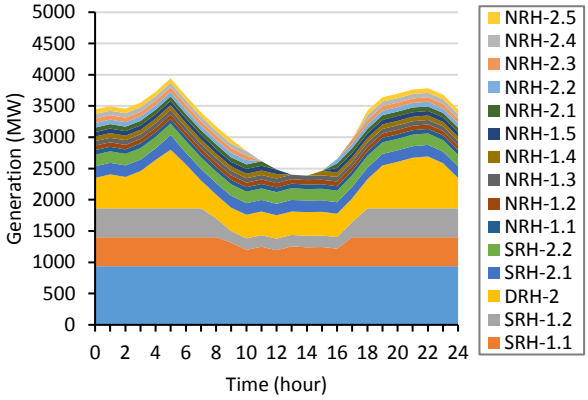

(c) 30% REPG Penetration level

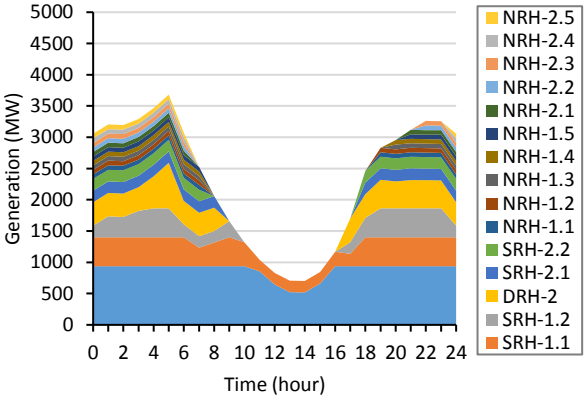

(d) 50% REPG Penetration level

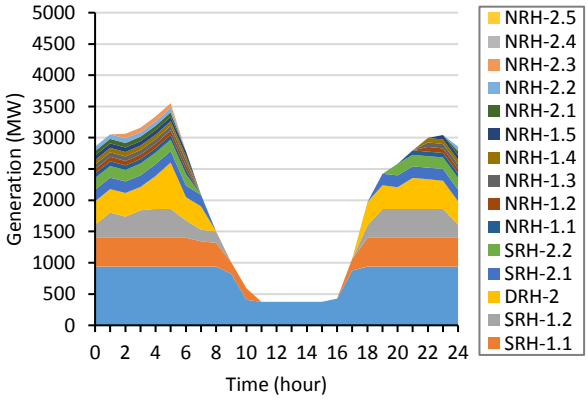

(e) 60% REPG Penetration level

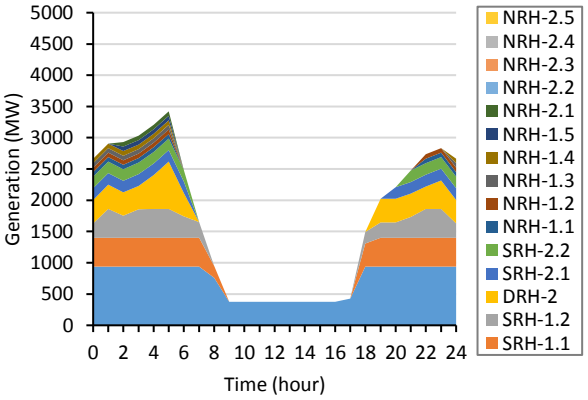

(f) 70% REPG Penetration level

C.2 Hourly Production profiles for Network 1: Dispatch method D

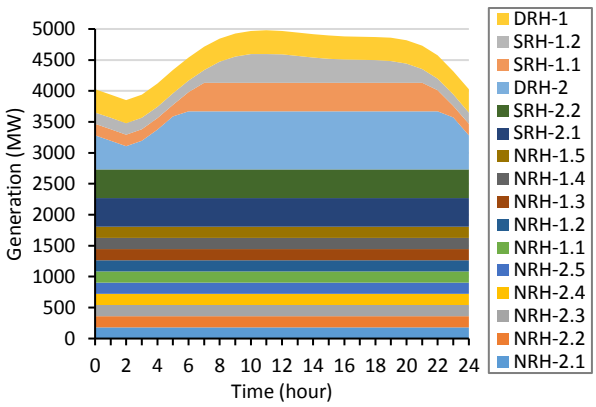

(a) 0% REPG Penetration level

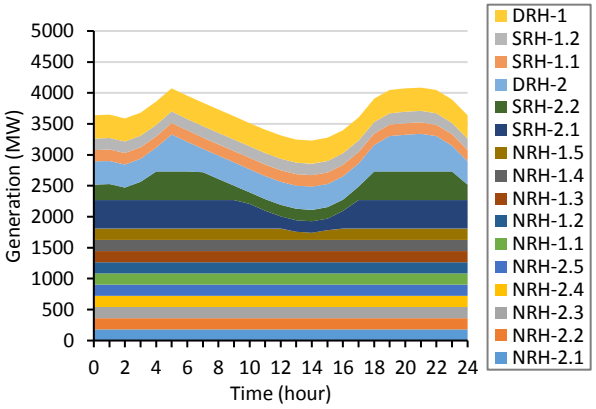

(b) 20% REPG Penetration level

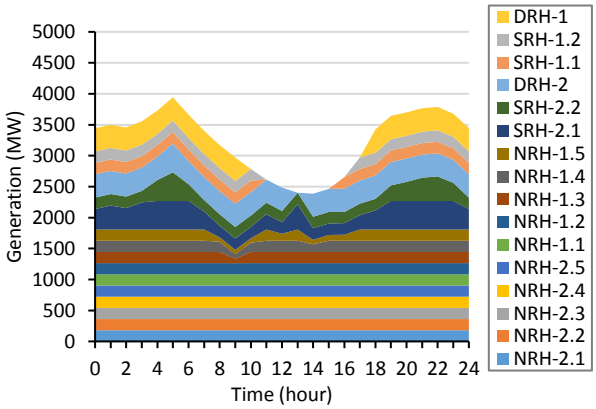

(c) 30% REPG Penetration level

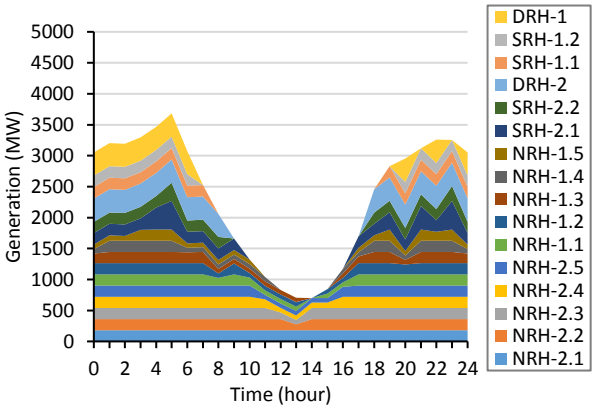

(d) 50% REPG Penetration level

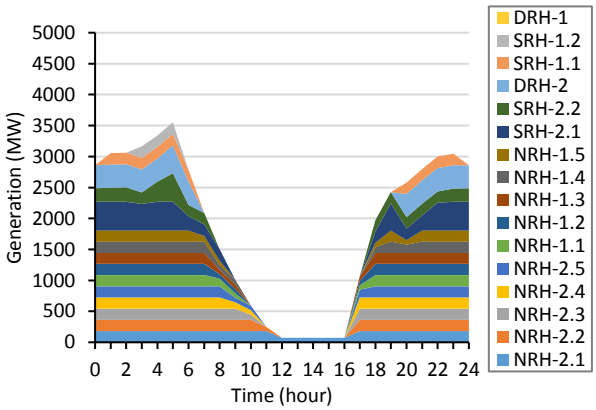

(e) 60% REPG Penetration level

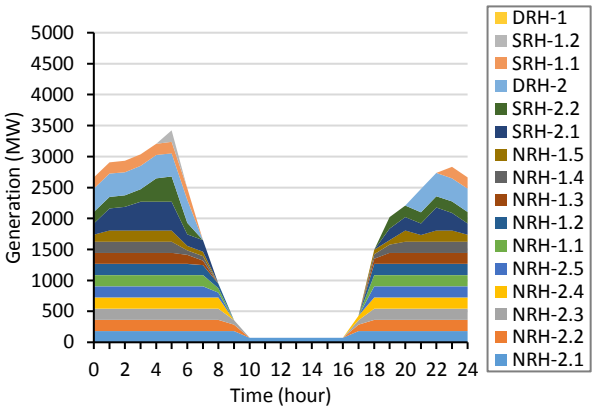

(f) 70% REPG Penetration level

C.3. Hourly Production profiles for different REPG penetration: Network 2 (dispatch method A)

(a) 0% REPG Penetration Level

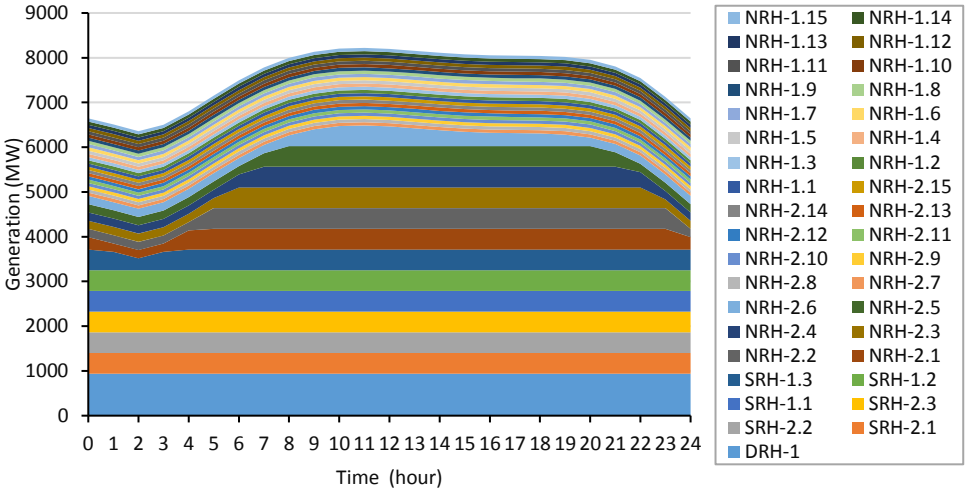

(b) 30% REPG Penetration Level

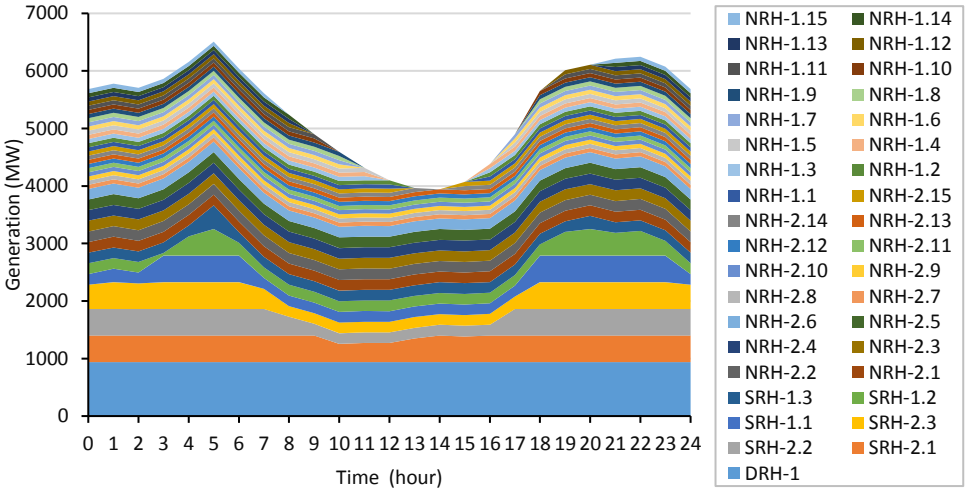

(c) 60% REPG Penetration Level

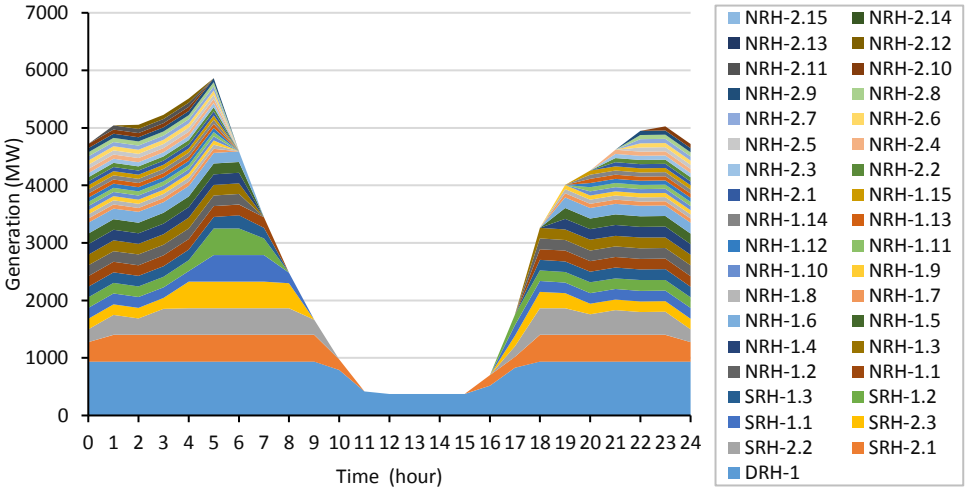

C.4. Hourly Production profiles for different REPG penetration: Network 3 (dispatch method A)

(d) 0% REPG Penetration Level

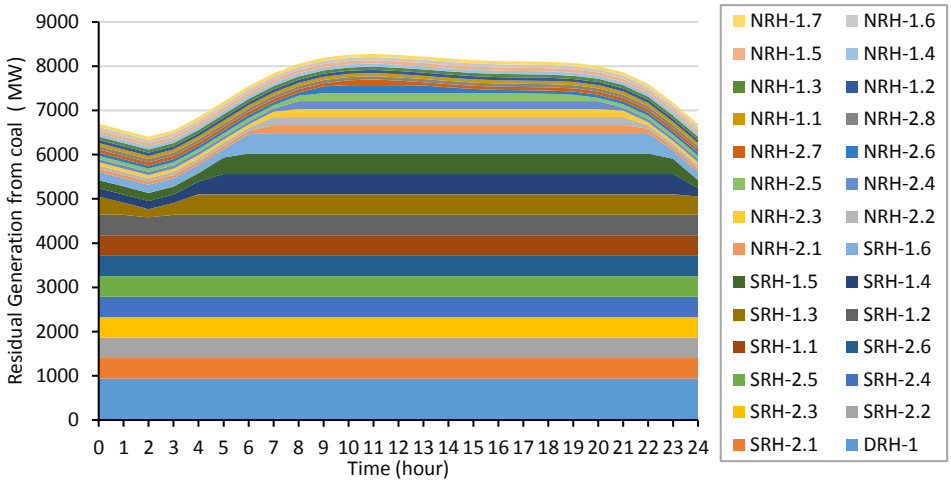

(e) 30% REPG Penetration Level

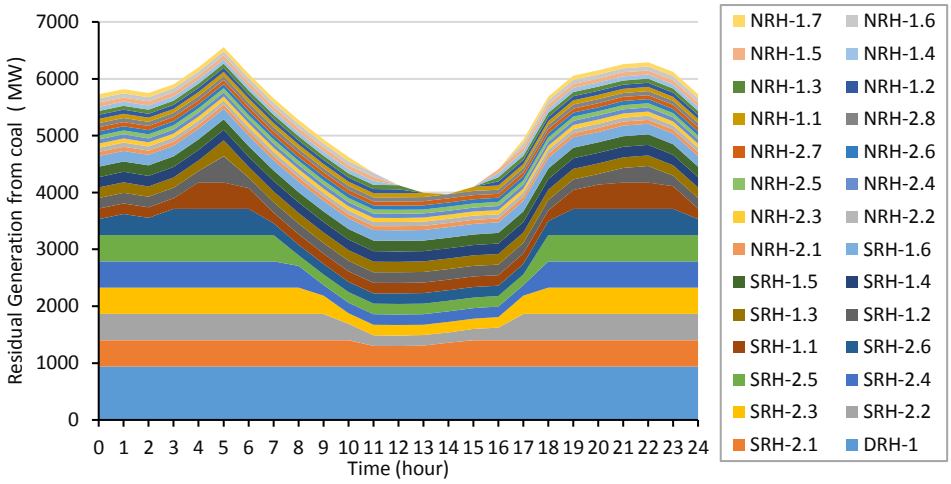

(f) 60% REPG Penetration Level

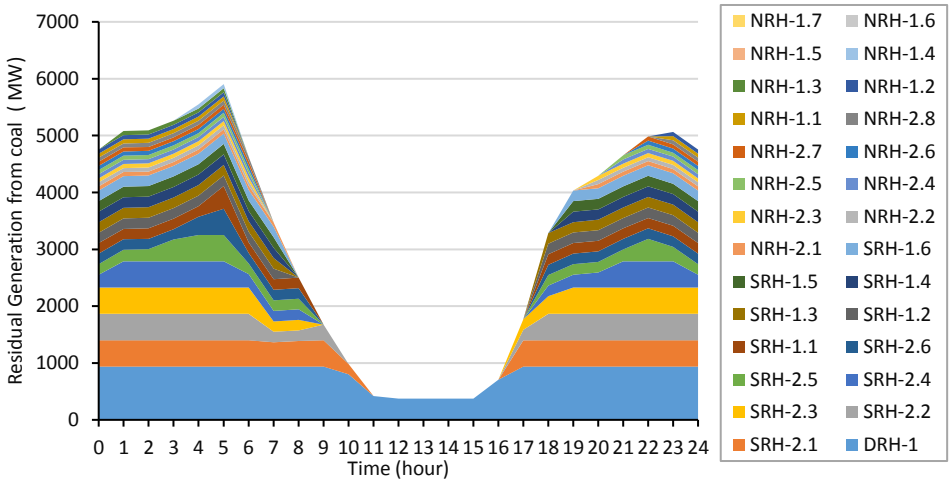

C.5. Hourly Production profiles for different REPG penetration: Network 4 (dispatch method A)

(g) 0% REPG Penetration Level

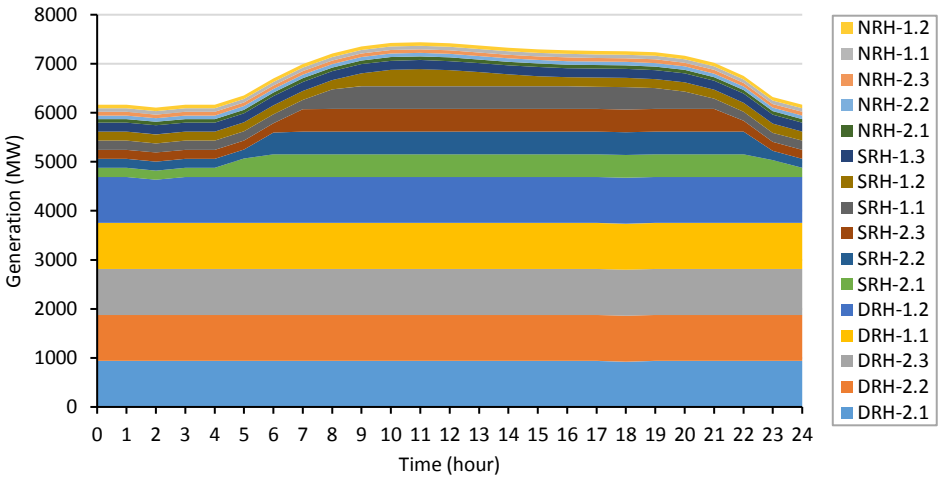

(h) 30% REPG Penetration Level

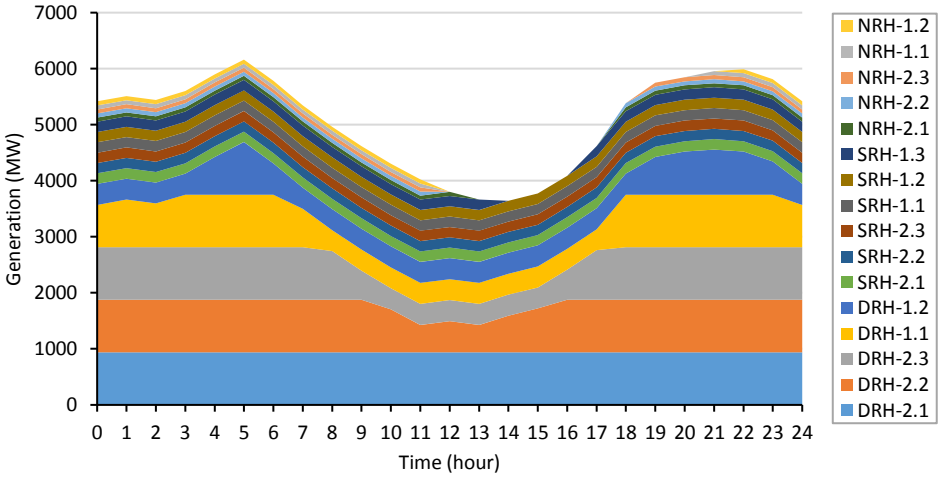

(i) 60% REPG Penetration Level

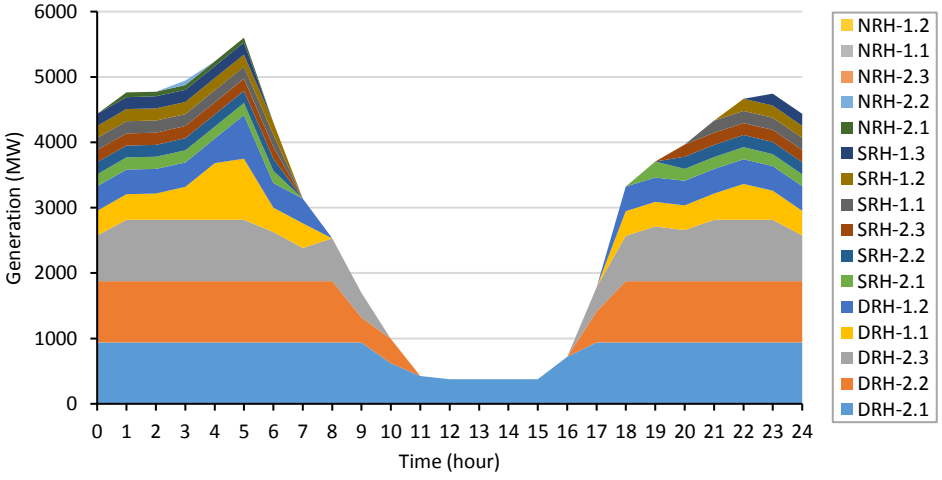

Appendix D. Fleet-wide CO_2: Impact of fuel quality